ACS SYMPOSIUM SERIES 1100

Progress in Controlled Radical Polymerization: Mechanisms and Techniques

EDITED BY
Krzysztof Matyjaszewski
Brent S. Sumerlin
Nicolay V. Tsarevsky

Downloaded by 89.163.35.42 on May 30, 2012 | http://pubs.acs.org
Publication Date (Web): March 20, 2012 | doi: 10.1021/bk-2012-1100.fw001

Progress in Controlled Radical Polymerization: Mechanisms and Techniques

Downloaded by 89.163.35.42 on May 30, 2012 | http://pubs.acs.org
Publication Date (Web): March 20, 2012 | doi: 10.1021/bk-2012-1100.fw001

ACS SYMPOSIUM SERIES **1100**

Progress in Controlled Radical Polymerization: Mechanisms and Techniques

Krzysztof Matyjaszewski, Editor
Carnegie Mellon University
Pittsburgh, Pennsylvania

Brent S. Sumerlin, Editor
Southern Methodist University
Dallas, Texas

Nicolay V. Tsarevsky, Editor
Southern Methodist University
Dallas, Texas

Sponsored by the
ACS Division of Polymer Chemistry, Inc.

American Chemical Society, Washington, DC

Distributed in print by Oxford University Press, Inc.

Downloaded by 89.163.35.42 on May 30, 2012 | http://pubs.acs.org
Publication Date (Web): March 20, 2012 | doi: 10.1021/bk-2012-1100.fw001

Downloaded by 89.163.35.42 on May 30, 2012 | http://pubs.acs.org
Publication Date (Web): March 20, 2012 | doi: 10.1021/bk-2012-1100.fw001

Library of Congress Cataloging-in-Publication Data

Progress in controlled radical polymerization : mechanisms and techniques /
Krzysztof Matyjaszewski, Brent S. Sumerlin, Nicolay V. Tsarevsky, editor[s] ; sponsored
by the ACS Division of Polymer Chemistry, Inc.
p. cm. -- (ACS symposium series ; 1100)
Includes bibliographical references and index.
ISBN 978-0-8412-2699-9
1. Addition polymerization. 2. Radicals (Chemistry) I. Matyjaszewski, K. (Krzysztof)
II. Sumerlin, Brent S. III. Tsarevsky, Nicolay V. IV. American Chemical Society.
Division of Polymer Chemistry, Inc.
TP156.P6P76 2012
541′.224--dc23
2012005349

The paper used in this publication meets the minimum requirements of American National Standard for Information Sciences—Permanence of Paper for Printed Library Materials, ANSI Z39.48n1984.

Copyright © 2012 American Chemical Society

Distributed in print by Oxford University Press, Inc.

All Rights Reserved. Reprographic copying beyond that permitted by Sections 107 or 108 of the U.S. Copyright Act is allowed for internal use only, provided that a per-chapter fee of $40.25 plus $0.75 per page is paid to the Copyright Clearance Center, Inc., 222 Rosewood Drive, Danvers, MA 01923, USA. Republication or reproduction for sale of pages in this book is permitted only under license from ACS. Direct these and other permission requests to ACS Copyright Office, Publications Division, 1155 16th Street, N.W., Washington, DC 20036.

The citation of trade names and/or names of manufacturers in this publication is not to be construed as an endorsement or as approval by ACS of the commercial products or services referenced herein; nor should the mere reference herein to any drawing, specification, chemical process, or other data be regarded as a license or as a conveyance of any right or permission to the holder, reader, or any other person or corporation, to manufacture, reproduce, use, or sell any patented invention or copyrighted work that may in any way be related thereto. Registered names, trademarks, etc., used in this publication, even without specific indication thereof, are not to be considered unprotected by law.

PRINTED IN THE UNITED STATES OF AMERICA

Downloaded by 89.163.35.42 on May 30, 2012 | http://pubs.acs.org
Publication Date (Web): March 20, 2012 | doi: 10.1021/bk-2012-1100.fw001

Foreword

The ACS Symposium Series was first published in 1974 to provide a mechanism for publishing symposia quickly in book form. The purpose of the series is to publish timely, comprehensive books developed from the ACS sponsored symposia based on current scientific research. Occasionally, books are developed from symposia sponsored by other organizations when the topic is of keen interest to the chemistry audience.

Before agreeing to publish a book, the proposed table of contents is reviewed for appropriate and comprehensive coverage and for interest to the audience. Some papers may be excluded to better focus the book; others may be added to provide comprehensiveness. When appropriate, overview or introductory chapters are added. Drafts of chapters are peer-reviewed prior to final acceptance or rejection, and manuscripts are prepared in camera-ready format.

As a rule, only original research papers and original review papers are included in the volumes. Verbatim reproductions of previous published papers are not accepted.

ACS Books Department

Downloaded by 89.163.35.42 on May 30, 2012 | http://pubs.acs.org
Publication Date (Web): March 20, 2012 | doi: 10.1021/bk-2012-1100.pr001

Preface

This book and a following volume are addressed to chemists who are interested in radical processes and especially in controlled/living radical polymerization. They summarize the most recent accomplishments in the field.

The two volumes comprise the topical reviews and specialists' contributions presented at the American Chemical Society Symposium entitled *Controlled/ Living Radical Polymerization* that was held in Denver, Colorado, August 29 - September 1, 2011. The Denver Meeting was a sequel to the previous ACS Symposia held in San Francisco, California, in 1997, in New Orleans, Louisiana, in 1999, in Boston, Massachusetts, in 2002, in Washington, DC, in 2005 and in Philadelphia, in 2008. They were summarized in the ACS Symposium Series Volume 685: *Controlled Radical Polymerization*, Volume 768: *Controlled/Living Radical Polymerization: Progress in ATRP, NMP and RAFT,* Volume 854: *Advances in Controlled/Living Radical Polymerization,* Volume 944: *Controlled/Living Radical Polymerization: From Synthesis to Materials,* Volume 1023: *Controlled/Living Radical Polymerization: Progress in ATRP*, and Volume 1024: *Controlled/Living Radical Polymerization: Progress in RAFT, DT, NMP and OMRP.* The Denver Meeting was very successful with 96 lectures and 83 posters presented. This illustrates a continuous growth in comparison to the San Francisco Meeting (32 lectures), the New Orleans Meeting (50 lectures), the Boston Meeting (80 lectures), the Washington Meeting (77 lectures), and the Philadelphia Meeting (90 lectures).

The 41 chapters submitted for publication in the ACS Symposium series could not fit into one volume, and therefore we were asked by ACS to split them into two volumes. We decided to divide the chapters into volumes related to mechanisms and techniques (21 chapters) and materials (20 chapters).

The first chapter in this volume provides an overview of the current status of controlled/living radical polymerization (CRP) systems. The following three chapters discuss important issues relevant to all radical polymerization methods. The mechanistic and kinetic topics of ATRP are covered in seven chapters, and the next two are related to commercial aspects of ATRP. Two chapters discuss organometallic radical polymerization, and the last six present recent progress in reversible addition-fragmentation chain transfer polymerization and in reversible iodine transfer polymerization.

The accompanying volume contains seven chapters on macromolecular architecture, two chapters on materials for electronic applications, eight on hybrid materials and four on bio-related materials.

Forty-one chapters published in two volumes show that CRP has made significant progress within the last 15 years. New systems have been discovered;

In Progress in Controlled Radical Polymerization: Mechanisms and Techniques; Matyjaszewski, K., et al.;
ACS Symposium Series; American Chemical Society: Washington, DC, 2012.

substantial progress has been achieved in understanding the mechanism and kinetics of reactions involved in all CRP systems. Significant progress has been made towards a comprehensive relationship between molecular structure and macroscopic properties. Some commercial applications of CRP were announced at the Denver Meeting, and it is anticipated that new products made by CRP will be soon on the market.

The financial support for the symposium from the following organizations is acknowledged: ACS Division of Polymer Chemistry, Inc., Boston Scientific, CSIRO, DSM, Evonik, General Electric, Lubrizol, the National Science Foundation, PPG, Royal Chemical Society and Wiley-VCH.

Krzysztof Matyjaszewski

Department of Chemistry
Carnegie Mellon University
4400 Fifth Avenue
Pittsburgh, Pennsylvania 15213

Brent Sumerlin

Department of Chemistry
Southern Methodist University
3215 Daniel Avenue
Dallas, Texas 75275

Nicolay V. Tsarevsky

Department of Chemistry
Southern Methodist University
3215 Daniel Avenue
Dallas, Texas 75275

Downloaded by 89.163.35.42 on May 30, 2012 | http://pubs.acs.org
Publication Date (Web): March 20, 2012 | doi: 10.1021/bk-2012-1100.pr001

Downloaded by UNIV OF GUELPH LIBRARY on May 31, 2012 | http://pubs.acs.org
Publication Date (Web): March 20, 2012 | doi: 10.1021/bk-2012-1100.ot001

Editors' Biographies

Krzysztof Matyjaszewski

Krzysztof Matyjaszewski is the J.C. Warner University Professor of Natural Sciences and Director of the Center for Macromolecular Engineering at Carnegie Mellon University. He developed atom transfer radical polymerization, commercialized in the U.S., Europe, and Japan. He has co-authored 700 publications (cited ca. 50,000 times, h-index 114), co-edited 14 books, and holds 40 U.S. and 120 international patents. Matyjaszewski received the 2011 Wolf Prize in Chemistry, 2009 Presidential Green Chemistry Challenge Award, and from the American Chemical Society: 2011 Hermann Mark Award, 2011 Award in Applied Polymer Science, 2002 Polymer Chemistry Award, and 1995 Creative Polymer Chemistry Award. He is a member of the USA National Academy of Engineering, Polish Academy of Sciences, and Russian Academy of Sciences.

Brent S. Sumerlin

Brent S. Sumerlin graduated with a B.S. from North Carolina State University (1998) and a Ph.D. from the University of Southern Mississippi (2003) under the direction of Charles McCormick. After serving as a Visiting Assistant Professor at Carnegie Mellon University under the direction of Krzysztof Matyjaszewski (2003-2005), he joined the Department of Chemistry at Southern Methodist University (Dallas, Texas, USA) as an assistant professor in 2005 and was promoted to associate professor in 2009. In 2012, Prof. Sumerlin joined the Department of Chemistry at the University of Florida. Prof. Sumerlin has received several awards, including a NSF CAREER Award and an Alfred P. Sloan Research Fellowship.

Nicolay V. (Nick) Tsarevsky

Nicolay V. (Nick) Tsarevsky obtained a M.S. in theoretical chemistry and chemical physics from the University of Sofia, Bulgaria (1999) and a Ph.D. in chemistry from Carnegie Mellon University (CMU, 2005, under Krzysztof Matyjaszewski). He was visiting assistant professor at the CMU Department of Chemistry (2005-2006), associate director of the CRP Consortium (2006-2007), and CSO of ATRP Solutions, Inc. (2007-2010). He joined the Department of Chemistry at Southern Methodist University in 2010. Research interests include polymerization techniques, functional materials, coordination chemistry, catalysis, and the chemistry of hypervalent compounds. He is the (co)author of over 65 peer-reviewed papers or book chapters, a textbook, and several patents.

Chapter 1

Controlled Radical Polymerization: State-of-the-Art in 2011

Krzysztof Matyjaszewski*

Center for Macromolecular Engineering, Department of Chemistry, Carnegie Mellon University, 4400 Fifth Avenue, Pittsburgh, Pennsylvania 15213, USA
***E-mail: km3b@andrew.cmu.edu**

Downloaded by 89.163.35.42 on May 30, 2012 | http://pubs.acs.org
Publication Date (Web): March 20, 2012 | doi: 10.1021/bk-2012-1100.ch001

The state-of-the-art of controlled radical polymerization (CRP) in 2011 is presented. Atom transfer radical polymerization, stable radical mediated polymerization, and degenerate transfer processes, including reversible addition fragmentation chain transfer are the most often used CRP procedures. CRP opens new avenues to novel materials from a large range of monomers. Detailed structure-reactivity relationships and mechanistic understanding not only helps attain a better controlled polymerization but enables preparation of polymers with complex architectures. Correlation of macromolecular structure with final properties of prepared materials is a prerequisite for creation of new applications and commercialization of various CRP products.

In Progress in Controlled Radical Polymerization: Mechanisms and Techniques; Matyjaszewski, K., et al.;
ACS Symposium Series; American Chemical Society: Washington, DC, 2012.

Controlled/living radical polymerization (CRP) is among the most rapidly expanding areas of chemistry and polymer science (*1–5*).

The advent of controlled radical polymerization (CRP) (IUPAC recommends the term reversible-deactivation radical polymerization (RDRP), or controlled reversible-deactivation radical polymerization and discourages using “living radical polymerization”) (*6*) has opened new avenues to various advanced materials with precisely controlled molecular architecture.

The dynamic equilibria required in RDRP systems can be reached in two ways (*7*). One approach employs reversible deactivation of propagating radicals to form dormant species that can be intermittently re-activated either in the presence of a catalyst, as in atom transfer radical polymerization, ATRP (*8*), or spontaneously, as in stable radical mediated polymerization, SRMP (with aminoxyl radicals or organometallic species) (*9*). The kinetics of SRMP and ATRP generally follow a particular persistent radical effect (*10*).

The second approach employs degenerate transfer between propagating radicals and dormant species. Typical examples of degenerate-transfer radical polymerization, DTRP, include reversible-addition-fragmentation chain-transfer polymerization, RAFT or iodine transfer radical polymerization (*11*). Generally, for DTRP, an external source of radicals is necessary but dormant species can also be activated by Cu-based catalyst, without generation of new chains (*12*, *13*). RAFT kinetics is similar to conventional RP but may sometimes depend on the nature of radicals and initiators/transfer agents and can be accompanied by retardation.

RDRP is among the most rapidly developing areas of polymer science. They provide a versatile synthetic tool that enables preparation of new (co)polymers with controlled architecture and materials with properties that can be targeted for various advanced technologies and biomedicine. Figure 1 presents the cumulative number of papers published on ATRP, SMRP and RAFT, as well as overall RDRP (using terms living or controlled radical polymerization) during the last 16 years. The growth in the number of publications in all areas of RDRP reflects the increasing level of interest in this field, although currently many papers do not use terms related to RDRP in titles, abstract or keywords, as they have become well-known “classic” terms in polymer science. Nevertheless, a continuous increase in the number of publications on CRP can be noted. This is accompanied by an increase in the number of patent applications and symposia partially or entirely devoted to CRP (*14–19*).

Figure 1 illustrates the results of a recent SciFinder Scholar search using the following terms: *controlled radical polymn* or *living radical polymn* (“SUM CRP” in Figure 1); *ATRP or atom transfer (radical) polymn* (“SUM ATRP”, this search does not include terms such as metal mediated or metal catalyzed (living) radical polymerization); *NMP* or *SFRP* or *nitroxide mediated polymn* or *stable free polymn* (“SUM SFRP”) and *RAFT* (“SUM RAFT”). The latter two terms were refined with terms *radical polymn* and *polymer* or *polymn*, respectively, since the search coincides with other common chemical terms such as *N-methylpyrrolidone* or *raft-associated proteins*. In summary, over 18,000 papers have been published on various CRP systems since 1995 and more than 11,000 on ATRP. Figure 1 also

Downloaded by 89.163.35.42 on May 30, 2012 | http://pubs.acs.org
Publication Date (Web): March 20, 2012 | doi: 10.1021/bk-2012-1100.ch001

Downloaded by 89.163.35.42 on May 30, 2012 | http://pubs.acs.org
Publication Date (Web): March 20, 2012 | doi: 10.1021/bk-2012-1100.ch001

shows that recently more papers are published on specific CRP methods rather than on a generic CRP or LRP.

Generally, the same rate of polymerization (whether it is a conventional process or CRP), corresponds to the same radical concentration and to essentially the same number (concentration) of terminated chains. Typically, the fraction of terminated chains is between 1 and 10%. The remaining chains are in the dormant state, capable of reactivation, functionalization, chain extension to form block copolymers, etc. Since the proportion of terminated chains in the final product is small, they often do not affect the physical properties of the targeted materials.

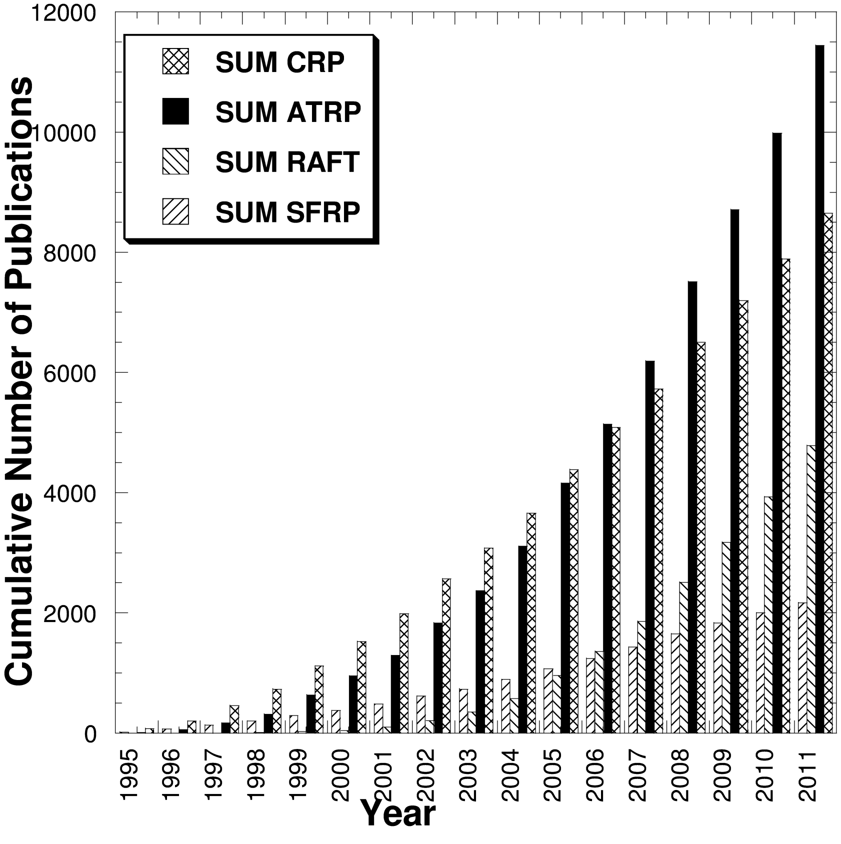

Figure 1. Results of SciFinder search on various CRP systems as of December 31, 2011. Detail explanation of terms is provided in the text.

Because termination always exists in any radical polymerization, including CRP systems, it is important to know how many chains have lost the ability to grow and cannot be further chain extended or functionalized. It is, therefore, useful to know how different reaction conditions affect chain end functionality in a CRP. Assuming, in the first approximation, a constant value of the rate coefficient of termination, predominant termination by disproportionation, and efficient initiation, one can derive a simple correlation between dead chain fraction (DCF), defined as a ratio between the concentration of terminated chains (T) and initial concentration of initiator (R-X) (*20*). This value depends on targeted degree of polymerization (DP_T, i.e. ratio of initial monomer concentration, $[M]_0$, to $[R\text{-}X]_0$), monomer conversion (*p*), propagation and termination rate constants (k_p, k_t) and reaction time, *t*. Equation 1 indicates that several strategies can be used to decrease the fraction of dead chains: reduction of the rate of polymerization (larger *t*), stopping the reaction at lower monomer conversion (smaller *p*), targeting lower DP_T, using higher initial monomer concentration (larger $[M]_0$) or choosing monomers that rapidly propagate, i.e., with a lower value of $k_t/(k_p)^2$.

$$\mathrm{DCF} = \frac{[\mathrm{T}]}{[\mathrm{R\text{-}X}]_0} = \frac{2\mathrm{DP}_\mathrm{T} k_\mathrm{t} [\ln(1-p)]^2}{[\mathrm{M}]_0 k_\mathrm{p}^2 t} \qquad (1)$$

Faster polymerization always leads to more termination. In radical polymerization, termination is often a diffusion-controlled process and differences between termination rate constants for different monomers is not large. However, propagation rate constants depend strongly on monomer structure. For example, at 80 °C, the value of k_p for styrene (St) is ca. two times smaller than that of methyl methacrylate (MMA) but nearly two orders of magnitude smaller than that of methyl acrylate (MA). Table 1 shows corresponding rate constants and values for 10% DCF (90% preserved chain end functionality) for these three monomers. Thus, it is possible to prepare poly(methyl acrylate) (PMA) with 10% DCF targeting $DP_T = 500$ at 60% conversion in 37 s. However, as highlighted by red bold entries in Table 1, the same control requires 13 hours for PMMA and 2.8 days for polystyrene (PSt)! Blue (italic underline) entries show the effect of DP_T for 500 and 100 values for PMA at 90% conversion. The former requires 4 minutes but the latter less than 1 minute. Finally, green (bold underlined) entries show that the same DCF = 10% for PSt and $DP_T = 100$ requires 3.5 days at 90% conversion but only 0.6 days at 60% conversion.

Downloaded by 89.163.35.42 on May 30, 2012 | http://pubs.acs.org
Publication Date (Web): March 20, 2012 | doi: 10.1021/bk-2012-1100.ch001

Downloaded by 89.163.35.42 on May 30, 2012 | http://pubs.acs.org
Publication Date (Web): March 20, 2012 | doi: 10.1021/bk-2012-1100.ch001

Table 1. Minimal time for the polymerization of MA, MMA and St with DCF = 10% [a] (*20*)

M	k_p *(M⁻¹ s⁻¹)*[b]	k_t *(M⁻¹ s⁻¹)*[b]	*DP*$_T$ *= 500*		*DP*$_T$ *= 100*	
			p = 60%	*p = 90%*	*p = 60%*	*p = 90%*
MA	47,400	1.10x10^8	**37 s**	*234 s*	7s	*47 s*
MMA	1,300	9.00x10^7	**13.3 h**	83.9 h	2.7 h	16.8 h
St	665	1.10x10^8	**2.8 d**	17.5 d	**0.6 d**	**3.5 d**

[a] Conditions: 80 °C, $[M]_0/[R\text{-}X]_0 = DP_T$, bulk polymerization. [b] k_p and k_t values were obtained or estimated from literature data (*21–25*). The value for k_t is the sum of k_{tc} (the combination rate constant) and k_{td} (the disproportionation rate constant).

The three "contour maps" in Figure 2 show how reaction time and conversion are correlated for the same DCF for the bulk polymerization of MA, MMA and St targeting the same DP_T (500) at 80 ºC. Each contour corresponds to the logarithmic value of DCF and the three solid lines show the relationship between reaction time and conversion for DCF = 5%, 10% and 20% respectively.

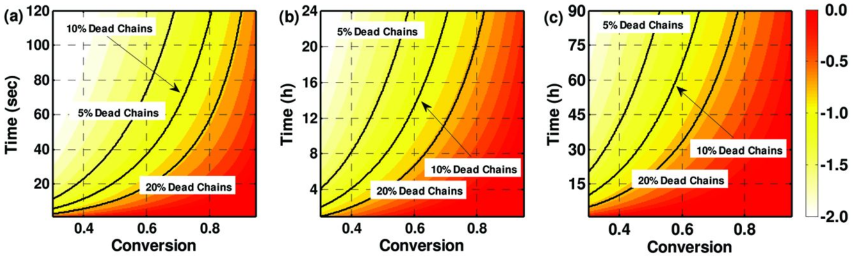

Figure 2. Contour maps for DCF as a function of conversion and polymerization time for different monomers. (a) MA; (b) MMA; (c) St. Conditions: 80 °C, $[M]_0/[R\text{-}X]_0$ = 500/1, bulk polymerization. Scale bar represents the logarithmic value of DCF (20).

The key to attaining control in a CRP is the reversible deactivation of radicals (or intermittent activation of dormant species). Their interconversion should be fast enough to provide a comparable probability of growth for all chains and, consequently, form polymers with narrow molecular weight distribution. Fine tuning of the exchange rate offers a possibility to design molecular weight distribution and also influence polymer properties. Such polymers will preserve chain end functionalities, will be capable of cross-propagation and block copolymer formation. On the other hand, due to continuous termination, polymers may loose functionality but still have low dispersity (especially if termination occurs at high conversion by disproportionation). Thus, the correlation between dispersity and functionality in CRP may be relatively weak.

Downloaded by 89.163.35.42 on May 30, 2012 | http://pubs.acs.org
Publication Date (Web): March 20, 2012 | doi: 10.1021/bk-2012-1100.ch001

Recent Progress

In introductory chapters for the previous ACS Symposia CRP proceedings (*14–19*), we referred to several challenges facing CRP processes:

1. Preservation of livingness without sacrificing the polymerization rate.
2. Controlled tacticity, sequence control and preparation of materials with complex macromolecular architecture.
3. Mechanistic understanding and comprehensive structure-reactivity correlation.
4. More environmentally friendly and inexpensive mediating agents.
5. Preparation of advanced inorganic/organic hybrid materials
6. New bioconjugates and bio-relevant materials.
7. Detailed structure-property correlation for new materials.
8. Identification of applications and commercialization of products

Some of these challenges have been addressed and significant progress has been made in all of the areas:

1. We discussed above that the proportion of terminated chains increases with the polymerization rate. However, it is possible to reduce the percentage of terminated chains at the same polymerization rate, by targeting lower conversion and lower molecular weight polymers. Since the proportion of terminated chains depends on the ratio of k_p/k_t, there is less termination for rapidly polymerizing acrylates than for styrene or methacrylates (*25*, *26*). There are possibilities to increase k_p/k_t ratio for the same monomer, by tuning various reaction conditions. For example, higher temperatures increase k_p much more than k_t, due to relatively higher activation energy of propagation (*27*) but there is a limit to the benefits of increasing temperature due to chain transfer (acrylates), self-initiation (St), depropagation (methacrylates) and other side reactions involving the mediating agent. Pressure is another important reaction parameter as radical propagation has a negative volume of activation while termination has a positive value. This strategy has been successfully applied to synthesize high MW polymers by RAFT and ATRP (*28–30*). Other strategies involve compartmentalization (*31*, *32*) in dispersed media, confined space, charge repulsion, complexation, etc. All these approaches are important as they allow increasing chain end functionality. It will be interesting to explore new complexing agents that could reduce bimolecular coupling by electrostatic repulsion. In a similar way, chain length dependent termination should enhance the k_p/k_t ratio at higher conversion.
2. Relatively low stereo- and chemoselectivities of radicals originate in the sp^2 hybridization and low polarity of radicals. Nevertheless, the addition of Lewis acids and other complexing or templating agents help enhance control of polymer tacticity and sequence distribution (*33–35*). One could also prepare dimeric or trimeric species and incorporate

Downloaded by 89.163.35.42 on May 30, 2012 | http://pubs.acs.org
Publication Date (Web): March 20, 2012 | doi: 10.1021/bk-2012-1100.ch001

these sequences directly into polymer chains. Another possibility is offered by synthesis of periodic polymers by timed incorporation of monomers with a very high tendency for alternation (e.g. phthalimide with styrene) (*36*, *37*). Polymers with controlled heterogeneity may be even more interesting than those with very regular structures (*38*). Controlled synthesis of polymers with one or more segments (*39*) displaying a distribution of chain lengths may help to generate polymers with new stable morphologies (*40*, *41*) that facilitate formation of bicontinuous morphologies for membranes, some biorelated applications or photovoltaics. The continuous change of composition along a chain in gradient copolymers significantly broadens glass transition and provides access to materials for vibration and noise dampening as well as more efficient surfactants. While the broad distribution of branches in gradient graft copolymers helps processing and may enhance properties of gels and networks. It must be stressed that one needs to control such heterogeneities in order to optimize and fine tune properties rather than just let them form spontaneously.

3. The new developments in the previously discussed areas originate in understanding the mechanism and kinetics of radical processes (*42–44*). Profound structure-reactivity correlation for monomers, radicals, dormant species and mediating agents using computational and experimental techniques helps develop an understanding of the systems and also selection of efficient initiators, mediating agents and design the sequence of monomer addition in block copolymerization (*44*).
4. There is a continuous search for new, more efficient, less expensive, environmentally friendly mediating agents. This includes identification of new ATRP catalysts that can be used at ppm amounts in benign media in the presence of reducing agents, new alkyl (pseudo)halide initiators, aminoxyl radicals applicable to methacrylates or can operate at lower temperatures, and also more environmentally friendly RAFT reagents (*8*, *9*, *11*, *44*, *45*). The basic principles correlating steric, polar, resonance and electronic properties exist but further development is needed, e.g. development of ATRP catalysts to efficiently polymerize vinyl acetate.
5. Covalent attachment of two incompatible systems can generate new hybrid materials with novel properties. These hybrids include some amphiphilic block copolymers and segmented copolymers with polar (acrylics) and non-polar (polyolefins) segments (*8*, *46–48*) that can act as efficient blend compatibilizers, surfactants and additives (*49*). Dense grafting from flat, cylindrical and spherical surfaces not only prevents particle aggregation but leads to a new class of nanocomposites with new electronic and mechanical properties.
6. Even more exciting is the area of bioconjugates. New biomaterials and bioconjugates based on water soluble components and especially stimuli responsive organic polymers could find applications in drug delivery systems and tissue engineering (*50–55*).
7. CRP provides access to a large variety of (co)polymers with controlled MW, MWD, topology, composition and functionality. However, a

full systematic evaluation of properties and potential applications of these materials is still underway. A thorough structure-property relationship for a large range of (co)polymers is very much needed. The final properties of the materials will depend not only on their molecular structure but also on processing, since processing affects their self-assembly to complex morphologies (*56*). Experimental evaluation of "libraries" with systematically varied parameters, together with computational/simulation or theoretical treatment, will help to predict properties of new systems and suggest new applications (cf. several chapters in this volume).

8. The detailed understanding of structure-property correlation is a prerequisite for specialty applications and eventual commercialization of new advanced materials produced by ATRP. However, in parallel, new cost efficient processes should be developed. During last several years several products prepared by CRP have been commercialized and new ones are expected soon (*2*, *4*).

Downloaded by 89.163.35.42 on May 30, 2012 | http://pubs.acs.org
Publication Date (Web): March 20, 2012 | doi: 10.1021/bk-2012-1100.ch001

New Challenges

There are several new or remaining challenges that could/should be addressed in the future.

1. **Competing equilibria.** Although CRP has the same stereo, chemo and regioselectivity as conventional RP, there could be some differences in degree of branching in acrylates or in copolymer composition (*57*, *58*). This stems from the various equilibria between active and dormant species competing with the radical crossover from one to another active species including tertiary and secondary systems in branching. These differences can be supplemented by different equilibria for initiating species (so called initialization) (*59*). The competing equilibria could be considered as a complication for system control but they could potentially open new possibilities to affect composition, branching, or rate and initiation efficiency.
2. **Aqueous media.** There has been a tremendous progress made in polymerization in water, both in homogeneous and in dispersed media (*32*, *60*). However, several aspects of aqueous systems require further studies, including solubility/transport phenomena, stability of mediating and dormant species and the effect of polar media on rate and equilibrium constants (*61*, *62*). Polymerization in water is attractive not only due to cost and environmental aspect but also important for bio-relevant systems, latexes, and segregation/compartmentalization.
3. **Complete monomer conversion with preserved control.** As discussed before, faster radical polymerization is accompanied by more pronounced termination reactions and a loss of control. Nevertheless, it is commercially important, in some systems, to essentially reach complete monomer conversion with preserved control over polymer architecture

and functionality. Some possibilities include CRP in aforementioned dispersed media, confined space, or complexing agents (*31*, *63*).

4. **"Universal" mediating agents.** Generally, for each CRP system there is a certain optimal mediator. Some ATRP catalysts are efficient for methacrylates but provide inadequate control for acrylates, acrylamides or vinyl acetate and vice versa. The same is true for nitroxides, organometallic species and RAFT reagents. It is tempting to seek to develop one reagent that would be applicable for the entire range of monomers and reaction conditions. Some successful attempts have been made by changing the activity of RAFT reagents by protonation (*45*, *64*, *65*), by using various reducing agents or even electrical current in ATRP (*66*, *67*) but more research should be done in this area.
5. **Functional groups for orthogonal chemistry.** Radical polymerization, in contrast to ionic and coordination polymerization, is tolerant of many functionalities. Many groups capable of robust orthogonal chemistry, such as "click" chemistry, epoxy transformation, thiol-ene reactions, have been incorporated into copolymers and this can be expanded to include materials with multiple hydrogen bonding, biodegradablity and many other functionalities (*49*, *68*, *69*).
6. **Smart-responsive systems.** CRP has been successfully used to synthesize polymers with functionalities that respond to various external stimuli such as: temperature, light, pH, ionic strength, sugar content, pressure, electric or magnetic fields (*70–75*). Especially interesting are amphiphilic segmented copolymers that lead to materials that can contract, expand, change solubility, hydrophilicity, etc. New opportunities are offered by hybrid materials, polymers at surfaces that can be self-cleaning (*76*), bioconjugates that can change activity upon stimulation. Self-healing systems also belong to this category (*77–81*). New "intelligent" materials synthesized by CRP should be precisely characterized to optimize their properties in the application.
7. **CRP polymers for energy and environment.** Advanced polymers prepared by CRP can meet the requirements of applications related to energy and the environment (*47*, *82–84*). Functional polymers prepared by CRP can be linked covalently to optoelectronically active polymers to generate bulk heterojunctions at the nanometer scale. They can be used as precursors for nanostructured graphitic carbons, and as electrode materials or membranes, both in fuel cells or water desalination. An environmental challenge for all vinyl polymers, including those made by CRP, is their controlled degradation, which is also critical for biomedical applications. How can vinyl polymers be efficiently degraded? One approach is to incorporate degradable moieties into the backbone by radical ring opening copolymerization, another would be to generate stars with degradable cores or precisely controlled networks with degradable crosslinkage.
8. **Commercialization.** Commercialization of CRP products is slower than anticipated. Although several advanced products have been on the market for several years, volume is relatively small and therefore

Downloaded by 89.163.35.42 on May 30, 2012 | http://pubs.acs.org
Publication Date (Web): March 20, 2012 | doi: 10.1021/bk-2012-1100.ch001

Downloaded by 89.163.35.42 on May 30, 2012 | http://pubs.acs.org
Publication Date (Web): March 20, 2012 | doi: 10.1021/bk-2012-1100.ch001

cost is high. Some initially used processes employed batch rather than continuous processes (*85*, *86*) and relied on less efficient mediators; such as TEMPO, less stable and more difficult to purify RAFT reagents, or ATRP catalysts that required high concentrations of Cu. Therefore, it is expected that introduction of new CRP procedures, including new nitroxides operating at lower temperatures, more stable RAFT reagents, low ppm Cu ATRP processes, such as ARGET and ICAR should, reduce costs, facilitate commercialization and consequently introduce new products to the marketplace. New mediating agents should be developed, processes that can lead to complete, or high, monomer consumption and to polymers with retained functionality. Structure-property correlations should be developed, not only for systems with ideal architecture but also for materials with some defects in a form of incomplete functionality, missing arms for stars, or polymers with higher dispersity. Some of these products not only could have sufficiently good properties, but also tolerate a broader processing regime, or even lead to materials with new morphologies and new properties.

These and other issues will be studied in a future and some results could be presented at the next ACS Symposium on CRP.

Acknowledgments

Support from the National Science Foundation (CHE 10-26060) and DMR (09-69301) is gratefully acknowledged.

References

1. Matyjaszewski, K.; Davis, T. P. *Handbook of Radical Polymerization*; Wiley-Interscience: Hoboken, 2002.
2. Matyjaszewski, K.; Spanswick, J. *Mater. Today (Oxford, U.K.)* **2005**, *8*, 26–33.
3. Braunecker, W. A.; Matyjaszewski, K. *Prog. Polym. Sci.* **2007**, *32*, 93–146.
4. Destarac, M. *Macromol. React. Eng.* **2010**, *4*, 165–179.
5. Mueller, A. H. E.; Matyjaszewski, K. *Controlled and Living Polymerizations: From Mechanisms to Materials*; Wiley-VCH: Weinheim, 2009.
6. Jenkins, A. D.; Jones, R. G.; Moad, G. *Pure Appl. Chem.* **2010**, *82*, 483–491.
7. Goto, A.; Fukuda, T. *Prog. Polym. Sci.* **2004**, *29*, 329–385.
8. Matyjaszewski, K.; Tsarevsky, N. V. *Nat. Chem.* **2009**, *1*, 276–288.
9. Bertin, D.; Gigmes, D.; Marque, S. R. A.; Tordo, P. *Chem. Soc. Rev.* **2011**, *40*, 2189–2198.
10. Fischer, H. *Chem. Rev.* **2001**, *101*, 3581.
11. Moad, G.; Thang, S. H. *Aust. J. Chem.* **2009**, *62*, 1379–1381.
12. Nicolay, R.; Kwak, Y.; Matyjaszewski, K. *Angew. Chem., Int. Ed.* **2010**, *49*, 541–544.

13. Kwak, Y.; Nicolay, R.; Matyjaszewski, K. *Aust. J. Chem.* **2009**, *62*, 1384–1401.
14. Matyjaszewski, K., Ed.; *Controlled Radical Polymerization*; ACS Symposium Series 685; American Chemical Society: Washington, DC, 1998.
15. Matyjaszewski, K., Ed.; *Controlled/Living Radical Polymerization. Progress in ATRP, NMP, and RAFT*; ACS Symposium Series 768; American Chemical Society: Washington, DC, 2000.
16. Matyjaszewski, K., Ed.; *Advances in Controlled/Living Radical Polymerization*; ACS Symposium Series 854; American Chemical Society: Washington, DC, 2003.
17. Matyjaszewski, K., Ed.; *Controlled/Living Radical Polymerization: From Synthesis to Materials*; ACS Symposium Series 944; American Chemical Society: Washington, DC, 2006.
18. Matyjaszewski, K., Ed.; *Controlled/Living Radical Polymerization: Progress in ATRP*; ACS Symposium Series 1023; American Chemical Society: Washington, DC, 2009.
19. Matyjaszewski, K., Ed.; *Controlled/Living Radical Polymerization: Progress in Progress in RAFT, DT, NMP and OMRP*; ACS Symposium Series 1024American Chemical Society: Washington, DC, 2009.
20. Zhong, M.; Matyjaszewski, K. *Macromolecules* **2011**, *44*, 2668–2677.
21. Buback, M.; Kurz, C. H.; Schmaltz, C. *Macromol. Chem. Phys.* **1998**, *199*, 1721–1727.
22. Beuermann, S.; Buback, M.; Davis, T. P.; Garcia, N.; Gilbert, R. G.; Hutchinson, R. A.; Kajiwara, A.; Kamachi, M.; Lacik, I.; Russell, G. T. *Macromol. Chem. Phys.* **2003**, *204*, 1338–1350.
23. Buback, M.; Gilbert, R. G.; Hutchinson, R. A.; Klumperman, B.; Kuchta, F. D.; Manders, B. G.; Odriscoll, K. F.; Russell, G. T.; Schweer, J. *Macromol. Chem. Phys.* **1995**, *196*, 3267–3280.
24. Buback, M.; Egorov, M.; Gilbert, R. G.; Kaminsky, V.; Olaj, O. F.; Russell, G. T.; Vana, P.; Zifferer, G. *Macromol. Chem. Phys.* **2002**, *203*, 2570–2582.
25. Barner-Kowollik, C.; Buback, M.; Egorov, M.; Fukuda, T.; Goto, A.; Olaj, O. F.; Russell, G. T.; Vana, P.; Yamada, B.; Zetterlund, P. B. *Prog. Polym. Sci.* **2005**, *30*, 605–643.
26. Barner-Kowollik, C.; Russell, G. T. *Prog. Polym. Sci.* **2009**, *34*, 1211–1259.
27. Beuermann, S.; Buback, M. *Prog. Polym. Sci.* **2002**, *27*, 191–254.
28. Kwiatkowski, P.; Jurczak, J.; Pietrasik, J.; Jakubowski, W.; Mueller, L.; Matyjaszewski, K. *Macromolecules* **2008**, *41*, 1067–1069.
29. Pietrasik, J.; Hui, C. M.; Chaladaj, W.; Dong, H.; Choi, J.; Jurczak, J.; Bockstaller, M. R.; Matyjaszewski, K. *Macromol. Rapid Commun.* **2011**, *32*, 295–301.
30. Arita, T.; Buback, M.; Janssen, O.; Vana, P. *Macromol. Rapid Commun.* **2004**, *25*, 1376–1381.
31. Zetterlund, P. B. *Macromolecules* **2010**, *43*, 1387–1395.
32. Zetterlund, P. B.; Kagawa, Y.; Okubo, M. *Chem. Rev.* **2008**, *108*, 3747–3794.
33. Kamigaito, M.; Satoh, K. *Macromolecules* **2008**, *41*, 269–276.

Downloaded by 89.163.35.42 on May 30, 2012 | http://pubs.acs.org
Publication Date (Web): March 20, 2012 | doi: 10.1021/bk-2012-1100.ch001

Downloaded by 89.163.35.42 on May 30, 2012 | http://pubs.acs.org
Publication Date (Web): March 20, 2012 | doi: 10.1021/bk-2012-1100.ch001

34. Satoh, K.; Matsuda, M.; Nagai, K.; Kamigaito, M. *J. Am. Chem. Soc.* **2010**, *132*, 10003–10005.
35. Hibi, Y.; Ouchi, M.; Sawamoto, M. *Angew. Chem., Int. Ed.* **2011**, *50*, 7434–7437.
36. Giuseppone, N.; Lutz, J. F. *Nature* **2011**, *473*, 40–41.
37. Lutz, J. F. *Polym. Chem.* **2010**, *1*, 55–62.
38. Matyjaszewski, K. *Science* **2011**, *333*, 1104–1105.
39. Boyer, C.; Soeriyadi, A. H.; Zetterlund, P. B.; Whittaker, M. R. *Macromolecules* **2011**, *44*, 8028–8033.
40. Listak, J.; Jakubowski, W.; Mueller, L.; Plichta, A.; Matyjaszewski, K.; Bockstaller, M. R. *Macromolecules* **2008**, *41*, 5919–5927.
41. Lynd, N. A.; Meuler, A. J.; Hillmyer, M. A. *Prog. Polym. Sci.* **2008**, *33*, 875–893.
42. Tang, W.; Kwak, Y.; Braunecker, W.; Tsarevsky, N. V.; Coote, M. L.; Matyjaszewski, K. *J. Amer. Chem. Soc.* **2008**, *130*, 10702–10713.
43. Lin, C. Y.; Coote, M. L.; Gennaro, A.; Matyjaszewski, K. *J. Amer. Chem. Soc.* **2008**, *130*, 12762–12774.
44. Lin, C.-Y.; Marque, S. R. A.; Matyjaszewski, K.; Coote, M. L. *Macromolecules* **2011**, *44*, 7568–7583.
45. Benaglia, M.; Chiefari, J.; Chong, Y. K.; Moad, G.; Rizzardo, E.; Thang, S. H. *J. Amer. Chem. Soc.* **2009**, *131*, 6914–6915.
46. Beija, M.; Marty, J. D.; Destarac, M. *Prog. Polym. Sci.* **2011**, *36*, 845–886.
47. Moad, G.; Chen, M.; Häussler, M.; Postma, A.; Rizzardo, E.; Thang, S. H. *Polym. Chem.* **2011**, *2*, 492–519.
48. Leblanc, A.; Grau, E.; Broyer, J. P.; Boisson, C.; Spitz, R.; Monteil, V. *Macromolecules* **2011**, *44*, 3293–3301.
49. Feldman, K. E.; Kade, M. J.; de Greef, T. F. A.; Meijer, E. W.; Kramer, E. J.; Hawker, C. J. *Macromolecules* **2008**, *41*, 4694–4700.
50. Oh, J. K.; Drumright, R.; Siegwart, D. J.; Matyjaszewski, K. *Prog. Polym. Sci.* **2008**, *33*, 448–477.
51. Lutz, J.-F.; Boerner, H. G. *Prog. Polym. Sci.* **2008**, *33*, 1–39.
52. Nicolas, J.; Mantovani, G.; Haddleton, D. M. *Macromol. Rapid Commun.* **2007**, *28*, 1083–1111.
53. Bordes, P.; Pollet, E.; Averous, L. *Prog. Polym. Sci.* **2009**, *34*, 125–155.
54. Siegwart, D. J.; Oh, J. K.; Matyjaszewski, K. *Prog. Polym. Sci.* **2012**, *37*, 18–37.
55. Le Droumaguet, B.; Nicolas, J. *Polym. Chem.* **2010**, *1*, 563–598.
56. Leibler, L. *Prog. Polym. Sci.* **2005**, *30*, 898–914.
57. Konkolewicz, D.; Sosnowski, S.; D'Hooge, D. R.; Szymanski, R.; Reyniers, M.-F.; Marin, G. B.; Matyjaszewski, K. *Macromolecules* **2011**, *44*, 8361–8373.
58. Matyjaszewski, K. *Macromolecules* **2002**, *35*, 6773–6781.
59. Van Den Dungen, E. T. A.; Matahwa, H.; McLeary, J. B.; Sanderson, R. D.; Klumperman, B. *J. Polym. Sci., Part A: Polym. Chem.* **2008**, *46*, 2500–2509.
60. Min, K.; Matyjaszewski, K. *Cent. Eur. J. Chem.* **2009**, *7*, 657–674.
61. Bortolamei, N.; Isse, A. A.; Magenau, A. J. D.; Gennaro, A.; Matyjaszewski, K. *Angew. Chem., Int. Ed.* **2011**, *50*, 11391–11394.

62. (a) Braunecker, W. A.; Tsarevsky, N. V.; Gennaro, A.; Matyjaszewski, K. *Macromolecules* **2009**, *42*, 6348−6360. (b) Averick, S.; Simakova, A.; Park, S.; Konkolewicz, D.; Magenau, A. J. D.; Mehl, R. A.; Matyjaszewski, K. *ACS Macro Lett.* **2012**, *1*, 6−10.
63. Gao, H.; Matyjaszewski, K. *Prog. Polym. Sci.* **2009**, *34*, 317–350.
64. Keddie, D. J.; Guerrero-Sanchez, C.; Moad, G.; Rizzardo, E.; Thang, S. H. *Macromolecules* **2011**, *44*, 6738–6745.
65. Benaglia, M.; Chen, M.; Chong, Y. K.; Moad, G.; Rizzardo, E.; Thang, S. H. *Macromolecules* **2009**, *42*, 9384–9386.
66. Magenau, A. J. D.; Strandwitz, N. C.; Gennaro, A.; Matyjaszewski, K. *Science* **2011**, *332*, 81–84.
67. di Lena, F.; Matyjaszewski, K. *Prog. Polym. Sci.* **2010**, *35*, 959–1021.
68. Golas, P. L.; Matyjaszewski, K. *Chem. Soc. Rev.* **2010**, *39*, 1338–1354.
69. Thomas, C. M.; Lutz, J. F. *Angew. Chem.* **2011**, *50*, 9244–9246.
70. Lee, H.-i.; Pietrasik, J.; Sheiko, S. S.; Matyjaszewski, K. *Prog. Polym. Sci.* **2010**, *35*, 24–44.
71. Murphy, E. B.; Wudl, F. *Prog. Polym. Sci.* **2010**, *35*, 223–251.
72. Chen, T.; Ferris, R.; Zhang, J.; Ducker, R.; Zauscher, S. *Prog. Polym. Sci.* **2010**, *35*, 94–112.
73. Urban, M. W. *Prog. Polym. Sci.* **2009**, *34*, 679–687.
74. Wu, D. Y.; Meure, S.; Solomon, D. *Prog. Polym. Sci.* **2008**, *33*, 479–522.
75. Smith, A. E.; Xu, X.; McCormick, C. L. *Prog. Polym. Sci.* **2010**, *35*, 45–93.
76. Dong, H.; Ye, P.; Zhong, M.; Pietrasik, J.; Drumright, R.; Matyjaszewski, K. *Langmuir* **2010**, *26*, 15567–15573.
77. Amamoto, Y.; Kamada, J.; Otsuka, H.; Takahara, A.; Matyjaszewski, K. *Angew. Chem., Int. Ed.* **2011**, *50*, 1660–1663.
78. Nicolay, R.; Kamada, J.; Van Wassen, A.; Matyjaszewski, K. *Macromolecules* **2010**, *43*, 4355–4361.
79. Kamada, J.; Koynov, K.; Corten, C.; Juhari, A.; Yoon, J. A.; Urban, M. W.; Balazs, A. C.; Matyjaszewski, K. *Macromolecules* **2010**, *43*, 4133–4139.
80. Canadell, J.; Goossens, H.; Klumperman, B. *Macromolecules* **2011**, *44*, 2536–2541.
81. Su, J.; Amamoto, Y.; Nishihara, M.; Takahara, A.; Otsuka, H. *Polym. Chem.* **2011**, *2*, 2021–2026.
82. Tang, C.; Wu, W.; Smilgies, D.-M.; Matyjaszewski, K.; Kowalewski, T. *J. Am. Chem. Soc.* **2011**, *133*, 11802–11809.
83. McCullough, L. A.; Matyjaszewski, K. *Mol. Cryst. Liq. Cryst.* **2010**, *521*, 1–55.
84. Chen, M.; Häussler, M.; Moad, G.; Rizzardo, E. *Org. Biomol. Chem.* **2011**, *9*, 6111–6119.
85. Hornung, C. H.; Guerrero-Sanchez, C.; Brasholz, M.; Saubern, S.; Chiefari, J.; Moad, G.; Rizzardo, E.; Thang, S. H. *Org. Process Res. Dev.* **2011**, *15*, 593–601.
86. Chan, N.; Cunningham, M. F.; Hutchinson, R. A. *Macromol. Rapid Commun.* **2011**, *32*, 604–609.

Downloaded by 89.163.35.42 on May 30, 2012 | http://pubs.acs.org
Publication Date (Web): March 20, 2012 | doi: 10.1021/bk-2012-1100.ch001

Chapter 2

The Mechanism of Stereoregulation in Free-Radical Polymerization of Bulky Methacrylates

Isa Degirmenci, Benjamin B. Noble, Ching Yeh Lin, and Michelle L. Coote*

**ARC Centre of Excellence for Free-Radical Chemistry and Biotechnology,
Research School of Chemistry, Australian National University,
Canberra ACT 0200, Australia
*E-mail: mcoote@rsc.anu.edu.au**

Theoretical calculations are performed to explore the origin of inherent tacticity in bulky methacrylates. Geometries and conformer distributions of monomers and oligomeric propagating radicals are calculated to study the impact of steric bulk and π-stacking interactions on the preferences for meso versus isotactic propagation. Consistent with the previous qualitative analyses by Satoh and Kamigaito, we have demonstrated a correlation between the preference for meso propagation and the steric bulk of the ester side chain, where the latter is measured as the volume of the side chain. We have also confirmed that syndiotactic methacrylates prefer linear chains, isotactic methacrylates prefer helical chains and the increasing isotactic preference with chain length can thus be understood in terms of the increasing helical tendency as substituents become more bulky. We also demonstrated that, whilst π-stacking interactions in aryl methacrylates are significant, the extent to which they influence the tacticity depends on their bulkiness and associated helical tendency. We have also provided an explanation for their solvent dependence in terms of the disruption of π-stacking conformations by the formation of inclusion complexes.

In Progress in Controlled Radical Polymerization: Mechanisms and Techniques; Matyjaszewski, K., et al.;
ACS Symposium Series; American Chemical Society: Washington, DC, 2012.

Introduction

While controlled radical polymerization regulates most aspects of the resulting polymer microstructure, a remaining and significant inadequacy of radical based techniques is the lack of stereochemical control in common radical polymerizations. Controlling the tacticity (stereochemistry) of a polymer is highly desirable because it influences its physical properties such as the melting point, solubility, density, crystallinity and mechanical strength (*1*, *2*). For instance, the melting points of isotactic, syndiotactic and atactic polypropene are 165 °C, 130 °C and 0 °C, respectively (*3*). Given the industrial significance of radical polymerization, much current research is aimed at finding inexpensive stereocontrol agents that are usable with ordinary monomers under practical reaction conditions (*4*). Two notable approaches to stereocontrol are polar solvent mediated radical polymerisation yielding syndiotactic polymers and Lewis acid mediated radical polymerisation yielding isotactic polymers (see Scheme 1) (*5*). While both approaches have had a lot of success in influencing polymer tacticity, neither can replicate the high stereoregularity of polymers produced by ionic or coordination methods. Additionally these approaches can be expensive to implement, are only applicable to monomers with polar substituents such as carbonyl groups, and are often incompatible with successful controlled radical polymerization processes.

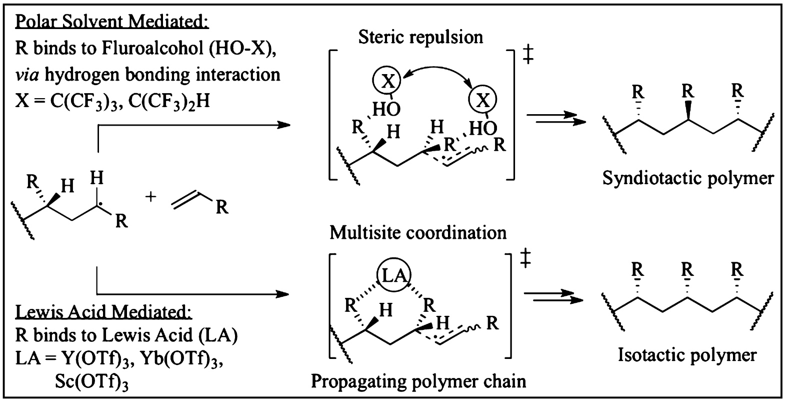
Polar Solvent Mediated:
R binds to Fluroalcohol (HO-X), *via* hydrogen bonding interaction
X = C(CF3)3, C(CF3)2H
Steric repulsion
X
HO
X
HO
R
H
H
R
R
‡
R R R
Syndiotactic polymer
R H H
+
R
R
Multisite coordination
LA
R H R
H
R
‡
R R R
Isotactic polymer
Lewis Acid Mediated:
R binds to Lewis Acid (LA)
LA = Y(OTf)3, Yb(OTf)3, Sc(OTf)3
Propagating polymer chain

Scheme 1. Current stereocontrol strategies in radical polymerisation: Lewis acid mediated and polar solvent mediated. (Adapted from Ref. (4)).

As a first step toward designing better stereocontrol strategies we have conducted a theoretical investigation into the mechanism of stereoregulation in free-radical polymerization in the absence of added control agents. For most monomers, the stereochemistry of the penultimate unit only weakly influences the terminal radical, primarily because of the planarity of the propagating radical and the relatively early position of the transition state. However, a number of exceptions have been documented in the experimental literature, typically involving monomers with side chains that are very bulky (*6*), chiral (*7*), highly aromatic (*8–10*) or complexed with metal ions (*11*). In such cases highly stereoregular polymers have been successfully prepared by radical polymerization. In this article we draw on our theoretical studies, as well as experimental evidence from the literature, to identify the principal factors affecting the stereochemistry in the polymerization of bulky methacrylates. Understanding the origin of stereoregulation in these special cases, and in particular the role of non-covalent interactions between substituents, can help us to design better control strategies for more conventional monomers.

Theoretical Background

The stereoregularity (or tacticity) of a polymer is determined by the relative orientation of substituents with respect to the C-C macromolecular backbone (see Scheme 2). Tacticity can be quantified by the relative fraction of racemo (*r*) and meso (*m*) diads or more precisely, by the fraction of syndiotactic (*rr*), isotactic (*mm*) and heterotactic triads (*rm*, *mr*). On the basis of diad structures, a syndiotactic polymer has $r \rightarrow 1$, an isotactic polymer has $m \rightarrow 1$ and a 'purely' atactic polymer has $r = m = 0.5$. On the basis of triad structures, a syndiotactic polymer has $rr \rightarrow 1$, an isotactic polymer has $mm \rightarrow 1$ and a 'purely' atactic polymer has $rm = mr = 0.5$. Polymers produced by radical polymerisation typically have a tacticity in the range of $r = 0.7$ to $m = 0.7$ depending on the type of monomer and the conditions used for the polymerisation reaction. In practical terms these polymers are considered atactic because they are neither syndiotactic nor isotactic.

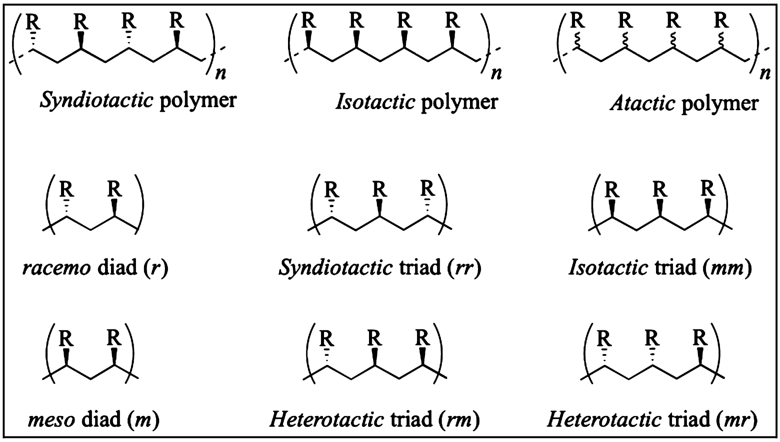

Scheme 2. Polymer tacticity nomenclature.

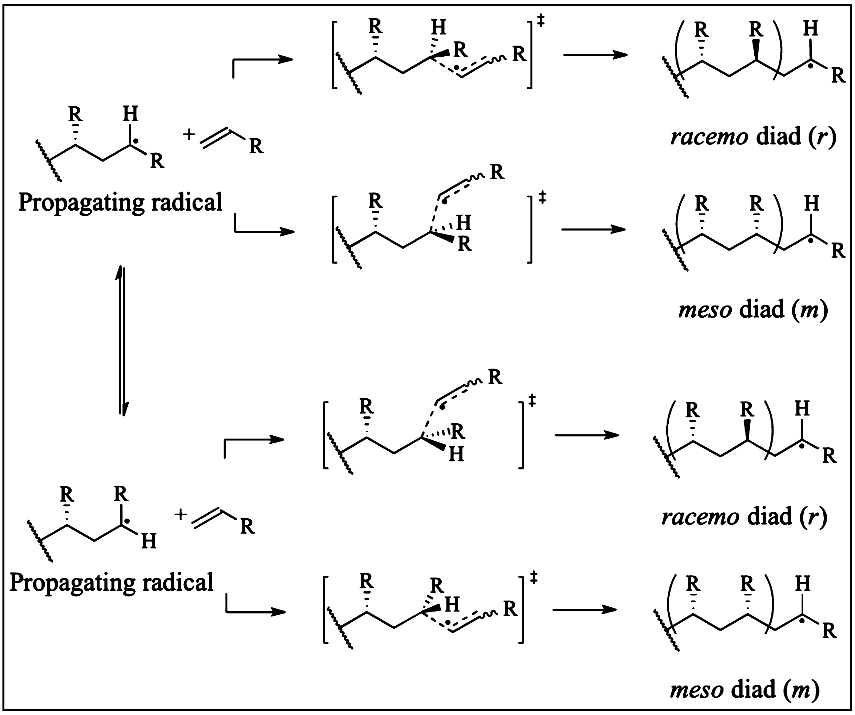

Scheme 3. Racemo and meso propagation of a polymer radical.

The concentrations of the various diads and triads are in turn determined by the relative orientation of the terminal substituent during the addition step (see Scheme 3). Thus the tacticity of a polymer merely reflects the kinetic selectivity of the propagating radical for different forms of monomer addition. Stereoregular polymers are formed when the stereochemistry at the penultimate unit of the polymer chain induces stereospecific monomer addition at the pro-chiral reactive center. It should be noted that the type of stereocenter formed in the propagation step will depend on *both* the conformation of the attacking the radical and the face from which the monomer attacks the (typically planar) radical center. Thus, in principle, a given conformation of the propagating radical can give rise to either type of stereocenter, according to the face from which the monomer attacks. The favoring of one propagating radical conformer over another is not sufficient to direct stereochemistry unless there is also an accompanying preference for the face of attack. However, theoretical studies of propagation reactions have found that attack usually occurs from the opposite face to the polymer chain (i.e. the first and fourth transition structures in Scheme 3) (*12*). For instance, Figure 1 shows our B3-LYP/6-31G(d) optimized racemo- and meso-like conformers of the methyl methacrylate propagating radical and their preferred transition structures. Each conformer in this case is expected to be selective for each stereoisomer and the favoring of one conformer over another provides a plausible mechanism of stereocontrol.

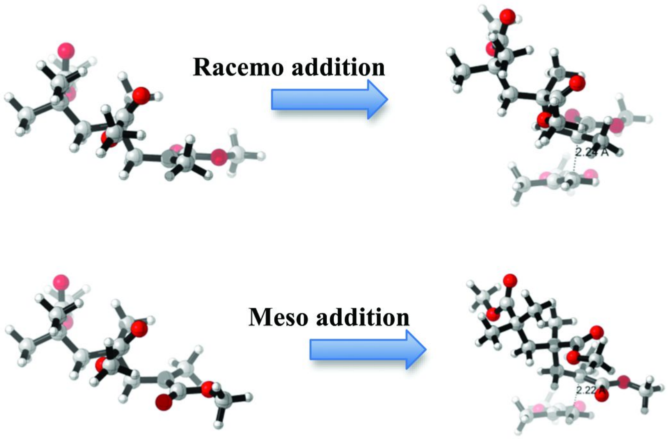

Figure 1. B3-LYP/6-31G(d) Optimized Geometries of the racemo and meso conformers of a trimeric poly(MMA) propagating radical and their preferred transition structures in each case.

Inherent Tacticity of Bulky Monomers

In their excellent review, Satoh and Kamigaito (*4*) highlighted an intriguing qualitative relationship between the steric bulk of a monomer and the tacticity of the resulting polymer. On the one hand, they noted methyl methacrylate (MMA) and other aliphatic methacrylic esters had a tendency to form syndiotactic rich polymers, presumably due to steric repulsion between the α-methyl groups and the ester groups. Somewhat counterintuitively, however, the syndiotactic preference decreases, rather than increases, as the ester side chain becomes more bulky, to the extent that some exceptionally bulky monomers form highly isotactic polymers. They suggested that these differing impacts of steric repulsions are due to changes in the chain structure as the size of the bulky groups increase. Whereas moderately bulky polymers might be expected to form linear growing chains for which syndiotactic structures would minimize steric repulsion, more bulky chains tend to form helical structures where it is the isotactic structures that are best able to orient the groups with minimal steric repulsion. Superimposed on these general trends, they also noted that some (but not all) bulky methacrylates with aromatic side chains can form highly syndiotactic polymers instead, a tendancy was affected by the solvent type. This indicates that other interactions, such as π-stacking can also contribute though the effect is not general.

In the present work, we have used theoretical calculations of monomer and propagating radical structures to test these ideas and place the relationship between steric bulk on inherent tacticity on a more quantitative footing. To this end, we considered the free-radical polymerization of a number of bulky methacrylate monomers as shown in Scheme 4. Table 1 summarizes the experimental tacticities of their resulting polymers, as produced under relatively consistent conditions (temperatures in the range 50-70°C; toluene or benzene solution). All experimental data are drawn from the review by Satoh and Kamigaito (*4*), except for the silicon containing methacrylates (M17-23), which are drawn from their more recent work (*13*). These data are reported in the literature as measured percentages of the isotactic (*mm*), heterotactic (*mr*) or syndiotactic (*rr*) triads. To simplify the analysis, we have converted these into a kinetic preference for meso versus racemo propagation using a simple Bernoullian model of propagation in which the reactivity is assumed to be dependent only on the stereochemistry of the penultimate unit. Under this model, the probability of meso propagation is given by $\%m = mm + mr/2$, the probability of racemo propagation is given by $\%r = rr + mr/2$, and their sum adds to 100%. To test this model, in Figure 2, we plot the experimentally observed triad fractions, *mm, mr* and *rr* against *%m*, and compare the data with the theoretical lines for Bernoullian statistics. The plot shows that the Bernoullian model provides an excellent description of the data, with M14 the only significant outlier. Interestingly, this species was studied at a different monomer concentration compared with the others, implying that solvent effects might have been responsible for its non-Bernoullian behavior. For the rest of the test set, these results imply that quantum-chemical studies need only take into account the stereochemistry of the penultimate unit of the polymer chain into account when predicting the stereochemistry; further *ab initio* testing of this result is currently underway.

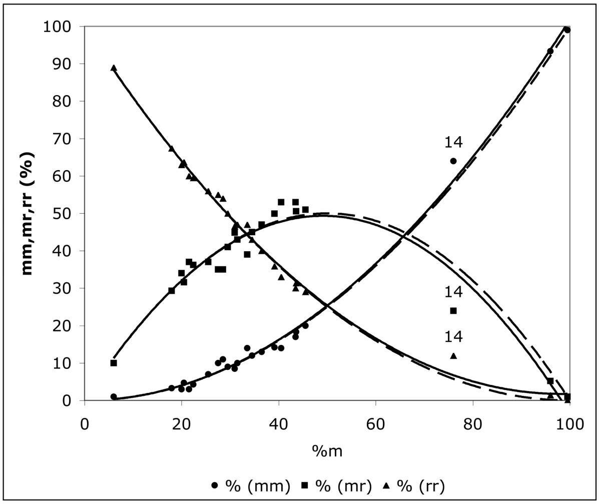

Figure 2. Isotactic (mm), heterotactic (mr), and syndiotactic (rr) triad fractions as a function of %m, the probability of meso propoagation, in the radical polymerisation of various methacrylates (in toluene or benzene solution, at 60±10 °C). %m was calculated according to the following equation, %m = mm + mr/2, by using the observed mm and mr values. The solid lines indicate the fitting of the data and the dashed lines indicate the theoretical lines for Bernoullian statistics $[mm = \%m^2,\ mr = 2\%m(1 - \%m),\ rr = (1 - \%m)^2]$.

Table 1. Experimental triad fractions and probabilities of meso propagation (%m) of bulky methacrylates, and corresponding volumes and solids of revolution of their pendant groups

Monomer	*% (mm)*	*% (mr)*	*% (rr)*	*% m*	*Volume (Å^3)*	*Solid of revolution (Å^3)*
M1	3	34	63	20.0	33	37
M2	3	37	60	21.5	88	119
M3 [c]	14	53	33	40.5	143	313
M4 [d]	10	35	55	27.5	112	201
M5 [c]	10	43	47	31.5	130	321
M6	11	35	54	28.5	184	394
M7	13	47	40	36.5	185	436
M8	9	41	50	29.5	98	162
M9	7	37	56	25.5	98	507
M10	12	45	43	34.5	117	284
M11	20	51	29	45.5	135	283
M12	17	53	30	43.5	169	540
M13 [c]	14	39	47	33.5	150	383
M14 [e]	64	24	12	76.0	283	563
M15	>99	<1	0	100	306	687
M16	1	10	89	6.0	189	487
M17	4.7	31.6	63.7	20.5	100	144
M18	4.3	36.2	59.5	22.4	158	349
M19	8.5	44.9	46.6	31.0	319	595
M20	3.3	29.3	67.4	18.0	155	350
M21	18.3	50.6	31.4	43.6	210	329
M22	14.2	49.9	35.9	39.2	286	829
M23	93.4	5.2	1.4	96.0	307	501

[a] The experimentally obtained stereoregularity results are taken from Ref. (*4*), except for M17-23 which are taken from Ref. (*13*). [b] Except where noted otherwise the polymerization temperature is 60°C and the solvent is benzene or toluene. [c] 50°C polymerization temperature. [d] 70°C polymerization temperature. [e] This was at the higher of the two monomer concentrations quoted in Ref. (*4*).

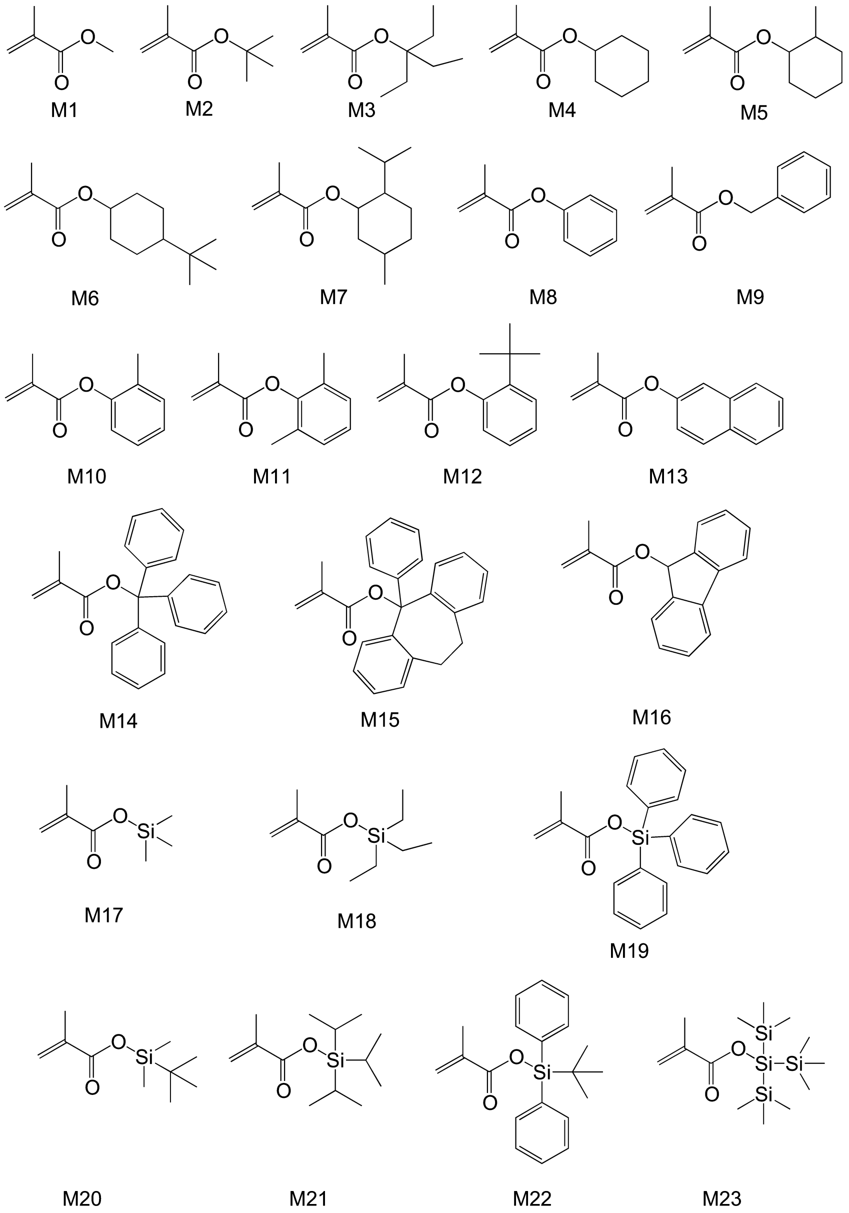
M1
M2
M3
M4
M5
M6
M7
M8
M9
M10
M11
M12
M13
M14
M15
M16
M17
M18
M19
M20
M21
M22
M23

Scheme 4. Monomers considered in the investigation of relationship between tacticity and steric bulk.

Steric Effects

To relate the stereopreferences in Table 1 to steric bulk, we calculated the B3-LYP/6-31G(d) optimized geometry for each monomer and then, using this optimized geometry, calculated the size of the monomer pendant group (defined here as the ester side chain) using two different methods. In the first method, we calculated the molecular volume of the pendent group using a simple space-filling model (CPK) based on the Van der Waals radii of the atoms. These calculations were performed in Spartan'08 software (*14*). In the second method, which we designed to mimic natural bulkiness of the moieties, we used the same optimized geometries but calculated the "solid of revolution" of the pendant group manually, as shown in Figure 3. To calculate the solid of revolution, the O–C or O–Si bond is set as the axis of the revolution, and the disc method was used for numerical summation with an increment of 0.001 Å. An in-house program used for the calculations can be downloaded from reference (*15*). The molecular volume and solid of revolution obtained are included in Table 1 (above), and are used to construct Figures 4 and 5, respectively.

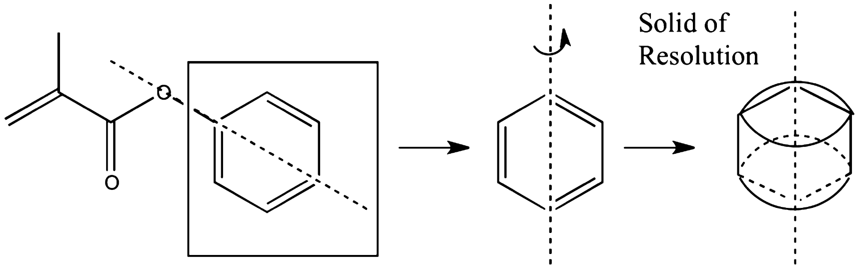

Figure 3. Schematic representation of manually calculated scanned volume of benzene ring in phenyl methacrylate.

Figure 4 shows the relationship between the molecular volume of the pendant group and the tacticity of the resulting polymer. This graph confirms that the smaller methacrylates have a low preference for meso propagation (i.e. are syndiotactic rich), but this meso propagation preference grows steadily as the steric bulk of the pendant group increases. While the graph shows a good correlation between the volume of the pendant group and the probability of meso propagation for most of the test set, various outliers are also evident. In particular, most of the silicon containing monomers (M17-23) tend to show a much lower preference for meso propagation than might have been expected on the basis of their steric bulk. This effect is most pronounced for the silyl monomers containing aromatic side chains (M19 and M22) but absent for the bulkiest non-silicon containing monomer (M23). It has been previously suggested (*13*) that the enhanced syndiotactic preference of most silicon-containing monomers is due to the longer silyl ester bond, relative to the corresponding alkyl ester bond, which dampens the steric crowding effect. Indeed, for the alkyl esters we have calculated an average O–C distance to be 1.456Å for aliphatic pendant group and 1.399Å for containing aromatic ring pendant group. In contrast, O–Si bond lengths are significantly longer (e.g., 1.727Å for the aromatic pendant groups), and this would indeed lessen the steric crowding. This reduced steric crowding may in turn facilitate more significant effects, such as enhanced opportunities for π-stacking and solvent interactions, and these may be responsible for the deviations of the aromatic monomers M19 and M22 from their corresponding non-silicon containing counterparts, and their differing behavior to the non-aromatic silyl monomer M23. Along related lines, another major outlier is the 9-fluorenyl methacrylate (M16), which is also highly syndiotactic despite having a large molecular volume. In this case, it is likely that favourable π-stacking interactions between the aromatic pendant groups outweighs any steric repulsion, causing them to prefer to align with each other, rather than orient away.

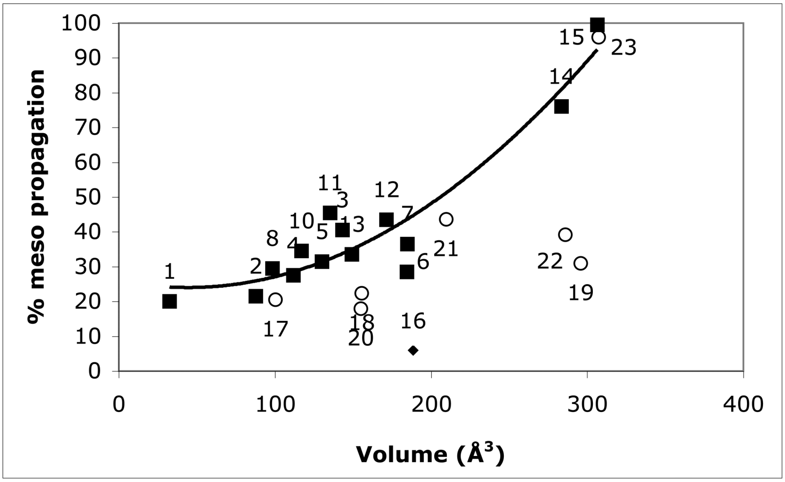

Figure 4. Relationship between the preference for meso propagation and pendant group bulkiness. Volume is calculated as the volume of space filling (CPK) using radii chosen to approximate van der Waals contact distances. The circles are the silicon-containing monomers (M17-23; omitted from data fitting), the diamond is M16 (also omitted), and the squares are the rest of the test set.

When moving from volume to solid of revolution (Figure 5) the relationship between steric bulk and %m is not improved. Had the side chains been freely rotating in the propagating radical, the solid of revolution should have provided a better measure of their effective steric bulk. The present results thus suggest the rotational barriers are likely to be significant. It is interesting to note that in Figure 5, apart from the previous outliers (M16-23), also M9 also veers away from the correlation. This species is the only one in the data set, which has a bulky side chain that is spaced from the ester oxygen by an intervening methylene group. This spacer group increases the solid of revolution, relative to the corresponding monomer without the spacer (M8) and, through relieving steric crowding, actually reduces %m. This spacer group effect echoes that of the siliyl-containing monomers, and may be useful when designing new monomers with tailored the stereochemistry.

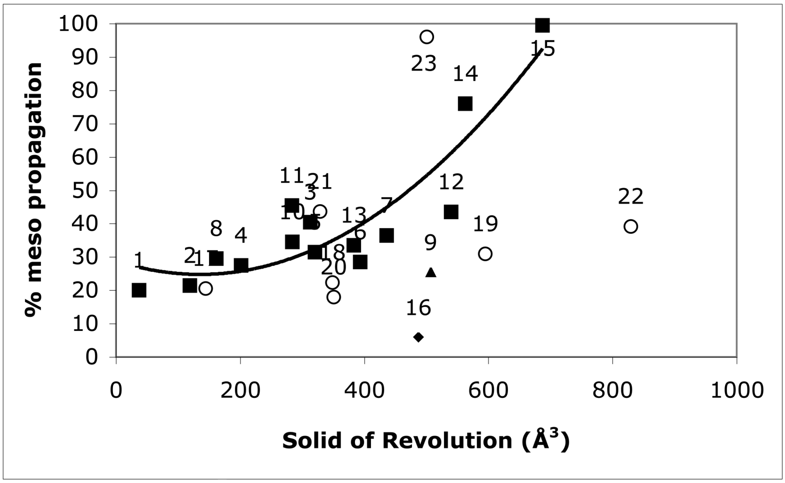

Figure 5. Relationship between the preference for meso propagation and the solid of resolution of the pendant group. The fitted line excludes the silyl monomers (M17-23), as well as M9 and M19.

Conformational Analysis

Based on the above results it is clear that one of the key influences on polymer tacticity is the steric bulk of the side chain, which, for moderately bulky methacrylate derivatives, induces a syndiotactic preference that decreases in a predictable manner with steric bulk to the extent that exceptionally bulky monomers give highly isotactic polymers instead. However, our results merely place known experimental trends on a quantitative footing. To understand the origin of the effects, it is necessary to examine the optimized structures of the propagating radicals and their propagation kinetics. In particular, it has been suggested in the literature that the syndiotactic rich and isotactic rich polymers are *both* consistent with the proposal that bulky groups undergo steric repulsion from each other —the differences in the tacticities that result from such interactions arise from the increasingly helical character of the polymer chain as steric bulk is increased (*4*). To explore whether this is indeed the case, we have used theory to predict the conformer distributions of oligomeric models of the propagating radicals in polymerization of MMA (M1). Owing to their very large size, we initially performed conformer searches using molecular mechanics force field (MMFF) calculations, before selecting the lowest linear and helical conformers and re-optimizing their geometries with the semi-empirical AM1 method. These calculations were performed in Spartan'08 software (*14*). Whilst neither method would be expected to be reliable for predicting the energetics of these reactions, we expect the main geometric features and broad qualitative trends in the relative conformer energies to be reasonably well captured due to significant systematic error cancellation (since we are comparing near identical species differing only in the rotations of some of their bonds).

Figure 6 shows the lowest energy linear and helical conformers of a heptamer model of syndiotactic poly(MMA), and their relative energies, at the AM1 level of theory. The lowest conformer (A) is the linear chain, with the helical chain (B) being significantly higher in energy. It should be noted that in both structures the acrylic side chains are oriented so as to maximize the distance between each other and thereby minimize their steric repulsion. Figure 7 shows the same analysis for isotactic poly(MMA). In this case, the linear and three different helical isotactic poly(MMA) chains are shown. The first helical structure (B) corresponds to rotation of the backbone between each unit by 20 degrees, the second (C) to rotation of approximately 100 degrees and the third (D) to rotation of about 130 degrees. All three helical structures lie below the linear conformation in this case with the last structure (D) having the global minimum energy for isotactic poly(MMA). We refer to this conformer as syndiotactic-like isotactic poly(MMA) due to its resemblance to the syndiotactic poly(MMA) in that acrylic side chains are again oriented to minimize steric interactions between each other. It should also be noted that the preferred syndiotactic structure (the linear conformer A in Figure 6) lies 6 kJ mol^{-1} below the preferred isotactic structure (the helical conformer D in Figure 7).

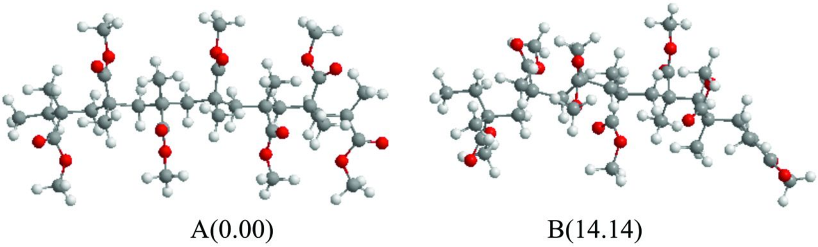

Figure 6. Conformational analysis for the seven member syndiotactic poly(MMA). Relative energies are in kJ/mol.

The conformational analysis of poly(MMA) indicates that, even for this small monomer, both syndiotactic and isotactic chains orient themselves so as to minimize the steric interactions between the ester side chains. In the case of syndiotactic poly(MMA), the conformation that best achieves this is a linear one which lies significantly below the corresponding helical conformers. In contrast, for isotactic poly(MMA) a helical chain (with an angle of rotation of 130°) best minimizes these interactions and lies significantly below the other isotactic conformations. Importantly, for poly(MMA) the (linear) syndiotactic conformation lies below the lowest energy (helical) isotactic conformation, consistent with the syndiotactic tendency in this monomer. At the same time, if (equivalent) helical conformers were to be considered, then the isotactic polymer would be more stabilized than the syndiotactic polymer. Thus if the helical tendency were to increase with increasing steric bulk, this would be expected to be accompanied by an increasing isotactic tendency.

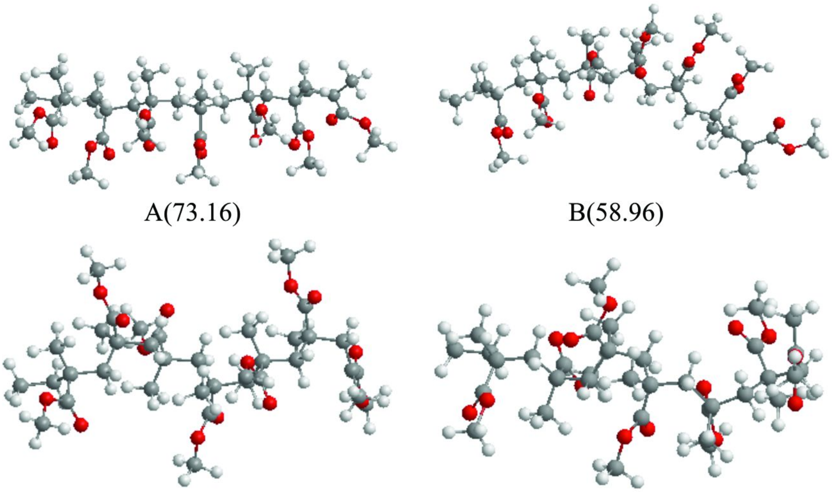

A(73.16)

B(58.96)

C(15.05)

D(0.00)

Figure 7. Conformational analysis for the seven member isotactic poly(MMA). Relative energies are in kJ/mol.

This conformational analysis therefore supports the explanation of Satoh and Kamigaito (*4*) for the seemingly counterintuitive switch from syndiotactic rich polymer to isotactic rich polymer with increasing bulkiness in terms of the increasing helical tendency of the polymer chains. Whilst this analysis is based on the conformers of pre-formed polymer radicals (i.e. on the thermochemistry), the steric interactions that govern these preferences are likely to be present to some extent in the transition states. More importantly, the conformation of the terminal unit of the reactant radicals does play a direct role. As explained earlier, since attack tends to occur from the opposite face of the attacking radical to the main polymer chain, the orientation of the terminal unit in the attacking the radical (relative to the penultimate unit) is typically preserved in the new stereocentre formed. Thus, to some extent, the stereochemistry of the resulting polymer will dependent on the relative concentrations of the syndiotactic-like and isotactic-like prochiral propagating radicals, in addition to their reactivities.

π-Stacking Interactions

Whilst the isotacticity increases with steric bulk for most of the bulky methacrylate monomers studied, some bulky methacrylates with aromatic side chains prefer syndiotactic polymers instead. As noted above, it has been suggested that this results from π-stacking interactions between the aromatic side chains (*4*). To examine whether these interactions are indeed significant, we have conducted conformational analyses on polymers of phenyl methacrylate (PhMA, M8) and also 9-fluorenyl methacrylate (FMA, M16). The former has a low-moderate side chain volume, while the latter is much larger. Both monomers show syndiotactic preferences but M8 fits nicely on the %m versus volume curve in Figure 4, whereas M16 is a major outlier. To ensure that the π-stacking interactions were properly taken into account in our theoretical model, we used the M06-2X density functional, which is known to be capable of modeling dispersion interactions (*16*, *17*). For poly(PhMA) we further improved the calculations using the MP2/6-311+G(d,p)//M06-2X/6-31G(d) level of theory; for the larger poly(FMA) we used the lower-cost M06-2X/6-31G(d) level of theory. These calculations were performed in Gaussian 09 software (*18*). Owing to the large size of the monomers, and the computational expense of these levels of theory, we considered only trimer models of the polymer chains.

Figure 8 shows the lowest energy conformers of trimeric isotactic poly(PhMA) and syndiotactic poly(PhMA) in the gas phase. It is clear that both stereoisomers prefer to orient themselves so as to maximize π-stacking interactions. The energy difference between the two chains is relatively small, but there is a slight preference toward syndiotactic poly(PhMA), consistent with experimental observations (%m = 29.5%). Our model studies indicate that the π-stacking interactions between the phenyl ester substituents are sufficient to overcome steric repulsion effects, and hence (at least in the absence of disrupting solvent effects) they prefer to orient themselves on the same side of the chain rather than opposite sides (i.e. the reverse of the situation in aliphatic bulky methacrylates). However, as in the previous section, the preferred orientation of the side chains can be achieved in either isotactic or syndiotactic polymers, according to whether the chain is linear or helical. Whether the polymer shows an overall preference for isotactic or syndiotactic polymer thus depends on the relative tendency to form linear versus helical chains, with the former favoring the isotactic tendency and the latter favoring the syndiotactic tendency. This is of course the opposite situation to the non-π-stacking bulky methacrylates where an increasing helical tendency is associated with an increasing preference for isotactic propagation. However, as poly(PhMA) is only moderately bulky, the differences between the linear isotactic and helical syndiotactic structures are themselves relatively small with just a slight preference for the latter. This is presumably why it does not appear as a major outlier in Figures 4 and 5.

To explore the impact of π-stacking interactions on tacticity, we need to consider a bulkier monomer, such as 9-fluorenyl methacrylate (FMA, M16), for which the helical tendency is expected to be more pronounced. In that case, based on the conformational analysis above, steric repulsion effects should lead to a strong isotactic preference whereas π-stacking effects should lead to a strong syndiotactic preference, which is what is observed experimentally. To confirm the π-stacking interactions in this polymer we conducted a conformational analysis on the trimeric propagating radicals of isotactic and syndiotactic poly(FMA) (Figure 9). Once again we find that both stereoisomers prefer conformations in which the side chains align with one another so as to maximize π-stacking interactions. For the isotactic polymer this means that the linear form (A) is favored in spite of its expected increase in steric strain over the helical form (B); for the syndiotactic isomer (C) this is best achieved in the helical form. However, although the helical syndiotactic structure (C) is favored over the linear isotactic structure (A) the energy difference is much smaller than anticipated. This could be in part

In Progress in Controlled Radical Polymerization: Mechanisms and Techniques; Matyjaszewski, K., et al.;
ACS Symposium Series; American Chemical Society: Washington, DC, 2012.

because the trimeric models are too short for the steric strain associated with the non-helical chains to be fully realized. It could also be due to the underestimation of dispersion effects by the M06-2X method. Ideally, we would perform MP2 calculations on yet larger models, but the computational expense is currently prohibitive. Nonetheless, our model calculations do confirm that π-stacking interactions are significant in this monomer, and that they stabilize conformers in which the side chains are aligned. This is the opposite situation to that observed in non-π stacking monomers such as MMA where steric effects lead to conformers in which the side chains are oriented away from one another, and this provides a reasonable explanation for their opposite stereochemical tendencies.

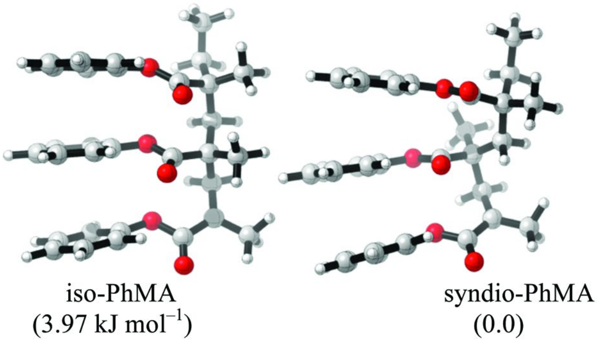

Figure 8. Trimeric growing chains of PhMA (M8).

Finally, it is worth noting that π-stacking interactions can sometimes be disrupted by solvent effects. In particular, small aromatic solvent molecules, such as benzene, can themselves form complexes between the aromatic side chains of aryl methacrylates. For example, we have located structures such as that shown in Figure 10 for the interaction of benzene with isotactic trimeric poly(PhMA). It can be seen that benzene can form a stable (by 13.04 kJ/mol relative to the isolated species) π-stacking complex with the phenyl rings on the pendant groups, displacing the intramolecular π-stacking interactions. These preliminary calculations were performed in the gas-phase (rather than in a solvent continuum) where the stabilization effect of the solvent-solute interactions is likely to be overemphasized but they nonetheless show that such interactions are possible. When such complexes form they would cause the tacticity preferences to reverse, and this is indeed seen experimentally. For instance 2-naphthyl methacrylate (M13) forms isotactic rich polymer in n-heptane but syndiotactic rich polymer in benzene (*4*). Interestingly, in poly(FMA) the syndiotactic structures (in Figure 10) give opportunities for aromatic solvent molecules to interact without disrupting the π-stacking network, and this may explain why syndiotactic preference of poly(FMA) is less disrupted by solvent effects.

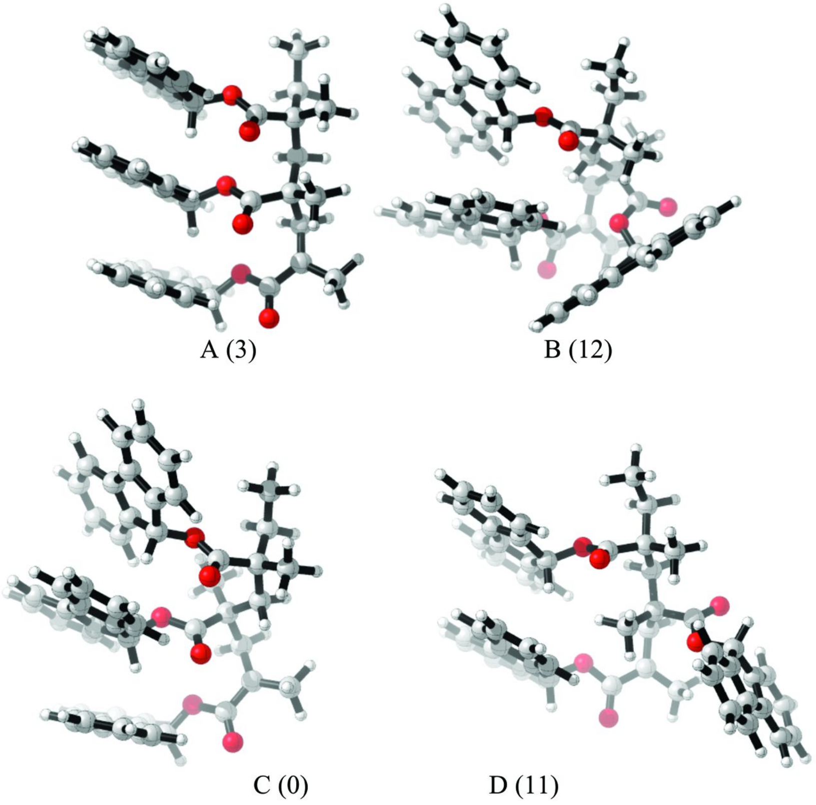

A (3) B (12)

C (0) D (11)

Figure 9. Trimeric growing chains of isotactic (A and B) and syndiotactic (C and D) poly(FMA) (M16). Relative energies (kJ/mol) are in brackets.

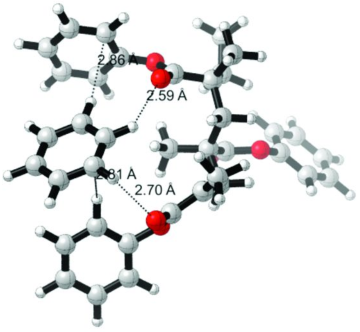

Figure 10. Influence of explicit solvent on the isotactic trimeric poly(PhMA).

Conclusions

In this work, we have used theoretical calculations to explore the origin of inherent tacticity in bulky methacrylates. Consistent with the previous qualitative analyses by Satoh and Kamigaito (*4*), we have demonstrated a quantitative relationship between the preference for meso propagation and the steric bulk of the ester side chain, where the latter is best measured as the scanned volume of the moiety. We have also confirmed that syndiotactic methacrylates prefer linear chains, isotactic methacrylates prefer helical chains and the increasing isotactic preference with chain length can be understood in terms of the increasing helical tendency as substituents become more bulky. We also demonstrated that, whilst π-stacking interactions in aryl methacrylates are significant, the extent to which they influence the tacticity depends on their bulkiness and associated helical tendency. We have also provided an explanation for their solvent dependence in terms of the disruption of π-stacking conformations by the formation of inclusion complexes.

Acknowledgments

MLC gratefully acknowledges generous financial support from the Australian Research Council (ARC) under their Centre of Excellence program, an ARC Future Fellowship and generous allocations on the National Facility of the National Computational Infrastructure.

References

1. Matyjaszewski, K.; Davis, T. P. *Handbook of Radical Polymerisation*; John Wiley and Sons, Inc.: New York, 2002.
2. Moad, G.; Solomon, D. H. *The Chemistry of Free Radical Polymerisation*, 2nd ed.; Elsevier Science: Oxford, U.K., 2006
3. Atkins, P.; et al. *Inorganic Chemistry*; Oxford University Press: Oxford, U.K., 2006
4. For an excellent review, see: Satoh, K.; Kamigaito, M. *Chem. Rev.* **2009**, *109*, 5120–5156.
5. Kamigaito, M.; Satoh, K. *Macromolecules* **2008**, *41*, 269–289.
6. Liu, W.; Koike, Y.; Okamoto, Y. *Polymer* **2004**, *45*, 5491–5495.
7. Porter, N. A.; Allen, T. R.; Breyer, R. A. *J. Am. Chem. Soc.* **1992**, *114*, 7676.
8. Nakano, T.; Yade, T.; Fukuda, Y.; Tamaguchi, T.; Okumura, S. *Macromolecules* **2005**, *38*, 8140.
9. Nakano, T.; Mori, M.; Okamoto, Y. *Macromolecules* **1999**, *32*, 2391.
10. Hoshikawa, N.; Hotta, Y.; Okamoto, Y. *J. Am. Chem. Soc.* **2003**, *125*, 12380.
11. Kaneko, Y.; Iwakiri, N.; Sato, S.; Kadokawa, J.-I. *Macromelcules* **2008**, *41*, 489.
12. For an early ab initio study of conformational effects in propagation see: Coote, M. L.; Davis, T. P.; Radom, L. *Macromolecules* **1999**, *32,* 5270−5276.
13. Ishitake, K.; Satoh, K.; Kamigaito, M.; Okamoto, Y. *Macromolecules* **2011**, *44*, 9108–9117.

14. *Spartan'08*; Wafeunction, Inc., Irvine CA.
15. Michelle Coote, Computer Aided Chemical Design. http://rsc.anu.edu.au/~cylin/scripts.html.
16. Zhao, Y.; Truhlar, D. G. *Theor. Chem. Acc.* **2008**, *120*, 215.
17. Zhao, Y.; Truhlar, D. G. *Acc. Chem. Res.* **2008**, *41*, 157.
18. *Gaussian 09*, Revision B.01; Frisch, M. J.; Trucks, G. W.; Schlegel, H. B.; Scuseria, G. E.; Robb, M. A.; Cheeseman, J. R.; Scalmani, G.; Barone, V.; Mennucci, B.; Petersson, G. A.; Nakatsuji, H.; Caricato, M.; Li, X.; Hratchian, H. P.; Izmaylov, A. F.; Bloino, J.; Zheng, G.; Sonnenberg, J. L.; Hada, M.; Ehara, M.; Toyota, K.; Fukuda, R.; Hasegawa, J.; Ishida, M.; Nakajima, T.; Honda, Y.; Kitao, O.; Nakai, H.; Vreven, T.; Montgomery, Jr., J. A.; Peralta, J. E.; Ogliaro, F.; Bearpark, M.; Heyd, J. J.; Brothers, E.; Kudin, K. N.; Staroverov, V. N.; Kobayashi, R.; Normand, J.; Raghavachari, K.; Rendell, A.; Burant, J. C.; Iyengar, S. S.; Tomasi, J.; Cossi, M.; Rega, N.; Millam, N. J.; Klene, M.; Knox, J. E.; Cross, J. B.; Bakken, V.; Adamo, C.; Jaramillo, J.; Gomperts, R.; Stratmann, R. E.; Yazyev, O.; Austin, A. J.; Cammi, R.; Pomelli, C.; Ochterski, J. W.; Martin, R. L.; Morokuma, K.; Zakrzewski, V. G.; Voth, G. A.; Salvador, P.; Dannenberg, J. J.; Dapprich, S.; Daniels, A. D.; Farkas, Ö.; Foresman, J. B.; Ortiz, J. V.; Cioslowski, J.; Fox, D. J. Gaussian, Inc.: Wallingford, CT, 2009.

Downloaded by OHIO STATE UNIV LIBRARIES on May 31, 2012 | http://pubs.acs.org
Publication Date (Web): March 20, 2012 | doi: 10.1021/bk-2012-1100.ch003

Chapter 3

Observations of Initial Steps of Radical Polymerizations by Time-Resolved and Steady-State Electron Spin Resonance Spectroscopy with the Aid of ATRP

Atsushi Kajiwara[*]

Department of Materials Science, Nara University of Education,
Takabatake-cho, Nara 630-8528, Japan
[*]E-mail: kajiwara@nara-edu.ac.jp

The initial steps of conventional radical polymerizations were investigated by both steady-state electron spin resonance (SS ESR) spectroscopy in combination with atom transfer radical polymerization (ATRP) technique and with time-resolved ESR (TR ESR) spectroscopy. The SS ESR/ATRP combination method can observe each initiation step by measurements of uniform oligomeric model propagating radicals. TR ESR spectra allowed direct observation of transient radicals (chain initiating radical) obtained by the addition reaction of a diphenylphosphinoyl radical to vinyl monomers. The addition rate constants (k_2) and activation energies (E_a) of diphenylphosphinoyl radical to the (meth)acrylates (initiation rate constants) were determined based on the TR ESR spectra. A combination of steady-state ESR and TR ESR provids information on both the initiation and propagation processes in radical polymerization of (meth)acrylates.

In Progress in Controlled Radical Polymerization: Mechanisms and Techniques; Matyjaszewski, K., et al.;
ACS Symposium Series; American Chemical Society: Washington, DC, 2012.

Downloaded by OHIO STATE UNIV LIBRARIES on May 31, 2012 | http://pubs.acs.org
Publication Date (Web): March 20, 2012 | doi: 10.1021/bk-2012-1100.ch003

Introduction

Steady-state electron spin resonance (SS ESR) spectroscopic studies directed at clarifying the fundamentals of radical polymerizations have been conducted ((*1–6*)). A combination of ESR and atom transfer radical polymerization (ATRP) provided significant new information on the properties of radicals in radical polymerizations, e. g. dependency of chain length, dynamics, and reactivity (hydrogen transfer) of propagating radicals (*7–12*). Previously, it has been extremely difficult, even impossible, to obtain such information from ESR spectra during conventional radical polymerizations.

This research work is intended as an investigation of the initial steps of conventional radical polymerizations by both SS ESR/ATRP combination method and time-resolved ESR (TR ESR) spectroscopy. Radical reactions in the initial stages of polymerizations usually occur much faster than those in propagation processes. SS ESR spectroscopy cannot be applied to observe the initital stages as is. There are two approaches to examine the initial stages of radical polymerizations using ESR. One is SS ESR study of each uniform oligomeric model propagating radicals like dimer, trimer, tetramer, pentamer, and so on. The uniform oligomeric model radicals can be generated from corresponding precursors synthesized by ATRP (*13–15*). Both steric and electronic structural information can be obtained from the measurements of the model radicals. The other is TR ESR spectroscopy. Radical reactions in the initial sage of polymerizations usually occur much faster than those in propagation processes, such that SS ESR spectroscopy cannot be applied. One of the roles of this technique is to enhance spectral resolution by elimination of most of the noise-contributing components. Applying field modulation provides the first derivative shape of the resulting spectra, which means that the time resolution of the SS ESR is at most 10^{-4} s (*16*). A TR ESR technique has been developed in order to observe processes that are faster than 10^{-4} s (*16–18*). Therefore TR ESR spectroscopy is a tool that can provide many details of reaction dynamics of transient radicals in solution (*19–28*). A time scale down to 10^{-7} s has been achieved by the TR ESR technique. The purpose of TR ESR is both the identification of transient radicals and examination of the concentration (rise and decay) profiles of the radicals. Since TR ESR spectra can be detected on the basis of chemically induced dynamic electron spin polarization (CIDEP) phenomena, TR ESR spectra are obtained in enhanced emission or absorption feature without modulation (*16–18*). Results on both SS ESR/ATRP combination method and TR ESR spectroscopy for investigation of initial stages of radical polymerizations of (meth)acrylates will be shown in this paper.

Downloaded by OHIO STATE UNIV LIBRARIES on May 31, 2012 | http://pubs.acs.org
Publication Date (Web): March 20, 2012 | doi: 10.1021/bk-2012-1100.ch003

Results and Discussion

SS ESR/ATRP Combination Method

Uniform model propagating radicals of dimeric, trimeric, tetrameric, and pentameric *tert*-butyl methacrylate (*t*BMA) were generated from corresponding radical precursors prepared by ATRP and were observed by SS ESR. Clear and well-resolved spectra were observed as shown in Figure 1. Typical SS ESR spectra for trimeric and pentameric model propagating radicals are shown as examples along with their structures. SS ESR spectra of these uniform oligomeric model radicals observed at 150 °C were simulated with an isotropic simulation program, indicating smooth rotation around C_α-C_β bonds. The SS ESR spectrum of the dimeric model radical (H-*t*BMA-*t*BMA•) can be simulated with almost equivalent values for the hyperfine splitting constants (hfc's) of two β-methylene protrons. This means that in the dimer, the rotation around C_α-C_β bond is very smooth. Apparently, the coupling constant of two β-methylene protons changed from equivalent to inequivalent as the chain length increased. Even at 150 °C, the trimeric, tetrameric, and pentameric model radicals showed inequivalent values of hfc for the β-methylene protons. The different electronic environments between the two β-methylene protons increased with increasing chain length. From the values of the hfc, dihedral angles between pπ-orbital and C_β-H bonds can be calculated as shown in Figure 2 in the Newman projections. These findings indicate that electronic structures of propagating radicals change considerably in the first several steps. The dimer showed almost equivalent β-protons, however the trimer already showed a deviated conformation from a symmetrical structure. The presence of two monomer units may cause asymmetry and the asymmetry increased in tetramer and pentamer.

In the cases of acrylates, it is difficult to conduct similar measurements on chain length dependence due to frequent occurrence of back biting reactions larger than trimeric model radicals. Figure 3 shows temperature dependent SS ESR spectroscopic change of dimeric model radical of *t*BA. No radical migration occurred in the dimer. Since the absolute values of the hfc's are proportional to those of spin density, detailed discussion on electronic structure of the dimeric model radical can be done from the values of hfc's. Structural insight can be obtained from these spectra in the initial stages of radical polymerizations of *t*BA. Since there is no method to evaluate addition rate constants of these oligomeric radicals in the present stage, kinetic information cannot be obtained from the spectra directly. Kinetic investigations would require another method as shown below.

In Progress in Controlled Radical Polymerization: Mechanisms and Techniques; Matyjaszewski, K., et al.;
ACS Symposium Series; American Chemical Society: Washington, DC, 2012.

Downloaded by OHIO STATE UNIV LIBRARIES on May 31, 2012 | http://pubs.acs.org
Publication Date (Web): March 20, 2012 | doi: 10.1021/bk-2012-1100.ch003

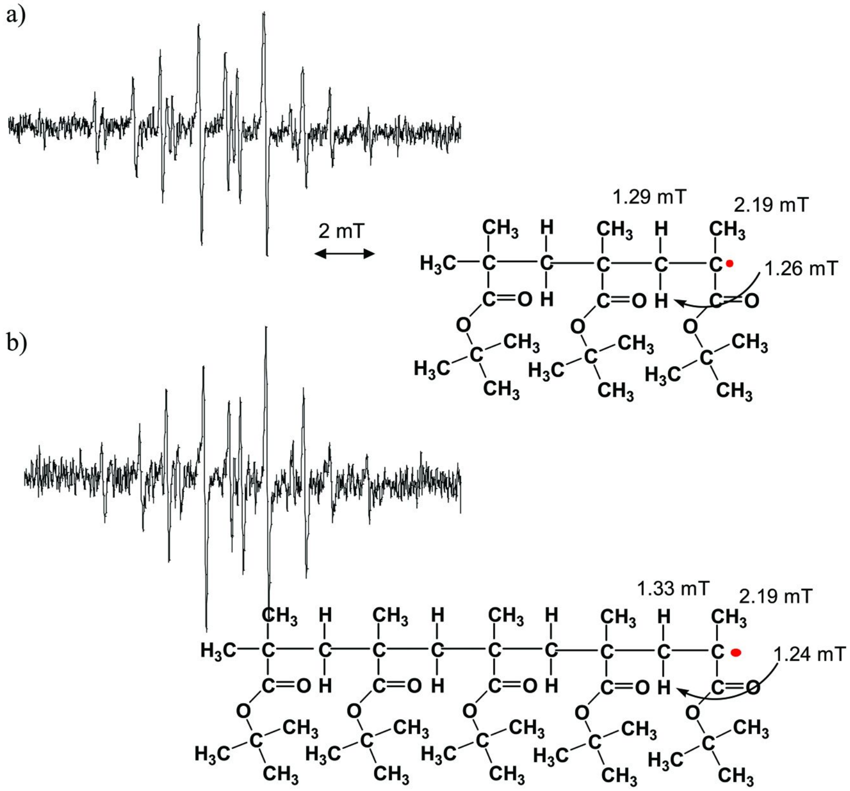

Figure 1. SS ESR spectra of trimeric (a) and pentameric (b) model propagating radicals of tBMA observed at 150 °C along with their structures and hfc's.

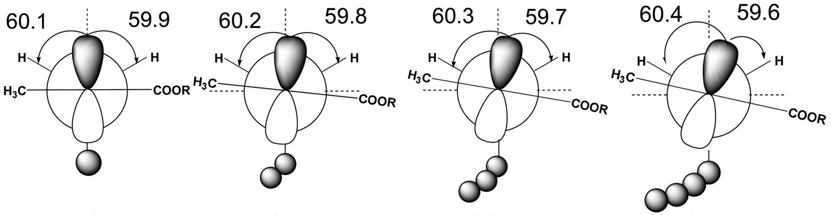

(a) (b) (c) (d)

Figure 2. Newman projections of averaged structures of dimeric (a), trimeric (b), tetrameric (c), and pentameric (d) model propagating radicals of tBMA with their dihedral angles (degree).

Downloaded by OHIO STATE UNIV LIBRARIES on May 31, 2012 | http://pubs.acs.org
Publication Date (Web): March 20, 2012 | doi: 10.1021/bk-2012-1100.ch003

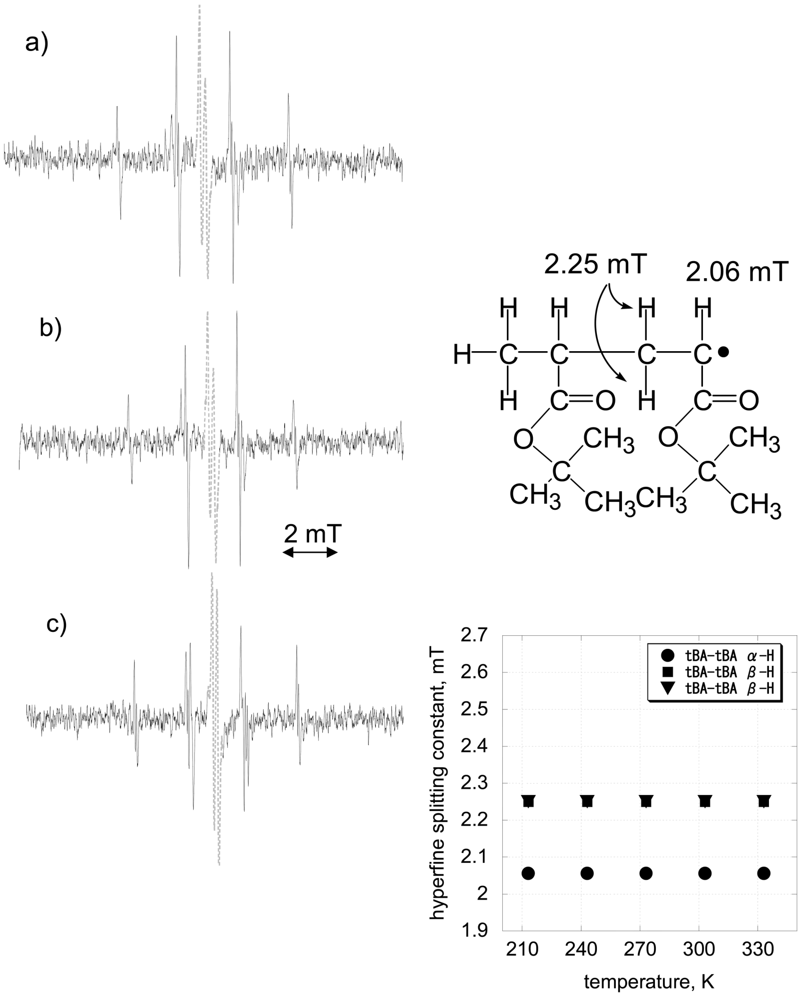

Figure 3. SS ESR spectra of dimeric model propagating radical of tBA at 60 °C (a), 30 °C (b), and 0 °C (c) along with the structure of the radicals and a plot of temperature dependent values of hfc's.

TR ESR Measurements

TR ESR spectra of TMDPO recorded in a magnetic field of 320 ± 25 mT in the absence and presence of *tert*-butyl acrylate (*t*BA) are shown in Figure 4 and 5 (*23–25*). The TR ESR spectrum obtained by photolysis of TMDPO in toluene (0.1 M) in the absence of *t*BA showed three characteristic spectroscopic lines (Figure 4). TMDPO provided both phosphorous-centered and carbon-centered radicals. The lines at 302.8 and 339.3 mT can be assigned to the doublet signals of the phosphorous-centered radical (diphenylphosphinoyl radical) whose spin quantum number is 1/2 with hfc of 36.5 mT and the line at 322.6 mT is due to the carbon-centered radical (2,4,6-trimethylbenzoyl radical) (*21*). In the presence of *t*BA, new signals, along with the signals from the diphenylphosphinoyl radical and the 2,4,6-trimethylbenzoyl radical, which are obtained by the photolysis of TMDPO, appeared in the magnetic field around the resonance line of the 2,4,6-trimethylbenzoyl radical as shown in Figure 5.

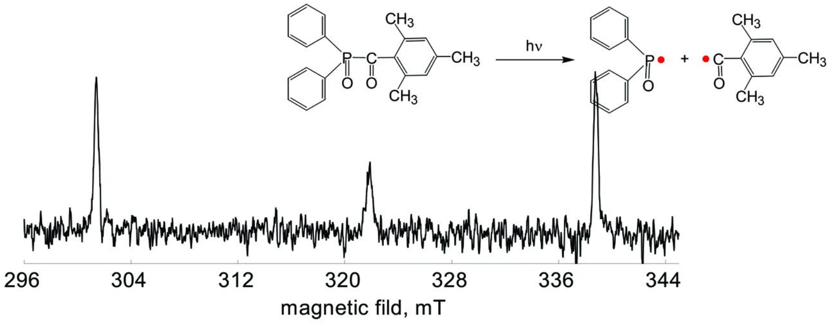

Figure 4. TR ESR spectrum of TMDPO only at 25 °C.

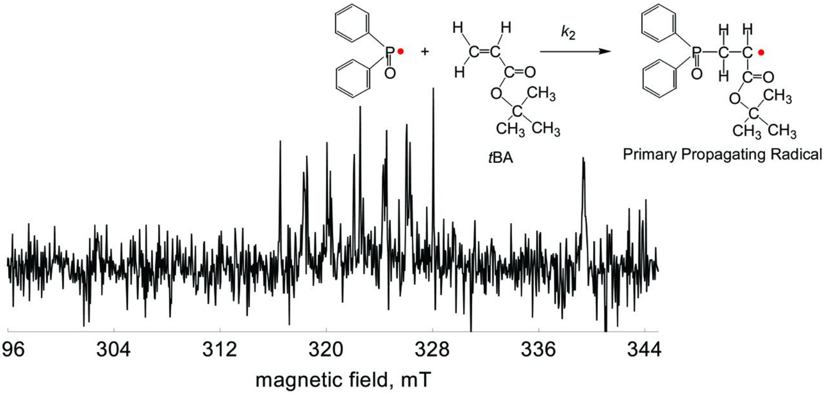

Figure 5. TR ESR spectrum of TMDPO in the presence of tBA at 25 °C.

A clear and well-resolved spectrum was observed in the presence of *t*BA. The spectrum was ascribable to two sets of *t*BA radicals. The presence of the relatively large doublet (5.97 mT) due to the phosphorous nucleus is an evidence of the structure of the chain initiating radical as shown in Figure 6. The smaller hfc value of phosphorous nucleus than that in diphenylphosphinoyl radical is reasonable for the distant interaction in the chain initiating radical (Figure 5). Thus, it was reasonably assigned to a radical obtained by an addition reaction of the diphenylphosphinoyl radical to *t*BA.

Temperature dependent spectroscopic changes of TR ESR spectra of *t*BA are shown in Figure 6. Broadening of some of the spectroscopic lines was observed clearly with lowering temperatures. Splitting lines due to β-methylene protons were broadened. This broadening is due to both slower rotational motion around

Downloaded by OHIO STATE UNIV LIBRARIES on May 31, 2012 | http://pubs.acs.org
Publication Date (Web): March 20, 2012 | doi: 10.1021/bk-2012-1100.ch003

C_α-C_β bond at lower temperatures and p-π interaction between phenyl ring and p-orbital of the radical. These spectra showed that chain initiating radicals were observed in the temperature range. Addition reactions to form the chain initiating radicals could be examined at these temperatures.

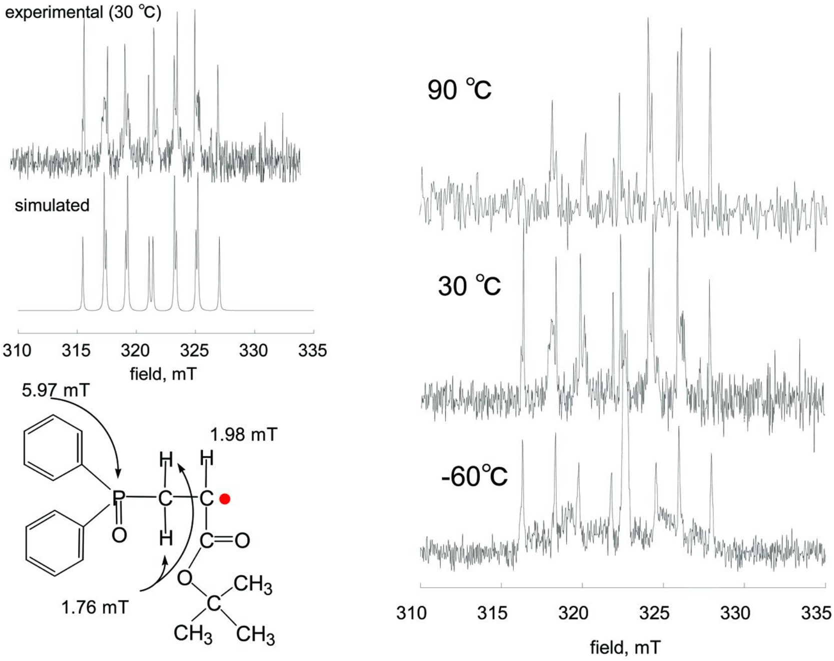

Figure 6. TR ESR spectra of chain initiating radical of tBA and its simulated spectrum and structure. Temperature dependent changes are also shown.

TR ESR spectroscopy can also provide kinetic information. In principle, a TR ESR spectrum has two axes. One is the magnetic field and the other is time. Time profile of the signal contains kinetics information. Since TR ESR spectra rose immediately after the laser pulse irradiation and the signal rapidly decayed according to the transient nature of the radicals, each spectroscopic line in Figure 7 shows rise and decay time profiles. Time profiles of the spectroscopic lines of TR ESR signals in Figure 4 after laser pulse irradiation are shown in Figure 7. The spectroscopic lines are due to diphenylphosphinoyl radical at 339.3 mT (solid line), 2,4,6-trimethylbenzoyl radical at 322.6 mT (dashed line) and one of the new signals (324.1 mT) that appeared in the presence of *t*BA (dotted line). It is clear that the new signals appear more slowly than that of radicals produced by the photolysis of TMDPO. This suggests that the new signals are secondary radicals (chain initiating radials) obtained by the addition of the diphenylphosphinoyl radical to *t*BA. As shown in the next figure (Figure 8), in the presence of *t*BA, the decay rate of the signal of the diphenylphosphinoyl radical becomes faster with increasing *t*BA concentration, which suggests that the increase in the decay rate is caused by the addition reaction of the diphenylphosphinoyl radical to *t*BA to form a chain initiating radical.

Downloaded by OHIO STATE UNIV LIBRARIES on May 31, 2012 | http://pubs.acs.org
Publication Date (Web): March 20, 2012 | doi: 10.1021/bk-2012-1100.ch003

Downloaded by OHIO STATE UNIV LIBRARIES on May 31, 2012 | http://pubs.acs.org
Publication Date (Web): March 20, 2012 | doi: 10.1021/bk-2012-1100.ch003

The effect of addition of *t*BA on the decay rate of the signals of the diphenylphosphinoyl radical and the 2,4,6-trimethylbenzoyl radical generated by the photolysis of TMDPO were investigated. While the decay rate of the diphenylphosphinoyl radical increased with increasing *t*BA concentration, the decay rate of the 2,4,6-trimethylbenzoyl radical scarcely changed with increasing concentration of the *t*BA. This finding shows that the diphenylphosphinoyl radical is much more reactive with *t*BA than the 2,4,6-trimethylbenzyoyl radical. The dependence of the decay rate of the diphenylphosphinoyl radical on the concentration of *t*BA followed first-order kinetics. Accordingly, the initiation rate constants for addition of the diphenylphosphinoyl radical to *t*BA were estimated from the relationship between concentration of *t*BA and the observed decay rate by the previously reported method (*23*, *25*) .

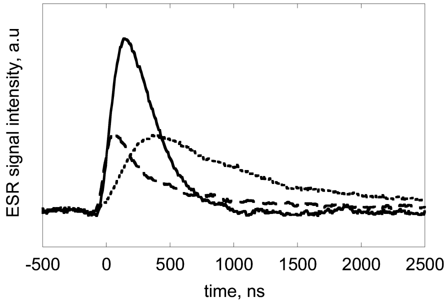

Figure 7. Time profiles of TR ESR spectra of phosphorous-centered radical (solid line), carbon-centered radical (dashed line), and chain initiating radical (dotted line) at 25 °C.

The decays of ESR signals due to the diphenylphosphinoyl radicals in the laser photolysis of TMDPO in the presence of varying concentrations of *t*BA are shown in Figure 8. The rate of decay became faster with increasing concentration of *t*BA. The first-order plots for the signal intensities gave linear relationships in both the absence and presence of the monomers. The apparent first-order rate constant (k') increased with increasing monomer concentration. The plots of the k' values against the monomer concentrations yielded linear relationships. Accordingly, k' follows

$$k' = k_1 + k_2[\mathrm{M}]$$

where k_1 is the first-order decay constant in the absence of the monomer, and k_2 is the bimolecular rate constant for the addition reaction of the diphenylphosphinoyl radical with the vinyl monomer, which corresponds to the initiation rate constant for the radical polymerization of a vinyl monomer with TMDPO as photo-initiator. These rate constants are on the order of 10^6-10^7 $s^{-1}M^{-1}$, which is 1 or 2 orders of magnitude larger than those of carbon-centered radicals, whose rate constants have been determined to be on the order of 10^4-10^5 $s^{-1}M^{-1}$ (*20*). Similar results were observed in the TR ESR measurements conducted in the presence of various kinds of acrylates and methacrylates.

Absolute rate constants for the addition of diphenylphosphinoyl radicals to *n*BA and *t*BA were obtained by Weber and Turro by both TR Fourier transform ESR and TR continuous wave ESR under ambient conditions (*28*). The values for *t*BA are almost identical to that obtained in this research. Further detailed analysis will clarify correlations between the values of both the steric and electronic structures of the acrylates.

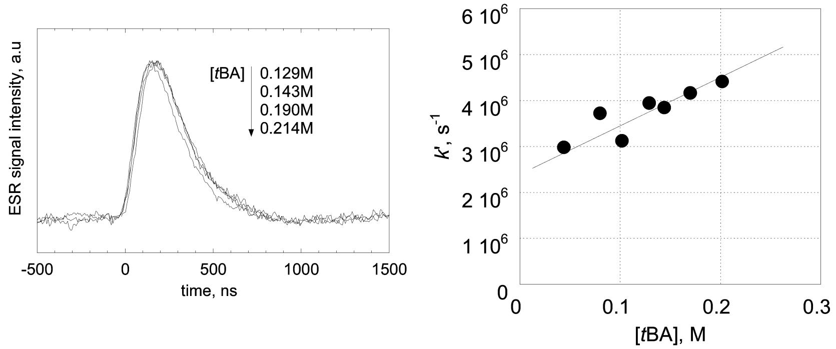

Figure 8. Time profiles of TR ESR spectra of phosphorous-centered radical at 339.3 mT in the presence of tBA (left) and plots of k' against [tBA] (right) at 25 °C.

As shown in Figure 6, TR ESR spectroscopy can be performed at various temperatures. The k_2 values can also be estimated at various temperatures. From these results, the activation energy (E_a) of the addition reaction can be estimated from these k_2 values by Arrhenius plots (Figure 9). From the slope of the plot, E_a was determined to be (12.0±3.9) kJ mol^{-1}. The E_a values of various (meth)acrylates were estimated in the same way as for *t*BA and are summarized in Table 1.

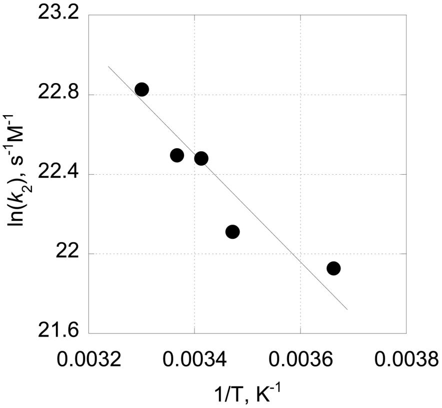

Figure 9. Arrhenius plot of addition reaction of diphenylphosphinoyl radical to tBA.

Downloaded by OHIO STATE UNIV LIBRARIES on May 31, 2012 | http://pubs.acs.org
Publication Date (Web): March 20, 2012 | doi: 10.1021/bk-2012-1100.ch003

Table 1. Activation energies (E_a) for addition reaction of diphenylphosphinoyl radical to monomers

monomer	E_a, kJ mol^{-1}
tert-Butyl acrylate	12.0±3.9
Dodecyl acrylate	8.7±3.7
Adamantyl acrylate	4.7±2.3
tert-Butyl methacrylate	17.8±4.2
Phenyl methacrylate	7.0±5.2
Adamantyl methacrylate	12.5±6.4

For the cases of (meth)acrylates as mentioned above, both SS ESR spectra of propagating radicals and TR ESR spectra of chain initiating radicals were observed. On the other hand, there are some cases that SS ESR spectra of propagating radicals have not been observed. For example, for radical polymerizations of *N*-vinyl carbazole (*N*VCz), SS ESR spectra of propagating radicals are very difficult to detect. No one has observed clear and well-resolved SS ESR spectra of the propagating radicals of *N*VCz. Figure 10 shows a TR ESR spectrum of *N*VCz initiated by TMDPO at 25 °C along with its simulated spectrum. Proposed structure of the chain initiating radical is also shown in the Figure. Clear and well-resolved spectrum was observed and this is clear evidence for the occurrence of radical addition of diphenylphosphinoyl radical to *N*VCz. Although hyperfine splitting from α- and β-protons were clearly observed, that from nitrogen nucleus was not clear. The spin density at the nitrogen nucleus is considered to be too small to show clear splitting probably due to highly delocalized spin density in the carbazole ring. Absolute values of hfc's would provide important information on the electronic structure of the chain initiating radicals of *N*VCz. This is a first step for examination of propagating radicals of *N*VCz. Preparation of oligomeric model radical precursors by ATRP may be a next step to conduct detailed analysis of the polymerization steps of *N*VCz. For the kinetics analysis, the value of k_2 at 25 °C was also estimated to be 4.06×10^6 M^{-1}s^{-1}.

Downloaded by OHIO STATE UNIV LIBRARIES on May 31, 2012 | http://pubs.acs.org
Publication Date (Web): March 20, 2012 | doi: 10.1021/bk-2012-1100.ch003

Downloaded by OHIO STATE UNIV LIBRARIES on May 31, 2012 | http://pubs.acs.org
Publication Date (Web): March 20, 2012 | doi: 10.1021/bk-2012-1100.ch003

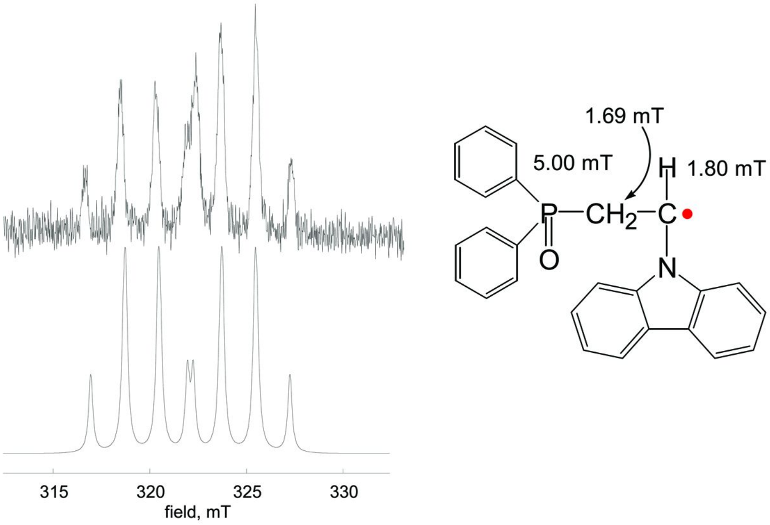

Figure 10. TR ESR spectrum of TMDPO in the presence of NVCz at 25 °C along with its simulated spectrum and structure.

Conclusion

Initial steps of conventional radical polymerizations of various kinds of monomers were investigated by both SS ESR/ATRP combination method and TR ESR spectroscopy. The SS ESR/ATRP combination method clearly showed gradual change of chemical properties of radicals from electronic structural information on values of hfc's observed in SS ESR measurements of dimeric, trimeric, tetrameric, and pentameric model propagating radicals. TR ESR spectra of transient radicals (the chain initiating radical) obtained by the addition reaction of a diphenylphosphinoyl radical to various kinds of (meth)acrylate monomers were clearly observed. Initiation rate constants (addition rate constants (k_2) of diphenylphosphinoyl radical to the (meth)acrylate monomers) were determined by the monomer concentration dependence of the decay rate of the diphenylphosphinoyl radical. Activation energies (E_a) of the addition reactions were also determined by temperature dependent measurements.

Therefore ESR can provide important information on both initiation and propagation processes. Many attempts have been made to reveal the properties of various kinds of (meth)acrylate radicals in radical polymerizations and this research work has added new information from a slightly different angle. Research works on basic chemistry of conventional radical polymerizations still can provide interesting information and combination of controlled radical polymerization technique and conventional ESR spectroscopy provided significant new information.

Downloaded by OHIO STATE UNIV LIBRARIES on May 31, 2012 | http://pubs.acs.org
Publication Date (Web): March 20, 2012 | doi: 10.1021/bk-2012-1100.ch003

Experimental

SS ESR/ATRP Combination Method

Dimeric model radical precursors were synthesized by atom transfer radical addition (ATRA) using a molar excess of initiator compared to monomer, in presence of a Cu^I/Cu^{II}PMDETA complex. The obtained products were a mixture of dimer, trimer, tetramer, pentamer and further oligomers. The dimers were separated and purified from the mixtures by repeated column chromatography. Purity and molecular weights of the purified materials were confirmed using GPC, ^1H NMR, and electron spray ionization mass spectroscopy. Dimeric model radicals were generated by a reaction of the uniform dimers with organotin compounds under irradiation. The generated radicals were observed by ESR spectroscopy by means of a JEOL JES RE-2X ESR spectrometer equipped with a universal cavity. Measurement temperature was controlled by a JEOL DVT2 variable-temperature accessory. ESR measurements were mainly performed in mesitylene at 150 and 120 °C and in toluene at 90, 60, 30, 0, -30 and -60 °C. Spectroscopic simulation was carried out by a JEOL IPRIT data analysis system.

TR ESR Spectroscopy

Diphenyl(2,4,6-trimethylbenzoyl)phosphine oxide (TMDPO, Aldrich) was purified by recrystallization from ethanol before use. Acrylates were purified by distillation just before use. A toluene solution of TMDPO (0.1 M) containing various concentrations of monomers was taken in an ESR sample cell. Laser pulses were irradiated by using a Q-switched Nd:YAG laser (Spectra Physics Quantaray DCR-2) operated at the third harmonic (20 mJ/flash at 355 nm with a 6-ns fwhm). For the measurements of the time-resolved ESR, a JEOL JES RE-2X spectrometer, equipped with a WBPA2 wide band pre-amplifier, was operated without magnetic field modulation, and the data were stored in a Tektronix TDS520A digital oscilloscope. Magnetic fields at resonance signals were determined by an Echo Electronics ES-FC5 NMR field meter. Measurement temperature was controlled by a JEOL DVT2 variable-temperature accessory. Data analysis was conducted by CIDEP software provided by JEOL Ltd.

Acknowledgments

The author is grageful to engineers at JEOL Resonance Inc. for cooperative developments of measurement and analysis systems of time-resolved electron spin resonance spectroscopy. Adamantyl (meth)acrylates were provided by Idemitsu Kosan Co. Ltd.

References

1. Fischer, H. *Adv. Polym. Sci.* **1968**, *5*, 463.
2. Kamachi, M. *Adv. Polym. Sci.* **1987**, *82*, 207.
3. Yamada, B.; Westmoreland, D. G.; Kobatake, S.; Konosu, O. *Prog. Polym. Sci.* **1999**, *24*, 565.
4. Spichty, M.; Giese, B.; Matsumoto, A.; Fischer, H.; Gescheidt, G. *Macromolecules* **2001**, *34*, 723.
5. Willemse, R. X. E.; van Herk, A. M.; Panchenko, E.; Junkers, T.; Buback, M. *Macromolecules* **2005**, *38*, 5098.
6. Buback, M.; Hesse, P.; Junkers, T.; Sergeeva, T.; Theis, T. *Maromolecules* **2008**, *41*, 288.
7. Kajiwara, A.; Maeda, K.; Kubo, N.; Kamachi, M. *Macromolecules* **2003**, *36*, 526.
8. Kajiwara, A; Nanda, A. K.; Matyjaszewski, K. *Macromolecules* **2004**, *37*, 1378.
9. Kajiwara, A.; Matyjaszewski, K. *Advanced ESR Methods in Polymer Research*; Wiley Interscience: Hoboken, NJ, 2006; Chapter 5, pp 101−132.
10. Kajiwara, A. Electron Spin Resonance Study of Methacrylate Radicals Generated from Purified Oligomers Prepared by Atom Transfer Radical Polymerization. In *Controlled/Living Radical Polymerization*; Matyjaszewski, K., Ed.; ACS Symposium Series 944; American Chemical Society: Washington, DC, 2006; Chapter 9, pp 111−124.
11. Kajiwara, A. *Macromolecular Symp.* **2007**, *248*, 50.
12. Kajiwara, A. Electron Spin Resonance (ESR) Observation of Radical Migration Reactions in the Polymerization of Alkyl Acrylates. In *Controlled/Living Radical Polymerization: Progress in ATRP*; Matyjaszewski, K., Ed.; ACS Symposium Series 1023; American Chemical Society: Washington, DC, 2009; Chapter 4, pp 49−59.
13. Wang, J. -S.; Matyjaszewski, K. *J. Am. Chem. Soc.* **1995**, *117*, 5614.
14. Wang, J. -S.; Matyjaszewski, K. *Macromolecules* **1995**, *28*, 7901.
15. Giese, B.; Damm, W.; Wetterich, F.; Zeitz, H.-G. *Tetrahedron Lett.* **1992**, *33*, 1863.
16. Weil, J. A.; Bolton, J. R. *Electron Paramagnetic Resonance*, 2nd ed.; Wiley, Hoboken, NJ, 2007
17. Kevan, L., Schwartz, R. N., Eds.; *Time-Domain Electron Spin Resonance*; Wiley, New York, 1979.
18. Lepley, A. R., Closs, G. L., Eds.; *Chemically Induced Magnetic Polarization*; Wiley-Interscience: New York, 1973.
19. Sumiyoshi, T.; Henne, A.; Lechtken, P.; Schnabel, W. *Z. Naturforsch.* **1984**, *A39*, 434.
20. Sumiyoshi, T.; Schnabel, W. *Polymer* **1985**, *26*, 141.
21. Kamachi, M.; Kuwata, K.; Sumiyoshi, T.; Schnabel, W. *J. Chem. Soc., Perkin Trans. 2* **1988**, 961.
22. Mizuta, Y.; Morishita, N.; Kuwata, K. *Chem. Lett.* **1999**, 311.
23. Kajiwara, A.; Konishi, Y.; Morishima, Y.; Schanbel, W.; Kuwata, K.; Kamachi, M. *Macromolecules* **1993**, *26*, 1656.

Downloaded by OHIO STATE UNIV LIBRARIES on May 31, 2012 | http://pubs.acs.org
Publication Date (Web): March 20, 2012 | doi: 10.1021/bk-2012-1100.ch003

24. Kamachi, M.; Kajiwara, A.; Saegusa, K.; Morishima, Y. *Macromolecules* **1993**, *26*, 7369.
25. Kajiwara, A. *Macromol. Rapid Commun.* **2009**, *30*, 1975.
26. Sluggett, G. W.; McGarry, P. F.; Koptyug, I. V.; Turro, N. J. *J. Am. Chem. Soc.* **1996**, *118*, 7367.
27. Weber, M.; Khudyakov, I. V.; Turro, N. J. *J. Phys. Chem. A* **2002**, *106*, 1938.
28. Weber, M.; Turro, N. J. *J. Phys. Chem. A* **2003**, *107*, 3326.

Downloaded by OHIO STATE UNIV LIBRARIES on May 31, 2012 | http://pubs.acs.org
Publication Date (Web): March 20, 2012 | doi: 10.1021/bk-2012-1100.ch003

Downloaded by STANFORD UNIV GREEN LIBR on May 31, 2012 | http://pubs.acs.org
Publication Date (Web): March 20, 2012 | doi: 10.1021/bk-2012-1100.ch004

Chapter 4

Terminal Monomer Units in Dormant and Active Copolymer Chains

Lebohang Hlalele[a] and Bert Klumperman*,[a,b]

[a]Department of Chemistry and Polymer Science, University of Stellenbosch, Private Bag X1 , Matieland 7602, South Africa
[b]Laboratory of Polymer Chemistry, Eindhoven University of Technology, P.O. Box 513, 5600 MB Eindhoven, The Netherlands
***E-mail: bklump@sun.ac.za**

Experimental and simulation results comparing radical ratios and terminal monomer units for dormant species in the copolymerization of styrene with methyl acrylate and *n*-butyl acrylate are reported. The copolymerization of styrene and methyl acrylate was considered under conventional radical copolymerization conditions. Styrene and *n*-butyl acrylate copolymerization was conducted via controlled/living radical copolymerization (LRcP), using a nitroxide as a mediator. From the results it can be concluded that the fraction of styrene-terminal active chains is much larger than the fraction of styrene-terminal dormant chains. From the results it can be concluded that the fraction of styrene-terminal active chains decreases with time in the LRcP. Good agreement is obtained between the experimental data and simulated data.

In Progress in Controlled Radical Polymerization: Mechanisms and Techniques; Matyjaszewski, K., et al.;
ACS Symposium Series; American Chemical Society: Washington, DC, 2012.

Downloaded by STANFORD UNIV GREEN LIBR on May 31, 2012 | http://pubs.acs.org
Publication Date (Web): March 20, 2012 | doi: 10.1021/bk-2012-1100.ch004

Introduction

Since the pioneering work on controlled/living radical polymerization, much work has been done to date on homo- and copolymerization reactions. A lot of attention has been directed towards understanding and comparing the kinetic and mechanistic features in both controlled/living radical copolymerization (LRcP) and conventional free radical copolymerization (FRcP) (*1–5*). However, very little experimental data has been published in the literature in which the radical ratios in a copolymerization system have been compared for an LRcP *vs.* a free radical copolymerization (FRcP) system. Kelemen *et al.* studied the radical ratios for the FRcP of styrene and methyl acrylate at different initial feed compositions (*6*). They employed the use of radical trapping agents to terminate polymer chains that grew under free radical conditions. In a copolymerization reaction, two distinct chain end radicals are possible. Recent work in our group on the study of terminal units in a nitroxide-mediated LRcP of styrene and *n*-butyl acrylate has indicated a significant difference between the terminal monomer unit in a dormant chain, compared to the terminal unit in a chain trapped during FRcP (*7*). Due to mediation of the copolymerization with a nitroxide species, the term LRcP will be used to refer to the class of controlled radical copolymerizations governed by the reversible deactivation mechanism.

In this contribution, we report on the determination of terminal monomer units in active chains (from FRcP) and dormant chains (from LRcP). A comparative simulation study of the copolymerization reactions is reported. Predici simulation of conventional free radical styrene/methyl acrylate copolymerization compared to the controlled styrene/*n*-butyl acrylate copolymerization simulation under the implicit penultimate unit model for both conventional and controlled radical polymerizations are discussed. It is assumed, within reasonable approximation that the two acrylate monomers should behave in relatively similar fashion.

Experimental

Materials

The alkoxyamine 2-methyl-2-[*N*-*tert*-butyl-*N*-(1-diethoxyphosphoryl-2,2-dimethylpropyl)-aminooxy]propionic acid (MAMA-DEPN) was synthesized as described elsewhere (*8–11*). Styrene and *n*-butyl acrylate (Plascon Research Centre, Stellenbosch University, South Africa) were washed with 10 % aqueous solution of sodium hydroxide and then washed with distilled deionised water and dried with anhydrous magnesium sulphate. The respective monomers were then distilled under reduced pressure and stored at low temperatures. Deuterated dimethyl sulphoxide (DMSO-d_6, Cambridge Isotope Laboratories, 99%) was used as received.

Downloaded by STANFORD UNIV GREEN LIBR on May 31, 2012 | http://pubs.acs.org
Publication Date (Web): March 20, 2012 | doi: 10.1021/bk-2012-1100.ch004

Styrene/*n*-butyl acrylate copolymerization procedure. Styrene and *n*-butyl acrylate LRcPs were followed via *in situ* ^{31}P NMR at 120 °C at different monomer feed compositions in DMSO-d_6. The ^{31}P NMR spectra were acquired with a 4.75 μs (45°) pulse width, a 1.6 seconds acquisition time, a relaxation delay of 1 second and an average of 23 scans per spectrum. The NMR tube was first inserted into the magnet at 25 °C and the magnet fully shimmed on the sample and a spectrum collected to serve as reference at 25 °C. This was followed by removal of the sample from the magnet and the probe of the magnet was then heated to 120 °C and allowed to stabilize before introducing the sample into the cavity of the magnet. After re-insertion of the sample, additional shimming was performed to acquire optimum conditions. The first spectrum was acquired 3 – 5 minutes after the re-insertion, followed by periodic spectra acquisition every two minutes for 90 minutes. The spectra were processed manually using ACD Labs 10.0 NMR processor®.

In a typical copolymerization reaction, 30.3 mg MAMA-DEPN (0.0794 mmol), 0.1191 g styrene (1.1436 mmol), 0.1078 g *n*-butyl acrylate (0.8411 mmol) and 0.3094 g DMSO-d_6 were thoroughly mixed and introduced into a J-Young type NMR tube. The reaction mixture was degassed by three freeze-pump-thaw cycles and backfilled with nitrogen gas. The copolymerization was allowed to run for 90 minutes.

Simulations

The simulations of the copolymerization were carried out using the Predici software package (version 6.72.3). The implicit penultimate unit model was assumed for the simulations of both FRcP and LRcP processes. The implemented model and kinetic parameters employed are shown in Schemes 1 and Table 1, and Scheme 2 and Table 2, respectively.

Under the simulation conditions chosen for the FRcP, the chains initiated by radicals I• and R• propagate before they are irreversibly terminated by the nitroxide. At 70 °C, the nitroxide TEMPO can form a stable C – ON bond, in contrast to nitroxides such as DEPN. Due to relatively similar reactivity parameters of the two copolymerization systems, direct comparisons can be made, evaluating the fraction of the active radical species and that of the dormant species. Dormant species in LRcP undergo continuous reversible activation-deactivation cycles, whereas in FRcP, the chosen temperature is such that once trapping by the nitroxide occurs, there is no subsequent activation of such a species.

Downloaded by STANFORD UNIV GREEN LIBR on May 31, 2012 | http://pubs.acs.org
Publication Date (Web): March 20, 2012 | doi: 10.1021/bk-2012-1100.ch004

$$\begin{array}{llllllll}
I_2 & & & \longrightarrow & I\cdot & + & I\cdot & k_d\text{, eff} \\
I\cdot & + & S & \longrightarrow & PSS_1\cdot & & & 10\ k_p{}^S \\
I\cdot & + & A & \longrightarrow & PAA_1\cdot & & & 10\ k_p{}^A \\
RY & & & \longrightarrow & R\cdot & + & Y & k_{act} \\
R\cdot & + & S & \longrightarrow & PSS_1\cdot & & & 10\ k_p{}^S \\
R\cdot & + & A & \longrightarrow & PAA_1\cdot & & & 10\ k_p{}^A \\
PSS_i\cdot & + & S & \longrightarrow & PSS_{i+1}\cdot & & & k_p{}^{SSS} \\
PSS_i\cdot & + & A & \longrightarrow & PSA_{i+1}\cdot & & & k_p{}^{SSA} \\
PAS_i\cdot & + & S & \longrightarrow & PSS_{i+1}\cdot & & & k_p{}^{ASS} \\
PAS_i\cdot & + & A & \longrightarrow & PSA_{i+1}\cdot & & & k_p{}^{ASA} \\
PAA_i\cdot & + & A & \longrightarrow & PAA_{i+1}\cdot & & & k_p{}^{AAA} \\
PAA_i\cdot & + & S & \longrightarrow & PAS_{i+1}\cdot & & & k_p{}^{AAS} \\
PSA_i\cdot & + & A & \longrightarrow & PAA_{i+1}\cdot & & & k_p{}^{SAA} \\
PSA_i\cdot & + & S & \longrightarrow & PAS_{i+1}\cdot & & & k_p{}^{SAS} \\
PSS_i\cdot & + & Y & \longrightarrow & PSS_iY & & & k_c{}^S \\
PAS_i\cdot & + & Y & \longrightarrow & PAS_iY & & & k_c{}^S \\
PSA_i\cdot & + & Y & \longrightarrow & PSA_iY & & & k_c{}^A \\
PAA_i\cdot & + & Y & \longrightarrow & PAA_iY & & & k_c{}^A \\
PSS_i\cdot & + & PSS_i\cdot & \longrightarrow & D & & & k_{tc}{}^{SS} \\
PAA_i\cdot & + & PAA_i\cdot & \longrightarrow & D & & & k_{tc}{}^{AA} \\
PSA_i\cdot & + & PSA_i\cdot & \longrightarrow & D & & & k_{tc}{}^{AA} \\
PAS_i\cdot & + & PAS_i\cdot & \longrightarrow & D & & & k_{tc}{}^{SS} \\
PSS_i\cdot & + & PAA_i\cdot & \longrightarrow & D & & & k_{tc}{}^{SA} \\
PSS_i\cdot & + & PSA_i\cdot & \longrightarrow & D & & & k_{tc}{}^{SA} \\
PSS_i\cdot & + & PAS_i\cdot & \longrightarrow & D & & & k_{tc}{}^{SS} \\
PAA_i\cdot & + & PSA_i\cdot & \longrightarrow & D & & & k_{tc}{}^{AA} \\
PAA_i\cdot & + & PAS_i\cdot & \longrightarrow & D & & & k_{tc}{}^{SA} \\
PSA_i\cdot & + & PAS_i\cdot & \longrightarrow & D & & & k_{tc}{}^{SA}
\end{array}$$

Scheme 1. The penultimate unit model for the copolymerization of n-butyl acrylate (B) and styrene (S) mediated by nitroxides (LRcP), implemented into the Predici software package.

$$\mathrm{RY} \rightleftharpoons \mathrm{R}\cdot + \mathrm{Y} \qquad k_{act} / k_{deact}$$

$$\mathrm{R}\cdot + \mathrm{S} \longrightarrow \mathrm{PSS}_1\cdot \qquad k_{add}^{S}$$

$$\mathrm{R}\cdot + \mathrm{B} \longrightarrow \mathrm{PBB}_1\cdot \qquad k_{add}^{B}$$

$$\mathrm{PSS}_i\cdot + \mathrm{S} \longrightarrow \mathrm{PSS}_{i+1}\cdot \qquad k_p^{SSS}$$

$$\mathrm{PSS}_i\cdot + \mathrm{B} \longrightarrow \mathrm{PSB}_{i+1}\cdot \qquad k_p^{SSB}$$

$$\mathrm{PBS}_i\cdot + \mathrm{S} \longrightarrow \mathrm{PSS}_{i+1}\cdot \qquad k_p^{BSS}$$

$$\mathrm{PBS}_i\cdot + \mathrm{B} \longrightarrow \mathrm{PSB}_{i+1}\cdot \qquad k_p^{BSB}$$

$$\mathrm{PBB}_i\cdot + \mathrm{B} \longrightarrow \mathrm{PBB}_{i+1}\cdot \qquad k_p^{BBB}$$

$$\mathrm{PBB}_i\cdot + \mathrm{S} \longrightarrow \mathrm{PBS}_{i+1}\cdot \qquad k_p^{BBS}$$

$$\mathrm{PSB}_i\cdot + \mathrm{B} \longrightarrow \mathrm{PBB}_{i+1}\cdot \qquad k_p^{SBB}$$

$$\mathrm{PSB}_i\cdot + \mathrm{S} \longrightarrow \mathrm{PBS}_{i+1}\cdot \qquad k_p^{SBS}$$

$$\mathrm{PSS}_i\cdot + \mathrm{Y} \rightleftharpoons \mathrm{PSS}_i\mathrm{Y} \qquad k_c^{S} / k_d^{S}$$

$$\mathrm{PBS}_i\cdot + \mathrm{Y} \rightleftharpoons \mathrm{PBS}_i\mathrm{Y} \qquad k_c^{S} / k_d^{S}$$

$$\mathrm{PSB}_i\cdot + \mathrm{Y} \rightleftharpoons \mathrm{PSB}_i\mathrm{Y} \qquad k_c^{B} / k_d^{B}$$

$$\mathrm{PBB}_i\cdot + \mathrm{Y} \rightleftharpoons \mathrm{PBB}_i\mathrm{Y} \qquad k_c^{B} / k_d^{B}$$

$$\mathrm{PSS}_i\cdot + \mathrm{PSS}_i\cdot \longrightarrow \mathrm{D} \qquad k_{tc}^{SS}$$

$$\mathrm{PBB}_i\cdot + \mathrm{PBB}_i\cdot \longrightarrow \mathrm{D} \qquad k_{tc}^{BB}$$

$$\mathrm{PSB}_i\cdot + \mathrm{PSB}_i\cdot \longrightarrow \mathrm{D} \qquad k_{tc}^{BB}$$

$$\mathrm{PBS}_i\cdot + \mathrm{PBS}_i\cdot \longrightarrow \mathrm{D} \qquad k_{tc}^{SS}$$

$$\mathrm{PSS}_i\cdot + \mathrm{PBB}_i\cdot \longrightarrow \mathrm{D} \qquad k_{tc}^{SB}$$

$$\mathrm{PSS}_i\cdot + \mathrm{PSB}_i\cdot \longrightarrow \mathrm{D} \qquad k_{tc}^{SB}$$

$$\mathrm{PSS}_i\cdot + \mathrm{PBS}_i\cdot \longrightarrow \mathrm{D} \qquad k_{tc}^{SS}$$

$$\mathrm{PBB}_i\cdot + \mathrm{PSB}_i\cdot \longrightarrow \mathrm{D} \qquad k_{tc}^{BB}$$

$$\mathrm{PBB}_i\cdot + \mathrm{PBS}_i\cdot \longrightarrow \mathrm{D} \qquad k_{tc}^{SB}$$

$$\mathrm{PSB}_i\cdot + \mathrm{PBS}_i\cdot \longrightarrow \mathrm{D} \qquad k_{tc}^{SB}$$

Scheme 2. The penultimate unit model for the conventional radical copolymerization (FRcP) of methyl acrylate (A) and styrene (S), implemented into the Predici software package.

Downloaded by STANFORD UNIV GREEN LIBR on May 31, 2012 | http://pubs.acs.org
Publication Date (Web): March 20, 2012 | doi: 10.1021/bk-2012-1100.ch004

Table 1. Rate parameters used in the simulation of the nitroxide mediated copolymerization at 120 °C as depicted in Scheme 1

Coefficient	*A*	*E (kJ /mol)*	*Value (120 °C)*	*Refs*
k_{act}	2.4×10^{14} s^{-1}	112.3	0.289 s^{-1}	(*12*)
k_{deact}			5.0×10^{6} L mol^{-1} s^{-1}	(*13*)
k_p^{SS}	4.27×10^{7} L mol^{-1}s^{-1}	32.5		(*14*)
k_p^{BB}	2.31×10^{7} L mol^{-1}s^{-1}	18.1		(*15*)
r_S			0.74	(*7*)
r_B			0.23	(*7*)
s_S			0.48	(*16*)
s_B			0.06	(*16*)
k_c^{S}			2.6×10^{5} L mol^{-1}s^{-1}	(*13*)
k_d^{S}			7.5×10^{-3} L mol^{-1}s^{-1}	(*13*)
k_c^{B}			5×10^{5} L mol^{-1}s^{-1}	(*7*)
k_d^{B}			7×10^{-4} L mol^{-1}s^{-1}	(*7*)
k_{tc}^{SS}			1.8×10^{8} L mol^{-1}s^{-1}	(*13*)
k_{tc}^{BB}			7.34×10^{7} L mol^{-1}s^{-1}	(*13*)
k_{tc}^{SB}			1.0×10^{8} L mol^{-1}s^{-1}	Estimate

Downloaded by STANFORD UNIV GREEN LIBR on May 31, 2012 | http://pubs.acs.org
Publication Date (Web): March 20, 2012 | doi: 10.1021/bk-2012-1100.ch004

Table 2. Rate parameters used in the simulation of the conventional radical copolymerization at 70 °C as depicted in Scheme 1

Coefficient	*A*	*E* (*kJ /mol)*	*Value (70 °C)*	*Refs*
k_d	1.58×10^{15} s^{-1}	128.74	3.996×10^{-5} s^{-1}	(*6*)
eff			0.6	
k_{act}			4.9×10^{-4}	(*6*)
k_p^{SS}	4.27×10^{7} L mol^{-1}s^{-1}	32.5		(*14*)
k_p^{AA}	3.61×10^{6} L mol^{-1}s^{-1}	13.9		(*17*)
r_S			0.73	(*6*)
r_A			0.19	(*6*)
s_S			0.41	(*6*)
s_A			0.41	(*6*)
k_c^S			1.0×10^{8} L mol^{-1}s^{-1}	
k_c^A			5.0×10^{8} L mol^{-1}s^{-1}	
k_{tc}^{SS}			1.0×10^{8}L mol^{-1}s^{-1}	
k_{tc}^{AA}			1.0×10^{8} L mol^{-1}s^{-1}	
k_{tc}^{SA}			1.0×10^{8} L mol^{-1}s^{-1}	

Downloaded by STANFORD UNIV GREEN LIBR on May 31, 2012 | http://pubs.acs.org
Publication Date (Web): March 20, 2012 | doi: 10.1021/bk-2012-1100.ch004

Downloaded by STANFORD UNIV GREEN LIBR on May 31, 2012 | http://pubs.acs.org
Publication Date (Web): March 20, 2012 | doi: 10.1021/bk-2012-1100.ch004

Results and Discussion

For the LRcP experiments, the alkoxyamine employed was a DEPN-based alkoxyamine illustrated in Figure 1. The presence of phosphorus in the nitroxide structures allows for the copolymerization reactions to be followed via *in situ* ^{31}P NMR spectroscopy (*7*).

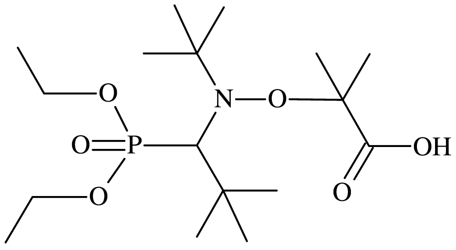

MAMA-DEPN

Figure 1. The structure of the DEPN-based alkoxyamine, MAMA-DEPN, used to initiate and mediate the copolymerization of styrene and n-butyl acrylate.

The evolution with time of the fraction of dormant chains with an acrylate as the terminal unit is illustrated in Figure 2. Detailed description of the simulation is described elsewhere (*7*). In contrast to the results illustrated in Figure 2, radical trapping experiments for an FRcP of styrene and methyl acrylate show behaviour completely opposite to that observed for the LRcP of styrene and *n*-butyl acrylate. The comparison between the fraction of dormant chains with an acrylate at the terminal unit for FRcP and LRcP processes is illustrated in Figure 3. For a FRcP, a direct correlation can be drawn between the ratio of the two radical species and the ratio of the trapped species. But such is not the case for the nitroxide mediated copolymerization.

From Figure 3, only at $f_A^0 \geq 0.9$ is a significant fraction of chains with an acrylate as the terminal monomer unit observed for conventional radical copolymerization. However, such is not the case for the nitroxide-mediated copolymerizations, where the fraction of dormant chains with acrylate as the terminal unit is observed to increase gradually with increasing initial fraction of the acrylate monomer in the monomer feed.

The evolution of the fraction of active chains with styrene as the terminal unit, for both FRcP and LRcP processes is illustrated in Figure 4. The difference in the two profiles illustrated in Figure 4 is attributed to the different radical reactivity ratios for the two systems. However, such a difference in the radical reactivity ratios does not disallow for the direct comparison of the two systems.

Downloaded by STANFORD UNIV GREEN LIBR on May 31, 2012 | http://pubs.acs.org
Publication Date (Web): March 20, 2012 | doi: 10.1021/bk-2012-1100.ch004

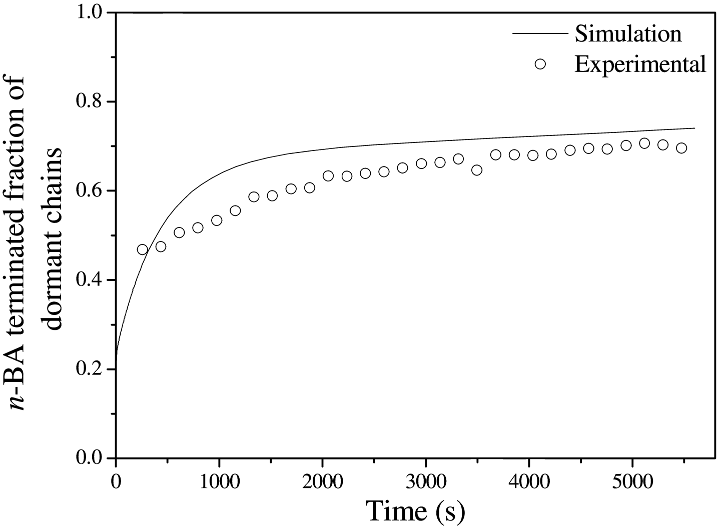

Figure 2. Experimental and simulated evolution of the fraction of dormant chains with n-butyl acrylate as the terminal monomer unit for the nitroxide mediated copolymerization of styrene and n-butyl acrylate for $f_A^0 = 0.71$.

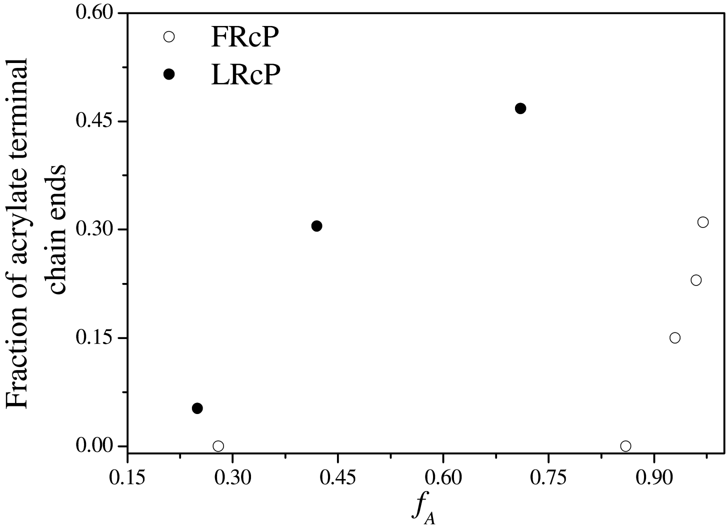

Figure 3. Evolution of nitroxide-terminated chains with an acrylate terminal monomer unit as a function of the fraction of the acrylate monomer in the feed taken at monomer conversion ca 5%.

According to Figures 3 and 4, the fraction of dormant species with a specific monomer as the terminal monomer unit cannot be correlated to the fraction of the respective active radicals in the LRcP system. The fraction of the respective radicals is identical in both FRcP and LRcP, as would be expected from the virtually identical copolymer composition data of the respective techniques.

For FRcP of an acrylate with styrene, where $r_S > r_A$ and $k_p^S << k_p^A$, a greater fraction of active chains will have the styrene moiety as the terminal monomer unit. However, in nitroxide-mediated LRcP involving an acrylate and styrene, activation and deactivation coefficients control that dormant species with an acrylate at the terminal monomer position are far long-lived relative to those with styrene. The result is an accumulation with time of dormant species with an acrylate at the terminal monomer position (Figure 2). This observation made for nitroxide-mediated LRcP also holds true in all reversible deactivation copolymerizations, whereas the situation in reversible-addition fragmentation chain transfer (RAFT) mediated copolymerization is slightly different due to the degenerative chain transfer process.

The simulated fraction of dormant chain ends with an acrylate terminal monomer unit, in LRcP and chain ends resulting from trapping experiments in FRcP are illustrated in Figure 5. The increase in fraction of dormant chain ends with an acrylate in LRcP is well in agreement with the observations reported in Figure 2. In LRcP, the increase in the fraction of dormant chain ends with an acrylate monomer unit is comparable to values reported in Figure 3 for corresponding feed composition. In Figure 5, the fraction of trapped living chain ends with acrylate terminal monomer unit in FRcP remains low, in agreement with results illustrated in Figure 3 for the corresponding feed composition.

For both FRcP and LRcP, similar fraction of active chains with respective terminal monomer unit are observed. However, a contrasting behaviour is observed in the comparison of the nitroxide-capped chain ends in LRcP with the active chain ends in LRcP and FRcP. In FRcP, the nitroxide-capped chain ends result from trapping of chains that grow under conventional free radical conditions by irreversible combination with TEMPO. In FRcP, the fraction of nitroxide-capped chain ends with terminal acrylate monomer unit can directly be correlated to the fraction of active chains with an acrylate terminal monomer unit. However, in LRcP the fraction of nitroxide-capped chain ends with an acrylate monomer unit increases with time due to the relatively smaller equilibrium constant (K). The smaller equilibrium constant implies that dormant chain ends with acrylate as the terminal monomer unit are long-lived relative to their counterparts with styrene as the terminal monomer unit. As such, the accumulation with time of the dormant chain ends with acrylate as the terminal monomer unit is observed in both simulation and experimental data.

Based on the results reported in this contribution, a hypothesis can be put forward with regard to the synthesis of styrene and acrylate block copolymers. Since one of the pre-requisites for a narrow molecular weight distribution is fast initiation, it would seem ideal to synthesize the styrene block first, and the acrylate block second. The macro-alkoxyamine of styrene decomposes faster than that of the acrylate counterpart.

Downloaded by STANFORD UNIV GREEN LIBR on May 31, 2012 | http://pubs.acs.org
Publication Date (Web): March 20, 2012 | doi: 10.1021/bk-2012-1100.ch004

Downloaded by STANFORD UNIV GREEN LIBR on May 31, 2012 | http://pubs.acs.org
Publication Date (Web): March 20, 2012 | doi: 10.1021/bk-2012-1100.ch004

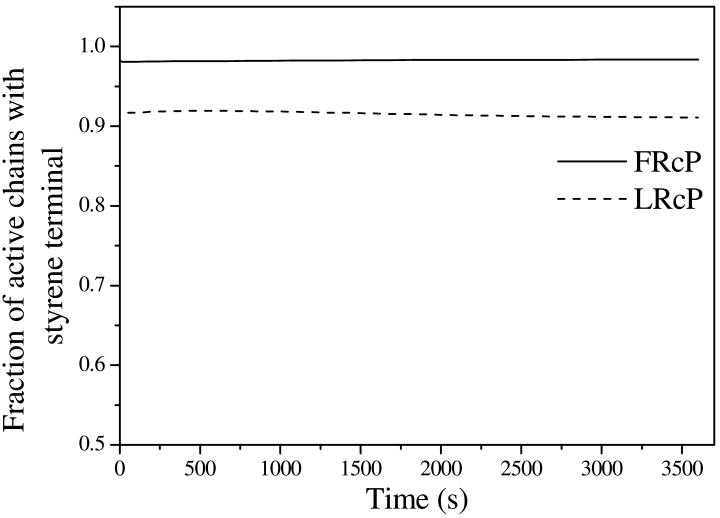

Figure 4. Simulated fraction of active chains with styrene as the terminal monomer unit as a function of time for $f_A^0 = 0.86$.

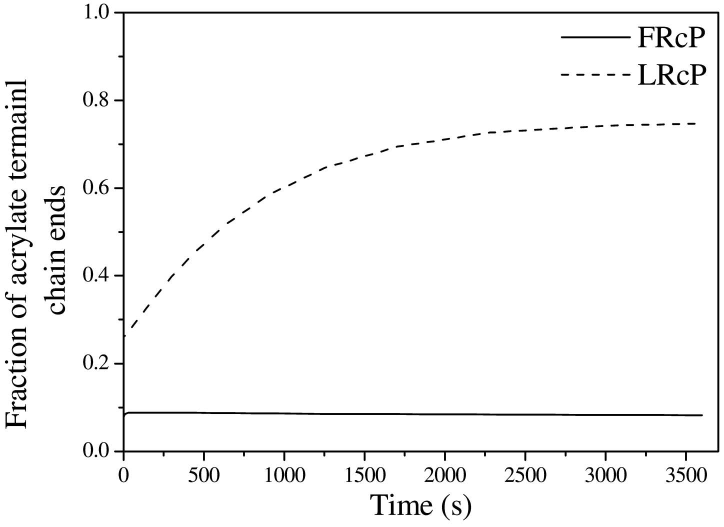

Figure 5. Simulated fraction of dormant and trapped chain ends with an acrylate terminal monomer unit as a function of time for $f_A^0 = 0.86$.

Downloaded by STANFORD UNIV GREEN LIBR on May 31, 2012 | http://pubs.acs.org
Publication Date (Web): March 20, 2012 | doi: 10.1021/bk-2012-1100.ch004

Conclusions

A comparison between FRcP and LRcP with respect to chains terminated with the nitroxide has been reported. Simulations via the Predici software package were conducted for both LRcP and FRcP showing good agreement with experimental data. In FRcP, the evolution of fraction of living chain ends (from irreversible trapping with a nitroxide) with a styrene or an acrylate as the terminal monomer unit, can be directly correlated to the respective fraction of active chains. The simulation revealed that the fractions of active chains with either styrene or acrylate are similar in both FRcP and LRcP, as would be expected. In LRcP, the fraction of active chains with either styrene or acrylate as terminal monomer unit is different to the fractions observed for living chain ends.

References

1. Abdollahi, M.; Mehdipour-Ataei, S.; Ziaee, F. *J. Appl. Polym. Sci.* **2007**, *105*, 2588–2597.
2. Arehart, S. V.; Matyjaszewski, K. *Macromolecules* **1999**, *32*, 2221–2231.
3. Chambard, G.; Klumperman, B.; German, A. L. *Polymer* **1999**, *40*, 4459–4463.
4. Davis, T. P.; O'Driscoll, K. F. *Polym. Int.* **1991**, *24*, 65–70.
5. de la Fuente, J. L.; Fernández-García, M.; Fernández-Sanz, M.; Madruga, E. L. *Macromol. Rapid Commun.* **2001**, *22*, 1415–1421.
6. Kelemen, P.; Klumperman, B. *Macromolecules* **2004**, *37*, 9338–9344.
7. Hlalele, L.; Klumperman, B. *Macromolecules* **2011**, *44* (17), 6683–6690.
8. Couturier, J. L.; Guerret, O.; Bertin, D.; Gigmes, D.; Marque, S.; Tordo, P. U.S. Patent 20060142511, 2006, assigned to Arkema, France.
9. Guerret, O.; Couturier, J.-L.; Le Mercier, C. U.S. Patent 7126021, 2006, assigned to Arkema, France.
10. Smith, L. I.; Emerson, O. H. *Org. Synth.* **1949**, *29*, 18–21.
11. Talaty, E. R.; Boese, C. A.; Adewale, S. M.; Ismail, M. S.; Provenzano, F. A.; Utz, M. J. *J. Chem. Educ.* **2002**, *79* (2), 221–224.
12. Bertin, D.; Gigmes, D.; Marque, S. R. A.; Tordo, P. *Macromolecules* **2005**, *38*, 2638–2650.
13. Chauvin, F.; Dufils, P.-E.; Gigmes, D.; Guillaneuf, Y.; Marque, S. R. A.; Tordo, P.; Bertin, D. *Macromolecules* **2006**, *39*, 5238–5250.
14. Beuermann, S.; Buback, M. *Progr. Polym. Sci.* **2002**, *27* (2), 191–254.
15. Barner-Kowollik, C.; Günzler, F.; Junkers, T. *Macromolecules* **2008**, *41*, 8971–8973.
16. Chambard, G. Control of Monomer Sequence Distribution: Strategic Approach Based on Novel Insights in Atom Transfer Radical Polymerization. Ph.D Dissertation, Technische Universiteit Eindhoven, Eindhoven, 2000.
17. van Herk, A. M. *Macromol. Theory Simul.* **2000**, *9*, 433–441.

Downloaded by UNIV OF GUELPH LIBRARY on May 31, 2012 | http://pubs.acs.org
Publication Date (Web): March 20, 2012 | doi: 10.1021/bk-2012-1100.ch005

Chapter 5

Possibilities for Photoinduced Controlled Radical Polymerizations

Mehmet Atilla Tasdelen,[1,2] Mustafa Çiftci,[1] Mustafa Uygun,[1] and Yusuf Yagci*,[1,3]

**[1]Istanbul Technical University, Faculty of Science and Letters,
Department of Chemistry, Maslak, TR-34469, Istanbul, Turkey
[2]Yalova University, Faculty of Engineering,
Department of Polymer Engineering, 77100 Yalova, Turkey
[3]King Abdulaziz University, Faculty of Science, Chemistry Department,
Jeddah, Saudi Arabia
*E-mail: yusuf@itu.edu.tr**

The purpose of this paper is to present the possibilities and limitations of photoinduced controlled radical polymerizations for the synthesis of well-defined polymers. Although there currently exist only a few examples, photochemical initiation can be applied to the all conventional controlled/living radical polymerizations including iniferter, nitroxide mediated radical, atom transfer radical polymerization and reversible addition-fragmentation chain transfer polymerizations. The photochemical initiation not only enables the easy control of the polymerization under ambient temperature even for heat-sensitive monomers but also tends to minimize side reactions like chain transfer or depolymerization.

Introduction

Photochemical reactions involve the absorption of light to create an excited species that may undergo a number of different reactions such as dissociation, isomerization, abstraction, electron or energy transfer, and bond formation (*1*). These reactions have been studied quite extensively in various fields including organic chemistry, molecular biology and electronics etc. Photoinduced chemical reactions can advantageously be utilized in the field of polymer chemistry (*2*).

In Progress in Controlled Radical Polymerization: Mechanisms and Techniques; Matyjaszewski, K., et al.;
ACS Symposium Series; American Chemical Society: Washington, DC, 2012.

Among them, photoinitiated polymerization has many advantages over other polymerization processes including that it is fast, uses little energy, and readily occurs at room temperature. It has been estimated that energy costs can be reduced 30% by switching from thermal polymerization to photoinitiated polymerization (*3*). Therefore, it has been the basis of numerous conventional applications in surface coatings, printing inks, adhesives, microelectronics, printing plates and three dimensional imaging and micro-fabrication processes.

In recent years, the controlled/living radical polymerization (C/LRP) became an established synthetic method to prepare new complex architectures of polymers such as block, graft, star and functional polymers with well-defined structures. The most widely studied C/LRP methods are atom transfer radical polymerization (ATRP) (*4*, *5*), reversible addition-fragmentation chain transfer polymerization (RAFT) (*6*), nitroxide-mediated radical polymerization (NMRP) (*7*). Most of these techniques so far can be performed at fairly elevated temperatures, mostly between 90 and 120 °C (*8*). Although with limited success, there have been a number of attempts to extend such control to polymerization conducted photochemically. Recent approaches with regard to achieving polymerization control in both cationic (*9–12*) and radical systems (*13–16*) are based on the stabilization of unstable growing species by the reversible formation of the corresponding covalent and dormant species that rapidly exchange. In this chapter, the synthetic possibilities for photoinduced controlled radical polymerizations and their mechanistic insights are discussed.

Downloaded by UNIV OF GUELPH LIBRARY on May 31, 2012 | http://pubs.acs.org
Publication Date (Web): March 20, 2012 | doi: 10.1021/bk-2012-1100.ch005

Photoiniferter-Based Controlled Radical Polymerization

The first step in the development of C/LRP dates back to the early 1980s when it was found that the use of iniferter (namely, agents that initiate, transfer, and terminate) systems exhibited a degree of livingness. This polymerization can be initiated by both thermal and photochemical activation and polymerize most vinyl monomers under mild reaction conditions. Photoiniferter-based polymerizations utilize dithiocarbamate derivatives that can initiate, terminate, and act as transfer agents during the polymerization. A large number of monomers, such as styrene, methyl methacrylate, *n*-butyl acrylate, acrylamide, acrylonitrile, and methacrylonitrile, can be polymerized in a controlled manner with various photoiniferters (Chart 1).

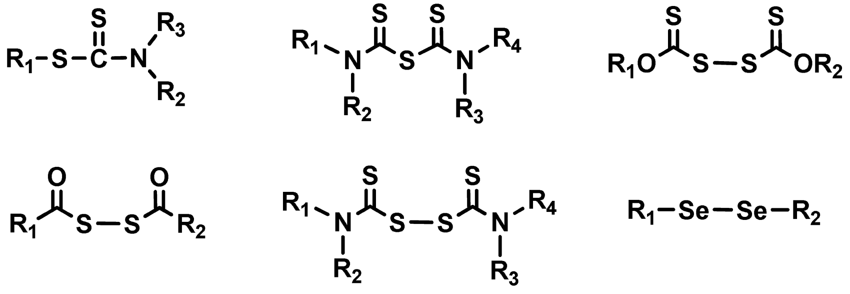

Chart 1. Examples of photoiniferters.

UV irradiation of a dithiocarbamate yields a reactive carbon radical and a relatively unreactive dithiocarbamyl radical. The carbon radical, reacting with the monomer molecules, initiate the radical polymerization and propagates the process upon addition of monomer molecules. Whereas, the dithiocarbamyl radical does reversibly terminate growing polymer chains ("capping/decapping") and, depending on reaction conditions, enables controlled radical polymerization during photoirradiation (Scheme 1). Simple evidence used to support this included the low polydispersities of the product (typically ranging from 1.2 to 2.0), a linear increasing trend of molecular weight with the conversion, and a formation of a related block copolymer.

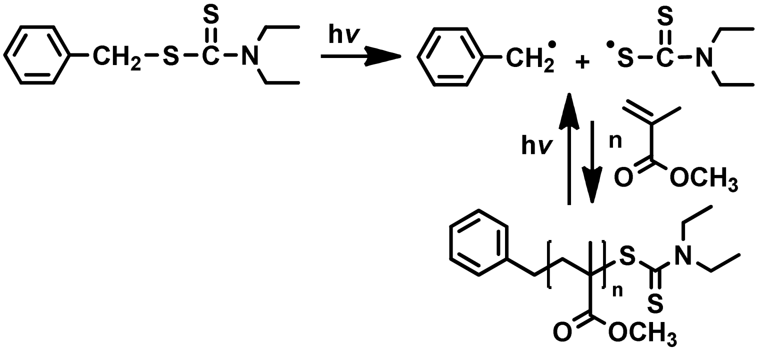

Scheme 1. C/LRP of methyl methacrylate using benzyl-N, N-diethyldithiocarbamate as photoiniferter.

A large number of monomers, such as styrene, methyl methacrylate, n-butyl acrylate, acrylamide, acrylonitrile, and methyl acrylonitrile, can be polymerized in a controlled manner with photoiniferters. However, for other monomers such as vinyl acetate and methyl acrylate, dithiocarbamates served as a weak initiator or terminator, depending on the reactivities of the monomers. The living character of the polymerization decreases from styrene to methyl methacrylate, and to disappear in the case of acrylates. There are a number of other factors that affect the living character of the polymerization such as photoiniferter structures (*17*, *18*), solvent (*19*), light intensity (*20*) and temperature. Steric effects contribute to the phoiniferter and monomer structures while solubility is affected by monomer, iniferter and solvent types. Since the photoiniferter itself is incorporated into the growing/propagating polymer chain during polymerization, a desirable end group functionality can be designed by careful choice of iniferter (*21*).

Photoinduced NMRP

NMRP, based on the use of nitroxyl radicals (nitroxides) or alkoxyamines, is also extensively studied photoinduced controlled radical polymerization method. Scaiano et al. (*22*) first proposed that the homolysis of TEMPO-based alkoxyamines (where TEMPO is 2,2,6,6-tetramethylpiperidinyloxy-4-yl radical) can be photosensitized by a xanthone or a pyrene molecule at their triplet

Downloaded by UNIV OF GUELPH LIBRARY on May 31, 2012 | http://pubs.acs.org
Publication Date (Web): March 20, 2012 | doi: 10.1021/bk-2012-1100.ch005

Downloaded by UNIV OF GUELPH LIBRARY on May 31, 2012 | http://pubs.acs.org
Publication Date (Web): March 20, 2012 | doi: 10.1021/bk-2012-1100.ch005

and singlet excited states (Chart 2). Although the photosensitization step was successful, only limited numbers of radicals were generated in these systems. On the other hand, they did not perform any polymerization study to see the relative contribution of these molecules in the polymerization.

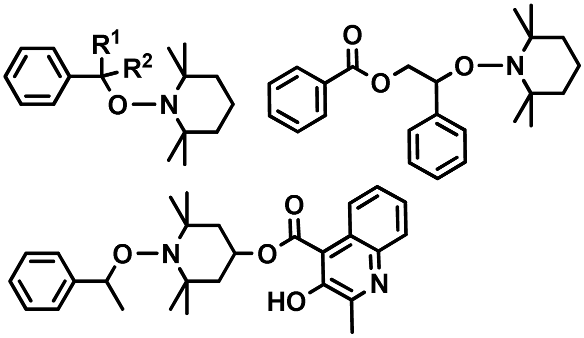

$R^1 = H; R^2 = H, R^1 = H; R^2 = CH_3, R^1 = CH_3; R^2 = CH_3,$
$R^1 = H; R^2 = C_2H_5, R^1 = H; R^2 = C_6H_5$

Chart 2. Examples of photosensitive TEMPO-based alkoxyamines.

Later on, Yoshida et al. (*23*) attempted to activate the radical generation process by using photoacid generator iodonium salt in the presence of TEMPO derivatives or alkoxyamines. However, this system is still unclear as the function of the iodonium salt is also not known. Several attempts were also made to covalently attach different chromophoric groups to the TEMPO moiety (*24*, *25*). Although, some success was achieved, the conditions for true C/LRP were not attained, because the energy transfer from the sensitizer ("antenna") to the C-O bond was not found to be efficient enough to activate the process (*32*, *33*). More recently, Neckers and Lalevee groups (*26*) reported new alkoxyamines possessing a chromophore group with various positions to facilitate the homolysis of alkoxyamine (Chart 3). The effect of the type and position of chromophore groups (xanthone or benzophenone), distance between the chromophore and the nitroxide group, and the structure of the leaving nitroxide on the polymerization was studied (*27–30*).

The first step in the process involves to the photodecomposition of the alkoxyamines with the concomitant formation of an initiating radical and a nitroxide (Scheme 2). The reversible reaction between the polymeric radical and the nitroxide leads to a reduction in the contribution of irreversible bimolecular termination. Usually, the chromophore group must be located on the nitroxide group to ensure reversible cleavage of the macroalkoxyamine during the photopolymerization process. It was demonstrated that photoinitiated NMRP of *n*-butyl acrylate using these compounds indicated a linear growth of the polymer chain combined with a partial living character. However, the photoinitiated NMRP gives rise to polydispersities considerably higher than those obtained by thermally initiated NRMP process.

Downloaded by UNIV OF GUELPH LIBRARY on May 31, 2012 | http://pubs.acs.org
Publication Date (Web): March 20, 2012 | doi: 10.1021/bk-2012-1100.ch005

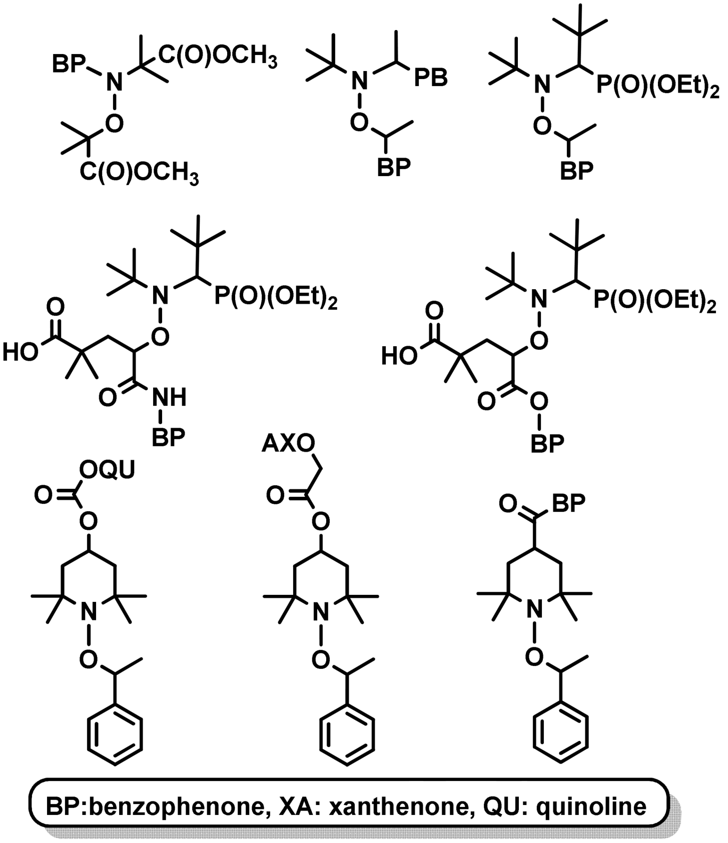
BP
C(O)OCH3
N
O
C(O)OCH3
PB
BP
P(O)(OEt)2
BP
HO
NH
BP
P(O)(OEt)2
O
BP
OQU
AXO
BP
BP:benzophenone, XA: xanthenone, QU: quinoline

Chart 3. Examples of photosensitive alkoxyamines possessing directly linked chromophore groups.

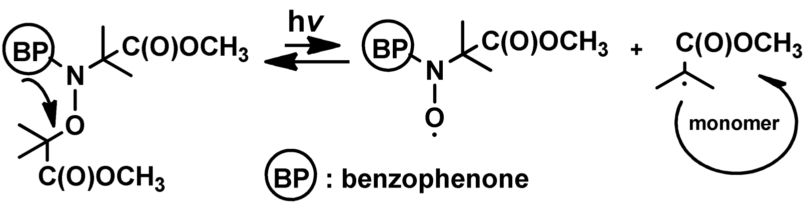
hν
BP
N
O
C(O)OCH3
C(O)OCH3
+
monomer
BP : benzophenone

Scheme 2. Photoinitiated nitroxide-mediated radical polymerization of vinyl monomers with an alkoxyamine possessing a chromophoric benzophenone molecule.

Downloaded by UNIV OF GUELPH LIBRARY on May 31, 2012 | http://pubs.acs.org
Publication Date (Web): March 20, 2012 | doi: 10.1021/bk-2012-1100.ch005

Photoinduced RAFT Polymerization

Photoinduced controlled radical polymerization of vinyl monomers by RAFT process has been also studied under UV and solar irradiation. Among various RAFT agents, dithiobenzoate and trithiocarbonate derivatives were found to be particularly useful in establishing a dynamic equilibrium between propagating radicals and dormant chains via RAFT mechanism under UV irradiation (Chart 4).

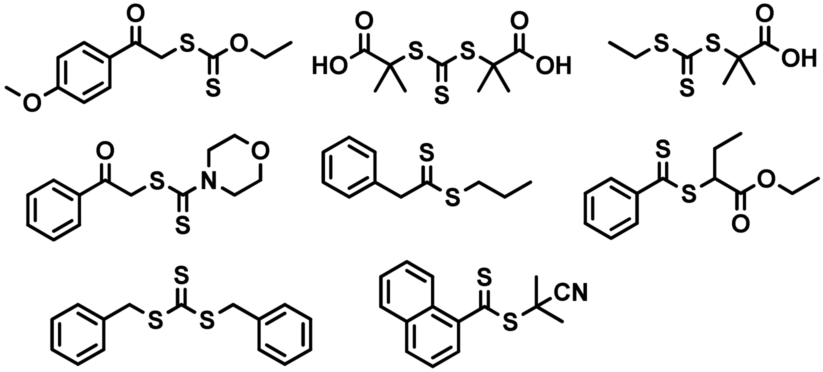

Chart 4. Examples of photosensitive RAFT agents.

The first successful photoinduced RAFT polymerization at low temperature was reported by Pan et al. (*31*) who polymerized styrene, methyl acrylate and butyl acrylate with a dibenzyl trithiocarbonate under UV light between 254 and 366 nm. In another study, Quinn et al. (*32*) used different types of RAFT agents such as 1-phenylethyl phenyldithioacetate in the styrene polymerization. It produced well-defined polymers with controllable molecular weight up to monomer conversions of 30%. Later on, Barner-Kowollik et. al. have studied the photoinitiated RAFT polymerization of acrylic acid in aqueous solutions at ambient temperature using S, S′-bis(α, α′-dimethyl-α″-acetic acid) trithiocarbonate and reached 50% conversion without losing the control (*33*). Cai and co-workers used S-ethyl-S′-(α, α′-dimethyl-α″-acetic acid) trithiocarbonate as RAFT agent for water-soluble monomers in combination with acylphosphine oxide as the photoinitiator under visible light irradiation. Well defined polymers were obtained with narrow polydispersities at conversions over 75% (*34*–*38*).

Zhu (*39*) and Yagci (*16*) independently reported the tandem polymerization concept by combination of photoiniferter and photoinduced RAFT polymerization. In these systems, both (i) photoiniferter and (ii) RAFT mechanisms are operative in the photoinduced controlled radical polymerization (Scheme 3). The results showed a good agreement between the theoretical molecular weight and experimental data with a PDI <1.3.

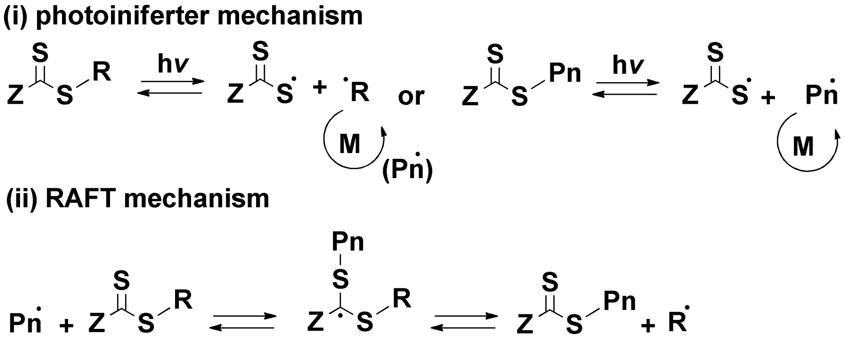

Scheme 3. Schematic representation of photoinitiated RAFT polymerization.

Several groups have also reported the synthesis of polystyrene (*31*, *40*), poly(butyl acrylate) (*31*, *40–42*), poly(methyl acrylate) (*31*), poly(methyl methacrylate) (*43*) and poly(styrene-*alt*-maleic anhydride) (*44*) via photoinduced RAFT polymerization. However, this method exhibits some limitations such as low conversions even at long polymerization times. The molecular weight distribution broadened significantly at long irradiation times due to the decomposition of the chain transfer agent moieties at the polymer ends. There have been a number of attempts to improve the photoinduced RAFT polymerization. For example, the degradation of chain transfer agent at the polymer ends can be minimized by cutting off the short-wave UV radiation using a filter or higher monomer conversion can be reached by addition of a commercially available photoinitiator to the polymerization media.

Photoinduced ATRP

The most versatile method of controlled radical polymerization is ATRP due to its simple polymerization procedure, functional group compatibility, and very good architectural and molecular weight control. A first attempt to integrate a photochemical activation in the ATRP is the use of a photoinitator in the reverse ATRP system. In this process, the initiating radicals originated from the decomposition of the photoinitiators (PI) can abstract the halogen atom (X) from the oxidized transition-metal species ($Cu^{II}X_2/L$) to form the reduced transition-metal species ($Cu^{I}X/L$) and the dormant species (I-X) or can react with the monomer to create a growing chain (I_P•) (Scheme 4). The situation then becomes exactly the same as in a classical ATRP. Therefore, propagation step is also required additional heat energy to achieve a fast initiation and a rapid and reversible deactivation. Interestingly, there is one report on ATRP of methyl methacrylate in the presence of ferric tri(*N*,*N*-diethyldithio carbamate) as the catalyst with 2,2-dimethoxy-2-phenylacetophenone as photoinitiator under UV light irradiation, the exact mechanism of the system is still unclear. And GPC results showed that the obtained polymers have quite high molecular weight distribution.

Downloaded by UNIV OF GUELPH LIBRARY on May 31, 2012 | http://pubs.acs.org
Publication Date (Web): March 20, 2012 | doi: 10.1021/bk-2012-1100.ch005

Downloaded by UNIV OF GUELPH LIBRARY on May 31, 2012 | http://pubs.acs.org
Publication Date (Web): March 20, 2012 | doi: 10.1021/bk-2012-1100.ch005

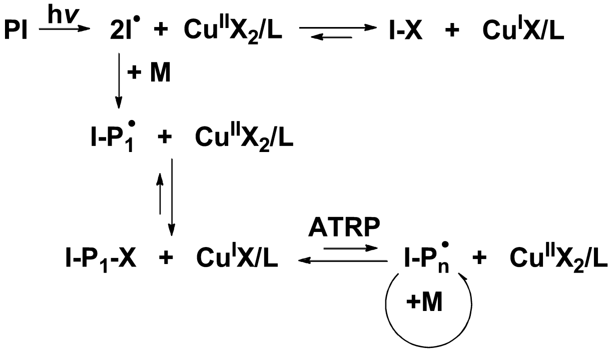

Scheme 4. Schematic representation of photoinitiated reverse ATRP process.

In another study, although authors claimed that light accelerates the rate of classical ATRP but also enhances the living character of the polymerization (*45*), k_{act} constants of ATRP system under UV and without UV irradiation were found quite similar, 0.10 and 0.092 M^{-1} s^{-1} (*46*). Recently, Matyjaszewski and others reported the combination of ATRP and photoiniferter polymerization of methyl methacrylate using a dithiocarbamate photoiniferter (*46–50*). Upon UV irradiation, dithiocarbamate molecules rapidly generate carbon-centered radicals that induce radical propagation and are deactivated by copper complex. In this system, the copper complex mainly facilitates deactivation of propagating radicals rather than activation of initiator, particularly, at low temperature (Scheme 5). Thus, inefficient chain transfer reactions in iniferter polymerization were eliminated by the fast deactivation of radicals by the copper complex.

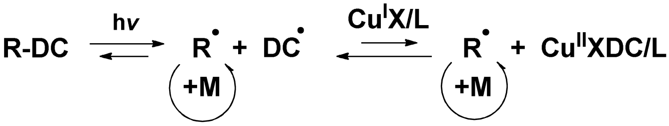

Scheme 5. General mechanism of ATRP with dithiocarbamate under UV Irradiation.

Quite recently, our group presented a new photoinduced controlled radical polymerization, which is mainly based on photochemical generation of activator in the ATRP (*14*, *15*). The polymerization can be operated by *in situ* photogeneration of Cu^IX/L as activator from the copper (II) species and the subsequent reaction of the activator with alkyl halide (Pn-X) resulting in the formation of active radical (Pn•) and $Cu^{II}X_2/L$. In the subsequent step, the radical adds to a monomer and rapidly deactivated by the $Cu^{II}X_2/L$ to form dormant species and Cu^IX/L (Scheme 6). The described photoredox process was also applied in copper-catalyzed azide-alkyne click reaction (*51*, *52*).

Downloaded by UNIV OF GUELPH LIBRARY on May 31, 2012 | http://pubs.acs.org
Publication Date (Web): March 20, 2012 | doi: 10.1021/bk-2012-1100.ch005

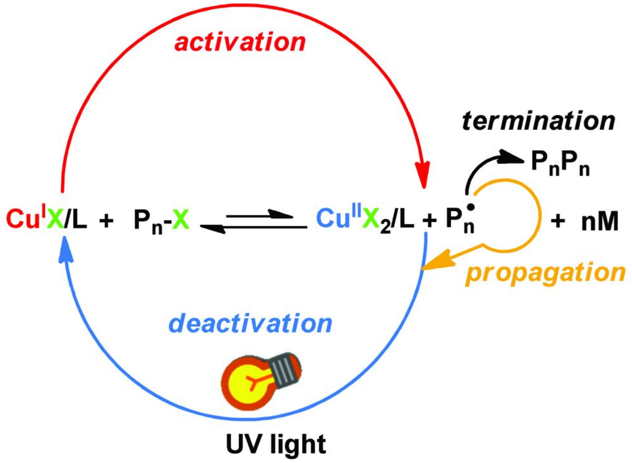
activation
termination
P_nP_n
$Cu^IX/L + P_n\text{-}X \rightleftharpoons Cu^{II}X_2/L + P_n^\bullet$
+ nM
propagation
deactivation
UV light

Scheme 6. Mechanistic scheme for photochemical generation of activator in the ATRP.

In the process, the excess of $Cu^{II}X_2/L$ deactivator resulting from irreversibly unavoidable radical-radical termination reactions is also continuously regenerated to the Cu^IX/L activator by light. However, it should be pointed out that, $Cu^{II}X_2/L$ complexes are usually less soluble in organic media than the corresponding Cu^IX/L complexes, often resulting to heterogeneous polymerizations. The use of small amount of methanol as solvent in the polymerization facilitates to conduct the process in homogeneous system, as methanol exclusively penetrates the solubility of $Cu^{II}X_2/L$ complexes in the polymerization mixture. By applying homogenous polymerization of MMA could significantly increase the rate of polymerization in comparison with, and the control over molecular weights under homogenous system was also improved. Furthermore, one can note that the molecular weight distribution of polymers prepared by homogenous system is relatively narrower (1.06~1.13) than the heterogeneous one (Figure 1).

As a part of continuous efforts to develop the photoinduced ATRP, the use of reverse ATRP, and simultaneous reverse and normal initiation (SR&NI) ATRP as alternative initiating systems were also reported (*13*). Photoinduced reverse ATRP was performed $Cu^{II}Cl_2$/PMDETA system in conjunction with several photoinitiators belonging to the *Type I a*nd *Type II* classes at room temperature. The polymerization of MMA could be initiated in the absence of alkyl halide; however, loss of control over the polymerization process was observed. Photoinduced SR&NI ATRP was successfully applied to MMA in the presence of alkyl halide. The molecular weights increased with conversion, and they were in good agreement with the theoretical values. Compared to the photoinduced reverse ATRP, it allowed better control over molecular weights with narrow molecular weight distributions (Figure 2). Notably, the chain extension reaction with the macroinitiator prepared by photoinduced SR&NI ATRP was more successful than photoinduced reverse ATRP.

Downloaded by UNIV OF GUELPH LIBRARY on May 31, 2012 | http://pubs.acs.org
Publication Date (Web): March 20, 2012 | doi: 10.1021/bk-2012-1100.ch005

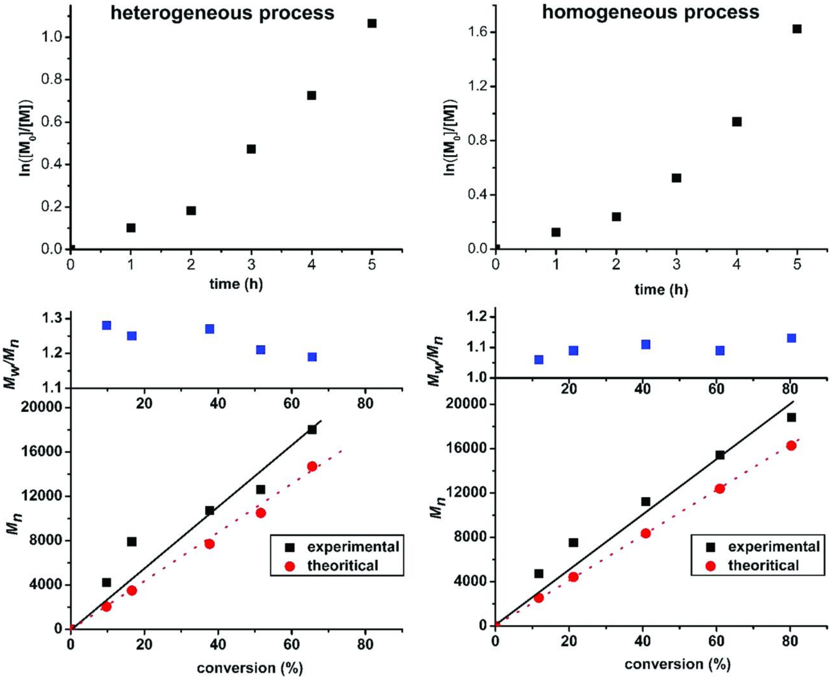

Figure 1. Kinetic plots and molecular weights and distributions of resulting polymers as a function of degree of conversion for photoinduced controlled radical polymerization of methyl methacrylate in the absence or the presence of methanol indicated. (Reproduced with permission from reference (36) Copyright 1994 Wiley).

The use of dyes including eosin Y and erythrosine B is a fairly flexible method to extend the spectral sensitivity of the photoinduced ATRP into the visible-light region. Photoinduced electron transfer from the excited dye to the $Cu^{II}Cl_2$ leads to formation of $Cu^{I}Cl$ which was surely responsible for the initiation of the C/LRP. In order to gain better understanding of the polymerization mechanism, several controlled experiments including in the absence of dye, alkyl halide or metal complexes were performed. When the polymerization was performed without dye (Table 1, entry 4) or $Cu^{II}Cl_2$/PMDETA complex (Table 1, entry 2) or without alkyl halide (Table 1, entry 3), either no polymer or a small amount of polymer with uncontrolled molecular weight was formed after the same polymerization time. Visible light-induced ATRP of MMA could be initiated by two different dyes such as eosin Y (Table 1, entry 4) or erythrosine B (Table 1, entry 5). The experimental molecular weights of polymers were in good agreement with the theoretical values, indicating high initiation efficiency. The molecular weight distribution remained narrow (1.2~1.4) and unimodal during the polymerization.

Downloaded by UNIV OF GUELPH LIBRARY on May 31, 2012 | http://pubs.acs.org
Publication Date (Web): March 20, 2012 | doi: 10.1021/bk-2012-1100.ch005

Table 1. Visible light-induced atom transfer radical polymerization[a] of methyl methacrylate at room temperature

Entry	*$[MMA]_0/[RX]_0/[MtX]_0/$ $[PMDETA]_0/[Dye]_0$*	*Conv. (%)*	*$M_{n,theo}$[b] ($g\ mol^{-1}$)*	*$M_{n,GPC}$[c] ($g\ mol^{-1}$)*	*M_w/M_n[c]*
1	200/1/0.1/1.1/0-	-	-	-	-
2	200/1/0/0/0.1-	-	-	-	-
3[d]	200/0/0.1/1.1/0.1	5	-	54500	3.60
4[d]	200/1/0.1/1.1/0.1	40	8300	11000	1.23
5[e]	200/1/0.1/1.1/0.1	52	10500	18400	1.38

[a] Polymerization experiments were performed at 400-500 nm, time = 120 min, light intensity = 45 mW cm^{-2}. [b] $M_{n,theo}$= ($[MMA]_0/[EtBP]_0$ x conversion x $M_{monomer}$). [c] Molecular weight ($M_{n,GPC}$) and distribution (M_w/M_n) were determined by gel permeation chromatography. [d] with Eosin Y. [e] with Erythrosine B.

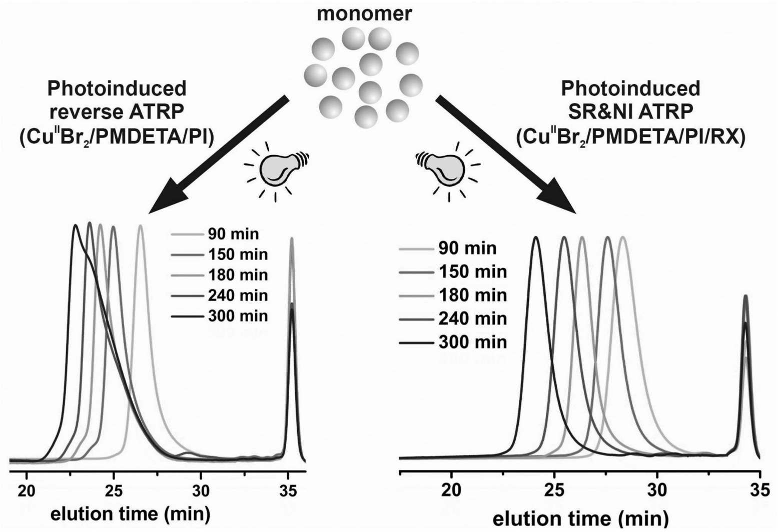

Figure 2. GPC traces of PMMA prepared by photoinduced reverse ATRP, and simultaneous reverse and normal initiation (SR&NI) ATRP.

Photoinduced Degenerative-Transfer Polymerization

Later on, Kamigaito et al. developed a visible light-induced controlled radical polymerization, based on degenerative iodine transfer processes, using a dinuclear manganese complex $[Mn_2(CO)_{10}]$ in conjunction with alkyl iodides (*53–55*). Upon absorption of light, $[Mn_2(CO)_{10}]$ undergoes to photochemical homolysis of the metal-metal bond to form the highly reactive metal-centered radical $[\bullet Mn(CO)_5]$, which can even activate the less reactive C-I dormant species (Scheme 7). This system was applicable to not only unconjugated monomer, vinyl acetate, but also conjugated monomers such as acrylates and styrene with the use of appropriate initiators.

In another example, Yamago et al. reported a photoinduced organotellurium-mediated controlled radical polymerization of meth(acrylate)s by direct photolysis of the C−Te bond of the dormant species (*56*, *57*). The proposed mechanism for the polymerization involves that the activation process mainly occurred by degenerative (exchange) chain transfer with a small contribution of reversible termination (Scheme 8). The main drawback of this technique is that organotellurium derivatives are sensitive to air and light, foul-smelling, and difficult to handle.

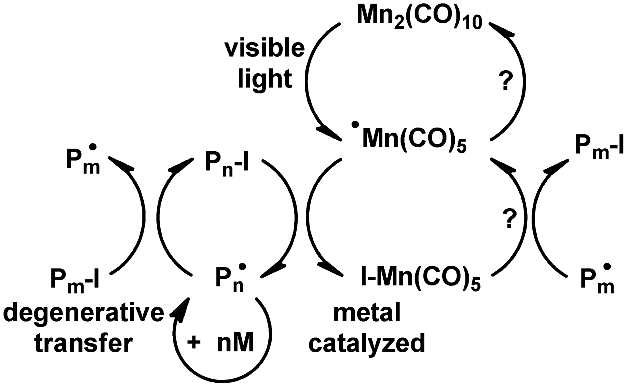
$Mn_2(CO)_{10}$
visible light
?
$^{\bullet}Mn(CO)_5$
$P_m^{\bullet}$
P_n-I
P_m-I
P_m-I
$P_n^{\bullet}$
I-Mn(CO)$_5$
?
$P_m^{\bullet}$
degenerative transfer
+ nM
metal catalyzed

Scheme 7. Proposed mechanism of photoinduced controlled radical polymerization with manganese decacarbonyl/alkyl iodide system.

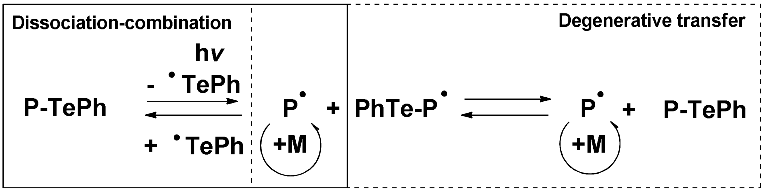
Dissociation-combination
P-TePh
hν
- $^{\bullet}$TePh
+ $^{\bullet}$TePh
$P^{\bullet}$ +
(+M)
Degenerative transfer
PhTe-$P^{\bullet}$
$P^{\bullet}$ + P-TePh
(+M)

Scheme 8. General mechanism of photoinduced organotellurium-mediated controlled radical polymerization.

Conclusion

In this contribution, new possible photoinduced controlled radical polymerizations for the synthesis of polymers with controlled architecture have been reported with particular references to recent works conducted in the area. It is still a challenge to prepare macromolecular materials with tailor-made properties employing photochemical techniques. We wish that advances in photoinitiated controlled polymerization systems will definitely open new pathways to achieve these complex macromolecular architectures.

Downloaded by UNIV OF GUELPH LIBRARY on May 31, 2012 | http://pubs.acs.org
Publication Date (Web): March 20, 2012 | doi: 10.1021/bk-2012-1100.ch005

References

1. Yagci, Y.; Jockusch, S.; Turro, N. J. *Macromolecules* **2010**, *43*, 6245–6260.
2. Tasdelen, M. A.; Yagci, Y. *Aust. J. Chem.* **2011**, *64*, 982–991.
3. Weiss, K. D. *Prog. Polym. Sci.* **1997**, *22*, 203–245.
4. Kamigaito, M.; Ando, T.; Sawamoto, M. *Chem. Rev.* **2001**, *101*, 3689–3745.
5. Matyjaszewski, K.; Xia, J. H. *Chem. Rev.* **2001**, *101*, 2921–2990.
6. Chiefari, J.; Chong, Y. K.; Ercole, F.; Krstina, J.; Jeffery, J.; Le, T. P. T.; Mayadunne, R. T. A.; Meijs, G. F.; Moad, C. L.; Moad, G.; Rizzardo, E.; Thang, S. H. *Macromolecules* **1998**, *31*, 5559–5562.
7. Hawker, C. J.; Bosman, A. W.; Harth, E. *Chem. Rev.* **2001**, *101*, 3661–3688.
8. Braunecker, W. A.; Matyjaszewski, K. *Prog. Polym. Sci.* **2007**, *32*, 93–146.
9. Kahveci, M. U.; Tasdelen, M. A.; Yagci, Y. *Polymer* **2007**, *48*, 2199–2202.
10. Kahveci, M. U.; Tasdelen, M. A.; Yagci, Y. *Macromol. Rapid Commun.* **2008**, *29*, 202–206.
11. Kahveci, M. U.; Tasdelen, M. A.; Cook, W. D.; Yagci, Y. *Macromol. Chem. Phys.* **2008**, *209*, 1881–1886.
12. Kahveci, M. U.; Uygun, M.; Tasdelen, M. A.; Schnabel, W.; Cook, W. D.; Yagci, Y. *Macromolecules* **2009**, *42*, 4443–4448.
13. Tasdelen, M. A.; Uygun, M.; Yagci, Y. *Macromol. Chem. Phys.* **2011**, *212*, 2036–2042.
14. Tasdelen, M. A.; Uygun, M.; Yagci, Y. *Macromol. Rapid Commun.* **2011**, *32*, 58–62.
15. Tasdelen, M. A.; Uygun, M.; Yagci, Y. *Macromol. Chem. Phys.* **2010**, *211*, 2271–2275.
16. Tasdelen, M. A.; Durmaz, Y. Y.; Karagoz, B.; Bicak, N.; Yagci, Y. *J. Polym. Sci., Part A: Polym. Chem.* **2008**, *46*, 3387–3395.
17. Otsu, T.; Matsunaga, T.; Kuriyama, A.; Yoshioka, M. *Eur. Polym. J.* **1989**, *25*, 643–650.
18. Otsu, T.; Matsunaga, T.; Doi, T.; Matsumoto, A. *Eur. Polym. J.* **1995**, *31*, 67–78.
19. Lalevee, J.; Allonas, X.; Jradi, S.; Fouassier, J. P. *Macromolecules* **2006**, *39*, 1872–1879.
20. Lalevee, J.; El-Roz, M.; Allonas, X.; Fouassier, J. P. *J. Polym. Sci., Part A: Polym. Chem.* **2007**, *45*, 2436–2442.
21. Otsu, T. *J. Polym. Sci., Part A: Polym. Chem.* **2000**, *38*, 2121–2136.
22. Scaiano, J. C.; Connolly, T. J.; Mohtat, N.; Pliva, C. N. *Can. J. Chem.* **1997**, *75*, 92–97.
23. Yoshida, E. *Colloid. Polym. Sci.* **2008**, *286*, 1663–1666.
24. Goto, A.; Scaiano, J. C.; Maretti, L. *Photochem. Photobiol. Sci.* **2007**, *6*, 833–835.
25. Hu, S.; Malpert, J. H.; Yang, X.; Neckers, D. C. *Polymer* **2000**, *41*, 445–452.
26. Guillaneuf, Y.; Bertin, D.; Gigmes, D.; Versace, D. L.; Lalevee, J.; Fouassier, J. P. *Macromolecules* **2010**, *43*, 2204–2212.
27. Versace, D. L.; Lalevee, J.; Fouassier, J. P.; Gigmes, D.; Guillaneuf, Y.; Bertin, D. *J. Polym. Sci., Part A: Polym. Chem.* **2010**, *48*, 2910–2915.

Downloaded by UNIV OF GUELPH LIBRARY on May 31, 2012 | http://pubs.acs.org
Publication Date (Web): March 20, 2012 | doi: 10.1021/bk-2012-1100.ch005

Downloaded by UNIV OF GUELPH LIBRARY on May 31, 2012 | http://pubs.acs.org
Publication Date (Web): March 20, 2012 | doi: 10.1021/bk-2012-1100.ch005

28. Versace, D. L.; Lalevee, J.; Fouassier, J. P.; Guillaneuf, Y.; Bertin, D.; Gigmes, D. *Macromol. Rapid Commun.* **2010**, *31*, 1383–1388.
29. Guillaneuf, Y.; Versace, D. L.; Bertin, D.; Lalevee, J.; Gigmes, D.; Fouassier, J. P. *Macromol. Rapid Commun.* **2010**, *31*, 1909–1913.
30. Versace, D. L.; Guillaneuf, Y.; Bertin, D.; Fouassier, J. P.; Lalevee, J.; Gigmes, D. *Org. Biomol. Chem.* **2011**, *9*, 2892–2898.
31. You, Y. Z.; Hong, C. Y.; Bai, R. K.; Pan, C. Y.; Wang, J. *Macromol. Chem. Phys.* **2002**, *203*, 477–483.
32. Quinn, J. F.; Barner, L.; Barner-Kowollik, C.; Rizzardo, E.; Davis, T. P. *Macromolecules* **2002**, *35*, 7620–7627.
33. Muthukrishnan, S.; Pan, E. H.; Stenzel, M. H.; Barner-Kowollik, C.; Davis, T. P.; Lewis, D.; Barner, L. *Macromolecules* **2007**, *40*, 2978–2980.
34. Lu, L.; Zhang, H. J.; Yang, N. F.; Cai, Y. L. *Macromolecules* **2006**, *39*, 3770–3776.
35. Lu, L. C.; Yang, N. F.; Cai, Y. L. *Chem. Commun.* **2005**, 5287–5288.
36. Jiang, W.; Lu, L.; Cai, Y. *Macromol. Rapid Commun.* **2007**, *28*, 725–728.
37. Shi, Y.; Liu, G.; Gao, H.; Lu, L.; Cai, Y. *Macromolecules* **2009**, *42*, 3917–3926.
38. Shi, Y.; Gao, H.; Lu, L.; Cai, Y. *Chem. Commun.* **2009**, 1368–1370.
39. Wang, X. Y.; Zhu, J.; Zhou, D.; Zhu, X. L. *Polymer* **2005**, *46*, 3515–3521.
40. Ran, R.; Yu, Y.; Wan, T. *J. Appl. Polym. Sci.* **2007**, *105*, 398–404.
41. Barth, J.; Buback, M.; Meiser, W.; Vana, P. *Macromolecules* **2010**, *43*, 51–54.
42. Meiser, W.; Barth, J.; Buback, M.; Kattner, H.; Vana, P. *Macromolecules* **2011**, *44*, 2474–2480.
43. Veetil, A. T.; Solomek, T.; Ngoy, B. P.; Pavlikova, N.; Heger, D.; Klan, P. *J. Org. Chem.* **2011**, *76*, 8232–8242.
44. Wu, D. C.; Hong, C. Y.; Pan, C. Y.; He, W. D. *Polym. Int.* **2003**, *52*, 98–103.
45. Guan, Z. B.; Smart, B. *Macromolecules* **2000**, *33*, 6904–6906.
46. Kwak, Y.; Matyjaszewski, K. *Macromolecules* **2010**, *43*, 5180–5183.
47. Li, P.; Qiu, K. Y. *Macromol. Rapid Commun.* **2002**, *23*, 1124–1129.
48. Li, P.; Qin, S. H.; Qin, D. Q.; Qiu, K. Y. *Polym. Int.* **2004**, *53*, 756–765.
49. Zhang, W.; Zhu, X. L.; Zhu, J.; Chen, J. Y. *J. Polym. Sci., Part A: Polym. Chem.* **2006**, *44*, 32–41.
50. Ishizu, K.; Katsuhara, H. *Des. Monomers Polym.* **2006**, *9*, 99–115.
51. Tasdelen, M. A.; Yagci, Y. *Tetrahedron Lett.* **2010**, *51*, 6945–6947.
52. Tasdelen, M. A.; Yilmaz, G.; Iskin, B.; Yagci, Y., *Macromolecules* **2012**, DOI: 10.1021/ma202438w.
53. Koumura, K.; Satoh, K.; Kamigaito, M. *Macromolecules* **2008**, *41*, 7359–7367.
54. Koumura, K.; Satoh, K.; Kamigaito, M. *Macromolecules* **2009**, *42*, 2497–2504.
55. Koumura, K.; Satoh, K.; Kamigaito, M. *J. Polym. Sci., Part A: Polym. Chem.* **2009**, *47*, 1343–1353.
56. Yamago, S. *Chem. Rev.* **2009**, *109*, 5051–5068.
57. Yamago, S.; Ukai, Y.; Matsumoto, A.; Nakamura, Y. *J. Am. Chem. Soc.* **2009**, *131*, 2100–2101.

Downloaded by CORNELL UNIV on May 31, 2012 | http://pubs.acs.org
Publication Date (Web): March 20, 2012 | doi: 10.1021/bk-2012-1100.ch006

Chapter 6

Highly Efficient Organic and Macromolecular Synthesis Using Sequential Copper Catalyzed Azide-Alkyne [3+2] Cycloaddition and ATRA/ATRP

Carolynne L. Ricardo and Tomislav Pintauer*

**Department of Chemistry and Biochemistry, Duquesne University,
308 Mellon Hall, 600 Forbes Avenue,
Pittsburgh, Pennsylvania 15282, USA
*E-mail: pintauert@duq.edu**

Catalyst regeneration technique in transition metal-mediated atom transfer radical polymerization (ATRP), addition (ATRA) and cyclization (ATRC) reactions utilizes environmentally benign reducing agents, which continuously regenerate transition metal complex in the lower oxidation state (activator) from the higher oxidation state (deactivator). This technique has been very successful in reducing the catalyst loadings from several thousands to 5-100 ppm levels. Consequently, this methodology has attracted further academic interest and its scope has been expanded to include sequential organic transformations such as ATRA/ATRC and ATRA/cyclopropanation. Additionally, copper-catalyzed azide-alkyne [3+2] cycloaddition (CuAAC) has been widely explored in combination with ATRP to generate a plethora of macromolecular structures. This chapter focuses on recent advances in small molecule synthesis using CuAAC and ATRA to form functionalized triazoles and polytriazoles.

In Progress in Controlled Radical Polymerization: Mechanisms and Techniques; Matyjaszewski, K., et al.;
ACS Symposium Series; American Chemical Society: Washington, DC, 2012.

Downloaded by CORNELL UNIV on May 31, 2012 | http://pubs.acs.org
Publication Date (Web): March 20, 2012 | doi: 10.1021/bk-2012-1100.ch006

Introduction and Background

Copper-Catalyzed Azide-Alkyne [3+2] Cycloaddition (CuAAC)

The term,“click chemistry” coined in 2001 serves as a guiding principle in the synthesis of compounds with desired functionality using “near perfect” reaction conditions (*1*). Typically, reactions classified under the “click chemistry” umbrella are defined by stringent set of criteria and among them, copper-catalyzed Huisgen [3+2] cycloaddition (CuAAC) popularized by the Meldal (*2*) and Sharpless (*3*) groups was the first to achieve the “click status” (Figure 1). To date, this reaction has dominated this area of research and even became synonymous with “click chemistry”, mainly due to its reliability, robustness, functional group tolerance, ability to withstand wide spectrum of solvents, and desirable properties of the resulting triazoles. Immense contributions have been made and wide arrays of applications found in various disciplines such as biology (*4*, *5*), chemistry (*1*, *6–8*), bioconjugation (*7*, *9*), drug discovery (*9–12*) and materials/polymer science (*8*, *13–16*).

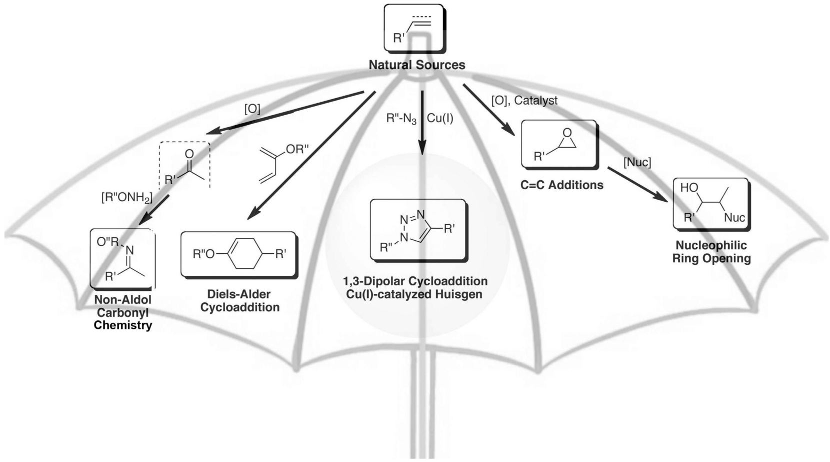
Natural Sources
[O]
[O], Catalyst
R"-N3
Cu(I)
[R"ONH2]
[Nuc]
C=C Additions
Nucleophilic Ring Opening
Non-Aldol Carbonyl Chemistry
Diels-Alder Cycloaddition
1,3-Dipolar Cycloaddition Cu(I)-catalyzed Huisgen

Figure 1. Selected reactions that meet the requirements for “click chemistry”classification.

The mechanism of copper catalyzed azide-alkyne [3+2] cycloaddition has been widely investigated using computational (*17–19*) and experimental (*3*, *20*, *21*) techniques. Regardless of the starting copper salt or complex (either Cu^I or Cu^{II}), it has been established that Cu^I is the active catalytic species in the coupling of azide and alkyne (*6*). The catalytic cycle begins with the coordination of the alkyne to the copper(I) center, resulting in the formation of a π-complex (Scheme 1). This step lowers the p*Ka* of terminal alkyne proton by approximately 10 units, enabling the conversion of the π-complex to a σ-acetylide copper(I) intermediate. Kinetic investigation (*20*) has revealed that the reaction rate is second-order with respect to the metal, suggesting the strong tendency of copper(I) acetylide species to form μ-coordinate bridged aggregates (*18*, *19*), the formation of which is highly dependent on the nature of the complexing ligand. The next step in the catalytic cycle is the coordination of the organic azide, which consequently activates the *N*-terminus for nucleophilic attack to the acetylide. This results in the formation of vinylidine-like structure, which subsequently converts to a more stable copper(I) triazolide. Lastly the catalytic cycle is completed by protonolysis, which yields the desired 1,2,3-triazole and regenerates the active copper(I) species.

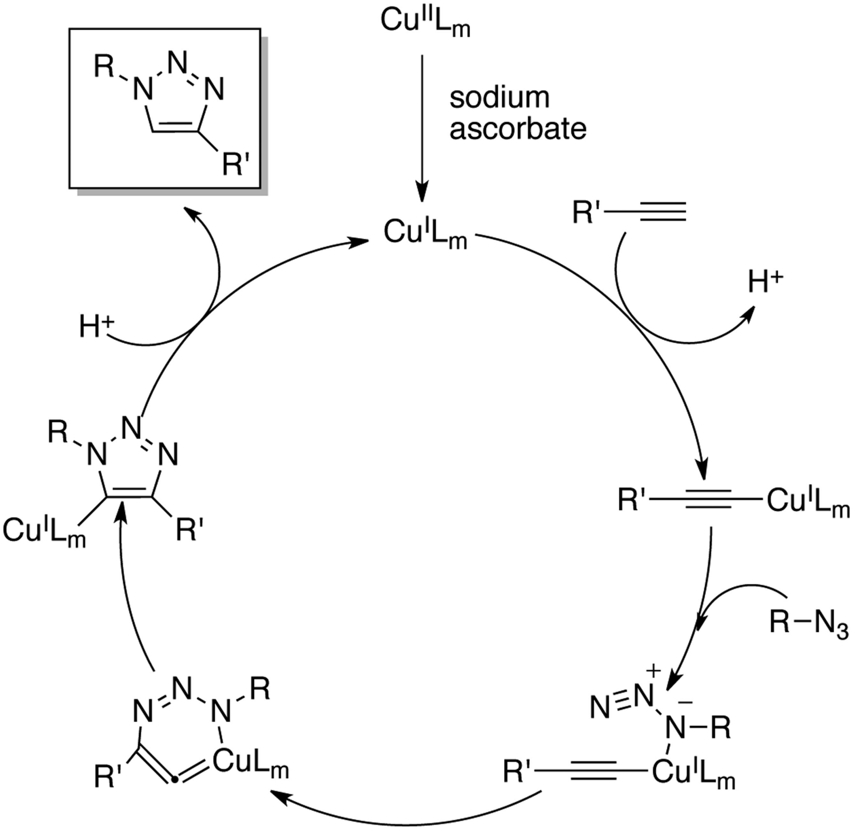

Scheme 1. Proposed mechanism for copper catalyzed azide-alkyne [3+2] cycloaddition.

Copper-Catalyzed Atom Transfer Radical Reactions in the Presence of Reducing Agents

Other C-C forming reactions that are becoming more synthetically useful are the transition-metal catalyzed atom transfer radical addition (ATRA) and its intramolecular counterpart, atom transfer radical cyclization (ATRC) (*22–29*). Traditionally, both were conducted in the presence of high catalyst loadings, therefore facing issues in product separation and catalyst recycling. Solution to

Downloaded by CORNELL UNIV on May 31, 2012 | http://pubs.acs.org
Publication Date (Web): March 20, 2012 | doi: 10.1021/bk-2012-1100.ch006

these problems was found for the mechanistically similar atom transfer radical polymerization (ATRP) (*30*, *31*) in which reducing agents were utilized to continuously regenerate the activator or copper(I) complex (Scheme 2). Catalyst regeneration technique has also been shown to be highly efficient in ruthenium and copper catalyzed ATRA and ATRC reactions (*32–47*). The presence of the reducing agents (free-radical diazo initiators, magnesium or ascorbic acid) successfully allowed the reduction in the amount of transition metal complex, and as a result, these reactions can now be conducted using very low amounts of the catalyst (*33–47*). Synthetic usefulness of this methodology has also been demonstrated in sequential organic transformations involving ATRA/ATRC (*43*, *44*, *48*, *49*) and ATRA/ring closure by reductive dehalogenation (*50–52*).

Downloaded by CORNELL UNIV on May 31, 2012 | http://pubs.acs.org
Publication Date (Web): March 20, 2012 | doi: 10.1021/bk-2012-1100.ch006

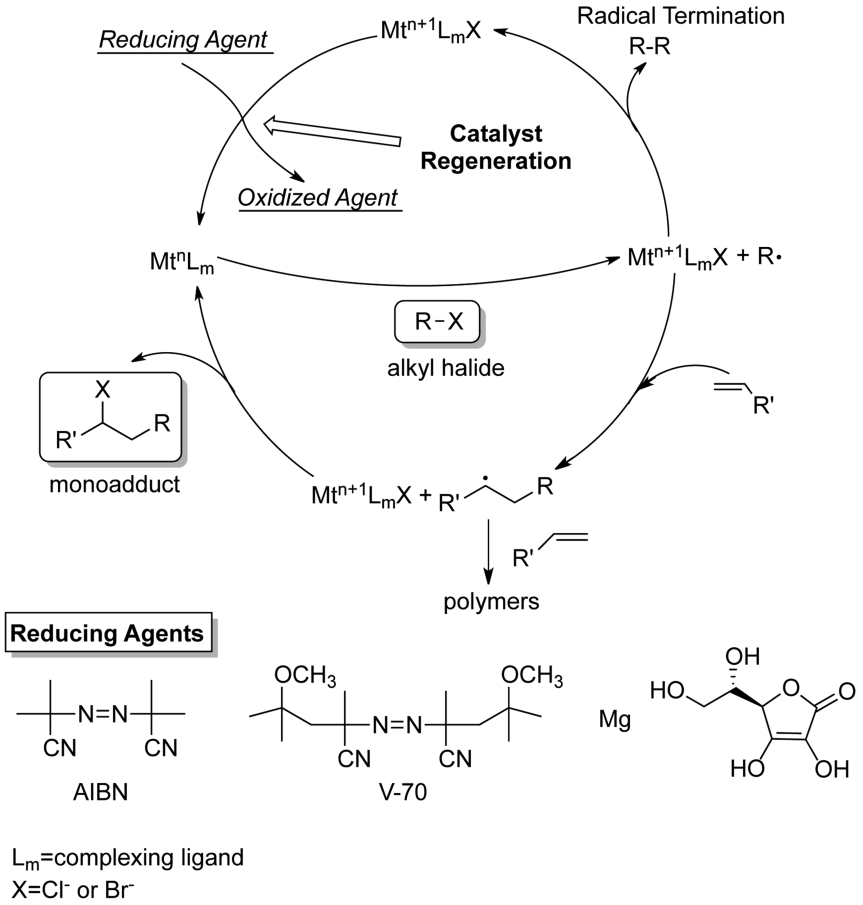
Reducing Agent
Mt^n+1LmX
Radical Termination
R-R
Catalyst Regeneration
Oxidized Agent
MtnLm
Mt^n+1LmX + R•
R−X
alkyl halide
R'
X
R'
R
monoadduct
Mt^n+1LmX + R'
R
R'
polymers
Reducing Agents
N=N
CN
CN
AIBN
OCH3
OCH3
N=N
CN
CN
V-70
Mg
OH
HO
O
O
HO
OH
Lm=complexing ligand
X=Cl- or Br-

Scheme 2. Proposed mechanism for transition metal catalyzed ATRA in the presence of reducing agents.

The proposed mechanism for copper catalyzed ATRA in the presence of reducing agents is shown in Scheme 2 (*26*, *27*). The role of the reducing agent is to continuously regenerate copper(I) from the copper(II) complex that accumulates in the reaction mixture as a result of unavoidable and often diffusion controlled radical-radical termination reactions. Catalytic cycle starts with a homolytic cleavage of the alkyl halide bond by the copper(I) complex to produce an alkyl radical, which subsequently adds across a carbon-carbon double bond of an alkene. The generated secondary radical is then trapped by irreversible abstraction of halogen atom from the copper(II) complex to form the desired monoadduct. This step regenerates the activator or copper(I) complex, completing the catalytic cycle. As indicated in Scheme 2, the competing side reactions in this process besides radical terminations by either coupling or disproportionation include repeating radical additions to alkene to form oligomers/polymers.

Downloaded by CORNELL UNIV on May 31, 2012 | http://pubs.acs.org
Publication Date (Web): March 20, 2012 | doi: 10.1021/bk-2012-1100.ch006

Synthesis of Macromolecular Structures by Combination of Copper Catalyzed [3+2] Azide-Alkyne Cycloaddition and ATRP

Click Chemistry in Materials/Polymer Chemistry

Although click chemistry was initially developed as a drug discovery tool, most successful applications thus far have been in the field of materials science/polymer chemistry (*6–8*, *13–16*, *53–55*). The union between “click chemistry” and controlled radical polymerization (CRP) techniques such as atom transfer radical polymerization (ATRP) (*31*, *56*, *57*), nitroxide-mediated polymerization (NMP) (*58*) and reversible addition-fragmentation polymerization (RAFT) has enabled the synthesis of macromolecular structures previously not accessible using classical free radical polymerization (*59*, *60*). Among the CRP methods, the first intensely exploited examples of combined azide-alkyne [3+2] cycloaddition and living radical polymerization involved ATRP (*13–16*). Strategies developed for the combination of these two reactions include the use of functional initiators (a), monomers bearing azido or acetylenic moieties (b, d-f), and post-polymerization modification typically consisting of converting the halogen into azido end groups (c, Figure 2). In recent years, an extensive range of new polymeric materials for macromolecular engineering and biological applications has been developed in conjunction with click chemistry; particularly multiblock copolymers (*61–63*), multisegmented block copolymers (*54*, *64–66*), micelles (*67–69*) and polymers with complex structures such as star polymers (*70–80*), brush and graft copolymers (*55*, *81–83*), dendrimers (*84*), hydrogels (*85*, *86*), model networks (*87*) and functionalized nanotubes (Figure 3) (*88*). At the same time, several polymeric techniques have been widely utilized in the preparation of water-soluble and biocompatible polymer therapeutics including polymer-drug conjugates (*89*), polymer-protein conjugates (*5*, *90*, *91*), glycopolymers/carbohydrate-polymer conjugates (*92*)(*93*), polymeric micelles to which drug is covalently-bound (*67–69*, *94*), and multi-component polyplexes that are being developed for non-viral vectors (*92*, *95*). Surface functionalization via ATRP and click chemistry has also been utilized in the synthesis of bionanoparticles (*67*, *96*).

Downloaded by CORNELL UNIV on May 31, 2012 | http://pubs.acs.org
Publication Date (Web): March 20, 2012 | doi: 10.1021/bk-2012-1100.ch006

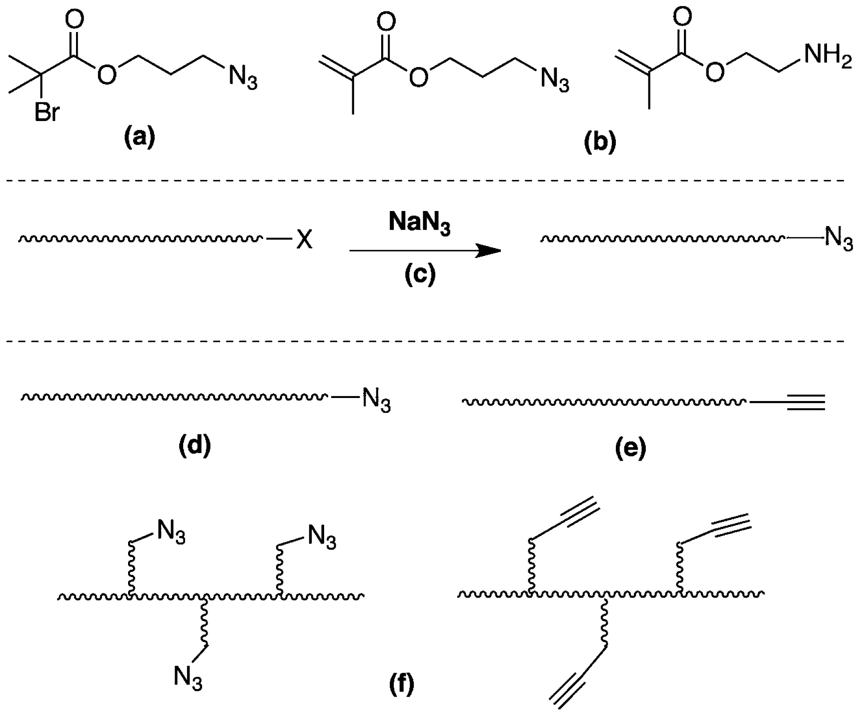
O
O
Br
N3
(a)
O
O
N3
O
O
NH2
(b)
X
NaN3
(c)
N3
N3
(d)
(e)
N3
N3
N3
(f)

Figure 2. Functional initiators (a), monomers (b), post-polymerization modification (c) and clickable macromonomers (d-f) utilized in combined ATRP and CuAAC.

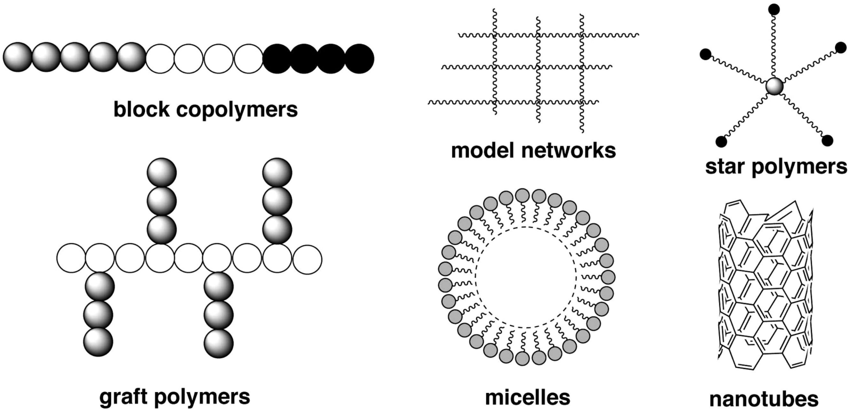
block copolymers
model networks
star polymers
graft polymers
micelles
nanotubes

Figure 3. Representative macromolecular structures constructed using combination of ATRP and click chemistry.

Downloaded by CORNELL UNIV on May 31, 2012 | http://pubs.acs.org
Publication Date (Web): March 20, 2012 | doi: 10.1021/bk-2012-1100.ch006

Common Mechanistic Features of Click Chemistry and ATRP

Several reasons for the compatibility of copper catalyzed ATRP and [3+2] azide-alkyne cycloaddition can be inferred from the reaction mechanisms. Firstly, both require the presence of the copper(I) species, however, in slightly different contexts. The Cu^I species in ATRP serve as an activator for the homolytic cleavage of the C-X bond and, at the same time, they are in dynamic equilibrium with their oxidized counterparts (Cu^{II}) in order to maintain low levels of propagating chain radicals (*31*, *56*, *57*). Copper(I)-catalyzed Huisgen azide-alkyne [3+2] cycloaddition on the other hand, requires high levels of Cu^I at all times during the course of the reaction (*6*, *21*). Secondly, both require the presence of nitrogen-based complexing ligands, which significantly accelerate the reaction rates. In ATRP, the presence of complexing ligands influences the redox potential, which can be directly correlated with catalyst activity and equilibrium constant for atom transfer (K_{ATRP}). Mechanistic investigations revealed that the copper catalyzed azide-alkyne [3+2] cycloaddition generally proceeds faster in the presence of aliphatic amine-based ligands due to their high basicity and enhanced lability (*97*). Additionally, faster rates were observed with tridentate ligands. It is believed that the saturation of the Cu^I center by the tetradentate ligands blocks the coordination of the incoming alkyne and azide. Finally, click chemistry, like ATRP, is highly tolerant to a wide range of reaction solvents.

Sequential and Simultaneous Combination of Click Chemistry and ATRP

As previously mentioned, ATRP was the first living radical polymerization method combined with click chemistry. This was demonstrated in the preparation of copolymers with 5-tetrazole units starting from homopolymers and copolymers (both random and block, including polymers on polystyrene or silica support) of acrylonitrile obtained via ATRP (*53*). Nitrile groups were subsequently functionalized by the reaction with NaN_3 in the presence of Lewis acid ($ZnCl_2$) to yield polymer derivatives of tetrazole after click functionalization (a, Scheme 3). The same research group also reported the synthesis of side-chain modified polymers from the ATRP of 3-azidopropyl methacrylate as the monomer (b, Scheme 3) (*55*). Copper-catalyzed click coupling of the azide moieties with various alkynes to form 1,2,3-triazoles proceeded efficiently at room temperature. Linear polystyrene bearing azido chain-ends coupled with multiple functional alkyne-containing substrates represented the first synthetic strategy to form three- and four-arm star polymers via the sequential ATRP and azide-alkyne cycloaddition protocols (c, Scheme 3) (*70*). Post-polymerization modification using the coupling procedure to generate the triazole groups was found to be fast and efficient under mild reaction conditions.

Downloaded by CORNELL UNIV on May 31, 2012 | http://pubs.acs.org
Publication Date (Web): March 20, 2012 | doi: 10.1021/bk-2012-1100.ch006

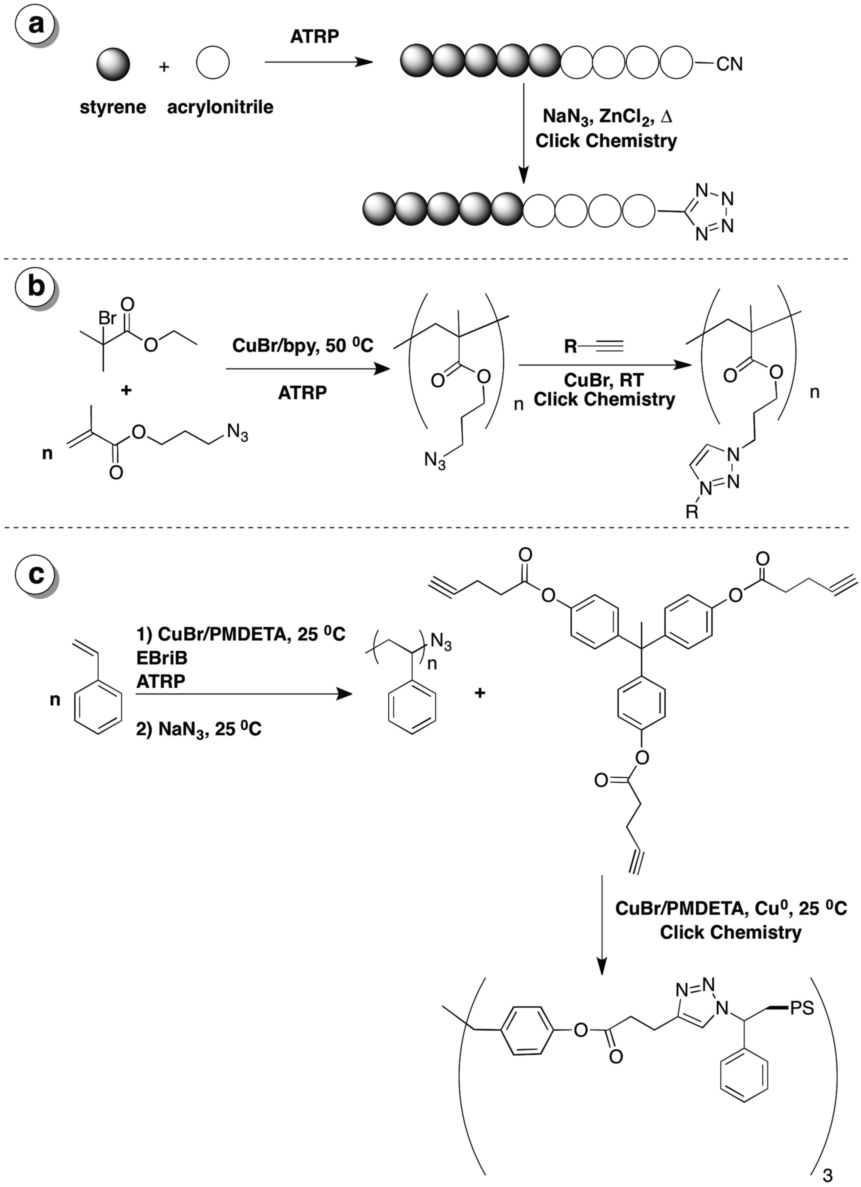
a
ATRP
styrene
acrylonitrile
CN
NaN3, ZnCl2, Δ
Click Chemistry
b
CuBr/bpy, 50 0C
ATRP
R
CuBr, RT
Click Chemistry
n
c
1) CuBr/PMDETA, 25 0C
EBriB
ATRP
2) NaN3, 25 0C
N3
CuBr/PMDETA, Cu0, 25 0C
Click Chemistry
PS
3

Scheme 3. First examples of sequential ATRP and click chemistry (53, 55, 70).

Downloaded by CORNELL UNIV on May 31, 2012 | http://pubs.acs.org
Publication Date (Web): March 20, 2012 | doi: 10.1021/bk-2012-1100.ch006

The successful click functionalization of polymers generated from ATRP has attracted considerable interest in developing strategies for the construction of other macromolecular architectures. In particular, quantitative yields of macrocyclic polymers have been achieved through the ATRP of styrene utilizing an alkyne-functionalized initiator, followed by nucleophilic displacement of the terminal halogen in the polymer and intramolecular click coupling (*98*). In a similar manner, cyclic polymer was also synthesized starting from *N*-isopropylacrylamide (NIPAM) serving as the monomer and the propargyl 2-chloropropionate as the functional initiator (a, Scheme 4) (*99*). As one of the most efficient ways to combine different molecular structures that are often found to be very challenging, click chemistry has played a major role in linking homopolymers to form block copolymers. Utilizing a modular approach, an initiator bearing a trisopropylsilyl (TIPS) protected acetylene was used in ATRA to synthesize homopolymers of polystyrene (PS), poly(*tert*-butyl acrylate) (P*t*BA) and poly(methyl acrylate) (PMA) (*100*). Terminal bromides were replaced by azides, followed by cleavage of the protecting group using *n*-tetrabutylammonium fluoride. Resulting homopolymers were linked together via copper(I)-catalyzed azide-alkyne cycloaddition forming an ABC block copolymer (b Scheme 4). Employing the same strategy, polymers with azide as well as alkyne functionalities were first prepared using ATRP. Subsequent click coupling provided amphiphilic block copolymers (*101*). Thermoresponsive microcapsules have also been prepared based on covalent layer-by-layer (LbL) assembly via 1,3-dipolar cycloaddition using clickable azido- and acetylene-functionalized poly(*N*-isopropylacrylamide) copolymers, which were synthesized by ATRP (*102*).

In essence, modular processes that sequentially combine ATRP and CuAAC have been proven to be powerful synthetic routes to functional polymers with complex macromolecular architectures. Both transformations were originally performed in separate steps. In recent reports, one-pot, two-step protocol has been developed for the combination of ATRP and CuAAC (*13*). This methodology enabled the synthesis of linear poly(methyl methacrylate) with triazole terminus (a, Scheme 5) (*103*) and triazole-derived hydrophilic methacrylic macromonomers (b, Scheme 5) (*104*). Another example includes the work of Dubois and co-workers, in which well-defined amphiphilic diblock copolymer, poly(ε-caprolactone)-*block*-poly(*N*,*N*-dimethylamino-2-ethyl methacrylate (PCL-*b*-PDMAEMA) was synthesized via ATRP of *N*,*N*-dimethylamino-2-ethyl methacrylate (DMAEMA) using azide-functionalized initiator (2-(2-azidoethoxy)ethyl bromisobutyrate), followed by *in situ* click coupling with α-isopropoxy-ω-4-pentynoate-poly(ε-caprolactone) (PCL-C≡CH) macromonomer (c, Scheme 5) (*105*).

Downloaded by CORNELL UNIV on May 31, 2012 | http://pubs.acs.org
Publication Date (Web): March 20, 2012 | doi: 10.1021/bk-2012-1100.ch006

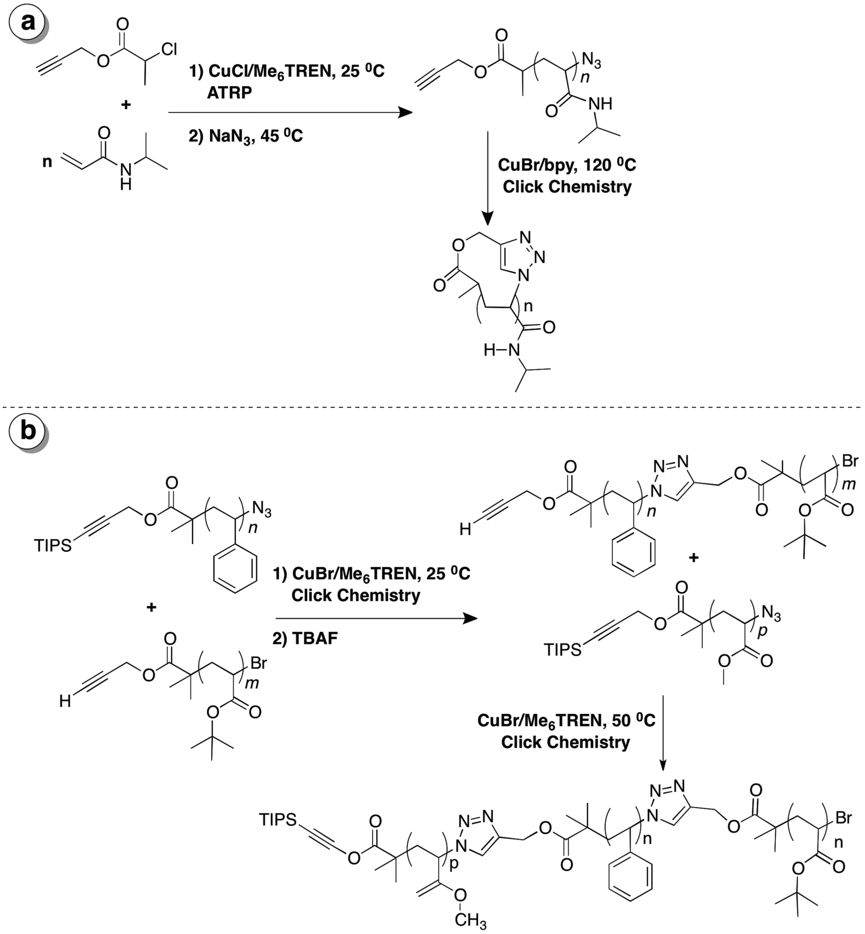
a
1) CuCl/Me6TREN, 25 0C
ATRP
2) NaN3, 45 0C
CuBr/bpy, 120 0C
Click Chemistry
b
TIPS
1) CuBr/Me6TREN, 25 0C
Click Chemistry
2) TBAF
CuBr/Me6TREN, 50 0C
Click Chemistry

Scheme 4. Functional macrocyclic (a) (99) and ABC block copolymers (b) (100) synthesized via sequential ATRP and click chemistry.

Downloaded by CORNELL UNIV on May 31, 2012 | http://pubs.acs.org
Publication Date (Web): March 20, 2012 | doi: 10.1021/bk-2012-1100.ch006

Recent reports also revealed that both organic transformations can be conducted simultaneously. Haddleton and co-workers reported the preparation of methacrylic polymers containing triazole groups in one-pot using ATRP catalyst, CuBr/*N*-ethylpyridineimine/triethylamine, alkyne-containing monomer (propargyl methacrylate) and an organic azide (a, Scheme 6) (*106*). Also, on the other hand, Drockenmuller's group described the elaborate preparation of random copolymers using two complementary tandem strategies based on one-pot combination of click chemistry and ATRP (*107*). In the first strategy, functionalized random copolymers were obtained from the simultaneous copolymerization of methyl methacrylate and propargyl acrylate and click coupling of a monofunctional azide. In another approach, copolymerization of methyl methacrylate and 11-azidoundecanoyl methacrylate followed by triazole formation utilizing monofunctional alkynes occurred simultaneously (b, Scheme 6) (*107*). Facile one-pot synthesis of miktoarm star terpolymers has been achieved by simultaneously conducting ATRP, ROMP and click chemistry using CuBr/PMDETA catalytic system, starting from trifunctional core molecule alkynyl(*-OH*)*-Br* and azide-terminated polystyrene (PS-N_3) (c, Scheme 6) . Simultaneous interpenetrating polymer networks (sIPNs) have also been synthesized via concurrent ATRP and click chemistry utilizing semi-(poly(polyethylene glycol)/poly(2-hydroxyethyl methacrylate) (PEG/PHEMA-sIPN) and poly(ethylene glycol)-diazide (N_3-PEG-N_3) (*85*). Functional microspheres, also referred to as therapeutics because of their potential applications as drug delivery vesicles and protecting shields for biomacromolecules, have also been prepared. This has been demonstrated by conducting simultaneous [3+2] azide-alkyne cycloaddition and dispersion ATRP utilizing ethynyl pyrene, azide-functionalized initiator and methyl methacrylate in the presence of Cu^IBr complexed to perfluorinated amine-based macroligand using a supercritical fluid (*108*).

In summary, rapid developments in materials/polymer chemistry as a result of the beneficial union of ATRP and CuAAC or "click chemistry" have been discussed. In less than a decade, a plethora of molecules with interesting architectures and important applications in various disciplines have emerged. These macromolecules have been synthesized by conducting ATRP and CuAAC sequentially in separate or one-pot reaction mixtures and simultaneously. The following sections will discuss recent developments in the area of small molecule synthesis using copper catalyzed azide-alkyne [3+2] cycloaddition and atom transfer radical addition (ATRA).

Downloaded by CORNELL UNIV on May 31, 2012 | http://pubs.acs.org
Publication Date (Web): March 20, 2012 | doi: 10.1021/bk-2012-1100.ch006

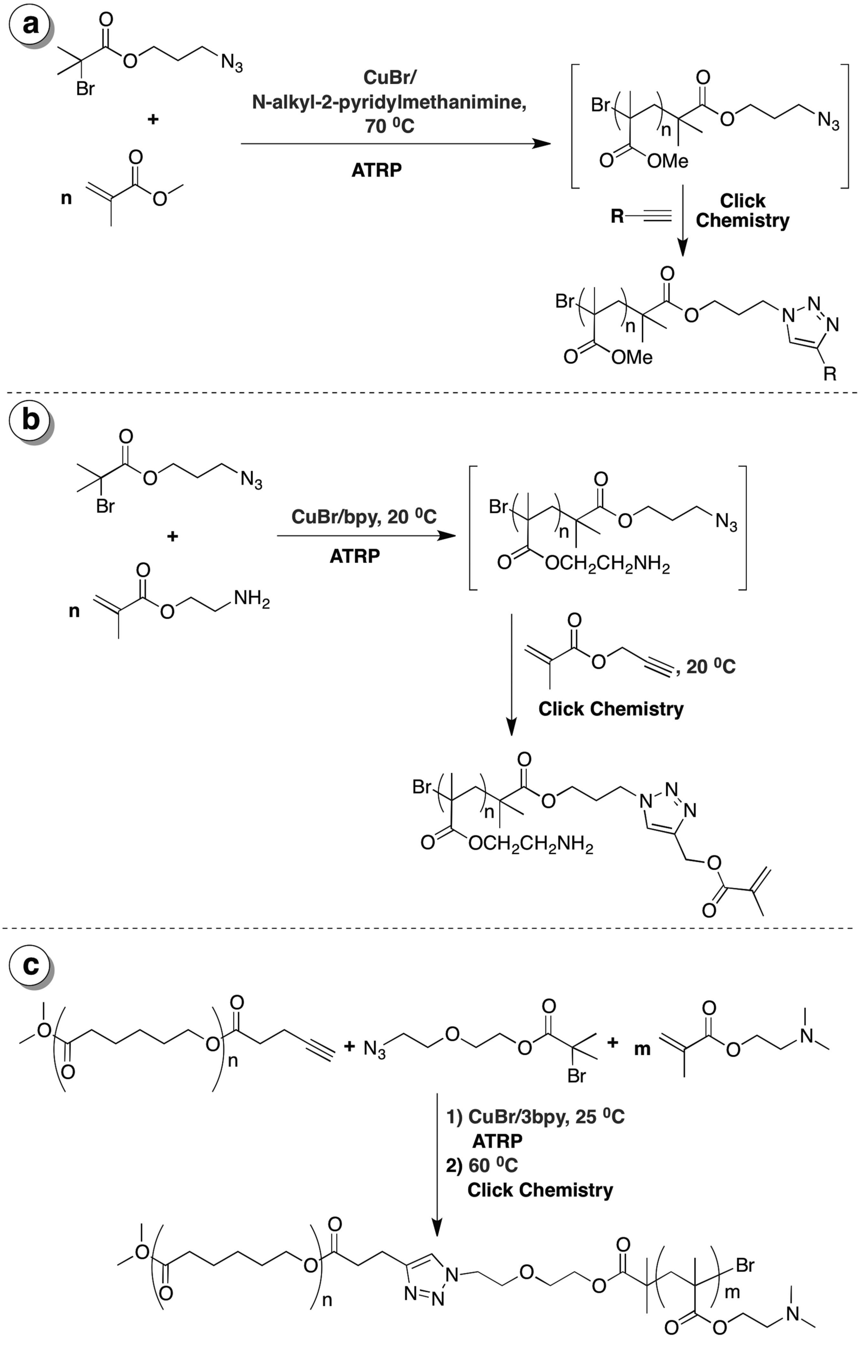
a
CuBr/
N-alkyl-2-pyridylmethanimine,
70 ⁰C
ATRP
Click
Chemistry
b
CuBr/bpy, 20 ⁰C
ATRP
, 20 ⁰C
Click Chemistry
c
1) CuBr/3bpy, 25 ⁰C
ATRP
2) 60 ⁰C
Click Chemistry

Scheme 5. Examples of polymers synthesized via one-pot sequential ATRP and click chemistry (103–105).

Downloaded by CORNELL UNIV on May 31, 2012 | http://pubs.acs.org
Publication Date (Web): March 20, 2012 | doi: 10.1021/bk-2012-1100.ch006

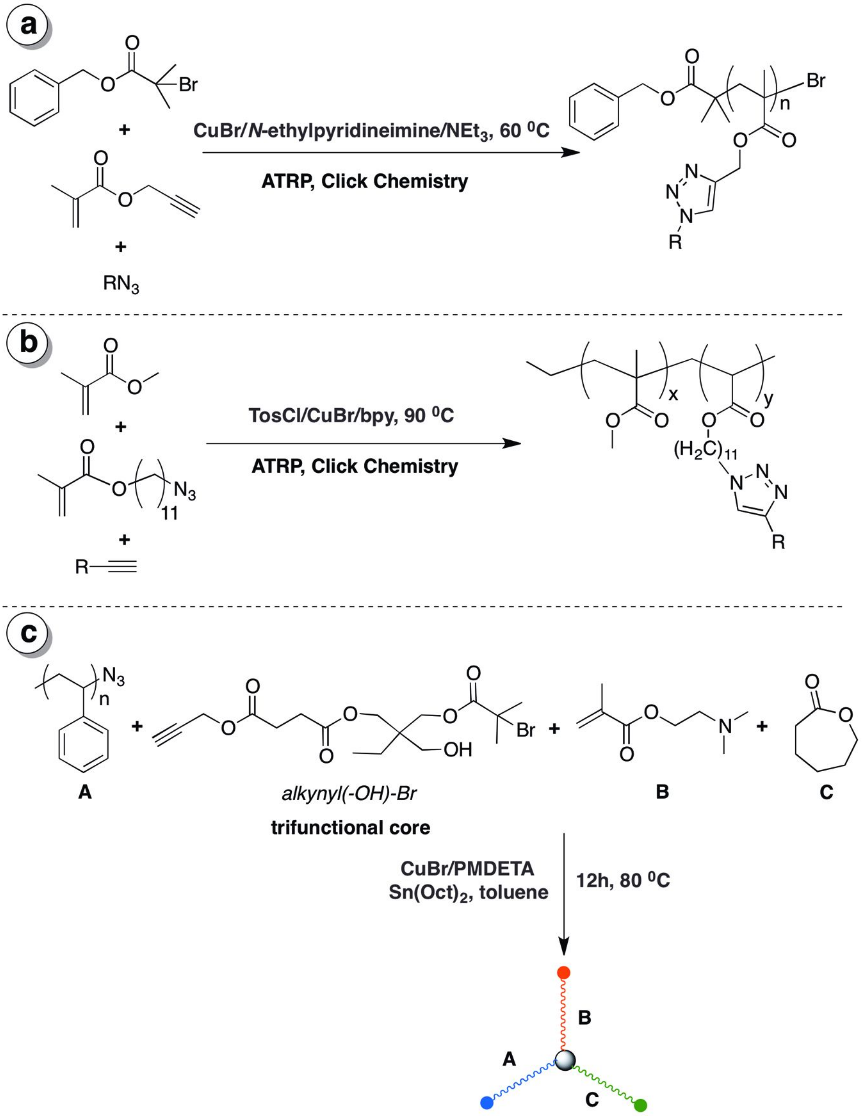
a
CuBr/N-ethylpyridineimine/NEt3, 60 0C
ATRP, Click Chemistry
RN3
b
TosCl/CuBr/bpy, 90 0C
ATRP, Click Chemistry
c
A
alkynyl(-OH)-Br
trifunctional core
B
C
CuBr/PMDETA
Sn(Oct)2, toluene
12h, 80 0C
A
B
C

Scheme 6. Examples of polymers synthesized in one-pot using simultaneous ATRP and click chemistry (78, 106, 107).

Synthesis of Triazolyl Alkyl Esters and Aryl Compounds

As discussed in the previous section, sequential reactions involving copper-catalyzed ATRP and azide-alkyne [3+2] cycloaddition have attracted considerable academic interest. This methodology provided means to rapid development of a plethora of functionalized molecules with complex macromolecular architectures (*6–8*, *13–16*, *53–55*). Despite its success and potential for various applications, the synthesis of small molecules appears to be somewhat neglected. Thus, we initiated a study on sequential reactions that would yield compounds bearing triazole and halide functionalities. The presence of the C-X (X=Br or Cl) bond in the resulting molecule is synthetically attractive because it offers versatility towards further organic transformations involving reduction, elimination, conversion to a Grignard reagent or free radical chemistry.

Based on literature reports, triazole formation via copper(I) catalyzed [3+2] azide-alkyne cycloaddition is commonly conducted via *in situ* reduction of Cu^{II} to Cu^{I} species by sodium ascorbate or ascorbic acid (*3*, *6*). At the same time, ATRA (*44*), ATRC (*44*) and ATRP (*109*, *110*) reactions utilize the same reducing agent to regenerate the copper(I) complex, which is needed to start the catalytic cycle by homolytically cleaving the carbon-halogen bond.

A logical step was taken in combining sequential azide-alkyne [3+2] cycloaddition and ATRA reactions in the presence of $[Cu^{II}(TPMA)X][X]$ (TPMA= tris(2-pyridyl)methylamine, X=Cl^- or Br^-) and ascorbic acid in one-pot sequential manner (Scheme 7) (*111*). Reactions utilizing azide functionalized alkenes (azidopropyl methacrylate(AzPM) and vinylbenzyl azide (VBA)), various alkynes (phenylacetylene (PhA), 3,4-difluorophenylacetylene (DFPhA), propargyl alcohol (PrOH), 2-methyl-3-butyn-2-ol (MBOH), methyl propiolate (MPr) and ethyl propiolate (EPr)) and alkyl halides (carbon tetrachloride (CCl_4), carbon tetrabromide (CBr_4), ethyl trichloroacetate (Cl_3CCO_2Et), methyl trichloroacetate (Cl_3CCO_2Me), ethyl dichloroacetate (Cl_2HCCO_2Et), methyl dichloroacetate (Cl_2HCCO_2Me), dichloroacetonitrile (CCl_2HCN) and 2-bromopropionitrile ($CHBr(CH_3)CN$)) yielded highly functionalized (poly)halogenated esters and aryls containing triazolyl group (Scheme 7 and 8).

As shown in Scheme 7, reactions were performed starting with azide-alkyne [3+2] cycloaddition catalyzed by $[Cu^{II}(TPMA)X][X]$ (X = Cl, Br) and ascorbic acid, followed by the addition of the alkyl halide in the second step. Initial set of reactions involved AzPM, various alkynes (Scheme 7) and CCl_4 (Table 1). For all alkynes, nearly quantitative yields of the triazolyl haloalkyl esters were obtained using 1.0 mol% of the copper catalyst (entries 1, 4, 7, 10, 13, and 16). Further decrease in catalyst loading to 0.5 mol% still resulted in very high yields of the desired monoadduct (entries 2, 5, 8, 11, 14, and 17). It is particularly important to notice that the reaction mixtures containing as low as 0.25 mol% of $[Cu^{II}(TPMA)Cl][Cl]$ still proceeded efficiently to afford the final product in yields greater than 80% (entries 6, 9, 15 and 18).

Downloaded by CORNELL UNIV on May 31, 2012 | http://pubs.acs.org
Publication Date (Web): March 20, 2012 | doi: 10.1021/bk-2012-1100.ch006

Downloaded by CORNELL UNIV on May 31, 2012 | http://pubs.acs.org
Publication Date (Web): March 20, 2012 | doi: 10.1021/bk-2012-1100.ch006

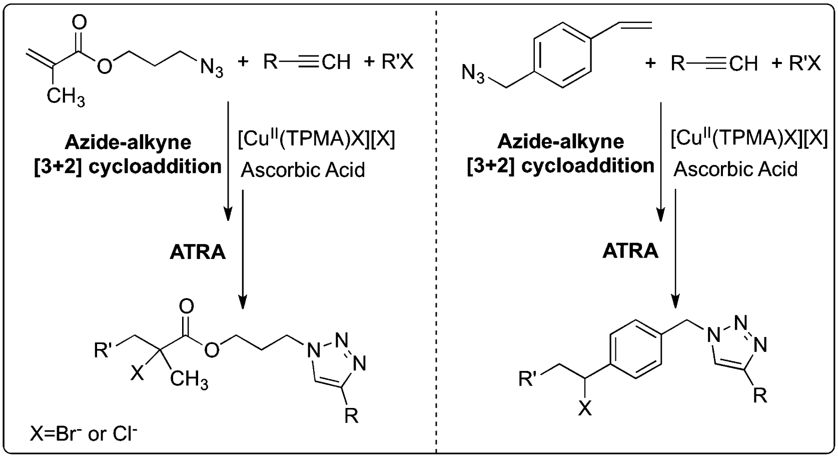
O
O
N3
CH3
+ R—≡CH + R'X
Azide-alkyne
[3+2] cycloaddition
[Cu^II(TPMA)X][X]
Ascorbic Acid
ATRA
R'
X
CH3
N
N
N
R
X=Br- or Cl-
N3
+ R—≡CH + R'X
Azide-alkyne
[3+2] cycloaddition
[Cu^II(TPMA)X][X]
Ascorbic Acid
ATRA
R'
X
R

Scheme 7. Copper-catalyzed sequential CuAAC and ATRA.

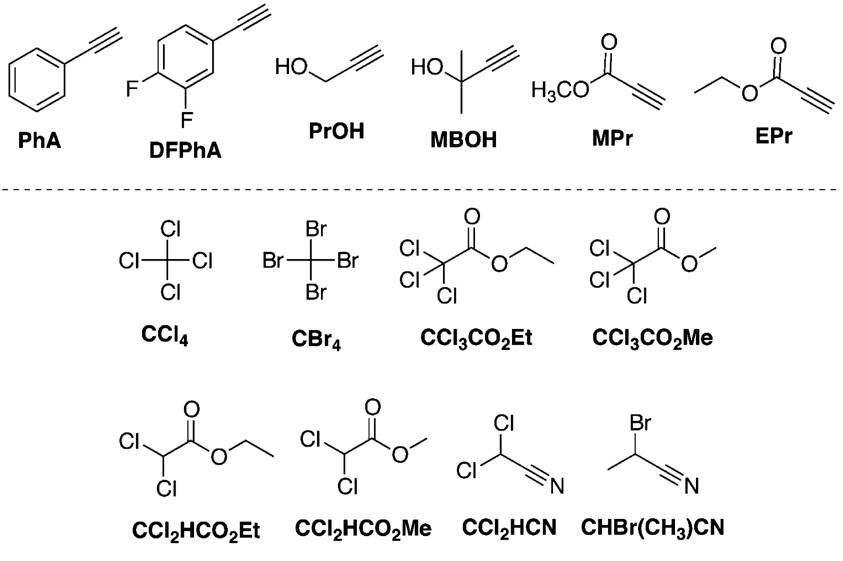
PhA
DFPhA
PrOH
MBOH
MPr
EPr
CCl4
CBr4
CCl3CO2Et
CCl3CO2Me
CCl2HCO2Et
CCl2HCO2Me
CCl2HCN
CHBr(CH3)CN

Scheme 8. Structures of alkynes and alkyl halides used in copper catalyzed azide-alkyne [3+2] cycloaddition and ATRA.

Additional experiments utilizing various alkyl halides such as CBr_4, CCl_3CO_2Et, CCl_3CO_2Me, CCl_2HCO_2Et, CCl_2HCO_2Me, CCl_2HCN and $CHBr(CH_3)CN$) and AzPM were also performed (Table 2). As expected, excellent yields of the final monoadduct were obtained using CBr_4 and catalyst loadings as low as 0.50 mol% (entries 2 and 12). The corresponding product in the case of methyl propiolate was isolated and characterized using single crystal X-ray crystallography (Figure 4). Sequential azide-alkyne [3+2] cycloaddition and ATRA also worked reasonably well for less active tri- and di-halogenated substrates using 1.0 mol% of the catalyst (entries 4, 6, 8, 14, 16, 18, 20, 22).

Downloaded by CORNELL UNIV on May 31, 2012 | http://pubs.acs.org
Publication Date (Web): March 20, 2012 | doi: 10.1021/bk-2012-1100.ch006

Table 1. Sequential azide-alkyne [3+2] cycloaddition and ATRA of CCl_4 catalyzed by $[Cu^{II}(TPMA)Cl][Cl]$ in the presence of ascorbic acid as a reducing agent

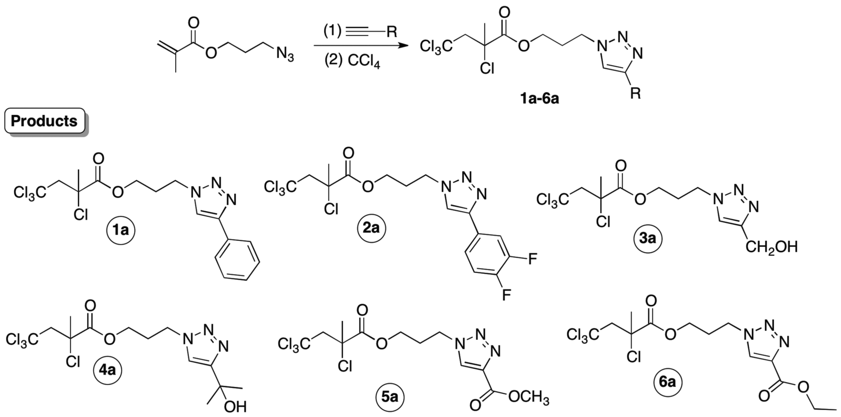

Entry[a]	Alkyne	Product	$[Cu^{II}]$[b]	t (h)[c]	Yield (%)[d]
1	PhA	1a	1.0	2	~100(91)[e]
2			0.50	3	90
3			0.25	3	78
4	DFPhA	2a	1.0	3	96
5			0.50	4	90
6			0.25	6	83
7	PrOH	3a	1.0	3	95(86)[e]
8			0.50	3	86
9			0.25	3	83
10	MBOH	4a	1.0	3	~100
11			0.50	3	86
12			0.25	3	74
13	MPr	5a	1.0	1	98
14			0.50	1	91
15			0.25	1	86
16	EPr	6a	1.0	3	~100(89)[e]
17			0.50	3	~100
18			0.25	3	85

[a] All reactions were performed in CH_3OH at 60 °C using $[AzPM]_0:[Alkyne]_0 = 1:1$, $[AzPM]_0=0.50M$. The amount of ascorbic acid in each system ranged between 20 and 25 eq. relative to copper(II) complex. For alkyne structures refer to Scheme 7. [b] Mole percent relative to alkyne. [c] Reaction time for azide-alkyne cycloaddition (time for ATRA reaction was 8 h for all substrates with $[AzPM]_0:[CCl_4]_0=1:1.25$). [d] The yield is based on the formation of the product and was determined by ^1H NMR spectroscopy using *p*-dimethoxybenzene as internal standard (relative errors are ±15%). [e] Isolated yield for the large scale reaction.

Downloaded by CORNELL UNIV on May 31, 2012 | http://pubs.acs.org
Publication Date (Web): March 20, 2012 | doi: 10.1021/bk-2012-1100.ch006

Table 2. Synthesis of functionalized triazoles using sequential CuAAC and ATRA of various alkyl halides in the presence ascorbic acid

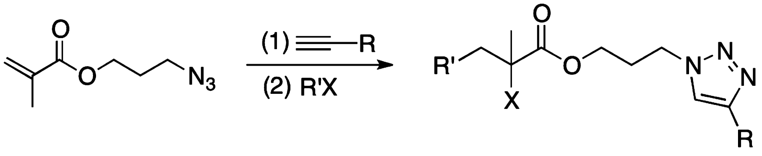

$\equiv$—**R** = PhA, MPr **R'X** = CBr$_4$, CCl$_3$CO$_2$Et, CCl$_2$HCO$_2$Et, CCl$_3$CO$_2$Me, CCl$_2$HCO$_2$Me, CCl$_2$HCN, CHBr(CH$_3$)CN

Entry[a]	*Alk.*	*RX*	*[Cu^{II}]*[b]	*t_1(h)/t_2(h)*[c]	*Yield (%)*[d]
1	PhA	CBr$_4$	1.0	2/8	99(90)[e]
2			0.50	2/8	96
3			0.25	6/8	80
4		CCl$_3$CO$_2$Et	1.0	2/24	82
5			0.50	2/24	72
6		CCl$_2$HCO$_2$Et	1.0	2/24	80
7			0.50	2/24	65
8		CCl$_2$HCN	1.0	2/24	85
9			0.50	2/24	70
10		CHBr(CH$_3$)CN	1.0	2/24	35
11	MPr	CBr$_4$	1.0	2/8	100(86)[e]
12			0.50	2/8	94
13			0.25	6/8	78
14		CCl$_3$CO$_2$Et	1.0	1/24	81
15			0.50	1/24	75
16		CCl$_3$CO$_2$Me	1.0	2/24	91
17			0.50	2/24	81
18		CCl$_2$HCO$_2$Et	1.0	2/24	80(73)[e]
19			0.50	2/24	75
20		CCl$_2$HCO$_2$Me	1.0	2/24	83
21			0.50	2/24	70
22		CCl$_2$HCN	1.0	2/24	83
23			0.50	2/24	78
24		CHBr(CH$_3$)CN	1.0	2/24	75
25			0.50	2/24	74

[a] All reactions were performed in CH$_3$OH at 60 °C using [AzPM]$_0$:[Alkyne]$_0$ = 1:1, [AzPM]$_0$=0.50M. The amount of ascorbic acid in each system ranged between 20 and 25 eq. relative to copper(II) complex. For alkyne structures refer to Scheme 7. [b] Mole percent relative to alkyne. [c] t_1=reaction time for azide-alkyne cycloaddition, t_2=reaction time for ATRA. For all alkyl halides 2 eq. were used relative to AzPM except for CCl$_4$ where only 1 eq. was utilized. [d] The yield is based on the formation of the product and was determined by ^{1}H NMR spectroscopy using *p*-dimethoxybenzene as internal standard (relative errors are ±15%). [e] Isolated yield for the large scale reaction.

Downloaded by CORNELL UNIV on May 31, 2012 | http://pubs.acs.org
Publication Date (Web): March 20, 2012 | doi: 10.1021/bk-2012-1100.ch006

Table 3. Sequential azide-alkyne cyloaddition and ATRA involving vinylbenzyl azide (VBA) and various alkynes alkyl halides catalyzed by $[Cu^{II}(TPMA)X][X]$ ($X=Br^-$ or Cl^-) in the presence of ascorbic acid

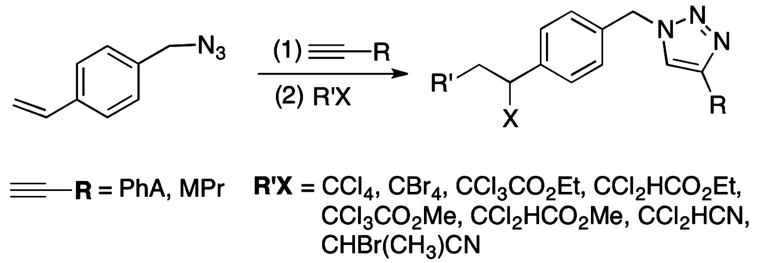
N3
(1) ≡—R
(2) R'X
R'
X
N
N
N
R
≡—R = PhA, MPr
R'X = CCl4, CBr4, CCl3CO2Et, CCl2HCO2Et, CCl3CO2Me, CCl2HCO2Me, CCl2HCN, CHBr(CH3)CN

Entry[a]	*Alk.*	*RX*	*[Cu^{II}]*[b]	*t_1(h)/t_2(h)*[c]	*Yield (%)*[d]
1	PhA	CCl_4	1.0	3/8	85(86)[e]
2			0.50	3/8	83
3		CCl_3CO_2Et	1.0	6/24	45
4		CCl_3CO_2Me	1.0	6/24	57
5	MPr	CCl_4	1.0	2/8	92(90)[e]
6			0.50	2/8	73
7		CCl_3CO_2Et	1.0	2/24	87
8			0.50	2/24	83
9		CCl_3CO_2Me	1.0	2/24	82(84)[e]
10			0.50	2/24	78
11		CCl_2HCO_2Et	1.0	2/24	43
12		CCl_2HCO_2Me	1.0	2/24	48
13		CCl_2HCN	1.0	2/24	46
14		$CHCl_3$	1.0	1/24	42
15		$CHBr(CH_3)CN$	1.0	2/24	26

[a] All reactions were performed in CH_3OH at 60 °C using $[VBA]_0$:$[Alkyne]_0$ = 1:1, $[VBA]_0$=0.50M. The amount of ascorbic acid in each system ranged between 20 and 25 eq. relative to copper(II) complex. For alkyne structures refer to Scheme 7. [b] Mole percent relative to alkyne. [c] t_1=reaction time for azide-alkyne cycloaddition, t_2=reaction time for ATRA. For all alkyl halides 2 eq. were used relative to VBA except for CCl_4 where only 1 eq. was utilized. [d] The yield is based on the formation of the product and was determined by ^1H NMR spectroscopy using *p*-dimethoxybenzene as internal standard (relative errors are ±15%). [e] Isolated yield for the large scale reaction.

Monohalogenated, 2-bromopropionitrile, yielded only 35 and 75% of the monoadduct in the case of phenylacetylene (entry 10) and methyl propiolate (entry 25), respectively. The decreased yield can be attributed to monoadduct reactivation resulting in the formation of oligomers/polymers. Another possibility is the competitive coordination of nitrile to the copper (I) centers, which competes with the alkyne complexation (*112*).

In addition to AzPM, a set of sequential azide-alkyne cyloaddition and ATRA reactions was also applied to a an aromatic substrate having azido and alkene functional groups vinylbenzyl azide (VBA). As indicated in Table 3, results obtained utilizing VBA are similar to AzPM. Generally, with 1.0 mol% of the catalyst relative to azide, yields greater than 80% were obtained using CCl_4 (entries 1 and 5). Modest yields of the monoadduct were still observed using trihalogenated alkyl halides (entries 3, 4, 7 and 9), but significantly decreased for dihalogenated ones (entries 11, 12 and 13). Lastly, the monoadduct formed from the azide-alkyne [3+2] cycloaddition of methyl propiolate to VBA followed by sequential ATRA of 2-bromopropionitrile was attained in only 26% yield (entry 15). Certainly, from the point of view of further synthetic modifications of the resulting sequential product such as conversion to a Grignard reagent, monohalogenated alkyl halides are of particular interest.

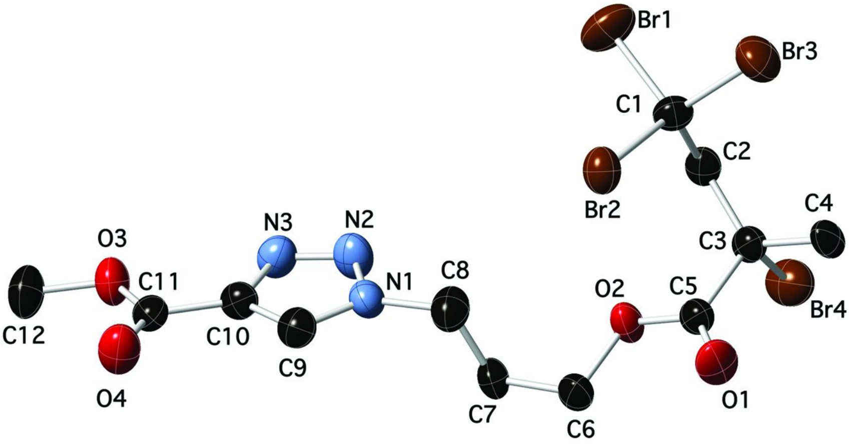

Figure 4. Molecular structure of the product (12a) formed from the sequential azide-alkyne [3+2] cycloaddition between azidopropyl methacrylate and methyl propiolate followed by ATRA of CBr_4 at 296 K, shown with 30% probability displacement ellipsoids. H-atoms have been omitted for clarity. (Reproduced with permission from reference (111). Copyright 2011 Wiley-VCH Verlag).

Downloaded by CORNELL UNIV on May 31, 2012 | http://pubs.acs.org
Publication Date (Web): March 20, 2012 | doi: 10.1021/bk-2012-1100.ch006

Synthesis of Functionalized Polytriazoles

Following the success of *in situ* catalyst regeneration in sequential reactions involving azide-alkyne [3+2] cycloaddition and ATRA, similar strategy was further expanded towards the synthesis of functionalized polytriazoles. For this particular synthesis, the procedure was modified such that the azide-alkyne [3+2] cycloaddition to form the triazoles was carried out in a ligand-free catalytic system followed by subsequent addition of tris(2-pyridyl)methylamine (TPMA) ligand in the ATRA step (Table 4) (*113*). Using this protocol, reactions between vinylbenzyl azide, tripropargylamine and tetrahalogenated methane (CCl_4 or CBr_4) proceeded efficiently providing the desired triazoles in nearly quantitative yields (>90%) using 10 mol-% of copper (entries 1 and 4). Increasing the reaction time for ATRA from 8 to 19 hours did not result in significant increase in the product yield (90%, entry 2). Furthermore, decreasing catalyst loading to 1.0 mol-% resulted in a significant decrease in the yield of the monoadduct (entry

3). The same trend was also observed in the case of CBr_4 (entries 4-6). The resulting brominated polytriazole was characterized using 1H NMR and high resolution mass spectroscopy (HRMS) (Figure 5). Positive ion mass spectrum indicated the presence of two molecular ion peaks, namely the protonated triazole (MH^+) and sodium ion (MNa^+). Sequential azide-alkyne [3+2] cycloaddition and ATRA reactions were also extended to less active alkyl halides such as methyl trichloroacetate (entries 7 and 8) and methyl dichloroacetate (entries 9 and 10). As indicated in Table 4, corresponding products were obtained in modest yields (50-80%). The presented methodology enables efficient synthesis of functionalized polytriazoles, which could have a potential use as chelating agents for a variety of transition metals.

Downloaded by CORNELL UNIV on May 31, 2012 | http://pubs.acs.org
Publication Date (Web): March 20, 2012 | doi: 10.1021/bk-2012-1100.ch006

Table 4. One-Pot Sequential Copper-Catalyzed [3+2] Azide-Alkyne Cycloaddition and ATRA in the Presence of Ascorbic Acid

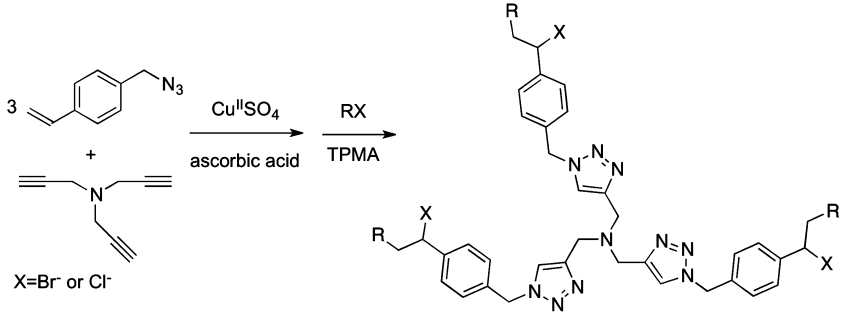

Entry[a]	*R-X*	*[Cu^{II}]*[b]	*t_1 [h]/t_2[h]*[c]	*Yield [%]*[d]
1	CCl_4	10	1/8	91(80)[e]
2	CCl_4	10	1/19	90
3	CCl_4	1.0	1/19	56
4	CBr_4	10	1/8	92(86)[e]
5	CBr_4	10	1/19	99
6	CBr_4	1.0	1/19	60
7	CCl_3CO_2Me	10	1/24	75(78)[e]
8	CCl_3CO_2Me	1.0	1/24	43
9	CCl_2HCO_2Me	10	1/24	66(43)[e]
10	CCl_2HCO_2Me	1.0	1/24	50

[a] All reactions were performed at 60 ^{0}C in MeOH using $[VBA]_0$:$[tripropargylamine]_0$=3:1, $[VBA]_0$=0.1 M. [b] Mol % relative to $[VBA]_0$. The amount of ascorbic acid was 20 equiv. relative to $Cu^{II}SO_4$. In the second step, 1.0 equiv. of TPMA relative to $CuSO_4$ and RX (CCl_4 or CBr_4=3.75 equiv., CCl_3CO_2Me or CCl_2HCO_2Me=6.0 equiv. relative to VBA) were added. [b] Mol % of $Cu^{II}SO_4$ relative to VBA. [c] t_1=time for click reaction, t_2=time for ATRA. [d] The yield is based on the formation of the triazole and was determined by ^{1}H NMR spectroscopy using *p*-dimethoxybenzene as internal standard (relative errors are ±15%). [e] Isolated yield after column chromatography.

Downloaded by CORNELL UNIV on May 31, 2012 | http://pubs.acs.org
Publication Date (Web): March 20, 2012 | doi: 10.1021/bk-2012-1100.ch006

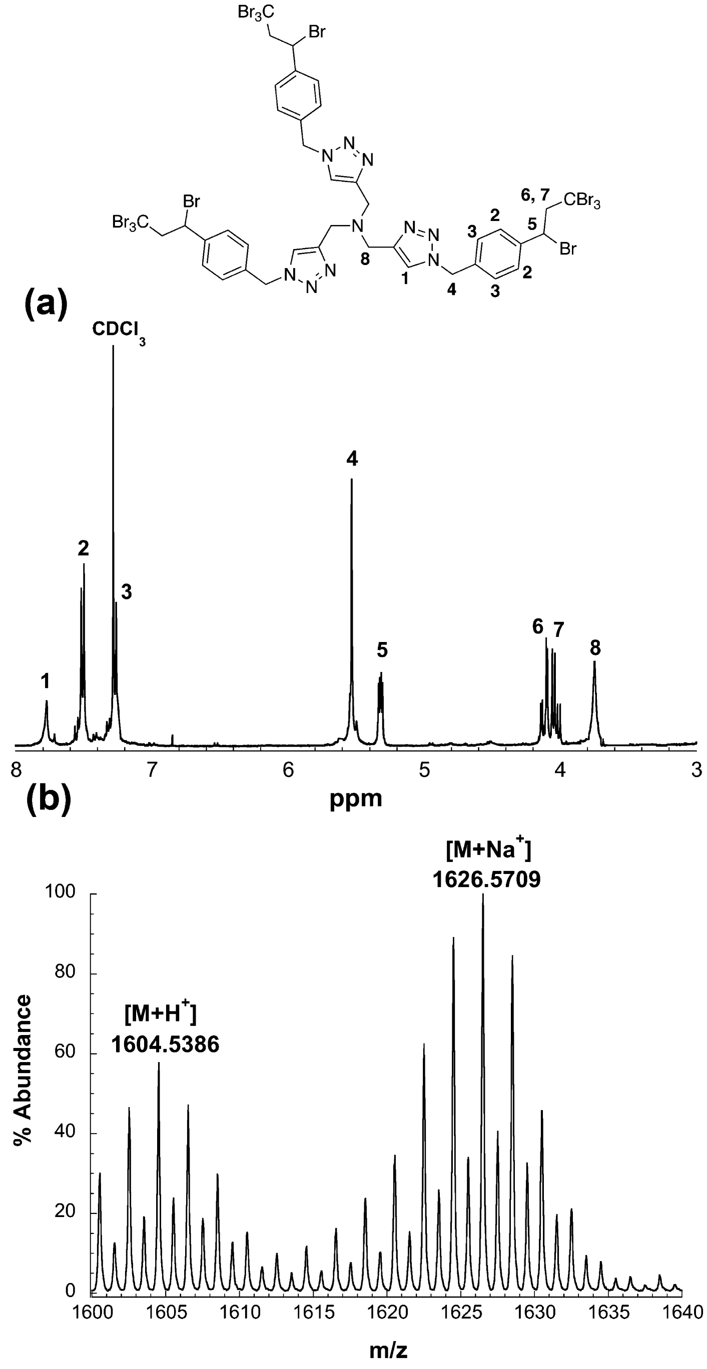

Figure 5. ^{1}H NMR (a) and HRMS (b) spectra of tris((1-(4-(1,3,3,3-tetrabromopropyl)benzyl)-1H-1,2,3-triazol-4-yl)methyl)amine (TBTA(CBr_4)$_3$).

Downloaded by CORNELL UNIV on May 31, 2012 | http://pubs.acs.org
Publication Date (Web): March 20, 2012 | doi: 10.1021/bk-2012-1100.ch006

Conclusions and Future Outlook

In summary, recent advances in the area of *in situ* catalyst regeneration in sequential copper-catalyzed azide-alkyne [3+2]cycloaddition and ATRA/ATRP have been reviewed. This technique allowed for the preparation of two types of functionalized triazoles. The first type represented the halogenated alkyl esters and aryls containing a triazolyl pendant that were formed from azide-alkyne cycloaddition and ATRA of alkyl halide utilizing $[Cu^{II}(TPMA)X][X]$ (X= Cl, Br) and ascorbic acid. A slightly different approach involving a ligand-free catalytic system ($CuSO_4$ and ascorbic acid) in the first step, followed by the addition of TPMA ligand and alkyl halide in the second one, afforded the formation of polyhalogened polytriazoles. The aforementioned methodologies could be synthetically useful since they utilize environmentally benign reducing agent, thus, harnessing a greener alternative for conducting such organic transformations. Furthermore, the presence of halide functionality in the final product offers versatility towards further organic transformations. Even more significant is the presence of the triazole group, which is extensively utilized for various applications in bioconjugation, drug discovery and medicine.

Acknowledgments

Financial support from National Science Foundation CAREER award (CHE 0844131) is greatly acknowledged.

References

1. Kolb, H. C.; Finn, M. G.; Sharpless, K. B. *Angew. Chem., Int. Ed.* **2001**, *40*, 2004–2021.
2. Tornoe, C. W.; Christensen, C.; Meldal, M. *J. Org. Chem.* **2002**, *67*, 3057–3064.
3. Rostovtsev, V. V.; Green, L. G.; Fokin, V. V.; Sharpless, K. B. *Angew. Chem., Int. Ed.* **2002**, *41*, 2596–2599.
4. Agard, N. J.; Prescher, J. A.; Bertozzi, C. R. *J. Am. Chem. Soc.* **2004**, *126*, 15046–15047.
5. Dirks, A. J.; van Berkel, S. S.; Hatzakis, N. S.; Opsteen, J. A.; van Delft, F. L.; Cornelissen, J. J. L. M.; Rowan, A. E.; van Hest, J. C. M.; Rutjes, F. P. J. T.; Nolte, R. J. M. *Chem. Commun.* **2005**, 4172–4174.
6. Meldal, M.; Tornoe, C. W. *Chem. Rev.* **2008**, *108*, 2952–3015.
7. Moses, J. E.; Moorhouse, A. D. *Chem. Soc. Rev.* **2007**, *36*, 1249–1262.
8. Binder, W. H.; Kluger, C. *Curr. Org. Chem.* **2006**, *10*, 1791–1815.
9. Kolb, H. C.; Sharpless, K. B. *Drug Discov. Today* **2003**, *8*, 1128–1137.
10. Amblard, F.; Cho, J. H.; Schinazi, R. F. *Chem. Rev.* **2009**, *109*, 4207–4220.
11. Hein, C.; Liu, X.-M.; Wang, D. *Pharm. Res.* **2008**, *25*, 2216–2230.
12. Najera, C.; Sansano, J. M. *Org. Biomol. Chem.* **2009**, *7*, 4567–4581.
13. Binder, W. H.; Sachsenhofer, R. *Macromol. Rapid Commun.* **2007**, *28*, 15–54.
14. Nandivada, H.; Jiang, X.; Lahann, J. *Adv. Mater.* **2007**, *19*, 2197–2208.

15. Golas, P. L.; Matyjaszewski, K. *QSAR Comb. Sci.* **2007**, *26*, 1116–1134.
16. Golas, P. L.; Matyjaszewski, K. *Chem. Soc. Rev.* **2010**, *39*, 1338–1354.
17. Himo, F.; Lovell, T.; Hilgraf, R.; Rostovtsev, V. V.; Noodleman, L.; Sharpless, K. B.; Fokin, V. V. *J. Am. Chem. Soc.* **2005**, *127*, 210–216.
18. Ahlquist, M.; Fokin, V. V. *Organometallics* **2007**, *26*, 4389–4391.
19. Straub, B. F. *Chem. Commun.* **2007**, 3868–3870.
20. Rodionov, V. O.; Fokin, V. V.; Finn, M. G. *Angew. Chem., Int. Ed.* **2005**, *44*, 2210–2215.
21. Bock, V. D.; Hiemstra, H.; van Maarseveen, J. H. *Eur. J. Org. Chem* **2006**, *2006*, 51–68.
22. Curran, D. P. *Synthesis* **1988**, 417–439.
23. Curran, D. P. *Synthesis* **1988**, 489–513.
24. Curran, D. P. *Comprehensive Organic Synthesis*; Pergamon: New York, 1992.
25. Iqbal, J.; Bhatia, B.; Nayyar, N. K. *Chem. Rev.* **1994**, *94*, 519–564.
26. Eckenhoff, W. T.; Pintauer, T. *Catal. Rev.: Sci. Eng.* **2010**, *51*, 1–59.
27. Pintauer, T. *Eur. J. Inorg. Chem.* **2010**, *2010*, 2449–2460.
28. Severin, K. *Curr. Org. Chem.* **2006**, *10*, 217–224.
29. Pintauer, T. "Greening" of Copper Catalyzed Atom Transfer Radical Addition (ATRA) and Cyclization (ATRC) Reactions. In *Controlled/Living Radical Polymerization: Progress in ATRP*; Matyjaszewski, K.; Ed.; ACS Symposium Series 1023; American Chemical Society: Washington, DC, 2009; pp 63−84. , *1023*, 63–84.
30. Wang, J.-S.; Matyjaszewski, K. *J. Am. Chem. Soc.* **1995**, *117*, 5614–5615.
31. Matyjaszewski, K.; Xia, J. *Chem. Rev.* **2001**, *101*, 2921–2990.
32. Quebatte, L.; Thommes, K.; Severin, K. *J. Am. Chem. Soc.* **2006**, *128*, 7440–7441.
33. Thommes, K.; Icli, B.; Scopelliti, R.; Severin, K. *Chem. Eur. J.* **2007**, *13*, 6899–6907.
34. Wolf, J.; Thommes, K.; Briel, O.; Scopelliti, R.; Severin, K. *Organometallics* **2008**, *27*, 4464–4474.
35. Fernandez-Zumel, M. A.; Thommes, K.; Kiefer, G.; Sienkiewicz, A.; Pierzchala, K.; Severin, K. *Chem. Eur. J.* **2009**, *15*, 11601–11607.
36. Lundgren, R. J.; Rankin, M. A.; McDonald, R.; Stradiotto, M. *Organometallics* **2008**, *27*, 254–258.
37. Nair, R. P.; Kim, T. H.; Frost, B. J. *Organometallics* **2009**, *28*, 4681–4688.
38. Eckenhoff, W. T.; Pintauer, T. *Inorg. Chem.* **2007**, *46*, 5844–5846.
39. Eckenhoff, W. T.; Garrity, S. T.; Pintauer, T. *Eur. J. Inorg. Chem.* **2008**, *2008*, 563–571.
40. Pintauer, T.; Eckenhoff, W. T.; Ricardo, C.; Balili, M. N. C.; Biernesser, A. B.; Noonan, S. T.; Taylor, M. T. *Chem. Eur. J.* **2009**, *15*, 38–41.
41. Balili, M. N. C.; Pintauer, T. *Inorg. Chem.* **2009**, *48*, 9018–9026.
42. Balili, M. N. C.; Pintauer, T. *Inorg. Chem.* **2010**, *49*, 5642–5649.
43. Balili, M. N. C.; Pintauer, T. *Dalton Trans.* **2011**, *40*, 3060–3066.
44. Taylor, M. J. W.; Eckenhoff, W. T.; Pintauer, T. *Dalton Trans.* **2010**, *39*, 11475–11482.
45. Clark, A. J.; Wilson, P. *Tetrahedron Lett.* **2008**, *49*, 4848–4850.

Downloaded by CORNELL UNIV on May 31, 2012 | http://pubs.acs.org
Publication Date (Web): March 20, 2012 | doi: 10.1021/bk-2012-1100.ch006

46. Munoz-Molina, J. M.; Caballero, A.; Diaz-Requejo, M. M.; Trofimenko, S.; Belderrain, T. R.; Perez, P. J. *Inorg. Chem.* **2007**, *46*, 7725–7730.
47. Munoz-Molina, J. M.; Belderrain, T. R.; Perez, P. J. *Inorg. Chem.* **2010**, *49*, 642–645.
48. Munoz-Molina, J. M.; Belderrain, T. R.; Perez, P. J. *Adv. Synth. Catal.* **2008**, *350*, 2365–2372.
49. Ricardo, C.; Pintauer, T. *J. Chem. Soc., Chem. Commun.* **2009**, 3029–3031.
50. Thommes, K.; Kiefer, G.; Scopelliti, R.; Severin, K. *Angew. Chem., Int. Ed.* **2009**, *48*, 8115–8119.
51. Fernández-Zúmel, M. A.; Buron, C.; Severin, K. *Eur. J. Org. Chem.* **2011**, 2272–2277.
52. Thommes, K.; Fernández-Zúmel, M. A.; Buron, C.; Godinat, A.; Scopelliti, R.; Severin, K. *Eur. J. Org. Chem.* **2011**, 249–255.
53. Tsarevsky, N. V.; Bernaerts, K. V.; Dufour, B.; Du Prez, F. E.; Matyjaszewski, K. *Macromolecules* **2004**, *37*, 9308–9313.
54. Tsarevsky, N. V.; Sumerlin, B. S.; Matyjaszewski, K. *Macromolecules* **2005**, *38*, 3558–3561.
55. Sumerlin, B. S.; Tsarevsky, N. V.; Louche, G.; Lee, R. Y.; Matyjaszewski, K. *Macromolecules* **2005**, *38*, 7540–7545.
56. Kamigaito, M.; Ando, T.; Sawamoto, M. *Chem. Rev.* **2001**, *101*, 3689–3746.
57. Tsarevsky, N. V.; Matyjaszewski, K. *Chem. Rev.* **2007**, *107*, 2270–2299.
58. Hawker, C. J.; Bosman, A. W.; Harth, E. *Chem. Rev.* **2001**, *101*, 3661–3688.
59. Moad, G.; Chiefari, J.; Chong, Y. K.; Krstina, J.; Mayadunne, R. T. A.; Postma, A.; Rizzardo, E.; Thang, S. H. *Polym. Int.* **2000**, *49*, 993–1001.
60. Rizzardo, E.; Chiefari, J.; Mayadunne, R.; Moad, G.; Thang, S. *Macromol. Symp.* **2001**, *174*, 209–212.
61. Kyeremateng, S. O.; Amado, E.; Blume, A.; Kressler, J. *Macromol. Rapid Commun.* **2008**, *29*, 1140–1146.
62. Opsteen, J. A.; van Hest, J. C. M. *Chem. Commun.* **2005**, 57–59.
63. Durmaz, H.; Dag, A.; Altintas, O.; Erdogan, T.; Hizal, G.; Tunca, U. *Macromolecules* **2006**, *40*, 191–198.
64. Golas, P. L.; Tsarevsky, N. V.; Sumerlin, B. S.; Walker, L. M.; Matyjaszewski, K. *Aust. J. Chem.* **2007**, *60*, 400–404.
65. Grieshaber, S. E.; Farran, A. J. E.; Lin-Gibson, S.; Kiick, K. L.; Jia, X. *Macromolecules* **2009**, *42*, 2532–2541.
66. Wang, W.; Li, T.; Yu, T.; Zhu, F. *Macromolecules* **2008**, *41*, 9750–9754.
67. Opsteen, J. A.; Brinkhuis, R. P.; Teeuwen, R. L. M.; Lowik, D. W. P. M.; van Hest, J. C. M. *Chem. Commun.* **2007**, 3136–3138.
68. Jiang, X.; Zhang, G.; Narain, R.; Liu, S. *Langmuir* **2009**, *25*, 2046–2054.
69. Yuan, W.; Li, X.; Gu, S.; Cao, A.; Ren, J. *Polymer* **2011**, *52*, 658–666.
70. Gao, H.; Matyjaszewski, K. *Macromolecules* **2006**, *39*, 4960–4965.
71. Gao, H.; Matyjaszewski, K. *J. Am. Chem. Soc.* **2007**, *129*, 6633–6639.
72. Altintas, O.; Hizal, G.; Tunca, U. *J. Polym. Sci., Part A: Polym. Chem.* **2006**, *44*, 5699–5707.
73. Altintas, O.; Yankul, B.; Hizal, G.; Tunca, U. *J. Polym. Sci., Part A: Polym. Chem.* **2006**, *44*, 6458–6465.

Downloaded by CORNELL UNIV on May 31, 2012 | http://pubs.acs.org
Publication Date (Web): March 20, 2012 | doi: 10.1021/bk-2012-1100.ch006

74. Altintas, O.; Yankul, B.; Hizal, G.; Tunca, U. *J. Polym. Sci., Part A: Polym. Chem* **2007**, *45*, 3588–3598.
75. Deng, G.; Ma, D.; Xu, Z. *Eur. Polym. J.* **2007**, *43*, 1179–1187.
76. Whittaker, M. R.; Urbani, C. N.; Monteiro, M. J. *J. Am. Chem. Soc.* **2006**, *128*, 11360–11361.
77. Liu, H.; Li, C.; Liu, H.; Liu, S. *Langmuir* **2009**, *25*, 4724–4734.
78. Zhang, Y.; Li, C.; Liu, S. *J. Polym. Sci., Part A: Polym. Chem* **2009**, *47*, 3066–3077.
79. Zhang, Y.; Liu, H.; Hu, J.; Li, C.; Liu, S. *Macromol. Rapid Commun.* **2009**, *30*, 941–947.
80. Li, C.; Ge, Z.; Liu, H.; Liu, S. *J. Polym. Sci., Part A: Polym. Chem* **2009**, *47*, 4001–4013.
81. Gao, H.; Matyjaszewski, K. *J. Am. Chem. Soc.* **2007**, *129*, 6633–6639.
82. Tsarevsky, N. V.; Bencherif, S. A.; Matyjaszewski, K. *Macromolecules* **2007**, *40*, 4439–4445.
83. Li, C.; Ge, Z.; Fang, J.; Liu, S. *Macromolecules* **2009**, *42*, 2916–2924.
84. Urbani, C. N.; Lonsdale, D. E.; Bell, C. A.; Whittaker, M. R.; Monteiro, M. J. *J. Polym. Sci., Part A: Polym. Chem* **2008**, *46*, 1533–1547.
85. Xu, L. Q.; Yao, F.; Fu, G. D.; Kang, E. T. *Biomacromolecules* **2010**, *11*, 1810–1817.
86. Pan, T.-T.; He, W.-D.; Li, L.-Y.; Jiang, W.-X.; He, C.; Tao, J. *J. Polym. Sci., Part A: Polym. Chem* **2011**, *49*, 2155–2164.
87. Johnson, J. A.; Lewis, D. R.; Diaz, D. D.; Finn, M. G.; Koberstein, J. T.; Turro, N. J. *J. Am. Chem. Soc.* **2006**, *128*, 6564–6565.
88. Li, H.; Cheng, F.; Duft, A. M.; Adronov, A. *J. Am. Chem. Soc.* **2005**, *127*, 14518–14524.
89. Chen, X.; McRae, S.; Parelkar, S.; Emrick, T. *Bioconjugate Chem.* **2009**, *20*, 2331–2341.
90. Lutz, J.-F.; Borner, H. G.; Weichenhan, K. *Macromolecules* **2006**, *39*, 6376–6383.
91. Agut, W.; Taton, D.; Lecommandoux, S. b. *Macromolecules* **2007**, *40*, 5653–5661.
92. Gupta, S. S.; Raja, K. S.; Kaltgrad, E.; Strable, E.; Finn, M. G. *Chem. Commun.* **2005**, 4315–4317.
93. Ladmiral, V.; Mantovani, G.; Clarkson, G. J.; Cauet, S.; Irwin, J. L.; Haddleton, D. M. *J. Am. Chem. Soc.* **2006**, *128*, 4823–4830.
94. Wan, X.; Liu, T.; Liu, S. *Biomacromolecules* **2011**, *12*, 1146–1154.
95. Wang, Q.; Chan, T. R.; Hilgraf, R.; Fokin, V. V.; Sharpless, K. B.; Finn, M. G. *J. Am. Chem. Soc.* **2003**, *125*, 3192–3193.
96. Zeng, Q.; Li, T.; Cash, B.; Li, S.; Xie, F.; Wang, Q. *Chem. Commun.* **2007**, 1453–1455.
97. Golas, P. L.; Tsarevsky, N. V.; Sumerlin, B. S.; Matyjaszewski, K. *Macromolecules* **2006**, *39*, 6451–6457.
98. Laurent, B. A.; Grayson, S. M. *J. Am. Chem. Soc.* **2006**, *128*, 4238–4239.
99. Xu, J.; Ye, J.; Liu, S. *Macromolecules* **2007**, *40*, 9103–9110.
100. Opsteen, J. A.; van Hest, J. C. M. *J. Polym. Sci., Part A: Polym. Chem* **2007**, *45*, 2913–2924.

Downloaded by CORNELL UNIV on May 31, 2012 | http://pubs.acs.org
Publication Date (Web): March 20, 2012 | doi: 10.1021/bk-2012-1100.ch006

101. Van Camp, W.; Germonpre, V.; Mespouille, L.; Dubois, P.; Goethals, E. J.; Du Prez, F. E. *React. Funct. Polym.* **2007**, *67*, 1168–1180.
102. Huang, C.-J.; Chang, F.-C. *Macromolecules* **2009**, *42*, 5155–5166.
103. Mantovani, G.; Ladmiral, V.; Tao, L.; Haddleton, D. M. *Chem. Commun.* **2005**, 2089–2091.
104. Topham, P. D.; Sandon, N.; Read, E. S.; Madsen, J.; Ryan, A. J.; Armes, S. P. *Macromolecules* **2008**, *41*, 9542–9547.
105. Mespouille, L.; Vachaudez, M.; Suriano, F.; Gerbaux, P.; Coulembier, O.; Degee, P.; Flammang, R.; Dubois, R. *Macromol. Rapid Commun.* **2007**, *28*, 2151–2158.
106. Geng, J.; Lindqvist, J.; Mantovani, G.; Haddleton, D. M. *Angew. Chem., Int. Ed.* **2008**, *47*, 4180–4183.
107. Damiron, D.; Desorme, M.; Ostaci, R.-V.; Al Akhrass, S.; Hamaide, T.; Drockenmuller, E. *J. Polym. Sci A: Polym. Chem* **2009**, *47*, 3803–3813.
108. Grignard, B.; Calberg, C.; Jerome, C.; Detrembleur, C. *J. Supercrit. Fluids* **2010**, *53*, 151–155.
109. Min, K.; Gao, H.; Matyjaszewski, K. *J. Am. Chem. Soc.* **2005**, *127*, 3825–3830.
110. Min, K.; Gao, H.; Matyjaszewski, K. *Macromolecules* **2007**, *40*, 1789–1791.
111. Ricardo, C. L.; Pintauer, T. *Eur. J. Inorg. Chem.* **2011**, 1292–1301.
112. Golas, P. L.; Tsarevsky, N. V.; Matyjaszewski, K. *Macromol. Rapid Commun.* **2008**, *29*, 1167–1171.
113. Ricardo, C. L.; Pintauer, T. *Israel J. Chem.* **2011**, accepted.

Downloaded by CORNELL UNIV on May 31, 2012 | http://pubs.acs.org
Publication Date (Web): March 20, 2012 | doi: 10.1021/bk-2012-1100.ch006

Downloaded by STANFORD UNIV GREEN LIBR on May 31, 2012 | http://pubs.acs.org
Publication Date (Web): March 20, 2012 | doi: 10.1021/bk-2012-1100.ch007

Chapter 7

Selecting the Optimal Reaction Conditions for Copper-Mediated Atom Transfer Radical Polymerization at Low Catalyst Concentration

Shannon R. Woodruff, Brad J. Davis, and Nicolay V. Tsarevsky*

Department of Chemistry, and Center for Drug Discovery, Design, and Delivery, Dedman College, Southern Methodist University, 3215 Daniel Avenue, Dallas, Texas 75275
***E-mail: nvt@smu.edu**

Atom transfer radical polymerization (ATRP) can be successfully carried out at low catalyst concentration in the presence of both non-radical or radical-based reducing agents. To be able to conduct controlled polymerizations, several important requirements should be met. The catalytically active complexes in both oxidation states should be very stable, even in the presence of excess destabilizing compounds, such as monomers and reducing agents or the products of their oxidation. The ratio of the stability constants of the higher to that of the lower oxidation state complexes should be large. The association constant of halide ions to the higher oxidation state metal complex (halidophilicity) should also be large, which guarantees both high catalytic activity and efficient radical deactivation. Reducing agents should be chosen that can only regenerate the lower oxidation state activating complex, but that cannot participate in side reactions with the monomer, polymer, or other reaction components. Only highly active ATRP initiators afford well-defined polymers with molecular weights close to the expected ones based on the monomer to initiator ratio.

Downloaded by STANFORD UNIV GREEN LIBR on May 31, 2012 | http://pubs.acs.org
Publication Date (Web): March 20, 2012 | doi: 10.1021/bk-2012-1100.ch007

Introduction

Atom transfer radical polymerization (ATRP), which was developed in the mid 1990s (*1*, *2*), has become one of the most popular controlled/"living" radical polymerization (CRP) (*3–5*) techniques. It allows for the synthesis of a plethora of well-defined polymers with controlled molecular weight, architecture, and placement of functional groups either at the chain ends or within the polymer chain (*6*). The process, shown in Figure 1, is based upon the reversible activation of an alkyl halide RX (X = Br, Cl) by a lower oxidation state metal complex (e.g., Cu^IL_m, as shown in the scheme, with L being a ligand), yielding the propagating radical $R^\bullet$ and the corresponding higher oxidation state metal halide complex ($XCu^{II}L_m$). The homolytic cleavage of the C-X bond by the Cu^I-based activating complex is characterized by the rate constant of activation, k_{act}, whereas the transfer of a halogen atom from the $XCu^{II}L_m$ complex (referred to as deactivator) to the propagating radical, which is accompanied with the formation of the Cu^I complex and the dormant alkyl halide species, is characterized with the rate constant of deactivation, k_{deact}. The equilibrium constant of the process K_{ATRP} can be expressed either as the ratio of the two rate constants, k_{act}/k_{deact}, or as the concentration ratio $([R^\bullet][XCu^{II}L_m])/([RX][Cu^IL_m])$.

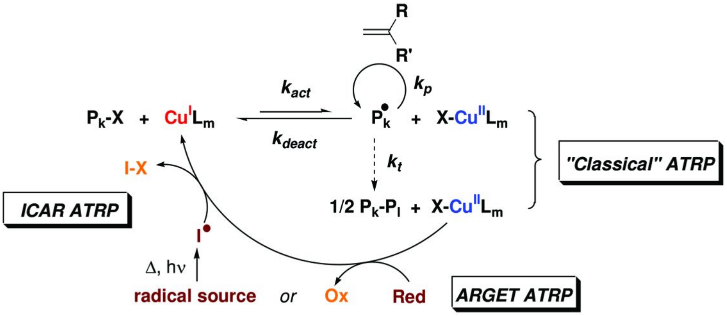

Figure 1. Mechanism of "classical" ATRP and of ICAR and ARGET ATRP.

The values of K_{ATRP} have been typically determined by monitoring the amount of Cu^{II} halide complex accumulated in systems containing initially the alkyl halide and the Cu^I-based activator (*7*). The mechanistic aspects of ATRP have been studied extensively, particularly for the Cu-mediated process, including factors determining catalytic activity and performance (*8*, *9*), effects of the alkyl halide initiator structure on the ATRP equilibrium constant (*10*, *11*), solvent effects (*12*), etc. Side reactions such as monomer coordination to the Cu^I center of the catalyst (*13*, *14*), disproportionation of the Cu^I-based activator (*15*), or dissociative loss of a halide ligand from the Cu^{II} halide-based deactivator (*16*), especially pronounced in protic media, and other competitive equlibria affecting the catalyst (*17*), have been also thoroughly studied.

In “classical” ATRP, the amount of catalyst needed to mediate the process is relatively large and often is equal to or close to the amount of the RX initiator. As the knowledge of the factors determining high catalytic activity accumulated, very active ATRP catalysts were developed that could be used at lower concentrations (*18*, *19*). However, in ATRP, as in any other radical polymerization, radical termination occurs and results in the irreversible conversion of Cu^I to Cu^{II}, a phenomenon known as the persistent radical effect (*20–22*). As a consequence, when the concentration of terminated chains starts to approach the concentration of activator initially present in the system, the polymerization will slow down and eventually stop. This can occur relatively early in the process, i.e., at low monomer conversion. A major step towards making ATRP a truly “green” process that could be successfully conducted at very low (often at single-digit ppm) amounts of catalyst was the realization that if a reducing agent was added to the system, it could continuously, throughout the reaction, regenerate the ATRP lower oxidation state activator, thus enabling the polymerization to proceed to high monomer conversion (*23*). The addition of reducing agents has also been utilized in other similar redox-active transition metal-mediated organic reactions, such as atom transfer radical addition or cyclization (*24*, *25*). Both non-radical (Sn^{II} compounds, amines, hydrazines, etc.) and radical source-based (e.g., radicals generated by the decomposition of AIBN) reducing agents have been successfully employed and the processes have been dubbed *activators regenerated by electron transfer* (ARGET) (*26*, *27*) and *initiators for continuous activator regeneration* (ICAR) ATRP (*28*), respectively (bottom of Scheme 1). A drawback of ICAR ATRP is the generation of polymer chains that do not originate from the alkyl halide initiator, but rather from the radical source used as a reducing agent. These additional chains may amount to 5-15 % of all the chains, depending on the amount of reducing agent used. In cases where pure block copolymers are desired, ICAR ATRP is not the most suitable synthetic method. Alternatively, in ARGET ATRP, non-initiating reducing agents are used, and the number of chains is solely determined by the amount of alkyl halide initiator. This technique is particularly useful in the synthesis of block copolymers that are not to be contaminated by homopolymers (*29*). However, in some cases, the reducing agents used in ARGET ATRP may participate in side reactions, leading to loss of reaction control. In those cases, ICAR ATRP may be preferred. The systems employing an excess of reducing agent allow an overall 10-1,000-fold decrease in the amount of catalyst compared to “classical” ATRP. The molecular weights (*30–32*) and degrees of chain-end functionalization (*32*) that can be attained are higher than those in “classical” ATRP systems with larger amounts of catalyst, mostly due to less pronounced redox reactions between the catalyst and the propagating radicals that limit the molecular weight of polymers, owing to the generation of inactive species (often cations or anions that are easily deactivated in the presence of nucleophiles or protic impurities, respectively) (*15*). Nucleophilic radicals (e.g., derived from styrene) can be oxidized by the ATRP Cu^{II}-based deactivating complex, whereas electrophilic radicals (e.g., derived from acrylates or acrylonitrile) can be reduced by the ATRP Cu^I-based activator, as shown in Figure 2.

Downloaded by STANFORD UNIV GREEN LIBR on May 31, 2012 | http://pubs.acs.org
Publication Date (Web): March 20, 2012 | doi: 10.1021/bk-2012-1100.ch007

Downloaded by STANFORD UNIV GREEN LIBR on May 31, 2012 | http://pubs.acs.org
Publication Date (Web): March 20, 2012 | doi: 10.1021/bk-2012-1100.ch007

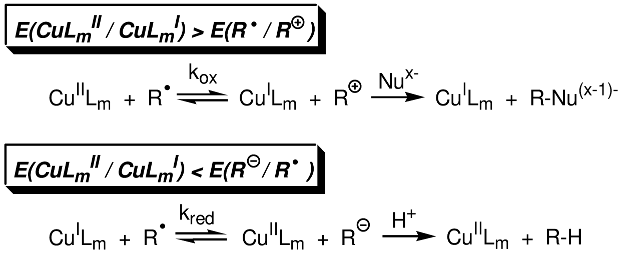
$E(CuL_m^{II} / CuL_m^{I}) > E(R^\bullet / R^\oplus)$
$Cu^{II}L_m + R^\bullet \underset{}{\overset{k_{ox}}{\rightleftharpoons}} Cu^{I}L_m + R^\oplus \xrightarrow{Nu^{x-}} Cu^{I}L_m + R\text{-}Nu^{(x-1)-}$
$E(CuL_m^{II} / CuL_m^{I}) < E(R^\ominus / R^\bullet)$
$Cu^{I}L_m + R^\bullet \overset{k_{red}}{\rightleftharpoons} Cu^{II}L_m + R^\ominus \xrightarrow{H^+} Cu^{II}L_m + R\text{-}H$

Figure 2. Radical oxidation and reduction and the subsequent chain "killing" reactions in ATRP.

The molecular weights that can be attained in ATRP depend upon the relative rates of propagation and radical "consumption" *via* the side redox reactions. The ratio of the two rates, which should be maximized, is inversely proportional to the catalyst concentration as shown by eq. 1. That is why low catalyst concentration techniques should be used for the synthesis of high molecular weight polymers.

$$\frac{R_p}{R_{ox}} = \frac{k_p[M]}{k_{ox}\left[Cu^{II}L_m\right]}; \quad \frac{R_p}{R_{red}} = \frac{k_p[M]}{k_{red}\left[Cu^{I}L_m\right]} \tag{1}$$

The factors that should be borne in mind while selecting the proper catalyst, initiator, reducing agent, and solvent in order to prepare well-defined polymers are discussed in this work.

Selecting the Components for Low Catalyst Concentration ATRP

The general rules for the rational selection of the catalyst and initiator for "classical" ATRP in various reaction media have been previously described. Some of the most important ones are (*8*, *11*): i) the ratio of the stability constants of the Cu^{II} and Cu^{I} complexes with the ligand L (for simplicity, 1:1 stoichiometry is assumed), i.e., β^{II}/β^{I}, should be as large as possible, which ensures high catalytic activity (high K_{ATRP}); ii) the rate constant of deactivation should be sufficiently large in order to obtain polymers with narrow molecular weight distributions, and iii) the halidophilicity $K_{Bromido}$ or $K_{Chlorido}$ should be high, which guarantees high activity as well as efficient deactivation even in protic solvents (*16*). The equation describing the dependence of the molecular weight distribution dispersity (M_w/M_n) on reaction parameters is (*33*, *34*):

$$\frac{M_w}{M_n} = 1 + \frac{1}{DP_n} + \left(\frac{k_p[RX]_0}{k_{deact}\left[XCu^{II}L_m\right]}\right)\left(\frac{2}{conv} - 1\right) \tag{2}$$

In systems, where the catalyst is present at very low concentration and where other components, namely reducing agents, have been added, some additional rules apply, which will be described below.

Catalytic Activity (K_{ATRP}) and Degree of Polymerization Control

As mentioned, to ensure high catalytic activity in ATRP, a high ratio of the stability constants β^{II}/β^{I}, and preferably also high halidophilicity of the $Cu^{II}L$ complex are required. High values of K_{ATRP} are important because they guarantee that a sufficiently large fraction of the Cu species present in the system is in the higher oxidation state, i.e., $XCu^{II}L_m$. Efficient deactivation of the propagating radicals (eq. 2), or more precisely, the addition of only a relatively small average number of monomer units during an activation-deactivation cycle (i.e., high ratio of $k_{deact}[XCu^{II}L_m]/k_p[M]$) is essential for generating polymers with narrow molecular weight distributions. It has been calculated that when tris(2-pyridylmethyl)amine (TPMA; high K_{ATRP} of the Cu^{I} complex), N,N,N′,N″,N″-pentamethyldiethylenetriamine (PMDETA; intermediate value of K_{ATRP}), and 2,2′-bipyridine (bpy; low K_{ATRP}) are used as the ligands for the ATRP catalyst under ICAR conditions, 90, 7, and only 0.3 % of the copper species are in the higher oxidation state, respectively. This means that the respective average numbers of monomer units added to the propagating radicals prior to each deactivation are 4, 9, and 230 (*28*). The concentrations of Cu^{II} complexes have also been determined in related Cu-mediated atom transfer radical addition reactions carried out in the presence of radical-based reducing agents (*35*, *36*). Due to the large number of monomer units added at each cycle in the case of bpy-based catalyst, the molecular weight distribution will be rather broad. In fact, the total amount of deactivator can be intentionally controlled by changing either the ligand or the total concentration of catalyst. This strategy can be utilized to obtain polymers with controlled molecular weight distribution widths (*37*, *38*).

Stability (Formation) Constants of the Catalytically-Active Complexes

Throughout this text, charges of complexes or ligands are omitted to simplify the mathematical expressions. For the simplest case, 1:1 stoichiometry, the degree of dissociation of the complex $Cu^{j}L$ (j = I or II) is concentration- or dilution-dependent. The same is true for the heterolytic dissociation of the Cu^{II}-X bonds in the deactivator $XCu^{II}L$ (which can be viewed as being formed through the association of a halide anion to the complex $Cu^{II}L$). All the complexes of interest can be represented as $Cu^{j}Y$, where Y is either L or the halide ligand in the Cu^{II}-based radical deactivator. If the complex $Cu^{j}Y$ is dissolved in the reaction medium at concentration $[Cu^{j}Y]_0$, part of it dissociates and after equilibrium has been established, the system contains non-dissociated $Cu^{j}Y$ and free Cu^{j} (and Y). From the mass balance, $[Cu^{j}Y] + [Cu^{j}] = [Cu^{j}Y]_0$, and therefore:

$$\frac{\left[Cu^{j}\right]}{\left[Cu^{j}Y\right]_0} = \frac{\left[Cu^{j}\right]}{\left[Cu^{j}Y\right]_{tot}} = \frac{\left[Cu^{j}\right]}{\left[Cu^{j}\right]+\left[Cu^{j}Y\right]} = \frac{-1+\sqrt{1+4\beta\left[Cu^{j}Y\right]_0}}{4\beta\left[Cu^{j}Y\right]_0} \qquad (3)$$

From eq. 3, the concentration of remaining complex $Cu^{j}Y$ can be calculated and is a function of both the stability constant β and the total concentration of Cu^{j} species. This dependence is shown in Figure 3. As seen, when the catalyst concentrations are low, and in ARGET and ICAR ATRP they can be as low as

Downloaded by STANFORD UNIV GREEN LIBR on May 31, 2012 | http://pubs.acs.org
Publication Date (Web): March 20, 2012 | doi: 10.1021/bk-2012-1100.ch007

10^{-5} M or less, only complexes with stability constants of at least $\beta \geq 10^8$ M^{-1} will not dissociate appreciably. If the initial complex concentration is 5×10^{-5} M, after dissociation the concentration of the remaining complex present in the system will be only 2.5×10^{-7} M if the stability constant is $\beta = 10^2$ M^{-1} (i.e., only 0.5 % of the initially present complex), 1.3×10^{-5} M if $\beta = 10^4$ M^{-1} (26 % of the initial concentration), 4.3×10^{-5} M if $\beta = 10^6$ M^{-1} (86 % of the initial), and 4.93×10^{-5} M if $\beta = 10^8$ M^{-1} (i.e., nearly all the complex, 98.6 % will remain intact). At higher dilutions, the stability of the complexes should be higher to ensure insignificant dissociation.

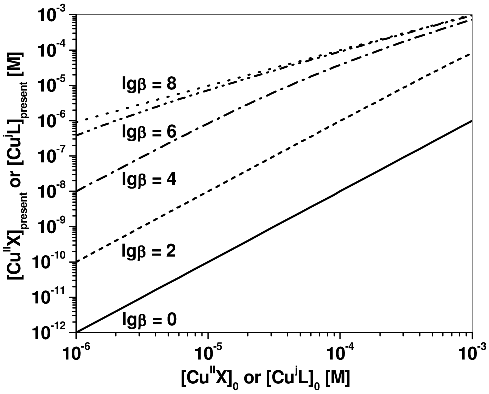

Figure 3. Concentration of complex actually present in the reaction mixture after dissociation as a function of the initial complex concentration for five different values of the stability constant β. The curves are valid for complexes with stoichiometry of 1:1 (L = ligand, j = I or II, and X = halide).

It should be borne in mind that if competitive equilibria can take place in the system, the stability constant β should be replaced with the conditional stability constant β^* in eq. 3, which takes into account all possible side reactions (*17*). Side reactions may include i) protonation of the ligand L, which often happens in ARGET ATRP in the presence of either acidic reducing agents (e.g., ascorbic acid) or acidic oxidation products of the reducing agents (e.g., gluconic acid formed in the oxidation of glucose); ii) competitive complexation of L with another metal ion, e.g., Sn^{II} or the product of its oxidation Sn^{IV}; iii) competitive complexation of the Cu^I or Cu^{II} center with a reaction component, e.g., monomer, polymer, reducing agent or its oxidation product. In the most general form, the conditional stability constant can be expressed by eq. 4, where the alpha coefficients take into account all possible competitive equilibria leading to destabilization of the complex of interest (*39*, *40*). Some of these coefficients can be equal to 1 if the corresponding side reaction does not take place. The stability constants β^M, β^P, β^{RA}, and β^{Ox} characterize the formation of complexes between Cu^j (j = I or II) and the monomer (*13*, *14*), polymer, reducing agent, and

Downloaded by STANFORD UNIV GREEN LIBR on May 31, 2012 | http://pubs.acs.org
Publication Date (Web): March 20, 2012 | doi: 10.1021/bk-2012-1100.ch007

its oxidized form, respectively, $\beta_1^{H,L}$, $\beta_2^{H,L}$, …, are the protonation constants of the ligand L (inverse of the acid dissociation constants of its protonated forms), and $\beta^{Mt,L}$ is the formation constant of the complex between the ligand L and a present metal ion Mt (e.g., the reducing agent or its oxidized product).

$$\beta^{*} = \frac{\beta}{\alpha^{M}\alpha^{S}\alpha^{RA}\alpha^{Ox}\alpha^{L,H}\alpha^{L,Mt}} =$$

$$= \frac{\beta}{\left(1+\beta^{M}[M]\right)\left(1+\beta^{P}[P]\right)\left(1+\beta^{RA}[RA]\right)\left(1+\beta^{Ox}[Ox]\right)\left(1+\beta_{1}^{L,H}\left[H^{+}\right]+\beta_{2}^{L,H}\left[H^{+}\right]^{2}+\ldots\right)\left(1+\beta^{L,Mt}[Mt]\right)} \quad (4)$$

When ligands that are relatively basic are used as the components of the ARGET ATRP catalyst (e.g., hexamethylated tris(2-aminoethyl)amine, Me_6TREN), to avoid protonation of the ligand by an acidic reducing agent (e.g., ascorbic acid) or its oxidation product (e.g., dehydroascorbic or gluconic acid), the ligand should be used in excess in order to "trap" the acidic reaction component. Similarly, if the reducing agent employed in an ARGET ATRP process is a metal compound able to coordinate to the ligand of the catalyst (e.g., Sn^{II} compound), an excess of the ligand with respect to Cu^{I} and Cu^{II} ought to be added to prevent decomplexation of the ligand from the Cu-based catalyst.

Knowing the stability constant of a catalytically active complex, one can determine whether or not the complex is suitable for ATRP under dilute conditions, i.e., for ARGET and ICAR ATRP. As an example, in order to determine if ICAR ATRP can be carried out in protic media, one has to know the value of the halidophilicity for the Cu^{II} complex in this media. Low halidophilicity, particularly at high dilutions, would lead to poor deactivation efficiency and therefore to poor polymerization control (eq. 2). Although the complexes of bpy are not suitable for ARGET or ICAR ATRP due to their low activity in ATRP, the halidophilicity of the Cu^{II} complex of bpy can be used to estimate the halidophilicity of Cu^{II} complexes derived from other ligands. Many values of bromido- and chloridophilicity of the Cu^{II} bpy complex in various water-organic solvent mixtures have been reported (*16*, *17*). As the amount of water in the system increases, the halidophilicity decreases markedly. The curves K_{Halido} vs. $[H_2O]$ can, in fact, be used to estimate the halidophilicity in the pure (water-free) solvent by extrapolation. The values for the chloridophilicity of the mentioned complex were measured in ethanol-water mixtures and compared to those previously reported (*16*) in methanol-water mixtures (Figure 4). At any composition, the chloridophilicity in the ethanol-containing solvents are 5-10 times higher than in the methanol-containing solvents. By extrapolation to $[H_2O]$ = 0 M, it can be estimated that the chloridophilicity of the Cu^{II} bpy complex is about an order of magnitude higher in ethanol than in methanol. The same trends are expected to be observed for the halidophilicities of complexes derived from other N-based ligands. Therefore, it is to be expected that if, for instance, ICAR ATRP is to be carried out in protic media, ethanol would be a much more

Downloaded by STANFORD UNIV GREEN LIBR on May 31, 2012 | http://pubs.acs.org
Publication Date (Web): March 20, 2012 | doi: 10.1021/bk-2012-1100.ch007

Downloaded by STANFORD UNIV GREEN LIBR on May 31, 2012 | http://pubs.acs.org
Publication Date (Web): March 20, 2012 | doi: 10.1021/bk-2012-1100.ch007

appropriate solvent than methanol, i.e., better defined polymers will be obtained in the former solvent due to the lower propensity of the deactivator to dissociate and lose its halide ligand. Indeed, the polymerization of 2-hydroxyethyl acrylate in ethanol (1:1 by vol.) at 65 °C under ICAR ATRP conditions ([HEA]$_0$: [diethyl 2-bromo-2-methylmalonate (Et$_2$BrMM)]$_0$: [AIBN]$_0$: [CuBr$_2$]$_0$: [TPMA]$_0$ = 200 : 1 : 0.05 : 0.02 : 0.02) was well-controlled, and afforded well-defined polymers of M_n = 23,650 g mol^{-1} and M_w/M_n = 1.16 at 29 % monomer conversion and M_n = 57,390 g mol^{-1} and M_w/M_n = 1.18 at 86 % monomer conversion (*41*).

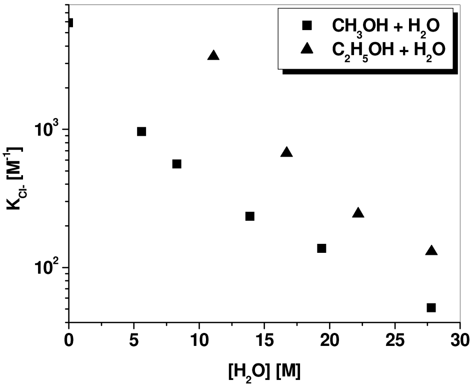

Figure 4. Chloridophilicity of Cu^{II}(bpy)$_2$ complexes in water-methanol and water-ethanol mixtures of various compositions.

Effect of the Reducing Agent

As mentioned above, both ICAR and ARGET ATRP have advantages and limitations. Generally, ARGET ATRP is the polymerization technique of choice when relatively inert monomers are polymerized in relatively inert solvents. The term "inert" refers to the inability of the reaction component to react with the reducing agent or the product of its oxidation. In some instances, such reactions do take place, which can be detrimental to polymerization control. It was recently reported (*42*) that Sn^{II} 2-ethylhexanoate and possibly the product of its oxidation (Sn^{IV} compound) can efficiently open the epoxide rings in both glycidyl methacrylate (GMA) and the corresponding polymer. As a result, when the ARGET ATRP of GMA was attempted in the presence of the mentioned Sn^{II} compound, poorly-defined polymers with polymodal molecular weight distributions were obtained. ICAR ATRP, on the other hand, yielded well-defined polymers of controlled molecular weight and narrow molecular weight distributions, even when high ratios of GMA to the initiator diethyl 2-bromo-2-methylmalonate (Et$_2$BrMM) of up to 600 were used (Figure 5), due to the absence of side reactions with the reducing agent (AIBN) (*42*).

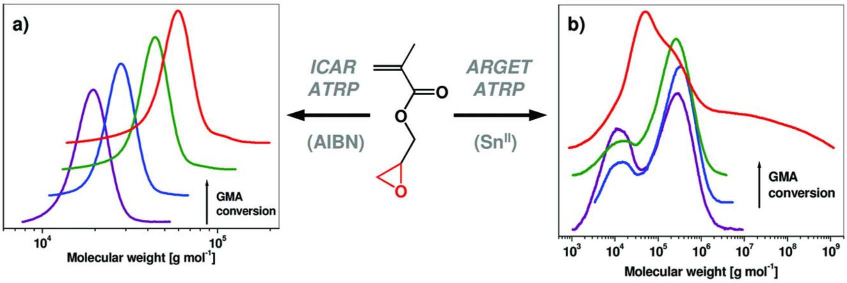

Figure 5. SEC traces of poly(glycidyl methacrylate) obtained under a) ICAR ATRP conditions: $[GMA]_0$ / $[Et_2BrMM]_0$ / $[CuBr_2]_0$ / $[TPMA]_0$ / $[AIBN]_0$ = 600 / 1 / 0.01 / 0.01 / 0.05; $[GMA]_0$ = 3.78 M in anisole / DMF at 60 °C. b) ARGET ATRP conditions: $[GMA]_0$ / $[Et_2BrMM]_0$ / $[CuBr_2]_0$ / $[Me_6TREN]_0$ / [Sn^{II} 2-ethylhexanoate$]_0$ = 200 / 1 / 0.01 / 0.05 / 0.05; $[GMA]_0$ = 3.78 M in anisole / DMF at 60 °C. Adapted from ref. (42) with permission. Copyright 2011, John Wiley and Sons.

In addition to the mentioned side reaction, Sn^{II}-based reducing agents or the Sn^{IV}-containing oxidation products can coordinate or react with monomers or polymers containing donor atoms or groups (e.g., pyridine or amine). Basic or nucleophilic reducing agents (e.g., amines or hydrazines) can either coordinate to the metal center of the catalyst or participate in nucleophilic substitution or elimination reactions with alkyl halide polymer chain ends. Nucleophilic substitution reactions are especially pronounced if the dormant polymeric species are a secondary halide, e.g., derived from styrene, and will be less important if the alkyl halide is tertiary, e.g., derived from methacrylates. For instance, both hydrazine and phenylhydrazine have been used as efficient reducing agents in ARGET ATRP (*28*). However, both compounds are nucleophilic and able to rapidly react with halogen-terminated polystyrene with the formation of the corresponding polymeric N-alkylated hydrazines. The reaction is faster with hydrazine, but both compounds can react with the dormant polystyrene chains, even at room temperature. Figure 6 shows the rate of consumption of 1-phenylethyl bromide (low molecular weight analogue of bromine-terminated polystyrene chains, 0.22 M) in reactions with hydrazine and phenylhydrazine (0.22 M) in DMSO at 27 °C, determined by ^{1}H NMR spectroscopy. Even at this low temperature, about 70 % of the alkyl halide is "lost" in about 1 h in the reaction with hydrazine.

In polymerization reactions, the concentration of alkyl halide chains may be comparable to the concentration used in the experiment shown in Figure 6 (e.g., when targeting degrees of polymerization of about 40 in bulk (8.73 M) styrene) or may be somewhat lower. However, due to the significant rate of the nucleophilic substitution, expected to be even higher at the higher polymerization temperatures (usually > 70 °C), chain end "killing" reactions *via* nucleophilic substitution in ARGET of styrene conducted in the presence of basic or nucleophilic reducing agents cannot be ignored and such compounds should be avoided.

Downloaded by STANFORD UNIV GREEN LIBR on May 31, 2012 | http://pubs.acs.org
Publication Date (Web): March 20, 2012 | doi: 10.1021/bk-2012-1100.ch007

Downloaded by STANFORD UNIV GREEN LIBR on May 31, 2012 | http://pubs.acs.org
Publication Date (Web): March 20, 2012 | doi: 10.1021/bk-2012-1100.ch007

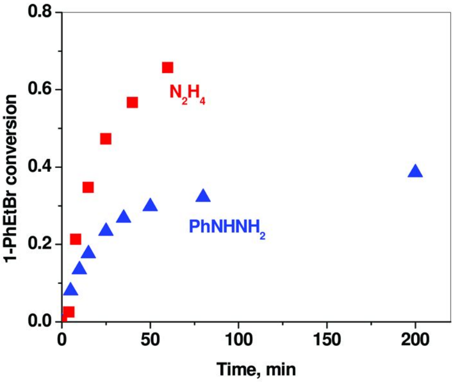

Figure 6. Reaction of 1-phenylethyl bromide (1-PhEtBr, 0.22 M) with hydrazine or phenylhydrazine (0.22 M) in DMSO-d_6 at 27 °C.

Selecting the Initiator and the Solvent

In any controlled polymerization (radical or ionic), fast and efficient initiation is essential for the synthesis of well defined polymers with molecular weights close to the ones determined by the ratio of the monomer to initiator and the monomer conversion. It was recognized early in the development of "living" polymerizations that high efficiency of initiation is needed to achieve narrow molecular weight distributions (*43*). In ATRP, an initiator should be chosen, which is characterized by fast initiation with respect to propagation. This is particularly important when comparatively low molecular weight polymers are to be synthesized. Also, this requirement is significant for the synthesis of block copolymers, where a well-defined block copolymer polyA-*b*-polyB is only obtained if the product of the K_{ATRP} of the polymeric halide of the first block (polyA-X) and the initiation rate constant, i.e., K_{ATRP}(polyA-X)×k_i(polyA$^\bullet$ + B) is larger than the product of the ATRP equilibrium constant of the alkyl halide derived from the second monomer multiplied by its propagation rate constant K_{ATRP}(polyB-X)×k_p(B) (*44*). The selection of active initiators is even more important in low catalyst-concentration ATRP reactions. For instance, it is known that 2-bromoisobutyrates are not the most appropriate initiators for the ATRP of methacrylates, due to the fact that Br-terminated dimers derived from methacrylates are 7-8 times more active than the "monomeric" analogue, 2-bromoisobutyrate (*45*, *46*). However, under "classical" ATRP conditions, well-defined polymethacrylates can be obtained even when 2-bromoisobutyrates are used as the initiators, particularly when the targeted degrees of polymerization at 100 % monomer conversion are of the order of 100 or higher. In ICAR ATRP, ethyl 2-bromoisobutyrate showed poor initiation efficiency in the polymerization of GMA even when the targeted degrees of polymerization were equal to 200. This was observed in several different solvents, namely, DMF, anisole and DMSO (Figure 7). As seen, the solvent did not affect the polymerization rate and high conversions (ca. 80 %) were reached within 9-10 hours in all studied solvents.

This is in accordance with simulations, indicating that the rate of ICAR ATRP is determined mostly by the decomposition rate of AIBN, which is not significantly influenced by the solvent (*28*).

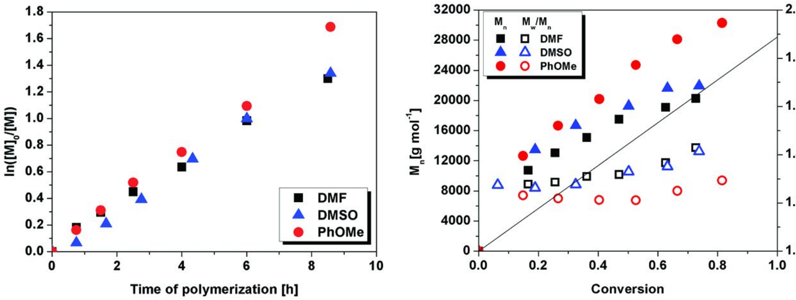

Figure 7. a) Kinetics and b) evolution of molecular weights and molecular weight distribution dispersities (M_w/M_n) with monomer conversion in the ICAR ATRP of GMA initiated by ethyl 2-bromoisobutyrate (EBiB) in several different solvents at 65 °C. $[GMA]_0$ / $[EBiB]_0$ / $[CuBr_2]_0$ / $[TPMA]_0$ / $[AIBN]_0$ = 200 / 1 / 0.04 / 0.04 / 0.1; $[GMA]_0$ = 3.78 M.

When the initiator was changed to Et_2BrMM, which is expected to have a higher K_{ATRP} value (due to the presence in the corresponding radical of two radical-stabilizing carboxylate groups attached to the tertiary carbon atom with the unpaired electron), the efficiency of initiation was markedly improved, as shown in Figure 8. In all studied solvents, the experimentally observed molecular weights were close to the theoretically expected ones based on the ratio of GMA to Et_2BrMM and the monomer conversion.

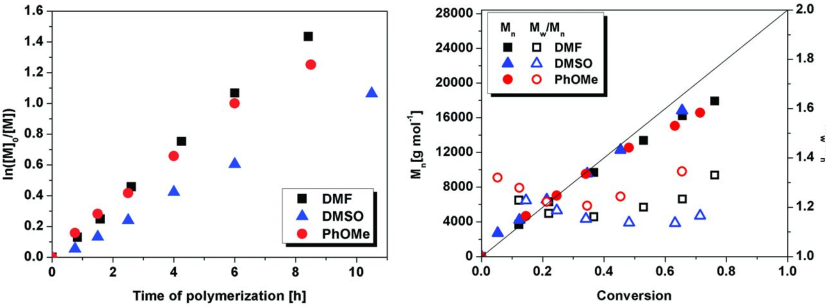

Figure 8. a) Kinetics and b) evolution of molecular weights and molecular weight distribution dispersities (M_w/M_n) with monomer conversion in the ICAR ATRP of GMA initiated by Et_2BrMM in several different solvents at 65 °C. $[GMA]_0$ / $[Et_2BrMM]_0$ / $[CuBr_2]_0$ / $[TPMA]_0$ / $[AIBN]_0$ = 200 / 1 / 0.04 / 0.04 / 0.1; $[GMA]_0$ = 3.78 M.

Downloaded by STANFORD UNIV GREEN LIBR on May 31, 2012 | http://pubs.acs.org
Publication Date (Web): March 20, 2012 | doi: 10.1021/bk-2012-1100.ch007

Downloaded by STANFORD UNIV GREEN LIBR on May 31, 2012 | http://pubs.acs.org
Publication Date (Web): March 20, 2012 | doi: 10.1021/bk-2012-1100.ch007

It is interesting to note that when another very active initiator was employed, 4-toluenesulfonyl chloride (TsCl), which has been shown to be among the best initiators for the ATRP of methacrylates, poor control was observed in DMSO (Figure 9), although the initiation efficiency and dispersities in the other two solvents tested (DMF and anisole) were good. This observation can plausibly be attributed to the high hygroscopicity of DMSO, which is exceptionally difficult to dry. Despite the fact that the solvents used in this study were kept over anhydrous Na_2SO_4, small amounts of water were still possibly present in DMSO. In the presence of small amounts of water and at elevated temperatures, TsCl can hydrolyze releasing two strong acids, 4-toluenesulfonic acid and hydrogen chloride. Both of these acids can open the epoxide ring of the monomer and/or the polymer. Indeed, at the conditions described in Figure 9, the reaction mixture in DMSO gelled in about 4 h. Hydrolysis cannot occur at an appreciable rate when Et_2BrMM is used as the ICAR ATRP initiator, which makes it the most appropriate for the controlled polymerization of GMA in various solvents.

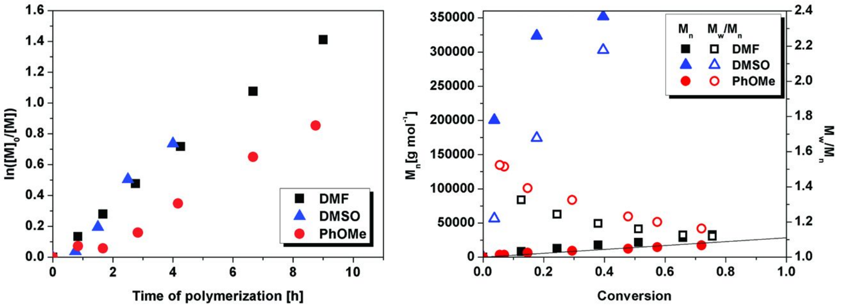

Figure 9. a) Kinetics and b) evolution of molecular weights and molecular weight distribution dispersities (M_w/M_n) with monomer conversion in the ICAR ATRP of GMA initiated by TsCl in several different solvents at 65 °C. $[GMA]_0 / [TsCl]_0 / [CuBr_2]_0 / [TPMA]_0 / [AIBN]_0 = 200 / 1 / 0.04 / 0.04 / 0.1$; $[GMA]_0 = 3.78$ M.

Conclusions

To select the proper reaction conditions for low catalyst concentration ATRP reactions, namely ICAR and ARGET ATRP, several important factors should be considered. The catalyst should be very active (to guarantee high concentration of deactivator and fast deactivation, and therefore narrow molecular weight distributions), i.e., the ratio of the stability constants of the Cu^{II} and Cu^{I} complexes β^{II}/β^{I} should be very high. Additionally, both individual stability constants should be sufficiently high, to ensure that an insignificant fraction of the catalyst dissociates at the high dilution conditions. If the catalyst is to be used at concentrations of the order of 10^{-5} M, the stability of the less stable Cu^{I} complex should be at least 10^{8} M^{-1}. Similarly, the halidophilicity of the Cu^{II} complex should be high. In ICAR and particularly in ARGET ATRP, the conditional stability constants of the complexes should be considered instead of β^{I} and β^{II}, because at low catalyst concentration, i.e., in the presence of large excess of the other reaction components, such as monomers, reducing agents and their oxidation products, etc., the complexes may be markedly destabilized. The solvent can also affect the values of the stability constants, including the halidophilicity, and its influence should be taken into consideration. Only very efficient initiators should be used in ICAR and ARGET ATRP, even more so than in "classical" systems employing higher catalyst amounts.

Acknowledgments

Financial support from the National Science Foundation (CHE-1111929) and Southern Methodist University (start-up funds to NVT) is gratefully acknowledged.

References

1. Wang, J.-S.; Matyjaszewski, K. *J. Am. Chem. Soc.* **1995**, *117*, 5614–5615.
2. Kato, M.; Kamigaito, M.; Sawamoto, M.; Higashimura, T. *Macromolecules* **1995**, *28*, 1721–1723.
3. Matyjaszewski, K., Davis, T. P., Eds.; *Handbook of Radical Polymerization*; Wiley: Hoboken, NJ, 2002.
4. Braunecker, W. A.; Matyjaszewski, K. *Prog. Polym. Sci.* **2007**, *32*, 93–146.
5. Mueller, A. H. E.; Matyjaszewski, K., Eds.; *Controlled and Living Polymerizations*; Wiley-VCH: Weinheim, 2009.
6. Matyjaszewski, K.; Tsarevsky, N. V. *Nature Chem.* **2009**, *1*, 276–288.
7. Tang, W.; Tsarevsky, N. V.; Matyjaszewski, K. *J. Am. Chem. Soc.* **2006**, *128*, 1598–1604.
8. Tsarevsky, N. V.; Tang, W.; Brooks, S. J.; Matyjaszewski, K. Factors Determining the Performance of Copper-Based Atom Transfer Radical Polymerization Catalysts and Criteria for Rational Catalyst Selection. In *Controlled/Living Radical Polymerization*; Matyjaszewski, K., Ed.; ACS Symposium Series 944; American Chemical Society: Washington, DC, 2006; pp 56−70.
9. Tsarevsky, N. V.; Matyjaszewski, K. *Chem. Rev.* **2007**, *107*, 2270–2299.
10. Tang, W.; Kwak, Y.; Braunecker, W.; Tsarevsky, N. V.; Coote, M. L.; Matyjaszewski, K. *J. Am. Chem. Soc.* **2008**, *130*, 10702–10713.
11. Tsarevsky, N. V.; Braunecker, W. A.; Tang, W.; Matyjaszewski, K. The Atom Transfer Radical Polymerization Equilibrium: Structural and Medium Effects. In *Controlled/Living Radical Polymerization: Progress in ATRP*; Matyjaszewski, K., Ed.; ACS Symposium Series 1023; American Chemical Society: Washington, DC, 2009; pp 85−96.
12. Braunecker, W. A.; Tsarevsky, N. V.; Gennaro, A.; Matyjaszewski, K. *Macromolecules* **2009**, *42*, 6348–6360.
13. Braunecker, W. A.; Pintauer, T.; Tsarevsky, N. V.; Kickelbick, G.; Matyjaszewski, K. *J. Organometal. Chem.* **2005**, *690*, 916–924.
14. Braunecker, W. A.; Tsarevsky, N. V.; Pintauer, T.; Gil, R. R.; Matyjaszewski, K. *Macromolecules* **2005**, *38*, 4081–4088.

Downloaded by STANFORD UNIV GREEN LIBR on May 31, 2012 | http://pubs.acs.org
Publication Date (Web): March 20, 2012 | doi: 10.1021/bk-2012-1100.ch007

15. Tsarevsky, N. V.; Braunecker, W. A.; Matyaszewski, K. *J. Organomet. Chem.* **2007**, *692*, 3212–3222.
16. Tsarevsky, N. V.; Pintauer, T.; Matyjaszewski, K. *Macromolecules* **2004**, *37*, 9768–9778.
17. Tsarevsky, N. V.; Braunecker, W. A.; Vacca, A.; Gans, P.; Matyjaszewski, K. *Macromol. Symp.* **2007**, *248*, 60–70.
18. Tang, H.; Arulsamy, N.; Sun, J.; Radosz, M.; Shen, Y.; Tsarevsky, N. V.; Braunecker, W. A.; Tang, W.; Matyjaszewski, K. *J. Am. Chem. Soc.* **2006**, *128*, 16277–16285.
19. Tsarevsky, N. V.; Braunecker, W. A.; Tang, W.; Brooks, S. J.; Matyjaszewski, K.; Weisman, G. R.; Wong, E. H. *J. Mol. Catal. A: Chem.* **2006**, *257*, 132–140.
20. Fischer, H. *J. Polym. Sci.: Part A: Polym. Chem.* **1999**, *37*, 1885–1901.
21. Fischer, H. *Chem. Rev.* **2001**, *101*, 3581–3610.
22. Goto, A.; Fukuda, T. *Prog. Polym. Sci.* **2004**, *29*, 329–385.
23. Pintauer, T.; Matyjaszewski, K. *Chem. Soc. Rev.* **2008**, *37*, 1087–1097.
24. Eckenhoff, W. T.; Pintauer, T. *Catal. Rev.: Sci. Eng.* **2010**, *52*, 1–59.
25. Pintauer, T. *Eur. J. Inorg. Chem.* **2010**, 2449–2460.
26. Jakubowski, W.; Matyjaszewski, K. *Angew. Chem., Int. Ed.* **2006**, *45*, 4482–4486.
27. Jakubowski, W.; Min, K.; Matyjaszewski, K. *Macromolecules* **2006**, *39*, 39–45.
28. Matyjaszewski, K.; Jakubowski, W.; Min, K.; Tang, W.; Huang, J.; Braunecker, W. A.; Tsarevsky, N. V. *Proc. Natl. Acad. Sci. U.S.A.* **2006**, *103*, 15309–15314.
29. Mueller, L.; Jakubowski, W.; Tang, W.; Matyjaszewski, K. *Macromolecules* **2007**, *40*, 6464–6472.
30. Pietrasik, J.; Dong, H.; Matyjaszewski, K. *Macromolecules* **2006**, *39*, 6384–6390.
31. Dong, H.; Tang, W.; Matyaszewski, K. *Macromolecules* **2007**, *40*, 2974–2977.
32. Jakubowski, W.; Kirci-Denizli, B.; Gil, R. R.; Matyjaszewski, K. *Macromol. Chem. Phys.* **2008**, *209*, 32–39.
33. Matyjaszewski, K. *Macromol. Symp.* **1996**, *111*, 47.
34. Litvinenko, G.; Mueller, A. H. E. *Macromolecules* **1997**, *30*, 1253.
35. Balili, M. N. C.; Pintauer, T. *Inorg. Chem.* **2009**, *48*, 9018–9026.
36. Balili, M. N. C.; Pintauer, T. *Inorg. Chem.* **2010**, *49*, 5642–5649.
37. Listak, J.; Jakubowski, W.; Mueller, L.; Plichta, A.; Matyjaszewski, K.; Bockstaller, M. R. *Macromolecules* **2008**, *41*, 2974–2977.
38. Jakubowski, W.; Tsarevsky, N. V.; McCarthy, P. Systematic Polymeric Libraries via Atom Transfer Radical Polymerization. In *Controlled/Living Radical Polymerization: Progress in ATRP*; Matyjaszewski, K., Ed.; ACS Symposium Series 1023; American Chemical Society: Washington, DC, 2009; pp 343−355.
39. Ringbom, A. *Complexation in Analytical Chemistry*; Interscience: New York, 1963.
40. Ringbom, A.; Still, E. *Anal. Chim. Acta* **1972**, *59*, 143.

Downloaded by STANFORD UNIV GREEN LIBR on May 31, 2012 | http://pubs.acs.org
Publication Date (Web): March 20, 2012 | doi: 10.1021/bk-2012-1100.ch007

41. Davis, B.; Jakubowski, W.; Tsarevsky, N. V. , unpublished data.
42. Tsarevsky, N. V.; Jakubowski, W. *J. Polym. Sci.: Part A: Polym. Chem.* **2011**, *49*, 918–925.
43. Litt, M. *J. Polym. Sci.* **1962**, *58*, 429.
44. Davis, K. A.; Matyjaszewski, K. *Adv. Polym. Sci.* **2002**, *159*, 1–157.
45. Nanda, A. K.; Matyjaszewski, K. *Macromolecules* **2003**, *36*, 8222–8224.
46. Lin, C. Y.; Coote, M. L.; Petit, A.; Richard, P.; Poli, R.; Matyjaszewski, K. *Macromolecules* **2007**, *40*, 5985–5994.

Downloaded by STANFORD UNIV GREEN LIBR on May 31, 2012 | http://pubs.acs.org
Publication Date (Web): March 20, 2012 | doi: 10.1021/bk-2012-1100.ch007

Chapter 8

Homobimetallic Ethylene− and Vinylidene−Ruthenium Complexes for ATRP

Yannick Borguet, Lionel Delaude, and Albert Demonceau*

Laboratory of Macromolecular Chemistry and Organic Catalysis,
University of Liège, Sart-Tilman (B.6a), B-4000 Liège, Belgium
***E-mail: A.Demonceau@ulg.ac.be**

The catalytic activity of a series of homobimetallic ruthenium complexes of the type [(*p*-cymene)Ru(μ-Cl)$_3$RuCl(L)(L′)] [L = C_2H_4 or a vinylidene ligand (=C=CHR); L′ = PPh_3, PCy_3, or an *N*-heterocyclic carbene ligand] was determined by investigating the atom transfer radical polymerisation of methyl methacrylate. The results clearly demonstrate that the ligands strongly affect the ability of the ruthenium complexes to favour the occurrence of a well-behaved ATRP.

Ruthenium–arene complexes are versatile and efficient catalyst precursors for various important organic transformations. This is due in part to the lability of the η^6-arene ligand that can be easily removed upon thermal or photochemical activation to release highly active, coordinatively unsaturated species. During the 1990s, we demonstrated that [$RuCl_2$(*p*-cymene)(PR_3)] complexes bearing basic and bulky phosphine ligands, such as tricyclohexyl-phosphine (PCy_3, see structure **1**, Scheme 1) were highly effective precatalysts for ring-opening metathesis polymerisation (ROMP) (*1*, *2*) and atom transfer radical polymerisation (ATRP) (*3*–*5*). The past decade also witnessed the experimental reality of stable nucleophilic *N*-heterocyclic carbenes (NHCs). These divalent carbon species are neutral, two-electron ligands with only little π-back-bonding tendency. They behave as phosphine mimics, yet they are better σ-donors and they form stronger bonds to metal centres than most phosphines. Their electronic and steric properties are liable to ample modification simply by varying the substituents on the heterocyclic ring. Therefore, NHCs have become ubiquitous ligands in organometallic chemistry and catalysis (*6–10*).

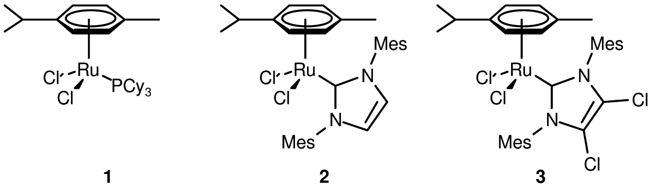

Scheme 1. Monometallic ruthenium–p-cymene complexes bearing a tricyclohexylphosphine or an NHC ligand.

In order to further expand the scope of ruthenium–arene catalyst precursors, we have adopted this class of ancillary ligands instead of phosphines to generate [$RuCl_2$(*p*-cymene)(NHC)] species, either preformed or *in situ* (*11*). Thus, complex **2** bearing the 1,3-dimesitylimidazolin-2-ylidene ligand displayed a remarkable activity for initiating ROMP of cyclooctene under visible light illumination (*12–14*), whereas complex **3** sporting a modified NHC ligand (4,5-dichloro-1,3-dimesitylimidazolin-2-ylidene) was an attractive challenger for promoting atom transfer radical addition (ATRA) (*15*) and polymerisation (*16*) processes.

Homobimetallic Ruthenium–Ethylene Complexes

In 2005, Severin and co-workers investigated the reaction of [$RuCl_2$-(*p*-cymene)]$_2$ with 1 equivalent of PCy_3 under an ethylene atmosphere. Under these conditions, the ruthenium dimer afforded a new type of molecular scaffold (**4**, Scheme 2) in which a RuCl(η^2-C_2H_4)(PCy_3) fragment was connected *via* three μ-chloro bridges to a ruthenium–(*p*-cymene) moiety. Complex **4** displayed an outstanding catalytic activity in ATRA reactions (*17*). By varying the nature of the arene ligand, the same group also synthesised the related homobimetallic complex **5** and successfully employed it as catalyst precursor for the ATRP of methacrylate monomers at a temperature of only 35 °C without the need of an additive such as Al(O*i*-Pr)$_3$ (*18*).

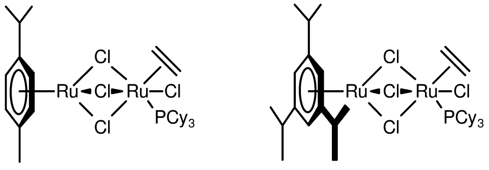

Scheme 2. Homobimetallic ruthenium–arene complexes bearing a tricyclohexylphosphine ligand.

In view of the enhancements brought about by the replacement of phosphines by NHCs in monometallic ruthenium–arene catalyst precursors of type **1**–**3**, we decided to investigate the effect of similar modifications on the catalytic activity of complexes of type **4**–**5**. The preparation of complexes **6** and **7** (Scheme 3) was rather straightforward and could be achieved in a single step by heating the commercially available $[RuCl_2(p\text{-cymene})]_2$ dimer with 1 equivalent of 1,3-dimesitylimidazolin-2-ylidene and 4,5-dichloro-1,3-dimesitylimidazolin-2-ylidene, respectively (*19*).

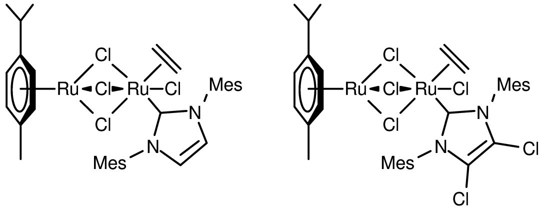

6 **7**

Scheme 3. Homobimetallic ruthenium–p-cymene complexes bearing an NHC ligand.

Table 1. Polymerisation of Methyl Methacrylate Initiated by Ethyl 2-Bromo-2-methylpropanoate and Catalysed by Ruthenium Complexes 4-7

Complex	*4*	*5*	*6*	*7*
Yield (%)	78	95	81	47
M_n *(g.mol^{-1})*	36 500	38 500	40 000	19 000
M_w/M_n	1.05	1.14	1.25	1.10

$[MMA]_0$:$[initiator]_0$:$[complex]_0$ = 800:2:1, 16 h at 85 °C.

The catalytic activity of the ruthenium–*N*-heterocyclic carbene complexes **6** and **7** was then investigated in the ATRP of methyl methacrylate and compared with that displayed by the ruthenium–PCy_3 analogues **4** and **5** (Table 1). With both complexes **6** and **7**, the molecular weights increased linearly with conversion. The semilogarithmic plot of $\ln([M]_0/[M]_t)$ *versus* time also followed a linear relationship, suggesting that radical polymerisation took place in a controlled fashion with both catalysts. The nature of the ancillary ligand significantly influenced the rate of reaction. The 1,3-dimesitylimidazolin-2-ylidene ligand afforded a much more active catalyst (**6**) than its dichloro derivative (**7**). Indeed, the pseudo-first order rate constant computed for complex **6** was three times larger than for complex **7**. Furthermore, in terms of kinetics, complex **6** was ranked between the *p*-cymene–tricyclohexylphosphine and the 1,3,5-triisopropylbenzene–tricyclohexylphosphine complexes **4** and **5**, respectively. When molecular weight distributions were examined, however, complex **4** took precedence over its congeners **5**–**7**. The polydispersity remained indeed as low as M_w/M_n = 1.05 with complex **4**, whereas complexes **5**–**7** led to PDIs ranging from 1.10 to 1.25 under the same experimental conditions.

In the next series of experiments, we investigated the ATRP of styrene at 110 °C (Table 2). Complex **4** proved once again its efficiency as a radical initiator, as it led to a well-behaved polymerisation process with a satisfactory control over the molecular weight distribution (M_w/M_n = 1.35) and no stilbene formation (*19*). Most interestingly, replacement of tricyclohexylphosphine by an NHC ligand led to a complete change of selectivity. Thus, when styrene was reacted with complexes **6** and **7** under the same experimental conditions that were employed for **4**, ATRP was totally suppressed and replaced by olefin metathesis (Scheme 4). Despite the presence of the initiator [(1-bromoethyl)-benzene], no polystyrene was isolated and a quantitative yield of stilbene (almost exclusively the (*E*)-isomer) was obtained within 30 min (*19*).

Table 2. ATRP vs Cross–Metathesis (CM) of Styrene

Complex		*Yield (%)*	M_n *(g.mol^{-1})*	M_w/M_n
4	ATRP	62	24 000	1.35
	CM	0		
6 or **7**	ATRP	0	–	–
	CM	100		

$[\text{Styrene}]_0:[\text{initiator}]_0:[\text{complex}]_0$ = 750:2:1, 16 h at 110 °C

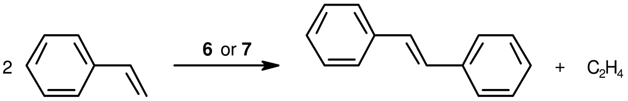

Scheme 4. Cross-metathesis of styrene.

The results described above indicate that an exchange of the PCy_3 ligand for an *N*-heterocyclic carbene ligand can have a pronounced influence on the catalytic behaviour of this type of dinuclear ruthenium complexes. We became thus interested to see how an exchange of the PCy_3 ligand for other phosphine ligands would influence the reactivity. In 2008, K. Severin and co-workers described the synthesis and structure of a related dinuclear ruthenium–ethylene complex (**8**) containing the PPh_3 ligand (Scheme 5) (*20*). Complex **8** was shown to be a potent catalyst for ATRA and ATRC reactions (*20*), but its activity in ATRP was not assessed, which prompted us to enter upon this study.

Again, methyl methacrylate was selected as the model monomer. At 60 and 85 °C (Figure 1), the polymerisation proceeded rather well, but the conversions culminated at 60–70%. This trend was also clearly reflected in the plots of $\ln([\text{MMA}]_0/[\text{MMA}]_t)$ *versus* time, which were linear at the beginning of the polymerisation and deviated afterwards from linearity (Figure 1). Furthermore, a linear evolution of M_n as a function of monomer conversion was observed and the polydispersities were as low as 1.05 (Table 3).

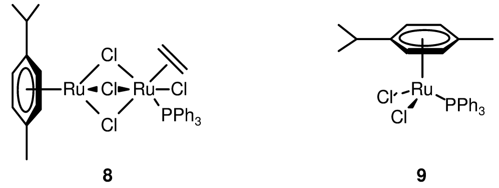

Scheme 5. Mono- and homobimetallic ruthenium–p-cymene complexes bearing a triphenylphosphine ligand.

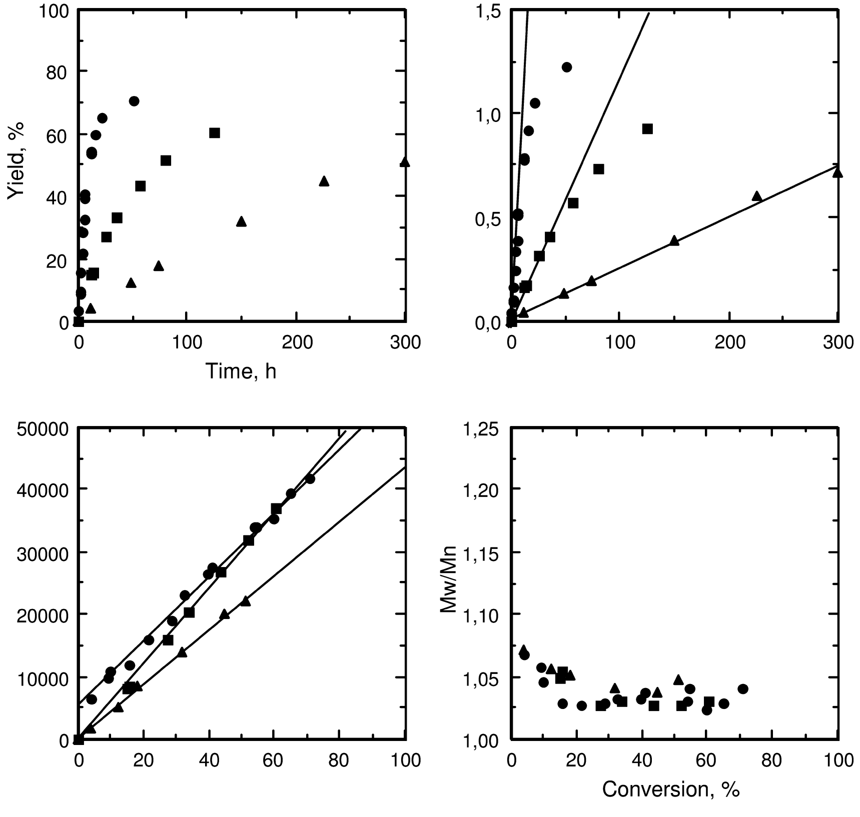

*Figure 1. Experimental data for the polymerisation of MMA initiated by ethyl 2-bromo-2-methylpropanoate and catalysed by complex **8** at 40 (σ), 60 (v), and 85 °C (λ). $[MMA]_0$:$[initiator]_0$:[complex **8**$]_0$ = 800:2:1.*

Complex **8** is also remarkable, as it is efficient at 40 °C (Table 3). It should be noted, indeed, that ruthenium-catalysed polymerisations of methacrylates are generally performed at temperatures of around 80–85 °C and that there are only a few Ru catalysts that allow one to work under milder conditions. The hydride complex $[RuH_2(PPh_3)_4]$, for example, was reported to catalyse the controlled polymerisation of MMA at 30 °C but significantly high catalyst concentrations (MMA/Ru = 200:1) and reaction times (300 h) were required (*21*). Although complex **8** seems to be less active than [$RuH_2(PPh_3)_4$] and **5** (*18*), it ranges nevertheless among the most active ruthenium catalysts for ATRP reactions described so far. Most importantly, the homobimetallic ruthenium complex **8** also greatly surpassed its monometallic counter-part **9**, which was found to be inefficient for the ATRP of MMA (*3–5*).

Table 3. Polymerisation of Methyl Methacrylate Initiated by Ethyl 2-Bromo-2-methylpropanoate and Catalysed by Ruthenium Complex 8

Temperature (°C)	*Reaction time (h)*	*Yield (%)*	M_n *(g.mol^{-1})*	M_w/M_n
40	12	4	1 850	1.07
	300	51	22 000	1.05
60	12	15	8 000	1.05
	80	52	32 000	1.03
85	12	54	34 000	1.03
	50	71	42 000	1.04

$[MMA]_0:[initiator]_0:[complex\ \mathbf{8}]_0 = 800:2:1$

Regarding the mechanism, it seems likely that, in a first step, the ethylene ligand in complexes **4**–**8** is cleaved off. The resulting coordinatively unsaturated ruthenium complex is then able to reversibly abstract a halogen atom from the initiator or subsequently from the growing polymer chain end. This mechanism is supported by the fact that the ethylene ligand in complexes **4** and **8** can be replaced by a halogen atom as evidenced by the isolation of the mixed valence Ru(II)–Ru(III) complex [(*p*-cymene)Ru(μ-Cl)$_3$RuCl$_2$(PR$_3$)] (R = Cy, *n*-Bu, and Ph) (*17*, *20*). In this respect, maximum MMA conversions of 60–70% monitored with complex **8** (Figure 1) might be explained by the accumulation of the mixed valence Ru(II)–Ru(III) complex **11** from the active catalytic species **10** (Scheme 6).

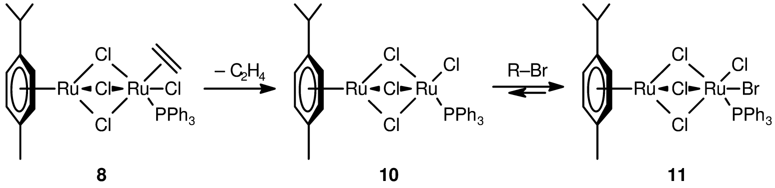

*Scheme 6. Oxidation of the Ru^{II}(η^2-C_2H_4) complex **8** to the Ru^{III}–Br complex **11**.*

Homobimetallic Ruthenium–Vinylidene Complexes

Metal–vinylidene complexes [ML_n(=C=CRR′)] are versatile organo-metallic species exhibiting a variety of reactivities, either in stoichiometric reactions, or in homogeneous catalysis (*22–25*). In particular, ruthenium–vinylidene complexes are good catalyst precursors for olefin metathesis, alkyne dimerisation, and enol ester synthesis from terminal alkynes and carboxylic acids (*22–29*). Ruthenium–vinylidene complexes **12**–**15** (Scheme 7) have also proven to be efficient catalysts for atom transfer radical addition (ATRA) (*30*), but to the best of our knowledge, their activity in ATRP has not been reported.

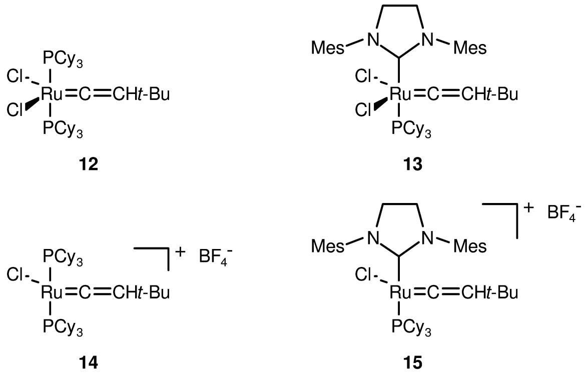
PCy3
Cl
Ru=C=CHt-Bu
Cl
PCy3
12
Mes
N
N
Mes
Cl
Ru=C=CHt-Bu
Cl
PCy3
13
PCy3
Cl
Ru=C=CHt-Bu
PCy3
+ BF4-
14
Mes
N
N
Mes
Cl
Ru=C=CHt-Bu
PCy3
+ BF4-
15

Scheme 7. Ruthemium–vinylidene complexes employed in ATRA (30).

Severin et al. reported recently the synthesis of two homobimetallic ruthenium–vinylidene complexes by displacing the ethylene ligand in **4** with *tert*-butylacetylene or phenylacetylene. Complexes **16** and **19** thus formed were fully characterised but their catalytic activity was not assessed (*31*).

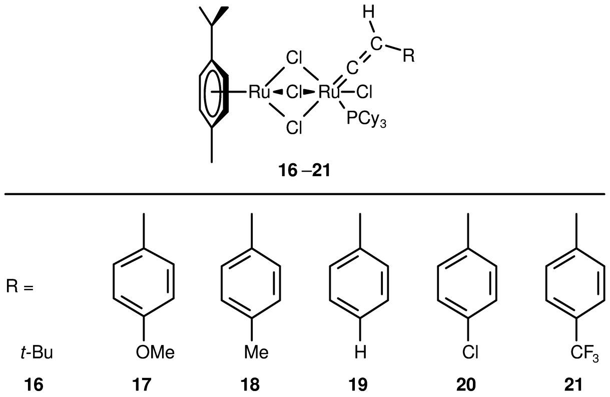
H
C
R
C
Cl
Ru
Cl
Ru
Cl
Cl
PCy3
16–21
R =
t-Bu
OMe
Me
H
Cl
CF3
16
17
18
19
20
21

Scheme 8. Homobimetallic ruthenium–PCy3 complexes bearing a vinylidene ligand.

Table 4. Polymerisation of Methyl Methacrylate Initiated by Ethyl 2-Bromo-2-methylpropanoate and Catalysed by Ruthenium Complexes 16–21

Complex	*Yield (%)*	*M_n (g.mol^{-1})*	*M_w/M_n*
16	66	31 000	1.6
17	77	37 500	1.6
18	61	31 000	1.35
19	49	23 000	1.15
20	36	25 000	1.15
21	37	20 000	1.25

$[MMA]_0$:$[initiator]_0$:$[complex]_0$ = 800:2:1, 24 h at 85 °C

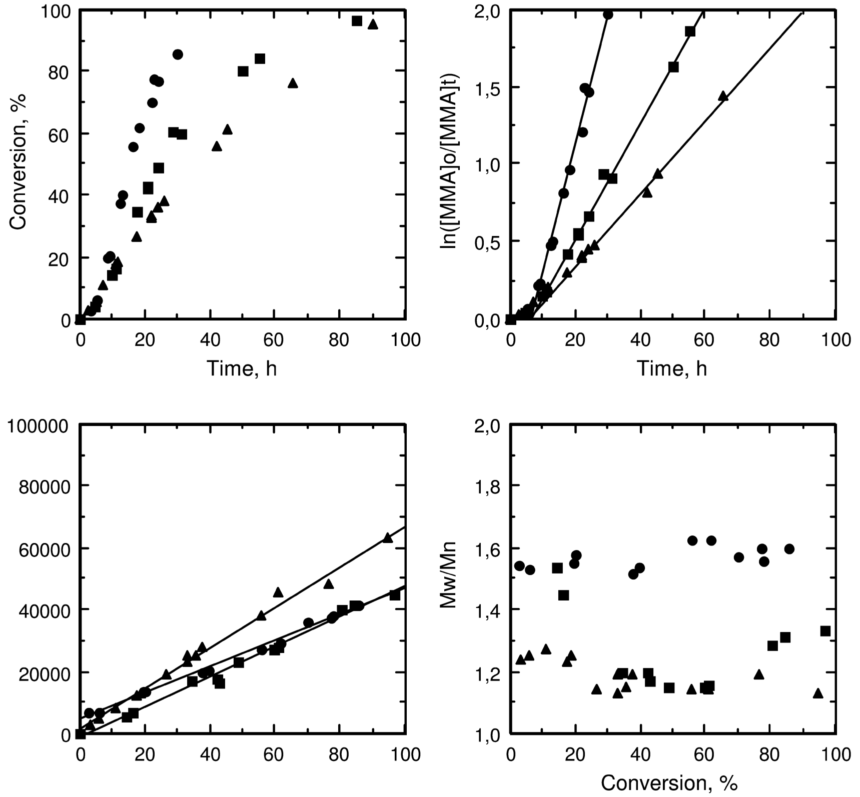

*Figure 2. Experimental data for the polymerisation of MMA initiated by ethyl 2-bromo-2-methylpropanoate and catalysed by complexes **17** (λ), **19** (ν), and **20** (σ). $[MMA]_0$:$[initiator]_0$:$[complex]_0$ = 800:2:1, 85 °C.*

Hence, we decided to study their behaviour in various ruthenium-promoted organic transformations. We also chose to prepare additional complexes bearing electron-donating or -withdrawing substituents on the phenylvinylidene ligand (complexes **17**–**18** and **20**–**21**, respectively (Scheme 8)) and to investigate their catalytic activity (*32*).

The activity of complexes **16**–**21** was then investigated for the ATRP of MMA using the standard experimental conditions (85 °C, with ethyl 2-bromo-2-methylpropanoate as the initiator). With all the ruthenium–vinylidene complexes under investigation, the molecular weights increased linearly with conversion. Furthermore, the semilogarithmic plot of $\ln([M]_0/[M]_t)$ *versus* time also followed a linear relationship. These results strongly suggest that the polymerisation took place in a controlled fashion. However, an induction period was clearly evidenced in the plots of conversion versus time and $\ln([M]_0/[M]_t)$ *versus* time (Figure 2).

Complexes **16**–**21**, however, differed from one another both in the polymerisation rate and the polydispersity of the polymers thus obtained. Examination of Table 4 and Figure 2 reveals that electron-rich ruthenium–vinylidene complexes (R = *t*-Bu (**16**), *p*-MeO-C_6H_4 (**17**), and *p*-Me-C_6H_4 (**18**)) were more active than their electron-poor counter-parts (R = *p*-Cl-C_6H_4 (**20**) and *p*-CF_3-C_6H_4 (**21**)). Furthermore, when the most active methoxy-substituted complex (**16**) was used, the molecular weight distribution was quite broad (M_w/M_n = 1.6) and remained almost constant throughout the entire run (Figure 2). With the phenylvinylidene complex (**19**), the molecular weight distribution decreased with conversion, before to increase to some extent (up to 1.3) at the end of the polymerisation. Thus, the lowest polydispersity (M_w/M_n = 1.15) was obtained after 40–60% conversion. Finally, with the chlorine-substituted complex (**20**), the polydispersity decreased from 1.25 at the beginning of the polymerisation to 1.15–1.20 after 25% conversion and did not change anymore during the remaining time of the polymerisation.

In view of the enhancements brought about by the replacement of the PCy_3 ligand with PPh_3 in homobimetallic ruthenium–ethylene catalyst precursors for ATRP (**4** Π **8**), we have adopted the same strategy to synthesise three homobimetallic ruthenium–vinylidene complexes containing the triphenyl-phosphine ligand (**22**–**24**, Scheme 9).

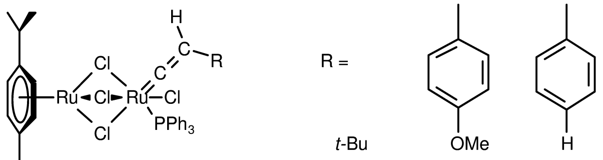

22–**24** **22** **23** **24**

Scheme 9. Homobimetallic ruthenium–PPh_3 complexes bearing a vinylidene ligand.

Table 5. Polymerisation of Methyl Methacrylate Initiated by Ethyl 2-Bromo-2-methylpropanoate and Catalysed by Ruthenium Complexes 22–24

Complex	*Reaction time (h)*	*Yield (%)*	*M_n (g.mol^{-1})*	*M_w/M_n*
22	16	25	12 000	1.20
	48	66	30 000	1.15
23	16	26	13 000	1.08
	48	65	30 000	1.05
24	16	25	10 500	1.09
	48	66	29 000	1.05

$[MMA]_0L:[initiator]_0:[complex]_0$ = 800:2:1, 85 °C

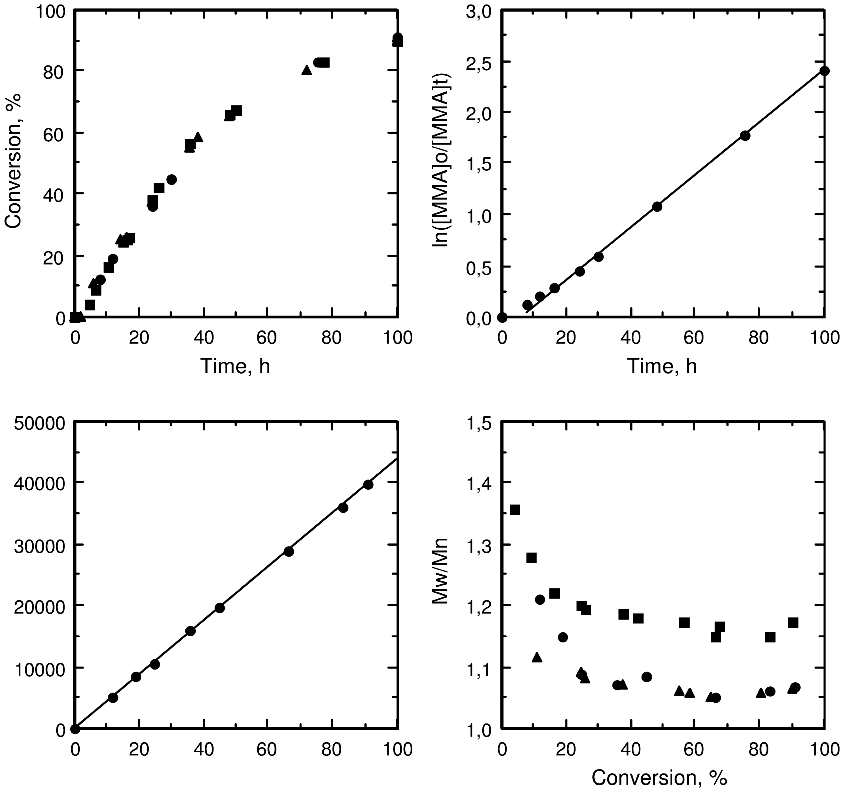

Figure 3. Experimental data for the polymerisation of MMA initiated by ethyl 2-bromo-2-methylpropanoate and catalysed by complexes ***22*** *(ν),* ***23*** *(σ), and* ***24*** *(λ). $[MMA]_0:[initiator]_0:[complex]_0$ = 800:2:1, 85 °C.*

Results from this study (Table 5) indicated that the introduction of the PPh_3 ligand was highly beneficial for the ATRP process. Indeed, ruthenium complexes bearing electron-donating vinylidenes (**22** and **23**), which gave a polydispersity index of around 1.6 when associated to PCy_3 (Table 4), furnished PMMAs with a much narrower molecular weight distribution (M_w/M_n = 1.05–1.2) when the bimetallic scaffold was coordinated to PPh_3. Quite surprisingly, complexes **22**–**24** were equipotent catalyst precursors (Table 5 and Figure 3), differing only slightly by the polydispersity indices. It should also be noted that the vinylidene complexes **22**–**24** were less active than the parent ruthenium–ethylene complex **8**. However, as mentioned before, with the latter complex, the conversion of MMA never exceeded 70–75%, whereas 90% conversion was reached in the presence of **22**–**24**. Furthermore, ruthenium–vinylidene complexes with a PPh_3 ligand (**22**–**24**) were also less active than the PCy_3 analogues (**16**, **17**, and **19**).

Again, with complexes **22**–**24**, the molecular weights increased linearly with conversion (Figure 3). The semilogarithmic plot of $\ln([M]_0/[M]_t)$ *versus* time also followed a linear relationship, although an induction period of a few hours was evidenced.

The reasons why the homobimetallic ruthenium–vinylidene complexes are active in ATRP are presently unclear. These complexes possess indeed two 18-electron ruthenium centres and, as such, should be unable to activate the carbon–halogen bond of the initiator or of the growing polymer chain end. On the other hand, the fact that an induction period was found for the ATRP of MMA indicates that the ruthenium–vinylidene complexes have to be activated prior to the ATRP process. There are in principle several plausible explanations for the formation of a coordinatively unsaturated 16-electron ruthenium species from the homobimetallic ruthenium–vinylidene complexes: either the splitting of the bimetallic scaffold into two different unsaturated ruthenium intermediates (Path A, Scheme 10), the opening of a μ-chloro bridge (Path B), or the release of the vinylidene ligand (Path C) (*33*). Further investigations are needed to clarify this point. However, the formation of the coordinatively unsaturated 16-electron ruthenium species according to path C (Scheme 10) could tentatively be explained by the metathetical transformation of the ruthenium–vinylidene complexes into the corresponding ruthenium–carbenes **25** and/or **26** (Scheme 11), which are highly unstable species (*34*–*37*). Although this process is well documented in olefin metathesis (*19*, *24*), in the present case it likely suffers from the low metathetical activity of methyl methacrylate. Consequently, induction periods observed in polymerisation of methyl methacrylate could result from structural modifications of the ruthenium–vinylidene complexes into the real active catalytic species, devoid of the vinylidene fragment.

It should also be noted that when the homobimetallic ruthenium–ethylene complex **4** was treated with a stoichiometric amount of acetylene in THF, the μ-carbide complex **28** was formed, presumably *via* the intermediate ruthenium–vinylidene complex **27** (Scheme 12) (*31*), suggesting thereby an alternative decomposition route for the ruthenium–vinylidene complexes under investigation.

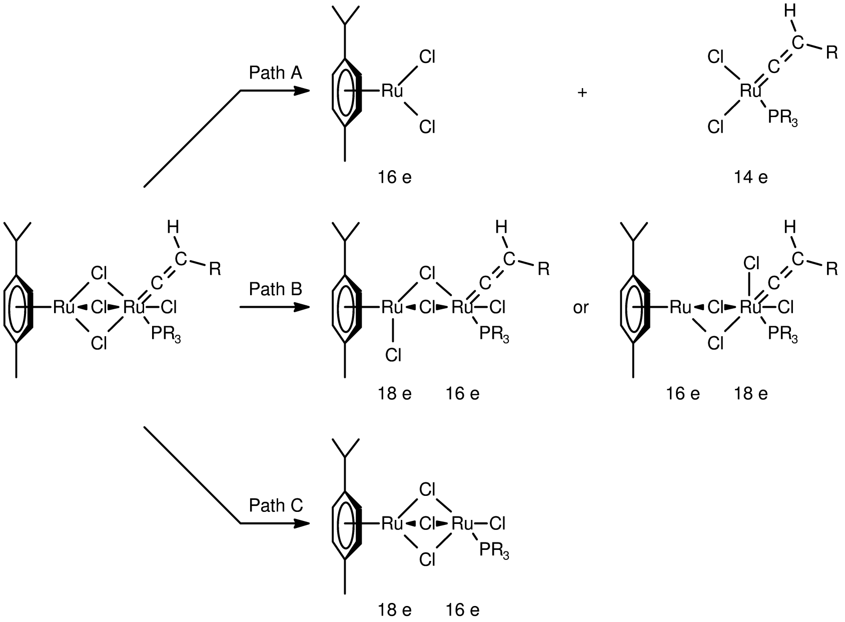
Path A
Path B
Path C
Ru
Cl
PR3
C
H
R
+
or
16 e
14 e
18 e
16 e
16 e
18 e
18 e
16 e

Scheme 10. Plausible explanations for the formation of coordinatively unsaturated 16-electron ruthenium species.

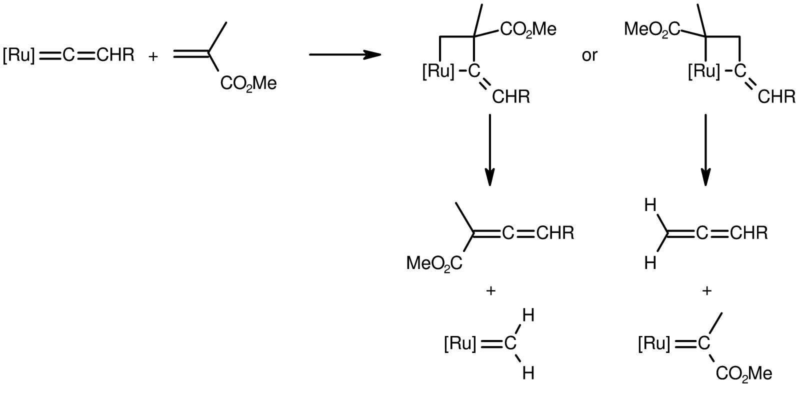
[Ru]=C=CHR
+
CO2Me
MeO2C
[Ru]-C
CHR
or
C=CHR
H
[Ru]=C

25

26

Scheme 11. Metathetical transformation of ruthenium–vinylidenes into ruthenium–carbenes.

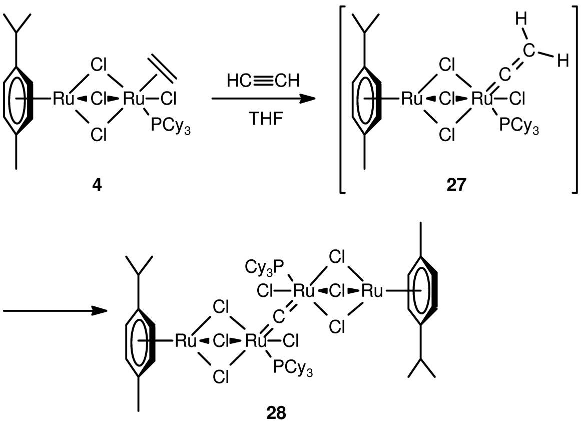

*Scheme 12. Formation of the ruthenium μ-carbide complex **28**.*

In the past decade, monometallic ruthenium catalysts have widely contributed to the development of ATRP (*3–5*, *38–40*). With the advent of homobimetallic ruthenium complexes as catalyst precursors, the following question arises: does the bimetallic scaffold remain intact throughout the polymerisation run? The answer is probably yes, although further investigations are needed to clarify this point. This answer is notably substantiated by the isolation of mixed valence Ru(II)–Ru(III) complexes [(*p*-cymene)Ru-(μ-Cl)$_3$RuCl$_2$(PR$_3$)] (R = Cy and Ph) (Scheme 6) upon heating a solution of complexes **4** or **8** in toluene at 40 °C in the presence of a large excess of CCl$_4$ (*17*, *20*). Interestingly, the X-ray structures of the mixed valence complexes demonstrated that both ruthenium fragments were connected *via* three chloro bridges, as in the parent compounds **4** and **8** (*17*, *20*).

It is also worth noting that homobimetallic ruthenium complexes **4** (bearing the PCy$_3$ ligand), **6** and **7** (bearing an NHC ligand) are usually synthesised at a temperature ranging from 60 to 75 °C, whereas complex **8** with the PPh$_3$ ligand is prepared at 110 °C for 2 days (*20*). A further indication that the μ-chloro bridges are viable at higher temperatures can be deduced from a recent paper of K. Severin and his co-workers (*41*). They found indeed that microwave heating at 130–150 °C facilitated arene exchange in reactions of [RuCl$_2$(arene)]$_2$ complexes with neutral chelate ligands to afford the bimetallic complexes **30** (Scheme 13) (*41*).

On the other hand, a process maintaining the three chloro bridges was also suggested for the metathetical transformation of homobimetallic ruthenium–benzylidene (**31**) and ruthenium–indenylidene (**32**) complexes into the corresponding ruthenium–ethylene complex (**4**), presumably *via* the highly unstable ruthenium–methylidene species (**33**) (Scheme 14) (*42*, *43*).

Based on these results, we are inclined to suggest that the catalytic species in ATRP is binuclear, with both ruthenium centres connected by three μ-chloro bridges (**10**), and devoid of ethylene or vinylidene ligand (Scheme 15).

Furthermore, the isolation of mixed valence Ru(II)–Ru(III) complexes [(*p*-cymene)Ru(μ-Cl)$_3$RuCl$_2$(PR$_3$)] (R = Cy, *n*-Bu, and Ph) (*17*, *20*) also suggests that the 16-electron ruthenium fragment does activate the carbon–halogen bonds of the initiator and polymer terminals, and return the halogen radical from the high oxidation-state bimetallic complex into polymer terminals. It should however be emphasised that the three μ-chloro bridges in bimetallic complexes **4**–**8**, **16**–**21**, **24**, **30**, and **32** have been evidenced by X-ray diffraction analysis, whereas in solution the situation could be different as ^{1}H, ^{13}C, and ^{31}P NMR spectroscopy gives no information on the exact number of chloro bridges.

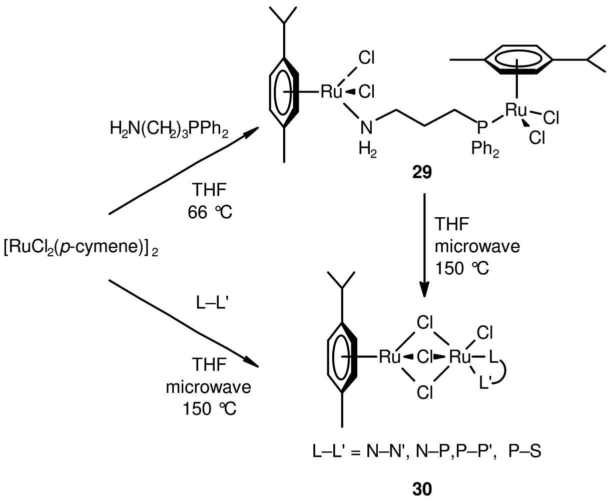
$H_2N(CH_2)_3PPh_2$
THF
66 °C
$[RuCl_2(p\text{-cymene})]_2$
L–L'
THF
microwave
150 °C
Ru
Cl
N
H_2
P
Ph_2
29
THF
microwave
150 °C
L–L' = N–N', N–P, P–P', P–S
30

Scheme 13. Microwave-assisted syntheses of dinuclear ruthenium complexes containing N–N'-, N–P-, P–P'-, and P–S-chelate ligands.

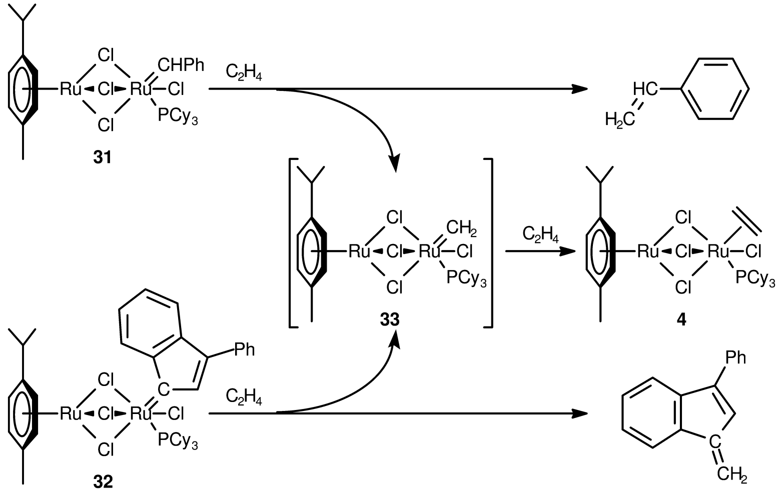
Ru
Cl
CHPh
PCy_3
31
C_2H_4
HC
H_2C
CH_2
33
C_2H_4
4
Ph
C
32
C_2H_4
CH_2

Scheme 14. Ethylenolysis of homobimetallic ruthenium–benzylidene and ruthenium–indenylidene complexes.

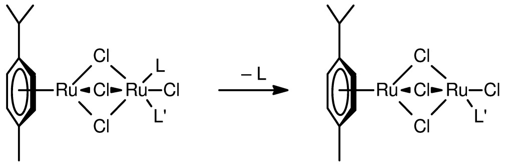

L = C_2H_4, C=CHR; L' = PR_3, NHC

4–8, **16–21**, **24**, **30**, **32** **10**

Scheme 15. Generation of the active species.

It also remains to explain the role of the binuclear scaffold on the high activity and controllability of the ATRP process. In this respect, it is of utmost importance to emphasise that the monometallic [$RuCl_2$(*p*-cymene)(PPh_3)] complex (**9**) was inefficient for the ATRP of MMA (*3–5*), whereas the corresponding homobimetallic ruthenium–ethylene (**8**) and –vinylidene complexes (**22**–**24**) promoted a highly controlled process, suggesting a cooperative effect between both metal fragments. Investigations in this line are in progress in our laboratory.

Conclusions

The catalytic activity of novel homobimetallic ruthenium–ethylene complexes (**4**–**8**) was investigated in the ATRP of MMA. Complex **6** bearing the 1,3-dimesitylimidazolin-2-ylidene ligand displayed faster reaction rates than its 4,5-dichloro derivative (**7**) and the related tricyclohexylphosphine-based complex **4**, although control was more effective with the latter catalyst. More importantly, complex **5** bearing the 1,3,5-triisopropylbenzene ligand instead of the commonly used *p*-cymene promoted a controlled ATRP of methacrylates at a temperature of only 35 °C, and the resulting polymers showed low polydispersities. The triphenylphosphine-based ruthenium–ethylene complex **8** was also a highly efficient catalyst precursor, as it provided an excellent control over the molecular weight and the molecular weight distribution. However, contrary to the related tricyclohexylphosphine-based system **4**, complex **8** did not allow conversions higher than 60–70%.

Ruthenium–vinylidene complexes **16**–**24** also promoted controlled radical polymerisations, albeit a short induction period was observed. Furthermore, ruthenium–vinylidene complexes **22**–**24** featuring a PPh_3 ligand afforded conversions higher than 90–95%, which stands in sharp contrast with the parent ruthenium–ethylene–PPh_3 complex **8**. The nature of the phosphine ligand also significantly influenced the course of the polymerisations. PCy_3 afforded indeed much more active catalysts than PPh_3. In addition, PCy_3 also led to broader molecular weight distributions than PPh_3. To sum up, the results clearly demonstrate that ancillary ligands exert a critical influence on the catalytic activity of homobimetallic ethylene– and vinylidene–ruthenium complexes and, in addition, these bimetallic complexes significantly broaden the application field of their monometallic predecessors **1**–**3**.

Experimental

The same protocol was followed for all the polymerisation tests of methyl methacrylate: ruthenium complex (0.0117 mmol) was placed in a glass tube containing a bar magnet and capped by a three-way stopcock. The reactor was purged of air (three vacuum–nitrogen cycles) before methyl methacrylate (1 mL, 9.35 mmol) and the initiator (ethyl 2-bromo-2-methylpropanoate 0.1 M in toluene, 0.25 mL) were added ($[MMA]_0$:$[initiator]_0$:$[complex]_0$ = 800:2:1). The mixture was heated in a thermostated oil bath for 16 or 24 h at 85 °C and, after cooling, dissolved in THF and the product precipitated in heptane. The polymer was filtered off and dried overnight under vacuum.

M_n and M_w/M_n were determined by size-exclusion chromatography with PMMA calibration.

Acknowledgments

We are grateful to the 'Fonds National de la Recherche Scientifique' (FRS–F.N.R.S.), Brussels, for the purchase of major instrumentation.

References

1. Demonceau, A.; Stumpf, A. W.; Saive, E.; Noels, A. F. *Macromolecules* **1997**, *30*, 3127–3136.
2. Jan, D.; Delaude, L.; Simal, F.; Demonceau, A.; Noels, A. F. *J. Organomet. Chem.* **2000**, *606*, 55–64.
3. Simal, F.; Demonceau, A.; Noels, A. F. *Angew. Chem., Int. Ed.* **1999**, *38*, 538–540.
4. Simal, F.; Sebille, S.; Hallet, L.; Demonceau, A.; Noels, A. F. *Macromol. Symp.* **2000**, *161*, 73–85.
5. Simal, F.; Jan, D.; Delaude, L.; Demonceau, A.; Spirlet, M.-R.; Noels, A. F. *Can. J. Chem.* **2001**, *79*, 529–537.
6. Jafarpour, L.; Nolan, S. P. *Adv. Organomet. Chem.* **2001**, *46*, 181–222.
7. Herrmann, W. A.; Weskamp, T.; Böhm, V. P. W. *Adv. Organomet. Chem.* **2001**, *48*, 1–69.
8. Herrmann, W. A. *Angew. Chem., Int. Ed.* **2002**, *41*, 1290–1309.
9. Dragutan, I.; Dragutan, V.; Delaude, L.; Demonceau, A. *Arkivoc* **2005**, *10*, 206–253.
10. Dragutan, V.; Dragutan, I.; Delaude, L.; Demonceau, A. *Coord. Chem. Rev.* **2007**, *251*, 765–794.
11. Delaude, L.; Demonceau, A.; Noels, A. F. *Curr. Org. Chem.* **2006**, *10*, 203–215.
12. Delaude, L.; Demonceau, A.; Noels, A. F. *Chem. Commun.* **2001**, 986–987.
13. Delaude, L.; Szypa, M.; Demonceau, A.; Noels, A. F. *Adv. Synth. Catal.* **2002**, *344*, 749–756.
14. Maj, A. M.; Delaude, L.; Demonceau, A.; Noels, A. F. *J. Organomet. Chem.* **2007**, *692*, 3048–3056.

15. Richel, A.; Delfosse, S.; Cremasco, C.; Delaude, L.; Demonceau, A.; Noels, A. F. *Tetrahedron Lett.* **2003**, *44*, 6011–6015.
16. Delaude, L.; Delfosse, S.; Richel, A.; Demonceau, A.; Noels, A. F. *Chem. Commun.* **2003**, 1526–1527.
17. Quebatte, L.; Solari, E.; Scopelliti, R.; Severin, K. *Organometallics* **2005**, *24*, 1404–1406.
18. Haas, M.; Solari, E.; Nguyen, Q. T.; Gautier, S.; Scopelliti, R.; Severin, K. *Adv. Synth. Catal.* **2006**, *348*, 439–442.
19. Sauvage, X.; Borguet, Y.; Noels, A. F.; Delaude, L.; Demonceau, A. *Adv. Synth. Catal.* **2007**, *349*, 255–265.
20. Wolf, J.; Thommes, K.; Briel, O.; Scopelliti, R.; Severin, K. *Organometallics* **2008**, *27*, 4464–4474.
21. Takahashi, H.; Ando, T.; Kamigaito, M.; Sawamoto, M. *Macromolecules* **1999**, *32*, 6461–6465.
22. Bruneau, C.; Dixneuf, P. H. *Acc. Chem. Res.* **1999**, *32*, 311–323.
23. Wakatsuki, Y. *J. Organomet. Chem.* **2004**, *689*, 4092–4109.
24. Bruneau, C.; Dixneuf, P. H. *Angew. Chem,. Int. Ed.* **2006**, *45*, 2176–2203.
25. *Metal Vinylidenes and Allenylidenes in Catalysis*; Bruneau, C., Dixneuf, P. H., Eds.; Wiley-VCH: Weinheim, 2008.
26. Opstal, T.; Verpoort, F. *Synlett* **2003**, 314–320.
27. Katayama, H.; Ozawa, F. *Coord. Chem. Rev.* **2004**, *248*, 1703–1715.
28. Ledoux, N.; Drozdzak, R.; Allaert, B.; Linden, A.; Van Der Voort, P.; Verpoort, F. *Dalton Trans.* **2007**, 5201–5210.
29. Borguet, Y.; Sauvage, X.; Zaragoza, G.; Demonceau, A.; Delaude, L. *Organometallics* **2011**, *30*, 2730–2738.
30. Opstal, T.; Verpoort, F. *Tetrahedron Lett.* **2002**, *43*, 9259–9263.
31. Solari, E.; Antonijevic, S.; Gauthier, S.; Scopelliti, R.; Severin, K. *Eur. J. Inorg. Chem.* **2007**, 367–371.
32. Borguet, Y.; Sauvage, X.; Zaragoza, G.; Demonceau, A.; Delaude, L. *Organometallics* **2010**, *29*, 6675–6686.
33. Borguet, Y.; Sauvage, X.; Bicchielli, D.; Delfosse, S.; Delaude, L.; Demonceau, A.; Bareille, L.; Le Gendre, P.; Moïse, C. In *Controlled/Living Radical Polymerization: Progress in ATRP*; Matyjaszewski, K., Ed.; ACS Symposium Series 1023; American Chemical Society: Washington, DC, 2009; pp 97–114.
34. Schwab, P.; Grubbs, R. H.; Ziller, J. W. *J. Am. Chem. Soc.* **1996**, *118*, 100–110.
35. Ulman, M.; Grubbs, R. H. *Organometallics* **1998**, *17*, 2484–2489.
36. Ulman, M.; Grubbs, R. H. *J. Org. Chem.* **1999**, *64*, 7202–7207.
37. Ulman, M.; Belderrain, T. R.; Grubbs, R. H. *Tetrahedron Lett.* **2000**, *41*, 4689–4693.
38. Kamigaito, M.; Ando, T.; Sawamoto, M. *Chem. Rev.* **2001**, *101*, 3689–3745.
39. Ouchi, M.; Terashima, T.; Sawamoto, M. *Acc. Chem. Res.* **2008**, *41*, 1120–1132.
40. Ouchi, M.; Terashima, T.; Sawamoto, M. *Chem. Rev.* **2009**, *109*, 4963–5050.
41. Albrecht, C.; Gauthier, S.; Wolf, J.; Scopelliti, R.; Severin, K. *Eur. J. Inorg. Chem.* **2009**, 1003–1010.

42. Sauvage, X.; Borguet, Y.; Zaragoza, G.; Demonceau, A.; Delaude, L. *Adv. Synth. Catal.* **2009**, *351*, 441–455.
43. Borguet, Y.; Sauvage, X.; Zaragoza, G.; Demonceau, A.; Delaude, L. *Beilstein J. Org. Chem.* **2010**, *6*, 1167–1173.

Chapter 9

Metal-Catalyzed Step-Growth Radical Polymerization of AA and BB Monomers for Monomer Sequence Regulation

Kotaro Satoh, Tomohiro Abe, and Masami Kamigaito*

**Department of Applied Chemistry, Graduate School of Engineering,
Nagoya University, Nagoya 464-8603, Japan
*E-mail: kamigait@apchem.nagoya-u.ac.jp**

Transition metal-catalyzed step-growth radical polymerizations between two α,ω-difunctional monomers were investigated. One of the monomers contained two non-conjugated carbon–carbon double bonds and the other possessed two active carbon–halogen bonds within a single molecule. $FeCl_2/P\textit{n}\text{-}Bu_3$ effectively induced the step-growth radical polymerization of these two bifunctional monomers, which possessed two C=C or C–Cl bonds connected via ester linkages, to produce relatively high-molecular-weight polymers ($M_w > 10{,}000$). By varying the initial feed ratio of the monomers, the end-functionalities were controlled to produce telechelic polyesters with C–Cl or C=C groups at the chain ends. Moreover, polyaddition reactions between the two monomers, into which vinyl monomer units were inset, generated various equivalents of sequence-regulated vinyl copolymers, such as *abbacc*-ordered copolymers, where *a*, *b*, and *c* represent vinyl chloride, styrene, and methyl acrylate, respectively.

Introduction

Metal-catalyzed atom transfer radical addition (ATRA), or the Kharasch reaction, is a highly efficient carbon–carbon bond forming radical reaction ((*1–3*)). Since the discovery of metal-catalyzed living radical polymerizations or atom transfer radical polymerizations (ATRP) in the mid 1990s (*4–8*), this chemistry has been widely applied to the chain-growth radical polymerization of vinyl monomers, which has begun a new era of precision polymer synthesis for a variety of controlled polymers, such as block, graft, and star polymers (Scheme 1A).

More recently, we developed a new class of transition-metal-catalyzed step-growth radical polymerizations or polyaddition using the same catalysts employed in metal-catalyzed chain-growth radical polymerizations (Scheme 1B) (*9*, *10*). The proposed reaction was performed on AB-type monomers possessing a reactive carbon–halogen bond (C–Cl) and an unconjugated carbon–carbon double bond (C=C) within a single molecule, and the reaction proceeded via the activation and deactivation of the carbon–halogen bond. In living chain-growth polymerization reactions, one reactive carbon–halogen bond at the terminus of each polymer chain is reversibly activated to react with the monomer. By contrast, a step-growth reaction occurs between reactive C–Cl and C=C bonds at the termini of monomers, oligomers, or polymers, and propagation is induced by the formation of a carbon–carbon backbone and inactive carbon–halogen pendants (*11*). Our novel polyaddition reaction was applied to synthesize a series of novel linear polymers. In particular, C–C bond forming reactions were combined with chain-growth living radical polymerizations to achieve unprecedented simultaneous chain- and step-growth polymerizations for the production of random copolymers of vinyl polymers and polyesters (*12*, *13*).

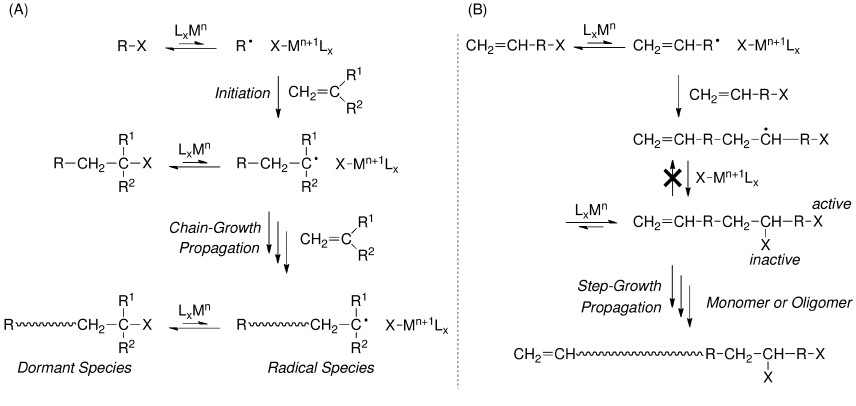

Scheme 1. Polymerizations Based on Metal-Catalyzed Atom Transfer Radical Addition: Chain-Growth or ATRP (A), Step-Growth or Polyaddition (B).

The regulation of monomer sequences in synthetic polymers, which is the holy grail of polymer synthesis, has attracted considerable attention. Natural macromolecules such as proteins and nucleic acids must possess a nearly perfect sequence to induce inherent functions (*14–16*). We developed a novel strategy for the synthesis of sequence-regulated vinyl copolymers via metal-catalyzed step-growth radical polymerization by focusing on the newly formed –CH_2–CHCl– unit, which is equivalent to a poly(vinyl chloride) repeating unit (*17*). A series of well-designed AB-type monomers were prepared from common vinyl monomers and employed in step-growth radical polymerization to produce *abc*- and *abcc*-sequence regulated copolymers with perfect vinyl chloride-styrene-acrylate sequences.

In this paper, we report the metal-catalyzed radical polyaddition of α,ω-difunctional compounds, i.e., AA- and BB-type monomers. One of the monomers possessed two carbon–carbon double bonds and the other contained two carbon–halogen bonds in a single molecule (**A1**–**A3** and **B1**–**B4** in Scheme 2, respectively). The intermolecular reaction yielded various types of linear polymer, including sequence-regulated vinyl copolymers derived from specifically designed monomers with prearranged united sequences.

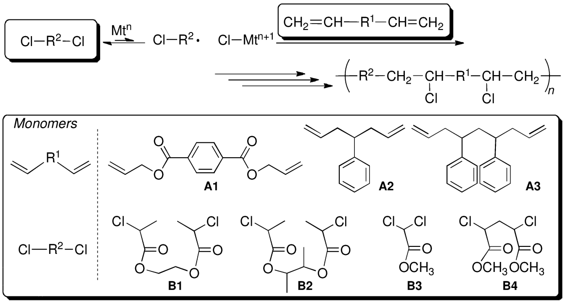

Scheme 2. Metal-Catalyzed Step-Growth Radical Polymerization between α,ω-Divinyl and α,ω-Dichloro Compounds.

Results and Discussion

Metal-Catalyzed Step-Growth Radical Polymerization between Divinyl and Dichloro Compounds

The metal-catalyzed polymerization of α,ω-difunctional ester-linked AA- and BB-type monomers (**A1** and **B1**, respectively) was investigated using $FeCl_2/Pn\text{-}Bu_3$ (*18*, *19*), which is effective for the step-growth polymerization of α,ω-heterofunctional ester-linked AB-type monomers (*9*). Figure 1 shows the conversion (A), number-average molecular weight (M_n) and molecular weight distribution (MWD: M_w/M_n) as a function of C=C bond consumption (B) and size-exclusion chromatography (SEC) curves (C) of the product of the polymerization of **A1** and **B1** with $FeCl_2/Pn\text{-}Bu_3$ in toluene at 100 °C. The consumption of **A1** was determined from the SEC curves, which were measured using a UV detector at 255 nm, while the consumption of C=C bonds in **A1** was monitored by ^{1}H NMR. However, the conversion of C–Cl bonds in **B1** could not be determined due to the overlapping peaks in the ^{1}H NMR spectra. The monomers were smoothly consumed, and the conversion of **A1** reached >90%. However, the conversion of C=C bonds was consistently lower than that of the monomer (Figure 1A). Specifically, at 73% monomer conversion, the C=C bond conversion was nearly half of that of the monomer (~40%). Similar results were obtained in the polymerization of ester-linked AB-type monomers (*12*).

The polymer molecular weight progressively increased in later stages of the polymerization and was close to the calculated values, which were based on the assumption that M_n increases inversely to the content of residual functional groups in step-growth polymerization. In addition, as the polymerization proceeded, the peaks of the SEC curves shifted to a higher molecular weight and the peak areas of the monomer decreased. These results indicate that most of the consumed monomer was converted into dimers during the initial stage of the polymerization and that significant undesirable reactions, such as intramolecular cyclization, did not occur. Subsequently, the reactions between oligomers proceeded in a step-growth manner to produce the polymers.

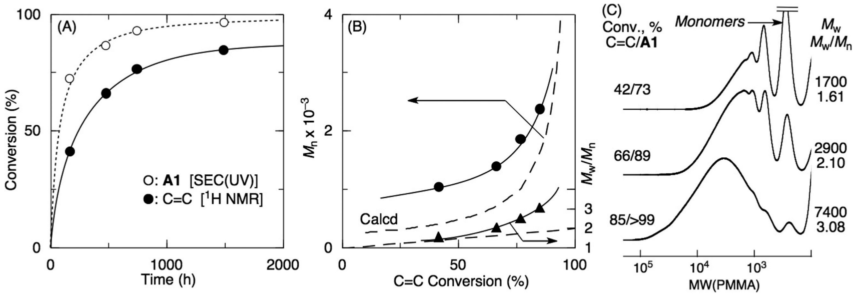

*Figure 1. Metal-catalyzed step-growth radical polymerization between **A1** and **B1** with $FeCl_2/Pn\text{-}Bu_3$: $[\mathbf{A1}]_0 = [\mathbf{B1}]_0 = 1.0$ M; $[FeCl_2]_0 = 100$ mM; $[Pn\text{-}Bu_3]_0 = 200$ mM in toluene at 100 °C.*

To identify the optimal conditions for the intermolecular polyaddition of **A1** and **B1**, copolymerization was investigated with a series of catalysts under various conditions (Table I). Although the monomer concentration ($[M]_{total} = 4.0$ M) did not affect the polymerization rate or the molecular weight of the products, an increase in the catalyst loading ($[FeCl_2]_0 = 200$ mM) accelerated the polymerization, leading to a high-molecular-weight polymer (M_w>10,000). In addition, the polymerization proceeded more rapidly at higher temperatures (120 °C). Similar to the polymerization of AB-type monomers, the addition of tin 2-ethylhexanoate [$Sn(EH)_2$] accelerated the polymerization of **A1** and **B1** in the $FeCl_2$/P*n*-Bu_3 system, in which the tin additive may act as a reducing agent for the oxidized Fe-species (*20*). This result suggests that a small amount of the metal catalyst was deactivated during the reaction and that the polymerization can be enhanced by reducing agents. In addition, other metal catalysts based on CuCl and multidentate amine ligands, such as *N*,*N*,*N*′,*N*″,*N*″-pentamethyldiethylene-triamine (PMDETA) and tris[2-(dimethylamino)ethyl]amine (Me_6TREN), were also examined in place of $FeCl_2$/P*n*-Bu_3 in the AA and BB polymerization (*21*, *22*). Cu-based systems were also effective for the polymerization of **A1** and **B1**; however, the polymerization was less well controlled and yielded lower C=C conversion rates and lower molecular weight polymers compared with using $FeCl_2$/P*n*-Bu_3.

Table I. Radical Polyaddition of A1 and B1 under Various Conditions[a]

System	*Temp. (°C)*	*Time (h)*	*C=C Conv. (%)*	M_n	M_w	M_w/M_n
$FeCl_2$/P*n*-Bu_3 [b]	100	1490	85	2400	7400	3.08
$FeCl_2$/P*n*-Bu_3 ($[FeCl_2]_0$ = 200 mM)	100	1030	86	2500	12000	4.78
$FeCl_2$/P*n*-Bu_3 ($[M]_{total}$ = 4.0 M) [b]	100	1200	88	2300	7700	3.29
$FeCl_2$/P*n*-Bu_3 [b]	120	240	88	2600	8100	3.11
$FeCl_2$/P*n*-Bu_3/Sn$(EH)_2$ [b,c]	100	216	87	2500	6300	2.57
$FeCl_2$/PCy_3 [b]	100	1900	64	1500	3000	2.00
$FeCl_2$/PPh_3 [b]	100	1900	46	950	1600	1.68
CuCl/PMDETA [d]	100	720	97	1600	5900	3.74
CuCl/PMDETA [d]	60	1990	46	1200	2100	1.79
CuCl/Me_6TREN [d]	60	1600	68	930	1500	1.61

[a] $[\mathbf{A1}]_0 = [\mathbf{B1}]_0$ = 1.0 M ($[M]_{total}$ = 2.0 M) in toluene. [b] $[FeCl_2]_0$ = 100 mM, [phosphine ligand]$_0$ = 200 mM. [c] $[Sn(EH)_2]_0$ = 45 mM. [d] $[CuCl]_0$ = 100 mM, [amine ligand]$_0$ = 400 mM.

A more detailed mechanism of the polymerization was determined using a combination of **A1** and **B2**, which allowed the total consumption of C=C and C–Cl groups in the monomer and polymerized products to be measured by ^{1}H NMR. The polyaddition of **A1** and **B2** was performed with $FeCl_2/PBu_3$ or CuCl/PMDETA in toluene. Figure 2 shows the consumption curves of the two functional groups, which were determined by ^{1}H NMR, along with those of **A1**, which were obtained using the SEC curves of the reaction mixture. Irrespective of the catalyst, the two functional groups were consumed simultaneously to afford the polymer. Although the molecular weights of the products were slightly lower than those obtained from **A1** and **B1**, the peak of the SEC curves shifted to a higher molecular weight. These results indicate that the polymer was generated via step-growth polymerization and continual ATRA between C–Cl and C=C bonds originating from the monomers.

The polyesters obtained from the combination of **A1** and **B1** or **B2** using $FeCl_2$/P*n*-Bu_3 were purified by preparative SEC to remove residual monomer and catalyst and analyzed by ^{1}H NMR (Figure 3). In the polymer spectra, a series of broad and relatively large peaks (***1***–***8***) were observed, which were assigned to the main-chain protons of the repeating units of the expected polyesters. The integral ratio of peaks originating from the α,ω-diene (***4***) and the dichloride (***6***) indicates that an equimolar amount of the two compounds was incorporated into the polymer via radical polyaddition. In addition to these signals, small peaks corresponding to double bonds (***a***–***c***) and reactive C–Cl bonds (***d*** and ***e***) at the chain ends were observed. These results indicate that the polymers were generated via the expected radical polyaddition reaction and that the chain end structures contained C–Cl or C=C bonds with equal probability. The thermal properties of the polyesters were also evaluated by differential scanning calorimetry (DSC). The glass transition temperatures (T_g) were relatively low (T_g = –8.5 °C [for **A1** and **B1**, M_n = 5400] and –7.6 °C [for **A1** and **B2**, M_n = 3500], respectively), and the melting points were not observed for both polymers, likely due to their low molecular weights, indicating that the products were amorphous polyesters.

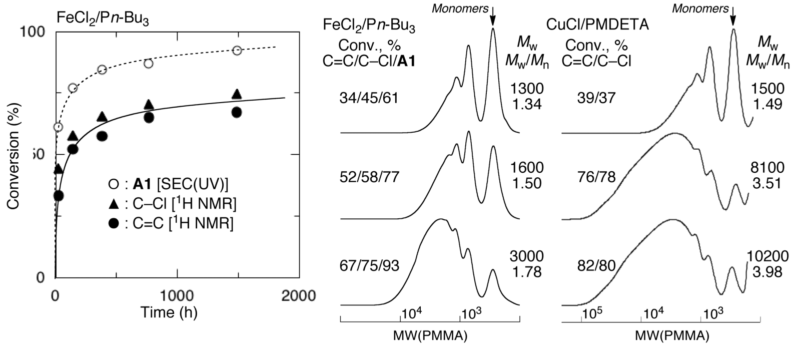

*Figure 2. Metal-catalyzed step-growth radical polymerization **A1** and **B2**: $[\textbf{A1}]_0 = [\textbf{B2}]_0$ = 1.0 M; $[FeCl_2$ or $CuCl]_0$ = 100 mM; $[Pn\text{-}Bu_3]_0$ = 200 mM; $[PMDETA]_0$ = 400 mM in toluene at 100 °C (for Fe) or 60 °C (for Cu).*

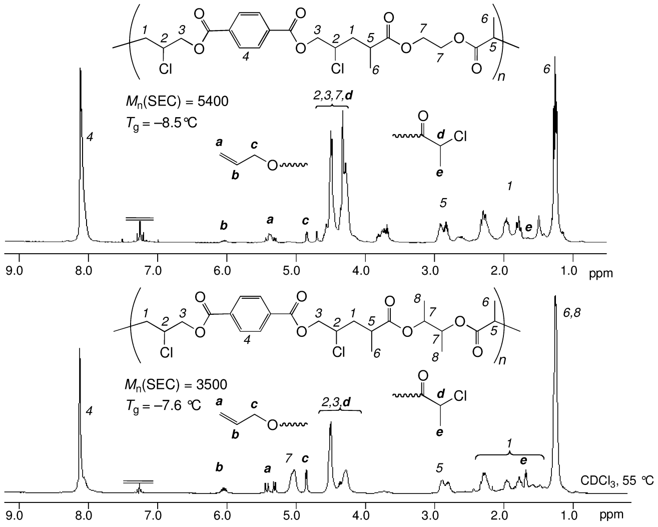

*Figure 3. ^1H NMR spectra ($CDCl_3$, r.t.) of the polymers obtained from **A1** and **B1** or **B2** with with $FeCl_2/Pn\text{-}Bu_3$.*

Synthesis of Homo-Telechelic Polymers by Step-Growth Radical Polymerization

Using a non-equivalent initial amount of AA and BB monomers, the proposed step-growth process can be used to produce homo-telechelic polymers, i.e., polymers with identical α- and ω-functional chain ends. For the synthesis of homo-telechelic polymers, the step-growth polymerization of **A1** and **B2** with $FeCl_2$/P*n*-Bu_3 in the presence of $Sn(EH)_2$ was examined by changing the initial feed ratio of the monomers ($[\mathbf{A1}]_0/[\mathbf{B2}]_0$ ratios of 4/1, 3/2, 1/1, 2/3, and 1/4 (Figure 4)). The reactions proceeded in all cases, even when non-equimolar feed ratios of the monomers were employed. Under these conditions, the conversion of functional groups reached the theoretical values. With an excess amount of **A1** ($[\mathbf{A1}]_0/[\mathbf{B2}]_0$ = 4/1 or 3/2), the consumption of C–Cl reached almost quantitative conversion, whereas that of C=C plateaued at approximately 25% and 66%, respectively, and vice versa. The highest polymer molecular weight was obtained when the initial monomer ratio was 1:1. These results also indicate that the polymerization proceeded in a step-growth manner via a 1:1 reaction between C–Cl and C=C bonds and that the terminal structure was dominated by the monomer with the highest content in the initial feed.

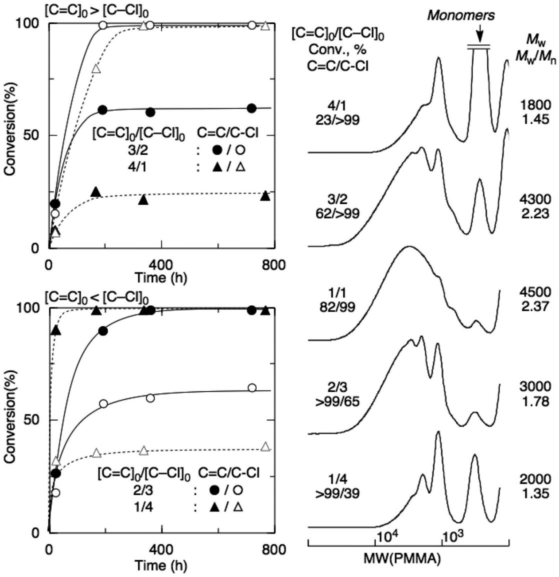

*Figure 4. Metal-catalyzed step-growth radical polymerization **A1** and **B2**: : $[\mathbf{A1}]_0 + [\mathbf{B2}]_0$ = 2.0 M; $[FeCl_2]_0$ = 100 mM; $[Pn\text{-}Bu_3]_0$ = 200 mM; $[Sn(EH)_2]_0$ = 45 mM in toluene at 100 °C.*

^{1}H NMR analyses of the products isolated by preparative SEC clearly showed the formation of homo-telechelic polymers (Figure 5). Polymers obtained from an equimolar amount of **A1** and **B2** exhibited the characteristic peaks of C=C (***a–c***) and C–Cl termini (***d*** and ***e***) (A). By contrast, at different initial feed ratios ($[\mathbf{A1}]_0/[\mathbf{B2}]_0$ = 3/2 and 2/3), only one structure was predominant at the termini of the polymers (B and C). Namely, α,ω-divinyl polymers were produced at $[C{=}C]_0 > [C{-}Cl]_0$, and vice versa.

Thus, the polymerization proceeded via a controlled process to produce a homo-telechelic polymer bearing well-defined α,ω-difunctionalized termini, and significant side reactions did not occur. Terminal C–Cl and C=C functionalities can be further utilized for various reactions such as transition-metal-catalyzed living radical polymerization (for C–Cl) and metathesis or thiol-ene reactions (for C=C), respectively.

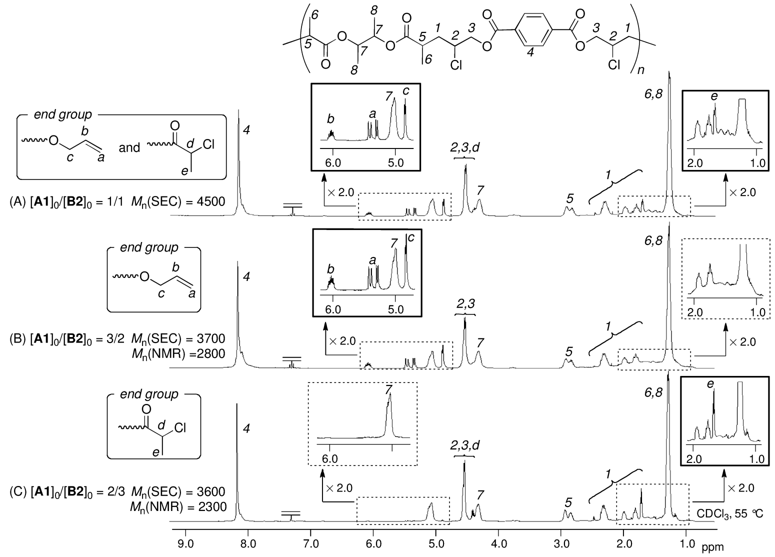

*Figure 5. ^{1}H NMR spectra ($CDCl_3$, r.t.) of the polymers obtained from **A1** and **B2** in the same experiments as for Figure 4.*

Sequence-Regulated Vinyl Copolymers from AA and BB Monomers

Step-growth radical polymerization is accompanied by the formation of a $-CH_2-CHCl-$ unit, which is equivalent to a poly(vinyl chloride) repeating unit. As a result, sequence-regulated vinyl copolymers were synthesized via the metal-catalyzed radical polyaddition of AB-type monomers, which was prepared from common vinyl monomers as building blocks (*17*). Here, α,ω-difunctional AA- and BB-type monomers (**A2**, **A3**, **B3**, and **B4**) were also designed to create novel families of sequence-regulated vinyl copolymers via intermolecular step-growth radical polymerization. The AA- and BB-type monomers were polymerized using Fe- and Cu-based systems under various conditions. Although appropriate conditions that enabled the synthesis of high-molecular-weight polymers with quantitative monomer conversions were not fully optimized, polymeric products were obtained using the CuCl/Me_6TREN system. Figure 6 shows the ^{1}H NMR spectra of the products after purification by preparative SEC (M_n = 630 [for **A2** and **B3**], 880 [for **A2** and **B4**], and 4100 [for **A3** and **B4**], respectively), in which the characteristic peaks of the main chain protons of styrene, methyl acrylate, and vinyl chloride repeating units were observed. Specifically, the polymerization of **A3** and **B4** resulted in the formation of a complex *abbacc*-sequenced copolymer, where *a*, *b*, and *c* represent vinyl chloride, styrene, and methyl acrylate, respectively. Thus, by designing and combining various monomers, the proposed metal-catalyzed radical polyaddition reaction can be used to produce complicated sequence-regulated vinyl copolymers.

Conclusions

In conclusion, metal-catalyzed radical step-growth polymerization of AA- and BB-type monomers was successfully performed to produce novel polymer structures including various polyesters and sequence-regulated vinyl copolymers. The proposed method produces synthetic vinyl polymers possessing periodically located functional groups, which leads to vinyl polymers with a highly ordered structure.

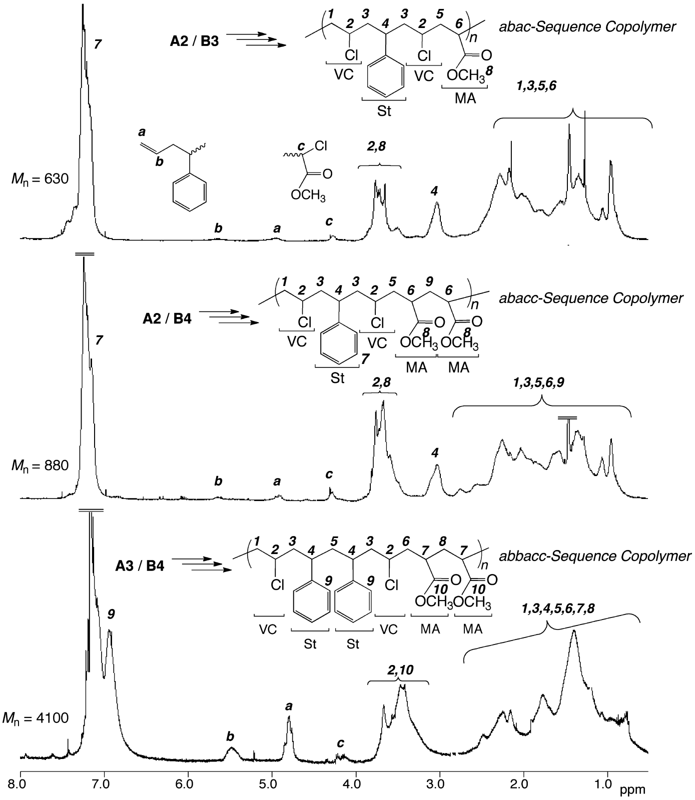

*Figure 6. ^{1}H NMR spectra ($CDCl_3$, r.t.) of the sequence-regulated polymers obtained by metal-catalyzed step-growth raidcal polymerization between **A2** or **A3** and **B3** or **B4** with CuCl/Me_6TREN: [AA monomer]$_0$ = [BB monomer]$_0$ = 2.0 (for **A2/B3** and **A2/B4**) or 1.0 M (for **A3/B4**); [CuCl]$_0$ = 100 mM; [Me_6TREN]$_0$ = 400 mM in toluene at 60 (for **A2/B3** and **A2/B4**) or 100 °C (for **A3/B4**).*

Experimental

Materials

Methyl acrylate (Tokyo Kasei, >99%) and styrene (Wako Chemicals, >98%) were distilled from calcium hydride under reduced pressure before use. $FeCl_2$ (Aldrich, 99.99%), CuCl (Aldrich, 99.99%), and $RuCl_2(PPh_3)_3$ (Aldrich, 97%), were used as received. All metal compounds were handled in a glove box (VAC Nexus) under a moisture- and oxygen-free argon atmosphere (O_2, <1 ppm). Toluene was distilled over sodium benzophenone ketyl and bubbled with dry nitrogen over 15 minutes just before use. P*n*-Bu_3 (KANTO, >98%), PCy_3 (KANTO, >97%), PPh_3 (KANTO, >98%), and $Sn(EH)_2$ (Aldrich, ~95%) were used as received. PMDETA and Me_6TREN were distilled from calcium hydride before use.

Synthesis of Monomers

Diallyl terephthalate (**A1**), ethylene bis(2-chloropropanoate) (**B1**), dimethylethylene bis(2-chloropropanoate) (**B2**) were synthesized from the corresponding acid chlorides and alcohols; i.e. terephthaloyl chloride (Tokyo Kasei; >99%) and allyl alcohol (Tokyo Kasei; > 99%) (for **A1**), 2-chloropropionyl chloride (Aldrich; > 97%) and ethylene glycol (Tokyo Kasei; > 99.5%) or 2,3-butanediol (Tokyo Kasei; > 97%, mixture of stereoisomers) (for **B1** and **B2**, respectively), and purified by distillation. Diallyl toluene (**A2**) was prepared by the reaction of benzal chloride (Tokyo Kasei; > 95%) and allylmagnesium bromide (Aldrich; 2.0 M in THF) and purified by distillation. A diallyl styrene dimer (**A3**) was prepared by $RuCl_2(PPh_3)_3$-catalyzed Kharasch addition between benzal chloride and styrene followed by $TiCl_4$-catalyzed allylation of the C–Cl bond adjacent to the styrene unit with allyltrimethylsilane (Tokyo Kasei; > 98%) (*23*) and purified by column chromatography on silica gel and distillation. Methyl dichloroacetate (**B3**) was distilled from calcium hydride before use. A dichloro MA dimer (**B4**) was prepared by the ruthenium-catalyzed Kharasch addition between **B3** with methyl acrylate and purified by column chromatography on silica gel and distillation.

Metal-Catalyzed Radical Polyaddition of AA- and BB-Type Monomers

Polymerization was carried out under dry nitrogen in baked glass tubes equipped with a three-way stopcock. A typical example for the polymerization is given below. A mixture of $FeCl_2$ (50.7 mg, 0.40 mmol) and P*n*-Bu_3 (0.20 mL, 0.80 mmol) in toluene (2.54 mL) was stirred for 24 h at 80 °C to give a homogeneous solution of $FeCl_2$(P*n*-Bu_3)$_2$ complex. After the solution was cooled to room temperature, **A1** (8.0 mmol) and **B1** (8.0 mmol) were added. The solution was evenly charged in seven glass tubes, and the tubes were sealed by flame under a nitrogen atmosphere. The tubes were immersed in thermostatic oil bath at 100 °C. In predetermined intervals, the polymerization was terminated by cooling the reaction mixtures to –78 °C. The conversion of **A1** was determined from the concentration of residual monomer measured by SEC using UV detector operating at 254 nm (1490 h, 97%). The quenched reaction mixture was diluted with toluene (30 mL), washed with dilute citric acid and water to remove complex residues, evaporated to dryness under reduced pressure, and vacuum-dried to give the product polymers (M_n = 2400, M_w = 7400, M_w/M_n = 3.08).

Measurements

^{1}H NMR spectra were recorded in $CDCl_3$ at room temperature on a JEOL ESC-400 spectrometer, operating at 400 MHz. Conversion of **A1**, number-average molecular weight (M_n), weight-average molecular weight (M_w), and molecular weight distribution (M_w/M_n) of the product polymers were determined by SEC in THF at 40 °C on two polystyrene gel columns [Shodex K-805L (pore size: 20–1000 Å; 8.0 mm i.d. × 30 cm) × 2; flow rate 1.0 mL/min] connected to a Jasco PU-980 precision pump, a Jasco 970-UV detector, and a Jasco 930-RI detector. The columns were calibrated against eight standard poly(MMA) samples (Shodex; M_p = 202–1,950,000; M_w/M_n = 1.02–1.09). Glass transition temperature (T_g) of the polymers were recorded on Q200 differential scanning calorimetry (TA Instruments Inc.). Samples were first heated to 100 or 150 °C at 10 °C/min., equilibrated at this temperature for 0 or 10 min, and cooled to –100 °C at 10 °C/min. After being held at this temperature for 20 min, the samples were then reheated to 200 °C at 10 °C/min. All T_g values were obtained from the second scan, after removing the thermal history.

Acknowledgments

This work was supported in part by a Grant-in-Aid for Young Scientists (S) (No. 19675003) by the Japan Society for the Promotion of Science, a Grant-in-Aid for Scientific Research (No. 23107515) on the Innovative Areas: “Fusion Materials” (Area no. 2206) from the Ministry of Education, Culture, Sports, Science and Technology, Japan, and the Global COE Program “Elucidation and Design of Materials and Molecular Functions.”

References

1. Kharasch, M. S.; Jensen, E. V.; Urry, W. H. *Science* **1945**, *102*, 128.
2. Minisci, F. *Acc. Chem. Res.* **1975**, *8*, 165–171.
3. Iqbal, J. P.; Bhatia, B.; Nayyar, N. K. *Chem. Rev.* **1994**, *94*, 519–564.
4. Kato, M.; Kamigaito, M.; Sawamoto, M.; Higashimura, T. *Macromolecules* **1995**, *28*, 1721–1723.
5. Wang, J.-S.; Matyjaszewski, K. *J. Am. Chem. Soc.* **1995**, *117*, 5614–5615.
6. Percec, V.; Barboiu, B. *Macromolecules* **1995**, *28*, 7970–7972.
7. Granel, C.; Dubois, P.; Jérôme, R.; Teyssié, P. *Macromolecules* **1996**, *29*, 8576–8582.
8. Haddleton, D. M.; Jasieczek, C. B.; Hannon, M. J.; Shooter, A. J. *Macromolecules* **1997**, *30*, 2190–2193.
9. Satoh, K.; Mizutani, M.; Kamigaito, M. *Chem. Commun.* **2007**, 1260–1262.

10. Mizutani, M.; Satoh, K.; Kamigaito, M. *Macromolecules* **2009**, *42*, 472–480.
11. Coessens, V.; Pyun, J.; Miller, P. J.; Gaynor, S. G.; Matyjaszewski, K. *Macromol. Rapid Commun.* **2000**, *21*, 103–109.
12. Mizutani, M.; Satoh, K.; Kamigaito, M. *J. Am. Chem. Soc.* **2010**, *132*, 7498–7507.
13. Mizutani, M.; Satoh, K.; Kamigaito, M. *Macromolecules* **2011**, *44*, 2382–2386.
14. Lutz, J. F. *Nat. Chem.* **2010**, *2*, 84–85.
15. Lutz, J. F. *Polym. Chem.* **2010**, *1*, 55–62.
16. Ouchi, M.; Badi, N.; Lutz, J. F.; Sawamoto, M. *Nat. Chem.* **2011**, *3*, 917–924.
17. Satoh, K.; Ozawa, S.; Mizutani, M.; Nagai, K.; Kamigaito, M. *Nat. Commun.* **2010**, *1*, 6.
18. Ando, T.; Kamigaito, M.; Sawamoto, M. *Macromolecules* **1997**, *30*, 4507–4510.
19. Matyjaszewski, K.; Wei, M.; Xia, J.; McDermott, N. E. *Macromolecules* **1997**, *30*, 8161–8164.
20. Jakubowski, W.; Matyjaszewski, K. *Macromolecules* **2005**, *38*, 4139–4146.
21. Xia, J.; Matyjaszewski, K. *Macromolecules* **1997**, *30*, 7697–7700.
22. Queffelec, J.; Gaynor, S. G.; Matyjaszewski, K. *Macromolecules* **2000**, *33*, 8629–8639.
23. Dau-Schmidt, J.-P.; Mayr, H. *Chem. Ber.* **1994**, *127*, 205–212.

Downloaded by UNIV OF GUELPH LIBRARY on May 31, 2012 | http://pubs.acs.org
Publication Date (Web): March 20, 2012 | doi: 10.1021/bk-2012-1100.ch010

Chapter 10

Tuning Polymer Properties through Competitive Processes

**Dominik Konkolewicz,*,1 Dagmar R. D'hooge,1,2
Stanislaw Sosnowski,3 Ryszard Szymanski,3
Marie-Françoise Reyniers,2 Guy B. Marin,2
and Krzysztof Matyjaszewski*,1**

**[1]Center for Macromolecular Engineering, Department of
Chemistry, Carnegie Mellon University, 4400 Fifth Avenue,
Pittsburgh, Pennsylvania 15213, USA
[2]Laboratory for Chemical Technology, Ghent University,
Krijgslaan 281 (S5), Gent, Belgium
[3]Center of Molecular and Macromolecular Studies,
Polish Academy of Sciences, Sienkiewicza 112,
90-363 Lodz, Poland
*E-mails: dominikk@andrew.cmu.edu (D.K.),
km3b@andrew.cmu.edu (K.M.)**

Competitive processes in controlled/living radical polymerization (CRP) are explored. Such processes occur in CRPs with two or more related small molecules or polymers that undergo activation, deactivation, and transformation reactions. For the CRP of acrylates and initiators for continuous activator regeneration atom transfer radical polymerization (ICAR ATRP), the polymer properties can be tuned by understanding competitive processes. In the CRP of acrylates, low branching levels require efficient deactivation, with low target chain lengths promotoing low branch levels. For ICAR ATRP, ATRP equilibrium in macromolecules must be established at low conversion for well-controlled polymers.

In Progress in Controlled Radical Polymerization: Mechanisms and Techniques; Matyjaszewski, K., et al.;
ACS Symposium Series; American Chemical Society: Washington, DC, 2012.

Downloaded by UNIV OF GUELPH LIBRARY on May 31, 2012 | http://pubs.acs.org
Publication Date (Web): March 20, 2012 | doi: 10.1021/bk-2012-1100.ch010

Introduction

Controlled/living radical polymerization (CRP) techniques have made a significant impact on the fields of polymer chemistry and materials science (*1*) since they can be used to synthesize polymers of predefined molecular weights and architecture through a free-radical mechanism (*1*, *2*). These CRP techniques offer similar control over molecular structure and architecture to traditional ionic polymerization, with the tolerance to functional groups and reaction conditions typical of free radical polymerization (FRP) (*3*). A wide variety of CRP techniques have been developed to date, including nitroxide mediated polymerization (NMP) (*4*, *5*), atom transfer radical polymerization (ATRP) (*6*–*8*), and reversible addition-fragmentation chain transfer (RAFT) polymerization (*3*, *9*, *10*).

In CRP, control over the polymer architecture is provided by the reversible deactivation of a propagating radical, which is the active species, to form a dormant species. This dormant, or capped, species is subsequently activated to reform the propagating radical, before returning to the dormant form after a few propagation steps (*1*, *2*). This leads, under ideal conditions, to the establishment of an equilibrium between the active and dormant species. Examples of the active dormant equilibria for NMP, ATRP and RAFT polymerization are shown in Scheme 1.

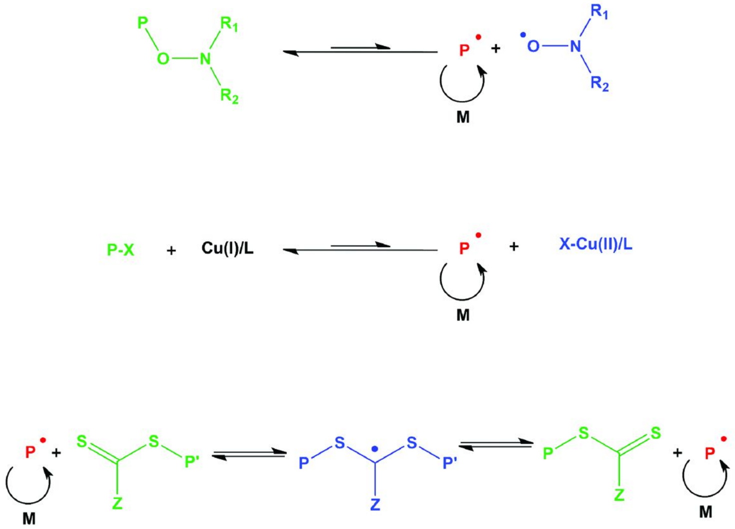

Scheme 1. The equilibrium between dormant (green) and active (red) species; top: NMP, middle: ATRP, bottom: RAFT polymerization.

In general, there are multiple distinct radical/dormant pairs involved in a CRP process. Each radical/dormant pair is subject not only to an activation-deactivation process but also to competing reactions that lead to an interchange between these distinct radical/dormant pairs. The presence of such interrelated or competitive radical/dormant pairs, can influence the balancing of the reaction rates and, hence, offers a handle to tune the properties of the resulting polymer by selecting the appropriate controlling agent and/or reaction conditions (*11*).

A simplified CRP model process subject to competitive equilibria and interconversions is shown in Scheme 2 and consists of only two radical/dormant pairs (P_A/P_AX and P_B/P_BX). When a macroradical of type A (P_A) interchanges to an active macroradical of type B (P_B) there are two competing fates. Either P_B becomes deactivated to form its dormant counterpart (P_BX), or it undergoes the transformation to reform P_A. The deactivation of P_B can induce a significant delay in the balancing of the two-way interconversions of P_A and P_B, whereas the conversion of P_B to P_A can significantly delay the establishment of an active dormant equilibrium in species of type B. Similarly, a competition exists when P_B changes to form P_A. It is worth noting that the general Scheme 2 and the concept of balancing of competitive processes can also be applied to CRP copolymerization processes (*12*, *13*).

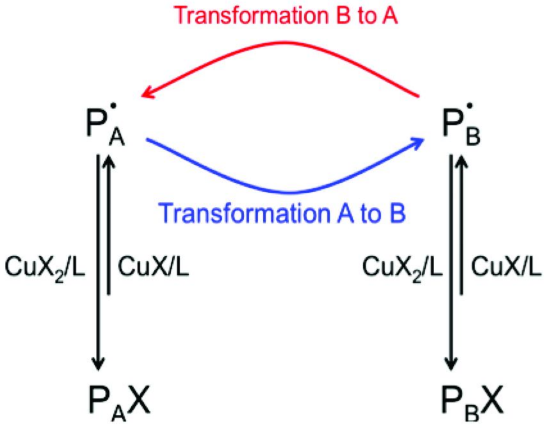

Scheme 2. Simplified CRP model process subject to competitive equilibria and interconversions; both activation-deactivation reactions involving species of type A and B, and transformations between species A and B are included.

In this chapter, the effect of competitive processes/equilibria on the control over polymer properties is first illustrated for the CRP of acrylates. Since the early work of Lovell et al. (*14*), active polyacrylate chains have been well-known to undergo transfer reactions, leading to the formation of tertiary mid-chain radicals in addition to the ‘regular’ secondary end-chain radicals (*15*). Upon propagation, these tertiary radicals result in quaternary carbons, or branch points, along the polymer backbone. Scheme 3 shows the transfer and branching in the CRP of acrylates, where ATRP is selected as the CRP technique. The transfer reactions in this scheme can be either intramolecular, typically occurring through a six-membered transition state, leading to short chain branches after monomer addition to the tertiary radical formed, i.e., tertiary propagation (*15*). This transfer process is also referred to as backbiting. Alternatively, the secondary radical from one active polymer chain can be transferred to a second chain, typically leading to a long

Downloaded by UNIV OF GUELPH LIBRARY on May 31, 2012 | http://pubs.acs.org
Publication Date (Web): March 20, 2012 | doi: 10.1021/bk-2012-1100.ch010

chain branch after tertiary propagation (*15*). However, as highlighted by Charleux et al. (*16*) the intramolecular transfer typically dominates the intermolecular one.

In general, branching alters the properties of the polymeric material, such as its viscosity and degree of crystallinity (*17*, *18*). Recently, Lovell et al. (*19*) found that CRP processes, most notably ATRP, reduce the branching fraction, or number of branch points per repeat unit, when compared to FRP. This result was first unexpected, since the radical formed in CRP has the same properties as the radical formed in FRP, and should undergo the same reactions, but was subsequently confirmed by direct atomic force microscopy (AFM) imaging of molecular brushes with backbones synthesized by either FRP or ATRP (*20*). Since branches can alter the properties of the resulting material, it is important to understand the origin of this decreased tendency for branching in CRP.

Initially, the reduction in branching was attributed to a strong chain-length dependence of the (intramolecular) transfer rate coefficient; oligomeric radicals were proposed to undergo transfer reactions more rapidly (*19*). Since in CRP, contrary to FRP, no oligomeric radicals are present at moderate conversions the reduction of branching in CRP could thus be explained (*19*). However, Reyes and Asua subsequently used kinetic Monte-Carlo (kMC) simulations to show that chain-length dependence alone cannot explain the decrease in branching in CRP compared to FRP (*21*). These authors proposed that the decrease in branching fraction occurs if the average time needed for the transfer reaction to occur, is higher than the transient radical lifetime (*21*). However, recent deterministic and kMC simulations starting from the concept of competitive processes showed that not only deactivation needs to be considered but that also the reverse activation is of importance (*11*). In the first part of this chapter, it will be shown that the branching content in polyacrylates can be altered from the free-radical limit to almost zero. Based on the understanding of the kinetics of the competitive processes presented in Scheme 3, the reaction conditions and controlling agent can be adjusted to cover a desired range of branching fractions.

Furthermore, to demonstrate the general nature of the concept of competitive processes, one of the more recently developed ATRP processes, namely initiators for continuous activator regeneration (ICAR) ATRP, is studied in light of these competitive processes (*22*). In this modified ATRP process, a conventional radical initiator is used to continuously regenerate the activator species needed for ATRP, from the deactivator species, which are formed by unavoidable radical termination reactions. In this way, low catalyst concentrations can be used with ICAR ATRP, often less than 100 ppm with respect to monomer (*22*).

In general, there are three different radical/dormant pairs in ICAR ATRP, as shown in Scheme 4: the ATRP initiator radicals, and their equivalent dormant species, the radicals derived from the conventional radical initiator, and their equivalent dormant species, as well as the macroinitiators and macroradicals. In addition, there are propagation reactions that form the macroradicals from the ATRP initiator radicals and the conventional initiator derived radicals. The second part of the chapter will show that to have good control over the polymer properties, i.e., to obtain both narrow molecular weight distributions and high end-group functionality, it is important to select reaction conditions that establish the ATRP equilibrium in the macromolecular species at low conversion.

Downloaded by UNIV OF GUELPH LIBRARY on May 31, 2012 | http://pubs.acs.org
Publication Date (Web): March 20, 2012 | doi: 10.1021/bk-2012-1100.ch010

Downloaded by UNIV OF GUELPH LIBRARY on May 31, 2012 | http://pubs.acs.org
Publication Date (Web): March 20, 2012 | doi: 10.1021/bk-2012-1100.ch010

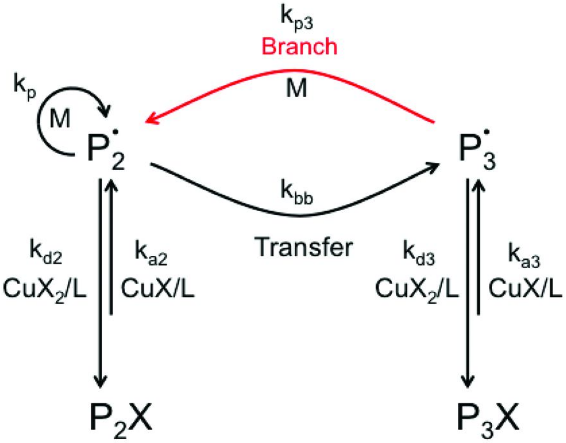
k_{p3}
Branch
M
k_p
M
$P_2^\bullet$
$P_3^\bullet$
k_{bb}
Transfer
k_{d2}
CuX_2/L
k_{a2}
CuX/L
k_{d3}
CuX_2/L
k_{a3}
CuX/L
P_2X
P_3X

Scheme 3. The ATRP of acrylates described in terms of competitive processes with P_2 referring to the secondary species, and P_3 referring to the tertiary species. Considered processes: activation-deactivation reactions for both secondary and tertiary species, as well as the intramolecular transfer reaction, which transforms a secondary to a tertiary radical, and the tertiary propagation reaction, which reforms the secondary radical; termination reactions not shown and intermolecular transfer neglected as indicated in text.

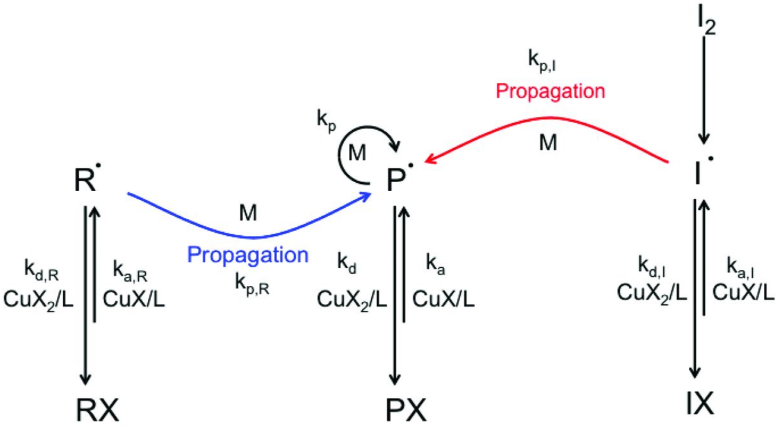
I_2
$k_{p,I}$
Propagation
M
k_p
M
$R^\bullet$
$P^\bullet$
$I^\bullet$
M
Propagation
$k_{p,R}$
$k_{d,R}$
CuX_2/L
$k_{a,R}$
CuX/L
k_d
CuX_2/L
k_a
CuX/L
$k_{d,I}$
CuX_2/L
$k_{a,I}$
CuX/L
RX
PX
IX

Scheme 4. The ICAR ATRP process described in terms of competitive processes. In this case R refers to the ATRP initiator derived species, P refers to the macromolecular species, and I refers to the conventional initiator derived species. All species undergo activation-deactivation reactions, and both small molecule species change into the macromolecular species by propagation; termination reactions not shown.

Kinetic Model

CRP/FRP of Acrylates

The following reaction scheme was implemented in the PREDICI® (v6.3.2) software package and used for the kMC simulations to study branching in the bulk ATRP of acrylates (Table 1):

Table 1. Reaction scheme used to study branching in the ATRP of acrylates

$$\mathrm{RX} + \mathrm{CuX} \xrightarrow{k_a} \mathrm{R}^{\bullet} + \mathrm{CuX_2} \tag{1}$$

$$\mathrm{R}^{\bullet} + \mathrm{CuX_2} \xrightarrow{k_d} \mathrm{RX} + \mathrm{CuX} \tag{2}$$

$$\mathrm{R}^{\bullet} + \mathrm{M} \xrightarrow{k_p} \mathrm{P}(1)^{\bullet} \tag{3}$$

$$\mathrm{P}(j)^{\bullet} + \mathrm{M} \xrightarrow{k_p} \mathrm{P}(j+1)^{\bullet} \tag{4}$$

$$\mathrm{P}(j)^{\bullet} + \mathrm{CuX_2} \xrightarrow{k_d} \mathrm{P}(j)\mathrm{X} + \mathrm{CuX} \tag{5}$$

$$\mathrm{P}(j)\mathrm{X} + \mathrm{CuX} \xrightarrow{k_a} \mathrm{P}(j)^{\bullet} + \mathrm{CuX_2} \tag{6}$$

$$\mathrm{P}(j)^{\bullet} \xrightarrow{k_{bb}} \mathrm{P_3}(j)^{\bullet} \tag{7}$$

$$\mathrm{P_3}(j)^{\bullet} + \mathrm{CuX_2} \xrightarrow{k_{d3}} \mathrm{P_3}(j)\mathrm{X} + \mathrm{CuX} \tag{8}$$

$$\mathrm{P_3}(j)\mathrm{X} + \mathrm{CuX} \xrightarrow{k_{a3}} \mathrm{P_3}(j)^{\bullet} + \mathrm{CuX_2} \tag{9}$$

$$\mathrm{P_3}(j)^{\bullet} + \mathrm{M} \xrightarrow{k_{p3}} \mathrm{P}(j+1)^{\bullet} \tag{10}$$

$$\mathrm{R}^{\bullet} + \mathrm{R}^{\bullet} \xrightarrow{k_{t0}} \mathrm{D} \tag{11}$$

Continued on next page.

Downloaded by UNIV OF GUELPH LIBRARY on May 31, 2012 | http://pubs.acs.org
Publication Date (Web): March 20, 2012 | doi: 10.1021/bk-2012-1100.ch010

Downloaded by UNIV OF GUELPH LIBRARY on May 31, 2012 | http://pubs.acs.org
Publication Date (Web): March 20, 2012 | doi: 10.1021/bk-2012-1100.ch010

Table 1. (Continued). Reaction scheme used to study branching in the ATRP of acrylates

$$P(j)^{\bullet} + R^{\bullet} \xrightarrow{k_{t0}} D(j) \qquad (12)$$

$$P(j)^{\bullet} + P(k)^{\bullet} \xrightarrow{k_t} D(j+k) \qquad (13)$$

$$P_3(k)^{\bullet} + R^{\bullet} \xrightarrow{k_{t0}} D(j) \qquad (14)$$

$$P(j)^{\bullet} + P_3(k)^{\bullet} \xrightarrow{k_t} D(j+k) \qquad (15)$$

$$P_3(j)^{\bullet} + P_3(k)^{\bullet} \xrightarrow{k_t} D(j+k) \qquad (16)$$

Here, R represents the ATRP initiator radical, RX the ATRP initiator, CuX the activator complex, CuX_2 the deactivator complex, M the monomer, P(j) a secondary macroradical containing j monomer units, $P_3(j)$ a tertiary macroradical containing j monomer units, P(j)X the secondary dormant species containing j monomer units, $P_3(j)X$ the tertiary dormant species containing j monomer units, and D(j) a dead species containing j monomer units. Furthermore, k_a and k_d are the ATRP activation and deactivation rate coefficients for secondary species, k_p is the secondary propagation rate coefficient, k_{bb} is the intramolecular transfer (or backbiting) rate coefficient, k_{a3} and k_{d3} are the ATRP activation and deactivation rate coefficients for tertiary species, k_{p3} is the tertiary propagation rate coefficient, k_{t0} is the termination rate coefficient for two small molecule radicals or a small molecule radical and a macroradical, and k_t is the termination rate coefficient for two macroradicals.

The branching fraction is calculated by two related approaches. The first is the instantaneous branching fraction, $f_{\mathrm{br,i}}$, which measures the rate at which branches are being formed at a given time and is determined as the ratio of the tertiary propagation rate to the total propagation rate. However, since the rate of secondary propagation is much higher than the rate of tertiary propagation $f_{\mathrm{br,i}}$ can be calculated by:

$$f_{br,i} = \frac{k_{p3}[P_3^{\bullet}]}{k_p[P^{\bullet}]} \qquad (17)$$

The second is the cumulative branching fraction, $f_{\mathrm{br,c}}$, or the total number of branches, per monomer unit, which is the experimentally measured quantity.This is total concentration of branch points, [B], found from the integral of k_{p3} [M] $[P_3\cdot]$ over the reaction time, divided by the monomer consumed:

Downloaded by UNIV OF GUELPH LIBRARY on May 31, 2012 | http://pubs.acs.org
Publication Date (Web): March 20, 2012 | doi: 10.1021/bk-2012-1100.ch010

$$f_{br,c} = \frac{[B]}{[M]_0 - [M]} \qquad (18)$$

where $[M]_0$ is the initial monomer concentration and [M] is the monomer concentration at the point of interest. Note that in a first approximation it has been assumed that the reaction volume remains constant throughout the polymerization. Similarly, the following reaction scheme was used to study branching in the bulk FRP of acrylates (Table 2):

Table 2. Reaction scheme used to study branching in the FRP of acrylates

$$I_2 \xrightarrow{k_i, f} 2\,I^{\bullet} \qquad (19)$$

$$I^{\bullet} + I^{\bullet} \xrightarrow{k_{t0}} D \qquad (20)$$

$$I^{\bullet} + M \xrightarrow{k_p} P(1)^{\bullet} \qquad (21)$$

$$P(j)^{\bullet} + M \xrightarrow{k_p} P(j+1)^{\bullet} \qquad (22)$$

$$P(j)^{\bullet} \xrightarrow{k_{bb}} P_3(j)^{\bullet} \qquad (23)$$

$$P_3(j)^{\bullet} + M \xrightarrow{k_{p3}} P(j+1)^{\bullet} \qquad (24)$$

$$P(j)^{\bullet} + I^{\bullet} \xrightarrow{k_{t0}} D(j) \qquad (25)$$

$$P(j)^{\bullet} + P(k)^{\bullet} \xrightarrow{k_t} D(j+k) \qquad (26)$$

$$P_3(k)^{\bullet} + I^{\bullet} \xrightarrow{k_{t0}} D(j) \qquad (27)$$

Continued on next page.

Table 2. (Continued). Reaction scheme used to study branching in the FRP of acrylates

$$P(j)^{\bullet} + P_3(k)^{\bullet} \xrightarrow{k_t} D(j+k) \qquad (28)$$

$$P_3(j)^{\bullet} + P_3(k)^{\bullet} \xrightarrow{k_t} D(j+k) \qquad (29)$$

All species have the same meanings as above, and I_2 is the conventional radical initiator, and $I^{\bullet}$ the conventional initiator derived radical. For sake of simplicity, in this theoretical investigation the initiator efficiency has been taken equal to one.

For both the CRP and FRP case, transfer was assumed to only occur by backbiting via a six-membered intramolecular process (*16*). Since this transition state involves a six-membered ring, strictly speaking oligomers consisting of one or two monomer units cannot undergo backbiting. This was explicitly accounted for in the kMC simulations, whereas this effect was not accounted for in the PREDICI® simulations. However, it will be shown that the PREDICI© results can be reliably used to formulate general insights for the difference in branching in the FRP and CRP of acrylates. The details of the kMC simulations have been previously published (*23*), with the discussed rate coefficients treated as real ("microscopic") rate constants. The rate coefficients were chosen to represent the polymerization of *n*-butyl acrylate at 70 °C (cf. Table 3). In particular, the conventional initiator dissociation rate coefficient is chosen to match that of azo bis(isobutyronitrile) AIBN, whereas the secondary ATRP activation and deactivation rate coefficients were based on representative values from the work of Tang et al. (*24*) On the other hand, the tertiary activation and deactivation rate coefficients were systematically varied, although 1 and 10^7 M^{-1} s^{-1} were taken as references values respectively.

Table 3. Kinetic parameters used in PREDICI® and kMC simulations of the bulk FRP and ATRP of n-butyl acrylate (70°C); for the ATRP case: tertiary activation/deactivation rate coefficient varied in the range 10^{-3} to 10^3 $M^{-1}s^{-1}$/10^4 to 10^8 $M^{-1}s^{-1}$ with 1/10^7 M^{-1} s^{-1} as reference value

Rate Coefficient	*Value*	*Reference*
k_a	1×10^0 M^{-1} s^{-1}	This work
k_d	1×10^8 M^{-1} s^{-1}	This work
f	1	This work
k_p	41400 M^{-1} s^{-1}	(*21*, *25*)
k_{bb}	1200 s^{-1}	(*21*, *26*)
k_{p3}	153 M^{-1} s^{-1}	(*21*, *27*)

Continued on next page.

Downloaded by UNIV OF GUELPH LIBRARY on May 31, 2012 | http://pubs.acs.org
Publication Date (Web): March 20, 2012 | doi: 10.1021/bk-2012-1100.ch010

Downloaded by UNIV OF GUELPH LIBRARY on May 31, 2012 | http://pubs.acs.org
Publication Date (Web): March 20, 2012 | doi: 10.1021/bk-2012-1100.ch010

Table 3. (Continued). Kinetic parameters used in PREDICI® and kMC simulations of the bulk FRP and ATRP of n-butyl acrylate (70°C); for the ATRP case: tertiary activation/deactivation rate coefficient varied in the range 10^{-3} to 10^{3} $M^{-1}s^{-1}$/10^{4} to 10^{8} $M^{-1}s^{-1}$ with 1/10^{7} M^{-1} s^{-1} as reference value

Rate Coefficient	*Value*	*Reference*
k_i	3.2×10^{-5} s^{-1}	(*28*)
k_{t0}	1×10^{9} M^{-1} s^{-1}	(*29*, *30*)
k_t	1×10^{8} M^{-1} s^{-1}	(*29*, *30*)

ICAR ATRP

The ICAR ATRP simulations were performed with methyl methacrylate (MMA) as monomer using the following reaction scheme (Table 4):

Table 4. Reaction scheme to study ICAR ATRP of MMA; for termination difference between termination by recombination and disproportionation accounted for

$$I_2 \xrightarrow{k_i, f} 2f\,I^{\bullet} \qquad (30)$$

$$I^{\bullet} + CuX_2 \xrightarrow{k_{d,I}} IX + CuX \qquad (31)$$

$$IX + CuX \xrightarrow{k_{a,I}} I^{\bullet} + CuX_2 \qquad (32)$$

$$I^{\bullet} + M \xrightarrow{k_{p,I}} P(1)^{\bullet} \qquad (33)$$

$$RX + CuX \xrightarrow{k_{a,R}} R^{\bullet} + CuX_2 \qquad (34)$$

$$R^{\bullet} + CuX_2 \xrightarrow{k_{d,R}} RX + CuX \qquad (35)$$

$$R^{\bullet} + M \xrightarrow{k_{p,R}} P(1)^{\bullet} \qquad (36)$$

Continued on next page.

Downloaded by UNIV OF GUELPH LIBRARY on May 31, 2012 | http://pubs.acs.org
Publication Date (Web): March 20, 2012 | doi: 10.1021/bk-2012-1100.ch010

Table 4. (Continued). Reaction scheme to study ICAR ATRP of MMA; for termination difference between termination by recombination and disproportionation accounted for

$$P(j)^{\bullet} + M \xrightarrow{k_p} P(j+1)^{\bullet} \qquad (37)$$

$$P(j)^{\bullet} + CuX_2 \xrightarrow{k_d} P(j)X + CuX \qquad (38)$$

$$P(j)X + CuX \xrightarrow{k_a} P(j)^{\bullet} + CuX_2 \qquad (39)$$

$$R^{\bullet} + R^{\bullet} \xrightarrow{k_{t0}} (2)D \qquad (40)$$

$$R^{\bullet} + I^{\bullet} \xrightarrow{k_{t0}} (2)D \qquad (41)$$

$$I^{\bullet} + I^{\bullet} \xrightarrow{k_{t0}} (2)D \qquad (42)$$

$$P(j)^{\bullet} + R^{\bullet} \xrightarrow{k_{t0}} D(j) \qquad (43)$$

$$P(j)^{\bullet} + I^{\bullet} \xrightarrow{k_{t0}} D(j) \qquad (44)$$

$$P(j)^{\bullet} + P(k)^{\bullet} \xrightarrow{k_t} D(j+k) \,/\, D(j) + D(k) \qquad (45)$$

In this scheme, the three radical/dormant pairs, i.e., the ATRP initiators/radicals, the conventional initiator derived dormant species/conventional initiator derived radicals and the macroinitiators/macroradicals are represented by (RX,R), (IX,I) and (PX,P) respectively. For all simulations, a temperature of 80°C is used and the activation/deactivation rate coefficients are treated as parameter values. An overview of the other kinetic coefficients is given in Table 5. For a detailed description of the solution strategy used to study the ICAR ATRP of MMA the reader is referred to D'hooge et al. (*31*)

Downloaded by UNIV OF GUELPH LIBRARY on May 31, 2012 | http://pubs.acs.org
Publication Date (Web): March 20, 2012 | doi: 10.1021/bk-2012-1100.ch010

Table 5. Kinetic coefficients used in simulations of the ICAR ATRP of MMA at 80 °C; activation and deactivation rate coefficients are treated as parameters; for termination the RAFT-CLD-T model is used; CLD-T: chain length dependent-termination (*30*, *34*, *35*)

Rate Coefficient	*Value*	*Reference*
k_i	2.5×10^{-4} M^{-1} s^{-1}	(*32*)
f	0.7	(*32*)
k_p	1300 M^{-1} s^{-1}	(*33*)
$k_{p,I}$	1300 M^{-1} s^{-1}	This work
$k_{p,R}$	1300 M^{-1} s^{-1}	This work

Results and Discussion

Branching in CRP/FRP of Acrylates

Predici® simulations for the FRP of acrylates are first presented in order to establish a reference case with no competitive activation-deactivation processes. In the FRP case, the only relevant process in Scheme 3 is the exchange of secondary radicals to tertiary radicals through backbiting reactions, and the transformation of tertiary radicals to secondary ones by tertiary propagation.

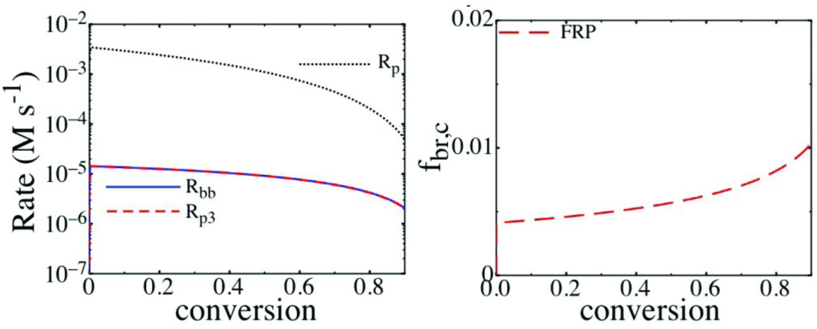

Figure 1. Rate data (left) and cumulative branching fraction (right) for bulk FRP of n-butyl acrylate under the conditions $[M]_0$:$[R_2]_0$ = 7000:1 (70 °C). Rates of secondary propagation (R_p), backbiting (R_{bb}), tertiary propagation or branching (R_{p3}) are shown, with the rate of tertiary propagation matching the rate of backbiting along the polymerization. Adapted with permission from Ref (11). Copyright 2011 American Chemical Society.

As can be seen in Figure 1 (left panel), under typical FRP conditions ($[M]_0$:$[R_2]_0$ = 7000:1; bulk), the rate of backbiting equals the rate of tertiary propagation (or branching) from the start of the polymerization, implying that the system is under steady-state conditions.

In contrast, as will be subsequently shown using three examples, the introduction of activation deactivation processes can cause the rate of transfer and the rate of branching to be out of balance for a significant portion of the polymerization. For instance, Figure 2 shows the rate data for two ATRP polymerizations of *n*-butyl acrylate ($[M]_0$:$[RX]_0$:$[CuX]_0$:$[CuX_2]_0$ = 200:1:0.29:0.029; bulk). All rate coefficients are identical, except that in the first case k_{d3} is 10^7 M^{-1} s^{-1}, with k_{a3} equal to 1 M^{-1} s^{-1}, while in the second case k_{d3} is 10^4 M^{-1} s^{-1}, with k_{a3} equal to 10^{-3} M^{-1} s^{-1} resulting in the same tertiary equilibrium constant of 10^{-7}.

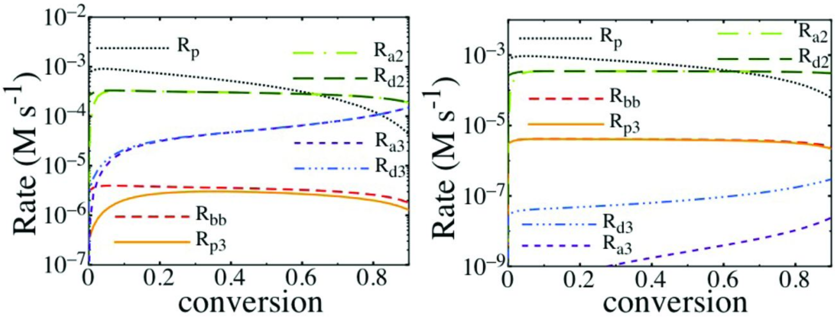

Figure 2. Rate data for the bulk ATRP of n-butyl acrylate under the conditions $[M]_0$:$[RX]_0$:$[CuX]_0$:$[CuX_2]_0$ = 200:1:0.29:0.029 (70 °C). Both have tertiary species equilibrium constants of 10^{-7} (reference value). The left has a tertiary radical deactivation rate coefficient 10^7 M^{-1} s^{-1} the right has a tertiary radical deactivation rate coefficient of 10^4 M^{-1} s^{-1}. These data show the rates of secondary radical propagation (R_p), backbiting (R_{bb}), tertiary radical propagation or branching (R_{p3}), secondary species ATRP activation (R_{a2}), secondary radical ATRP deactivation (R_{d2}), tertiary species ATRP activation (R_{a3}) and tertiary radical ATRP deactivation (R_{d3}). Adapted with permission from Ref (11). Copyright 2011 American Chemical Society.

It can be seen that the secondary ATRP equilibrium is rapidly established, however, the two systems have vastly different outcomes in establishment of the tertiary ATRP equilibrium and the balance between backbiting and tertiary propagation rates. In particular, as shown in the left panel of Figure 2, the system where k_{d3} equals 10^7 M^{-1} s^{-1}, reaches ATRP equilibrium in the tertiary species at ~10% conversion, while the backbiting rate is above the branching rate for the entire polymerization. The imbalance of interconversions of secondary and tertiary species is due to the slow balancing of interconversions constituting the competitive processes. This is because the tertiary radical formed by transfer has two competing fates, either to react with CuX_2 and become deactivated, or to react with monomer and to form a branch, re-forming the secondary radical. However, the rates of these processes are not sufficiently high to attain the balance of all interconversions.When k_{d3} is 10^7 M^{-1} s^{-1} the deactivation of the tertiary radical is very efficient, causing the dominant fate for the tertiary radical to be deactivation, which allows the tertiary system to reach ATRP equilibrium at low conversion. However, this efficient deactivation also causes the branching rate to be below the backbiting rate. In contrast, when the tertiary radical is deactivated inefficiently by CuX_2 (k_{d3} equal to 10^4 M^{-1} s^{-1}), the dominant reaction becomes

Downloaded by UNIV OF GUELPH LIBRARY on May 31, 2012 | http://pubs.acs.org
Publication Date (Web): March 20, 2012 | doi: 10.1021/bk-2012-1100.ch010

tertiary propagation, which leads to the formation of branches. In this case the rates of backbiting and branching equal for most of the reaction (as seen in the right panel of Figure 2), however, the ATRP equilibrium in the tertiary species is never reached.

Importantly, these competitive processes can alter not only the rates but also the properties of the resulting material. Figure 3 shows the effect of the deactivation rate coefficient on the branching fraction while maintaining the tertiary equilibrium constant at 10^{-7}. It follows that both the instantaneous (left) and cumulative (right) branching fractions are near the free radical limit when tertiary deactivation is inefficient (low k_{d3}) whereas the branching fractions are significantly below the free radical limit in the opposite scenario (high k_{d3}). This decrease in the branching fraction is caused by the effective formation of tertiary dormant species after backbiting. These tertiary dormant species are distinct from the branches, since the latter species are only formed upon propagation. Therefore, by forming a tertiary dormant species, the formation of the branch can be delayed, leading to a decrease in the branching fraction for a given conversion.

Downloaded by UNIV OF GUELPH LIBRARY on May 31, 2012 | http://pubs.acs.org
Publication Date (Web): March 20, 2012 | doi: 10.1021/bk-2012-1100.ch010

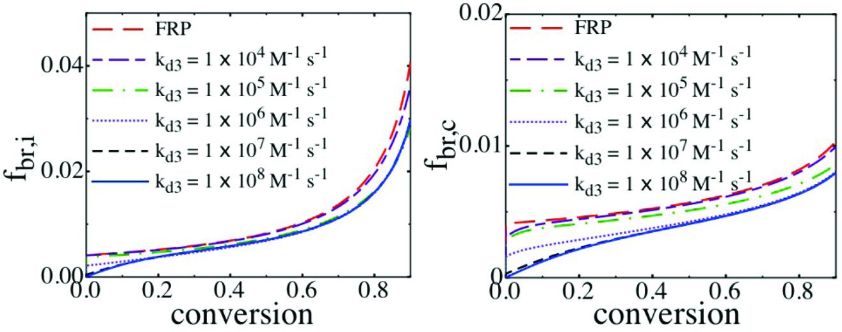

Figure 3. Branch fraction data for the bulk ATRP of n-butyl acrylate under the conditions $[M]_0:[RX]_0:[CuX]_0:[CuX_2]_0 = 200:1:0.29:0.029$ (70 °C). All systems have tertiary ATRP equilibrium constants of 10^{-7} (reference value). Left shows instantaneous branching fraction, right shows cumulative branching fraction data. Adapted with permission from Ref (11). Copyright 2011 American Chemical Society.

In order to confirm the validity of the previous findings, kMC simulations were also performed. Figure 4 shows the cumulative branching fraction determined for FRP ($[M]_0:[R_2]_0 = 7000:1$; bulk), and ATRP ($[M]_0:[RX]_0:[CuX]_0:[CuX_2]_0 = 200:1:0.29:0.029$; bulk) with $k_{d3} = 10^4$ M^{-1} s^{-1} and $k_{d3} = 10^7$ M^{-1} s^{-1}, using both kMC and PREDICI®. In all cases the branching fraction at sufficiently high conversion is the same regardless of the simulation technique. In addition, detailed analysis revealed that at low conversions the PREDICI® simulations can lead to higher cumulative branching values than the kMC simulations, which is attributed to the incorrect consideration of backbiting reactions for oligomeric species containing one or two monomer units for the former simulations (see Kinetic model). Despite these small discrepancies, these results indicate that the PREDICI® simulations can be used without compromising the conclusions drawn.

Downloaded by UNIV OF GUELPH LIBRARY on May 31, 2012 | http://pubs.acs.org
Publication Date (Web): March 20, 2012 | doi: 10.1021/bk-2012-1100.ch010

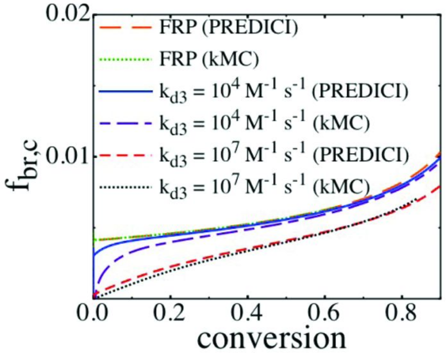

Figure 4. Comparison of simulated cumulative braching fractionin bulk FRP and ATRP using PREDICI® and kMC. FRP: $[M]_0$:$[I_2]_0$ = 7000:1, ATRP: $[M]_0$:$[RX]_0$:$[CuX]_0$:$[CuX_2]_0$ = 200:1:0.29:0.029. ATRP systems have tertiary ATRP equilibrium constants of 10^{-7} (reference value). Adapted with permission from Ref (11). Copyright 2011 American Chemical Society.

The influence of the (re)activation rate of the tertiary dormant species, for a fixed high tertiary deactivation rate coefficient, also highlights the importance of the competitive processes in Scheme 3. Since the activation rate coefficient is varied for a fixed deactivation rate coefficient, this examines the effect of the tertiary ATRP equilibrium constant (K_{ATRP-3}). In particular, it will be shown that a sufficiently high tertiary ATRP equilibrium constant causes a high branching fraction. In such case, although the tertiary radical is rapidly deactivated by reaction with CuX_2, it is also rapidly reformed due to the high tertiary activation coefficient. This is highlighted in Figure 5, which shows the rate data for two ATRP systems with k_{d3} = 10^7 M^{-1} s^{-1}, however, the left one has a low k_{a3} of 10^{-1} M^{-1} s^{-1}, while the right one has a high k_{a3} of 10^2 M^{-1} s^{-1}. For the first system (low tertiary ATRP equilibrium constant), although the secondary ATRP equilibrium is established at a conversion below 5%, the tertiary ATRP equilibrium is not established until a conversion of approximately 30%, and the rates of backbiting and branching do not match until very high conversion. This is due to the competing fates of the tertiary radical, namely deactivation and propagation. Here tertiary deactivation dominates, removing the branching pathway until a very high number of tertiary dormant species are formed. This mismatching of transfer and branching rates is a feature that is possible only due to the competitive processes in CRP. However, as shown in the right panel of Figure 5, if the reactivation is sufficiently rapid (high tertiary ATRP equilibrium constant) the competitive processes do not delay the equilibration in either the secondary or tertiary ATRP systems, nor is there an imbalance in the transfer and branching rates. This is because a system with rapid reactivation of the tertiary dormant species is unable to effectively trap the tertiary species and delay branching, since the tertiary radical is rapidly reformed and able to branch by reacting with monomer.

Downloaded by UNIV OF GUELPH LIBRARY on May 31, 2012 | http://pubs.acs.org
Publication Date (Web): March 20, 2012 | doi: 10.1021/bk-2012-1100.ch010

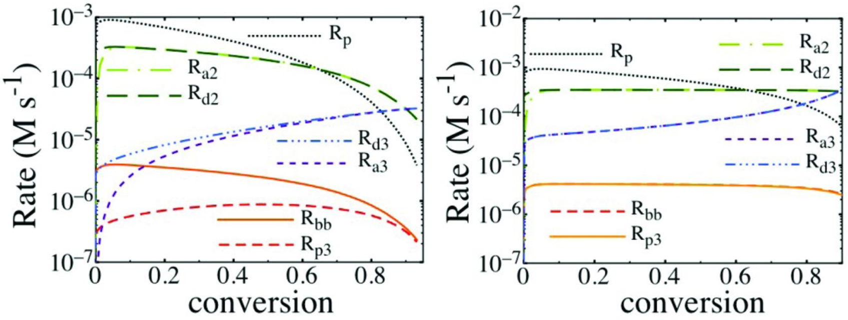

Figure 5. Rate data for the bulk ATRP of n-butyl acrylate under the conditions $[M]_0$:$[RX]_0$:$[CuX]_0$:$[CuX_2]_0$ = 200:1:0.29:0.029 (70 °C). Both have tertiary radical deactivation rate coefficients of 10^7 M^{-1} s^{-1}. The left has tertiary equilibrium constant 10^{-8} the right has tertiary equilibrium constant 10^{-5}. These data show the rates of secondary radical propagation (R_p), backbiting (R_{bb}), tertiary radical propagation or branching (R_{p3}), secondary ATRP species activation (R_{a2}), secondary radical deactivation (R_{d2}), tertiary species ATRP activation (R_{a3}) and tertiary radical deactivation (R_{d3}). Adapted with permission from Ref (11). Copyright 2011 American Chemical Society.

These observations are further highlighted by examining both the instantaneous and cumulative branching fractions as shown in Figure 6. Whenever the tertiary ATRP equilibrium constant is low, the branching fraction is far below the FRP limit, whereas a high equilibrium constant gives branching fractions that are nearly at the FRP limit. This is again due to fact that a low tertiary equilibrium constant effectively traps the tertiary radicals, forming tertiary dormant species and delaying the branch formation, whereas a high tertiary equilibrium constant rapidly reforms the tertiary radical, promoting branch formation. Furthermore, it follows that whenever the rate of backbiting and the rate of tertiary propagation match, the instantaneous branching fraction matches the FRP instantaneous branching fraction. When the tertiary ATRP equilibrium constant is high the transfer and tertiary propagation rates match for almost the whole polymerization. This implies that the instantaneous branching fraction is always near the FRP limit, and consequently the cumulative branching fraction is at the FRP limit for essentially the whole polymerization. In contrast when the tertiary ATRP equilibrium constant is low the rate of transfer only matches the rate of tertiary propagation at very high conversion. At this point the instantaneous branching fraction matches the FRP instantaneous branching fraction, however, the cumulative branching fraction is far below the FRP limit since the rate of branch formation was below the FRP limit for almost the whole polymerization.

In the previous two examples, the rate coefficients were varied to demonstrate the effect of the competitive processes in the ATRP of acrylates. In all simulations, the secondary activation-deactivation rate coefficients were kept fixed and the tertiary activation-deactivation rate coefficients were varied. However in practice it is difficult to choose or design two catalysts that will have different activation-deactivation rate coefficients for the tertiary species, but the same activation-deactivation rate coefficients for the secondary species. This is because if a catalyst is highly active, it should be active towards both secondary and tertiary species. Similarly, if a catalyst is highly deactivating, it should be highly deactivating towards both secondary and tertiary species. In contrast, it would be more convenient to vary the reaction conditions and be able to tune the branching fraction in that manner. As indicated previously (*11*), variations in the initial concentrations of CuX activator and CuX_2 deactivator affect only the absolute rates to a similar extent, and consequently similar polymer properties are obtained. Contrary, the initial initiator concentration can have a distinct effect on the branching fraction. In particular, the cumulative branching fraction decreases dramatically for higher initial initiator concentrations, i.e., when lower chain lengths are targeted, as clearly shown in Figure 7.

Downloaded by UNIV OF GUELPH LIBRARY on May 31, 2012 | http://pubs.acs.org
Publication Date (Web): March 20, 2012 | doi: 10.1021/bk-2012-1100.ch010

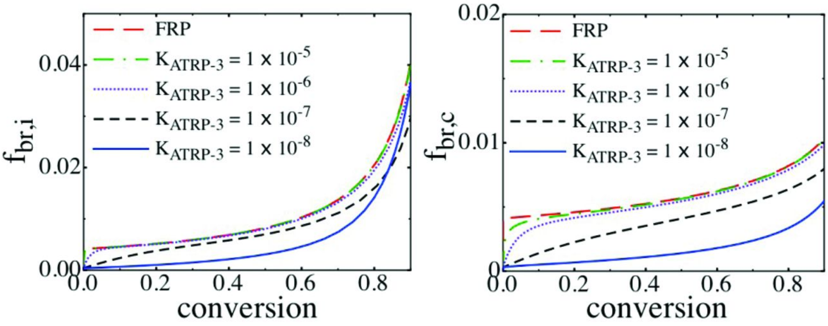

Figure 6. Branch fraction data for bulk ATRP of n-butyl acrylate under the conditions $[M]_0:[RX]_0:[CuX]_0:[CuX_2]_0$ = 200:1:0.29:0.029 (70 °C). All systems have tertiary deactivation rate coefficients of 10^7 M^{-1} s^{-1}. Left shows instantaneous branching fraction, right shows cumulative branching fraction data. Adapted with permission from Ref (11). Copyright 2011 American Chemical Society.

When the initial initiator concentration is changed, the rate of backbiting changes by the same factor as the rate of propagation at least up to intermediate conversions, leading to no net change in the rate of tertiary radical formation with conversion. In all cases, essentially all tertiary species formed by backbiting must be either a tertiary dormant species or have reacted with monomer to form a branch. However, with a higher targeted chain length, the total number of chains that can be trapped as tertiary dormant species is lower, due to the smaller number of end-groups, per monomer. Therefore, for the same monomer conversion the number of branches is higher with higher targeted chain lengths. In contrast, when the initial initiator concentration is relatively high, there are a relatively large number of tertiary deactivated species that can be formed, which leads to a low branching fraction.

Downloaded by UNIV OF GUELPH LIBRARY on May 31, 2012 | http://pubs.acs.org
Publication Date (Web): March 20, 2012 | doi: 10.1021/bk-2012-1100.ch010

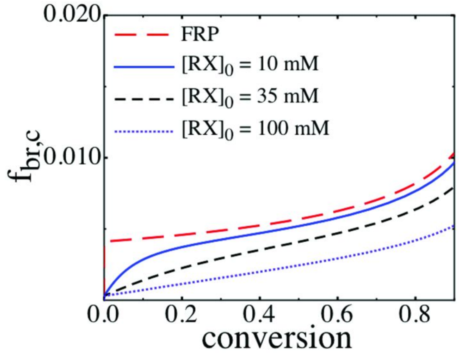

Figure 7. Cumulative branch fraction data for bulk ATRP of n-butyl acrylate under conditions $[M]_0:[CuX]_0:[CuX_2]_0 = 200:0.29:0.029$ *(70 °C). All have tertiary equilibrium constants of* 10^{-7}*, and tertiary deactivation rate coefficients of* 10^7 M^{-1} s^{-1} *(reference values).* $[M]_0:[RX]_0$ *was varied from 200:0.29 to 200:2.9. Adapted with permission from Ref (11). Copyright 2011 American Chemical Society.*

ICAR ATRP

The ICAR ATRP systems studied here highlight how the competitive processes phenomenon can affect the properties of polymers made by this technique under various conditions. Initially a system is chosen with relatively low ATRP equilibrium constant for all species. In particular, all activation rate coefficients are considered to be 1 M^{-1} s^{-1}, and all deactivation rate coefficients are 10^8 M^{-1} s^{-1}. Finally, the importance of active catalysts and initiators is demonstrated.

As can be seen in Figure 8, the reaction conditions for the ICAR ATRP must be chosen carefully. In particular, if the initial concentration of conventional initiator, $[I_2]_0$, is too high (0.1 with respect to ATRP initiator; green solid lines), the polymerization gives poor control over the macromolecular properties, with polydispersitiy indices (PDIs) remaining near 2 for the whole polymerization and number average chain length (x_n) values far above the value expected for that conversion. However, when the initial concentration of conventional initiator, $[I_2]_0$, is lower (0.02 with respect to ATRP initiator; red dashed lines), the control over the polymer properties is significantly better. In particular, the end-group functionality is much higher and the PDI drops after a conversion of ca. 25%.

The rate data corresponding to the system with a ratio $[I_2]_0:[RX]_0$ of 0.02:1 are shown in Figure 9. These rate data display the competitive equilibria effects, with the three radical/dormant pairs (ATRP radical/initiators, conventional initiator derived radicals/dormant species and macroradicals/macroinitiators) being out of equilibrium at low to intermediate conversions. In this case, the conventional initiator derived molecules are the first to have ‘matched’ activation and deactivation rates, with this occurring around 15% conversion. In contrast, the ATRP initiators are never in equilibrium except at almost complete ATRP initiator depletion, and the macromolecules do not reach an equilibrium until a

Downloaded by UNIV OF GUELPH LIBRARY on May 31, 2012 | http://pubs.acs.org
Publication Date (Web): March 20, 2012 | doi: 10.1021/bk-2012-1100.ch010

conversion of approximately 45%. However, at a conversion of approximately 40%, the activation and deactivation rates for the macromolecular species start to converge, which coincides with the point where the control over the polymer properties improves. This shows that well-controlled polymers can only be made by ICAR ATRP if all activation/deactivation rates are well-balanced. In particular, it is important that the ATRP equilibrium is established in the macromolecular species at a relatively low conversion. However, close inspection of Figure 9 shows that no further activator regeneration occurs at conversions around 50%, since both the activation and deactivation rate of the conventional initiator derived molecules tend to zero. This suggests that at this point, it is necessary to add extra conventional initiator to obtain a high conversion.

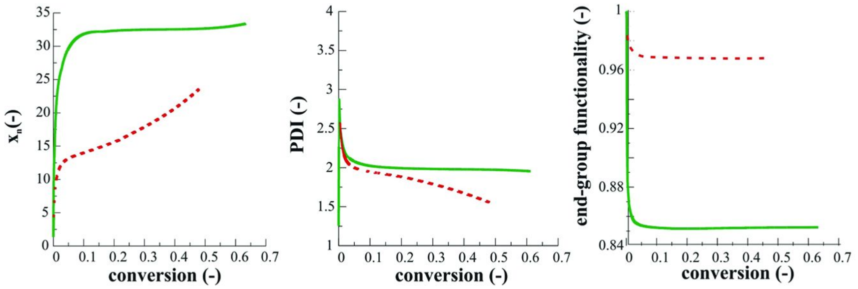

Figure 8. ICAR ATRP of MMA showing the effect of the initial conventional initiator concentration; on left: number average chain length (x_n); middle: polydispersity index (PDI) and right: end-group functionality all as a function of conversion under the conditions: 80 °C; $[M]_0$:$[RX]_0$=50; $[CuX]_0$=0 mol L^{-1}; 50 vol% solvent with respect to monomer; $[CuX_2]_0$:$[RX]_0$= 0.002; $[I_2]_0$:$[RX]_0$=0.02 and 0.1 (red dashed and green full lines). Adapted with permission from Ref (36). Copyright 2011 John Wiley and Sons.

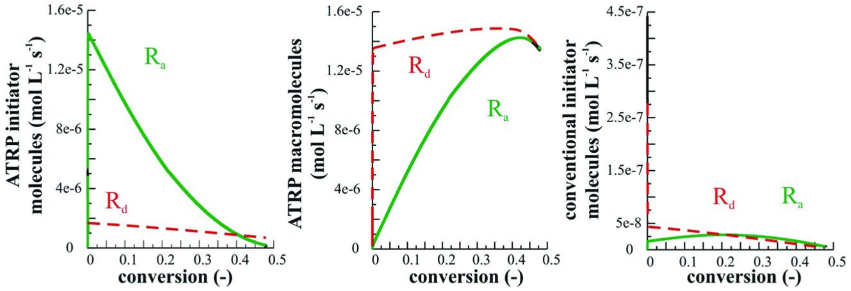

Figure 9. Activation and deactivation (R_a/R_d) rate data for the ICAR ATRP of MMA left: ATRP initiators middle: macromolecules right: conventional initiator derived molecules under the conditions: 80 °C; $[M]_0$:$[RX]_0$=50; $[CuX]_0$=0 mol L^{-1} ; 50 vol% solvent with respect to monomer; $[CuX_2]_0$:$[RX]_0$= 0.002; $[I_2]_0$=0.02 $[RX]_0$. Adapted with permission from Ref (36). Copyright 2011 John Wiley and Sons.

As shown in Figure 10, when conventional initiator is added at a conversion of 45%, the control over the polymer properties remains good up to high conversion. By the time the conversion exceeds 85% the polydisperisty indices are below 1.4, which is a very acceptable, and the end-group functionality is greater than 0.9 throughout the whole polymerization. Only at conversions very close to 45% the control over the polymer properties is slightly disturbed.

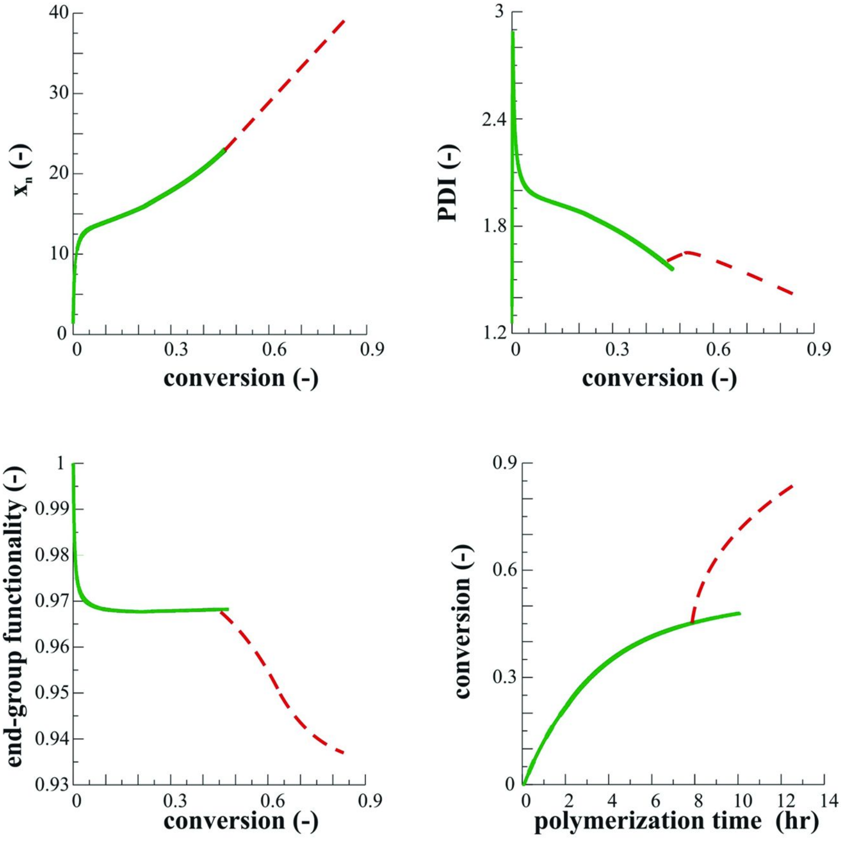

Figure 10. ICAR ATRP of MMA showing the effect of injection of extra conventional initiator (reestablishment of the initial concentration) at a conversion of 0.45 (red dashed) on top left number average chain length (x_n) top right polydispersity index (PDI) bottom left end-group functionality all as a function of conversion bottom right conversion profile under theconditions: 80 °C; $[M]_0$:$[RX]_0$=50; $[CuX]_0$=0 mol L^{-1}; 50 vol% solvent with respect to monomer; $[I_2]_0$=0.02$[RX]_0$; $[CuX_2]_0$:$[RX]_0$= 0.002. Adapted with permission from Ref (36). Copyright 2011 John Wiley and Sons.

Downloaded by UNIV OF GUELPH LIBRARY on May 31, 2012 | http://pubs.acs.org
Publication Date (Web): March 20, 2012 | doi: 10.1021/bk-2012-1100.ch010

In addition to the polymer properties and ATRP kinetics, it is also important to study the corresponding activation deactivation rate data. Figure 11 shows that, the rates are well-balanced once the equilibrium in macromolecular species is established. However, directly after the addition of the conventional initiator at 45% conversion some non-equilibration results for a narrow conversion range. This is due to rapid increase in the radical concentration, which can be explained by the increased rate of deactivation for the conventional initiator derived radicals immediately after the injection.

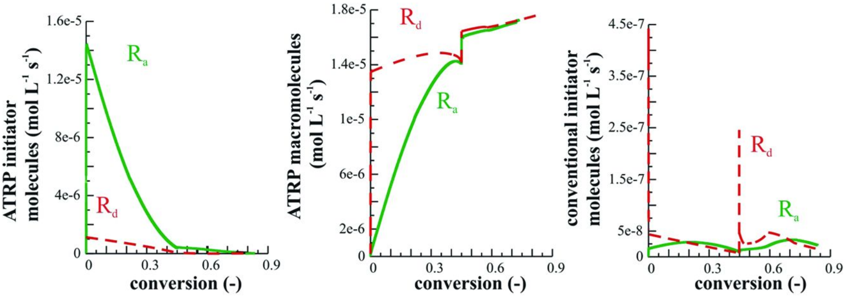

Figure 11. Activation and deactivation (R_a/R_d) rate data for the ICAR ATRP of MMA with the extra addition of conventional initiator at a conversion of 0.45 left: ATRP initiators middle: macromolecules right: conventional initiator derived molecules; initial conditions: 80 °C; $[M]_0:[RX]_0=50$; $[CuX]_0=0$ mol L^{-1} ; 50 vol% solvent with respect to monomer; $[CuX_2]_0:[RX]_0= 0.002$; $[I_2]_0=0.02\ [RX]_0$. Adapted with permission from Ref (36). Copyright 2011 John Wiley and Sons.

In the previous simulations, the activities of the various species toward activation/deactivation were assumed identical, with all species having activation rate coefficients of 10^0 M^{-1} s^{-1} and deactivation rate coefficients of 10^8 M^{-1} s^{-1}. If this assumption is invalid, a delay in equilibration for the macromolecular species, and, hence, a reduced control over polymer properties can result (*36*). Importantly, this disadvantage can be overcome by selecting a sufficiently active ATRP initiator and catalyst, as illustrated in Figure 12. In this case, the deactivation rate coefficients are all taken equal to 10^7 M^{-1} s^{-1}, and the small molecule activation rate coefficients are taken to be 10^3 M^{-1} s^{-1}, and the macromolecular species are characterized by a lower activation rate coefficient of 10^2 M^{-1} s^{-1}. It follows from this figure that polymers prepared with the more active ATRP initiator and catalyst are better defined already at a lower conversion. For example, polydispersity indices around 1.2 are observed at 30% conversion. Furthermore, due to the highly active catalyst, this system can sustain a single injection of conventional initiator.

Downloaded by UNIV OF GUELPH LIBRARY on May 31, 2012 | http://pubs.acs.org
Publication Date (Web): March 20, 2012 | doi: 10.1021/bk-2012-1100.ch010

Downloaded by UNIV OF GUELPH LIBRARY on May 31, 2012 | http://pubs.acs.org
Publication Date (Web): March 20, 2012 | doi: 10.1021/bk-2012-1100.ch010

Finally, the good control over polymer properties can be inferred from the rate plots in Figure 13. In this figure, the equilibrium for all three species is established at very low conversion, i.e, below 10%. This highlights that by carefully selecting an active catalyst and ATRP initiator the competitive activation/deactivation processes can be tuned from low conversion onwards leading to well controlled polymers.

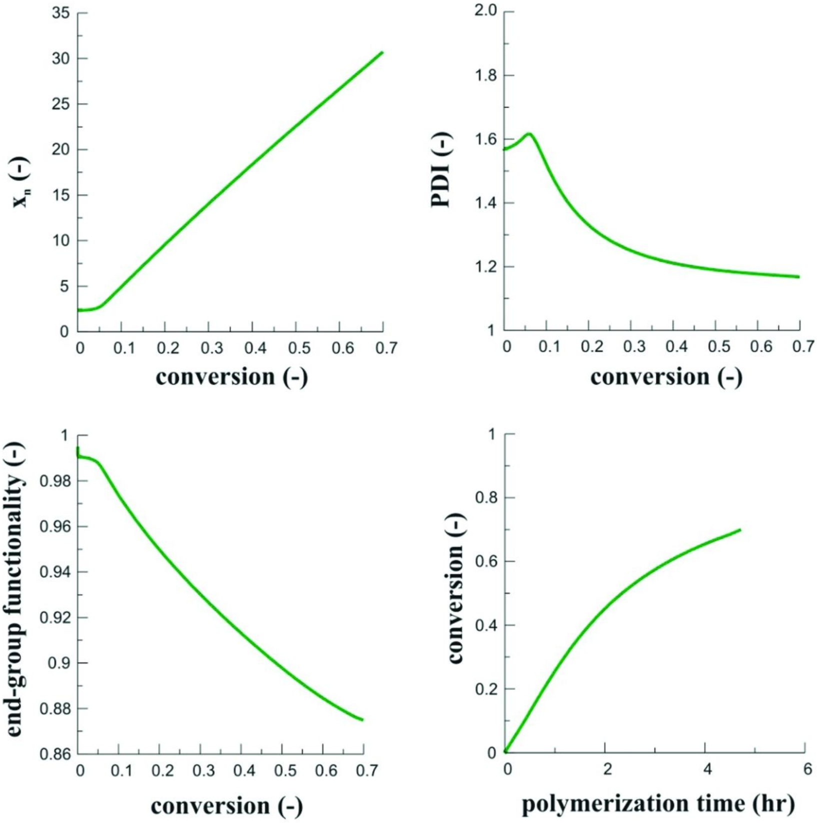

Figure 12. ICAR ATRP of MMA showing the effect of using a more active catalyst and a more active initiator on top left number average chain length (x_n) top right polydispersity index (PDI) bottom left end-group functionality all as a function of conversion bottom right conversion profile under the conditions: 80 °C; $[M]_0:[RX]_0=50$; $[CuX]_0=0$ mol L^{-1}; 50 vol% solvent with respect to monomer; $[I_2]_0=0.1[RX]_0$; $[CuX_2]_0:[RX]_0= 0.002$.

Downloaded by UNIV OF GUELPH LIBRARY on May 31, 2012 | http://pubs.acs.org
Publication Date (Web): March 20, 2012 | doi: 10.1021/bk-2012-1100.ch010

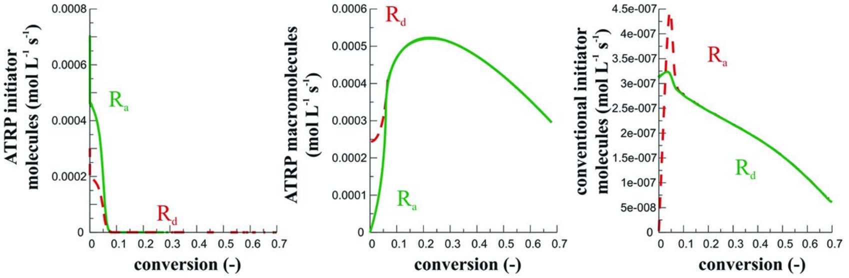

Figure 13. Activation and deactivation (R_a/R_d) rate data for the ICAR ATRP of MMA with active initiator and catalyst; left ATRP initiators middle macromolecules right conventional initiator derived molecules under the conditions: 80 °C; $[M]_0$:$[RX]_0$=50; $[CuX]_0$=0 mol L^{-1} ; 50 vol% solvent with respect to monomer; $[CuX_2]_0$:$[RX]_0$= 0.0025; $[I_2]_0$=0.1 $[RX]_0$.

Conclusions

The concept of competitive processes or equilibria was highlighted in this chapter for two important CRP systems. The first system was the CRP of acrylates, where secondary and tertiary species can undergo activation-deactivation reactions, as well as interconversion through transfer reactions, and tertiary propagation reactions. The second system studied was the ICAR ATRP of MMA, where there are activation-deactivation reactions in ATRP initiator molecules, conventional initiator derived molecules, and macromolecular species, with propagation transforming the small molecules into macromolecules.

The competitive processes phenomenon can change the branching fraction in a polyacrylate from having the same branching fraction as a polyacrylate made by FRP, to having a branching fraction significantly below the FRP limit. If the branching fraction in a polyacrylate synthesized by ATRP should be reduced below the FRP limit, it is important that the deactivation of secondary and tertiary radicals is efficient. In this case the tertiary radicals formed by unavoidable transfer reactions can be effectively trapped as dormant species delaying the branch formation process. Furthermore, a low targeted degree of polymerization should be chosen. The concepts developed here may be extended to other CRP processes, including NMP and RAFT polymerization. This is because in NMP there is a bond homolysis leading to a radical and nitroxide similar to ATRP activation although non-catalyzed, and the nitroxide itself may be substituted for the CuX2 deactivator complex. Similarly, for RAFT polymerization the degenerative transfer process may still be viewed in light of these competitive processes, if the propagating radical which exchanges with the chain of interest is viewed as the activator, and the thiocarbonylthio group is viewed as the deactivator.

In the case of ICAR ATRP, the competitive processes can deteriorate the establishment of the ATRP equilibrium in the macromolecular species. As shown in this chapter, the equilibrium in macromolecular species is needed at

Downloaded by UNIV OF GUELPH LIBRARY on May 31, 2012 | http://pubs.acs.org
Publication Date (Web): March 20, 2012 | doi: 10.1021/bk-2012-1100.ch010

low conversion to create polymers with low polydispersities, and well-controlled molecular weights and high livingness. The properties of the polymer may be improved by using an active initiator and a low initial amount of conventional initiator with respect to the initial amount of ATRP initiator. In certain cases, depending on the catalyst reactivity, multiple injections (or continuous feeding) of the conventional initiator may be needed to reach high conversion. These conclusions drawn from ICAR ATRP may be applied to RAFT polymerization, due to the kinetic similarity of these two processes.

Acknowledgments

The work was supported by the National Science Foundation (DMR 09-69301 and CHE 10-26060), The Polish Ministry of Science and Higher Education from the budget funds for science for years 2009-2012, The Fund for Scientific Research Flanders (FWO), the Interuniversity Attraction Poles Programme - Belgian State-Belgian Science Policy, and the Long Term Structural Methusalem Funding by the Flemish Government.

References

1. Braunecker, W. A.; Matyjaszewski, K. *Prog. Polym. Sci.* **2007**, *32*, 93–146.
2. Goto, A.; Fukuda, T. *Prog. Polym. Sci.* **2004**, *29*, 329–385.
3. Moad, G.; Rizzardo, E.; Thang, S. H. *Aust. J. Chem.* **2005**, *58*, 379–410.
4. Georges, M. K.; Veregin, R. P. N.; Kazmaier, P. M.; Hamer, G. K. *Macromolecules* **1993**, *26*, 2987–8.
5. Hawker, C. J.; Bosman, A. W.; Harth, E. *Chem. Rev.* **2001**, *101*, 3661–3688.
6. Kato, M.; Kamigaito, M.; Sawamoto, M.; Higashimura, T. *Macromolecules* **1995**, *28*, 1721–3.
7. Wang, J.-S.; Matyjaszewski, K. *J. Am. Chem. Soc.* **1995**, *117*, 5614–15.
8. Matyjaszewski, K.; Xia, J. *Chem. Rev.* **2001**, *101*, 2921–2990.
9. Chiefari, J.; Chong, Y. K.; Ercole, F.; Krstina, J.; Jeffery, J.; Le, T. P. T.; Mayadunne, R. T. A.; Meijs, G. F.; Moad, C. L.; Moad, G.; Rizzardo, E.; Thang, S. H. *Macromolecules* **1998**, *31*, 5559–5562.
10. Perrier, S.; Takolpuckdee, P. *J Polym. Sci., Part A: Polym. Chem.* **2005**, *43*, 5347–5393.
11. Konkolewicz, D.; Sosnowski, S.; D'hooge, D. R.; Szymanski, R.; Reyniers, M.-F.; Marin, G. B.; Matyjaszewski, K. *Macromolecules* **2011**, *44*, 8361–8373.
12. Ziegler, M. J.; Matyjaszewski, K. *Macromolecules* **2001**, *34*, 415–424.
13. Matyjaszewski, K. *Macromolecules* **2002**, *35*, 6773–6781.
14. Lovell, P. A.; Shah, T. H.; Heatley, F. *Polym Commun* **1991**, *32*, 98–103.
15. Junkers, T.; Barner-Kowollik, C. *J Polym. Sci., Part A: Polym. Chem.* **2008**, *46*, 7585–7605.
16. Farcet, C. l.; Belleney, J. l.; Charleux, B.; Pirri, R. *Macromolecules* **2002**, *35*, 4912–4918.
17. Aggarwal, S. L.; Sweeting, O. J. *Chem. Rev.* **1957**, *57*, 665–742.

18. White, J. L.; Dharod, K. C.; Clark, E. S. *J. App. Polym. Sci.* **1974**, *18*, 2539–2568.
19. Ahmad, N. M.; Charleux, B.; Farcet, C.; Ferguson, C. J.; Gaynor, S. G.; Hawkett, B. S.; Heatley, F.; Klumperman, B.; Konkolewicz, D.; Lovell, P. A.; Matyjaszewski, K.; Venkatesh, R. *Macromol. Rapid Commun.* **2009**, *30*, 2002–2021.
20. Yu-Su, S. Y.; Sun, F. C.; Sheiko, S. S.; Konkolewicz, D.; Lee, H.-i.; Matyjaszewski, K. *Macromolecules* **2011**, *44*, 5928–5936.
21. Reyes, Y.; Asua, J. M. *Macromol. Rapid Commun.* **2011**, *32*, 63–67.
22. Matyjaszewski, K.; Jakubowski, W.; Min, K.; Tang, W.; Huang, J. Y.; Braunecker, W. A.; Tsarevsky, N. V. *Proc. Natl. Acad. Sci. U. S. A.* **2006**, *103*, 15309–15314.
23. Szymanski, R. *e-Polymers* **2009** (44).
24. Tang, W.; Kwak, Y.; Braunecker, W.; Tsarevsky, N. V.; Coote, M. L.; Matyjaszewski, K. *J. Am. Chem. Soc.* **2008**, *130*, 10702–10713.
25. Asua, J. M.; Beuermann, S.; Buback, M.; Castignolles, P.; Charleux, B.; Gilbert, R. G.; Hutchinson, R. A.; Leiza, J. R.; Nikitin, A. N.; Vairon, J.-P.; van Herk, A. M. *Macromol. Chem. Phys.* **2004**, *205*, 2151–2160.
26. Plessis, C.; Arzamendi, G.; Alberdi, J. M.; van Herk, A. M.; Leiza, J. R.; Asua, J. M. *Macromol. Rapid Commun.* **2003**, *24*, 173–177.
27. Arzamendi, G.; Plessis, C.; Leiza, J. R.; Asua, J. M. *Macromol. Theory Simul.* **2003**, *12*, 315–324.
28. Bawn, C. E. H.; Verdin, D. *Trans. Faraday Soc.* **1960**, *56*, 815–822.
29. Smith, G. B.; Russell, G. T.; Heuts, J. P. A. *Macromol. Theory Simul.* **2003**, *12*, 299–314.
30. Johnston-Hall, G.; Monteiro, M. J. *J. Polym. Sci. Part A: Polym. Chem.* **2008**, *46*, 3155–3173.
31. D'hooge, D. R.; Reyniers, M.-F.; Marin, G. B. *Macromol. React. Eng.* **2009**, *3*, 185–209.
32. Moad, G.; Solomon, D. H., *The Chemistry of Free Radical Polymerization*; Elsevier Science, Ltd: Oxford, 1995.
33. Beuermann, S.; Buback, M.; Davis, T. P.; Gilbert, R. G.; Hutchinson, R. A.; Olaj, O. F.; Russell, G. T.; Schweer, J.; van Herk, A. M. *Macromol. Chem. Phys.* **1997**, *198*, 1545–1560.
34. Vana, P.; Davis, T. P.; Barner-Kowollik, C. *Macromol. Rapid Commun.* **2002**, *23*, 952–956.
35. Johnston-Hall, G.; Stenzel, M. H.; Davis, T. P.; Barner-Kowollik, C.; Monteiro, M. J. *Macromolecules* **2007**, *40*, 2730–2736.
36. D'hooge, D. R.; Konkolewicz, D.; Reyniers, M.-F.; Marin, G. B.; Matyjaszewski, K. *Macromol. Theory Simul.* **2011**, in press.

Downloaded by UNIV OF GUELPH LIBRARY on May 31, 2012 | http://pubs.acs.org
Publication Date (Web): March 20, 2012 | doi: 10.1021/bk-2012-1100.ch010

Downloaded by OHIO STATE UNIV LIBRARIES on May 31, 2012 | http://pubs.acs.org
Publication Date (Web): March 20, 2012 | doi: 10.1021/bk-2012-1100.ch011

Chapter 11

ATRPases: Using Nature's Catalysts in Atom Transfer Radical Polymerizations

Gergely Kali,[1,2] Tilana B. Silva,[1] Severin J. Sigg,[1] Farzad Seidi,[1] Kasper Renggli,[1] and Nico Bruns*,[1]

**[1]Department of Chemistry, University of Basel, Klingelbergstr. 80,
CH-4056 Basel, Switzerland**
**[2]Institute of Materials and Environmental Chemistry,
Chemical Research Center, Hungarian Academy of Sciences,
Pusztaszeri ut 59-67, P.O. Box 17, H-1525 Budapest, Hungary**
***E-mail: nico.bruns@unibas.ch**

Enzymes are environmentally friendly, non-toxic catalysts that have found many applications in synthetic polymer chemistry. However, until very recently no examples of enzyme-catalyzed, controlled radical polymerizations were known. Here we review the nascent field of biocatalytic atom transfer radical polymerization (ATRP). The heme proteins horseradish peroxidase, hemoglobin and catalase, as well as the copper-containing enzyme laccase have been reported to display catalytic activity in activators regenerated by electron transfer (ARGET) ATRP of two model monomers, *N*-isopropylacrylamide and poly(ethylene glycol) methyl ether acrylate. Bromine-terminated polymers, low polydispersity indices, linear increase in molecular weight with conversion as well as first-order kinetics indicate ATRP-type mechanisms. However, the first examples of biocatalytic ATRP also show that enzymes are much more complex catalysts than conventional ones.

In Progress in Controlled Radical Polymerization: Mechanisms and Techniques; Matyjaszewski, K., et al.;
ACS Symposium Series; American Chemical Society: Washington, DC, 2012.

Downloaded by OHIO STATE UNIV LIBRARIES on May 31, 2012 | http://pubs.acs.org
Publication Date (Web): March 20, 2012 | doi: 10.1021/bk-2012-1100.ch011

Introduction

Controlled radical polymerization reactions that allow the synthesis of polymers with predetermined molecular weights, with narrow molecular weight distributions and with functional end groups have propelled polymer science into the position of key contributor to advanced materials, nanosciences, and modern soft matter research. Such "living" polymerizations are used e.g. to synthesize amphiphilic blockcopolymers, which are needed as building blocks of self-assembled nano-objects. Atom transfer radical polymerization (ATRP) is one of the most widely used controlled radical polymerizations (*1*). ATRP tolerates the presence of various functional groups and can be conducted in aqueous media (*2*). Thus, it is not surprising that ATRP has even been carried out in the presence of proteins, e.g. in order to synthesize protein-polymer conjugates by grafting polymers from an initiator attached to enzymes (*3*, *4*), a topic covered in other chapters of this book. Such hybrids are potential candidates for applications ranging from switchable biocatalysts to stealth therapeutic proteins.

Conventional ATRP has some drawbacks. It is carried out with transition metal complexes as catalysts, most often Cu(I) complexes. These catalysts are difficult to remove from the polymer product. Due to the (mild) toxicity of transition metal ions and amine ligands, the catalysts interfere with the application of the resulting polymers in biomedical and food grade applications (*2*, *5*). Moreover, copper ion and amine ligand residues in polymers also represent a problem for technical applications in plastics, as they cause unwanted coloration (*5*).

Three approaches have been followed in order make ATRP environmentally more favorable, i.e. greener and the resulting polymers more compatible with medical and food grade requirements. One approach is the substitution of copper complexes with non-toxic catalysts that are based e.g. on iron ions (*6*, *7*). However, iron-based ATRP catalysts often have poorer catalytic properties compared to their copper counterparts. The second approach is to reduce the amount of catalyst needed by designing catalysts with higher activity and better performance or by changing the experimental protocol (*1*, *2*). In particular, the development of techniques such as *activators regenerated by electron transfer* (ARGET) ATRP, and *initiators for continuous activator regeneration* (ICAR) ATRP has permitted a reduction in catalyst concentration to the ppm range. Both methods use reagents (a reducing agent in ARGET, a radical source in ICAR), to continuously regenerate the activating Cu(I) species from Cu(II) species that otherwise accumulate due to termination reactions of radicals. The third approach is to remove the catalyst from the polymerization solution at the end of the reaction, e.g. by simple filtration over aluminium oxide columns, scavenging with ion exchange resins, and using Cu-complexes immobilized on solid supports (*2*, *5*).

Enzymes have been explored as catalyst in many fields of synthetic chemistry, including polymer chemistry (*8*)–(*10*). They are an environmentally friendly, often non-toxic and biodegradable alternative to conventional catalysts. Moreover, they often are highly substrate-, regio-, and stereo-selective, can open new synthetic routes, and have been found to be active catalysts both in water and in non-aqueous media, such as organic solvents and supercritical CO_2. Well-explored enzyme-catalyzed polymerizations include polycondensations and ring-opening polymerizations of polyesters and polyamides (*11–13*). The most prominent biocatalyst for these reactions is immobilized *Candida antarctica* lipase B (CALB) which is sold under the trade name Novozyme 435 (*14*). Other biocatalytic polymer syntheses are oxidative polymerizations of phenols (*15*), polymerization of polysaccharides (*16*, *17*), and enzyme-mediated radical initiation for the polymerization of vinyl monomers (*18–20*).

Although many enzymes and proteins contain metal atoms at their catalytically active sites, no report of a controlled radical polymerization with enzymes or proteins as catalyst has been known until very recently, when our group (*21*, *22*) and a team from Singapore (*23*) discovered, in parallel and independent of each other, first examples of enzyme-catalyzed ATRP. Prior to these findings, heme enzymes such as horseradish peroxidase (HRP) were extensively studied for their ability to catalyze free radical polymerizations of vinyl monomers (*18*, *19*) and aromatic compounds (*24–26*), by generating radicals from peroxides. Free radical polymerization, however, does not yield the well-defined polymers obtainable by ATRP and other controlled radical polymerizations.

In this chapter, we will review the emerging field of biocatalytic ATRP.

Downloaded by OHIO STATE UNIV LIBRARIES on May 31, 2012 | http://pubs.acs.org
Publication Date (Web): March 20, 2012 | doi: 10.1021/bk-2012-1100.ch011

Horseradish Peroxidase and Hemoglobin

In an ongoing project, we developed *N*,*N*,*N′*,*N′*-tetraethyldiethylene triamine (TEDETA)-based ATRP catalysts that were conjugated to proteins, such as bovine serum albumin (BSA), fluorescent proteins, and a hollow protein cage, the thermosome (THS) from *Thermoplasma acidophilum* (*27*, *28*). These conjugates are the first examples of protein-catalyst conjugates for ATRP. The proteins act as a functional support for the catalyst, e.g. by providing a handle to effectively remove the catalyst from solution, or to trace its location. Furthermore, the protein cage was used as a nanoreactor that allows the confinement of ATRP in nanoscale compartments. Polymerizations of *N*-isopropylacrylamide (NIPAAm) were carried out under ARGET ATRP conditions with the protein-catalyst conjugates. In the course of our work we planned to attach the ATRP catalysts to another protein, hemoglobin (Hb). However, a control experiment that involved native Hb, the reducing agent ascorbic acid, the ATRP initiator 2-hydroxyethyl-2-bromoisobutyrate (HEBIB), and NIPAAm in water surprisingly resulted in the formation of poly(*N*-isopropylacrylamide) (PNIPAAm). As the reaction mixture did not contain any conventional ATRP catalyst, any peroxides, or any other radical sources, the radicals that formed the polymer were most likely generated by the transfer of the bromine from the initiator to the enzyme. The discovery of possible catalytic activity by a native protein in an ATRP sparked our interest, and we investigated the heme protein Hb and heme enzyme HRP as catalysts for ARGET ATRP (Figure 1).

Downloaded by OHIO STATE UNIV LIBRARIES on May 31, 2012 | http://pubs.acs.org
Publication Date (Web): March 20, 2012 | doi: 10.1021/bk-2012-1100.ch011

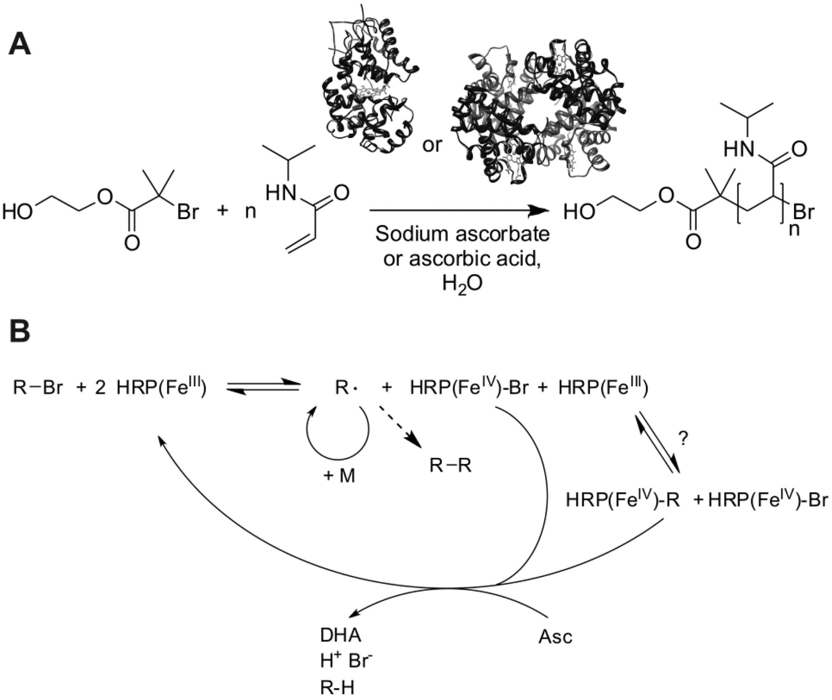

Figure 1. A) HRP- or Hb-catalyzed polymerization of NIPAAm under ARGET ATRP conditions. B) Possible mechanism of HRP's ATRPase activity. (Asc = sodium ascorbate, DHA = dehydroascorbic acid).

In our first report, we demonstrated that HRP, a monomeric enzyme with an Fe(III) protoporhyrin IX group at its active site, is a catalyst in the polymerization of NIPAAm under ARGET ATRP conditions at room temperature (*21*). The polymerization exhibits a degree of controlled character and involves reversible atom transfer between the enzyme and the initiator or the growing polymer chain. Thus, we proposed naming this newly discovered enzymatic activity ATRPase activity. PNIPAAm was obtained with relatively low molecular weight distributions (PDI $\geq$ 1.44). The bromine-content of a sample was analyzed by neutron activation analysis and showed a bromine chain-end functionality of 67%. The reaction followed first order kinetics, another requirement for a controlled polymerization (Figure 2a). However, the molecular weights were higher than the theoretical, as calculated from the monomer-to-initiator ratio, and did not increase with conversion, as would be expected for a conventional ATRP (Figure 2b). Possible explanations are slow initiation and that the deactivation reaction of the atom transfer equilibrium is not efficient enough to shift the equilibrium adequately to the side of the dormant species. Furthermore, the ATRPase mechanism is most likely more complex than the mechanism of conventional ATRP. Long dormant chains could be disfavored during reactivation due to steric hindrance at the active site of the enzyme, and side reactions could compete with the atom transfer mechanism, such as a reaction of polymer radicals with the metal center of HRP in its resting state, which would terminate chain growth. Another possibility is that polymer size is controlled by an affinity of the polymer chain to the enzyme in a tethering, processive-type of polymerization, which has been described for enzymes that synthesize polysaccharides (*29*). Thus, the exact mechanism of ATRPase activity remains to be elucidated and will be the subject of future work. Great care has been taken to characterize the HRP and to investigate its structural integrity during the reaction. Systematic variation of pH showed a pH-dependence of the catalytic performance typical for enzymes, with a maximal conversion at pH 7.0. Circular dichroism (CD) spectroscopy revealed no changes in the secondary structure of the enzyme, SDS and native gel electrophoresis as well as MALDI-TOF mass spectrometry showed that no enzyme-polymer conjugates formed (Figure 3). UV-Vis spectra of the enzyme were almost identical before and after the polymerization, and revealed that the peroxidase was in its Fe(III) resting state. These experiments allowed us to conclude that HRP is structurally stable under the reaction conditions and provided a first insight into the enzyme's redox states involved in the reaction.

Hb proved to be a more complex catalyst than HRP (*22*), most likely due to the fact that it consists of four subunits that influence each other and that it did not evolve to handle electron transfer reactions as efficiently as HRP. Moreover, Hb has surface-accessible cysteine residues that were found to act as chain transfer agents, effectively resulting in polymer chains that grew from the protein. This side-reaction was suppressed by blocking the accessible cysteines with a maleimide reagent. ARGET ATRP of NIPAAm with Cys-blocked Hb resulted in Br-terminated polymers (as determined by neutron activation analysis and a chain extension experiment), but with a lower degree of chain end-functionality than in the case of HRP. The PDIs of the polymers were higher, often around 2.0. The polymerization kinetics were of first order. Again, no increase in molecular weight with conversion was observed, and molecular weights were much higher than expected. The Hb showed only ATRPase activity in acidic conditions, which were also necessary to avoid the formation of green Hb, most likely a product due to porphyrin-to-protein crosslinking in the presence of radicals (*30*). The optimum activity was found to be at pH 3.7 in pure water. Characterization of the protein before, during, and after the polymerization revealed that it underwent some conformational changes, albeit the overall structure was preserved. Cys-blocked Hb did not result in any protein-polymer conjugates. The redox state changes during the polymerization were observed by UV-Vis spectroscopy. The Hb was in its methemoglobin form (Fe(III) state) before addition of ascorbic acid. The reducing agent reduced only the β-subunits to their Fe(II) state, which most likely reacted with the alkylbromide to form a radical species and Fe(III). The fact that a bromine-terminated polymer was obtained shows that the reaction also proceeded in the reverse reaction, i.e. that reversible atom transfer occurred. However, the ATRP equilibrium might compete with similar side reactions as in the case of HRP, e.g. quenching of radicals by the protein and other termination reactions. Interestingly, not only pure Hb but also fresh human erythrocytes were able to be used as catalyst for these ARGET ATRP-type polymerizations. Polymerization of NIPAAm with red blood cells resulted in polymers with PDI = 2.09 at 40% conversion. The polymerization was conducted to full conversion at

Downloaded by OHIO STATE UNIV LIBRARIES on May 31, 2012 | http://pubs.acs.org
Publication Date (Web): March 20, 2012 | doi: 10.1021/bk-2012-1100.ch011

the cost of broader molecular weight distributions. Not surprisingly, the degree of control over the polymerization exhibited by erythrocytes was lower than with pure Cys-blocked Hb, given the fact that a crude blood sample contains many molecules that can interact with radicals, e.g. cysteine residues on proteins.

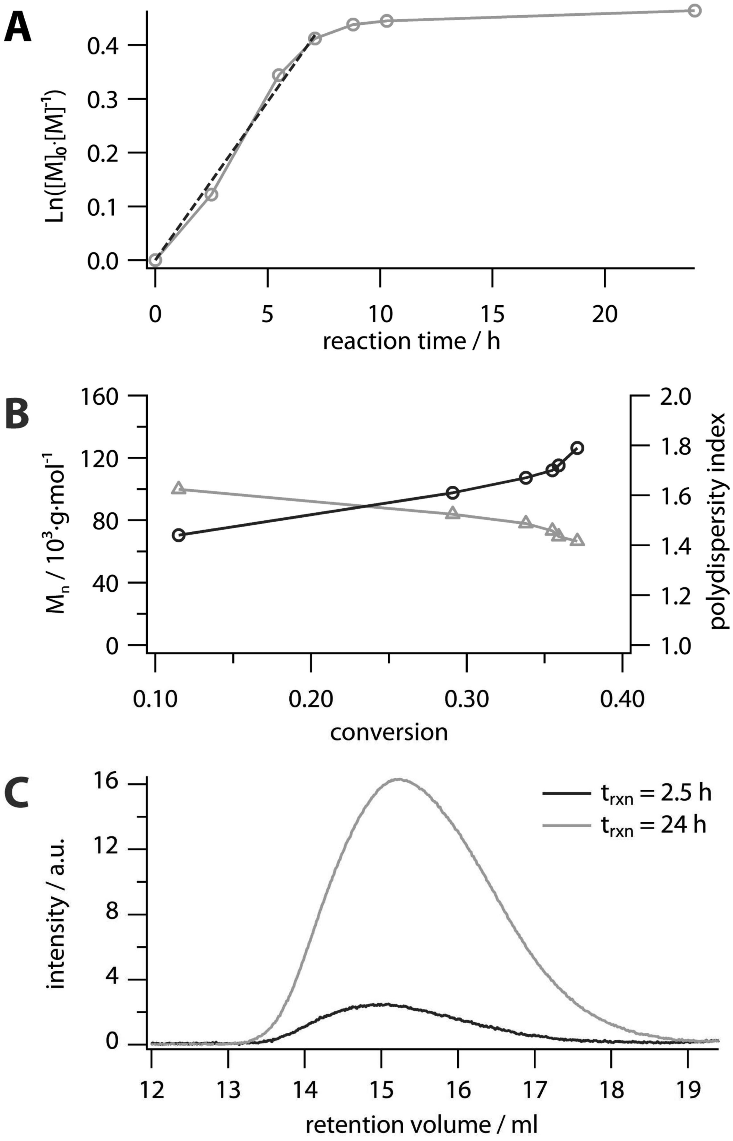

Figure 2. (A) kinetic plot, (B) molecular weight (Δ) and PDI (○) as a function of conversion and (C) selected GPC traces of an HRP-catalyzed polymerization of NIPAAm under ARGET ATRP conditions. (Reaction conditions: Ratio of HEBIB/NIPAAm/HRP 1:68:0.034; ratio ascorbate/HRP 33:1; buffered aqueous solution, pH 6.0; room temperature). (Reproduced with permission from reference (21). Copyright 2011 Wiley-VCH Verlag GmbH & Co. KGaA).

Downloaded by OHIO STATE UNIV LIBRARIES on May 31, 2012 | http://pubs.acs.org
Publication Date (Web): March 20, 2012 | doi: 10.1021/bk-2012-1100.ch011

Downloaded by OHIO STATE UNIV LIBRARIES on May 31, 2012 | http://pubs.acs.org
Publication Date (Web): March 20, 2012 | doi: 10.1021/bk-2012-1100.ch011

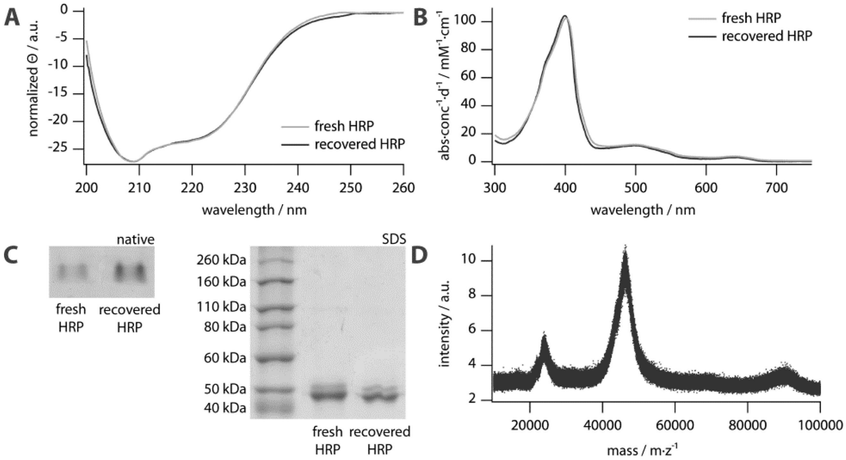

Figure 3. Characterization of HRP before and after polymerization of NIPAAm under ARGET ATRP conditions at pH 6.0 for 16 h. A) circular dichroism spectra, B) UV/Vis spectra, C) native and SDS gel electrophoresis. D) MALDI-TOF mass spectrum of recycled HRP shows the molecular ion peak of HRP$^+$ at m/z 44000, HRP^{2+} at m/z 22000, HRP dimer$^+$ at m/z 88000 and HRP trimer^{2+} weak at m/z 66000. (Reproduced with permission from reference (21). Copyright 2011 Wiley-VCH Verlag GmbH & Co. KGaA).

Catalase, Laccase, and Horseradish Peroxidase

In parallel with and independent of our research, di Lena and coworkers found the copper-containing enzyme laccase to initiate free radical polymerization by dehalogenation of an alkylbromide in the presence of ascorbic acid (*20*). The monomer polyethylenglycol methylether methacrylat (PEGMA) was polymerized in aqueous solution using the initiator ethyl 2-bromoisobutyrate (EBIB), while methylmethacrylate (MMA), styrene (St), 2-hydroxyethyl methacrylate (HEMA), and divinylbenzene (DVB) were polymerized in emulsion. The free radical polymerizations yielded partially insoluble polymers with very high molecular weights and very broad molecular weight distributions. Control of the enzyme-initiated radical polymerization was achieved by the addition of a chain transfer agent for reversible addition-fragmentation chain transfer polymerization, resulting in RAFT polymerization. In their follow-up paper, di Lena and coworkers found conditions under which the heme-enzyme catalase (CBL) polymerized poly(ethylene glycol) methyl ether acrylate (PEGA) in a controlled, ARGET-ATRP-type reaction in aqueous solution using bromopropionitrile (BPN) as initiator (Figure 4) (*23*). Laccase and HRP were also investigated in a limited set of reactions. First order polymerization kinetics during the initial phase of the polymerization, linear increase of molecular weight with conversion (although with a non-zero intercept), low molecular weight distributions (PDI between 1.2

and 1.7) and the fact that bromine-terminated chains were obtained (as determined by NMR and a chain extension experiment) show that the polymerizations followed a controlled atom-transfer mechanism.

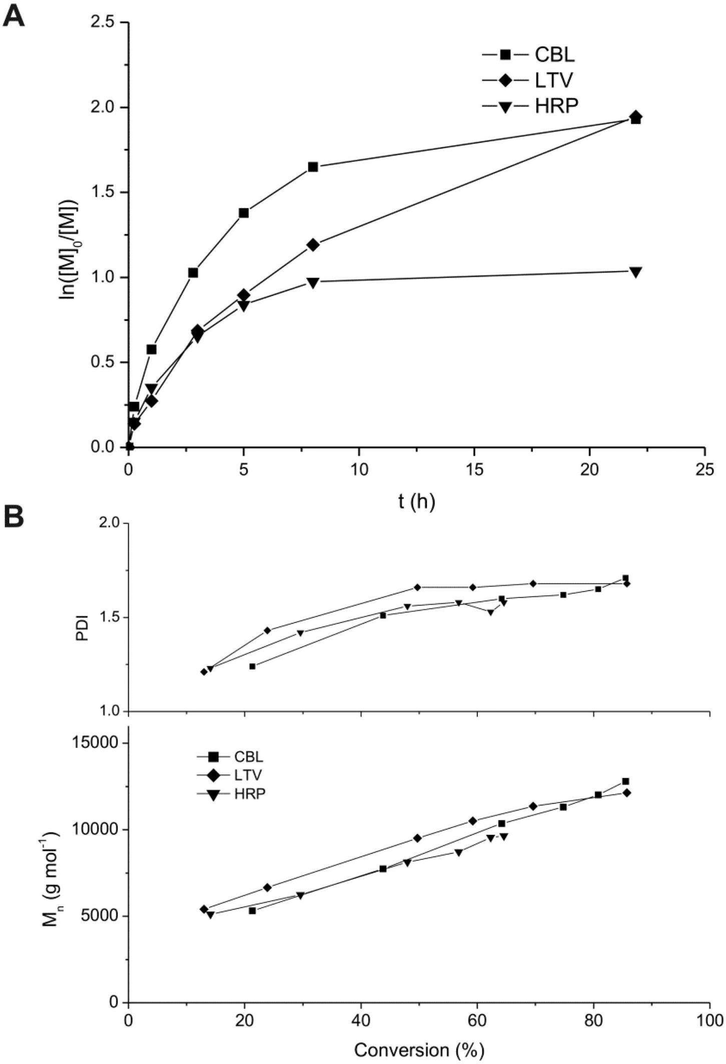

Figure 4. Selected polymerizations of PEGA catalyzed by catalase (CBL), laccase (LTV), and horseradish peroxidase (HRP). (A) kinetic plot and (B) molecular weight and PDI as a function of conversion. (Reaction conditions: Ratio of BPN/PEGA 1:35; ratio BPN/ ascorbic acid/CBL subunits 1:8.2:0.0096; ratio BPN/ ascorbic acid/LTV 1:8.2:0.0013; ratio BPN/ ascorbic acid/HRP 1:8.2:0.0030; water; 60 °C.). (Data are from reference (23).

Downloaded by OHIO STATE UNIV LIBRARIES on May 31, 2012 | http://pubs.acs.org
Publication Date (Web): March 20, 2012 | doi: 10.1021/bk-2012-1100.ch011

As no direct characterization of the enzymes was provided, the stability of the proteins under the reaction conditions and the effect of pH remain unclear, and could be clarified in future work. Most of the reactions in the ARGET-ATRP paper were carried out at 60 °C under acidic conditions (*23*). However, catalase is known to denature between 42 and 62 °C in water, with full denaturation taking place at 62 °C (*31*). Laccase rapidly loses its native activity at 60 °C at pH 6 (*32*), and HRP has a melting temperature of 62 °C at pH 7.4 (*33*). On the other hand, a polymerization carried out with CBL at 40 °C gave similar results regarding evolution of molecular weight and PDI than the reactions with CBL at 60 °C, which could indicate that the catalase was stable at elevated temperatures. Nevertheless, the value of the publication lies in its thoroughly conducted polymerization reactions that provide proof that catalase, laccase and HRP are ATRPases which allow biocatalytic, controlled radical polymerizations to be carried out.

Downloaded by OHIO STATE UNIV LIBRARIES on May 31, 2012 | http://pubs.acs.org
Publication Date (Web): March 20, 2012 | doi: 10.1021/bk-2012-1100.ch011

Conclusions

With a growing world population, increasing demand and endangered natural resources it is obvious that the environmental impact of chemical synthesis has to be lowered. The so-called green-chemistry approach calls for replacing toxic reagents with those that are non-toxic, and using feedstocks from renewable resources. Enzymes are ideal green catalysts, as they are non-toxic, environmentally friendly, and obtained from living organisms. The first findings that certain native enzymes and proteins can mediate ARGET ATRP have been reviewed in this chapter. Such ATRPase activity is important both from a basic scientific point of view, as ATRP represents a novel type of reaction carried out by enzymes, and from an applications point of view, as proteins and enzymes are non-toxic and do not contaminate the product with traces of transition metal complexes, thus representing an environmentally friendly alternative to conventional ATRP catalysts. Polymers synthesized with these enzymes will most likely be suitable for biomedical and food-grade applications.

We are still at the beginning of understanding the underlying principles and influencing factors governing this new enzymatic reaction and many open questions remain. Also, it is obvious that the catalytic performance of ATRPases is, at the present stage, not comparable to the well-established ATRP catalysts based on transition metal complexes. However, the initial reports on ATRPase activity will pave the way for further studies on biocatalytic ATRP. Given the fact that only a few metallo-enzymes have been probed for ATRPase activity, and that the parameter space of pH, buffers, solvents, temperature, monomers, reducing agents, etc. has only been touched upon, it is likely that the performance of enzymes in ATRP can be significantly increased. Moreover, biotechnology offers a wide range of well-established tools to improve the performance of biocatalysts, ranging from rational design to directed evolution, which could be used to the benefit of biocatalytic, controlled radical polymerizations.

In Progress in Controlled Radical Polymerization: Mechanisms and Techniques; Matyjaszewski, K., et al.;
ACS Symposium Series; American Chemical Society: Washington, DC, 2012.

Downloaded by OHIO STATE UNIV LIBRARIES on May 31, 2012 | http://pubs.acs.org
Publication Date (Web): March 20, 2012 | doi: 10.1021/bk-2012-1100.ch011

Acknowledgments

Generous financial support by a Marie Curie Intra European Fellowship (ThermosomeNanoReact, GA 237110) and a Marie Curie European Reintegration Grant (ProteinATRP, GA 277120) within the 7th European Community Framework Programme, by the NCCR Nanoscale Science as well as a Sciex-NMS^{ch} fellowship (FP-PROT ATRP, 10.041) is gratefully acknowledged. We thank Mark Inglin for editing and proofreading the manuscript.

References

1. Braunecker, W. A.; Matyjaszewski, K. *Prog. Polym. Sci.* **2007**, *32*, 93–146.
2. Tsarevsky, N. V.; Matyjaszewski, K. *Chem. Rev.* **2007**, *107*, 2270–2299.
3. Grover, G. N.; Maynard, H. D. *Curr. Opin. Chem. Biol.* **2010**, *14*, 818–827.
4. Gauthier, M. A.; Klok, H.-A. *Polym. Chem.* **2010**, *1*, 1352–1373.
5. Mueller, L.; Matyjaszewski, K. *Macromol. React. Eng.* **2010**, *4*, 180–185.
6. di Lena, F.; Matyjaszewski, K. *Prog. Polym. Sci.* **2010**, *35*, 959–1021.
7. Ouchi, M.; Terashima, T.; Sawamoto, M. *Chem. Rev.* **2009**, *109*, 4963–5050.
8. Kobayashi, S.; Makino, A. *Chem. Rev.* **2009**, *109*, 5288–5353.
9. Loos, K., Ed.; *Biocatalysis in Polymer Chemistry*; Wiley-VCH: Weinheim, 2010.
10. Palmans, A. R. A., Heise, A., Eds.; *Enzymatic Polymerisation*; Adv. Polym. Sci., 237; Springer: Berlin, Heidelberg, 2010.
11. Miletić, N.; Loos, K.; Gross, R. A. In *Biocatalysis in Polymer Chemistry*; Loos, K., Ed.; Wiley-VCH: 2010; pp 83−129.
12. Cheng, H. N. In *Biocatalysis in Polymer Chemistry*; Loos, K., Ed.; Wiley-VCH: 2010; pp 131−141.
13. Veld, M. A. J.; Palmans, A. R. A. *Adv. Polym. Sci.* **2010**, *237*, 55–78.
14. Mei, Y.; Miller, L.; Gao, W.; Gross, R. A. *Biomacromolecules* **2003**, *4*, 70–74.
15. Uyama, H. In *Biocatalysis in Polymer Chemistry*; Loos, K., Ed.; Wiley-VCH: 2010; pp 165−185.
16. van der Vlist, J.; Loos, K. In *Biocatalysis in Polymer Chemistry*; Loos, K., Ed.; Wiley-VCH Verlag GmbH & Co. KGaA: 2010; pp 211−246.
17. van der Vlist, J.; Loos, K. *Adv. Polym. Sci.* **2010**, *237*, 21–54.
18. Singh, A.; Kaplan, D. *Adv. Polym. Sci.* **2006**, *194*, 211–224.
19. Hollmann, F. In *Biocatalysis in Polymer Chemistry*; Loos, K., Ed.; Wiley-VCH: Weinheim, 2010; pp 143−164.
20. Ng, Y.-H.; di Lena, F.; Chai, C. L. L. *Polym. Chem.* **2011**, *2*, 589–594.
21. Sigg, S. J.; Seidi, F.; Renggli, K.; Silva, T. B.; Kali, G.; Bruns, N. *Macromol. Rapid Commun.* **2011**, *32*, 1710–1715.
22. Silva, T. B.; Seidi, F.; Charan, H.; Sigg, S. J.; Renggli, K.; Kali, G.; Bruns, N., 2011, manuscript in preparation.
23. Ng, Y.-H.; di Lena, F.; Chai, C. L. L. *Chem. Commun.* **2011**, *47*, 6464–6466.
24. Reihmann, M.; Ritter, H. *Adv. Polym. Sci.* **2006**, *194*, 1–49.
25. Walde, P.; Guo, Z. *Soft Matter* **2011**, *7*, 316–331.
26. Ochoteco, E.; Mecerreyes, D. *Adv. Polym. Sci.* **2010**, *237*, 1–19.

27. Bruns, N.; Renggli, K.; Seidi, F.; Kali, G. *Polym. Prepr. (Am. Chem. Soc., Div. Polym. Chem.)* **2011**, *52*, 521–522.
28. Bruns, N.; Pustelny, K.; Bergeron, L. M.; Whitehead, T. A.; Clark, D. S. *Angew. Chem., Int. Ed.* **2009**, *48*, 5666–5669.
29. May, J. F.; Splain, R. A.; Brotschi, C.; Kiessling, L. L. *Proc. Natl. Acad. Sci. U.S.A.* **2009**, *106*, 11851–11856.
30. Reeder, B. J. *Antioxid. Redox Signaling* **2010**, *13*, 1087–1123.
31. Bartoszek, M.; Kściuczyk, M. *J. Mol. Struct.* **2005**, *744-747*, 733–736.
32. Kurniawati, S.; Nicell, J. A. *Bioresour. Technol.* **2008**, *99*, 7825–7834.
33. Liu, J.-Z.; Wang, T.-L.; Huang, M.-T.; Song, H.-Y.; Weng, L.-P.; Ji, L.-N. *Protein Eng., Des. Sel.* **2006**, *19*, 169–173.

Downloaded by OHIO STATE UNIV LIBRARIES on May 31, 2012 | http://pubs.acs.org
Publication Date (Web): March 20, 2012 | doi: 10.1021/bk-2012-1100.ch011

Downloaded by STANFORD UNIV GREEN LIBR on May 31, 2012 | http://pubs.acs.org
Publication Date (Web): March 20, 2012 | doi: 10.1021/bk-2012-1100.ch012

Chapter 12

ARGET ATRP of BMA and BA: Exploring Limitations at Low Copper Levels

Kevin A. Payne, Michael F. Cunningham,* and Robin A. Hutchinson*

**Department of Chemical Engineering, Queen's University,
Kingston, ON, K7L 3N6 Canada
*E-mails: michael.cunningham@chee.queensu.ca (M.F.C.);
robin.hutchinson@chee.queensu.ca (R.A.H.)**

Batch ARGET ATRP of butyl methacrylate (BMA) and butyl acrylate (BA) was systematically investigated over a range of initiator, catalyst, and reducing agent loadings to produce material with a target molecular weight of 5,000 g·mol^{-1}. Reducing copper catalyst loading to 36 molar ppm with respect to monomer (800 chains per Cu atom) in the BMA system, however, led to a significant decrease in polymerization rate and initiator efficiency. Rate was recovered with a large excess of reducing agent, with some loss of livingness. Similar trends were observed for BA polymerization, but initiator efficiencies were significantly higher than found with BMA. Achieving reasonable rates of polymerization while maintaining control of livingness at low catalyst levels requires a trade-off between catalyst and reducing agent loadings.

Atom Transfer Radical Polymerization (ATRP) is a form of Controlled/Living Radical Polymerization (CRP/LRP) in which the polymerization is mediated by a metal that has *n* and *n+1* oxidation states. The reaction mechanism with the most common catalyst choice, copper, is shown in Figure 1. The forward activation reaction with rate coefficient k_{act} creates the radical as Cu^{I} is oxidized to Cu^{II}, with the rate coefficient for the reverse deactivation reaction (k_{deact}) several orders of magnitude greater than k_{act} such that the radical typically adds only a few monomer units before deactivating (*1–6*). A well-controlled and living system exhibits a narrow polymer molar mass distribution (MMD) with minimal

In Progress in Controlled Radical Polymerization: Mechanisms and Techniques; Matyjaszewski, K., et al.;
ACS Symposium Series; American Chemical Society: Washington, DC, 2012.

Downloaded by STANFORD UNIV GREEN LIBR on May 31, 2012 | http://pubs.acs.org
Publication Date (Web): March 20, 2012 | doi: 10.1021/bk-2012-1100.ch012

termination such that the entire MMD shifts to higher values with increasing conversion. The concern for normal ATRP is the accumulation of the Cu^{II} species due to loss of radicals by termination, and by oxidation of Cu^{I} by impurities such as oxygen. The resulting reduction in polymerization rate necessitates operation with an elevated Cu level approaching 1 catalyst species per chain. The copper must then be removed from the polymer product once the reaction is complete, as it produces discoloration.

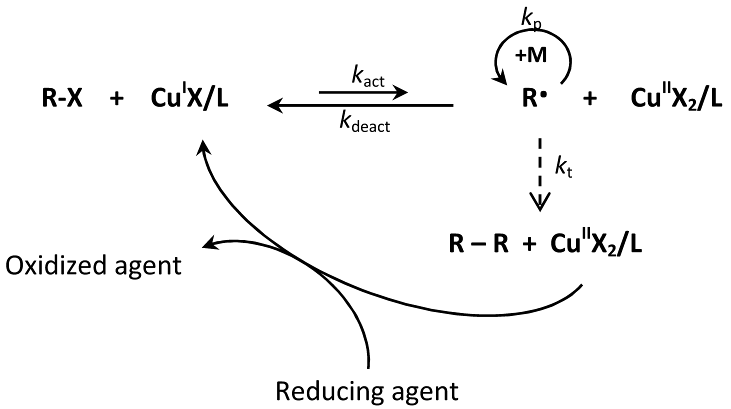

Figure 1. Mechanism for ARGET ATRP. The Cu^{I} activator is constantly regenerated from Cu^{II} by the reducing agent.

Matyjaszewski et al. have recently developed a modified version of ATRP known as ARGET, for "activators regenerated by electron transfer", through which catalyst concentration can be lowered to parts per million (ppm) levels with respect to monomer while still maintaining a reasonable polymerization rate and molecular weight (MW) control. The technique employs the more oxidatively stable Cu^{II} species as a starting material, along with an excess of an additional reagent which reduces deactivator (whose concentration has built up due to termination) to regenerate Cu^{I} activating species, as seen in Figure 1 (*7*, *8*).

The rate expression for the ATRP system, which also holds for ARGET ATRP, is written as

$$R_{\mathrm{p}} = k_{\mathrm{p}}[M][R-X]\frac{k_{\mathrm{act}}[Cu^{I}X/L]}{k_{\mathrm{deact}}[Cu^{II}X_2/L]} \qquad (1)$$

where $K_{ATRP} = k_{act}/k_{deact}$ is the ATRP equilibrium constant, k_p is the propagation rate coefficient of the monomer, [M] is monomer concentration, [R-X] is the concentration of dormant chains, $[Cu^{I}]$ and $[Cu^{II}]$ are the concentration of activator and deactivator species present in the system with (pseudo) halide *X* and ligand *L* (*8*). Usually, as most chains are in the dormant state at any instant in time, [R-X] is approximated by $[R\text{-}X]_o$, the amount of alkyl halide initiator added to the system.

The polymer dispersity index (PDI) may be estimated by eq 2,

$$PDI = \frac{\mathrm{Mw}}{\mathrm{Mn}} = 1 + \frac{1}{\mathrm{DP}_{\mathrm{nT}}} + \left(\frac{[R-X]_{\mathrm{o}} k_{\mathrm{p}}}{k_{\mathrm{deact}}[Cu^{II}X_2 / L]} \right) \left(\frac{2}{x} - 1 \right) \quad (2)$$

where x is polymer conversion, Mn and Mw are the number-average and weight-average polymer molar masses, respectively, and $\mathrm{DP}_{\mathrm{nT}}$ is the target chain length. The latter quantity is given by $[\mathrm{M}]_{\mathrm{o}}/[\mathrm{R\text{-}X}]_{\mathrm{o}}$, the ratio of the initial molar concentrations of monomer and initiator, respectively (*2*). The target molar mass (Mn_{T}) at full conversion can be calculated by eq 3,

$$\mathrm{Mn}_{\mathrm{T}} = \frac{m_{\mathrm{monomer}}}{\eta_{\mathrm{init}}} \quad (3)$$

where m_{monomer} is the mass of monomer and η_{init} is the number of moles of initiator added to the reactor. The initiator efficiency (f_{init}) is estimated by

$$f_{\mathrm{init}} = \frac{\mathrm{Mn}_{\mathrm{T}}}{\mathrm{Mn}_{\mathrm{exp}}} \cdot x \quad (4)$$

where $\mathrm{Mn}_{\mathrm{exp}}$ is the number-average molar mass obtained from size exclusion chromatography (SEC).

Recently, Zhong and Matyjaszewski (*9*) have derived a relationship to estimate dead chain fraction (DCF), under the assumption that the radical concentration does not change significantly.

$$\mathrm{DCF} = \frac{[T]}{f_{\mathrm{init}}[R-X]_{\mathrm{o}}} = \frac{2\mathrm{DP}_{\mathrm{nT}} k_{\mathrm{t}} \left(\ln(1-x) \right)^2}{f_{\mathrm{init}}[M]_{\mathrm{o}} k_{\mathrm{p}}^2 t} \quad (5)$$

[T] is the concentration of terminated chains, $[\mathrm{R\text{-}X}]_{\mathrm{o}}$ is the concentration of chains (initiator) added to the system, k_t is the termination rate constant and t is the reaction time (*9*). We have modified eq 5 by adding an initiator efficiency factor, f_{init}, to correct for deviation from quantitative initiation. This equation shows that DCF increases with increasing conversion and target chain length, and decreases with reduced reaction rate (longer t to reach the same value of x).

Previous work in low Cu ARGET ATRP has been performed for target chain lengths of 100-200 units with molar concentrations of Cu as low as ~2 ppm with respect to monomer. The number of polymer molecules being mediated per catalyst molecule is often 100 (*8*, *10*, *11*), although studies at over 1000 chains per Cu have been reported (*7*, *12*, *13*). This previous work finds that an increase in the number of chains mediated per Cu molecule results in longer reaction times, sometimes requiring over 20 hours to achieve a conversion greater than 40%. Termination as well as transfer can be minimized by limiting the targeted chain length, as these reactions increase in proportion to chain length and conversion (*14*). Zhong and Matyjaszewski suggested that the combination of higher $\mathrm{DP}_{\mathrm{nT}}$

Downloaded by STANFORD UNIV GREEN LIBR on May 31, 2012 | http://pubs.acs.org
Publication Date (Web): March 20, 2012 | doi: 10.1021/bk-2012-1100.ch012

Downloaded by STANFORD UNIV GREEN LIBR on May 31, 2012 | http://pubs.acs.org
Publication Date (Web): March 20, 2012 | doi: 10.1021/bk-2012-1100.ch012

and lower conversion should give fewer dead chains when targeting a desired chain length and still achieving a reasonable polymerization rate (*9*). However, this strategy requires additional separation of unconverted monomer and higher Cu levels from the polymer.

The purpose of this experimental study is to determine practical operating regimes for the ARGET ATRP system in a batch reactor. For industry to consider adoption of ARGET ATRP chemistry, the system must include limited reaction time with minimal copper levels to be competitive with conventional free radical polymerization (FRP) processes. The reaction conditions investigated include changes in monomer type, chain length (initiator loading), the initial concentrations of catalyst, reducing agent, and initiator, as well as the ratios of the catalyst to reducing agent and initiator to catalyst/reducing agent. In this work, the catalyst concentration was lowered to 34-37 ppm on a molar basis relative to monomer. Unless otherwise stated, the target molecular weight for each reaction was 5,000 $g \cdot mol^{-1}$, while the solvent content was 30 wt%; the short chain length and high polymer content are applicable to the coatings industry (*15*, *16*). Thus, the reactions are run with as many as 800 chains per Cu molecule, with typical reaction times of 6 hours. Loss of control and termination at higher monomer conversion are problems that are particularly apparent in this type of system (low DPnT and large number of chains), and as such are a major hindrance in the ability to lower catalyst levels.

Experimental

Materials

Butyl methacrylate (BMA; 99%, Aldrich), butyl acrylate (BA; 99%, Aldrich), copper(II) bromide ($CuBr_2$, 99% Aldrich), anisole (99%, Aldrich), ethyl α-bromoisobutyrate (EBiB; 98%, Aldrich), and tin(II) 2-ethylhexanoate ($Sn(EH)_2$, 95%, Aldrich) were used as received.

Procedure

All polymerizations were carried out under batch conditions in a 100 mL two-neck round-bottom flask in a thermostated oil bath with a condenser to prevent loss of solvent or monomer. The catalyst [Cu(II)TPMABr]Br was synthesized according to the literature (*17*) and dissolved in 10 g of anisole by sonication for 20 minutes. $[TPMA]:[Cu^{II}]$ was kept at a 1:1 molar ratio for all reactions. 35 g of monomer was mixed with the catalyst and anisole in a round-bottom flask. The mixture was purged under nitrogen and stirred at 250 rpm for 40 minutes before heating to the desired reaction temperature. The initiator ethyl α-bromoisobutyrate (EBiB) was dissolved in 2.5 g of anisole and injected into the round-bottom flask using a degassed syringe. After approximately 10 minutes, the reducing agent, tin(II) 2-ethylhexanoate ($Sn(EH)_2$), which was dissolved in 2.5 g of anisole and purged with nitrogen, was injected, marking the beginning of the reaction. Samples were taken with a deoxygenated syringe at various times throughout the reaction, with polymerizations assumed to stop upon exposure to air.

Analytical Methods

Conversion was calculated by gravimetry and molecular weight was measured by size exclusion chromatography (SEC) using a Waters 2960 separation module with Styragel packed columns HR 0.5, HR 1, HR 3, HR 4, and HR 5E (Waters Division Millipore) coupled with a refractive index detector operating at 40 °C. THF was used as eluent and the flow rate was set to 1.0 mL·min^{-1}. The detector was calibrated with eight narrow polystyrene standards, ranging from 347 to 355000 g·mol^{-1}. The molecular weights of poly(BMA), and poly(BA) samples were obtained by universal calibration using known Mark-Houwink parameters for polystyrene ($K = 11.4 \times 10^{-5}$ dL·g^{-1}, $a = 0.716$) (*18*), poly(BMA) ($K = 14.8 \times 10^{-5}$ dL·g^{-1}, $a = 0.664$) (*18*), and poly(BA) ($K = 7.4 \times 10^{-5}$ dL·g^{-1}, $a = 0.750$) (*19*).

Results

Initiator Loading

Butyl methacrylate (BMA) was polymerized at 70 °C, with the target polymer MW altered by changing the [M]:[R-X] ratio, thus changing the number of chains in the system and also the number of chains that each catalyst molecule has to initiate and regulate. The catalyst and reducing agent loadings were adjusted in this set of initial experiments to ensure a constant molar ratio relative to initiator of [R-X]:[Cu]:[Sn] = 1:0.01:0.1. A summary of the results, which compare well with those previously published for a target chain length of 200 (*12*), is presented in Table I. The target MWs corresponding to [BMA]:[R-X] ratios of 400:1, 100:1, 70:1, and 35:1 are 56,800 g·mol^{-1}, 14,200 g·mol^{-1}, 10,000 g·mol^{-1} and 5,000 g·mol^{-1}, respectively. Note that all tabulated results are for the final sample in each reaction, and that the added Cu levels are presented on a molar basis with respect to initial monomer content (ppm or µmol·mol^{-1}).

The experimental profiles are plotted in Figure 2. The increased initiator concentration that results from lowering the target chain length leads to an increased polymerization rate (Figure 2a), as expected from eq 1. Mn increased linearly with conversion (Figure 2b), and PDI was <1.3 for all cases (Figure 2c). What is most noteworthy is the apparent increase in initiator efficiency that occurs with reaction time (Figure 2d), as estimated from polymer Mn values by eq 4. Efficiencies are less than unity in all cases, and indicate that the activation of R-X is slow and not complete. This situation is most obvious at the lowest Cu levels (<30 ppm, $DP_{nT} = 400$), for which the reduced initiator efficiency as well as the reduced $[R\text{-}X]_o$ value contributes to the lower rate of polymerization.

Downloaded by STANFORD UNIV GREEN LIBR on May 31, 2012 | http://pubs.acs.org
Publication Date (Web): March 20, 2012 | doi: 10.1021/bk-2012-1100.ch012

Table I. Batch ARGET ATRP of BMA at 70 °C with 30 wt% anisole and [R-X]:[Cu]:[Sn] = 1:0.01:0.1

Initial Ratio [M]:[R-X]:[Cu]:[Sn]	*Cu (ppm)*[a]	*Time (min)*	*Conversion*	*Mn_{exp} (g·mol^{-1})*	*Initiator Efficiency*
400:1:0.01:0.1	28	360	0.43	36200	0.64
200:1:0.01:0.1[b]	50	300	0.59	18500	0.64
100:1:0.01:0.1	100	360	0.95	18529	0.72
70:1:0.01:0.1	143	300	0.96	13156	0.73
35:1:0.01:0.1	285	120	0.87	6954	0.62

[a] Cu level reported as a molar ratio with respect to initial monomer concentration.
[b] Previously reported (*12*).

Downloaded by STANFORD UNIV GREEN LIBR on May 31, 2012 | http://pubs.acs.org
Publication Date (Web): March 20, 2012 | doi: 10.1021/bk-2012-1100.ch012

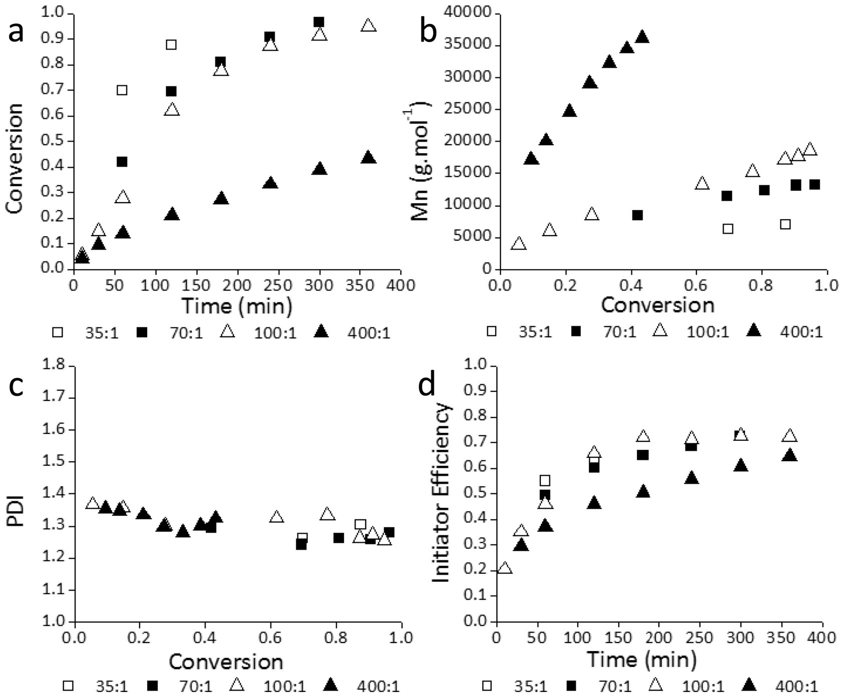

Figure 2. Batch ARGET ATRP of BMA with varying initiator loading at 70 °C: (a) monomer conversion versus time; (b) number-average molecular weight (Mn) and (c) polydispersity index (PDI) as a function of conversion; (d) initiator efficiency versus time. Legend shows initial molar ratios of [M]:[R-X], with [R-X]:[Cu]:[Sn] = 1:0.01:0.1.

The polymer MMDs for the BMA polymerizations with target chain lengths of 70 and 400 are shown in Figure 3; both systems have a similar PDI (Figure 2c) despite the difference in DP_{nT}. The MMDs exhibit a low MW tail which remains visible even at increased reaction times. This tail may be the result of termination of low MW chains early in the batch, or may be an indication of slow initiation in the system. The latter explanation is consistent with the initiator efficiencies shown in Figure 2d. As the decrease in DP_{nT} (and resulting increase in rate) was achieved by a simultaneous increase in initiator and copper levels, the effect of varying copper level at constant DP_{nT} was examined in the next set of experiments.

Downloaded by STANFORD UNIV GREEN LIBR on May 31, 2012 | http://pubs.acs.org
Publication Date (Web): March 20, 2012 | doi: 10.1021/bk-2012-1100.ch012

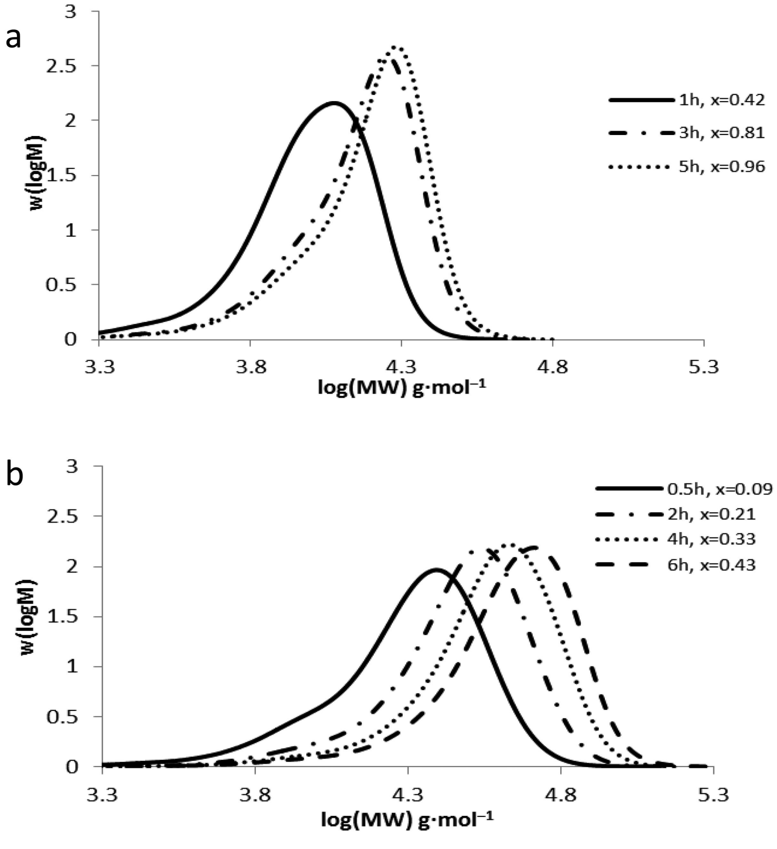

Figure 3. MMDs of pBMA produced by batch ARGET ATRP AT 70 °C, sampled hourly to confirm living nature of polymerization: (a) [M]:[R-X]:[Cu]:[Sn]=70:1:0.01:0.1; (b) [M]:[R-X]:[Cu]:[Sn]=400:1:0.01:0.1.

Effect of Decreased Catalyst and Reducing Agent Loading

To measure the effect of decreased catalyst level, the amounts of Cu and reducing agent were kept at a constant molar ratio of $[Cu(II)TPMABr_2]:[Sn(EH)_2]$ = 1:10 while reducing the catalyst loading from 285 to 36 ppm at constant

Downloaded by STANFORD UNIV GREEN LIBR on May 31, 2012 | http://pubs.acs.org
Publication Date (Web): March 20, 2012 | doi: 10.1021/bk-2012-1100.ch012

monomer and initiator levels. The ratio of catalyst to number of chains was therefore decreased from one Cu per 100 chains to one Cu per 800 chains, assuming 100% initiator efficiency, while maintaining a target chain length of 35 (Mn_T = 5,000 g·mol^{-1}). A summary of the experiments is presented in Table II and plotted as Figure 4.

Table II. Batch ARGET ATRP of BMA with varying catalyst levels and 30 wt% anisole at 70 °C with Mn_T = 5,000 g·mol^{-1}, maintaining [Cu]:[Sn] at 1:10

Initial Ratio [M]:[R-X]:[Cu]:[Sn]	*Cu (ppm)*	*Time (min)*	*Conversion*	*Mn_{exp} (g·mol^{-1})*	*Initiator Efficiency*
35:1:0.01:0.1	285	120	0.88	6954	0.62
35:1:0.005:0.05	145	360	0.88	8726	0.50
35:1:0.005:0.05	145	360	0.85	8707	0.48
35:1:0.0025:0.025	72	300	0.69	7863	0.44
35:1:0.00125:0.0125	36	360	0.44	8778	0.25

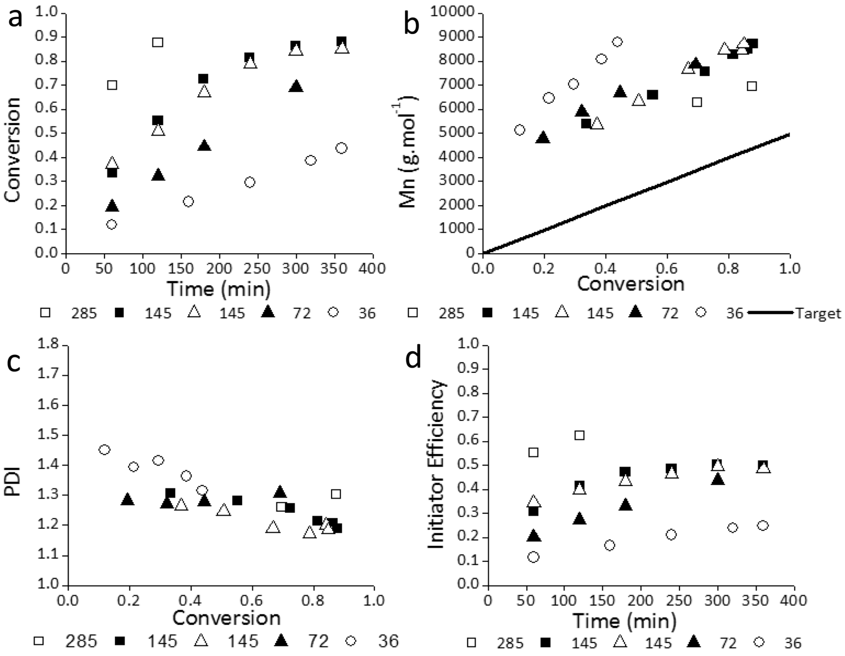

Figure 4. Batch ARGET ATRP of BMA with decreasing catalyst loading for target Mn = 5,000 g·mol^{-1} at 70 °C (see Table II): (a) monomer conversion versus time; (b) number-average molecular weight (Mn) and (c) polydispersity index (PDI) as a function of conversion; (d) initiator efficiency versus time. The Cu level (ppm) in the legend is presented on a molar basis with respect to monomer.

Downloaded by STANFORD UNIV GREEN LIBR on May 31, 2012 | http://pubs.acs.org
Publication Date (Web): March 20, 2012 | doi: 10.1021/bk-2012-1100.ch012

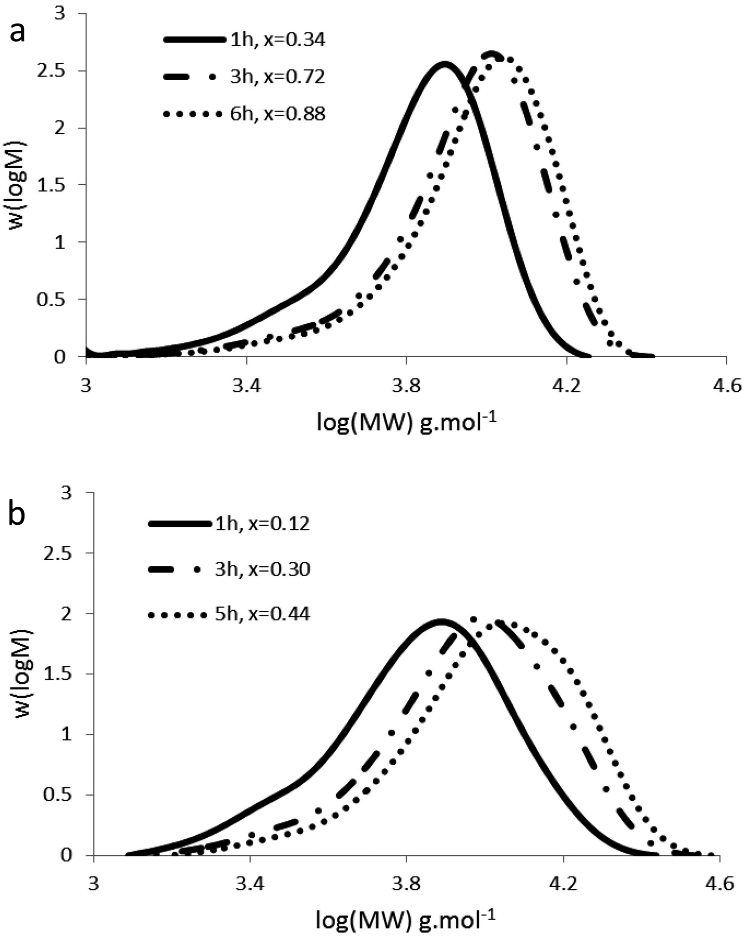

Figure 5. MMDs of pBMA produced by batch ARGET ATRP at 70 °C, sampled hourly to confirm living nature of polymerization. Copper concentration of (a) 145 ppm and (b) 36 ppm on a molar basis with respect to monomer.

Assuming that a constant ratio of catalyst to reducing agent preserves a similar Cu^I/Cu^{II} ratio across varying catalyst levels, there should not be a decrease in reaction rate with lower catalyst concentrations (eq 1). However, it is clear from the monomer conversion profiles (Figure 4a) that the polymerization rate decreases significantly with decreasing catalyst concentration, as has been seen previously in other ARGET systems with higher Mn_T (*8*, *12*, *20*). The experimental Mn values are well above the target chain length (Figure 4b), with the difference becoming greater as the Cu level is decreased from 285 ppm to 36 ppm. The estimated decrease in initiator efficiency (Figure 4d) matches the trends seen in the conversion profiles, suggesting that the decrease in effective chain concentration causes the decrease in the reaction rate. The polymer MMDs (Figure 5) have an observable high MW shoulder as well as a significant short chain population at the reduced copper level of 36 ppm (Figure 5b), indicating the gradual loss of control and difficulty with uniform initiation, respectively. Estimates of catalyst equilibrium at various initial copper loadings will be discussed in a later section.

Effect of Varying Catalyst and Reducing Agent Loading

The first set of BMA experiments indicated that a reasonable polymerization rate and MW control could be maintained while lowering the target MW of the polymer to 5,000 g·mol^{-1}. However, the copper levels were increased proportionally with [R-X], such that the experiment had a Cu level of 285 ppm relative to monomer. As the Cu level was reduced from 285 to 36 ppm at a constant [Cu]:[Sn] ratio of 1:10 (Table II), there was a significant decrease in polymerization rate and initiator efficiency. Thus, the next investigation was to determine the effect of increasing the reducing agent ($Sn(EH)_2$) loading while keeping a constant ratio of [M]:[R-X]:[Cu]. The experiments are summarized in Table III with the results presented in Figure 6. The initiator efficiency was also plotted with respect to conversion, as shown in Figure 7.

Downloaded by STANFORD UNIV GREEN LIBR on May 31, 2012 | http://pubs.acs.org
Publication Date (Web): March 20, 2012 | doi: 10.1021/bk-2012-1100.ch012

Table III. Batch ARGET ATRP of BMA at 70 °C with varying reducing agent levels and 30 wt% anisole with a constant molar ratio of [M]:[R-X]:[Cu] = 35:1:0.00125. Mn_T is constant at 5,000 g·mol^{-1}

Initial Ratio [Cu]:[Sn]	*Cu (ppm)*	*Time (min)*	*Conversion*	*Mn_{exp} (g·mol^{-1})*	*Initiator Efficiency*
1:10	36	360	0.44	8778	0.25
1:20	36	360	0.45	8915	0.26
1:40	34	300	0.45	8473	0.26
1:100	37	360	0.94	11237	0.42

The results shown earlier (Figure 4) demonstrated that reducing the Cu level from 145 to 36 ppm while maintaining a [Cu]:[Sn] ratio of 1:10 led to a marked reduction in polymerization rate and initiator efficiency, with almost 88% conversion seen at the higher Cu level and approximately 44% conversion at the lower Cu level. Increasing the reducing agent loading at 36 ppm Cu has minimal impact on the reaction rate until a Cu:Sn ratio of 1:100 is reached, at which point a large increase in polymerization rate, especially after 2 hours, was observed (Figure 6a). This increase was also found in previous studies for systems where the chain to Cu ratio is lower (*20–22*). A methyl acrylate conversion of 93% was achieved in 3.3 hours versus 87% in 5 hours when the reducing agent (ascorbic

In Progress in Controlled Radical Polymerization: Mechanisms and Techniques; Matyjaszewski, K., et al.;
ACS Symposium Series; American Chemical Society: Washington, DC, 2012.

acid) to catalyst ratio was lowered from 100:1 to 10:1 for a system with 100 chains per Cu molecule (*20*). Using Sn(EH)$_2$ at 90 °C with 200 chains per Cu molecule, 97% versus 87% conversion of BMA was achieved in 6 hours when the [Sn]:[Cu] ratio was changed from 40:1 to 10:1 (*21*). The effect of reducing agent on BMA conversion profiles is much larger for our system with 800 chains per Cu molecule. According to eq 1, the decreased polymerization rates found at decreased Cu levels may result from a lower [Cu^I]/[Cu^{II}] ratio in the system, an effect partially remedied with a large excess of reducing agent. Note that the Mn profiles (Figure 6b) are similar for all experiments in this set; however, apparent initiator efficiency (number of chains) continues to rise for x>0.5 with [Sn]:[Cu] at the 100:1 ratio (Figures 6d and 7). The combination of low Cu levels and a high number of chains per Cu molecule requires that higher levels of reducing agent be used. Thus, the same rates and Mn values (initiator efficiencies) are achieved with 36 ppm Cu and 3560 ppm Sn as with 145 ppm Cu and 1450 ppm Sn.

Downloaded by STANFORD UNIV GREEN LIBR on May 31, 2012 | http://pubs.acs.org
Publication Date (Web): March 20, 2012 | doi: 10.1021/bk-2012-1100.ch012

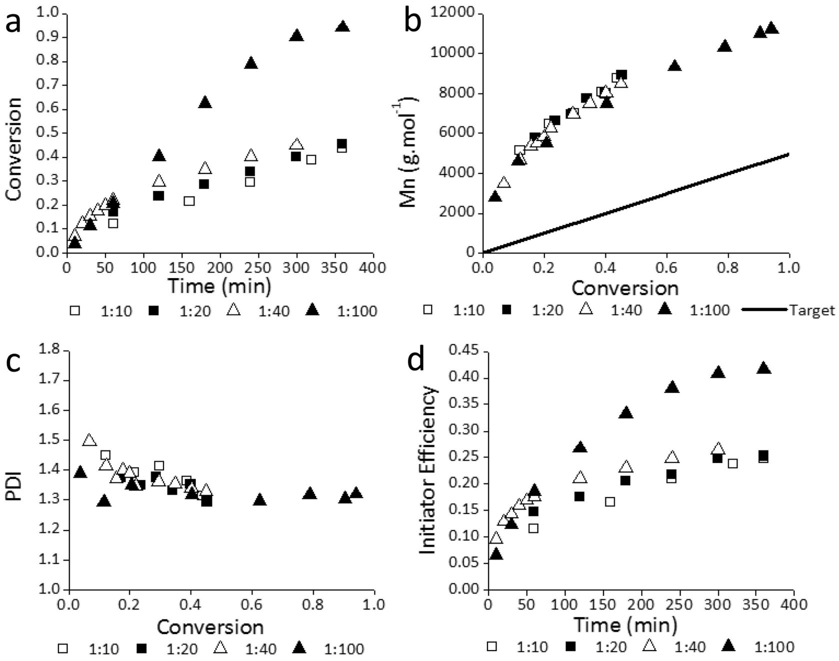

Figure 6. Batch ARGET ATRP of BMA with 36 ppm Cu and varying reducing agent level at 70 °C: (a) monomer conversion versus time, (b) number-average molecular weight (Mn) and (c) polydispersity index (PDI) as a function of conversion; (d) initiator efficiency versus time. Molar [Cu]:[Sn] ratios are presented in the legend, with [M]:[R-X]:[Cu] = 35:1:0.00125.

Downloaded by STANFORD UNIV GREEN LIBR on May 31, 2012 | http://pubs.acs.org
Publication Date (Web): March 20, 2012 | doi: 10.1021/bk-2012-1100.ch012

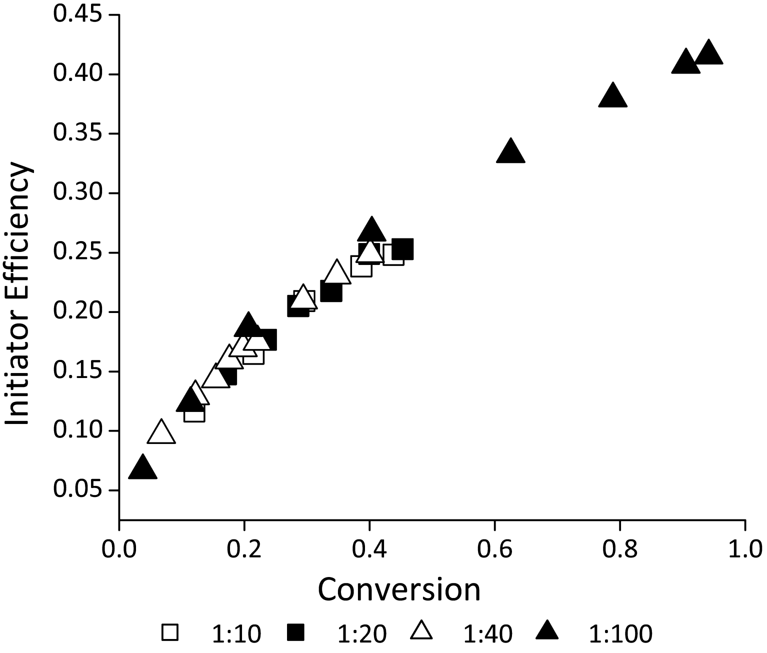

Figure 7. Initiator efficiency versus conversion for batch ARGET ATRP of BMA with 36 ppm Cu and varying reducing agent level at 70 °C. Molar ratios in the legend are presented as [Cu]:[Sn] with [M]:[R-X]:[Cu] = 35:1:0.00125.

It is also interesting to examine the polymer MMDs produced with the highest level of reducing agent (Figure 8). Once again, a tail on the low MW side of the MMD is observed, consistent with the slow activation of initiator indicated by initiator efficiency. However, the polymer MMD is broader (PDI of 1.3) when compared to that obtained with 145 ppm Cu (Figure 5a, PDI of 1.2). Thus, the abundance of reducing agent, while effectively increasing the rate of monomer conversion, also results in a less controlled polymerization. The increased Cu level of 145 ppm allows for more chains to be activated and mediated with good control compared to the low Cu case (36 ppm) with an increased reducing agent concentration.

To estimate the combined impact of varying reducing agent and catalyst loadings for the experiments with DP_{nT} = 35, the initial rates of polymerization were also compared. By rearranging the simplified rate equation, $R_p = k_p[M][R\cdot]$, the radical concentration was determined by dividing the slope of the kinetic plot by the propagation rate constant. The catalyst ratio was then determined using eq 6.

$$f_{\text{init}}\frac{[Cu^{I}]}{[Cu^{II}]}=\frac{[R\cdot]}{K_{\text{ATRP}}[R-X]_{\text{o}}} \qquad (6)$$

Downloaded by STANFORD UNIV GREEN LIBR on May 31, 2012 | http://pubs.acs.org
Publication Date (Web): March 20, 2012 | doi: 10.1021/bk-2012-1100.ch012

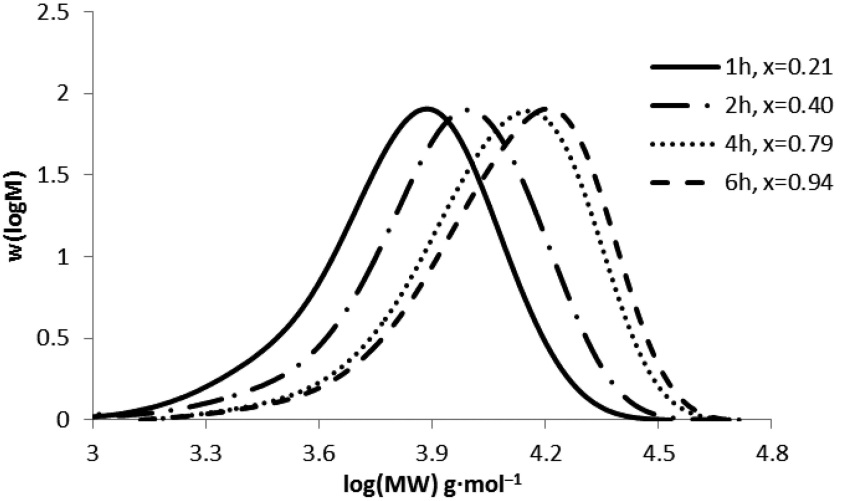

Figure 8. MMDs of pBMA produced by batch ARGET ATRP at 70 °C, sampled hourly to confirm living nature of polymerization. [M]:[R-X]:[Cu]:[Sn] = 35:1:0.00125:0.125.

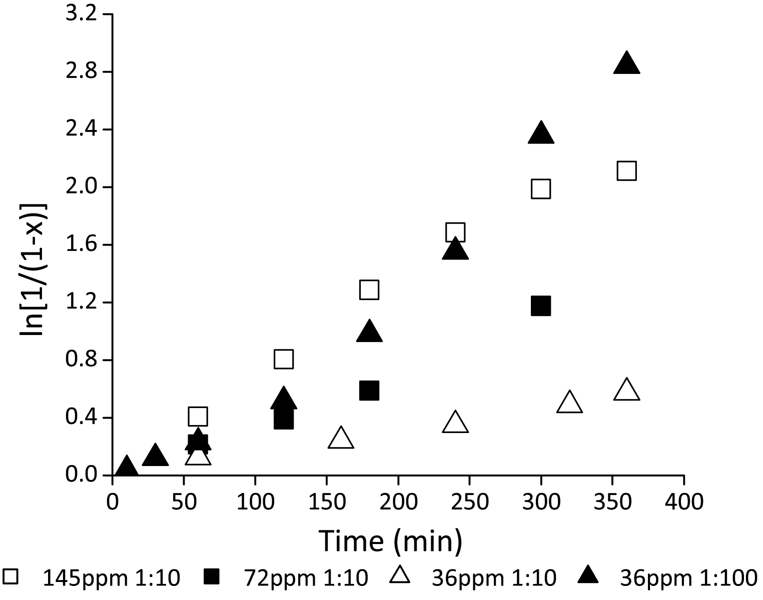

Figure 9. Kinetic plot of batch ARGET ATRP of BMA at 70 °C with varying Cu and reducing agent levels. Cu concentration presented on a molar basis with respect to monomer. Molar ratios in the legend are presented as [Cu]:[Sn] with [M]:[R-X] = 35:1.

This method assumes a constant radical concentration, an assumption that is verified by linearity in the kinetic plot of ln[1/(1-x)] vs time. As seen in Figure 9, there is some deviation from linearity observed at longer times. For the reaction with 36 ppm Cu and a Cu:Sn ratio of 1:100, the upward curvature is consistent with an increasing number of chains in the system, while the reaction with 145 ppm Cu has a slight downward curvature consistent with a buildup of Cu^{II} in the system.

Nonetheless, the expected linear relationship is observed up to three hours, allowing the use of eq 6 to estimate the product of $[Cu^{I}]/[Cu^{II}]$ and initiator efficiency from the initial concentration of initiator and an estimate of $K_{ATRP} = 2.88 \times 10^{-5}$ extrapolated from the literature (*23–25*). Results are shown in Figure 10. The two highest reducing agent concentrations (1424 and 3654 ppm) at the lowest copper loading of 36 ppm have an increased value of $(f_{init}[Cu^{I}]/[Cu^{II}])$ compared to the lower Sn loadings. However, the highest level of reducing agent is required to match the increased reaction rate found at the higher copper loading of 145 ppm. This result suggests that there is not enough reducing agent present to continuously reduce Cu^{II} to Cu^{I} if the low Cu level (36 ppm) must regulate a large number of chains (800:1, assuming 100% initiator efficiency). There is a definite trade-off between the amount of reducing agent and the amount of copper necessary to maintain good control and a reasonable polymerization rate.

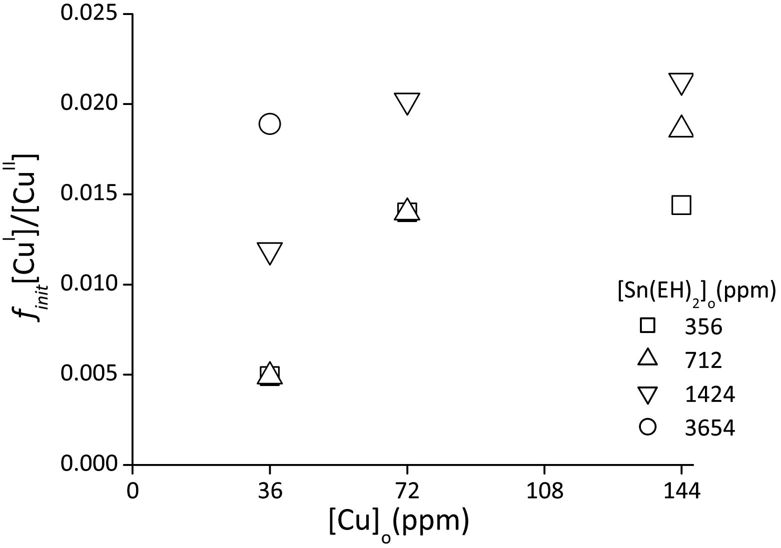

Figure 10. ARGET ATRP catalyst ratios at various initial copper and reducing agent loadings at 70 °C under batch conditions, as estimated from initial rates of polymerization. Concentrations are molar ratios with respect to monomer. [M]:[R-X] = 35:1 for all cases.

Downloaded by STANFORD UNIV GREEN LIBR on May 31, 2012 | http://pubs.acs.org
Publication Date (Web): March 20, 2012 | doi: 10.1021/bk-2012-1100.ch012

Downloaded by STANFORD UNIV GREEN LIBR on May 31, 2012 | http://pubs.acs.org
Publication Date (Web): March 20, 2012 | doi: 10.1021/bk-2012-1100.ch012

Comparison of BMA and BA

Butyl acrylate (BA) has a higher k_p value than BMA and therefore is expected to exhibit a higher polymerization rate. The comparison of BA to BMA was conducted at 90 °C, in order to achieve higher rates of monomer conversion than those found at 70 °C for BMA with low Cu levels; results are summarized in Table IV and shown in Figure 11. The chain length was changed from DPn = 35 for BMA to DPn = 39 for BA in order to maintain a target MW of 5,000 $g \cdot mol^{-1}$. The experiments at the higher Cu level were conducted at a Cu:Sn ratio of 1:10, while those at the lower Cu level were run at the ratio of 1:40.

Table IV. Batch ARGET ATRP of BMA and BA with varying catalyst levels and 30 wt% anisole at 90 °C. Mn_T was constant at 5,000 $g \cdot mol^{-1}$

Initial Ratio [M]:[R-X]:[Cu]:[Sn]	*Monomer*	*Cu (ppm)*	*Conversion at 360 min*	*Mn_{exp} ($g \cdot mol^{-1}$)*	*Initiator Efficiency*
35:1:0.005:0.05	BMA	145	0.72	6452	0.55
39:1:0.005:0.05	BA	130	0.88	5561	0.79
35:1:0.00125:0.05	BMA	35	0.80	10331	0.39
39:1:0.00125:0.05	BA	34	0.86	5491	0.78

As expected, there is an increase in the polymerization rate from BMA to BA (Figure 11a), although the profiles level off at close to the same conversion for the two systems. The increased polymerization rate is markedly greater at 35 ppm Cu than at 145 ppm Cu. There is also a significant increase in the initiator efficiency for BA compared to BMA (Figure 11d). A constant initiator efficiency of 0.7-0.8 for BA is found at both Cu levels, compared to the slow increase over time observed for BMA; the efficiency for BMA also exhibits a significant increase as Cu is increased from 35 to 145 ppm. Due to the higher initiator efficiency, the Mn_{exp} values for poly(BA) are much closer to the target value of 5,000 $g \cdot mol^{-1}$ (Figure 11b). The polymer MMD for BA at 130 ppm Cu (Figure 12) does not have the low MW tail seen with BMA in Figure 5; however, a pronounced low MW tail is seen for the 34 ppm Cu BA experiment, a finding also reflected in the slightly higher value of PDI (Figure 11c).

This comparison indicates that EBiB is activated earlier in the BA system, as opposed to throughout the reaction for the BMA system. The increased efficiency with BA has been reported in the literature (*10*), although another comparison of methyl acrylate and methyl methacrylate suggests that acrylate binds more strongly to Cu^I than methacrylate and hinders the rate of polymerization (*26*, *27*). To minimize side reactions with the catalyst complex, excess ligand has been recommended (*7*, *10*). Increasing the ratio of [TPMA]:[Cu^{II}] from 1:1 to 6:1 had a negligible effect on the conversion and initiator efficiency profiles for our system (results not shown), indicating monomer coordination is not a major contributor to the difference in rate.

Downloaded by STANFORD UNIV GREEN LIBR on May 31, 2012 | http://pubs.acs.org
Publication Date (Web): March 20, 2012 | doi: 10.1021/bk-2012-1100.ch012

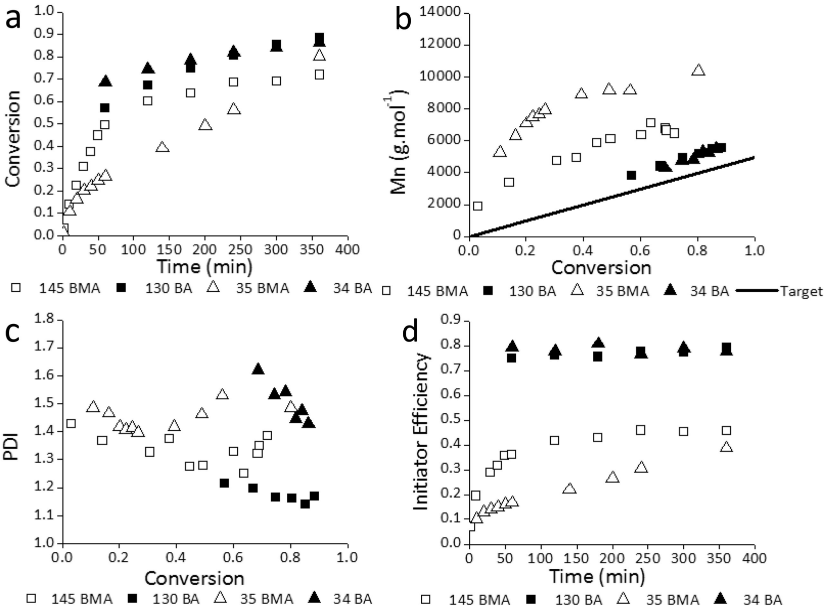

Figure 11. Batch ARGET ATRP of BMA and BA at 90 °C: (a) monomer conversion versus time, (b) number-average molecular weight (Mn) and (c) polydispersity index (PDI) as a function of conversion; (d) initiator efficiency versus time. Legend shows ppm Cu levels for experiments with BMA (open symbols) and BA (closed symbols); see Table IV for further experimental details.

Table V. Batch ARGET ATRP of BA with varying reducing agent levels at 90 °C with 30 wt% anisole. Molar ratio of [M]:[R-X]:[Cu] = 39:1:0.00125 is constant in all cases

Initial Ratio [Cu]:[Sn]	*Cu (ppm)*	*Time (min)*	*Conversion*	*Mn$_{exp}$ (g·mol^{-1})*	*Initiator Efficiency*
1:10	31	240	0.68	4721	0.72
1:20	34	240	0.70	4646	0.75
1:40	34	360	0.86	5491	0.78
1:100	39	360	0.99	6572	0.75

As shown in Figure 13a and summarized in Table V, varying the amount of reducing agent added to the BA system with 36 ppm Cu has a lesser effect on polymerization rate and initiator efficiency compared to BMA polymerizations. The largest effect is observable at the initial stages of the polymerization. Rates level off quickly, as do the estimated efficiency values at 0.7-0.8, independent of the amount of added Sn (Figure 13d). The increased polymerization rate observed at short times with higher Sn levels is most likely caused by a shift in the [Cu^{I}]:[Cu^{II}] ratio, as well as the faster activation of initiator. The data indicate an upper limit to the achievable initiator efficiency that is unaltered by copper or reducing agent levels. In all cases the initial PDI is high (>1.6) and decreases to 1.4 as the reaction proceeds to near full conversion (Figure 13c). The slower initiation observed with the 1:10 Cu:Sn ratio leads to an appreciable low MW tail; even with Cu:Sn at 1:40, a low MW tail is observed in the MMD of poly(BA) produced at a Cu level of 34 ppm (Figure 12). While increasing the concentration of reducing agent still has a clear effect on BA polymerization rate for these low Cu experiments, the impact is smaller than observed for BMA polymerization, in agreement with a previous comparison in literature conducted with a higher Mn_T (*12*).

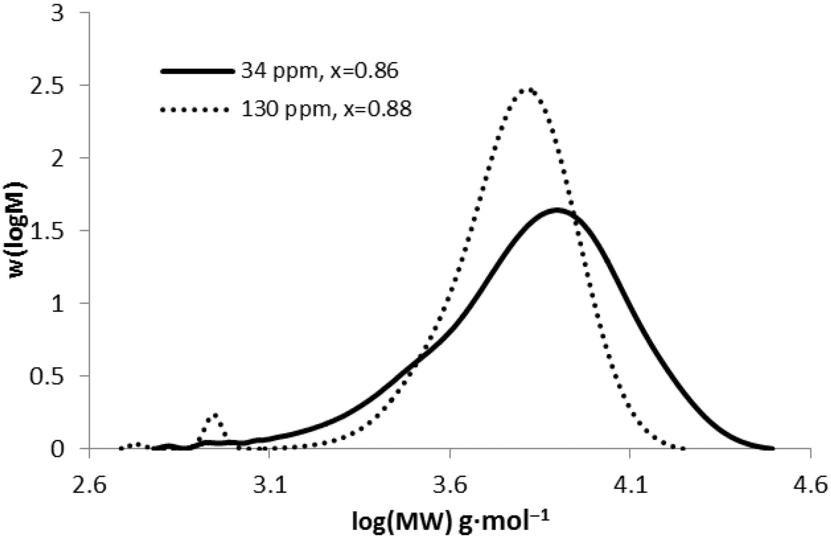

Figure 12. MMDs of pBA (final samples) produced by batch ARGET ATRP at 90 °C. Cu concentration specified on a molar basis with monomer. [M]:[R-X]:[Sn] = 39:1:0.05.

Downloaded by STANFORD UNIV GREEN LIBR on May 31, 2012 | http://pubs.acs.org
Publication Date (Web): March 20, 2012 | doi: 10.1021/bk-2012-1100.ch012

Downloaded by STANFORD UNIV GREEN LIBR on May 31, 2012 | http://pubs.acs.org
Publication Date (Web): March 20, 2012 | doi: 10.1021/bk-2012-1100.ch012

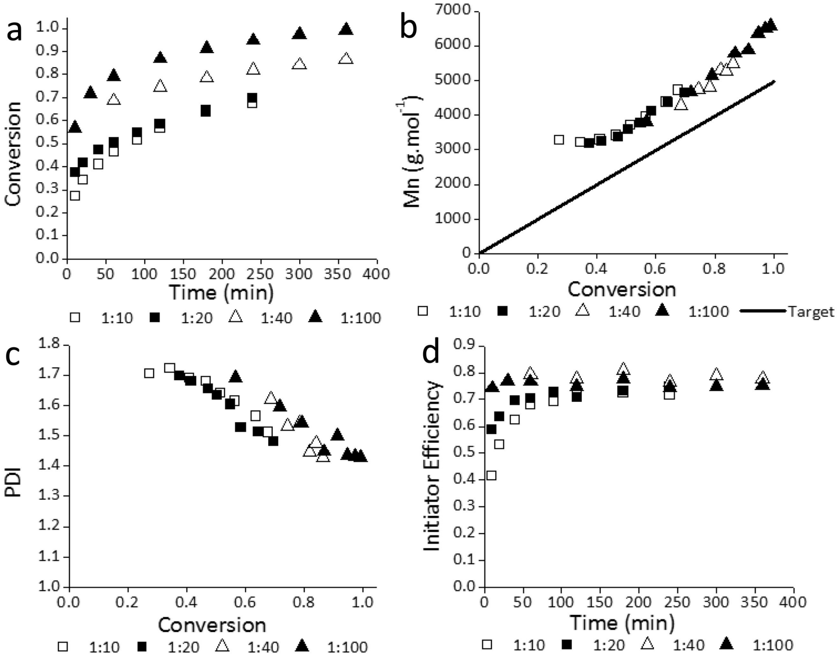

Figure 13. Batch ARGET ATRP of BA with varying reducing agent levels at 90 °C and 36 ppm Cu: (a) monomer conversion versus time, (b) number-average molecular weight (Mn) and (c) polydispersity index (PDI) as a function of conversion; (d) initiator efficiency versus time. Molar ratios in the legend presented as [Cu]:[Sn] with [M]:[R-X]:[Cu] = 39:1:0.00125.

Conclusions

A systematic study investigating the impact of reaction conditions on the rate of monomer conversion and polymer MW has been conducted for ARGET ATRP with low Cu concentrations. Decreasing the DP_{nT} value by increasing initiator concentration while keeping the Cu to initiator level constant led to an expected increase in rate. However, initiator efficiency was observed to increase slowly throughout the reaction, indicating chain formation was not instantaneous. The Cu level was then decreased to 36 molar ppm relative to monomer for Mn_T = 5,000 g·mol^{-1}, such that there were 800 chains to be mediated by each Cu molecule assuming 100% initiator efficiency. Under these conditions, the decrease in Cu concentration caused a significant decrease in polymerization rate and estimated intitiator efficiency. At this low Cu level, the amount of reducing agent had to be subsequently increased, with only a large excess having an impact on polymerization rate and initiator efficiency. A definite trade-off between catalyst level and reducing agent level is evident, with 1:100 [Cu]:[Sn] resulting in high conversion in 6 hours at 36 ppm Cu, comparable to a polymerization conducted with 145 ppm Cu and 1:10 [Cu]:[Sn].

The initiator efficiency for BA increased rapidly to a essentially constant level of 0.7-0.8, a value consistently higher than the steadily increasing efficiency observed for BMA polymerization with 36 ppm Cu. Increasing the concentration of reducing agent in the BA system had a smaller impact on polymerization rate and initiator efficiency than found for BMA. However, the poly(BA) produced had higher PDI values than found for BMA with PDI narrowing with conversion to a final value of 1.3-1.4.

Recently, the first model of ARGET ATRP examining the effect of reducing agent on polymerization rate has been published (*13*). The data presented here summarize a systematic study of the combined effects of Cu and Sn concentrations, information that will be essential to improve understanding and aid further model development. Studies are also underway to explore the effect of temperature and monomer composition (copolymerization) on initiator efficiency and rate under low Cu conditions.

Downloaded by STANFORD UNIV GREEN LIBR on May 31, 2012 | http://pubs.acs.org
Publication Date (Web): March 20, 2012 | doi: 10.1021/bk-2012-1100.ch012

References

1. Wang, J.-S.; Matyjaszewski, K. *J. Am. Chem. Soc.* **1995**, *117*, 5614–5615.
2. Matyjaszewski, K.; Xia, J. *Chem. Rev.* **2001**, *101*, 2921–2990.
3. Wang, J.-S.; Matyjaszewski, K. *Macromolecules* **1995**, *28*, 7901–7910.
4. Grimaud, T.; Matyjaszewski, K. *Macromolecules* **1997**, *30*, 2216–2218.
5. Percec, V.; Barboiu, B. *Macromolecules* **1995**, *28*, 7970–7972.
6. Wang, J.-L.; Grimaud, T.; Matyjaszewski, K. *Macromolecules* **1997**, *30*, 6507–6512.
7. Jakubowski, W.; Min, K.; Matyjaszewski, K. *Macromolecules* **2006**, *39*, 39–45.
8. Matyjaszewski, K.; Jakubowski, W.; Min, K.; Tang, W.; Huang, J.; Braunecker, W. A.; Tsarevsky, N. V. *Proc. Natl. Acad. Sci. U.S.A.* **2006**, *103*, 15309–14.
9. Zhong, M.; Matyjaszewski, K. *Macromolecules* **2011**, *44*, 2668–2677.
10. Jakubowski, W.; Matyjaszewski, K. *Angew. Chem.* **2006**, *118*, 4594–4598.
11. Mueller, L.; Matyjaszewski, K. *Macromol. React. Eng.* **2010**, *4*, 180–185.
12. Chan, N.; Cunningham, M. F.; Hutchinson, R. A. *Macromol. Chem. Phys.* **2008**, *209*, 1797–1805.
13. Li, X.; Wang, W.-J.; Li, B.-G.; Zhu, S. *Macromol. React. Eng.* **2011**, *5*, 467–478.
14. Matyjaszewski, K. *Macromolecules* **1998**, *31*, 4710–7.
15. Chan, N.; Cunningham, M. F.; Hutchinson, R. A. *Macromol. React. Eng.* **2010**, *4*, 369–380.
16. Destarac, M. *Macromol. React. Eng.* **2010**, *4*, 165–179.
17. Britovsek, G. J. P.; England, J.; White, A. J. P. *Inorg. Chem.* **2005**, *44*, 8125–34.
18. Hutchinson, R. A.; Beuermann, S.; Paquet, D. A.; McMinn, J. H. *Macromolecules* **1997**, *30*, 3490–3493.
19. Penzel, E.; Goetz, N. *Angew. Makromol. Chem.* **1990**, *178*, 191–200.
20. Min, K.; Gao, H.; Matyjaszewski, K. *Macromolecules* **2007**, *40*, 1789–1791.

In Progress in Controlled Radical Polymerization: Mechanisms and Techniques; Matyjaszewski, K., et al.;
ACS Symposium Series; American Chemical Society: Washington, DC, 2012.

21. Chan, N.; Boutti, S.; Cunningham, M. F.; Hutchinson, R. A. *Macromol. React. Eng.* **2009**, *3*, 222–231.
22. Matyjaszewski, K.; Dong, H.; Jakubowski, W.; Pietrasik, J.; Kusumo, A. *Langmuir* **2007**, *23*, 4528–31.
23. Seeliger, F.; Matyjaszewski, K. *Macromolecules* **2009**, *42*, 6050–6055.
24. Tang, W.; Tsarevsky, N. V.; Matyjaszewski, K. *J. Am. Chem. Soc.* **2006**, *128*, 1598–604.
25. Tang, W.; Matyjaszewski, K. *Macromolecules* **2007**, *40*, 1858–1863.
26. Braunecker, W. A.; Tsarevsky, N. V.; Pintauer, T.; Gil, R. R.; Matyjaszewski, K. *Macromolecules* **2005**, *38*, 4081–4088.
27. Braunecker, W. A.; Pintauer, T.; Tsarevsky, N. V.; Kickelbick, G. *J. Organomet. Chem.* **2005**, *690*, 916–924.

Downloaded by STANFORD UNIV GREEN LIBR on May 31, 2012 | http://pubs.acs.org
Publication Date (Web): March 20, 2012 | doi: 10.1021/bk-2012-1100.ch012

Downloaded by UNIV OF GUELPH LIBRARY on May 31, 2012 | http://pubs.acs.org
Publication Date (Web): March 20, 2012 | doi: 10.1021/bk-2012-1100.ch013

Chapter 13

Adapting Atom Transfer Radical Polymerization to Industrial Scale Production: The *Ultimate ATRP*^{SM} Technology

Wojciech Jakubowski[*]

ATRP Solutions, Inc., 855 William Pitt Way, Pittsburgh, Pennsylvania 15238
[*]E-mail: wjakubowski@atrpsolutions.com

Atom transfer radical polymerization (ATRP) is among the most powerful controlled/living radical polymerization techniques and it is anticipated that many new products containing polymers made by this technique will be introduced in the US within the next several years. The major factors which constrain the commercial application of ATRP are high copper catalyst concentration and the special handling procedures which are required to avoid catalyst oxidation. Recently developed catalytic systems for ATRP alleviate these problems but were successfully applied only on the laboratory scale. The new *Ultimate ATRP*^{SM} technology is presented that has a much greater potential to be used on industrial scale. There are several advantages of the proposed method compared to the currently used ICAR (initiators for continuous activator regeneration) ATRP.

In Progress in Controlled Radical Polymerization: Mechanisms and Techniques; Matyjaszewski, K., et al.;
ACS Symposium Series; American Chemical Society: Washington, DC, 2012.

Downloaded by UNIV OF GUELPH LIBRARY on May 31, 2012 | http://pubs.acs.org
Publication Date (Web): March 20, 2012 | doi: 10.1021/bk-2012-1100.ch013

Introduction

Atom transfer radical polymerization (ATRP) is among the most powerful controlled/living radical polymerization techniques (*1–3*). The ATRP process was discovered in 1995 and can be applied to the polymerization of a broad spectrum of radically (co)polymerizable monomers (*4*). Examples of the new well-defined polymeric materials prepared using ATRP in the past decade include block copolymers, branched polymers, polymeric stars, brushes, blends, composites, and bioconjugates (*1*, *5*). These custom materials have potential to improve the performance of commercial products in the areas of personal care and cosmetics, detergents and surfactants, paints, pigments and coatings, adhesives, thermoplastic elastomers, biocompatible materials and drug delivery systems (*6*). It is anticipated that many new products containing polymers made by this technique will be introduced in the US within the next several years.

Materials made by ATRP are entering broad market segments, estimated for $200 billion dollars (*7*). Carnegie Mellon has signed several commercial licenses for ATRP and Kaneka from Japan and Dionex from the US have already commercialized products made by ATRP (*6*, *8*, *9*). The major factors which constrain the commercial application of ATRP are high copper catalyst concentration and the special handling procedures which are required to avoid catalyst oxidation (*10*). Other challenges which are of great importance when producing polymers on a high scale include the handling of exothermic reactions, building simple automated processes as well as driving polymerization reaction to high conversion in short times (*11*).

Recent research has resulted in the development of ATRP initiation systems that alleviates the problem with high catalyst concentration and catalyst oxidation. These new systems called ARGET (Activators ReGenerated by Electron Transfer) (*12*, *13*) and ICAR (Initiators for Continuous Activator Regeneration) ATRP (*14*) allow a decrease in the amount of catalyst needed from 10,000 ppm to 10 ppm or less, where its removal or recycling would be unwarranted for most industrial applications (Figure 1). Furthermore, ARGET/ICAR ATRP can be performed in the presence of limited amounts of air and produces polymers with higher attainable molecular weight and with higher chain end functionality than normal ATRP process (*15–20*). These systems were successfully applied to the preparation of a variety of polymer materials including homo, block and random copolymers, and the development of a straightforward process for the preparation of molecular brushes on a flat surface and star copolymers (*19*, *21–25*). Thus, these new techniques made a huge step towards making ATRP an industrially viable process.

ARGET and ICAR ATRP have only been shown to be successful for laboratory scale batch procedures. In order to perform polymerization on a higher scale, these systems have to be further modified to fit industrially feasible processes. Herein we describe the new *Ultimate ATRP*^{SM} technology which has great potential to solve major problems in scaling-up the ATRP technology (*26*).

Downloaded by UNIV OF GUELPH LIBRARY on May 31, 2012 | http://pubs.acs.org
Publication Date (Web): March 20, 2012 | doi: 10.1021/bk-2012-1100.ch013

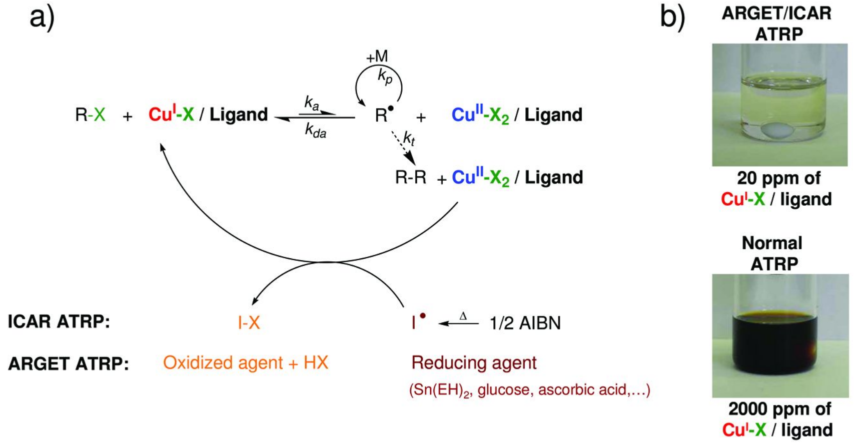

Figure 1. a) Mechanism for ICAR (and ARGET) ATRP where Cu^I activator is constantly regenerated by organic radicals or environmentally acceptable reducing agents (e.g. FDA approved compounds, sugars etc.), b) appearance of reaction mixtures containing typical catalyst concentration used in ICAR/ARGET ATRP and traditional ATRP.

Results and Discussion

The New *Ultimate ATRP^{SM}* Technology

ATRP has been successfully applied to the preparation of many polymeric materials on the R&D laboratory scale. Today, over 4 scientific publications containing the word 'ATRP' are published every day and 5 US patents are submitted per week (250 per year). ATRP is efficient in the preparation of polymers at small scale, however, scaling ATRP to commercial quantities has proven challenging. Since this polymerization method has a relatively complicated mechanism, internal R&D departments of most of the companies have difficulty transferring this technology to manufacturing and performing polymerization in full-scale production.

There is a critical need for a robust process which enables the cost-effective scaling of ATRP from the 10 gram scale to the 1 ton scale. A process which enables cost effective scaling of ATRP technology is tremendously valuable in that it will enable companies to access over 10 years of strategic ATRP-related intellectual property (R&D) and go to the market with products developed with these high performance polymers. ARGET and ICAR ATRP may be considered as one of the largest recent breakthroughs in the ATRP process since its discovery in 1995 since they provide a huge step towards the development of a viable 'green' ATRP processes for industrial scale production of specialty polymers. Although, they have only been shown to be successful for laboratory scale batch procedures. In order to perform polymerization on a higher scale, these systems have to be further modified to fit industrially feasible processes.

We have developed a new process which allows an efficient, safe and cost effective ATRP scale-up. The proposed mechanism of the *Ultimate ATRP*^{SM} process is shown on Figure 2. It relies on precise control of the Cu^{II}/Cu^{I} ratio during the polymerization process by feeding radical initiator to the polymerization mixture at a controlled rate.

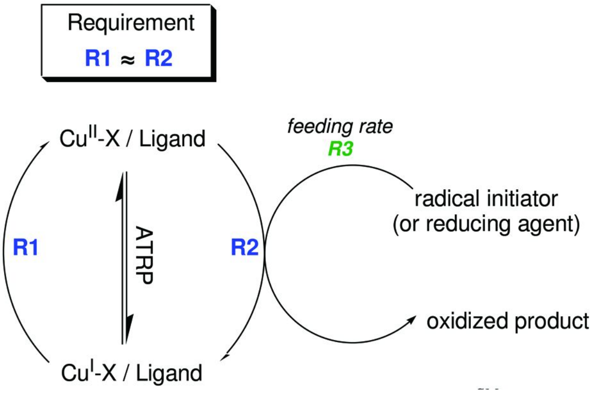

Figure 2. Proposed mechanism of the Ultimate ATRP^{SM} *process (R1 – is determined by the radical termination reactions; R2 – is determine by radical initiator decomposition rate and reaction with* Cu^{II}*-X and/or monomer; R3 – is determined manually and can be varied in the wide range).*

Main Features of the *Ultimate ATRP*^{SM} Technology

Feeding of radical initiator in the *Ultimate ATRP*^{SM} method should occur at such a rate that the amount of radical initiator added can properly compensate all the termination reactions (that had occurred since the last addition) and convert only the appropriate amount of Cu^{II} to Cu^{I}. In order to achieve a well controlled system, rates R1 and R2 should be similar as depicted on Figure 2. If this requirement is fulfilled then only a very small amount of radical initiator will be instantaneously present in the polymerization system. A use of high temperatures with radical initiators with high decomposition rates is a key element for the process to be successful. The difference in the radical concentration in the *Ultimate ATRP*^{SM} process vs. ICAR ATRP system is presented on Figure 3. Instead of adding the entire amount of radical initiator at the beginning of the reaction, only as much as needed is fed to the system during the entire process. This guarantees that concentration of AIBN in the polymerization mixture is very low at any given time of the reaction.

Downloaded by UNIV OF GUELPH LIBRARY on May 31, 2012 | http://pubs.acs.org
Publication Date (Web): March 20, 2012 | doi: 10.1021/bk-2012-1100.ch013

Downloaded by UNIV OF GUELPH LIBRARY on May 31, 2012 | http://pubs.acs.org
Publication Date (Web): March 20, 2012 | doi: 10.1021/bk-2012-1100.ch013

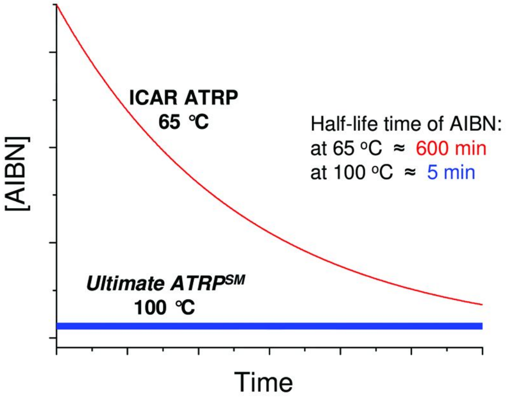

Figure 3. Theoretical representation of the AIBN concentration during the polymerization via the Ultimate ATRP^{SM} process and ICAR ATRP.

This polymerization design is characterized by features which may solve very important challenges when performing the reaction on a bigger scale:

a) *No need of precise temperature control* – the only requirement is to keep the temperature high enough to quickly decompose the radical initiator, while still allowing sufficient time for distribution throughout the reaction mixture after addition.

b) *Safe process for exothermic reactions* – the effect of the exothermic reaction is diminished by very low instantaneous concentration of radical initiator. The reaction stops after the tiny amount of initiator is consumed and excess Cu^{II} is formed. If local temperature would increase, due to a poor heat exchange or local overheating, the excess reduction of Cu^{II} to Cu^{I} is easily contained and limited to only the amount of the initiator present.

c) *Shorter reaction times and reduced amounts of solvents* – due to the use of higher reaction temperatures, reactions are faster (the rate constant of propagation increases with temperature much more than that of termination) and lower amount of solvent can be used (viscosity is lower at high temperature)

d) *Full automation possible* – as only tiny amounts of radical initiator are present at any instant in the polymerization medium, the reaction stops as soon as feeding is stopped. Thus, the rate of polymerization is controlled by the feeding of radical initiator and is stopped in any emergency conditions by stopping addition. This feature also increases the reproducibility of the polymerization results.

e) *Lower amounts of catalyst and radical initiator* – due to low concentration of the catalyst and radical initiator in the polymerization mixture, catalyst and radical initiator based side reactions are minimized.

Downloaded by UNIV OF GUELPH LIBRARY on May 31, 2012 | http://pubs.acs.org
Publication Date (Web): March 20, 2012 | doi: 10.1021/bk-2012-1100.ch013

Polymerization of Styrene (St) via the *Ultimate ATRP*^{SM} Process

To achieve successful polymerization via the *Ultimate ATRP*^{SM} method, it is crucial to design the feeding rate of radical initiator for a specific type of monomer, temperature, type of radical initiator, concentrations and ratios of all reagents, etc. Herein we present the results for polymerization of styrene. Figure 3a shows the kinetic plot for the polymerization of St with 50 ppm of $CuBr_2$ and small excess of tris(2-pyridylmethyl)amine (TPMA) ligand. The solution of 2,2′-azo-bis(isobutyronitrile) (AIBN) in toluene was fed with the constant rate 0.008 equivalents vs. diethyl 2-bromo-2-methylmalonate (DEBMM) per hour. The feeding was stopped and the heating mantle was turned off after 9 h. It can be seen from the kinetic plot that the reaction stopped immediately after stopping the addition of AIBN solution. Next, polymerization was successfully restarted at 110 °C using the same feed rate of the AIBN solution. Although viscosity significantly increased at the end of the polymerization process, the heat transfer and incorporation of AIBN were efficient. Figure 3b presents the change of temperature inside and on the outside wall of the reactor. The temperature profile suggests good heat transfer as the difference in the temperature from both thermocouples does not change during the reaction. No exothermic effect was observed during the polymerization of St. This is due to several factors, such us: i) utilization of feeding method, ii) low amount of catalyst used, iii) relatively small scale of the reaction and iv) type of monomer.

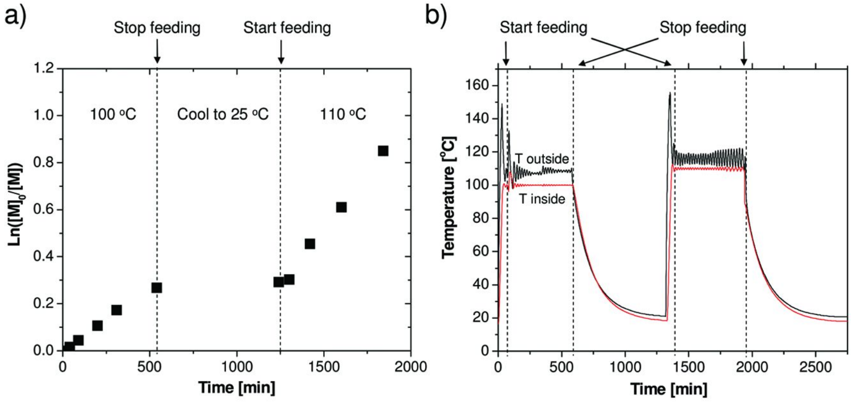

Figure 3. a) Kinetic plot and b) change of temperature inside and outside the reactor during the polymerization of St using the Ultimate ATRP^{SM} *process. Experimental conditions: St / DEBMM /* $CuBr_2$ */ TPMA / AIBN = 1000 / 1 / 0.05 / 0.15 / fed; bulk at 100-110 °C; 50 ppm of Cu; feeding rate = 3.33 mL/h (0.008 eq. of AIBN vs. DEBMM in 1 h).*

Figure 4 presents molecular weight and polydispersity (PDI) vs. conversion and gel permeation chromatography (GPC) traces of PSt prepared via the *Ultimate ATRP*^{SM} process. Molecular weight control was excellent and followed theoretical values based on quantitative initiation. Due to initiation of new polymer chains with AIBN, molecular weights were slightly lower than theoretical values at the

Downloaded by UNIV OF GUELPH LIBRARY on May 31, 2012 | http://pubs.acs.org
Publication Date (Web): March 20, 2012 | doi: 10.1021/bk-2012-1100.ch013

end of the polymerization process. Nevertheless, molecular weight distribution decreased during the reaction time from 1.32 to 1.18. GPC traces shifted smoothly to higher molecular weights with conversion. These results clearly prove that the process was fully controlled and can be automated.

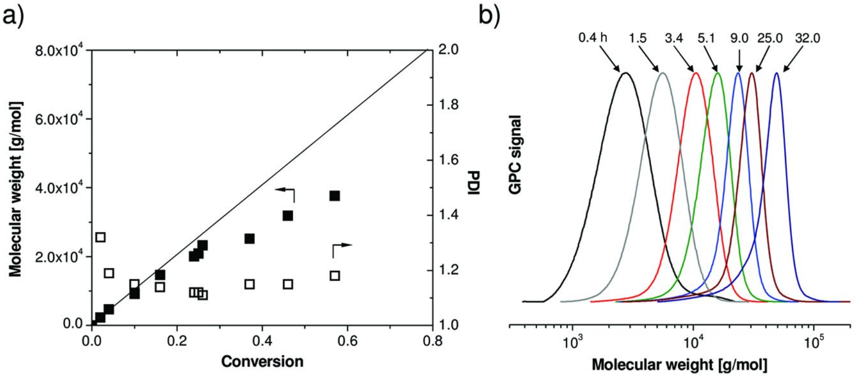

Figure 4. a) Molecular weights and polydispersities as a function of conversion and b) GPC traces during the polymerization of St using the Ultimate ATRP^{SM} process. Experimental conditions: see Figure 3.

Chain-End Functionality of PSt Macroinitiators Prepared via the *Ultimate ATRP^{SM}* Process

Polymers prepared using ATRP have a halogen atom at a majority of the polymer chain ends. The halogen functionality allows synthesis of block copolymers which are of great industrial significance (*27*, *28*). The halogen functionality may also participate in post-polymerization reactions such as chain-end modifications to other functional groups (*29*). Thus, high chain-end functionality for polymers prepared by ATRP is very important. However, the halogen functionality may be lost during the polymerization process due to side reactions and termination processes. Use of high amounts of radical initiator (such as AIBN) may also negatively influence the number of living polymer chains.

The synthesis of PSt macroinitiator with high chain-end functionality and high molecular weight via normal ATRP is challenging due to side reactions such as β-H elimination in the presence of CuX/ligand complex (*16*, *30*). The utilization of the *Ultimate ATRP^{SM}* method allows to decrease amount of side reactions due to low Cu/ligand content and produce PSt macroinitiaor with high chain-end functionality and high molecular weights. In order to evaluate chain-end functionality of polymers prepared by the new method, a block copolymer was synthesized. Figure 5 presents GPC traces before and after chain extension of two different PSt macroinitiators ($M_{n,GPC}$ = 8,100 g/mol at 81% conversion; $M_{n,GPC}$ = 1,600 g/mol at 82% conversion) prepared via the *Ultimate ATRP^{SM}* process. Both chain extensions resulted in well defined block copolymers proving that polymers prepared via the new method had high chain-end functionality.

Downloaded by UNIV OF GUELPH LIBRARY on May 31, 2012 | http://pubs.acs.org
Publication Date (Web): March 20, 2012 | doi: 10.1021/bk-2012-1100.ch013

Polymerization of *n*-Butyl Acrylate (*n*BA) via the *Ultimate ATRP^{SM}* Process

As in the polymerization of St, to achieve successful polymerization of *n*BA via the *Ultimate ATRP^{SM}* process, it is critical to properly design the feeding rate of radical initiator, temperature, type of radical initiator, concentrations and ratios of all reagents, etc. Polymerization of acrylate type of monomer via ATRP may be very challenging due to generation of high amounts of heat (*31*). These exothermic effects may be very difficult to handle when the process is performed in the large reaction vessels. In order to keep control over the polymerization process and its kinetics, the temperature inside the reactor should be maintain close to the targeted value.

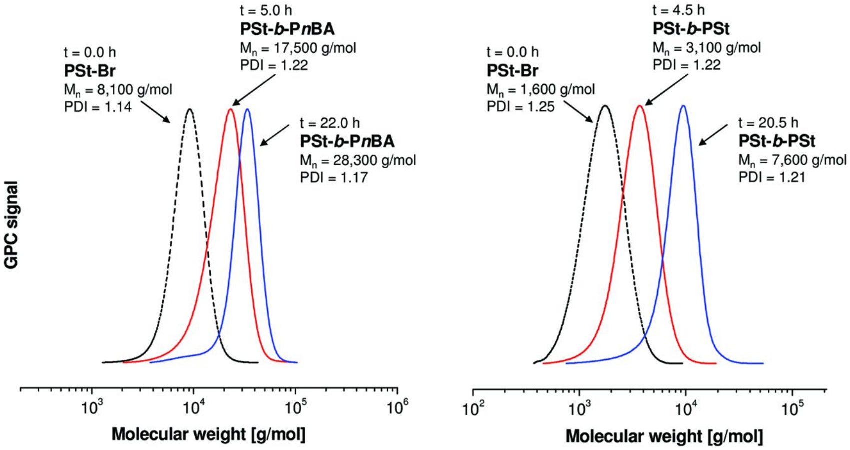

Figure 5. GPC traces of PSt macroinitiators prepared via the Ultimate ATRP^{SM} process and resulting PSt-b-PnBA block copolymer and PSt-b-PSt prepared by traditional ARGET and ICAR ATRP. Experimental conditions for chain extension with nBA: nBA / PSt / $CuBr_2$ / TPMA / $Sn(EH)_2$ = 300 / 1 / 0.01 / 0.05 / 0.1; [nBA] = 4.4 M, Cu catalyst: 33 ppm vs. monomer, T = 60 °C, in anisole (40 % v/v vs. monomer). Experimental conditions for chain extension with St: St / PSt / $CuBr_2$ / Me_6TREN / AIBN = 100 / 1 / 0.005 / 0.03 / 0.1; [St] = 7.6 M, Cu catalyst: 50 ppm vs. monomer, T = 70 °C, in DMF (15 % v/v vs. monomer).

Figure 6a presents the evolution of temperature during the polymerization of *n*BA via ARGET ATRP performed in 1 L reactor. It is clear that addition of a weak reducing agent such as tin(II) 2-ethylhexanoate ($Sn(EH)_2$) to the reaction mixture at 30 °C started the polymerization process with a significant exothermic effect (heating mantle was turned off and next turned on after 320 min and set at 60 °C). When using the *Ultimate ATRP^{SM}* method these exothermic effects can be minimized and control over the polymerization can be maintained. Figure 6b shows the evolution of temperature inside and on the outside wall of the reactor

Downloaded by UNIV OF GUELPH LIBRARY on May 31, 2012 | http://pubs.acs.org
Publication Date (Web): March 20, 2012 | doi: 10.1021/bk-2012-1100.ch013

during the polymerization of *n*BA via the *Ultimate ATRP*^{SM} process performed in a 1 L reactor. Feeding rate of the radical initiator was slow at the beginning of the polymerization process and next increased, resulting in a small exothermic effect. As soon as the temperature reached a targeted value, feeding of the readical initator was decresed. It is clear that by adjusting the feeding rate of the radical initiator, the exothermic effect can be relatively well controlled.

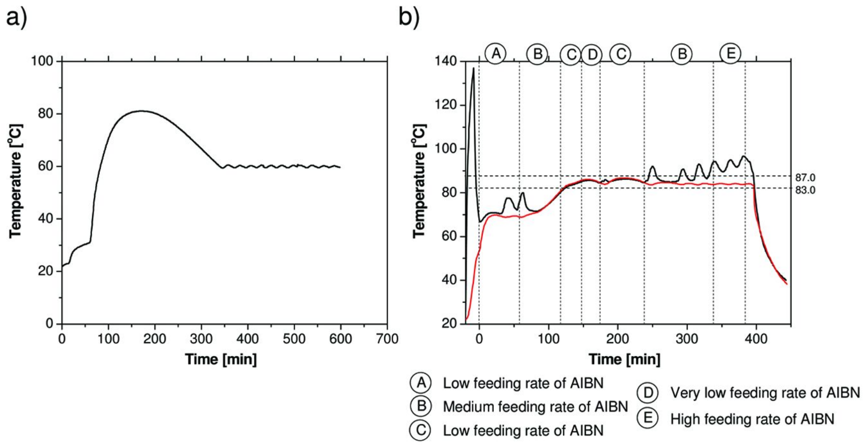

Figure 6. Change of temperature inside and outside the reactor during the polymerization of nBA via a) ARGET ATRP and b) the Ultimate ATRP^{SM} *process. Experimental conditions for ARGET ATRP: nBA / EtBiB /* $CuBr_2$ */ TPMA /* $Sn(EH)_2$ *= 500 / 1 / 0.025 / 0.075 / 0.1; [nBA] = 5.8 M, Cu catalyst: 50 ppm vs. monomer, T = 60 °C, in anisole (20 % v/v vs. monomer). Experimental conditions for the Ultimate ATRP*^{SM} *process: nBA / EtBiB / CuBr /* $CuBr_2$ */* Me_6TREN */ V-70 = 200 / 1 / 0.01 / 0.005 / 0.05 / fed; ; [nBA] = 5.8 M, Cu catalyst: 75 ppm vs. monomer, T = 85 °C, in toluene (20 % v/v vs. monomer), feeding rate was varied.*

Figure 7a presents molecular weight and polydispersity (PDI) vs. conversion and GPC traces of P*n*BA prepared via the *Ultimate ATRP*^{SM} process. Molecular weight control was excellent and followed theoretical values based on quantitative initiation. Molecular weight distribution decreased during the reaction time from 1.72 to 1.32. Figure 7b presents GPC traces which shifted smoothly to higher molecular weights with conversion. The kinetic plot was linear but a short induction period was observed (Figure 7c). This is probably due to the time needed to convert Cu^{II} species to Cu^{I} activator as well as scavenge some small amount of impurities (e.g. oxygen from air, monomer inhibitor). Nonetheless, high conversion was reached (91%) and well-defined polymer was obtained ($M_{n,GPC}$ = 17,800 g/mol, PDI = 1.32). These results clearly prove that the polymerization process was fully controlled and exothermic effects were efficiently diminished.

Downloaded by UNIV OF GUELPH LIBRARY on May 31, 2012 | http://pubs.acs.org
Publication Date (Web): March 20, 2012 | doi: 10.1021/bk-2012-1100.ch013

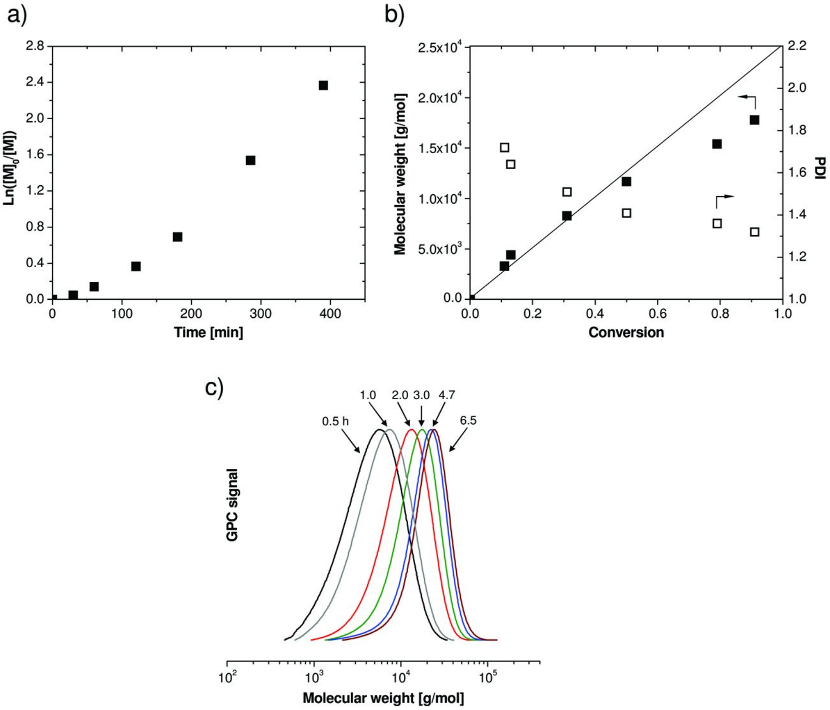

Figure 7. a) Kinetic plot, b) molecular weights and polydispersities as a function of conversion and c) evolution of GPC traces during the Ultimate ATRP^{SM} process of nBA. Experimental conditions: see Figure 6b.

Summary

Polymers made by ATRP are slowly entering the US market. It is very important to develop fully scalable systems to accelerate this process and make ATRP an efficient and cost effective method for polymer production. Herein, we proposed the *Ultimate ATRP^{SM}* process which is envisioned as a straightforward and safe method for industrial scale-up. It relies on a control of the ratio of Cu^{I} and Cu^{II} species in the polymerization mixture. Due to a very small amount of radical initiator instantaneously present in the polymerization reactor it is possible to make ATRP a fully automated system. The polymerization reaction can be stopped and restarted by ‘pressing the button’ on the feeding device. The *Ultimate ATRP^{SM}* technology allows the polymerization process to be performed with lower amounts of radical initiator and solvents and in shorter times. It also introduces safety and reproducibility to the ATRP process during a higher scale production. As presented above, the *Ultimate ATRP^{SM} method* was successfully applied to the polymerization of St and *n*BA. The presented feeding method may also be used for polymerization of methacrylate type monomers and in other controlled radical polymerization techniques (e.g. RAFT), results from these experiments will be presented in forthcoming publications.

Downloaded by UNIV OF GUELPH LIBRARY on May 31, 2012 | http://pubs.acs.org
Publication Date (Web): March 20, 2012 | doi: 10.1021/bk-2012-1100.ch013

Experimental

Materials

Styrene (St) (Sigma-Aldrich, 99%) and *n*-butyl acrylate (*n*BA) (Sigma-Aldrich, 99%) were used as received. Tris(2-dimethylaminoethyl)amine (Me_6TREN, 98 %) and tris(2-pyridylmethyl)amine (TPMA, 98 %) are commercially available from ATRP Solutions, Inc. (www.atrpsolutions.com). Diethyl 2-bromo-2-methylmalonate (DEBMM) (Sigma-Aldrich, 98%), ethyl 2-bromoisobutyrate (EtBiB) (Sigma-Aldrich, 98 %), copper(II) bromide ($CuBr_2$) (Sigma-Aldrich, 99%), tin(II) 2-ethylhexanoate ($Sn(EH)_2$) (Sigma-Aldrich, 95%), toluene (Sigma-Aldrich, 99.5%), N,N-dimethylformamide (DMF) (Aldrich, 99%), 2,2′-azo-bis(isobutyronitrile) (AIBN) (Aldrich, 99%) and 2,2′-azobis(4-methoxy-2.4-dimethyl valeronitrile) (V-70) (Wako, 96%) were used as received.

Analysis

Molecular weight (M_n) and polydispersity index (PDI) were determined by gel permeation chromatography (GPC), conducted with a Waters 515 pump and Waters 2414 differential refractometer using PSS columns (Styrogel 10^5, 10^3, 10^2 Å) in THF as an eluent at 35 °C and at a flow rate of 1 mL/min. Linear polystyrene standards were used for calibration. Conversion of monomers was determined using a Shimadzu GC 14-A gas chromatograph equipped with a FID detector using a J&W Scientific 30 m DB WAX Megabore column with DMF as an internal standard. Conversion was calculated by detecting the decrease of the monomer peak area relative to the peak areas of the standards.

1 L Reactor Setup

Polymerization experiments were performed in a 1 L Ace Glass reactor equipped with overhead IKA stirrer and heated with a heating mantle. The temperature inside the reactor was monitored using an internal thermocouple and a second thermocouple was placed outside the reactor, between the wall of the reactor and the heating mantle. A solution of radical initiator in toluene (degassed) was fed at a defined rate into Ace Glass reactor using NE-1000 syringe pump.

General Procedure for the Polymerization of St via the *Ultiamte ATRP^{SM}* Process

A solution of catalyst was made by dissolving $CuBr_2$ (78.0 mg, 34.9×10^{-2} mmol) and TPMA (304 mg, 104×10^{-2} mmol) in 35.0 mL of DMF. This solution was added to a 1 L Ace Glass reactor together with St (800 mL, 6.98 mol) and DEBMM (1.34 mL, 6.98 mmol). The mixture was purged with nitrogen for 1.5 h and the reactor was heated to 100 °C using a heating mantle. Next, a solution of AIBN (115 mg, 69.8×10^{-2} mmol) in 40.0 mL of degassed toluene was fed into the reactor at a constant rate (3.33 mL/h) using a syringe pump. Samples were withdrawn at regular time intervals and analyzed by GC and GPC to follow the progress of the reaction. Reaction was stopped after 9 h (feeding was stopped) and polymerization solution was left to cool overnight. Next, reaction was restarted by heating the reaction vessel to 110 °C and feeding of AIBN solution with a constant rate (3.33 mL/h).

Chain Extension of the PSt Macroinitiator with *n*BA via ARGET ATRP

A solution of catalyst was made by dissolving $CuBr_2$ (2.4 mg, 1.1×10^{-2} mmol) and TPMA (15.3 mg, 5.25×10^{-2} mmol) in 1.0 ml of DMF. This solution was added to a 100 mL Schlenk flask together with PSt macroinitiator (8.82 g, $M_{n,GPC}$ = 8,100 g/mol, PDI=1.14), *n*BA (45.0 mL, 0.32 mol) and anisole (27.0 mL). The mixture was flushed with nitrogen for 0.7 h and the flask was placed in the oil bath thermostated at 60 °C. An initial sample was taken before the reducing agent, $Sn(EH)_2$ (34.1 μL, 10.5×10^{-2} mmol), was added. Samples were withdrawn at regular intervals and analyzed by GC and GPC to follow the progress of the reaction.

General Procedure for the Polymerization of *n*BA via the *Ultimate ATRP*^{SM} Process

1 L Ace Glass reactor was charged with *n*BA (700 mL, 4.90 mol), EtBiB (3.60 mL, 24.5 mmol) and 140 ml of toluene. The mixture was purged with nitrogen for 1.5 h and the reactor was heated to 55 °C using a heating mantle. A solution of catalyst was made by dissolving CuBr (24.5 mg, 34.9×10^{-2} mmol) $CuBr_2$ (24.4 mg, 12.3×10^{-2} mmol) and Me_6TREN (324 μL, 122×10^{-2} mmol) in 10.0 mL of degassed DMF. This solution was added to a reactor. Next, a solution of V-70 (227 mg, 73.6×10^{-2} mmol) in 30.0 mL of degassed acetone was fed into the reactor at various rates using a syringe pump. Samples were withdrawn at regular time intervals and analyzed by GC and GPC to follow the progress of the reaction.

General Procedure for the Polymerization of *n*BA via ARGET ATRP

A solution of catalyst was made by dissolving $CuBr_2$ (54.8 mg, 24.5×10^{-2} mmol) and TPMA (214 mg, 73.6×10^{-2} mmol) in 10.0 mL of DMF. This solution was added to a 1 L Ace Glass reactor together with nBA (700 mL, 4.90 mol), EtBiB (1.44 mL, 9.81 mmol) and 140 ml of anisole . The mixture was purged with nitrogen for 1.5 h and the reactor was heated to 35 °C using a heating mantle. An initial sample was taken before the reducing agent, $Sn(EH)_2$ (318 μL, 98.1×10^{-2} mmol), was added. The heating mantle temperature was set to 60 °C after exothermic effect was gone (~320 min).

Acknowledgments

The author would like to thank National Science Foundation Small Business Innovation Research for the financial support (#0912338 and #1026575) and Laura Mueller and Patrick McCarthy for helpful dicussions.

Downloaded by UNIV OF GUELPH LIBRARY on May 31, 2012 | http://pubs.acs.org
Publication Date (Web): March 20, 2012 | doi: 10.1021/bk-2012-1100.ch013

References

1. Matyjaszewski, K.; Tsarevsky, N. V. *Nat. Chem.* **2009**, *1*, 276.
2. Braunecker, W. A.; Matyjaszewski, K. *Prog. Polym. Sci.* **2007**, *32*, 93.
3. Matyjaszewski, K.; Davis, T. P. *Handbook of Radical Polymerization*; Wiley Interscience: Hoboken, NJ, 2002.
4. Wang, J.-S.; Matyjaszewski, K. *J. Am. Chem. Soc.* **1995**, *117*, 5614.
5. Matyjaszewski, K.; Gnanou, Y.; Leibler, L. *Macromolecular Engineering. Precise Synthesis, Materials Properties, Applications*; Wiley-VCH: Weinheim, 2007.
6. Matyjaszewski, K.; Spanswick, J. *Mater. Today* **2005**, *8*, 26.
7. Spanswick, J.; Pike, B. Opportunities in Controlled Radical Polymerization. In *Controlled/Living Radical Polymerization: Progress in RAFT, DT, NMP & OMRP*; Matyjaszewski, K., Ed.; ACS Symposium Series 1023; American Chemical Society: Washington, DC, 2009; pp 385−396.
8. McCarthy, P.; Chattopadhyay, M.; Millhauser, G. L.; Tsarevsky, N. V.; Bombalski, L.; Matyjaszewski, K.; Shimmin, D.; Avdalovic, N.; Pohl, C. *Anal. Biochem.* **2007**, *366*, 1.
9. McCarthy, P.; Tsarevsky, N. V.; Bombalski, L.; Matyjaszewski, K.; Pohl, C. Grafting Chromatographic Stationary Phase Substrates by Atom Transfer Radical Polymerization. In *Controlled/Living Radical Polymerization*; Matyjaszewski, K., Ed.; ACS Symposium Series 944; American Chemical Society: Washington, DC, 2006; pp 252−268.
10. Tsarevsky Nicolay, V.; Matyjaszewski, K. *Chem. Rev.* **2007**, *107*, 2270.
11. Chan, N.; Cunningham, M. F.; Hutchinson, R. A. *Macromol. React. Eng.* **2010**, *4*, 369.
12. Jakubowski, W.; Matyjaszewski, K. *Angew. Chem., Int. Ed.* **2006**, *45*, 4482.
13. Jakubowski, W.; Min, K.; Matyjaszewski, K. *Macromolecules* **2006**, *39*, 39.
14. Matyjaszewski, K.; Jakubowski, W.; Min, K.; Tang, W.; Huang, J.; Braunecker, W. A.; Tsarevsky, N. V. *Proc. Natl. Acad. Sci. U.S.A.* **2006**, *103*, 15309.
15. Mueller, L.; Jakubowski, W.; Matyjaszewski, K.; Pietrasik, J.; Kwiatkowski, P.; Chaladaj, W.; Jurczak, J. *Eur. Polym. J.* **2010**, *47*, 730.
16. Jakubowski, W.; Kirci-Denizli, B.; Gil, R. R.; Matyjaszewski, K. *Macromol. Chem. Phys.* **2008**, *209*, 32.
17. Kwiatkowski, P.; Jurczak, J.; Pietrasik, J.; Jakubowski, W.; Mueller, L.; Matyjaszewski, K. *Macromolecules* **2008**, *41*, 1067.
18. Dong, H.; Tang, W.; Matyjaszewski, K. *Macromolecules* **2007**, *40*, 2974.
19. Matyjaszewski, K.; Dong, H.; Jakubowski, W.; Pietrasik, J.; Kusumo, A. *Langmuir* **2007**, *23*, 4528.
20. Pietrasik, J.; Dong, H.; Matyjaszewski, K. *Macromolecules* **2006**, *39*, 6384.
21. Tsarevsky, N. V.; Jakubowski, W. *J. Polym. Sci., Part A: Polym. Chem.* **2011**, *49*, 918.
22. Burdynska, J.; Cho, H. Y.; Mueller, L.; Matyjaszewski, K. *Macromolecules* **2010**, *43*, 9227.
23. Jakubowski, W.; Tsarevsky, N. V.; McCarthy, P. Systematic Polymeric Libraries via Atom Transfer Radical Polymerization. In *Controlled/Living*

Downloaded by UNIV OF GUELPH LIBRARY on May 31, 2012 | http://pubs.acs.org
Publication Date (Web): March 20, 2012 | doi: 10.1021/bk-2012-1100.ch013

Radical Polymerization: Progress in RAFT, DT, NMP & OMRP; Matyjaszewski, K., Ed.; ACS Symposium Series 1023; American Chemical Society: Washington, DC, 2009; pp 343−355.

24. Listak, J.; Jakubowski, W.; Mueller, L.; Plichta, A.; Matyjaszewski, K.; Bockstaller, M. R. *Macromolecules* **2008**, *41*, 5919.
25. Mueller, L.; Jakubowski, W.; Tang, W.; Matyjaszewski, K. *Macromolecules* **2007**, *40*, 6464.
26. Jakubowski, W.; Spanswick, J. U.S. Patent application 12/653,937, 2011.
27. Hadjichristidis, N.; Pispas, S.; Floudas, G. *Block Copolymers: Synthetic Strategies, Physical Properties, and Applications*; John Wiley & Sons, Inc.: Hoboken, NJ, 2003.
28. Davis, K. A.; Matyjaszewski, K. *Adv. Polym. Sci.* **2002**, *159*, 1.
29. Coessens, V.; Pintauer, T.; Matyjaszewski, K. *Prog. Polym. Sci.* **2001**, *26*, 337.
30. Lutz, J.-F.; Matyjaszewski, K. *J. Polym. Sci., Part A: Polym. Chem.* **2005**, *43*, 897.
31. Levere, M. E.; Willoughby, I.; O'Donohue, S.; de Cuendias, A.; Grice, A. J.; Fidge, C.; Becer, C. R.; Haddleton, D. M. *Polym. Chem.* **2010**, *1*, 1086.

Downloaded by UNIV OF GUELPH LIBRARY on May 31, 2012 | http://pubs.acs.org
Publication Date (Web): March 20, 2012 | doi: 10.1021/bk-2012-1100.ch013

Chapter 14

Radical Coupling of Polymers Formed by Cobalt-Mediated Radical Polymerization

Antoine Debuigne, Marie Hurtgen, Christine Jérôme, and Christophe Detrembleur[*]

Center for Education and Research on Macromolecules (CERM),
Chemistry Department, University of Liege (ULg), Sart-Tilman, B6A,
4000 Liege, Belgium
[*]E-mail: christophe.detrembleur@ulg.ac.be

Considerable progress has been recently made in cobalt-mediated radical polymerization (CMRP), a controlled radical polymerization system based on the temporary deactivation of the polymer chains by a cobalt complex, like the improvement of the mechanistic understanding, the extension to a range of monomers and the preparation of novel architectures. However, the real breakthrough in this field concerns the development of efficient radical coupling methods for polymer precursors preformed by CMRP. This book chapter aims to describe the general principle and main characteristics of such radical coupling techniques involving dienes, nitrones, fullerenes or carbon nanotubes. Well-defined and complex architectures obtained by these techniques are provided in order to illustrate their potential for macromolecular engineering.

In Progress in Controlled Radical Polymerization: Mechanisms and Techniques; Matyjaszewski, K., et al.;
ACS Symposium Series; American Chemical Society: Washington, DC, 2012.

In the last two years, considerable progress has been made in the field of cobalt-mediated radical polymerization (CMRP) (*1–8*), a controlled radical polymerization system based on the temporary deactivation of the growing radical chains by a cobalt complex. The mechanistic understanding of this technique enhanced and the experimental parameters influencing the kinetics and the level of control are well identified today. The range of monomers whose polymerization can be controlled by the *bis*(acetylacetonato)cobalt(II) ($Co(acac)_2$) has been recently extended to vinyl ethyl imidazolium bromide (VEtImBr) (*9*), *N*-vinyl caprolactam (*N*VCL) (*10*) and poly(ethylene glycol) acrylate monomer (PEGA) (*11*). New diblock copolymers involving either an ionic liquid sequence like PVEtImBr (*9*), a thermosensitive block as P*N*VCL (*10*) or a PEGA stealthy segment (*11*), have been prepared by CMRP.

Besides these interesting achievements, a real breakthrough has been made in the field of CMRP. This advance does not concern the controlled polymerization system by itself but it strongly widens the scope of CMRP from the macromolecular engineering point of view. It concerns the development of efficient radical coupling methods for polymer precursors preformed by CMRP (*12–14*). Such polymers are capped by a cobalt complex and can release the radical chains upon activation via the Co-C bond cleavage. Although direct recombination of the radical chains is possible, disproportionation invariably competes with the desired coupling reaction. Fortunately, the use of coupling agents can specifically lead to the dimerization of the chains as discussed below.

This contribution aims to describe the radical coupling methods successfully developed for CMRP precursors and to demonstrate that it is a perfect complementary tool for CMRP, particularly for the design of symmetrical structures. The discussion is organized in three sections corresponding to the coupling agents used until now, i.e. conjugated dienes (*9*, *12–15*), nitrones (*16*) and carbon based materials (*17–19*). In each section, general principles and main characteristics of the coupling method are provided and their macromolecular engineering potential is illustrated by the synthesis of novel macromolecules including symmetrical triblocks, stars and H-sape polymers, etc.

Experimental Section

Radical Coupling with Conjugated Dienes

Under inert atmosphere, a 100 fold excess of diene compared to the cobalt is added to solution of a polymer synthesized by CMRP as described elsewhere. The medium is stirred for 2h at room temperature. The coupling product is then purified by precipitation in order to remove the cobalt(II) complex released in the reaction medium. The extent of coupling X_c is calculated based on the molecular weight of the polymer measured by size exclusion chromatography before and after the coupling reaction following the equation: $X_c = 2[1-(Mn\ initial/Mn\ final)]$. For more details see reference (*12*).

Radical Coupling with Nitrones

Under inert atmosphere, a PVAc precursor is formed by CMRP from an alkyl-cobalt(III) initiator ($(Co(acac)_2(\text{-}CH(OCOCH_3)CH_2)_{<4}\text{-}R_0)$ at 40°C. After about 60% conversion, the residual monomer is removed under reduced pressure at room temperature (rt). To the PVAc-$Co(acac)_2$ under argon is added a toluene solution of alkyne bearing nitrone (2 equiv. compared to the cobalt) and the medium is stirred overnight at 40°C. The final product is precipitated 2 times in heptane and dried at 40°C under vacuum overnight.

In a Schlenk tube are placed PVAc-alkyne-PVAc, PEG-N_3 (1 equiv), PMDETA (5 equiv) in DMF. The solution is further degassed by three freeze–thaw–pump cycles and left under argon. CuBr (5 equiv) is added to the solution under argon. The tube is stirred at room temperature for 24 h. The solution is passed through a neutral alumina column to remove CuBr-PMDETA complex. The final star shaped $PVAc_2$-PEG is recovered by precipitation in a methanol/water (1/4) mixture. For more details see reference (*16*).

Radical Coupling with Fullerenes

Under inert atmosphere, a polymer synthesized by CMRP is dissolved in 1,2,4-trichlorobenzene (TCB) and added in an 8-fold excess to a solution of C_{60} in TCB. The medium is stirred for 20h at 30°C. The resulting polymer/C_{60} nanohybrid is then purified by precipitation in order to remove the cobalt(II) complex released in the reaction medium. The ungrafted polymer is removed by centrifugal filtration (cut-off: 30000 Da). The grafting reaction onto C_{60} is evidenced by size exclusion chromatography with dual detection (refractive index and UV at 290 nm). The functionality of the star-shaped nanohybrid is calculated based on the molecular weight of the polymer measured by SEC before and after reaction onto C_{60} following the equation : x = Mn, star/Mn precursor. For more details see reference (*18*).

Radical Coupling with Carbon Nanotubes

Under inert atmosphere, a PVAc-$Co(acac)_2$ is formed by CMRP of VAc using a mixture of V70 and cobalt(II) acetylacetonate ($Co(acac)_2$) ($[V70]/[Co(acac)_2]=3.25$) at 30°C for 40h. A sample is picked out for the monomer conversion (45 %) and the SEC analysis (Mn = 6000 g/mol; Mw/Mn = 1.4). Residual monomer is then removed under vacuum followed by the addition of methanol at 0°C. The methanolic solution of PVAc-$Co(acac)_2$ is then added to a degassed suspension of CNTs in methanol (PVAc-$Co(acac)_2$/CNTs = ~ 37 w/w), and the mixture is placed in an ultrasonic bath for 2 min followed by the addition of a low amount of distilled water. After 20 h at 30°C, the mixture is cooled down to room temperature, diluted and filtrated. The CNTs are then washed several times with methanol to remove ungrafted PVAc. The washing steps consist in the dispersion of modified CNTs within methanol, the treatment in an ultrasonic bath for 10 min and filtration. After drying under vacuum for 24h at 40°C, the modified CNTs are characterized by thermogravimetric analysis (TGA) in order to quantify the amount of grafted polymer (20 wt%). For more details see reference (*19*).

Results and Discussion

Radical Coupling with Conjugated Dienes

A recent attempt to control the radical polymerization of conjugated dienes in the presence of Co(acac)$_2$ leads us to discover a novel chain coupling reaction, designated as Cobalt-Mediated Radical Coupling (CMRC) (*12–14*). When a solution of polymer formed by CMRP is treated with a large excess of isoprene at room temperature, the cross addition takes place leading to allyl radical terminated chains (*14*). However, further polymerization of isoprene does not occur because of the low propagation rate constant of this monomer at room temperature. Moreover, deactivation of the allyl radicals by the cobalt is unfavorable, as suggested by the low bond dissociation enthalpy calculated for an allyl-Co(acac)$_2$ model compound (~1 Kcal) (*14*). Therefore, the allyl radical terminated chains undergo bimolecular termination reactions mainly by coupling, as observed for polyisoprene. The doubling of the molecular weight of the CMRP precursor is thus obtained instead of the formation of a diblock. The measured extent of coupling is usually above 95%. The CMRC concept has been successfully applied to various homopolymers preformed by CMRP. Nevertheless, this reaction becomes most important when applied to diblocks (*9*, *12*, *13*) or α-functional precursors (*15*).

For example, the CMRC process has been applied to a PVAc-*b*-PVEtImBr-Co(acac)$_2$ diblock copolymer **2** leading to the corresponding PVAc and PVEtImBr triblock copolymer (Figure 1) (*9*). The diblock **2** is obtained by sequential copolymerization of VAc **1** in bulk at 40°C and VEtImBr at 30°C in a DMF/MeOH (2/1) mixture. At 50% of VEtImBr conversion, a large excess of isoprene compared to the cobalt is injected and provokes an almost quantitative coupling of the chains and the formation of a well-defined symmetrical triblock PVAc-*b*-PVEtImBr-*b*-PVAc **3** which presents a polymer ionic liquid as central block. In this particular case, the CMRC has been conducted without removal of the residual VEtImBr (*9*). A simple purification by precipitation allows recovering the final copolymer free of unreacted monomer and cobalt. Considering the molar masses of the triblock copolymer, it is clear that CMRC is not restricted to low molecular weight precursors. Other well-defined symmetrical triblock copolymers based on PVAc, polyacrylonitrile (PAN) (*12*), P*N*VCL (*10*) and poly(*N*-vinylpyrrolidone) (P*N*VP) (*13*), have been prepared following the same convergent CMRC strategy.

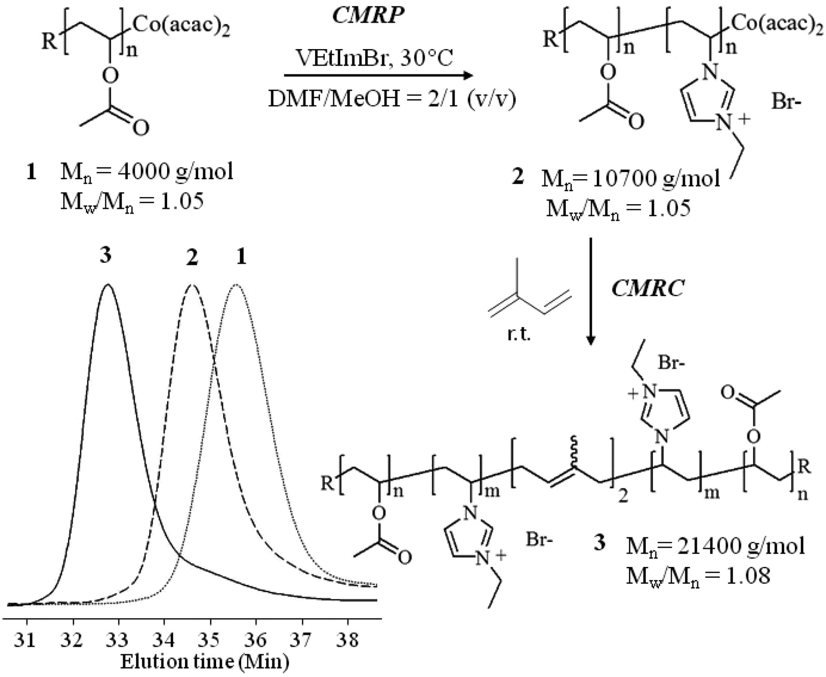

Figure 1. General strategy and SEC chromatograms for the synthesis of a symmetrical PVAc-b-PVEtImBr-b-PVAc triblock copolymer.

The CMRC reaction also paves the way to α,ω-telechelic polymers by isoprene addition onto α-functional CMRP polymers (Figure 2). Recently, a well-defined α-hydroxy-P*N*VP-Co(acac)$_2$ **4** was prepared by the photoinitiated polymerization of *N*VP at 0°C in methanol using a hydroxyl-functional azoinitiator (VA-086) and Co(acac)$_2$ as controlling agent (*15*). The use of photochemistry in the initiation step is crucial since the decomposition temperature of the functional azoinitiator (VA-086) is much higher than the temperature (90°C) prescribed for an ideal Co(acac)$_2$-mediated polymerization (0°C - room temperature) (*15*). An α,ω-dihydroxy-telechelic P*N*VP **5** (45400 g/mol, Ip = 1.08) has been obtained for the first time by isoprene addition to the α-functional P*N*VP **4**. In spite of the quite high molar mass of the P*N*VP precursor, the CMRC reaction is almost complete as shown by the shift of the SEC chromatograms towards lower elution volumes. Finally, the hydroxyl functions at the extremities of P*N*VP **5** have been used to initiate the ring-opening polymerization (ROP) of ε−caprolactone (CL) in the presence of tin octoate (Sn(Oct)$_2$) at 110°C. The desired PCL(18600)-*b*-P*N*VP(45400)-*b*-PCL(18600) **6** symmetrical triblock copolymer has been obtained accordingly. Such amphiphilic copolymer **6** based on a biocompatible P*N*VP and biodegradable PCL sequences forms vesicles in water which is unusual for a triblock having a hydrosoluble central block (*15*). In this case, the P*N*VP segment forms loops at the surface and in the water pool of the vesicle while PCL blocks form the membrane. In order words, it is the first example of flower like vesicles assemblies.

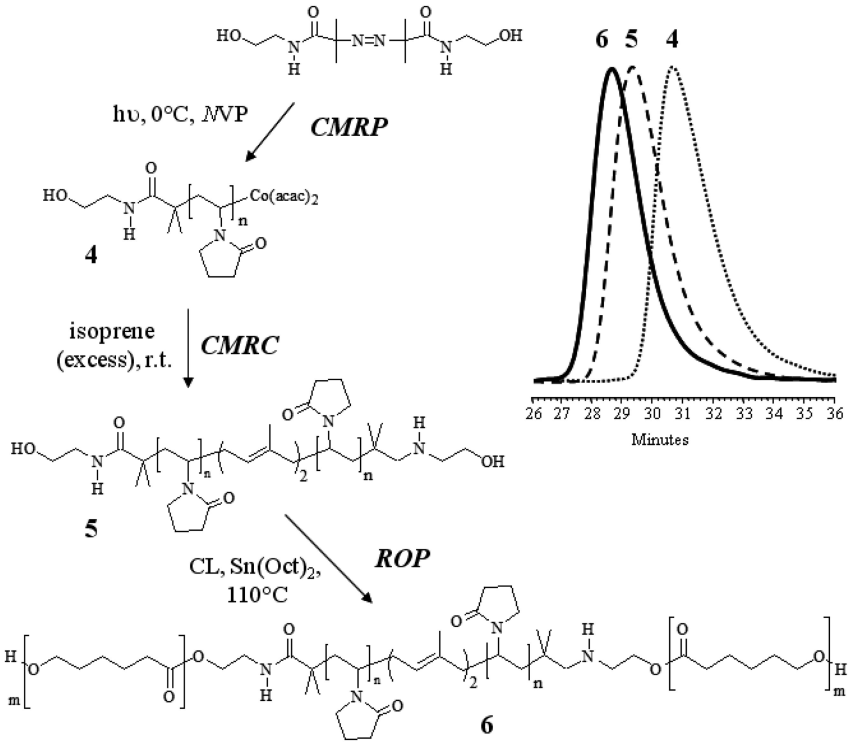

Figure 2. General strategy and SEC chromatograms for the synthesis of α,ω-telechelic PNVP and symmetrical PCL-b-PNVP-b-PCL triblock copolymers.

The incorporation of isoprene units in the middle of the coupling product is a key feature of CMRC (*14*). A detailed study based on NMR and mass spectrometry demonstrates that a large majority of the chains contains exactly two isoprene units per chain. On the other hand, several dienes with different substitution, including compounds functionalized by alcohol or ester moieties, have been considered as coupling agents in the CMRC process. In all the cases, the efficiency of coupling is not altered and the incorporation of diene in the backbone is confirmed which paves the way to the mid-chain functionalization of polymers (*14*). Nevertheless, the inserted reactive functions, like alcohols, have not been exploited for further modifications of the polymers yet.

Radical Coupling with Nitrones

Besides CMRC, another radical coupling method is useful to dimerize polymer chains preformed by CMRP (*16*). This two-step process, called nitrone-mediated radical coupling (NMRC) (*20*), takes advantage of the well-known spin-trap ability of nitrones (*21*). Typically, a nitrone undergoes a first radical addition with formation of a nitroxide-terminated polymer which captures a second radical chain. The final coupling product has a twice higher molar mass compared to the initial polymer and contains an alkoxyamine function in the middle of the backbone. NMRC, derived from the electron-spin capturing polymerization (ESCP) (*22–26*) based on the coupling of radical chains produced by a free radical polymerization process, was first applied to polymers prepared by atom transfer radical polymerization (ATRP). The radical species were generated in the presence of a nitrone upon treatment of the halogen-terminated chains with a copper catalyst. Very good coupling efficiencies were observed. The implementation of NMRC to CMRP precursors has been quite straightforward (*16*). The homolytic activation of the PVAc-Co(acac)$_2$ or PAN-Co(acac)$_2$ bonds is promoted by thermal treatment in the presence of two equivalents of nitrone. An almost perfect doubling of the molar mass is then observed by size exclusion chromatography (SEC) and the presence of an alkoxyamine moiety in the polymer backbone is evidenced by NMR and Electrospray Ionization Mass Spectrometry (ESI-MS).

Compared to CMRC, NMRC offers similar coupling efficiencies at least for polymers with molar masses around 10000 g/mol (*16*). However, the nitrone-assisted method is superior for the mid-chain functionalization. Indeed, in contrast to CMRC, the use of a functional nitrone leads specifically to the insertion of one function per chain. For example, a PVAc-Co(acac)$_2$ **7** formed by CMRP in bulk has been treated with an alkyne bearing nitrone and formed a well-defined alkyne mid-chain functionalized PVAc **8** (Mn = 9400g/mol, Ip =1.10) (Figure 3) (*16*). The latter is an interesting precursor for the synthesis of mikto-arm copolymers. Indeed, the alkyne group in mid-chain position has been used to graft an azide-terminated poly(ethylene oxide) (PEO) chain **9** through the well-known copper catalyzed azide alkyne cycloaddition (CuAAC) reaction. The expected well-defined PVAc$_2$PEO star copolymer **10** (Mn = 10800g/mol, Ip =1.09) was recovered (*16*). The exact same strategy was applied to PVAc-*b*-PAN-Co(acac)$_2$ precursors leading to the corresponding (PVAc-*b*-PAN)$_2$-PEO mikto-arm copolymer. Interestingly, H-shape copolymers have been synthesized by CuAAC reaction between alkyne mid-chain function derivatives with telechelic diazide PEO chains (*16*).

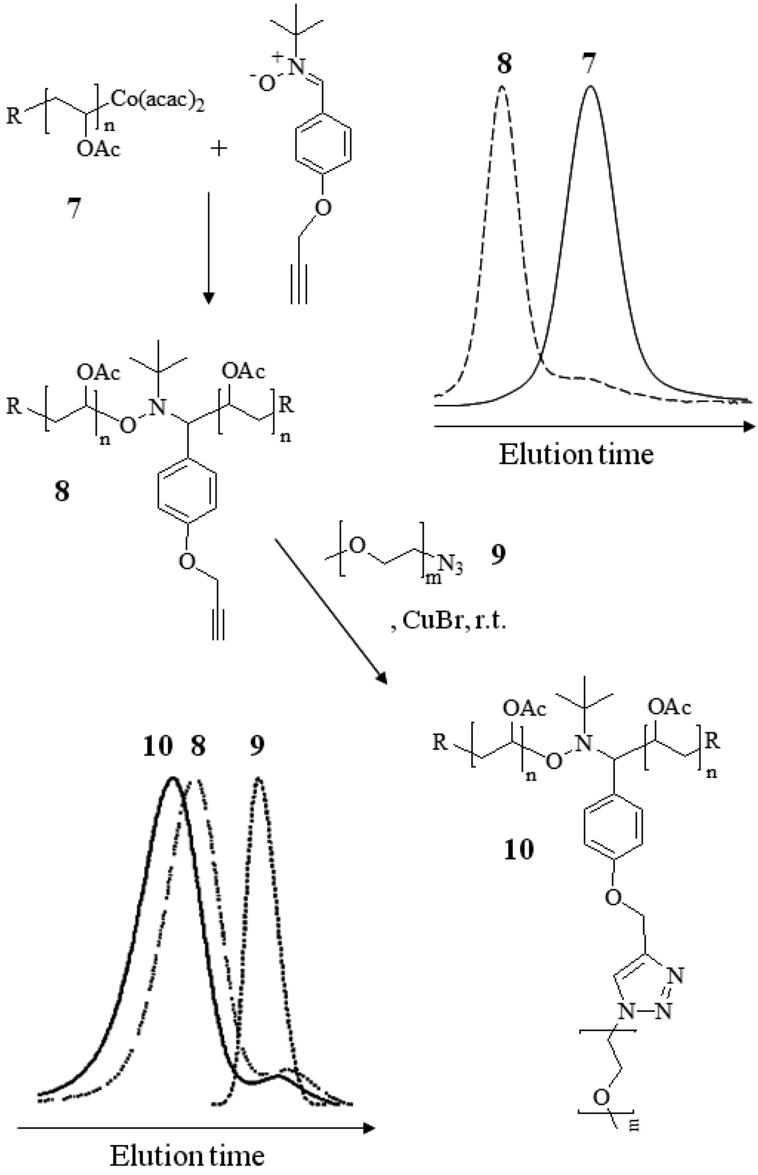
R
Co(acac)$_2$
n
OAc
7
+
O
N
O
8
7
Elution time
OAc
OAc
R
N
O
R
n
n
8
O
O
N$_3$
m
9
, CuBr, r.t.
OAc
OAc
R
O
N
R
n
n
10
O
N
N
N
O
m
10 8 9
Elution time

Figure 3. General strategy and SEC chromatograms for the synthesis of PVAc$_2$-PEG stars by combination of NMRC carried out on CMRP precursors and copper catalyzed azide-alkyne cycloaddition (CuAAC).

Radical Coupling with Carbon Based Materials

Unsaturated carbon-based materials such as fullerenes or carbon nanotubes (CNT) behave as radical sponges and can be regarded as multifunctional coupling agents due to the abundance of unsaturated sites.

In particular, C_{60} has a more pronounced curvature and therefore reactivity than CNT towards radicals. Its reaction with a macroradical results in the formation of a fullerenyl radical that is then deactivated by the addition of a second polymer chain. This sequence can occur multiple times, which constitutes a straightforward route towards star-shaped polymers having a central C_{60} core. The radical addition onto C_{60} was first applied to macroradicals prepared by ATRP (*27–30*), NMP (*31*, *32*) and more recently, RAFT polymerization (*33*). The implementation to various CMRP precursors was also successful and achieved by the thermal activation of polymer-Co(acac)$_2$ in the presence of C_{60}. Depending on the molecular structure of the CMRP precursor, the grafting reaction onto C_{60} can lead to interesting architectures.

This is well exemplified by the grafting of poly(poly(ethylene glycol) acrylate-*co*-vinyl acetate) (P(PEGA-*co*-VAc)) onto C_{60} (Figure 4). These copolymers **11** have been prepared by the Co(acac)$_2$-mediated statistical copolymerization of vinyl acetate with PEG acrylate initiated by a preformed alkylcobalt(III) adduct (*11*). The resulting graft copolymer **11** is characterized by a strong gradient imparted by the extreme difference of reactivity between the conjugated (PEGA) and the non-conjugated (VAc) monomers. The gradient is such that the copolymer tends towards a block structure. Previous reports also deal with the synthesis of gradient copolymers of vinyl acetate and acrylic monomers by controlled radical polymerizations (*34*, *35*). Upon addition of an eight-fold excess of **11** onto C_{60}, the corresponding P(PEGA-*co*-VAc)/C_{60} nanohybrid **12** is formed (Figure 4). The grafting reaction is evidenced by SEC with UV detection that is sensitive to C_{60}-containing species. The nanohybrid **12** was isolated from the ungrafted polymer chains **11** by centrifugal filtration on appropriate membranes. In nanohybrid **12**, an average of six polymer chains were attached to C_{60}, as determined by SEC. Although the precursor polymer **11** is amphiphilic (*11*), the star-like architecture of **12** with an outer-shell of PEG grafts renders it water-soluble.

A similar strategy was applied for the synthesis of PVAc/C_{60} (*18*) and water-soluble P*N*VP-*co*-PVAc/C_{60} nanohybrids (*17*). Also, the hydrolysis of PVAc into poly(vinyl alcohol) (PVOH) led to hydrosoluble PVOH/C_{60} nanohybrids (*18*).

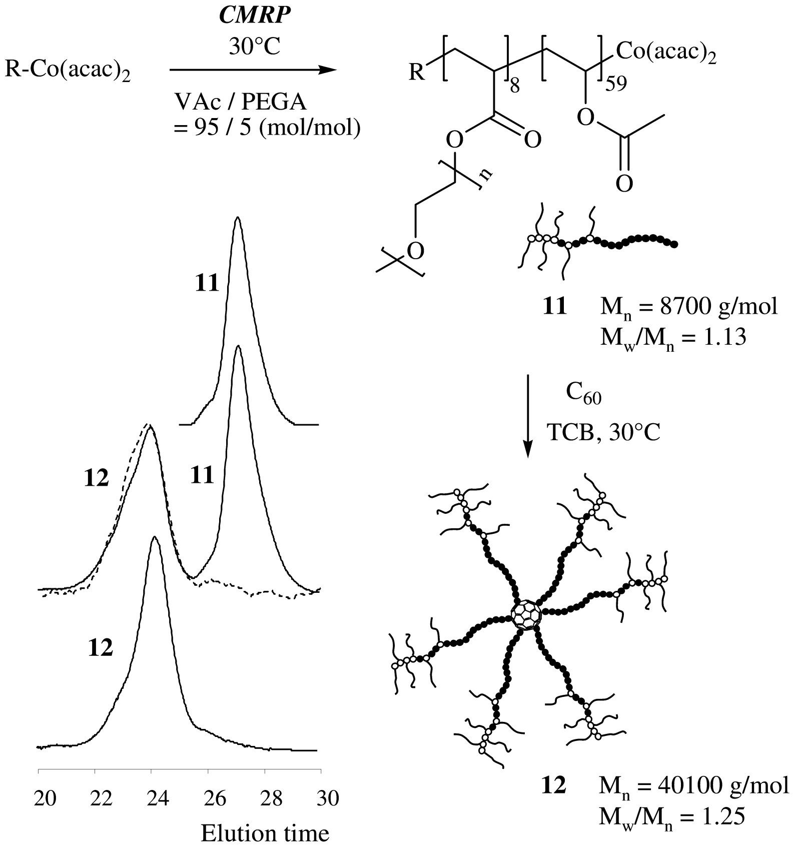
CMRP
30°C
R-Co(acac)2
VAc / PEGA
= 95 / 5 (mol/mol)
R
8
59
Co(acac)2
O
O
O
O
O
n
O
11
11 Mn = 8700 g/mol
Mw/Mn = 1.13
C60
TCB, 30°C
12
11
12
12 Mn = 40100 g/mol
Mw/Mn = 1.25
20
22
24
26
28
30
Elution time

Figure 4. General strategy and SEC chromatograms (dotted line: UV detection) for the synthesis of P(PEGA-co-VAc) diblock graft copolymers and P(PEGA-co-VAc)/C_{60} nanohybrids.

Carbon nanotubes (CNTs) are also reactive towards radicals such that the grafting of pre-formed polymers by radical additions was successfully applied to CNTs. In that respect, various well-defined polymers, including block copolymers, prepared by controlled radical polymerization techniques such as atom transfer radical polymerization (ATRP) (*36*, *37*) and nitroxide mediated polymerization (NMP) (*38–41*) were grafted onto CNTs. Recently, CMRP was implemented for the covalent anchoring of PVAc chains onto CNTs (*19*). Upon mild thermal treatment at 30°C in methanol, the C-Co bond at the PVAc chain end (**13**, Figure 5) cleaves and releases PVAc radical that is rapidly trapped by the sp^2 carbons of CNTs. The so-modified CNTs (CNTs-g-PVAc, **14**, Figure 5) are now soluble in good solvents of PVAc such as toluene and tetrahydrofuran for instance. By treatment of **14** by a mixture of acetic acid and hydrochloric acid in water, PVAc is hydrolysed at 72% leading to CNTs grafted by poly(vinyl acetate)-co-poly(vinyl alcohol) (CNTs-g-P(VAc-co-VOH), **15**, Figure 5). This copolymer being a good stabilizer for dispersion polymerization of vinyl monomers, **15** has been used as a co-stabilizer for the methyl methacrylate (MMA) dispersion polymerization in methanol (*19*). Poly(methyl methacrylate) (PMMA) microspheres decorated by CNTs are therefore collected at the end of the reaction. Using **15** as a dispersion stabilizer has therefore demonstrated to be a powerful strategy to localize selectively CNTs at the surface of polymer microspheres and to form highly conducting nanocomposites at low CNTs content.

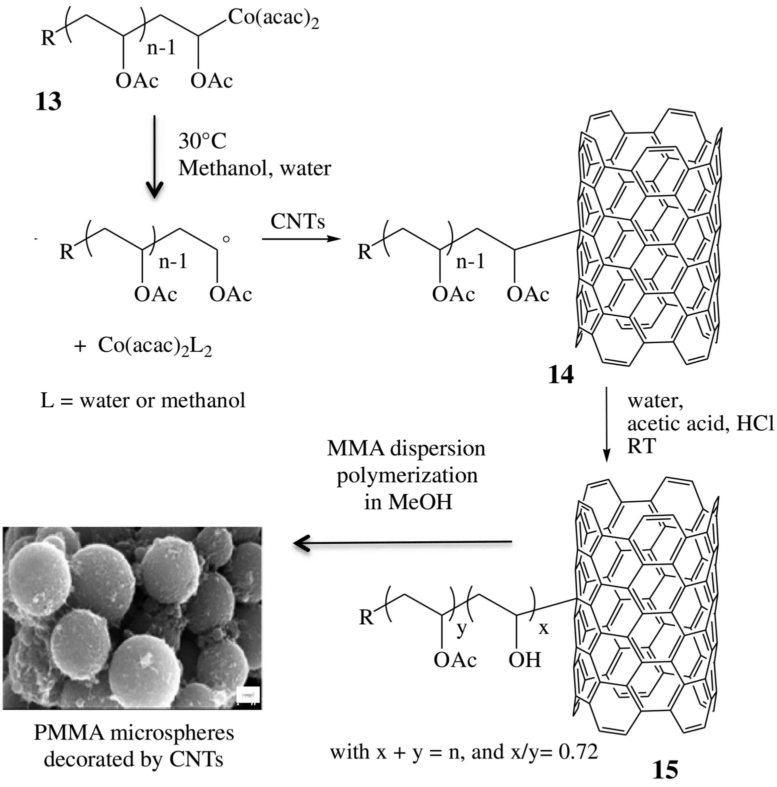
R
n-1
Co(acac)2
OAc
OAc
13
30°C
Methanol, water
R
n-1
OAc
OAc
+ Co(acac)2L2
L = water or methanol
CNTs
R
n-1
OAc
OAc
14
water,
acetic acid, HCl
RT
MMA dispersion
polymerization
in MeOH
R
y
x
OAc
OH
15
with x + y = n, and x/y= 0.72
PMMA microspheres
decorated by CNTs

Figure 5. General strategy and Scanning Electron Microscopy (SEM) for the synthesis of PVAC and PVOH grafted carbon nanotubes and PMMA microspheres decorated with CNTs.

Conclusion

This book chapter emphasizes the relevance of the combination of CMRP and various radical coupling methods, particularly for the preparation of telechelic, mid-chain functionalized, H-shape polymers, stars or symmetrical triblock copolymers. Several coupling agents have been successfully investigated and specificities of each system are discussed above. For example, the use of dienes is recommended in order to reach high coupling efficiencies for precursors with molar masses above 10000 g/mol. However, the precise mid-chain functionalization of the polymer remains difficult by CMRC. In contrast, a single reactive function, like an alkyne, can be inserted in the middle of the polymer chain when using a functional nitrone as coupling agent. In this case, further modification of the alkyne paves the way to the synthesis of complex architectures as mikto-arm and H-shape polymers. Compared to CMRC and NMRC, fullerenes and carbon nanotubes are able to trap more than two chains leading to carbon based multi-arms hybride materials. In general, the radical coupling of polymer chains preformed by controlled radical polymerization (CRP) is more and more investigated and is proving to be a perfect complementary tool for CRP, and CMRP in particular.

Acknowledgments

The authors from Liege are indebted to the "Belgian Science Policy" for financial support in the frame of the "Interuniversity Attraction Poles Programme (PAI VI/27) - Functional Supramolecular Systems", and to the "Fonds National de la Recherche Scientifique" (FRS-F.N.R.S., Belgium). A.D., M.H. and C.D. are thankful to the FRS-F.N.R.S. The authors thank G. Cartigny for skilful assistance and Wako for kindly providing them with V-70.

References

1. Hurtgen, M.; Detrembleur, C.; Jerome, C.; Debuigne, A. *Polym. Rev.* **2011**, *51*, 188.
2. Debuigne, A.; Poli, R.; Jerome, C.; Jerome, R.; Detrembleur, C. *Prog. Polym. Sci.* **2009**, *34*, 211.
3. Debuigne, A.; Poli, R.; Jérôme, R.; Jérôme, C.; Detrembleur, C. Key Role of Metal-Coordination in Cobalt-Mediated Radical Polymerization of Vinyl Acetate. In *Controlled/Living Radical Polymerization: Progress in RAFT, DT, NMP & OMRP*; Matyjaszewski, K., Ed.; ACS Symposium Series 1024; American Chemical Society: Washington, DC, 2009; pp 131−147.
4. Maria, S.; Kaneyoshi, H.; Matyjaszewski, K.; Poli, R. *Chem. Eur. J.* **2007**, *13*, 2480.
5. Wayland, B. B.; Peng, C.-H.; Fu, X.; Lu, Z.; Fryd, M. *Macromolecules* **2006**, *39*, 8219.
6. Debuigne, A.; Caille, J.-R.; Jerome, R. *Angew. Chem., Int. Ed.* **2005**, *44*, 1101.

7. Arvanitopoulos, L. D.; Greuel, M. P.; King, B. M.; Shim, A. K.; HarwoodH. J. Photochemical Polymerizations Initiated and Mediated by Soluble Organocobalt Compounds. In *Controlled Radical Polymerization*; Matyjaszewski, K., Ed.; ACS Symposium Series 685; American Chemical Society: Washington, DC, 1998; pp 316−331.
8. Wayland, B. B.; Poszmik, G.; Mukerjee, S. L.; Fryd, M. *J. Am. Chem. Soc.* **1994**, *116*, 7943.
9. Detrembleur, C.; Debuigne, A.; Hurtgen, M.; Jerôme, C.; Pinaud, J.; Fèvre, M.; Coupillaud, P.; Vignolle, J.; Taton, D. *Macromolecules* **2011**, *44*, 6397.
10. Hurtgen, M.; Liu, J.; Debuigne, A.; Jérôme, C.; Detrembleur, C. *Polym. Chem.* 2012, DOI: 10.1002/pola.25045.
11. Hurtgen, M.; Debuigne, A.; Fustin, C.-A.; Jerome, C.; Detrembleur, C. *Macromolecules* **2011**, *44*, 4623.
12. Debuigne, A.; Jerome, C.; Detrembleur, C. *Angew. Chem., Int. Ed.* **2009**, *48*, 1422.
13. Debuigne, A.; Poli, R.; De Winter, J.; Laurent, P.; Gerbaux, P.; Wathelet, J.-P.; Jerome, C.; Detrembleur, C. *Macromolecules* **2010**, *43*, 2801.
14. Debuigne, A.; Poli, R.; De, W. J.; Laurent, P.; Gerbaux, P.; Dubois, P.; Wathelet, J.-P.; Jerome, C.; Detrembleur, C. *Chem. Eur. J.* **2010**, *16*, 1799.
15. Debuigne, A.; Schoumacher, M.; Riva, R.; Willet, N.; Zhu, X.; Ruetten, S.; Jérôme, C.; Detrembleur, C. *Chem. Commun.* **2011**, *47*, 12703.
16. Detrembleur, C.; Debuigne, A.; Altintas, O.; Conradi, M.; Wong, E. H. H.; Jérôme, C.; Barner-Kowollik, C.; Junkers, T. *Poly. Chem.***2012**, *3,* 135−147.
17. Hurtgen, M.; Debuigne, A.; Mouithys-Mickalad, A.; Jerome, R.; Jerome, C.; Detrembleur, C. *Chem. Asian J.* **2010**, *5*, 859.
18. Detrembleur, C.; Stoilova, O.; Bryaskova, R.; Debuigne, A.; Mouithys-Mickalad, A.; Jérôme, R. *Macromol. Rapid Commun.* **2006**, *27*, 498.
19. Thomassin, J.-M.; Molenberg, I.; Huynen, I.; Debuigne, A.; Alexandre, M.; Jerome, C.; Detrembleur, C. *Chem. Commun.* **2010**, *46*, 3330.
20. Wong, E. H. H.; Altintas, O.; Stenzel, M. H.; Barner-Kowollik, C.; Junkers, T. *Chem. Commun.* **2011**, *47*, 5491.
21. Wong, E. H. H.; Junkers, T.; Barber-Kowollik, C. *Polym. Chem.* **2011**, *2*, 1008.
22. Wong, E. H. H.; Junkers, T.; Barner-Kowollik, C. *J. Polym. Sci., Part A: Polym. Chem.* **2008**, *46*, 7273.
23. Wong, E. H. H.; Stenzel, M. H.; Junkers, T.; Barner-Kowollik, C. *J. Polym. Sci., Part A: Polym. Chem.* **2009**, *47*, 1098.
24. Junkers, T.; Wong, E. H. H.; Stenzel, M. H.; Barner-Kowollik, C. *Macromolecules* **2009**, *42*, 5027.
25. Wong, E. H. H.; Stenzel, M. H.; Junkers, T.; Barner-Kowollik, C. *Macromolecules* **2010**, *43*, 3785.
26. Zang, L.; Wong, E. H. H.; Barner-Kowollik, C.; Junkers, T. *Polymer* **2010**, *51*, 3821.
27. Zhou, P.; Chen, G.-Q.; Hong, H.; Du, F.-S.; Li, Z.-C.; Li, F.-M. *Macromolecules* **2000**, *33*, 1948.

28. Audouin, F.; Renouard, T.; Schmaltz, B.; Nuffer, R.; Mathis, C. *Polymer* **2005**, *46*, 8519.
29. Audouin, F.; Nuffer, R.; Mathis, C. *J. Polym. Sci., Part A: Polym. Chem.* **2004**, *42*, 3456.
30. Ravi, P.; Dai, S.; Tan, C. H.; Tam, K. C. *Macromolecules* **2005**, *38*, 933.
31. Okamura, H.; Terauchi, T.; Minoda, M.; Fukuda, T.; Komatsu, K. *Macromolecules* **1997**, *30*, 5279.
32. Ford, W. T.; Lary, A. L.; Mourey, T. H. *Macromolecules* **2001**, *34*, 5819.
33. Zhou, G.; Harruna, I. I.; Zhou, W. L.; Aicher, W. K.; Geckeler, K. E. *Chem. Eur. J.* **2007**, *13*, 569.
34. Koumura, K.; Satoh, K.; Kamigaito, M. *J Polym. Sci., Part A: Polym. Chem.* **2009**, *47*, 1343.
35. Kaneyoshi, H.; Matyjaszewski, K. *Macromolecules* **2005**, *38*, 8163.
36. Jeon, J.-H.; Lim, J.-H.; Kim, K.-M. *Polymer* **2009**, *50*, 4488.
37. Wu, H.-X.; Tong, R.; Qiu, X.-Q.; Yang, H.-F.; Lin, Y.-H.; Cai, R.-F.; Qian, S.-X. *Carbon* **2007**, *45*, 152.
38. Lou, X.; Detrembleur, C.; Pagnoulle, C.; Jerome, R.; Bocharova, V.; Kiriy, A.; Stamm, M. *Adv. Mater.* **2004**, *16*, 2123.
39. Lou, X.; Detrembleur, C.; Sciannamea, V.; Pagnoulle, C.; Jerome, R. *Polymer* **2004**, *45*, 6097.
40. Liu, Y.; Yao, Z.; Adronov, A. *Macromolecules* **2005**, *38*, 1172.
41. Homenick, C. M.; Sivasubramaniam, U.; Adronov, A. *Polym. Int.* **2008**, *57*, 1007.

Downloaded by PENNSYLVANIA STATE UNIV on June 1, 2012 | http://pubs.acs.org
Publication Date (Web): March 20, 2012 | doi: 10.1021/bk-2012-1100.ch015

Chapter 15

Investigation of Bis(acetylacetonato)iron(II) as a Moderator for the Radical Polymerization of Vinyl Acetate

Zhigang Xue[1,2] and Rinaldo Poli[*,1,3]

[1]CNRS, LCC (Laboratoire de Chimie de Coordination),
Université de Toulouse, UPS, INPT, 205, route de Narbonne,
F-31077 Toulouse, France
[2]Current address: Department of Chemistry and Chemical Engineering,
Huazhong University of Science and Technology, Wuhan 430074, China
[3]Institut Universitaire de France, 103, bd Saint-Michel, 75005 Paris, France
[*]E-mail: rinaldo.poli@lcc-toulouse.fr

The radical polymerization of vinyl acetate is moderated by $Fe(acac)_2$ by the organometallic route (OMRP) under both reversible termination (RT) and degenerative transfer (DT) conditions through the formation of thermally labile organometallic Fe_{III} dormant species. Control under OMRP conditions is improved by the presence of Lewis bases, especially PMe_2Ph. The controlling ability, however, is negatively affected by a slow radical trapping rate. Iron(II) phthalocyanine, on the other hand, inhibits completely the radical polymerization of vinyl acetate.

Introduction

Organometallic mediated radical polymerization (OMRP) (*1*, *2*) has become a tool in controlling the polymerization of less reactive monomers such as vinyl acetate (VAc). OMRP rests on the use of organometallic dormant species that can easily and reversibly generate the growing radical chain by homolytic cleavage of the metal-carbon bond. This may be possible either by direct dissociative bond breaking, as shown in Scheme 1, or by associative radical exchange (also known as degenerative transfer) if an independent radical source is available and if the metal coordination sphere allows it, Scheme 2. Hence, organometallic compounds are

In Progress in Controlled Radical Polymerization: Mechanisms and Techniques; Matyjaszewski, K., et al.;
ACS Symposium Series; American Chemical Society: Washington, DC, 2012.

Downloaded by PENNSYLVANIA STATE UNIV on June 1, 2012 | http://pubs.acs.org
Publication Date (Web): March 20, 2012 | doi: 10.1021/bk-2012-1100.ch015

of great relevance in controlled radical polymerization, provided that they contain sufficiently weak, thermally fragile metal-carbon bonds.

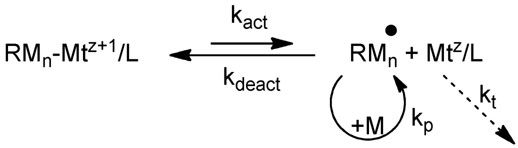

Scheme 1. OMRP mechanism by reversible termination (Mt = metal, L = ligand, M = monomer, R = initiating radical/chain end).

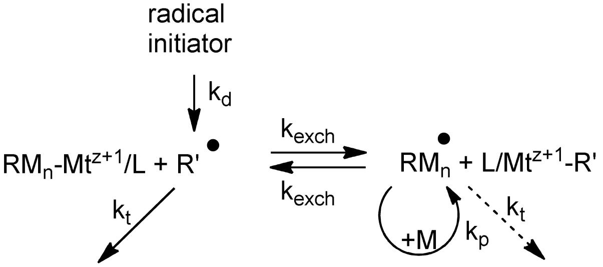
radical initiator
k_d
$RM_n\text{-}Mt^{z+1}/L + R'^{\bullet}$
k_t
k_{exch}
k_{exch}
$RM_n^{\bullet} + L/Mt^{z+1}\text{-}R'$
+M
k_p
k_t

Scheme 2. OMRP mechanism by associative radical exchange (degenerative transfer). Symbols as in Scheme 1.

The OMRP technique is still rather limited in terms of the choice of the transition metal, with only a handful of complexes having proven successful. The largest number of contributions makes use of cobalt complexes, after the first reports of the controlled polymerization of acrylates with porphyrin or glyoxime cobalt complexes by Wayland and Harwood (*3*, *4*) and a greater number of recent report for many monomers including vinyl acetate (*5*). Certain complexes of Ti (*6–9*), Mo (*10*), Cr (*11–13*), Os and V (*14*, *15*), have been successfully employed as OMRP trapping agents, but it would be of interest to develop controlling systems based on iron in light of its low cost and biocompatibility.

Iron-based complexes have attracted particular attention as catalysts in atom transfer radical polymerization (ATRP), the other major controlled polymerization strategy that makes use of transition metal complexes (*16–19*). Certain $FeCl_2$ complexes with dimine ligands have been invoked to reversibly trap polymer radical chains, but β-H elimination and atom transfer processes interplay and even dominate the radical polymerization process (*20–22*). Only one report appears to be available on the use of Fe within a pure OMRP approach, and only for the polymerization of styrene, using various macrocyclic Fe^{II} complexes in AIBN-initiated polymerization (*23*). Given the application value of iron in polymerization, further development of OMRP using iron complexes as trapping agents seems warranted, particularly for less reactive monomers such as VAc since methods to insure good control for the polymerization of this important monomer are still limited. Herein we report, for the first time, the iron-based organometallic mediated radical polymerization of VAc.

Downloaded by PENNSYLVANIA STATE UNIV on June 1, 2012 | http://pubs.acs.org
Publication Date (Web): March 20, 2012 | doi: 10.1021/bk-2012-1100.ch015

Experimental Section

Materials

Vinyl acetate (VAc, 99+%, Acros) was passed through a column filled with neutral alumina, dried over CaH_2, distilled under reduced pressure, and stored in a freezer under nitrogen. Pyridine (py, 99.5%, SDS) and triethylamine (TEA, 99%, Acros) were dried over CaH_2 and distilled under reduced pressure. Iron(II) acetylacetonate ($Fe(acac)_2$, 99.95%, Aldrich), 2,2′-azobis(4-methoxy-2,4-dimethylvaleronitrile) (V-70, Wako), and dimethylphenylphosphine (DMPP, 97%, Acros) were used without further purification.

Instrumentation

Size-exclusion chromatography (SEC) of PVAc was carried out in THF (flow rate: 1 mL min^{-1}) at 35°C on a 300 x 7.5 mm PL gel 5 micrometer mixed-D column, equipped with multiangle light scattering and refractive index detectors. ^1H (300 MHz) NMR spectra were recorded on a Bruker DPX-300 instrument.

Standard OMRP of VAc Initiated by V-70 in the Presence of $Fe(acac)_2$

A Schlenk flask (25 mL) was charged with $Fe(acac)_2$ (55 mg, 0.216 mmol) and the required excess amount of V-70. The flask was sealed with a rubber septum and was cycled three times between vacuum and nitrogen to remove oxygen. Degassed toluene (10 mL) (in solution polymerization), VAc (10 mL, 108.06 mmol) and the ligand (if applicable) were then added to the flask through degassed syringes. The solution was stirred for 20 min at room temperature. After three additional freeze-pump-thaw cycles, the flask was immersed in a thermostated oil bath at 30°C. At timed intervals, samples were withdrawn from the flask with a degassed syringe. The monomer conversion was determined gravimetrically after removal of the unconverted monomer under reduced pressure and the resulting residue was used for SEC characterization.

Results and Discussion

Vinyl Acetate Polymerization under Reversible Termination Conditions

As mentioned in the introduction, iron(II) phthalocyanine was shown to insure the controlled growth of polystyrene by OMRP through the reversible termination mechanism (*23*). We have tested the same system as a controlling agent for the polymerization of VAc initiated by V-70 [V-70 is the trade name of 2,2′-azobis(4-methoxy-2,4-dimethylvaleronitrile)], a thermal radical initiator with a half-life of 10 h at 30°C. The bulk polymerization, without additional ligands (30°C, [VAc]:[Fe]:[V-70] = 500:0.8:1) was completely inhibited. No conversion was observed even after raising the temperature to 60 °C. The same irreversible trapping behavior had previously been found for cobalt porphyrins in the polymerization of VAc, whereas the same compound controls

Downloaded by PENNSYLVANIA STATE UNIV on June 1, 2012 | http://pubs.acs.org
Publication Date (Web): March 20, 2012 | doi: 10.1021/bk-2012-1100.ch015

the polymerization of acrylates (*24*). According to DFT calculations, acrylate and styrene associated radicals form much weaker bonds, relative to the vinyl acetate associated radical, to halogen atoms (in the ATRP dormant species) (*25*), to dithiocarboxyl radicals (in the RAFT dormant species) (*26*) and to transition metal complexes, for instance systems based on Cr^{II} and Co^{II} (*11*, *27*). On the other hand, the PVAc radical chain was found to be reversibly released from dormant species based on the bis(acetylacetonate) system, PVAc-$Co(acac)_2(L)$ (L = Lewis base such as pyridine, DMF, DMSO, H_2O, …) (*28–30*). Hence, the oxygen-based coordination sphere on R-$Co^{III}(acac)_2$ appears to considerably weaken the Co^{III}-C bond compared to a nitrogen-based environment. For this reason, we considered it interesting to test the commercially available $Fe(acac)_2$ for the radical polymerization of VAc.

To probe the ability of Fe(acac)2 to trap and reversibly release the growing PVAc radical chains, initial polymerizations tests were run in bulk with a $[Fe(acac)_2]$:[V-70] ratio of 1:0.8 and a [VAc]:$[Fe(acac)_2]$ ratio of 500:1. The use of 0.8 equivalents of V-70, generating in principle 1.6 equivalents of primary radicals, effectively affords a nearly stoichiometric amount of initiating chains once the initiator efficiency factor is taken into account. The results are reported in Table 1. Without the iron complex, the polymerization was very fast at 30°C and yielded very high molecular weights and dispersities (Đ = M_w/M_n) (Table 1, entries 1 and 2). In the presence of $Fe(acac)_2$, an induction time was observed since no significant amount of polymer was found after 5 h (Table 1, entry 3), followed by a much slower polymerization relative to the iron-free conditions. This indicates radical trapping by $Fe(acac)_2$. The molecular weights of the resulting polymer are much higher than the values expected for a well controlled process, indicating that only a small fraction of the iron centers is operating as chain growth moderators. However, the resulting polymer had relatively low dispersities (Đ = 1.29-1.36) and the M_n increased more or less proportionally with the conversion. All these results are consistent with a controlled polymerization, although the controllability is far from ideal, when compared with that of reported for Co systems (*28*, *29*, *31–37*).

When carried out under more diluted conditions (50% v/v in toluene, see Table 1, entries 6-8), the polymerization was expectedly much slower, reaching only a 34% conversion in 312 h. The molecular weights were once again higher than the theoretical ones, but now much less so than from the bulk experiment, indicating improved efficiency of the $Fe(acac)_2$ trapping agent. Hence, a greater fraction of the iron centers appear to play a role in the moderation of chain growth in the more dilute solution. The possibility that chain transfer to the solvent might account for this molecular weight reduction seems excluded, because previous work has shown that a PVAc with M_n in perfect agreement with the theory is obtgained under the same conditions (30°C, 50% v/v in toluene) when controlled by a cobalt complex (*36*). This phenomenon may be related to solution equilibria involving the $Fe(acac)_2$ species. Indeed, it is known that this compound adopts a tetranuclear structure in solution (*38*), in equilibrium with less aggregated species that are favored at high dilution (*39*), see Scheme 3. This suggests that the polymer dormant chain has a small mixed-valent $Fe(acac)_2$ oligomer as chain end, PVAc-$[Fe(acac)_2]_x$ with only one Fe^{III} center and (x-1) Fe^{II} centers, the value of x being concentration dependent. Note that the polymer growth was sustained well beyond the time needed to generate new radicals (7 half-lives or approximately 70 h). This demonstrates the reversible release of the PVAc chains from the PVAc-[Fe(acac)$_2$]$_x$ dormant species, as expected for an OMRP mechanism.

Table 1. Radical Polymerization of VAc mediated by Fe(acac)$_2$[a]

entry	*Fe(acac)$_2$*	*Medium*	*time (h)*	*Conv (%)*[b]	$M_{n,th}$[c]	$M_{n,SEC}$	*Đ*
1	No	Bulk	5	48.5		168000	1.70
2	No	Bulk	7	78.2		178000	3.76
3	Yes	Bulk	5	0			
4	Yes	Bulk	14	10.1	4350	61600	1.31
5	Yes	Bulk	22	34.2	14720	152000	1.29
6	Yes	50%[d]	22	8.8	3790	26000	1.46
7	Yes	50%[d]	56	19.4	8340	29830	1.35
8	Yes	50%[d]	312	34.0	14600	34510	1.26

[a] Conditions: 30°C, [VAc]:[Fe(acac)$_2$]:[V-70] = 500:1:0.8. [b] From gravimetry. [c] $M_{n,th}$ = ([VAc]$_0$/[Fe(acac)$_2$]$_0$)M_{VAc} × Conv.(%); M_{VAc} is the molecular weight of the monomer, VAc. [d] 50% v/v in toluene.

Downloaded by PENNSYLVANIA STATE UNIV on June 1, 2012 | http://pubs.acs.org
Publication Date (Web): March 20, 2012 | doi: 10.1021/bk-2012-1100.ch015

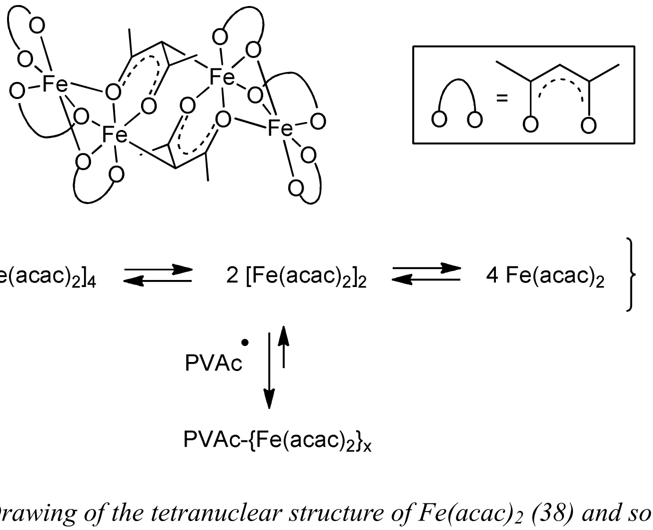

Scheme 3. Drawing of the tetranuclear structure of Fe(acac)$_2$ (38) and solution equilibria with less aggregated species (39).

Downloaded by PENNSYLVANIA STATE UNIV on June 1, 2012 | http://pubs.acs.org
Publication Date (Web): March 20, 2012 | doi: 10.1021/bk-2012-1100.ch015

It was shown for the Co(acac)$_2$-mediated VAc polymerization that the addition of coordinating ligands such as pyridine (py), triethylamine (TEA), and H_2O provided faster polymerizations relative to the ligand-free system (*5*, *28*, *30*), for which no reversible release of the growing PVAc radicals occurred (the controlled polymerization with ligand-free Co(acac)$_2$ only occurred by degenerative transfer polymerization) (*5*, *28*). The Fe/Co comparison shows that the (acac)$_2$Fe-PVAc bond is homolytically more fragile than the (acac)$_2$Co-VAc bond, since reversible release of the PVAc radical chains from the iron system occurs in the absence of ligands. We wondered, however, whether the controlling ability of the Fe(acac)$_2$ system could be modulated, as for the Co(acac)$_2$ system, by the addition of Lewis bases (L). An additional reason for using Lewis bases is that these are known to add to Fe(acac)$_2$ resulting in disaggregation and formation of mononuclear Fe(acac)$_2$(L)$_2$ species (*40*), hence perhaps helping to obtain molecular weights in better agreement with the theoretical values for a controlled process. More polymerization experiments were therefore carried out for VAc/Fe(acac)$_2$/V-70 in the presence of added ligands. The results, shown in Table 2, are again consistent with a certain degree of control for the polymerizations (low dispersities, M_n increasing with conversion in most cases).

In order to directly compare with the Co(acac)$_2$ system (*28*), the polymerizations in the presence of py, TEA, and H_2O were conducted with the same ligand excess, namely with [L]:[Fe(acac)$_2$] = 30. The polymerization rate in the presence of py was slightly slower, relative to the ligand-free conditions (*cf.* 34.2% conversion in 22 h without ligand, run 5 in Table 1, *vs.* 36% conversion in 39 h in the presence of py, run 2 in Table 2) and it was lower still in the presence of TEA (only 23.3% conversion in 209 h, run 6 in Table 2). The observed M_n values of these polymers were again greater than expected. The same behavior was observed in the presence of H_2O. Water was immiscible at the beginning of the reaction but then the mixture became clear and the polymerization proceeded at a rate comparable to the ligand-free system.

The polymerization was also tested in the presence of bis(diphenylphosphino)ethane (DPPE), and dimethylphenylphosphine, PMe_2Ph (DMPP). Since phosphine ligands and particularly chelating diphosphines should in principle bind metals more strongly, a P/Fe ratio of 2 was used in these cases (*i.e.* [DPPE]/[Fe(acac)$_2$] = 1:1 and [DMPP]/[Fe(acac)$_2$] = 2:1). A well-defined Fe(acac)$_2$(DPPE) complex has been described in the literature (*41*) and we have recently obtained the X-ray structure for this compound (*42*). Also in these cases, the polymerizations were slower than for the ligand-free system, the M_n were greater than the theoretical values but increased with conversion, and the dispersities were low. Note that the DMPP system gave a much lower rate of polymerization, a smaller discrepancy between observed and calculated molecular weight, and narrower dispersities (Đ = 1.16-1.21).

The effect of added Lewis bases on the polymerization rate is therefore opposite for Fe(acac)$_2$ than for Co(acac)$_2$, where the polymerization was accelerated by the presence of Lewis bases. The reason for the acceleration for the cobalt system is the greater stabilization of Co^{II}(acac)$_2$, by addition of two L molecules and formation of Co(acac)$_2$(L)$_2$, relative to the PVAc-Co^{III}(acac)$_2$ dormant species, which can also add one L ligand (but not two) to form

PVAcCo^{III}(acac)$_2$(L). For the Fe system, the results indicate that the Lewis base is able to stabilize the Fe^{III} dormant species comparatively better than Fe(acac)$_2$.

An additional experiment was run in the presence of a [DMPP]/[Fe(acac)$_2$] ratio of 1:1, while maintaining all other parameters unchanged (bulk, 30°C, [VAc]/[Fe(acac)$_2$] = 500 and [V-70]/[Fe(acac)$_2$] = 0.8). The results, shown in Figure 1, indicate that the monomer consumption follows the expected first order rate law, that the M_n values are greater than the calculated ones but now only by a factor of 2 at the highest conversions, that M_n grows more or less proportionally with conversion, and that the Đ values are rather low. Apparently, the DMPP ligand is not able to react quantitatively and desaggregate Fe(acac)$_2$. This is confirmed by a recent NMR study (*42*).

The size-exclusion chromatograms (SEC) of PVAc mediated by Fe(acac)$_2$ are shown in Figure 2. They confirm the monomodal distribution of the molecular weights throughout the polymerization, with only a small shoulder on the low molecular weights side, visible at low conversions, probably related to a small amount of termination processes at the beginning of the polymerization. Note that also in this case the polymerization was sustained well beyond the time needed to generate new radicals, confirming the reversible release of growing chains from the [(acac)$_2$Fe/DMPP]-PVAc dormant species according to an OMRP-RT mechanism.

Downloaded by PENNSYLVANIA STATE UNIV on June 1, 2012 | http://pubs.acs.org
Publication Date (Web): March 20, 2012 | doi: 10.1021/bk-2012-1100.ch015

Table 2. Bulk Polymerization of VAc in the presence of added ligands[a]

entry	*L*	*[L/Fe]*	*time (h)*	*Conv (%)*	$M_{n,th}$[b]	$M_{n,GPC}$[c]	*Đ*
1	py	30	17	14.0	6030	44010	1.16
2	py	30	39	36.0	15480	68280	1.33
3	py	30	116	58.6	25200	93910	1.33
4	TEA	30	20	6.6	2820	30500	1.16
5	TEA	30	112	18.8	8100	33050	1.22
6	TEA	30	209	23.3	10030	30960	1.25
7	H_2O	30	20	30.4	13050	120400	1.36
8	DPPE	1	17	13.1	5620	52030	1.29
9	DPPE	1	39	44.9	19340	99930	1.22
10	DMPP	2	17.5	7.1	3070	20860	1.17
11	DMPP	2	44.5	11.7	5030	25490	1.19
12	DMPP	2	374	34.3	14760	39710	1.21

[a] Conditions: 30°C; [VAc]:[Fe(acac)$_2$]:[V-70] = 500:1:0.8. [b] From gravimetry. [c] $M_{n,th}$ = ([VAc]$_0$/[Fe(acac)$_2$]$_0$)M_{VAc} × Conv.(%); M_{VAc} is the molecular weight of the monomer, VAc.

In Progress in Controlled Radical Polymerization: Mechanisms and Techniques; Matyjaszewski, K., et al.;
ACS Symposium Series; American Chemical Society: Washington, DC, 2012.

Downloaded by PENNSYLVANIA STATE UNIV on June 1, 2012 | http://pubs.acs.org
Publication Date (Web): March 20, 2012 | doi: 10.1021/bk-2012-1100.ch015

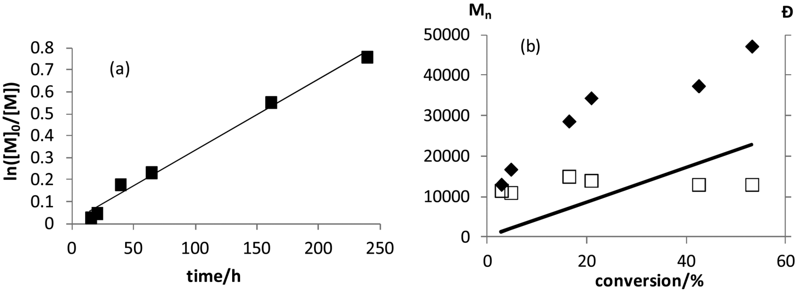

Figure 1. Bulk polymerization of VAc at 30°C controlled by Fe(acac)$_2$ in the presence of DMPP. [VAc]:[Fe(acac)$_2$]:[DMPP]:[V-70] = 500:1:1:0.8. (a) First order kinetics plot. (b) SEC-determined number-average molecular weight and polydispersity index as a function of monomer conversion. The solid line indicates the molecular weights calculated for one chain per Fe atom.

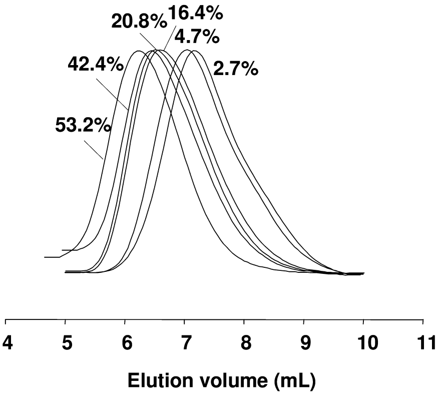

Figure 2. SEC chromatograms for PVAc from the OMRP mediated by Fe(acac)$_2$. Conditions are as shown in Figure 1.

Vinyl Acetate Polymerization under Degenerative Transfer Conditions

As already mentioned, the VAc polymerization mediated by Co(acac)$_2$ in the absence of Lewis bases and in the presence of an excess amount of radicals continuously injected from V-70 proceeds rapidly and in a controlled fashion by a degenerate transfer mechanism (Scheme 2). In other words, the (acac)$_2$Co-PVAc dormant species is able to associatively exchange radical chains very rapidly. It was of interest to verify whether a similar associative exchange may occur on (acac)$_2$Fe-PVAc, since the two complexes should be isostructural. A polymerization carried out in toluene (50% v/v) in the presence of 8 equivalents of V-70 was much faster relative to that with 0.8 equivalents of initiator under the same conditions (see Figure 3a).

Downloaded by PENNSYLVANIA STATE UNIV on June 1, 2012 | http://pubs.acs.org
Publication Date (Web): March 20, 2012 | doi: 10.1021/bk-2012-1100.ch015

Conversion reached 46.5% in 72 h, yielding PVAc with a molecular weight of 20000. In this case, the molecular weights matched quite well the theoretical ones, while the dispersities were not too high (Đ = 1.36-1.50). This observation suggests that the PVAc-$[Fe(acac)_2]_x$ dormant species are more readily broken down into mononuclear chain ends, PVAc-$Fe(acac)_2$, in the presence of a greater concentration of radicals, therefore generating one growing chain per Fe center. A mononuclear chain end is also presumably necessary in order to allow the associative radical exchange. Hence, the role of transfer agent in degenerate transfer polymerization seems confirmed for the dormant PVAc-$Fe(acac)_2$ species.

As shown in Figure 3, the conversion increased rapidly at the beginning of the polymerization and then slowed down after 72 h (ca. 7 half-lives) but continued at a reduced rate, indicating the installation of control by reversible termination, as described in the previous section. Interplay between associative and dissociative radical exchange processes has already been demonstrated for a few cobalt systems (*36*, *43*, *44*). The polymerization was also carried out at 40°C under the same conditions (50% v/v in toluene, [V-70]/[Fe] = 8:1), where the half-life of V-70 is about 200 min. Also in this case, there is a break in the polymerization kinetics plot, with a slowing down of the process after ca. 7 half-lives (ca. 25 h). In the OMRP-RT regime, the rate is first order in monomer and the rate constant is greater at the higher temperature, as expected. The measured molecular weights were in agreement with the theoretical values until the end of the degenerative transfer process, when excess radicals maintain the iron complex in the oxidation state III in the organometallic dormant state. Subsequently, in the reversible termination regime, the M_n values evolve less and eventually become smaller than the calculated ones, presumably because of the formation of additional polymer chains by catalyzed chain transfer reactions, since the inevitable terminations accumulate again $Fe(acac)_2$, which may act as a chain transfer catalyst. A similar behavior (M_n falling below the theoretical value in the OMRP regime) was previously observed for the polymerization of VAc mediated by a cobalt bis(diketonato) derivative (*36*).

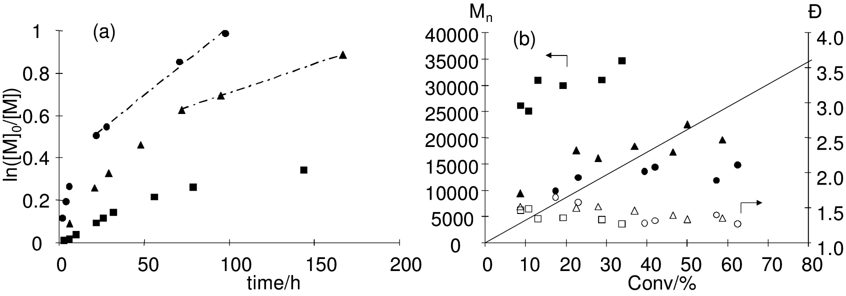

Figure 3. (a) Kinetic plots of ln($[M]_0$/[M]) vs time and (b) dependence of molecular weights, M_n (filled symbols), and molecular weight distributions, M_w/M_n (open symbols), on the monomer conversion for the OMRP of VAc with different ratios of V-70 to Fe in toluene (50% v/v). [VAc]:[$Fe(acac)_2$] = 500:1. ■: V-70/Fe = 0.8:1, 30 °C; ▲: V-70/Fe = 8:1, 30 °C; ●: V-70/Fe = 8:1, 40 °C.

Conclusions

In conclusion, we have demonstrated the ability of Fe(acac)$_2$ to moderate the radical polymerization of VAc, via both the reversible termination and the degenerative transfer mechanisms, with formation of an organometallic dormant species. It is the first report of a controlled polymerization of VAc using an iron complex, and the first report of a controlled radical polymerization by degenerative transfer polymerization with an iron complex for any monomer. In fact, we are not aware of any report where a degenerate transfer polymerization is clearly demonstrated for complexes of a metal other than cobalt as transfer agents. Addition of Lewis bases under reversible termination conditions has the effect of slowing down the polymerization process, indicating greater stabilization of the dormant PVAc-Fe^{III}(acac)$_2$ species relative to the trapping Fe$_{II}$(acac)$_2$ species by Lewis base coordination. The Lewis base, especially PMe$_2$Ph, slightly improves controllability (molecular weight and molecular weight distribution). While the principles of reversible termination and associative radical exchange have been established, the controlling ability of this system is however poor, compared with that of other systems and notably of Co(acac)$_2$/L (*30*). These results, however, are encouraging for further exploration of iron complexes as controlling systems within the OMRP approach.

Acknowledgments

We are grateful to the European Commission (project “METMED-CRP”, grant PIIF-GA-2009-235249), to the “Agence Nationale de la Recherche” (grant ANR-Blanc “OMRP”) and to the Centre National de la Recherche Scientifique for support of this work.

References

1. Poli, R. *Angew. Chem., Int. Ed.* **2006**, *45*, 5058.
2. Smith, K. M.; McNeil, W. S.; Abd-El-Aziz, A. S. *Macromol. Chem. Phys.* **2010**, *211*, 10.
3. Arvanatitopoulos, L. D.; Greuel, M. P.; Harwood, H. J. *Polym. Prep.* **1994**, *35*, 549.
4. Wayland, B. B.; Poszmik, G.; Mukerjee, S. *J. Am. Chem. Soc.* **1994**, *116*, 7943.
5. Debuigne, A.; Poli, R.; Jérôme, C.; Jérome, R.; Detrembleur, C. *Prog. Polym. Sci.* **2009**, *34*, 211.
6. Asandei, A. D.; Moran, I. W. *J. Am. Chem. Soc.* **2004**, *126*, 15932.
7. Asandei, A. D.; Moran, I. W. *J. Polym. Sci., Part A: Polym. Chem.* **2005**, *43*, 6039.
8. Asandei, A. D.; Moran, I. W. *J. Polym. Sci., Part A: Polym. Chem.* **2006**, *44*, 1060.
9. Asandei, A. D.; Saha, G. *J. Polym. Sci., Part A: Polym. Chem.* **2006**, *44*, 1106.
10. Le Grognec, E.; Claverie, J.; Poli, R. *J. Am. Chem. Soc.* **2001**, *123*, 9513.

Downloaded by PENNSYLVANIA STATE UNIV on June 1, 2012 | http://pubs.acs.org
Publication Date (Web): March 20, 2012 | doi: 10.1021/bk-2012-1100.ch015

11. Champouret, Y.; Baisch, U.; Poli, R.; Tang, L.; Conway, J. L.; Smith, K. M. *Angew. Chem., Int. Ed.* **2008**, *47*, 6069.
12. Champouret, Y.; MacLeod, K. C.; Baisch, U.; Patrick, B. O.; Smith, K. M.; Poli, R. *Organometallics* **2010**, *29*, 167.
13. Champouret, Y.; MacLeod, K. C.; Smith, K. M.; Poli, R. *Organometallics* **2010**, *29*, 3125.
14. Allan, L. E. N.; Cross, E. D.; Francis-Pranger, T. W.; Hanhan, M. E.; Jones, M. R.; Pearson, J. K.; Perry, M. R.; Storr, T.; Shaver, M. P. *Macromolecules* **2011**, *44*, 4072–4081.
15. Shaver, M. P.; Hanhan, M. E.; Jones, M. R. *Chem. Commun.* **2010**, *46*, 2127.
16. Kamigaito, M.; Ando, T.; Sawamoto, M. *Chem. Rev.* **2001**, *101*, 3689.
17. Ouchi, M.; Terashima, T.; Sawamoto, M. *Acc. Chem. Res.* **2008**, *41*, 1120.
18. Ouchi, M.; Terashima, T.; Sawamoto, M. *Chem. Rev.* **2009**, *109*, 4963.
19. di Lena, F.; Matyjaszewski, K. *Progr. Polym. Sci.* **2010**, *35*, 959.
20. Shaver, M. P.; Allan, L. E. N.; Rzepa, H. S.; Gibson, V. C. *Angew. Chem., Int. Ed. Eng.* **2006**, *45*, 1241.
21. Shaver, M. P.; Allan, L. E. N.; Gibson, V. C. *Organometallics* **2007**, *26*, 4725.
22. Allan, L. E. N.; Shaver, M. P.; White, A. J. P.; Gibson, V. C. *Inorg. Chem.* **2007**, *46*, 8963.
23. Kanagasabapathy, S.; Serero, D.; Silie, D.; Prost, S.; Ruiz-Guerrero, R.; Claverie, J. *Res. Discl.* **1998**, P1595.
24. Enikolopyan, N. S.; Smirnov, B. R.; Ponomarev, G. V.; Belgovskii, I. M. *J. Polym. Sci., Part A: Polym.* **1981**, *19*, 879.
25. Gillies, M. B.; Matyjaszewski, K.; Norrby, P.-O.; Pintauer, T.; Poli, R.; Richard, P. *Macromolecules* **2003**, *36*, 8551.
26. Matyjaszewski, K.; Poli, R. *Macromolecules* **2005**, *38*, 8093.
27. Debuigne, A.; Michaux, C.; Jérôme, C.; Jérôme, R.; Poli, R.; Detrembleur, C. *Chem. Eur. J.* **2008**, *14*, 7623.
28. Maria, S.; Kaneyoshi, H.; Matyjaszewski, K.; Poli, R. *Chem. Eur. J.* **2007**, *13*, 2480.
29. Debuigne, A.; Champouret, Y.; Jérôme, R.; Poli, R.; Detrembleur, C. *Chem. Eur. J.* **2008**, *14*, 4046.
30. Debuigne, A.; Poli, R.; Jérôme, R.; Jérôme, C.; Detrembleur, C. Key Role of Metal-Coordination in Cobalt-Mediated Radical Polymerization of Vinyl Acetate. In *Controlled/Living Radical Polymerization: Progress in RAFT, DT, NMP & OMRP*; Matyjaszewski, K., Ed.; ACS Symposium Series 1024; American Chemical Society: Washington, DC, 2009; pp 131−147.
31. Debuigne, A.; Caille, J. R.; Jérôme, R. *Angew. Chem., Int. Ed.* **2005**, *44*, 1101.
32. Debuigne, A.; Caille, J. R.; Detrembleur, C.; Jerome, R. *Angew. Chem., Int. Ed.* **2005**, *44*, 3439.
33. Kaneyoshi, H.; Matyjaszewski, K. *Macromolecules* **2005**, *38*, 8163.
34. Kaneyoshi, H.; Matyjaszewski, K. *Macromolecules* **2006**, *39*, 2757.
35. Peng, C. H.; Scricco, J.; Li, S.; Fryd, M.; Wayland, B. B. *Macromolecules* **2008**, *41*, 2368.
36. Santhosh Kumar, K. S.; Gnanou, Y.; Champouret, Y.; Daran, J.-C.; Poli, R. *Chem. Eur. J.* **2009**, *15*, 4874.

Downloaded by PENNSYLVANIA STATE UNIV on June 1, 2012 | http://pubs.acs.org
Publication Date (Web): March 20, 2012 | doi: 10.1021/bk-2012-1100.ch015

37. Santhosh Kumar, K. S.; Li, Y.; Gnanou, Y.; Baisch, U.; Champouret, Y.; Poli, R.; Robson, K. C. D.; McNeil, W. S. *Chem. Asian J.* **2009**, *4*, 1257.
38. Cotton, F. A.; Rice, G. W. *New J. Chem.* **1977**, *1*, 301.
39. Buckingham, D. A.; Gorges, R. C.; Henry, J. T. *Austr. J. Chem.* **1967**, *20*, 281.
40. Buckingham, D. A.; Gorges, R. C.; Henry, J. T. *Austr. J. Chem.* **1967**, *20*, 497.
41. Ittel, S. D. *Inorg. Chem.* **1977**, *16*, 1245.
42. Xue, Z.; Daran, J.-C.; Champouret, Y.; Poli, R. *Inorg. Chem.* **2011**, *50*, 11543–11551.
43. Wayland, B. B.; Peng, C.-H.; Fu, X.; Lu, Z.; Fryd, M. *Macromolecules* **2006**, *39*, 8219.
44. Peng, C.-H.; Fryd, M.; Wayland, B. B. *Macromolecules* **2007**, *40*, 6814.

Downloaded by PENNSYLVANIA STATE UNIV on June 1, 2012 | http://pubs.acs.org
Publication Date (Web): March 20, 2012 | doi: 10.1021/bk-2012-1100.ch015

Chapter 16

Some Recent Developments in RAFT Polymerization

**Graeme Moad,[*] Erika Bicciocchi, Ming Chen, John Chiefari,
Carlos Guerrero-Sanchez, Matthias Haeussler, Shadi Houshyar,
Daniel Keddie, Ezio Rizzardo, San H. Thang, and John Tsanaktsidis**

**CSIRO Materials Science and Engineering, Bag 10, Clayton South,
Victoria 3169, Australia
[*]E-mail: graeme.moad@csiro.au**

Downloaded by CORNELL UNIV on May 31, 2012 | http://pubs.acs.org
Publication Date (Web): March 20, 2012 | doi: 10.1021/bk-2012-1100.ch016

This paper reviews some recent developments in RAFT Polymerization at CSIRO. We report the successful use of switchable RAFT agents for controlling the polymerization of *N,N*-dimethylacrylamide in aqueous media and the dependence of RAFT agent activity on acid type and acid strength. For best results a stoichiometric amount of a strong acid should be used. We describe new RAFT agents (N-*aryl*-*N*-(4-pyridinyl) dithiocarbamates, aryl trithiocarbonates). We assess the for scope for RAFT single unit monomer insertion and describe its application in the synthesis of block copolymers containing organic semiconductor segments. Finally we briefly summarize methods of transforming RAFT synthesized polymers and disclose a potential click process based on successive 1,3-doplar addition steps for quantitatively transforming RAFT end groups.

Introduction

Control of radical polymerization with the addition of thiocarbonylthio compounds that serve as reversible addition fragmentation chain transfer (RAFT) agents was first reported in 1998 (*1*, *2*). Since that time substantial research carried out in these laboratories and elsewhere (*3–11*) has shown that RAFT polymerization is a reversible deactivation radical polymerization (RDRP) (*12*); an extremely versatile process that satisfies most of the established criteria

In Progress in Controlled Radical Polymerization: Mechanisms and Techniques; Matyjaszewski, K., et al.;
ACS Symposium Series; American Chemical Society: Washington, DC, 2012.

for a living polymerization (*13*, *14*). It can be applied to form homopolymers or copolymers from most monomers amenable to radical polymerization all with narrow or controlled molar mass distributions. Stars, blocks, microgel and hyperbranched structures, supramolecular assemblies and other complex architectures are accessible.

This paper will review recent developments in RAFT polymerization made in our laboratories. These developments include switchable RAFT agents (*15–17*) and their application in aqueous media (*18*), aryl trithiocarbonates (*19*), processes for single unit monomer insertion (*20*) and their application to the synthesis of block copolymers containing organic semiconductor segments (*21*) and a potential new click process for transforming RAFT end groups (*22*).

Downloaded by CORNELL UNIV on May 31, 2012 | http://pubs.acs.org
Publication Date (Web): March 20, 2012 | doi: 10.1021/bk-2012-1100.ch016

Switchable RAFT Agents

The polymerization of most monomers can be controlled by the RAFT process. However, the RAFT agent (ZC(=S)S-R) needs to be selected according to the monomer used (*23–25*). Explanation follows from a consideration mechanism of the reversible chain transfer step in RAFT polymerization (Scheme 1) and the properties of the propagating radicals.

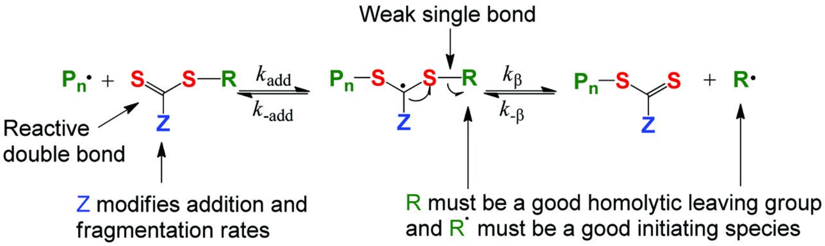
Weak single bond
$P_n^\bullet$ + S=C(Z)S—R
k_{add}
k_{-add}
P_n—S–C•(Z)–S—R
k_β
$k_{-\beta}$
P_n—S–C(Z)=S + R•
Reactive double bond
Z modifies addition and fragmentation rates
R must be a good homolytic leaving group and R• must be a good initiating species

Scheme 1. Mechanism for reversible addition-fragmentation chain transfer (RAFT) with thiocarbonylthio RAFT agents.

Monomers fall into two main classes. The 'more-activated' monomers (MAMs) are characterized by the monomer double bond being conjugated to an aromatic ring (e.g., styrene (St)), another double bond (e.g., butadiene) or a carbonyl group (e.g., methyl methacrylate (MMA), *N*-hydroxypropylmethacrylamide (HPMAm), *N,N*-dimethylacrylamide (DMAm)). The 'less activated' monomers (LAMs) often have an oxygen or nitrogen lone pair adjacent to the monomer double bond (e.g., vinyl acetate (VAc), *N*-vinylpyrrolidone (NVP), *N*-vinylcarbazole (NVC)). RAFT agents such as dithioesters (Z=aryl or alkyl) or trithiocarbonates (Z=alkylthio), suitable for controlling polymerization of (MAMs) inhibit or strongly retard polymerizations of LAMs. This can be largely attributed to the relatively poor homolytic leaving group ability of propagating radicals with a terminal LAM unit and side reactions that ensue from the consequent slow rates of fragmentation. On the other hand, RAFT agents suitable for controlling polymerizations of LAMs, such as

N,*N*-dialkyl- or *N*-alkyl-*N*-aryl dithiocarbamates and alkyl xanthates have a low reactivity towards propagating radicals with a terminal MAM unit and are ineffective in controlling polymerization of MAMs.

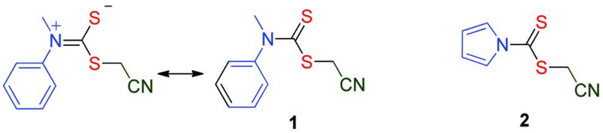

Scheme 2. Dithiocarbamate RAFT agents.

The low reactivity of dithiocarbamates and xanthates is attributed to the importance of the zwitterionic canonical structures which reduce the double bond character of the thiocarbonyl group (e.g., cyanomethyl methyl(phenyl)carbamodithioate (**1**); Scheme 2) (*23*, *26*). Dithiocarbamates where such delocalization is disfavored by the nitrogen lone pair being part of an aromatic ring system (e.g., cyanomethyl pyrrole-1-carbodithioate (**2**); Scheme 2) show activity similar to that of the dithioesters (*23*, *26*). The general guidelines for selection of Z (Figure 1) (*4*–*7*) indicate that the synthesis of polyMAM-*block*-polyLAM with low dispersity is not possible using the usual range RAFT agents.

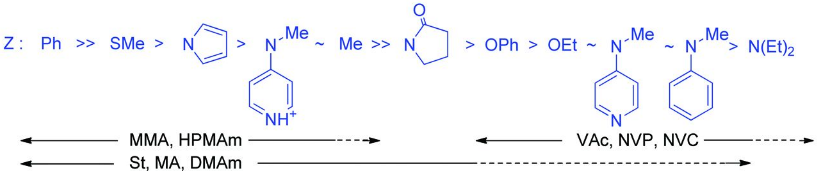

Figure 1. Guidelines for selection of 'Z' group of RAFT agents (Z-C(=S)S-R) in various polymerizations (4–7) Addition rates decrease and fragmentation rates increase from left to right. A dashed line indicates poor control.

We have recently introduced switchable RAFT agents. The *N*-(4-pyridinyl)-*N*-methyldithiocarbamates (**3**-**6**, Scheme 3) (*15*–*17*) provide excellent control over polymerization of LAMs. The properties of **3** as a RAFT agent are similar to those of **1**. Addition of an equivalent of a protic or Lewis acid, provides **3-H$^+$-6-H$^+$** which are effective in controlling the polymerization of more activated monomers MAMs. Importantly, these RAFT agents allow a convenient and direct synthesis of polyMAM-*block*-polyLAM with narrow molar mass distributions. The efficiency of the protonated dithiocarbamate in controlling the polymerization of MAMs suggests the importance of the canonical form in a positive charge is localized on the dithiocarbamate nitrogen. This hypothesis is supported by molecular orbital calculations (*17*). In recent work we have utilized high throughput methodology in determining the effect of the type and amount of acid on the efficiency of the process (*18*), provided a demonstration of switchable RAFT in aqueous media (*18*), and explored a wider range of switchable RAFT agents (*27*).

Downloaded by CORNELL UNIV on May 31, 2012 | http://pubs.acs.org
Publication Date (Web): March 20, 2012 | doi: 10.1021/bk-2012-1100.ch016

Downloaded by CORNELL UNIV on May 31, 2012 | http://pubs.acs.org
Publication Date (Web): March 20, 2012 | doi: 10.1021/bk-2012-1100.ch016

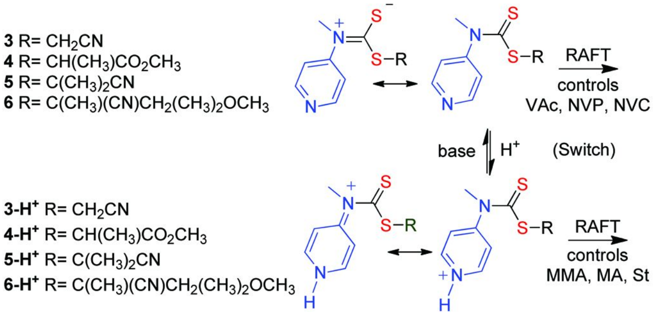
3 R= CH2CN
4 R= CH(CH3)CO2CH3
5 R= C(CH3)2CN
6 R= C(CH3)(CN)CH2(CH3)2OCH3
RAFT
controls
VAc, NVP, NVC
base
H+
(Switch)
3-H+ R= CH2CN
4-H+ R= CH(CH3)CO2CH3
5-H+ R= C(CH3)2CN
6-H+ R= C(CH3)(CN)CH2(CH3)2OCH3
RAFT
controls
MMA, MA, St

Scheme 3. Switchable N-methyl-N-(4-pyridinyl) dithiocarbamate RAFT Agents.

There has been recent emphasis on RAFT polymerization in aqueous media for a variety of reasons which include (*28*, *29*): (i) perceived environmental benefits, (ii) control over polymerization of monomers with cationic, anionic, zwitterionic and neutral polar groups which have limited solubility in organic media, (iii) the need to perform polymerization under physiological conditions. Thus, it was of significant interest to establish the effectiveness of switchable RAFT agents in aqueous media (*18*).

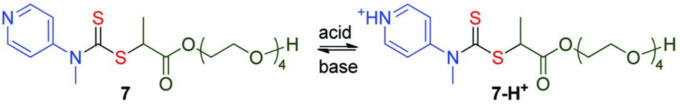
7
acid
base
7-H+

Scheme 4. Aqueous soluble switchable RAFT agent.

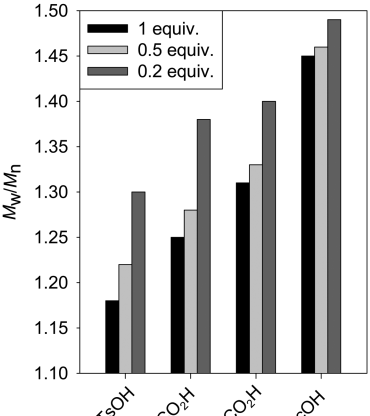

Figure 2. Dependence of dispersity (Đ=M_w/M_n) on the type and concentration of acid for high conversion polymerizations of DMAm. (figure reproduced from reference (18) © American Chemical Society).

Downloaded by CORNELL UNIV on May 31, 2012 | http://pubs.acs.org
Publication Date (Web): March 20, 2012 | doi: 10.1021/bk-2012-1100.ch016

We observed in our initial studies, for polymerizations in organic media, that the acid used to form the protonated RAFT agent should be a strong acid (e.g., 4-toluenesulfonic acid), and the acid should be added in a stoichiometric amount. The use of less than a stoichiometric amount of acid or of a weaker acid (e.g., acetic acid) provided poorer control (higher dispersities). A more quantitative study of the influence of acid type and concentration has been performed for polymerization of DMAm in water. Some results are shown in Figure 2 (*18*). The results have been rationalized in terms of the pK$_a$ of *N*-methyl-*N*-(4-pyridinium) dithiocarbamates (that for **7-H$^+$** in 20% dimethyl sulfoxide/water was determined as 3.13) (*18*). The polymerizations were performed with the tetraethyleneglycol macro-RAFT agent (**7**; Scheme 4) which provided enhanced water solubility for the initial RAFT agent in its neutral (unswitched) form.

While polymerizations of DMAm with **3-H$^+$**, **4-H$^+$** or **7-H$^+$** in aqueous medium were successful, polymerizations of LAM (specifically NVP) with **7** in water were problematical due to the inherent instability of the NVP-based macro RAFT agents in aqueous media (*30*, *31*) which was aggravated by even trace amounts of acid. The recent work of Destarac and coworkers suggests that this problem might be overcome with room temperature polymerization (*32*). Block copolymers were successfully prepared from the DMAm macro-RAFT agent in organic media (Figure 3) (*18*).

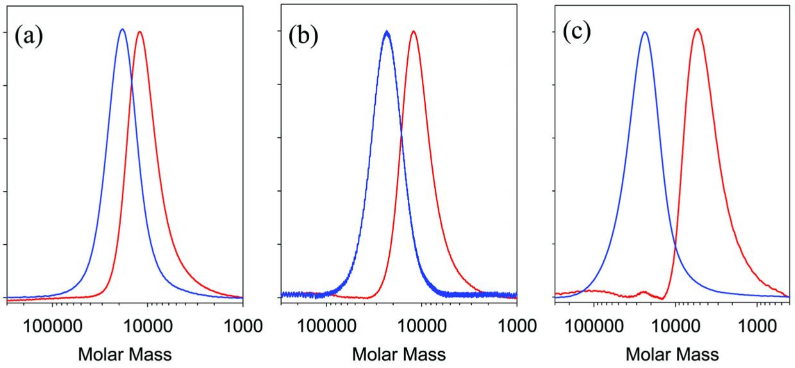

*Figure 3. Gel permeation chromatograms of (a) PDMAm **3-H$^+$** (M_n = 10000, Đ = 1.17) (—) and PDMAm-block-PNVC **3** (M_n = 16400, Đ = 1.13) (—), (b) PDMAm **3-H$^+$** (M_n = 10000, Đ = 1.17) (—) and PDMAm-block-PVAc **3** (M_n = 20100, Đ = 1.15) (—) and (c) PDMAm **3-H$^+$** (M_n = 3660, Đ = 1.27) (—) and PDMAm-block-PNVP **3** (M_n = 16000, Đ = 1.19) (—). (figure adapted from reference (18) © American Chemical Society).*

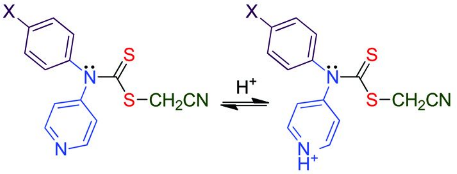

8

Scheme 5. Switchable N-aryl-N-(4-pyridinyl) dithiocarbamates.

N-Aryl-*N*-4-pyridinyl dithiocarbamates (**8**; Scheme 5, X=OCH_3, H, F, CN) have been evaluated in polymerizations of MA, NVC and VAc. These RAFT agents appear more effective (dispersities are lower) than the analogous *N*-methyl-*N*-(4-pyridinium) dithiocarbamates (**3**) with LAMs in the unswitched (neutral) form and more active with MAMs in the switched (protonated) form (*27*). Activity is enhanced by electron withdrawing 'X'. For example, C_{tr}^{app} for **8** in VAc polymerization increases from 42 with X=OCH_3 to >320 with X=CN.

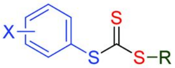
9

Scheme 6. Aryl trithiocarbonate RAFT agent.

Aryl trithiocarbonates (**9;** Scheme 6) have C_{tr}^{app} higher than those of analogous alkyl trithiocarbonates (*19*). The values of C_{tr}^{app} for the benzyl aryl trithiocarbonates (**9**, R=CH_2Ph; 0.029 M) in bulk styrene polymerization at 110 °C fall within the range 10-25 depending on the substituents on the aryl ring (X) and are higher than that of benzyl dodecyl trithiocarbonate for which C_{tr}^{app} was determined to be 8.9 (*19*). Benzyl 3,5-bis(trifluoromethyl)phenyl trithiocarbonate had highest C_{tr}^{app} amongst the series studied.

The *S*-(4-pyridinyl) *S*-benzyl trithiocarbonate (**10**) can be switched to become a more active RAFT agent (Scheme 7) (*19*). Both the unprotonated (**10**) and protonated form (**10-H**$^+$) are only effective with MAMs. Values of *Đ* for < 4 h reaction time in RAFT polymerizations of St at 70 °C with **10-H**$^+$ (trifluoroacetate) were significantly lower that with **10** though the polymerizations with **10-H**$^+$ were slightly retarded with respect to the similar polymerization with the **10**. Consistent with this observation, C_{tr}^{app} in St polymerization estimated on the basis of the residual RAFT agent for **10-H**$^+$ RAFT agent appeared ~25% higher (37 for **10-H**$^+$ *vs* 30 for **10**) (*19*).

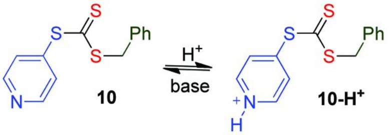

Scheme 7. Switchable S-(4-pyridinyl) S-benzyl trithiocarbonate.

Single Unit Monomer Insertion

Techniques for reversible-deactivation radical polymerization (RDRP) (*12*), such as RAFT, have provided a powerful toolkit, allowing unprecedented level of control over polymer structure. However, the precise control over molar mass and monomer sequence, as is achieved by nature in protein or polynucleotide biosynthesis, remains as a "Holy Grail" in the field of polymer synthesis (*33*). In this context we have recently undertaken a study of scope and limitations of RAFT single unit monomer insertion for synthesis of new macro-RAFT agents (Z-C(=S)S-$(M)_n$-R) by sequential insertion of multiple monomers (M) one-at-a-time into an initial (low molar mass) RAFT agent (Z-C(=S)S-R) (*20*, *21*).

Downloaded by CORNELL UNIV on May 31, 2012 | http://pubs.acs.org
Publication Date (Web): March 20, 2012 | doi: 10.1021/bk-2012-1100.ch016

Downloaded by CORNELL UNIV on May 31, 2012 | http://pubs.acs.org
Publication Date (Web): March 20, 2012 | doi: 10.1021/bk-2012-1100.ch016

McLeary, Klumperman and colleagues (*34–40*) observed that complete conversion of the initial RAFT agent to a species incorporating a single monomer unit is common to many well-behaved RAFT polymerizations (including those of styrene (*34*, *37*), methyl acrylate (MA) (*36*, *39*), *N*-vinylpyrollidone (*38*) and vinyl acetate (VAc) (*38*)) and that the time required for this step was correlated with a period of slow polymerization observed with those systems.

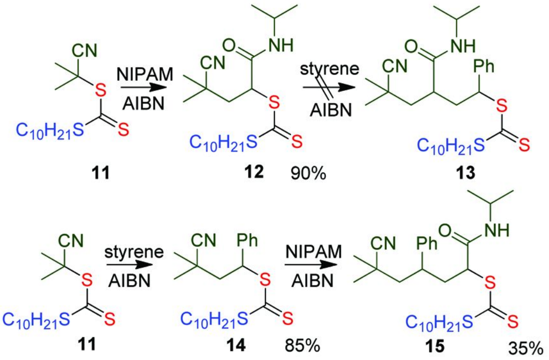

Scheme 8. Process for RAFT single unit monomer insertion.

The first examples of RAFT single unit monomer insertion were reported by Zard and coworkers who applied xanthate transfer chemistry to prepare “macro-RAFT agents” by selectively inserting a single unit of a less-activated monomer (LAM) into a xanthate RAFT agent (*41–46*). We previously established RAFT single unit monomer or macromonomer insertion process as a useful method of forming macro-RAFT agents (*47*, *48*) and have applied this in making block copolymers based on fully conjugated polymers (*vide infra*) (*21*). For the process to succeed, the transfer constant of the RAFT agent must be high – such that there is < 1 monomer addition per active cycle – and initiation by ‘R’ should be efficient and substantially more facile than subsequent propagation steps (*49*).

Single unit monomer insertion into cyanoisopropyl trithiocarbonates (e.g., **11**) proceeds in high yields for many MAMs (these include St (*20*), *N*-isopropylacrylamide (NIPAM) (*20*) and 2-vinylthiophene (*21*)). Our preferred reaction conditions involve use of a stoichiometric amount of monomer and RAFT agent and 10-20 mole% of azobis(isobutyronitrile) (AIBN) initiator. Attempted insertion of a second unit of the same monomer under similar reaction conditions invariably resulted in oligomerization.

Further experiments showed that insertion of a St into the NIPAM macro-RAFT agent **12** did not proceed and insertion of NIPAM into the St macro-RAFT agent **14** was selective but slow (Scheme 8) (*20*). With a two-fold excess of monomer over **14** and an extended reaction time, a 35% isolated yield of **15** was obtained. No oligomerization was detected.

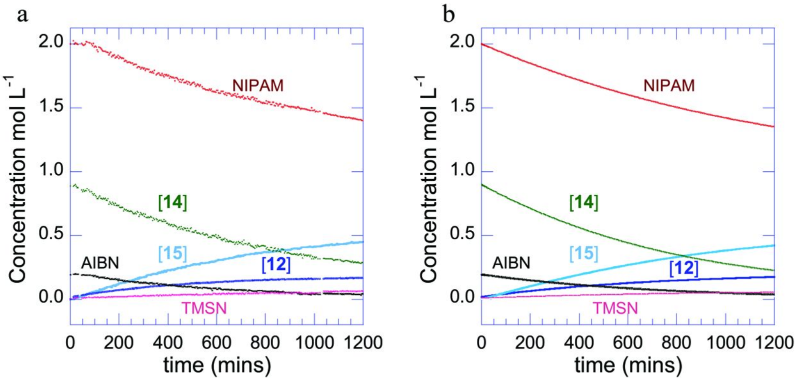

Figure 4. Concentration of species vs time observed during RAFT insertion of NIPAM (1.0 M) into styrene macro-RAFT agent ***14*** *(0.94 M) with AIBN (0.20 M) initiator at 66 °C; (a) experimental results; (b) results of kinetic simulation using Predici™. AIBN = azobisisobutyonitrile; TMSN = tetramethylsuccinonitrile; other species defined in Scheme 8. For rate constants used in simulation see ref. (20). (adapted from ref (20) © Royal Society of Chemistry).*

We attributed the low rates of reaction to the intermediate formed by addition of cyanoisopropyl radicals to the RAFT agent partitioning strongly in favor of starting materials (*20*). The cyanoisopropyl radical is a substantially better homolytic leaving group than radicals with a terminal St or NIPAM unit (*50*). For reaction to proceed we therefore require that the cyanoisopropyl radical first add NIPAM to provide a radical that is a poorer homolytic leaving group. This step necessarily leads to the NIPAM macro-RAFT agent **12** being formed as a by-product. It was possible to predict the yields of the various products by kinetic simulation using Predici™ (Figure 4) (*20*).

We conclude that multiple single unit insertion is possible. However, issues with respect to the formation initiator-derived by-products must be solved before the process becomes viable as a synthetic method. Possible solutions are currently being examined.

Block Copolymers Based on Organic Semiconductors

Fully conjugated polymers, such as those that see use in organic semiconductors, cannot be directly made by RAFT or other RDRP methods (e.g., atom transfer radical polymerizations (ATRP), nitroxide mediated polymerization (NMP)). Nonetheless, RDRP can be used to form materials which comprise segments of these polymers either as blocks or grafts. RDRP can also be used to form polymers which contain conjugated polymer segments as pendant units. We have recently reviewed the use of RAFT for the synthesis of optoelectronic polymers (*51*). One significant advantage of RAFT polymerization in the context of optoelectronic applications is that no undesirable metal species are introduced during the polymerization process (*51*).

Downloaded by CORNELL UNIV on May 31, 2012 | http://pubs.acs.org
Publication Date (Web): March 20, 2012 | doi: 10.1021/bk-2012-1100.ch016

Downloaded by CORNELL UNIV on May 31, 2012 | http://pubs.acs.org
Publication Date (Web): March 20, 2012 | doi: 10.1021/bk-2012-1100.ch016

There are three processes whereby a RAFT synthesized polymer can be combined with fully conjugated polymers to form block copolymers. The post polymerization “grafting to” strategy involves coupling of a RAFT-synthesized polymer to a semiconductor segment. The “grafting through” strategy involves RAFT (co)polymerization of a (macro)monomer with pendant semiconductor functionality. The “grafting from” strategy wherein macro-RAFT agents based on organic semiconductor or analogous oligomeric species are prepared by end-group modification of an organic semiconductor.

RAFT synthesized block copolymers based on poly(3-hexylthiophene) (P3HT) were reported by Iovu *et al.* (*52*) Yang *et al.* (*53*) and Palaniappan et al. (*54*) They prepared ‘Z’-connected blocks where the thiocarbonylthio functionality in the product is positioned at the block juncture. This means that the block will be lost on thiocarbonylthio group removal/transformation (refer Scheme 9). This is of significance since the presence of the thiocarbonylthio group has been shown to be detrimental to some optoelectronic applications (*48*, *55*, *56*).

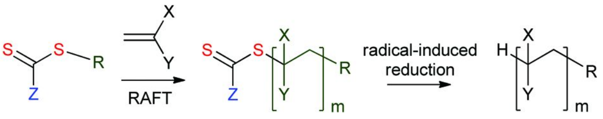

Scheme 9. Overall process for RAFT polymerization and thiocarbonylthio end group removal.

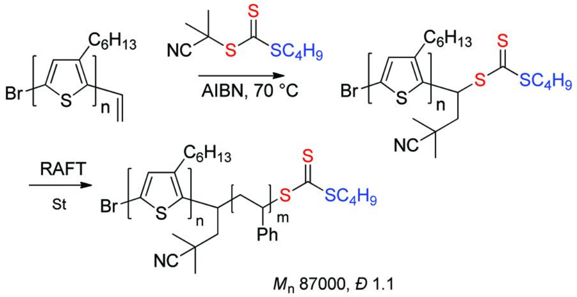

Scheme 10. Synthesis of poly(3-hexylthiophene) macro-RAFT agents and use to form poly(3-hexylthiophene)-block-polystyrene (21).

Downloaded by CORNELL UNIV on May 31, 2012 | http://pubs.acs.org
Publication Date (Web): March 20, 2012 | doi: 10.1021/bk-2012-1100.ch016

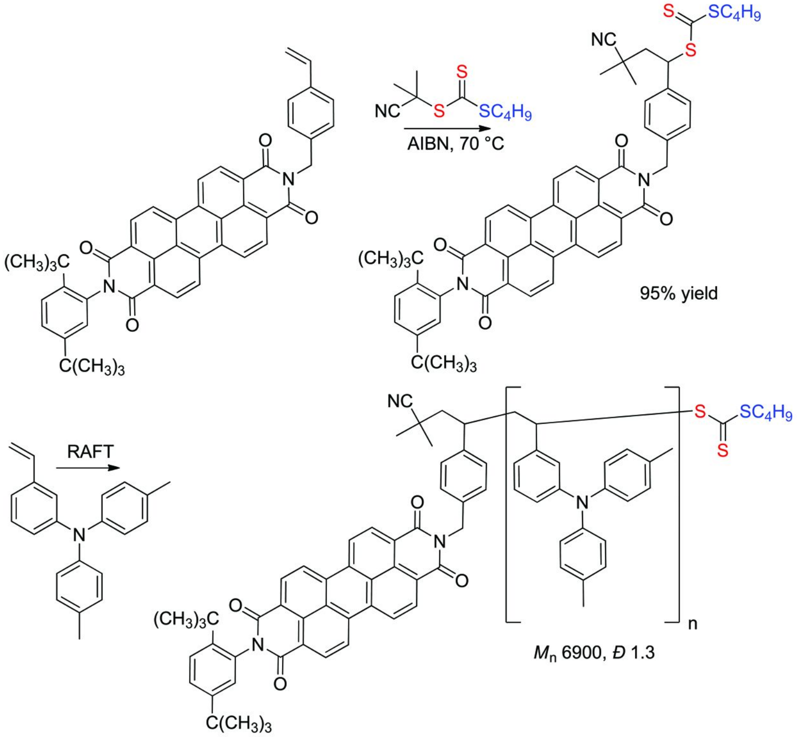

Scheme 11. Synthesis of perylene diimide macro-RAFT agents and use to form poly(triarylamine) block copolymer (21).

When ‘R’-connected macro-RAFT agent are used the thiocarbonyl thio functionality is retained at the chain end. Rajaram *et al.* (*57*) used this strategy to form a P3HT block copolymer. However, The RAFT agent possessed a relative long connecting chain between the polythiophene chain and the thiocarbonylthio group that included a potentially hydrolyzable amide linkage.

Transformation of a vinyl compound to a macro-RAFT agent by single unit macromonomer insertion provides a route to ‘R’-connected block copolymers with a very short block linkage that does not contain potentially hydrolyzable ester or amide groups. Thus, RAFT single unit monomer insertion was used to form macro-RAFT agents based on organic semiconductor segments, poly(3-hexylthiophene) and perylene diimide, as shown in Scheme 10 and Scheme 11 respectively (*21*). In the latter case, near quantitative (>95%) conversion of the precursor ‘macromonomer’ to the macro RAFT agent was achieved with appropriate choice of reaction conditions. The macro-RAFT agents were then used to synthesize block copolymers (*21*).

A New RAFT-Click Reaction?

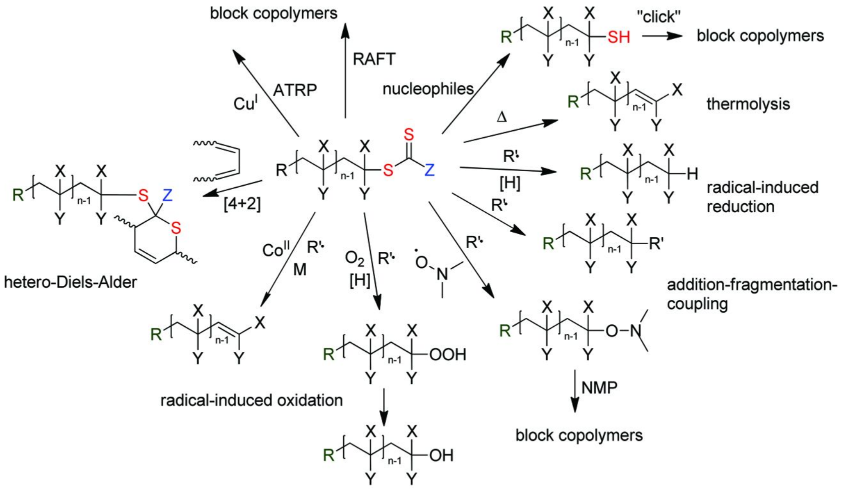
block copolymers
RAFT
ATRP
Cu^I
nucleophiles
"click"
block copolymers
SH
thermolysis
Δ
R'·
[H]
radical-induced reduction
R'·
addition-fragmentation-coupling
[4+2]
hetero-Diels-Alder
Co^{II}
R'·
M
O$_2$
R'·
[H]
radical-induced oxidation
OOH
OH
NMP
block copolymers
R
X
Y
S
Z
n-1

Scheme 12. Processes for RAFT end-group transformation (R'· = radical, [H] = hydrogen-atom donor, M = monomer, Co^{II} = square planar cobalt complex). Adapted from reference (9) © Society of Chemical Industry.

Many methods are now available for removing or transforming the thiocarbonylthio-groups in RAFT-synthesized polymers. All have advantages and limitations depending on the intended application. The thiocarbonyl functionality present in RAFT-synthesized polymers, once seen as a limitation to the wide-spread adoption of RAFT polymerization, is now seen as an enabling functionality in addressing the needs of the biomedical, optoelectronic, nanotechnology and other sectors. We have recently reviewed end-group transformation reactions and these are summarized in Scheme 12 (*9*).

Notable amongst these reactions in the present context is the hetero-Diels-Alder reaction in which thiocarbonyls of electron-deficient RAFT agents (or macro-RAFT agents) act as a dieneophile with suitable dienes (*58*, *59*). Suitable RAFT agents are those where 'Z' is pyridyl, phosphonate or phenylsulfonyl. To achieve acceptable rates the reaction is typically catalyzed by trifluoroacetic acid. The process has been developed as a route to block copolymers, star polymers, graft copolymers and modified surfaces.

We have found that diazomethane undergoes a facile 1,3-dipolar cycloaddition with dithiobenzoate RAFT agents and with dithiobenzoate end-groups of polymers formed by RAFT polymerization (*22*). Thus, 2-cyanoprop-2-yl dithiobenzoate on treatment with one equivalent of diazomethane at room temperature provided stereoisomeric 1,3-dithiolanes in very high (>95%) yield (Scheme 13) (*22*). No catalyst was used or required for essentially instantaneous reaction. Under similar conditions, the trithiocarbonate group (e.g., 2-cyano-2-propyl dodecyl trithiocarbonate) does not react with diazomethane.

Downloaded by CORNELL UNIV on May 31, 2012 | http://pubs.acs.org
Publication Date (Web): March 20, 2012 | doi: 10.1021/bk-2012-1100.ch016

Downloaded by CORNELL UNIV on May 31, 2012 | http://pubs.acs.org
Publication Date (Web): March 20, 2012 | doi: 10.1021/bk-2012-1100.ch016

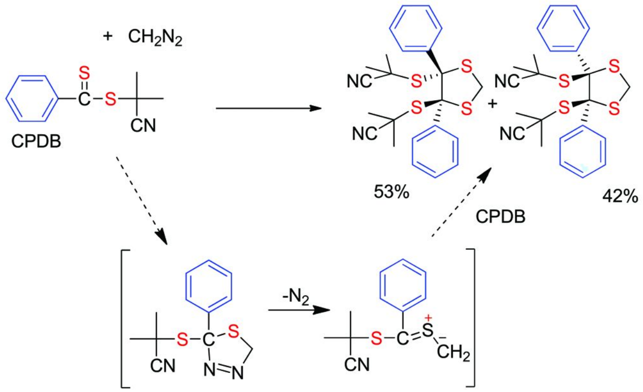

Scheme 13. Reaction of cyanoisopropyl dithiobenzoate with diazomethane (22).

A low molar mass RAFT-synthesized poly(methyl methacrylate) (PMMA) with dithiobenzoate end-groups undergoes similar reaction as indicated by immediate decolorization and a quantitative doubling of molar mass (Figure 5). Higher molar mass PMMA are also rapidly and completely decolorized by diazomethane but provided a product with a bimodal molar mass distribution. This is attributed to (a) the higher concentration of dead chains present in higher molar mass PMMA formed as a consequence of termination during RAFT polymerization, and (b) the unimolecular collapse of the intermediate ylide to a thiirane end group which becomes competitive with interpolymer 1,3-cycloaddition for, more slowly diffusing, higher molar mass chains.

Mloston *et al.* (*60*) have reported some time ago that the thiadiazole intermediates formed by reaction of phosphonodithioformates with diazomethane are stable at -65 °C and can be quantitatively converted to the ylide on warming to -35 °C. They also found that the ylide could be trapped by various dipolarophiles (*60*).

These observations suggest a potential new "click reaction" for end-functionalizing RAFT-synthesized polymers by sequential treatment of a polymer with diazomethane (or other diazo-compound) and a dipolarophile (A=B) (Scheme 14). When the dipolarophile is another macro-RAFT agent the product will be a block copolymer.

Before using term "click reaction" a strict set of criteria should be satisfied. The characteristics of "click" reactions are a) high yields with by-products (if any) that are simply removed by non-chromatographic processes, b) high regiospecificity and stereospecificity, c) insensitivity to oxygen and water, d) mild, solventless reaction conditions, e) orthogonality with other reactions, and f) amenability to a wide variety of readily available starting materials. A large number of recent reviews have focused on the combination of "click" chemistry and polymer chemistry (*61–67*). It is doubtful if many of the reactions mentioned in these reviews meet all of the criteria just mentioned. Barner-Kowollik et al. (*68*) have recently provided an interpretation of these criteria suitable for polymer chemists.

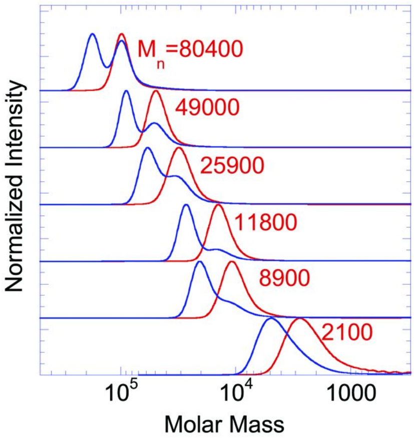

Figure 5. Molar mass distributions for RAFT-synthesized poly(methyl methacrylate) before (—) and after (---) treatment with diazomethane. Precursor molar masses were as indicated. Figure reproduced from ref. (22).

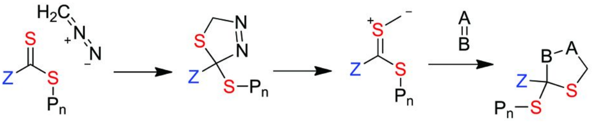

Scheme 14. A New RAFT-Click Reaction. A=B is a dipolarophile (22).

The present reaction under consideration satisfies criteria a – the reaction uses stoichiometric amounts of reagents and the yields are high (apparently quantitative) when at least of the reaction partners is of low molar mass – it fails b – the reaction produces a mixture of diastereomers – it satisfies c – there is no oxygen or water sensitivity – it fails d – the conditions are mild but a solvent is required – it satisfies e and f. Clearly it is too early to call the reaction a click process. Nonetheless there is potential which will be examined in proposed future work.

Conclusions

In this review, we have described new RAFT agents (switchable RAFT agents (*15–18*), aryl trithiocarbonates (*19*)). Switchable RAFT agents have been shown to be effective in aqueous media (*18*). We also discuss the scope and limitations of RAFT single unit monomer insertion (*20*). The process is very effective for inserting a single unit of monomer or macromonomer into an initial RAFT agent when it can provide very high yields (>90%) with appropriate choice of reaction conditions. The method has been applied to the synthesis of block copolymers containing organic semiconductor segments (*21*). However, issues with respect to the formation initiator-derived by-products must be solved before the process becomes viable as a synthetic method for sequential insertion of

Downloaded by CORNELL UNIV on May 31, 2012 | http://pubs.acs.org
Publication Date (Web): March 20, 2012 | doi: 10.1021/bk-2012-1100.ch016

multiple monomer units 'one-at-a-time' (*20*). We also reported a new process for transforming dithiobenzoate end groups which involves sequential treatment of the RAFT-synthesized polymer with a diazo-compound, such as diazomethane, and a dipolarophile (*22*). The reaction requires stoichiometric amounts of reagents and is rapid and quantitative.

References

1. Chiefari, J.; Chong, Y. K.; Ercole, F.; Krstina, J.; Jeffery, J.; Le, T. P. T.; Mayadunne, R. T. A.; Meijs, G. F.; Moad, C. L.; Moad, G.; Rizzardo, E.; Thang, S. H. *Macromolecules* **1998**, *31*, 5559–62.
2. Le, T. P.; Moad, G.; Rizzardo, E.; Thang, S. H. Polymerization with Living Characteristics. Patent WO9801478, 1998.
3. Moad, G.; Rizzardo, E.; Thang, S. H. *Polymer* **2008**, *49*, 1079–1131.
4. Moad, G.; Rizzardo, E.; Thang, S. H. *Acc. Chem. Res.* **2008**, *41*, 1133–1142.
5. Moad, G.; Rizzardo, E.; Thang, S. H. *Aust. J. Chem.* **2005**, *58*, 379–410.
6. Moad, G.; Rizzardo, E.; Thang, S. H. *Aust. J. Chem.* **2006**, *59*, 669–692.
7. Moad, G.; Rizzardo, E.; Thang, S. H. *Aust. J. Chem.* **2009**, *62*, 1402–1472.
8. Boyer, C.; Bulmus, V.; Davis, T. P.; Ladmiral, V.; Liu, J.; Perrier, S. *Chem. Rev.* **2009**, *109*, 5402–5436.
9. Moad, G.; Rizzardo, E.; Thang, S. H. *Polym. Int.* **2011**, *60*, 9–25.
10. Barner-Kowollik, C. *Handbook of RAFT Polymerization*; Wiley-VCH: Weinheim, Germany, 2008.
11. Boyer, C.; Stenzel, M. H.; Davis, T. P. *J. Polym. Sci., Part A: Polym. Chem.* **2011**, *49*, 551–595.
12. Jenkins, A. D.; Jones, R. I.; Moad, G. *Pure Appl. Chem.* **2010**, *82*, 483–491.
13. Darling, T. R.; Davis, T. P.; Fryd, M.; Gridnev, A. A.; Haddleton, D. M.; Ittel, S. D.; Matheson, R. R., Jr.; Moad, G.; Rizzardo, E. *J. Polym. Sci., Part A: Polym. Chem.* **2000**, *38*, 1706–1708.
14. Quirk, R. P.; Lee, B. *Polym. Int.* **1992**, *27*, 359–67.
15. Benaglia, M.; Chiefari, J.; Chong, Y. K.; Moad, G.; Rizzardo, E.; Thang, S. H. *J. Am. Chem. Soc.* **2009**, *131*, 6914–6915.
16. Benaglia, M.; Chen, M.; Chong, Y. K.; Moad, G.; Rizzardo, E.; Thang, S. H. *Macromolecules* **2009**, *42*, 9384–9386.
17. Moad, G.; Benaglia, M.; Chen, M.; Chiefari, J.; Chong, Y. K.; Keddie, D. J.; Rizzardo, E.; Thang, S. H. Block Copolymer Synthesis through the Use of Switchable RAFT Agents. In *Non-Conventional Functional Block Copolymers*; Theato, P., Kilbinger, A. F. M., Coughlin, E. B., Eds.; ACS Symposium Series 1066; American Chemical Society: Washington, DC, 2011; pp 81−102.
18. Keddie, D. J.; Guerrero-Sanchez, C.; Moad, G.; Rizzardo, E.; Thang, S. H. *Macromolecules* **2011**, *44*, 6738–6745.
19. Bicciocchi, E.; Chong, Y. K.; Giorgini, L.; Moad, G.; Rizzardo, E.; Thang, S. H. *Macromol. Chem. Phys.* **2010**, *211*, 529–538.
20. Houshyar, S.; Keddie, D.; Moad, G.; Mulder, R.; Saubern, S.; Tsanaktsidis, J. *Polym. Chem.* **2012**, DOI:10.1039/C2PY00529H.

Downloaded by CORNELL UNIV on May 31, 2012 | http://pubs.acs.org
Publication Date (Web): March 20, 2012 | doi: 10.1021/bk-2012-1100.ch016

21. Chen, M.; Haeussler, M.; Moad, G.; Rizzardo, E. *Org. Biomol. Chem.* **2011**, *9*, 6111–6119.
22. Chen, M.; Moad, G.; Rizzardo, E. *Aust. J. Chem.* **2011**, *64*, 433–437.
23. Chiefari, J.; Mayadunne, R. T. A.; Moad, C. L.; Moad, G.; Rizzardo, E.; Postma, A.; Skidmore, M. A.; Thang, S. H. *Macromolecules* **2003**, *36*, 2273–2283.
24. Moad, G.; Chiefari, J.; Krstina, J.; Postma, A.; Mayadunne, R. T. A.; Rizzardo, E.; Thang, S. H. *Polym. Int.* **2000**, *49*, 993–1001.
25. Moad, G.; Barner-Kowollik, C. The Mechanism and Kinetics of the RAFT Process: Overview, Rates, Stabilities, Side Reactions, Product Spectrum and Outstanding Challenges. In *Handbook of RAFT Polymerization*; Barner-Kowollik, C., Ed.; Wiley-VCH: Weinheim, Germany, 2008; pp 51−104.
26. Mayadunne, R. T. A.; Rizzardo, E.; Chiefari, J.; Chong, Y. K.; Moad, G.; Thang, S. H. *Macromolecules* **1999**, *32*, 6977–6980.
27. Keddie, D. J.; Guerrero-Sanchez, C.; Moad, G.; Mulder, R.; Rizzardo, E.; Thang, S. H. *Macromolecules* **2012**to be submitted.
28. Lowe, A. B.; McCormick, C. L. *Prog. Polym. Sci.* **2007**, *32*, 283–351.
29. Smith, A. E.; Xu, X.; McCormick, C. L. *Prog. Polym. Sci.* **2010**, *35*, 45–93.
30. Pound, G.; Eksteen, Z.; Pfukwa, R.; McKenzie, J. M.; Lange, R. F. M.; Klumperman, B. *J. Polym. Sci., Part A: Polym. Chem.* **2008**, *46*, 6575–6593.
31. Pound, G.; McKenzie, J. M.; Lange, R. F. M.; Klumperman, B. *Chem. Commun.* **2008**, 3193–3195.
32. Guinaudeau, A.; Mazieres, S.; Wilson, D. J.; Destarac, M. *Polym. Chem.* **2012**, *3*, 81–84.
33. Lutz, J.-F. *Polym. Chem.* **2010**, *1*, 55–62.
34. McLeary, J. B.; Calitz, F. M.; McKenzie, J. M.; Tonge, M. P.; Sanderson, R. D.; Klumperman, B. *Macromolecules* **2004**, *37*, 2383–2394.
35. McLeary, J. B.; Calitz, F. M.; McKenzie, J. M.; Tonge, M. P.; Sanderson, R. D.; Klumperman, B. *Macromolecules* **2005**, *38*, 3151–3161.
36. McLeary, J. B.; McKenzie, J. M.; Tonge, M. P.; Sanderson, R. D.; Klumperman, B. *Chem. Commun.* **2004**, 1950–1951.
37. McLeary, J. B.; Tonge, M. P.; Klumperman, B. *Macromol. Rapid. Commun.* **2006**, *27*, 1233–1240.
38. Pound, G.; McLeary, J. B.; McKenzie, J. M.; Lange, R. F. M.; Klumperman, B. *Macromolecules* **2006**, *39*, 7796–7797.
39. van den Dungen, E. T. A.; Matahwa, H.; McLeary, J. B.; Sanderson, R. D.; Klumperman, B. *J. Polym. Sci., Part A: Polym. Chem.* **2008**, *46*, 2500–2509.
40. van den Dungen, E. T. A.; Rinquest, J.; Pretorius, N. O.; McKenzie, J. M.; McLeary, J. B.; Sanderson, R. D.; Klumperman, B. *Aust. J. Chem.* **2006**, *59*, 742–748.
41. Zard, S. Z. *Angew. Chem., Int. Ed. Engl.* **1997**, *36*, 672–685.
42. Quiclet-Sire, B.; Zard, S. Z. *Top. Curr. Chem.* **2006**, *264*, 201–236.
43. Quiclet-Sire, B.; Zard, S. Z. *Chem. Eur. J.* **2006**, *12*, 6002–6016.
44. Quiclet-Sire, B.; Zard, S. Z. *Org. Lett.* **2008**, *10*, 3279–3282.
45. Lebreux, F.; Quiclet-Sire, B.; Zard, S. Z. *Org. Lett.* **2009**, *11*, 2844–2847.
46. Quiclet-Sire, B.; Revol, G.; Zard, S. Z. *Tetrahedron* **2010**, *66*, 6656–6666.

Downloaded by CORNELL UNIV on May 31, 2012 | http://pubs.acs.org
Publication Date (Web): March 20, 2012 | doi: 10.1021/bk-2012-1100.ch016

47. Chen, M.; Ghiggino, K. P.; Mau, A. W. H.; Rizzardo, E.; Sasse, W. H. F.; Thang, S. H.; Wilson, G. J. *Macromolecules* **2004**, *37*, 5479–5481.
48. Chen, M.; Ghiggino, K. P.; Rizzardo, E.; Thang, S. H.; Wilson, G. J. *Chem. Commun.* **2008**, 1112–1114.
49. Moad, G.; Chong, Y. K.; Mulder, R.; Rizzardo, E.; Thang, S. H. New Features of the Mechanism of RAFT Polymerization. In *Controlled/Living Radical Polymerization: Progress in RAFT, DT, NMP & OMRP*; Matyjaszewski, K., Ed.; ACS Symposium Series 1024; American Chemical Society: Washington, DC, 2009; pp 3−18.
50. Chen, M.; Moad, G.; Rizzardo, E. *J. Polym. Sci., Part A: Polym. Chem.* **2009**, *47*, 6704–6714.
51. Moad, G.; Chen, M.; Häussler, M.; Postma, A.; Rizzardo, E.; Thang, S. H. *Polym. Chem.* **2011**, *2*, 492–519.
52. Iovu, M. C.; Craley, C. R.; Jeffries-El, M.; Krankowski, A. B.; Zhang, R.; Kowalewski, T.; McCullough, R. D. *Macromolecules* **2007**, *40*, 4733–4735.
53. Yang, C.; Lee, J. K.; Heeger, A. J.; Wudl, F. *J. Mater. Chem.* **2009**, *19*, 5416–5423.
54. Palaniappan, K.; Hundt, N.; Sista, P.; Nguyen, H.; Hao, J.; Bhatt, M. P.; Han, Y.-Y.; Schmiedel, E. A.; Sheina, E. E.; Biewer, M. C.; Stefan, M. C. *J. Polym. Sci., Part A: Polym. Chem.* **2011**, *49*, 1802–1808.
55. Farinha, J. P. S.; Relogio, P.; Charreyre, M.-T.; Prazeres, T. J. V.; Martinho, J. M. G. *Macromolecules* **2007**, *40*, 4680–4690.
56. Kitchin, A. D.; Velate, S.; Chen, M.; Ghiggino, K. P.; Smith, T. A.; Steer, R. P. *Photochem. Photobiol. Sci.* **2007**, *6*, 853–856.
57. Rajaram, S.; Armstrong, P. B.; Kim, B. J.; Frechet, J. M. J. *Chem. Mater.* **2009**, 1775–1777.
58. Inglis, A. J.; Sinnwell, S.; Stenzel, M. H.; Barner-Kowollik, C. *Angew. Chem., Int. Ed. Engl.* **2009**, *48*, 2411–2414.
59. Sinnwell, S.; Inglis, A. J.; Davis, T. P.; Stenzel, M. H.; Barner-Kowollik, C. *Chem. Commun.* **2008**, 2052–2054.
60. Mloston, G.; Urbaniak, K.; Gulea, M.; Masson, S.; Linden, A.; Heimgartner, H. *Helv. Chim. Acta* **2005**, *88*, 2582–2592.
61. Evans, R. A. *Aust. J. Chem.* **2007**, *60*, 384–395.
62. Iha, R. K.; Wooley, K. L.; Nystrom, A. M.; Burke, D. J.; Kade, M. J.; Hawker, C. J. *Chem. Rev.* **2009**, *109*, 5620–5686.
63. Binder, W. H.; Sachsenhofer, R. *Macromol. Rapid. Commun.* **2007**, *28*, 15–54.
64. Binder, W. H.; Sachsenhofer, R. *Macromol. Rapid. Commun.* **2008**, *29*, 952–981.
65. Sumerlin, B. S.; Vogt, A. P. *Macromolecules* **2009**, *43*, 1–13.
66. Golas, P. L.; Matyjaszewski, K. *Chem. Soc. Rev.* **2010**, *39*, 1338–1354.
67. Kempe, K.; Krieg, A.; Becer, C. R.; Schubert, U. S. *Chem. Soc. Rev.* **2012**, *41*, 176–191.
68. Barner-Kowollik, C.; Du Prez, F. E.; Espeel, P.; Hawker, C. J.; Junkers, T.; Schlaad, H.; Van Camp, W. *Angew. Chem., Int. Ed. Engl.* **2011**, *50*, 60–62.

Downloaded by CORNELL UNIV on May 31, 2012 | http://pubs.acs.org
Publication Date (Web): March 20, 2012 | doi: 10.1021/bk-2012-1100.ch016

Chapter 17

Aqueous RAFT/MADIX Polymerization: Same Monomers, New Polymers?

Mathias Destarac,*,[1] Issam Blidi,[1] Olivier Coutelier,[1]
Aymeric Guinaudeau,[1] Stéphane Mazières,[1] Eric Van Gramberen,[2]
and James Wilson[2]

[1]Université Paul Sabatier, Laboratoire Hétérochimie Fondamentale
et Appliquée, UMR-CNRS 5069, Bât 2R1, 118 route de Narbonne,
31062 Toulouse cedex 9, France
[2]Rhodia Opérations, Centre de Recherches et Technologies d'Aubervilliers,
52 rue de la Haie Coq, 93308 Aubervilliers Cedex, France
***E-mail : destarac@chimie.ups-tlse.fr**

Downloaded by STANFORD UNIV GREEN LIBR on June 1, 2012 | http://pubs.acs.org
Publication Date (Web): March 20, 2012 | doi: 10.1021/bk-2012-1100.ch017

Thanks to their specific reactivity in RAFT/MADIX polymerization, *O*-ethyl xanthates are chain transfer agents of choice for controlling the polymerization of "less-activated" monomers (LAMs). In particular, hydrophilic LAMs can be polymerized in water by means of either water-soluble or hydrophobic xanthates in some appropriate conditions. Through the description of successful aqueous RAFT/MADIX polymerization of *N*-vinylpyrrolidone, diallydimethylammonium chloride and vinylphosphonic acid monomers, which strongly differ in their chemical nature and physicochemical properties of the resulting polymers, it is expected that various original water-soluble copolymers with complex architectures will be available in the future.

Introduction

Since the early nineties, the unceasing development of reversible-deactivation radical polymerization technologies (*1*) (RDRP) has been offering synthetic chemists the ability to design an nearly limitless range of more or less complex macromolecular architectures. Among them, double hydrophilic block copolymers (DHBCs) are widely studied water-soluble copolymers that

Downloaded by STANFORD UNIV GREEN LIBR on June 1, 2012 | http://pubs.acs.org
Publication Date (Web): March 20, 2012 | doi: 10.1021/bk-2012-1100.ch017

can combine blocks with distinct physicochemical properties, *e.g.* neutral and polyelectrolyte blocks (*2*). These materials can exhibit stimuli-responsive properties, *i.e.* they either undergo morphological transitions induced by an external stimulus like changes in temperature, solvent polarity, ionic strength, pH, or can lead to nanostructured aggregates with oppositely charged surfactants (*3*), polymers (*4*) or inorganic nanoparticles (*5*). Although all the RDRP strategies can potentially be used to synthesize DHBCs, RAFT/MADIX (*6*, *7*) is by far the most straightforward approach for controlling the polymerization of water-soluble monomers in aqueous media, thereby directly leading to a great variety of DHBCs in water (*8–10*). Whereas aqueous RAFT/MADIX solution polymerizations of many so-called “more-activated” monomers (MAMs) like hydrophilic (meth)acrylates, acrylamido and styrenic monomers have been widely reported in the literature (*8*), a very limited number of studies have dealt with “less-activated” monomers (LAMs) like diallyl (*10*) and vinyl monomers (*11*). As it is now well-established that *O*-ethyl xanthates are RAFT/MADIX agents of choice for controlling the polymerization of the main LAM monomers like vinyl acetate (*12*), *N*-vinylpyrrolidone (NVP) (*13*) and *N*-vinylcaprolactam (*14*) in organic media, we recently concentrated our efforts on their use for hydrophilic LAMs in aqueous solution. A first example consisted in the successful RAFT/MADIX polymerization of diallyldimethylammonium chloride (DADMAC) mediated by a *O*-ethyl xanthate-terminated low molar mass polyacrylamide (*10*). More recently, poly(*N*-vinylpyrrolidone) (PVP) of controlled M_n and low dispersities ($Đ = M_w/M_n$) was synthesized in water at room temperature with the Rhodixan A1 transfer agent, namely *O*-ethyl-*S*-(1-methoxycarbonyl)ethyldithiocarbonate (*11*). First promising results on RAFT/MADIX polymerization of vinyl phosphonic acid (VPA) in water mediated by a water-soluble carboxy-functional xanthate (*15*) encouraged us to further explore the strengths and limitations of this challenging system.

This work aims to illustrate the great potential of *O*-ethyl xanthates for polymerizing the aforementioned LAM monomers by RAFT/MADIX in water with unprecedented control. The numerous resulting opportunities for the access to novel DHBCs will be exemplified through the synthesis of PDADMAC-based diblock copolyampholytes.

Experimental

Unless otherwise stated, materials, experimental procedure and instrumentation are described in ref.10 for DADMAC, ref. 15 for VPA and ref. 11 for NVP.

Materials

2-[(ethoxythiocarbonyl)thio] propionic acid (X1) was prepared according to a procedure described elsewhere (*16*).

Synthesis of O-ethyl-S-(1-carboxy)methyl Dithiocarbonate (X2)

Ethylxanthic acid potassium salt (7.2 g, 44.92 mmol) was dissolved in 60 mL of ethanol in a 250 mL round-bottomed flask. The reaction mixture was stirred overnight with 2-bromoacetic acid (6.24 g, 44.90 mmol) at room temperature and then dissolved in CH_2Cl_2 and washed with H_2O. The organic phase was dried and evaporated to obtain the desired xanthate as a crystalline solid (4 g, 49.5%).

^{1}H-NMR ($CDCl_3$, 300.13 MHz): δ [ppm]: 1.36 (t, 3H, CH_3CH_2, $^3J_{HH}$ = 6.90 Hz), 3.91 (s, 2H, CH_2COOH), 4.60 (q, 2H, CH_3CH_2, $^3J_{HH}$ = 6.90 Hz), 10.35 (s, COOH). ^{13}C-NMR ($CDCl_3$, 75.48 MHz) δ [ppm]: 13.68 (CH_3CH_2), 37.61 (CH_2COOH), 70.92 (CH_3CH_2), 174.55 (CO), 211.97 (CS).

RAFT/MADIX Polymerization of VPA

A typical polymerisation procedure is as follows: X2 (31.9 mg, 0.177 mmol), VPA (500 mg, 4.62 mmol), AIBA (9.35 mg, 0.034 mmol) and distilled water (615 mL) were put together in a Schlenk flask. The solution was then degassed by gently bubbling argon for 15 mins. After that, the reaction mixture was heated at 65°C for 24 hours in a thermostated oil bath. 54.7% of VPA was converted into polymer at the end of the reaction as determined by ^{31}P NMR. $M_{n\,th}$=1640 g mol^{-1}, $M_{n\,NMR}$=1460 g mol^{-1}, $M_{n\,MALS}$=2270 g mol^{-1}, $Đ$=1.32.

Synthesis of VPA-X1 1:1 Adduct

X1 (719 mg, 3.7 mmol), VPA (200 mg, 1.85 mmol), AIBA (3.74 mg, 0.013 mmol) and distilled water (245 mL) were added to a Schlenk flask. The solution was then degassed by gently bubbling argon for 15 min. After that, the reaction mixture was heated at 65°C for 24 hours in a thermostated oil bath. The mixture was then purified by extraction of the residual amount of xanthate X1 with dichloromethane. The aqueous phase was then freeze-dried to remove water. The monoadduct was obtained as a mixture of diastereisomers (viscous oil, 280 mg, 51% yield).

^{1}H-NMR (D_2O, 300.13. MHz): δ (ppm) =1.05 (m, 3H, CH_3-CH), 1.35 (m, 3H, CH_3-CH_2O), 1.62, 1.98 and 2.28 (m, 2H, CH-CH_2-CH), 2.65 (m, 1H, CH-CO_2H), 4.01 (m, 1H, CH-PO$(OH)_2$), 4.55 (m, 2H, CH_3 CH_2-O).

^{31}P-NMR (D_2O, 121.50 MHz): δ (ppm) =19.5 (d).

Instrumentation

For PVPA samples, size exclusion chromatography (SEC) was performed on an Agilent 1100 HPLC system, a 18 angle Multi-Angle Light Scattering (MALS) DAWN-Heleos-II (Wyatt Technology), an OptilaRex Refractometer (Wyatt Technology) and a set of 2 columns (Shodex SB-806M and SB-802.5) thermostated at 30°C. Number-average molar masses ($M_{n\,MALS}$) and dispersities $Đ$ were determined with the SEC-RI-MALS line described above. Water (NaCl

Downloaded by STANFORD UNIV GREEN LIBR on June 1, 2012 | http://pubs.acs.org
Publication Date (Web): March 20, 2012 | doi: 10.1021/bk-2012-1100.ch017

100 mmol.L^{-1}, NaH_2PO_4 25 mmol.L^{-1}, Na_2HPO_4 25 mmol.L^{-1}, buffer solution at pH=7) was used as eluent with a flow rate of 1.0 mL.min^{-1}. PAA-PDADMAC copolymer samples were eluted through three SB 806 M HQ Shodex columns in a 1 M NH_4NO_3 solution of water/acetonitrile 80/20 wt.-% containing 10 ppm PDADMAC (flow rate: 1 mL.mn^{-1}) (*10*).

Results and Discussion

Vinylphosphonic Acid (VPA)

In contrast to most of the main classes of functional monomers, RDRP of phosphonic acid-containing monomers was surprisingly never reported in the academic literature. Instead, the polymerization of alkyl ester derivatives of phosphonic monomers was considered in few cases (*17*, *18*). Therefore, the possibility of directly synthesizing a poly(phosphonic acid) from an unprotected phosphonic monomer in water remains highly challenging and looks advantageous from both economic and environmental standpoints. In this respect, VPA (*19*) is a very attractive monomer because it is one of the few industrially available phosphonic monomer with a reasonable cost. Moreover, it polymerises under homogeneous aqueous conditions to yield watersoluble PVPA. It has been only recently that free-radical polymerization of VPA started to be studied in detail by several research groups (*20–22*). In this contribution, we aim to report RDRP of VPA by means of an aqueous RAFT/MADIX process mediated by the carboxy-functional *O*-ethyl-xanthate X2 and a *O*-ethyl xanthate/VPA 1/1 adduct (so-called monoadduct, Scheme1).

Downloaded by STANFORD UNIV GREEN LIBR on June 1, 2012 | http://pubs.acs.org
Publication Date (Web): March 20, 2012 | doi: 10.1021/bk-2012-1100.ch017

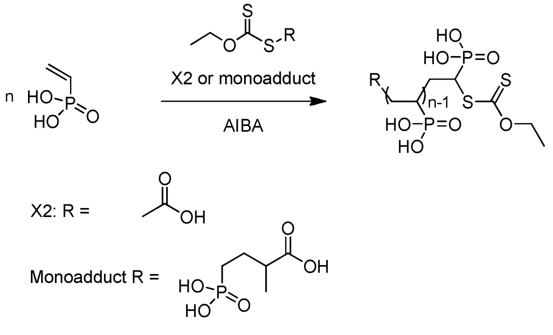

Scheme 1. Aqueous RAFT/MADIX polymerization of vinylphosphonic acid mediated by a carboxy-functional xanthate (X2 or monoadduct).

Experimental conditions were defined from free-radical polymerization of VPA at various temperatures and for different concentrations of AIBA initiator and VPA. A polymerization temperature of 65 °C with AIBA and VPA concentrations of 56 mmol.L^{-1} and 7.52 mol.L^{-1}, respectively, were found to be the best compromise to obtain both high VPA conversion (>80%) and sufficiently high molecular weight (M_n~9000 g.mol^{-1}, table 1, entry 1-4) for efficient RAFT/MADIX polymerization. Bearing in mind the low M_n values obtained for

Downloaded by STANFORD UNIV GREEN LIBR on June 1, 2012 | http://pubs.acs.org
Publication Date (Web): March 20, 2012 | doi: 10.1021/bk-2012-1100.ch017

xanthate-free experiments, we considered VPA polymerization in the presence of two different concentrations of xanthate X2, corresponding to theoretical M_n values of 1000 and 3000 g.mol^{-1} (Table 1, entry 5-14). ^{31}P NMR was found to be very useful to follow both conversion and polymer end-group. In fact, VPA has a characteristic chemical shift in deuterated water at 15.5 ppm and PVPA exhibits a broad signal in the range 29-32 ppm (Scheme 2). The characteristic signal of the VPA terminal unit next to the *O*-ethyl xanthate group has been identified by synthesising a xanthate:VPA monoadduct (Scheme 1) that mimics the PVPA-X2 chain end. A characteristic signal at 19.5 ppm can be observed (Scheme 2). In PVPA obtained in the presence of X2, a similar, but broader peak is visible at 19-20 ppm, which attests that X2 acts like a chain transfer agent during polymerization. Hence, VPA conversion and M_n of the xanthate-terminated chains ($M_{n\ \mathrm{NMR}}$) could be easily determined by simple mathematical expressions using relative peak integrations for monomer, polymer and VPA terminal unit.

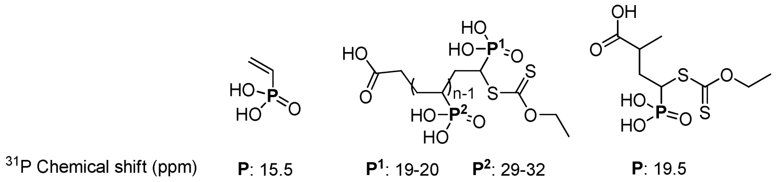

Scheme 2. VPA, PVPA-X2 and VPA/X1 monoadduct structures and corresponding chemical shifts in ^{31}P NMR. VPA conversion (%)=$(I_{P1}+I_{P2})/(I_{P1}+I_{P2}+I_{residual\ VPA})$ and $DP_{n\ NMR}=(I_{P1}+I_{P2})/I_{P1}$, with I_{P1}, I_{P2} and $I_{residual\ VPA}$ the integration of the corresponding phosphorous signals.

Compared to the xanthate-free VPA polymerization, polymerization in the presence of X2 is slowed down to a conversion of 49-60% after 24h (Table 1, entries 5-14). However, it can be clearly observed in Table 1 and on SEC-RI traces (Figure 1b) that X2 plays its role by regulating M_n. Assuming that all the chains are capped with the dithiocarbonate group, we could observe that $M_{n\ \mathrm{NMR}}$ values increase virtually linearly with VPA conversion for the two experiments in relatively good agreement with theoretical values (Figure 1a), except at low conversions (<20%) were $M_{n\ \mathrm{NMR}}$ are slightly higher than expected. This seems to indicate that the xanthate is quantitatively consumed relatively early in the reaction, after which its dithiocarbonate fragment caps the PVPA chain. The somewhat slow reaction of X2 could be explained by the relative difficulty for the carboxyethyl leaving group to fragmentate at first. The same trend in M_n evolution was observed when analysing PVPA by SEC-RI-MALS. For both targeted M_n of 1000 and 3000 g/mol, we also observed higher molecular weight than expected at early conversion followed by an evolution of M_n that increased with conversion.

Dispersity values were found to decrease with conversion as expected. In contrast to results obtained by ^{31}P NMR when X2 has fully reacted, $M_{n\ MALS}$ is systematically higher than expected by a 2-3 fold factor (Table 1). We attribute this difference to the errors of the MALS analysis in this low molecular weight range. This difference could as well indicate a slow reversible transfer during the polymerization, leading to higher molecular weight polymers than targeted.

Downloaded by STANFORD UNIV GREEN LIBR on June 1, 2012 | http://pubs.acs.org
Publication Date (Web): March 20, 2012 | doi: 10.1021/bk-2012-1100.ch017

Table 1. Aqueous RAFT/MADIX polymerization of VPA at different concentrations of xanthates (X2 or VPA-X1). $[VPA]_0$=7.52 mol.L^{-1}, $[AIBA]_0$=56 mmol.L^{-1}, T=65°C

Entries	*[Xanthate] (mmol.L^{-1})*	*t (h)*	*Conv^a (%)*	*$M_{n\ th}$^{b} (g.mol^{-1})*	*$M_{n\ NMR}$^{c} (g.mol^{-1})*	*$M_{n\ MALS}$^{d} (g.mol^{-1})*	*Đ*
1	0	1	35.5	--	--	11800	1.64
2		4	75.4	--	--	14170	1.65
3		8	84.1	--	--	9440	1.86
4		24	84.5	--	--	8980	1.85
5	[X2] 990	1	10.3	260	470	--	--
6		2	20.0	340	540	2170	1.13
7		4	34.3	460	600	1360	1.40
8		8	46.5	650	690	1650	1.34
9		24	48.8	680	710	1720	1.33
10	[X2] 288	1	20.2	750	830	3650	1.67
11		2	29.3	1010	990	2280	1.58
12		4	38.0	1250	1150	2080	1.51
13		8	48.2	1540	1430	2260	1.31
14		24	54.8	1640	1460	2270	1.32
15	[VPA-X1] 1066	1	28.5	480	480	1300	1.38
16		2	36.1	580	580	1510	1.45
17		4	47.6	660	750	1600	1.31
18		8	55.1	720	860	1670	1.33
19	[VPA-X1] 275	1	21.8	950	1130	1970	2.16
20		2	35.5	1350	1570	2020	1.55
21		4	49.6	1770	1840	2180	1.55
22		8	56.9	1980	2330	2420	1.47
23		24	61.4	2120	2000	2500	1.45

[a] determined by ^{31}P NMR. [b] $M_{n\ th}$=($[VPA]_0$/$[xanthate]_0$))*Conv*M(VPA)+ M(xanthate). [c] determined by ^{31}P NMR. [d] measured by SEC-RI-MALS.

Downloaded by STANFORD UNIV GREEN LIBR on June 1, 2012 | http://pubs.acs.org
Publication Date (Web): March 20, 2012 | doi: 10.1021/bk-2012-1100.ch017

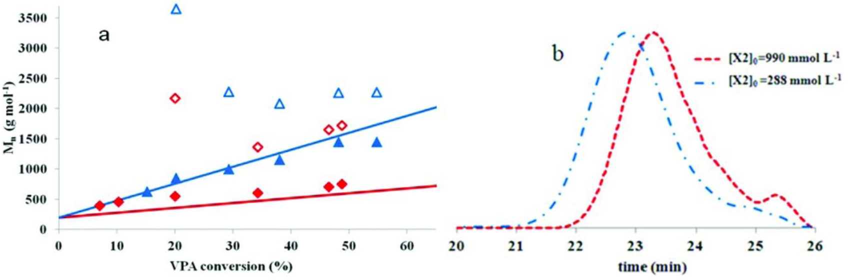

Figure 1. (a)Evolution of $M_{n\ NMR}$ and $M_{n\ MALS}$ during RAFT/MADIX polymerization of VPA in water at different initial concentrations of X2. Conditions of Table 1. Full lines represent the theoretical evolution of M_n for a controlled RAFT/MADIX polymerization. $M_{n\ th}$=1000 g.mol^{-1} (diamonds) and 3000 g.mol^{-1} (triangles). Filled symbols correspond to $M_{n\ NMR}$ and open symbols to $M_{n\ MALS}$ (b) SEC-RI chromatograms of the corresponding PVPAs after 24h reaction.

To ensure that the polymer chains grow according to a reversible transfer process, and that the dithiocarbonate fragment capped on a VPA unit could be reactivated, the 1/1 xanthate/VPA monoadduct VPA-X1 was tested in polymerization. It is worth mentioning that a slightly different xanthate was used in the synthesis process in order to overcome the slow fragmentation process of X2. When using VPA-X1 to target PVPA with M_n of 1000 and 3000 g mol^{-1}, we observed that the xanthate end group could be reactivated leading to the formation of end-capped PVPA. Indeed, following the evolution of VPA-X1 by ^{31}P NMR, we could observe a slow consumption of the monoadduct (sharp doublet at 19.5 ppm) into the corresponding xanthate end-capped PVPA (broad signal in the range 19-20 ppm) confirming the reactivation process of the xanthate end-group (Figures 2 and 3). $M_{n\ MALS}$ of the corresponding PVPAs were found to be higher than both $M_{n\ th}$ and $M_{n\ NMR}$, which confirmed the results obtained with X2 and was explained by a slow reversible chain transfer process between dormant and active PVPA chains.

In summary, RAFT/MADIX polymerization of VPA was successfully performed in pure water at 65°C with the AIBA initiatior in the presence of water-soluble carboxy-functional xanthates X2 and VPA/X1. It was demonstrated that the starting xanthate fully reacts with VPA oligoradicals to yield low molar mass xanthate-capped PVPAs. By using a model xanthate for mimicing the PVPA macro-chain transfer agent, NMR studies and SEC-RI-MALS analysis confirmed that the xanthate terminal group could be slowly and reversibly transferred, leading to an increase of M_n during polymerization.

Downloaded by STANFORD UNIV GREEN LIBR on June 1, 2012 | http://pubs.acs.org
Publication Date (Web): March 20, 2012 | doi: 10.1021/bk-2012-1100.ch017

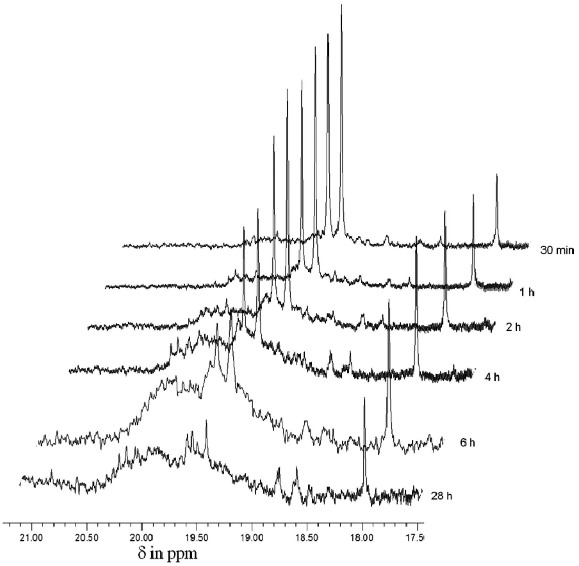

Figure 2. Evolution of ^{31}P NMR spectrum with time in the range 17.5-22 ppm during the RAFT/MADIX polymerization of VPA in water with initial concentration of [VPA-X1] = 1066 mmol.L^{-1}(sharp signal at 18 ppm corresponds to monomer impurity).

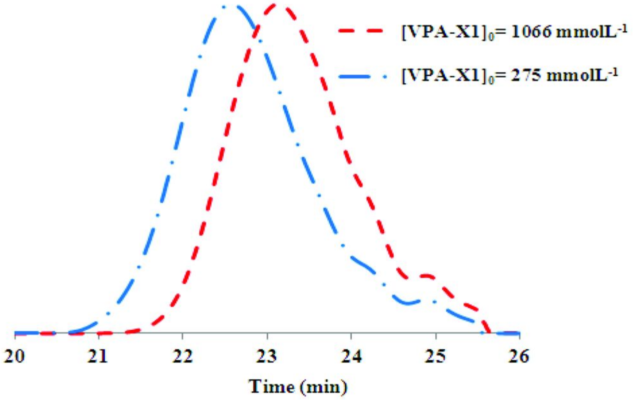

Figure 3. SEC-RI chromatograms of VPA in water at different initial concentrations of VPA-X1, targeting $M_{n\ th}$=1000 g mol^{-1},and 3000 g mol^{-1} after 24h reaction.

N-Vinylpyrrolidone (NVP)

In recent years, *O*-ethyl xanthates were by far the most employed chain transfer agents for RAFT/MADIX polymerization of NVP due to their high efficiency in controlling both molecular weights and and narrow molecular weight distributions of PVPs up to high conversions (*13*, *23*, *24*). However, it has been reported that NVP monomer undergoes side reactions in the presence of acid-functional xanthates, water and impurities (*13*). It was also demonstrated that the *O*-ethyl xanthate group at the end of PVP chains is thermally unstable and can lead to sulfur-free unsaturated chain ends during the polymerisation (*23*). Therefore, it was suggested to work at moderated temperatures (<60°C) and to avoid water as a polymerisation medium which strongly limited the development of RDRP of NVP, a widespread industrial water-soluble monomer (*13*). These numerous drawbacks could be recently avoided by polymerizing NVP at ambient temperature in water in the presence of Rhodixan A1 and using the t-butyl hydroperoxyde (tBuOOH) / ascorbic acid (Asc Ac) redox initiating system (Scheme 3).

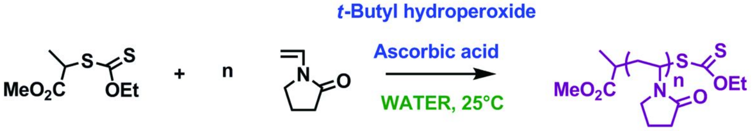

Scheme 3. Synthetic scheme for redox-initiated RAFT/MADIX polymerization of NVP in water at ambient temperature.

In order to identify efficient redox couples, a systematic study was carried out on many oxidant/reducing agent pairs likely to initiate aqueous NVP polymerisation at 25°C (Table 2). Redox couples 1-3 of Table 2 did not give any reaction, systems 4-8 yielded by-products and did not initiate polymerization of NVP and initiators 9 and 10 gave PVP. From these results, it was established that several conditions must be fulfilled in order to initiate NVP polymerization in an efficient manner; firstly, the difference between the oxidizing and reducing potentials of respectively oxidant and reducing agents must be great enough to generate radicals at a sufficient rate. Then, the oxidizing agent potential should be low enough in order to prevent the direct oxidation of NVP. Importantly, as side reactions between NVP and water are catalyzed in acidic media, it is crucial to maintain a sufficiently high pH and to avoid the presence of strong acids in the redox couple. In a similar fashion that benzoyl peroxide (entries 1,2), persulfate ions (entries 4-5) are known to generate side reactions with NVP. In the presence of a reducing agent, $SO_4^{\cdot -}$ radicals are produced at room temperature and react with water to yield acidic protons among other species. This acidity catalyses hydrolysis and coupling reaction of NVP (*13*). The corresponding by-products have been observed and perfectly characterized by ^{1}H NMR. Entries 6, 7 and 8 failed mainly because either the oxidant or the reducing agent -or both- are too acidic. The H_2O_2/ascorbic acid couple (entry 9) appeared to be ineffective

Downloaded by STANFORD UNIV GREEN LIBR on June 1, 2012 | http://pubs.acs.org
Publication Date (Web): March 20, 2012 | doi: 10.1021/bk-2012-1100.ch017

and allowed very limited conversion (x<0.1). High concentrations of ascorbic acid were needed to increase NVP conversion, which concomitantly led to the formation of a significant amount of NVP hydrolysis product. Finally, the couple *t*-BuOOH/ Asc Ac turned out to be the most efficient initiator and allowed the formation of PVP with high conversion after 24 h without side reactions.

Table 2. Radical polymerization of NVP with various redox couples. T = 25°C, $[NVP]_0$ = 6,2 mol.L^{-1}, $[oxidant]_0$ = $[reducing\ agent]_0$ = 1,2.10^{-1} mol.L^{-1}, t_r = 24 hours

Entry	*Redox couple*	*E⁰ (eV)*	*pKa*	*Ref.*
1	BPO / DMA	0.4/-0.9	n.a	
2	BPO / DMPT	0.4/NA	n.a	(*25*)
3	$KBrO_3$ / $Na_2S_2O_3$	1.5/0.1	0.7/7	
4	$Na_2S_2O_8$ / $Na_2S_2O_3$	2.1/0.1	Weak acid /7	(*26*)
5	$(NH_4)_2S_2O_8$ / $HOCH_2SO_3Na$	2.1/NA	Weak acid/n.a	(*26*)
6	PMS / Glycolic acid	2.1/-0.1	0.2/3.8	(*27*)
7	$KHSO_5$	2.1	0.2	
8	*t*-BuOOH / Glycolic acid	1.5/-0.1	Weak acid /3.8	
9	H_2O2 / Ascorbic acid	1.8/-0.3	Weak acid /4.1	(*28*)
10	*t*-BuOOH / Ascorbic acid	1.5/-0.3	Weak acid /4.1	

Benzoyl peroxide (BPO); N,N-Dimethylaniline (DMA); N,N-Dimethyl paratoluidine (DMPT); Tert-butyl hydroperoxide (t-BuOOH); Peroxymonosulfate ($KHSO_5$. n.a: not available.

RAFT/MADIX polymerization was conducted at an initial NVP concentration of 6.2 mol.L^{-1} (66 wt.%). Under these conditions at pH=6.5, Rhodixan A1 at a concentration of 3.8 g.mol^{-1} (i.e. $M_{n\ th}$=18300 g.mol^{-1}) was soluble in the aqueous NVP solution (*11*). M_n values measured by SEC in DMF/LiCl using PMMA standards (Figure 3a) increased linearly with conversion and are in good agreement with the theoretical values even at low conversions. Dispersity values are very low (1.15<Đ<1.30, Figure 3b) and in the same range as those for RAFT/MADIX polymerisation of NVP in bulk or organic media. The ^{1}H NMR spectroscopy of the PVP confirmed not only the microstructure and the presence of the xanthate moiety at the polymer ends, but also the absence of the known by-products due to hydrolysis or coupling of NVP (*11*). In order to demonstrate the influence of reaction conditions (solvent, temperature and type of initiator) on both the formation of by-products from side reactions with NVP and loss of the xanthate chain-end functionality, the redox initiation at room temperature was compared with three other initiation systems: AIBN in bulk at 60°C, V-50 at 50°C and ACVA at 80°C (66% aqueous NVP solution in both

Downloaded by STANFORD UNIV GREEN LIBR on June 1, 2012 | http://pubs.acs.org
Publication Date (Web): March 20, 2012 | doi: 10.1021/bk-2012-1100.ch017

cases). Figure 4 shows the evolution of M_n and Đ values the different initiating systems. Evolutions of M_n are linear and the dispersities values are quite low. Macromolecular characteristics for the redox initiating follow the same trend, with even better controlled M_n than those using more conventional systems.

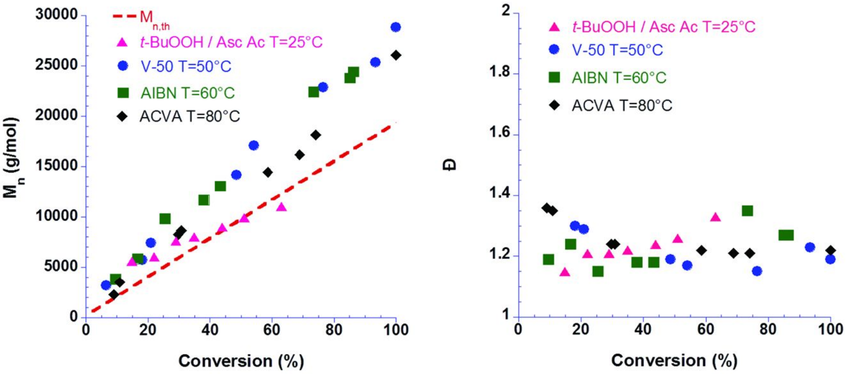

Figure 4. Dependence of M_n (a) and Đ=M_w/M_n (b) on monomer conversion in the aqueous RAFT/MADIX polymerisation of NVP, initiated with the t-BuOOH/Acsorbic acid redox couple at 25°C (▲), V-50% in water at 50°C (●), AIBN in bulk at 60°C (■) and ACVA in water at 80°C (◆). The dashed line represent the theoretical evolution of M_n for a controlled polymerization. M_n was determined by SEC in DMF/LiCl with PMMA standards.

MALDI-TOF MS analysis was performed on PVPs originated from the different initiation modes under various reaction conditions (Figure 5). A low molar mass PVP was synthesised with the tBuOOH/ Asc Ac at 25°C in water ($M_{n\ th}$=1500 g.mol^{-1}, $M_{n\ NMR}$=1600 g.mol^{-1} with 97% conversion after 24 h). The structures corresponding to the major population and one of the minor populations are $CH_3OCOCH_3CH\text{-}(NVP)_{n-1}\text{-}CH{=}CH(C_4H_6NO)$, A being cationised with sodium and B with potassium. This observation brings additional evidence that the R substituent of the xanthate agent fragments and efficiently reinitiates polymerization. However, the xanthate moiety of the polymer has disappeared in favor of a double bond. The loss of the xanthate moiety is due to its fragmentation by the MALDI-TOF laser, as previously reported by Destarac et al. (*29*) ^{1}H NMR analysis and the strong absorption of the PVP-XA$_1$ samples in the UV range at 290 nm, which is characteristic of the presence of the –S(C=S)- group in the polymer, support this assumption (*11*). The expected population $CH_3OCOCH_3CH\text{-}(NVP)_n\text{-}S(C{=}S)OCH_2CH_3$ cationised with potassium was nevertheless observed and corresponds to the second minor population C. AIBN was used to initiate NVP polymerization in bulk at 60°C ($M_{n\ th}$=3000 g.mol-1). 85% conversion was reached after 6h. ^{1}H NMR and MALDI-TOF MS analysis showed that a PVP with similar controlled characteristics to that obtained by redox initiation was formed after this time. If the heating was maintained for 24h, the PVP-Rhodixan A1 was modified, and four different populations could

Downloaded by STANFORD UNIV GREEN LIBR on June 1, 2012 | http://pubs.acs.org
Publication Date (Web): March 20, 2012 | doi: 10.1021/bk-2012-1100.ch017

Downloaded by STANFORD UNIV GREEN LIBR on June 1, 2012 | http://pubs.acs.org
Publication Date (Web): March 20, 2012 | doi: 10.1021/bk-2012-1100.ch017

be detected. Along with A which was the major population, D, E and G have been identified (Figure 5b). Only F could not be attributed. It is believed that D and E were originated from the transformation of the terminal xanthate moiety with temperature according to a concerted mechanism. The corresponding end-group has been also detected by ^{1}H NMR and therefore do not result from the MALDI-TOF MS laser fragmentation. Population G contains a cyanoisopropyl fragment which comes from the initiation with AIBN at one end and a terminal insaturation at the other hand. V-50 and ACVA were used at 50°C and 80°C respectively for NVP polymerization in water with Rhodixan A1. The results looked similar for both initiators. For the RAFT/MADIX polymerization of NVP at 80°C with ACVA initiation ($M_{\mathrm{n\ th}}$ = 3100 g/mol), NVP conversion was about 98% after 2h of reaction. The ^{1}H NMR did not show the *O*-ethyl xanthate chain end moiety and indicated the presence of many identified by-products and chain-end modifications. After 24h, the MALDI-TOF spectrum shows four different identified populations (Figure 5c). Surprisingly, the major one (H) correspond to an aldehyde end group and has already been reported by Pound et al. (*23*), when a preformed PVP-*O*-ethyl xanthate was placed into water and heated for several hours. Populations I and J result from PVPs terminated by a hydrogen atom which may come from a termination mechanism by disproportionation or a hydrogen transfer reaction, and K from polymer chains initiated with ACVA radicals. From these results, it appears that the azo-initiated polymerization of NVP at 50°C and above, when performed either in bulk or in aqueous solution, generate by-products and causes the loss of the xanthate chain end. This may happen during polymerization in some cases, especially in water at high temperature, or after leaving the synthesized PVP at high temperature in the reaction mixture for a longer period of time.

To confirm these results, an elemental analysis has been performed on the obtained PVPs. The results are gathered in Table 3. The experimental percentage of sulfur is slightly less than expected considering the theoretical values for the redox initiation (1.82 instead of 2.52 wt%), but is very stable over time, even after five days (1.75 wt%). On the opposite, the sulfur percentage is quite low after 6h of polymerization with the AIBN system (1.15 wt%), and decrease dramatically after 24h (0.31%). With the V-50 and ACVA initiators, the sulfur percentages are very low (less than 1 wt%), indicating a rapid loss of the xanthate functionality during polymerization. The effect is even more pronounced with ACVA at 80°C than for V-50 at 50°C. After 24 h, less than 0.2 wt% of sulfur is left in the polymer in both cases.

In conclusion, the RAFT/MADIX polymerization of NVP could be successfully controlled at 25°C in water with a suitable redox initiating system without side reactions on monomer and xanthate terminal group, even after five days. In contrast, thermal initiation with azo compounds generally gave rise to numerous by-products and side reactions, whose proportion was increased at high temperature and long heating times, and in water as reaction medium. In particular, using AIBN in bulk, NVP polymerization was reasonably controlled but attention should be paid in order to minimize side reactions that might occur if the formed PVP is left for too long at high temperature.

Downloaded by STANFORD UNIV GREEN LIBR on June 1, 2012 | http://pubs.acs.org
Publication Date (Web): March 20, 2012 | doi: 10.1021/bk-2012-1100.ch017

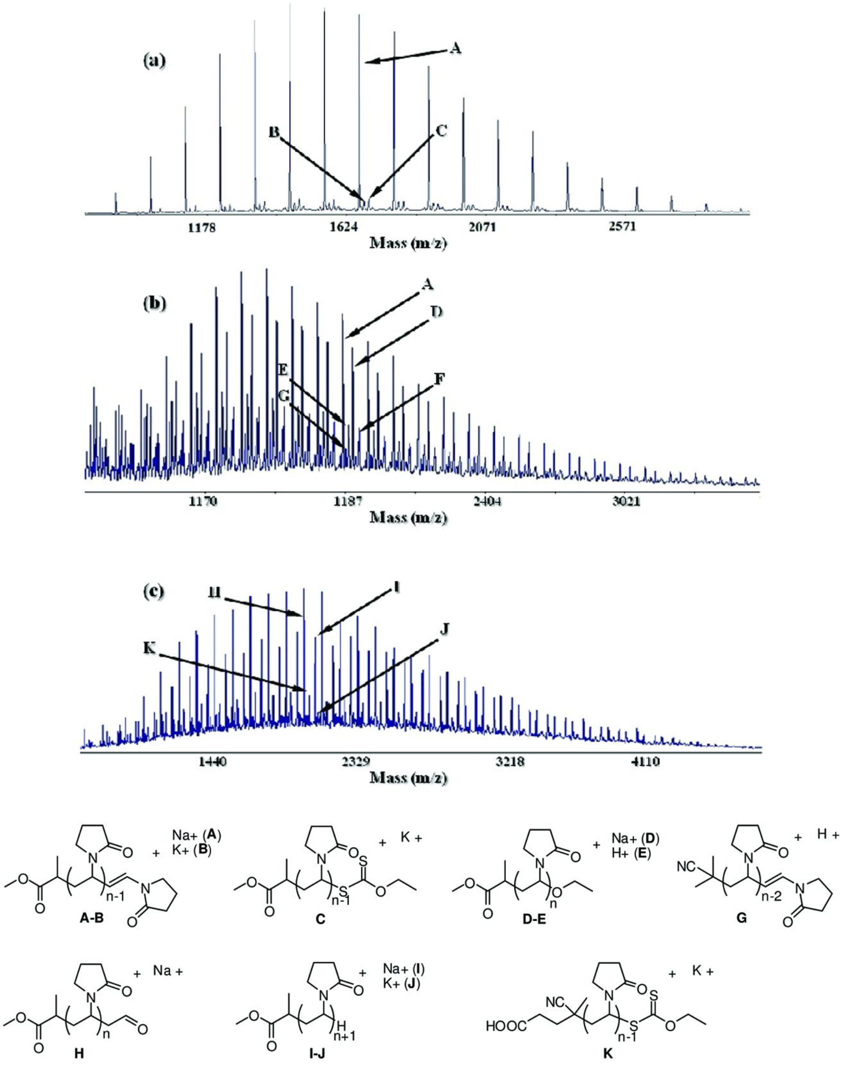

Figure 5. MALDI-TOF mass spectra and identified populations A-K of PVPs initiated in different conditions (a) t-BuOOH / ascorbic acid in water at 25°C (b) AIBN in bulk at 60°C (c) and ACVA in water at 80°C. Reaction time=24h.

Table 3. Elemental analyses of RAFT/MADIX PVPs synthesized with redox and azo initiations

Initiating systems	*Theoretical S (weight %)*	*Experimental S (weight %)*
Redox (25°C, 24 h)	2,52	1,82
Redox (25°C, 5 days)	2,52	1,75
AIBN (60°C, 6h)	2,00	1,15
AIBN (60°C, 24 h)	2,00	0,31
V-50 (50°C, 8 h)	2,20	0,78
V-50 (50°C, 24 h)	2,20	0,23
ACVA (80°C, 2 h)	2,52	< 0,2
ACVA (80°C, 24 h)	2,52	< 0,2

Downloaded by STANFORD UNIV GREEN LIBR on June 1, 2012 | http://pubs.acs.org
Publication Date (Web): March 20, 2012 | doi: 10.1021/bk-2012-1100.ch017

Diallydimethylammonium Chloride (DADMAC)

Our group recently reported that *O*-ethyl xanthates could allow the synthesis of PDADMAC with controlled M_n in water at 50°C according to a RAFT/MADIX mechanism (*10*). A fast and quantitative chain transfer to starting xanthate ensures the molecular weight control of the PDADMACs whereas a relatively slow reversible chain transfer process during polymerization is responsible for relatively large dispersities ($1.8 < Đ < 2.0$). First neutral-cationic DHBCs which comprise a polyacrylamide block and a PDADMAC block of controlled M_n and composition could be successfully synthesized.

We modified this synthetic strategy and replaced the neutral block by a weak polyacid block, like polyacrylic acid (PAA). AA was fully polymerized at 70°C with the ACVA initiator in water with a minimum of ethanol co-solvent to solubilize the hydrophobic xanthate. Ethanol was then evaporated under vacuum and DADMAC was considered for chain extension.

Conditions were found for aqueous SEC analysis of the obtained copolymerss. Polyethylene oxide (PEO) calibration was not satisfactory to produce relevant M_n data (Table 4) with lower than expected $\mathrm{M_n}$ values for the diblocks of higher M_n, but dispersities were relatively low ($1.50 < Đ < 1.70$) for DADMAC-based polymers. Most importantly, all the SEC chromatograms looked as expected for a RDRP, with a clear shift between first and second block, which was more pronounced for the longer second blocks (Figure 6) (*30*). These original diblock copolyampholytes comprise a weak polyacid block and a polyquaternary ammonium block. They were recently used to control the pH and salt stability, size and zeta potential of polymer-inorganic oxide nanoparticles (*31*).

Downloaded by STANFORD UNIV GREEN LIBR on June 1, 2012 | http://pubs.acs.org
Publication Date (Web): March 20, 2012 | doi: 10.1021/bk-2012-1100.ch017

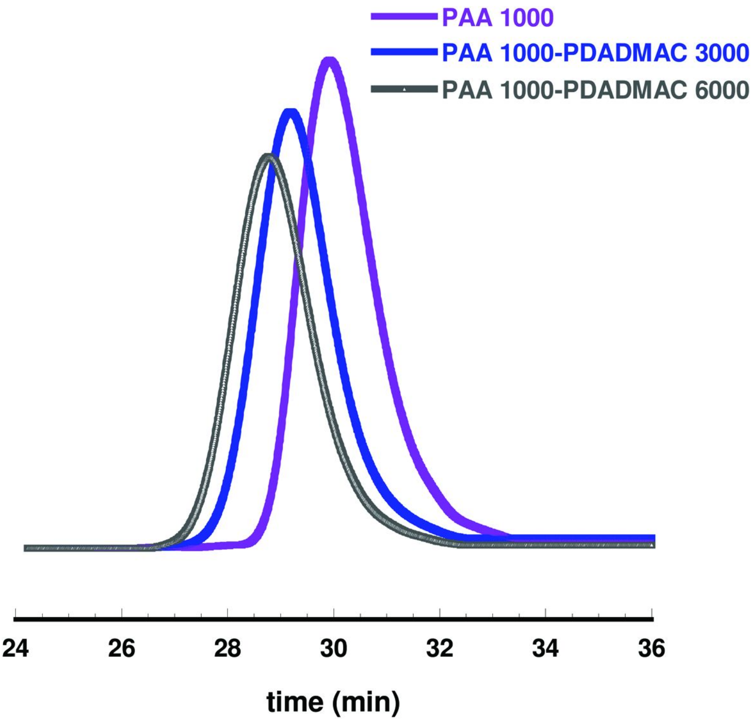

Figure 6. Aqueous SEC chromatograms of PAA-PDADMAC diblock copolymers.

Table 4. PAA-PDADMAC block copolymers synthesized in the presence of Rhodixan A1 and initiated by V-50 in water at 50°C

PAA-PDADMAC Theoretical M_n	*DADMAC* [a] *Conv. (%)*	$M_{n\,SEC}$ [b] *(g* moL^{-1}*)*	*Ð*
500-1500	65.9	1000	1.64
500-1000	99.1	2500	1.50
1000-3000	79.1	2400	1.52
1000-6000	74.0	3000	1.66
1500-45000	84.2	2500	1.50
1500-9000	80.0	4200	1.70

[a] By ^{1}H NMR. [b] PEO calibration.

Downloaded by STANFORD UNIV GREEN LIBR on June 1, 2012 | http://pubs.acs.org
Publication Date (Web): March 20, 2012 | doi: 10.1021/bk-2012-1100.ch017

Conclusion

The efficient aqueous RAFT/MADIX polymerization of three less-activated monomers –one anionic, one neutral, one cationic- using a *O*-ethyl xanthate reversible chain transfer agent is seen as an opportunity to derive original double hydrophilic block copolymers based on VPA, NVP and DADMAC which are all readily industrially available. Block copolymers of these LAMs either together or in combinaison with more-actived monomers compatible with RAFT/MADIX polymerization will be considered in the future.

References

1. Jenkins, D. A.; Jones, R. G.; Moad, G. *Pure Appl. Chem.* **2010**, *82*, 483–491.
2. Cölfen, H. *Macromol. Rapid Commun.* **2001**, *22*, 219–252.
3. Hervé, P.; Destarac, M.; Berret, J.-F.; Lal, J.; Oberdisse, J.; Grillo, I. *Europhys. Lett.* **2002**, *58*, 912–918.
4. Pispas, S. *J. Phys. Chem. B* **2007**, *111*, 8351–8359.
5. Bouyer, F.; Sanson, N.; Destarac, M.; Gérardin, C. *New J. Chem.* **2006**, *30*, 399–408.
6. Barner-Kowollik, C. *Handbook of RAFT Polymerization*; Barner-Kowollik, C., Ed.; Wiley-VCH: Weinheim, 2008.
7. Taton, D.; Destarac, M.; Zard, S. Z. *Handb. RAFT Polym.* **2008**, 373–421.
8. Lowe, A. B.; McCormick, C. L. *Prog. Polym. Sci.* **2007**, *32*, 283–351.
9. Taton, D.; Wilczewska, A.; Destarac, M. *Macromol. Rapid Commun.* **2001**, *22*, 1497–1503.
10. Destarac, M.; Guinaudeau, A.; Geagea, R.; Mazières, S.; Van Gramberen, E.; Boutin, C.; Chadel, S.; Wilson, D. J. *J. Polym. Sci., Part A: Polym. Chem.* **2010**, *48*, 5163–5171.
11. Guinaudeau, A.; Mazières, S.; Wilson, D. J.; Destarac, M. *Polym. Chem.* **2012**, *3* (1), 81–84.
12. (a) Charmot, D.; Corpart, P.; Adam, H.; Zard, S. Z.; Biadatti, T.; Bouhadir. G. *Macromol. Symp.* **2000**, *150*, 23−32. (b) Stenzel, M. H.; Cummins, L.; Roberts, G. E.; Davis, T. P.; Vana, P.; Barner-Kowollik, C. *Macromol. Chem. Phys.* **2003**, *204*, 1160−1168.
13. Pound, G.; Eksteen, Z.; Pfukwa, R.; McKenzie, J. M.; Lange, R. F. M.; Klumperman, B. *J. Polym. Sci., Part A: Polym. Chem.* **2008**, *46*, 6575–6593.
14. Beija, M.; Marty, J.-D.; Destarac, M. *Chem. Commun.* **2011**, *47*, 2826–2828.
15. Blidi, I.; Geagea, R.; Coutelier, O.; Violleau, F.; Destarac, M. *ACS Polym. Prepr., (Am. Chem. Soc., Div. Polym. Chem.)* **2011**, *52* (2), 636–637.
16. Fleet, R.; McLeary, J. B.; Grumel, V.; Weber, W. G.; Matahwa, H.; Sanderson, R. D. *Macromol. Symp.* **2007**, *255*, 8–19.
17. Boutevin, B.; Hervaud, Y.; Boulahna, A.; El Asri, M. *Macromolecules* **2002**, *35*, 6511–6516.
18. Rixens, B.; Severac, R.; Boutevin, B.; Lacroix-Desmazes, P. *J. Polym. Sci., Part A: Polym. Chem.* **2006**, *44*, 13–24.
19. Macarie, L.; Ilia, G. *Prog. Polym. Sci.* **2010**, *35*, 1078–1092.

20. David, G.; Boyer, C.; Tayouo, R.; Seabrook, S.; Ameduri, B.; Boutevin, B.; Woodward, G.; Destarac, M. *Macromol. Chem. Phys.* **2008**, *209*, 75–83.
21. David, G.; Boutevin, B.; Seabrook, S.; Destarac, M.; Woodward, G.; Otter, G. *Macromol. Chem. Phys.* **2007**, *208*, 635–642.
22. Bingöl, B.; Meyer, W. H.; Wagner, M.; Wegner, G. *Macromol. Rapid Commun.* **2006**, *27*, 1719–1724.
23. Pound, G.; McKenzie, J. M.; Lange, R. F. M.; Klumperman, B. *Chem. Commun.* **2008**, 3193–3195.
24. Wan, D.; Satoh, K.; Kamigaito, K.; Okamoto, Y. *Macromolecules* **2005**, *38*, 10397–10405.
25. Punyani, S.; Deb, S.; Singh, H. *J. Biomater. Sci., Polym. Ed* **2007**, *18*, 131–145.
26. Kurenkov, V. F.; Zhelonkina, T. A.; Galibeev, S. S.; Lobanov, F. I. *Russ. J. Appl. Chem.* **2004**, *77*, 1165–1168.
27. Srivastava, A.; Behari, K. *J. Appl. Polym. Sci.* **2006**, *100*, 2480–2489.
28. Taghizadeh, M. T.; Salehi, M. T. *Iran. J. Polym. Sci. Technol.* **1995**, *4*, 262–267.
29. Destarac, M; Brochon, C.; Catala, J-M.; Zard, S. Z. *Macromol. Chem. Phys.* **2002**, *203*, 2281–2289.
30. Destarac, M. Patent WO 2009059887, Rhodia Operations, 2009.
31. Destarac, M.; Crinière, G.; Pitois, C. European Patent 2219774 A1, Rhodia Operations, 2010.

Downloaded by STANFORD UNIV GREEN LIBR on June 1, 2012 | http://pubs.acs.org
Publication Date (Web): March 20, 2012 | doi: 10.1021/bk-2012-1100.ch017

Chapter 18

Reversible Addition-Fragmentation Chain Transfer Polymerization under Microwave Heating Conditions

William L. A. Brooks and Brent S. Sumerlin*

Department of Chemistry, Southern Methodist University,
3215 Daniel Avenue, Dallas, Texas 75275, USA
***E-mail: bsumerlin@smu.edu**

The use of reversible addition-fragmentation chain transfer (RAFT) polymerization has led to the controlled synthesis of a wide variety of macromolecular architectures while maintaining molecular weight control, narrow molecular weight distributions, and functionality. Despite its demonstrated promise, in some cases it would be advantageous to accelerate the synthesis of polymers by RAFT to allow rapid screening of polymers for a variety of potential applications. In many instances, microwave heating, which has demonstrated significant potential in small molecule chemistry, has been employed to increase RAFT polymerization rates without deleterious consequences on reaction control. While it is largely accepted that rate acceleration is likely the result of thermal effects, microwave-assisted RAFT has proved to be an efficient method to prepare well-defined polymers in an accelerated manner.

Introduction

With the discovery of controlled radical polymerization (CRP) techniques, the number and type of controlled architectures possible for polymers was widened considerably, as many vinyl monomers could be controllably polymerized through a radical mechanism (*1*). Of the CRP methods, the three most commonly cited techniques are stable free radical polymerization (SFRP) (*2–4*), atom transfer radical polymerization (ATRP) (*5–10*), and reversible addition-fragmentation chain transfer (RAFT) polymerization (*11–13*). RAFT is promising because of its tolerance to a wide range of monomers, functional groups, and reaction conditions (*1*, *14*). RAFT involves the radical addition to, and fragmentation from, thiocarbonylthio chain transfer agents (CTAs), such as dithioesters, trithiocarbonates, and xanthates. Under ideal circumstances, the rate of a RAFT polymerization should be comparable to that of a conventional radical polymerization conducted under identical conditions. This expected similarity in rates assumes the intermediate radical formed upon the addition of a radical to a thiocarbonylthio species quickly fragments and that the resulting fragment derived from the CTA quickly reinitiates (*15*, *16*). Under these conditions, the overall propagating radical concentration and reaction rate would the same for a RAFT polymerization and a conventional radical polymerization conducted in the absence of a CTA. In practice, the kinetics for RAFT polymerizations are sometimes retarded as compared to conventional polymerizations. Additionally, depending on the specifics of the polymerization and the purity of the reagents, inhibition periods have also been observed (*17*, *18*).

Recently, microwave-assisted synthesis has been applied to RAFT polymerizations. The use of microwave-irradiation as a heating source is a well established precedent in small molecular organic chemistry, with reactions often exhibiting accelerated reaction rates with a reduced tendency to form unwanted side products (*19*). More recently, microwave synthesis has been expanded to the field of polymer chemistry, both as an approach to rapid polymerization (*20–25*) and as a route for accelerated post-polymerization modification (*26–29*). Microwave-irradiation has seen a more limited use in controlled polymerizations, and there have been conflicting reports as to what benefits microwave-irradiation offers. These discrepancies may well be due to the widely varying reaction conditions under which the polymerizations were performed. There have been reports of microwave-assisted SFRP (*30–34*), including Schubert et al., who noticed no rate increase for the nitroxide mediated polymerization (NMP) of methyl acrylate (MA) (**M1**) and *tert*-butyl acrylate (*t*BA) (**M2**) (*30*), or Zhu and coworkers, who observed a marked increase in rate during the NMP of styrene (Sty) (**M3**) (Figure 2) (*31*, *32*). Many examples of microwave-assisted ATRP have also been reported (*35–46*). However, reports of microwave-assisted RAFT polymerizations have been rather limited (*47–55*), and the degree to which the reactions have exhibited control has been mixed. Herein, we overview recent developments in the field of microwave-assisted RAFT polymerization.

RAFT Polymerizations Performed under Microwave-Irradiation

Zhu and coworkers were the first to report RAFT polymerization being performed using microwave-irradiation as a heating source (*47*). A modified domestic microwave with a power rating of 90-900 W was employed to polymerize styrene, both with and without initiator (Figure 1).

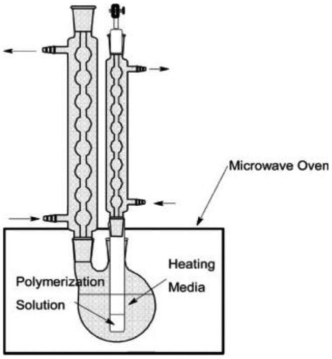

Figure 1. Scheme of the modified domestic microwave oven. Reproduced with permission from Ref. (47). Copyright 2006, John Wiley & Sons.

There are difficulties inherent to the use of a microwave not dedicated to chemical synthesis, namely an inhomogeneous electromagnetic field and fixed power output rather than a dynamically changing output to maintain a constant temperature. In an attempt to maintain isothermal conditions, solvent systems were employed such that the reflux temperature of the solvent would serve as an internal temperature control for the reaction. Reactions with azobisisobutyronitrile (AIBN) initiator were heated to 72 °C in refluxing hexane, and reactions without initiator were heated to 98 °C in a mixture of hexane and CCl_4. Following three freeze-pump-thaw cycles, the RAFT CTA 2-cyanoprop-2-yl 1-dithionaphthalate (CPDN) (**C1**) (Figure 3) was vacuum-sealed in an ampoule along with styrene and, if initiator was included, AIBN. The kinetics determined for reactions performed under microwave-irradiation were compared to measurements taken from an identical polymerization performed using conventional heating techniques. For both microwave and conventional heating, the resulting polymers had molecular weights close to theoretical values and narrow molecular weight distributions ($M_w/M_n \approx 1.2$), along with linear pseudo first-order kinetic plots.

The polymerizations performed using microwave-irradiation had apparent rate constants of propagation (k_p^{app}) 5.4 times greater than conventional heating for reactions with initiator and 6.2 times greater for thermally initiated polymerizations. The living nature of the polymerizations was verified by chain extension of macro-RAFT agents (macroCTAs) prepared under microwave-irradiation. A polystyrene macroCTA ($M_n \approx$ 8,460 g/mol, $M_w/M_n \approx 1.12$) was chain extended with styrene ($[\text{styrene}]_o$:$[\text{macroCTA}]_o$:$[\text{initiator}]_o$ = 500:1:0.5) to verify end group retention. Again, the microwave-assisted polymerization proceeded much faster than during conventional heating, with the microwave-irradiated polymerization completing in 25 min ($M_n \approx$ 23,650 g/mol; $M_w/M_n \approx 1.23$), while conventional heating took 24 h ($M_n \approx$ 25,700 g/mol; $M_w/M_n \approx 1.25$). Chain extension was also performed under microwave irradiation in the absence of initiator ($[\text{styrene}]_o$:$[\text{macroCTA}]_o$ = 1000:2), the molecular weight reaching 19,600 g/mol ($M_w/M_n \approx 1.26$) within 60 min.

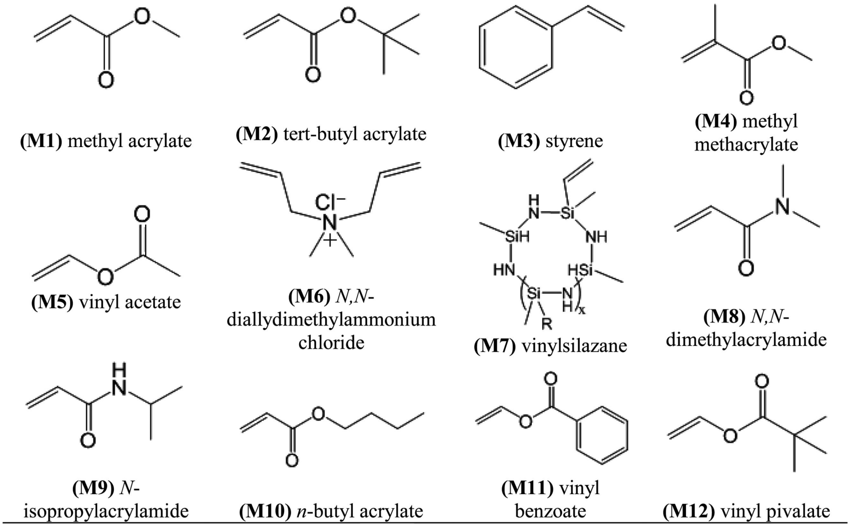

(M1) methyl acrylate

(M2) tert-butyl acrylate

(M3) styrene

(M4) methyl methacrylate

(M5) vinyl acetate

(M6) *N,N*-diallydimethylammonium chloride

(M7) vinylsilazane

(M8) *N,N*-dimethylacrylamide

(M9) *N*-isopropylacrylamide

(M10) *n*-butyl acrylate

(M11) vinyl benzoate

(M12) vinyl pivalate

Figure 2. Various monomers used for microwave-assisted RAFT.

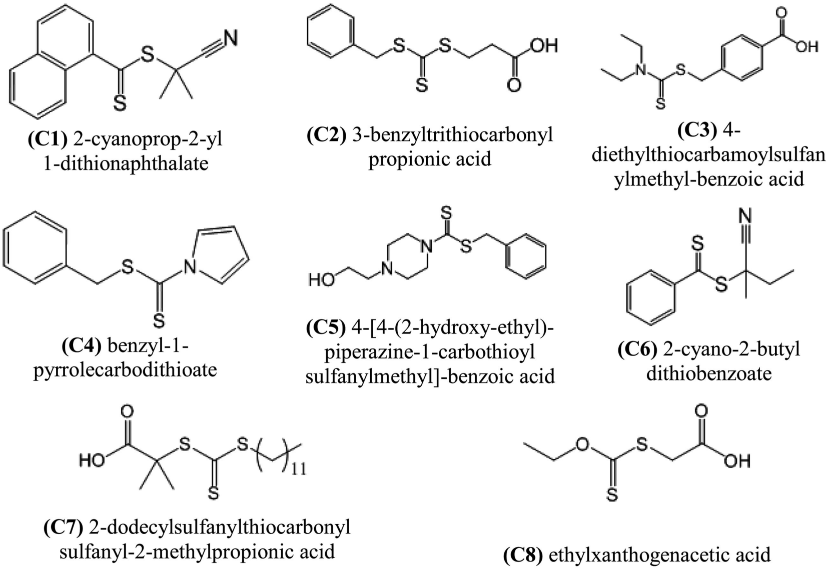

(C1) 2-cyanoprop-2-yl 1-dithionaphthalate

(C2) 3-benzyltrithiocarbonyl propionic acid

(C3) 4-diethylthiocarbamoylsulfanylmethyl-benzoic acid

(C4) benzyl-1-pyrrolecarbodithioate

(C5) 4-[4-(2-hydroxy-ethyl)-piperazine-1-carbothioyl sulfanylmethyl]-benzoic acid

(C6) 2-cyano-2-butyl dithiobenzoate

(C7) 2-dodecylsulfanylthiocarbonyl sulfanyl-2-methylpropionic acid

(C8) ethylxanthogenacetic acid

Figure 3. Various chain transfer agents used for microwave-assisted RAFT.

Perrier and coworkers investigated the bulk RAFT polymerizations of methyl acrylate, methyl methacrylate (MMA) (**M4**), and styrene (*48*). Enhanced reaction rates were observed for the microwave polymerization of methyl acrylate and methyl methacrylate, both relatively polar monomers, compared to conventional heating. The reaction rates were 152% faster for MA and 254% faster for MMA, with the molecular weight distributions for microwave polymerizations being narrower than for comparable polymerizations performed under conventional heating. The same accelerated reaction rate was not seen for styrene, a nonpolar, microwave-transparent monomer. In a second study, Perrier and Rannard et al. examined the reaction kinetics of methyl acrylate, vinyl acetate (VAc) (**M5**), and styrene (*49*). As with the previous study, all polar monomers exhibited increased reaction rates while maintaining molecular weight control. To determine if the higher rates of polymerization could be explained by higher radical concentrations, Perrier et al. examined the dissociation rate of AIBN under both microwave and conventional heating conditions by NMR spectroscopy, with no appreciable difference being observed for the dissociation rate under the two different heating conditions.

Microwave-assisted RAFT polymerization was extended by Agarwal and coworkers to *N,N*-diallydimethylammonium chloride (DADMAC) (**M6**) (*50*), a monomer that polymerizes via a ring closing mechanism that results primarily in 5-member rings along the backbone. Good polymerization control was observed under microwave heating conditions in aqueous media with ammonium persulfate used as an initiator and 3-benzyltrithiocarbonyl propionic acid (**C2**) as the CTA. During microwave-irradiation, the reaction vial was simultaneously cooled using a stream of compressed air; this feature, common to many commercial microwave reactors, will hereafter be referred to as *enhanced microwave (EMW)* conditions. During EMW irradiation, the reaction vial is simultaneously cooled by the flowingair while being heated to the programmed temperature via microwave irradiation. Under these isothermal conditions, the simultaneous heating and cooling requires higher levels of microwave radiation than required for uncooled microwave reactions, accentuating any effects that arise specifically from microwave heating. The EMW polymerization of DADMAC resulted in rates that were approximately 520% and 280% faster than conventionally heated polymerizations at 30 min and 4 h respectively, without sacrificing molecular weight control.

Kim and coworkers employed microwave-assisted RAFT polymerization for the synthesis of vinylsilazane (**M7**), a precursor to silicon carbide and silicon nitride ceramics (*51*). The polymerization of vinylsilazane requires extended times under conventional heating conditions, and often the polymerizations lack sufficient molecular weight control. Three CTAs were employed, 4-diethyl thiocarbamoylsulfanylmethyl-benzoic acid (DTBA) (**C3**), benzyl-1-pyrrolecarbodithioate (BPCD) (**C4**), and4[4-(2-hydroxy-ethyl)-piperazine-1-carbothioylsulfanylmethyl]-benzoic acid (HPCB) (**C5**). Under microwave-irradiation, the polymerizations required only 2.4 h to reach high conversion, while 48-60 h was required by conventional heating. Additionally, microwave polymerizations led to greater molecular weight control, with the molecular weight distributions observed during the microwave polymerizations being narrower ($M_w/M_n \approx$ 1.07-1.12) than was seen for the conventionally heated reactions ($M_w/M_n \approx$ 1.02-2.16). While all three RAFT agents were capable of controlling the polymerization under microwave conditions, HPCB was less successful at controlling the polymerization during conventional heating.

Hoogenboom, Schubert, and coworkers compared the kinetics for the polymerization of MMA at both low and high temperatures, with initiator at 70 °C and without initiator at 120 °C, 150 °C, and 170 °C, under microwave and conventional heating conditions (*52*). The CTA 2-cyano-2-butyl dithiobenzoate (CBDB) (**C6**) was chosen to control the polymerization. Stock solutions were prepared with MMA, CBDB, and, for lower temperature reactions, AIBN. Toluene was chosen for the solvent for the reactions carried out at 70 °C ($[MMA]_0$:$[CBDB]_0$:$[AIBN]_0$ = 100:1:0.25), while bulk conditions were used for reactions performed at 120 °C, 150 °C, and 180 °C ($[MMA]_0$:$[CBDD]_0$ = 234:1). Reactions with AIBN were compared to previously reported reactions performed using conventional heating (*56*, *57*). For reactions performed at 70 °C, no appreciable reaction rate difference was observed between microwave-assisted and conventionally heated reactions (Figure 4). For both reaction types, the pseudo first-order kinetic plots remained linear to extended reaction times, and the microwave kinetics closely mirrored that of the conventional RAFT polymerizations, with both exhibiting an inhibition period of approximately 1 h and having essentially the same k_p^{app}. For the initiator-free reactions, autoinitiation by MMA was proposed, rather than degradation of CBDB, to yield initiating radicals. For initiator-free reactions, the reaction rate increased significantly with increasing temperature, with the polymerization at 180 °C being essentially uncontrolled, and reactions performed at 150 °C resulted in relatively broad molecular weight distributions ($M_w/M_n \approx 2.0$), although at higher conversion the measured M_n values were close to theoretical values.

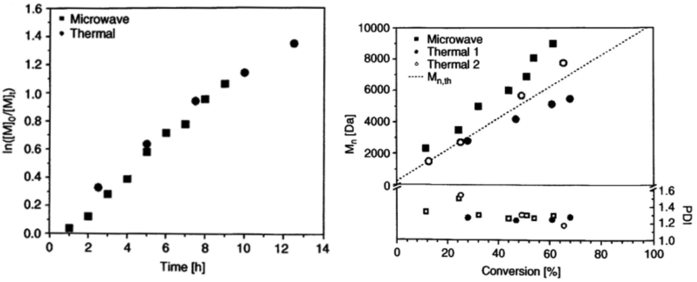

Figure 4. Plot of ln([M]$_o$/[M]) vs. time and M$_n$ and PDI vs. monomer conversion for the polymerization of MMA mediated by CBDB. [MMA]:[CBDB]:[AIBN]=100:1:0.25, [MMA]=2.2M. Reproduced with permission from Ref. (52). Copyright 2009, CSIRO.

Our group used microwave-assisted RAFT for the homopolymerization and block copolymerization of multiple monomers, including *N,N*-dimethylacrylamide (DMA) (**M8**), *N*-isopropylacrylamide (NIPAM) (**M9**), methyl acrylate, and *n*-butyl acrylate (BA) (**M10**) with 2-dodecylsulfanylthiocarbonylsulfanyl-2-methyl propionic acid (DMP) (**C7**) as the RAFT agent (*53*). The reactions performed under microwave-irradiation had significantly accelerated reactions rates as compared to polymerizations heated conventionally (Table 1). The microwave polymerization of DMA ($[DMA]_o$:$[CTA]_o$:$[I]_o$ = 100:1:0.05) had apparent rate constants much higher than for polymerizations performed under conventional heating; the apparent rate constant was 3 times greater for conventional microwave heating and 16.5 times greater for enhanced microwave heating than was observed for polymerizations performed under conventional heating (Figure 5). Similarly, accelerated rates were observed for the microwave-assisted polymerizations of NIPAM. For both DMA and NIPAM polymerizations, inhibition periods up to 35 min were observed during polymerization performed under conventional heating, with no inhibition being observed under microwave-assisted RAFT. Despite the enhanced reaction rates observed during microwave-assisted polymerizations, weight control was maintained.

Table 1. Apparent rate constants for the homopolymerizations of DMA and NIPAM under conventional heating (CH), microwave heating (MW), and enhanced microwave heating (EMW) conditions. Reproduced with permission from Ref. (*53*). Copyright 2009, American Chemical Society.

			$k_p^{app} \times 10^3\ s^{-1}$		
monomer	$[M]_o$:$[CTA]_o$:$[I]_o$	*Temp. (°C)*	*EMW*	*MW*	*CH*
DMA	[100]:[1]:[0.05]	70	6.6 ± 0.01	1.2 ± 0.1	0.4 ± 0.01
DMA	[200]:[1]:[0.05]	70	4.0 ± 0.04	0.7 ± 0.01	0.3 ± 0.47
DMA	[400]:[1]:[0.05]	70	1.2 ± 0.03	n/a	0.2 ± 0.01
DMA	[100]:[1]:[0.005]	70	1.1 ± 0.02	n/a	0.1 ± 0.01
NIPAM	[100]:[1]:[0.05]	60	1.4 ± 0.16	0.3 ± 0.02	0.1 ± 0.01
NIPAM	[200]:[1]:[0.05]	60	0.6 ± 0.05	0.2 ± 0.02	n/a

There has been ongoing debate as to the cause of enhanced reactions rates observed during microwave reactions, with the prevailing theory being that acceleration is ultimately the result of higher than expected temperatures. Unfortunately, measuring the bulk temperature of microwave reactions is not trivial. Using conventional metal thermocouples is not possible, as the thermocouple would interact with the microwave radiation. There have been internal fiber optic probes developed for some microwave reactors that actually measure bulk temperature from within the reaction vial. However, these suffer from fluctuations in measured temperatures based on the depth of the probe in the solution and the rate at which the solution is stirred (*58*). Often, the reaction temperatures are monitored by an external IR sensor that measures the temperature of the vessel, rather than the temperature of the internal solution directly. It is assumed that this temperature accurately represents the temperature of the solution, although this may not always be the case, especially for reactions performed under enhanced microwave conditions, given the cooling of the reaction vessel by an external stream of compressed air. For many microwave reactors, the power output of the microwave can be dynamically adjusted in accordance with the IR sensor to maintain a nearly constant reaction temperature during the course of the reaction.

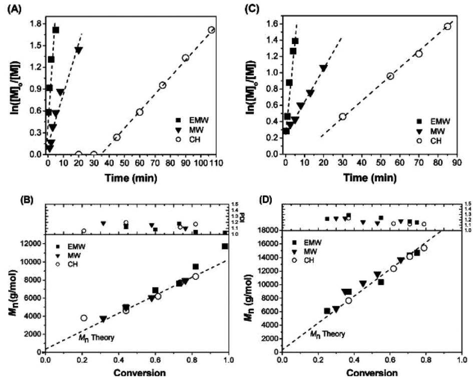

Figure 5. (A) Pseudo first-order kinetic plot and (B) number average molecular weight (M_n) vs. conversion for polymerization of DMA. [DMA]:[CTA]:[AIBN] = 100:1:0.05; (C) Pseudo first-order kinetic plot and (D) number average molecular weight (M_n) vs. conversion for polymerization of DMA. [DMA]:[CTA]:[AIBN] = 200:1:0.05. Reproduced with permission from Ref. (53). Copyright 2009, American Chemical Society.

The potential uncertainty in the solution temperature during microwave reactions has led to the suggestion that the accelerated rates are a result of purely thermal effects, i.e., higher than expected reaction temperatures leading to higher rates. In many cases these thermal effects are not easily duplicated by conventional heating (e.g., superheating at atmospheric pressure, selective heating of polar catalysts or reagents in non-polar media, and absence of wall effects caused by an inverted temperature profile) (*58*). For these reasons, the potential discrepancy between targeted and actual temperatures is sometimes suggested as the reason for accelerated reaction rates often observed during microwave-irradiation.

Sumerlin et al. attempted to account for this temperature uncertainty as it pertained to microwave-assisted RAFT by determining the true temperature of the polymerizations. Reactions were paused immediately before the actual temperature of the reaction solution was measured using an external thermocouple. The temperatures measured at the onset of the reaction were found to overshoot the preset temperature (82 °C measured vs. 70 °C programmed) before equilibrating to the programmed temperature after a few minutes. This unexpected temperature increase can be explained as either overheating by the microwave instrument, overheating due to the sudden reaction exotherm that resulted from the rapid onset of polymerization, or both. Model conventionally heated polymerizations were performed at temperatures slightly higher than were observed during microwave polymerizations (82 °C via microwave vs. 85 °C via conventional heating). If the higher reactions rates were simply a result of the higher initial temperature, then the model polymerizations performed at higher temperatures should have kinetics similar to those measured for microwave-assisted RAFT. However, the model polymerizations performed under conventional heating conditions were still two times slower than those carried out under microwave radiation. Even more telling is the fact that the model conventionally heated polymerizations showed decreased molecular weight control and broader molecular weight distributions than those conducted under microwave heating.

It is important to consider the effect that microwave-assisted RAFT has on the structure of the final polymer, particularly end group retention, as this will have a direct impact on post-polymerization end group modification and chain extension efficiency in block copolymerization. Higher polymerization rates that result from higher radical concentrations in microwave polymerizations would lead to an increased tendency for termination events, degenerative chain transfer, and end group loss that would lead to less efficient chain extension. Our group employed UV-Vis spectroscopy to probe the degree of trithiocarbonate end group fidelity during the microwave-assisted RAFT polymerization of DMA and NIPAM. End group retention was also verified by chain extension of macroCTAs prepared under microwave-assisted RAFT with DMA, NIPAM, MA, and BA (Figure 6). All resulting polymerizations showed a high degree of end group retention with a highly efficient chain extension reaction being observed. These results suggest the accelerated rates observed in microwave-assisted RAFT are not necessarily accompanied by end group loss, and that polymers synthesized using microwave-irradiation can serve as efficient macroCTAs for quick, effective block copolymer synthesis. This successful end group retention will likely be key to the application of RAFT polymerizations under microwave irradiation.

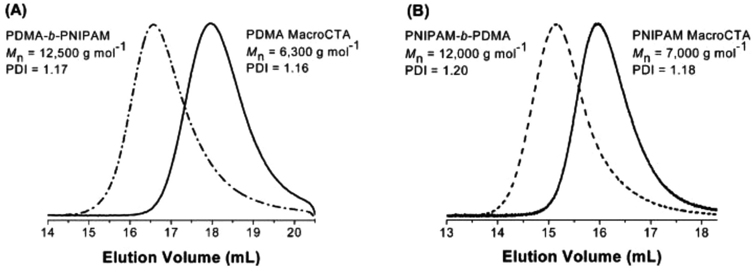

Figure 6. Size exclusion chromatography traces for macroCTA and block copolymers prepared by the enhanced microwave (EMW) approach. (A) PDMA macroCTA and PDMA-b-PNIPAM block copolymer; (B) PNIPAM macroCTA and PNIPAM-b-PDMA block copolymer. Reproduced with permission from Ref. (53). Copyright 2009, American Chemical Society.

One such application has already been reported by Hawker and Stucky et al. Using both a hydrophilic and amphiphilic CTA, PDMA macroCTAs were prepared and used as chain transfer agents for the precipitation polymerization of NIPAM by microwave-assisted RAFT (*54*). The reactions exhibited good control and were highly efficient even with high solids content. Thermoresponsive core crosslinked micelles were prepared by the addition of a difunctional acrylamido crosslinker, and these thermoresponsive nanoparticles were conjugated to fluorescein-labeled albumin using carboxylic acid functionalities present on the RAFT agent.

Sumerlin and coworkers also expanded the use of microwave-assisted polymerization to macromolecular design via the interchange of xanthates (MADIX) (*55*), a subset of RAFT that employs xanthates as chain transfer agents. Due to the higher reactivity of vinyl esters, careful preparation and CTA selection is often necessary to minimize inhibition periods and degenerative chain transfer (*59–63*). Enhanced reaction kinetics were observed for the homopolymerization of vinyl acetate with ethylxanthogenacetic acid (**C8**), a commercially available xanthate CTA. The conventionally heated polymerizations were carried out at both 70 °C and 80 °C, with the microwave polymerization at 70 °C being 14 and 7 times faster by microwave heating, respectively (Figure 7). The resulting molecular weight distributions were narrow at lower conversions, and the final molecular weight distributions were narrower for the microwave-MADIX polymerizations. The MADIX-prepared PVAc homopolymers performed well as macroCTAs for block copolymerizations with other vinyl ester monomers (Figure 8), including vinyl benzoate (VBz) (**M11**) and vinyl pivalate (VPv) (**M12**).

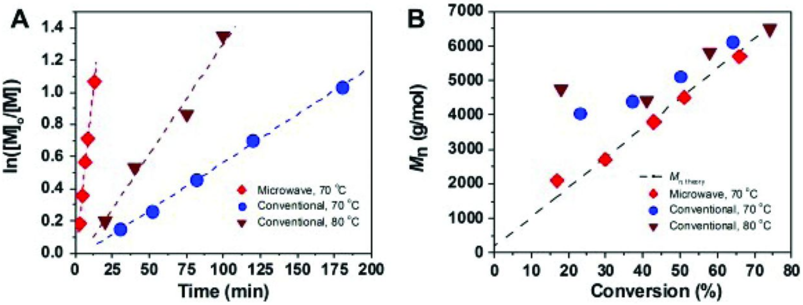

Figure 7. (A) Pseudo first-order kinetic plot and (B) number average molecular weight (M_n) vs. conversion for the RAFT polymerization of vinyl acetate with molar ratios of [vinyl acetate]:[EXGA]:[AIBN] = 100:1:0.2. Reproduced with permission from Ref. (55). Copyright 2011, Elsevier.

Although the examples above indicate RAFT polymerizations performed under microwave-irradiation often exhibit enhanced reaction kinetics, the mechanism for these accelerated rates has not been fully elucidated. In a computational model developed by Vivaldo-Lima and coworkers, several possible mechanisms for the accelerated rates were investigated, including several propagation, termination, and chain transfer possibilities (*64*). The model was compared to the previously reported microwave-RAFT polymerization of styrene in the presence of 2-cyanoprop-2-yl 1-dithionaphthalate, reported by Zhu et al.

(*47*) Vivaldo-Lima and coworkers determined that a mechanism that accounted for radical autoinitiation from monomer was able to predict the molecular weight plots observed experimentally. However, the calculated molecular weight distributions were much broader at low conversion than measured experimentally. Nonetheless, it was suggested that microwave-induced radical formation could account for the increase reaction rate observed during the microwave-assisted polymerization.

A second computational model was developed by Zetterlund and Perrier, comparing the model results to experimental findings reported earlier by Perrier (*49*, *65*). This model focused on sources of initiation and investigated the effect on reaction rate constants, combining all possible propagation steps and termination steps into single terms describing each process respectively. The authors presented three possible mechanisms for the increase in reaction rates: an increase in reaction temperature under microwave conditions, microwave-enhanced rates of propagation (k_p) and addition to the RAFT agent ($k_{-\beta}$), and microwave-specific initiation events (Figure 9).

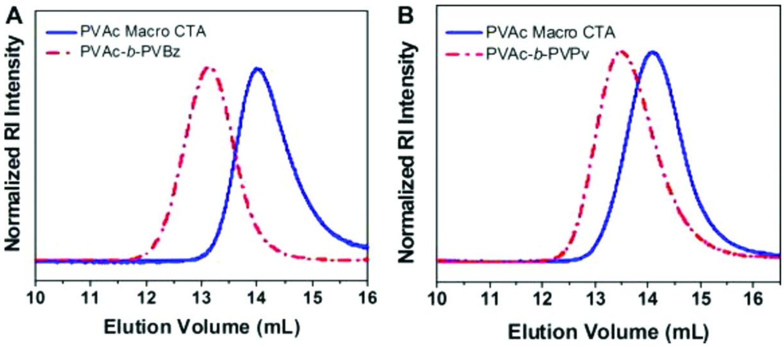

Figure 8. Size exclusion chromatography traces for a (A) PVAc macroCTA and PVAc-b-PVBz) block copolymer and (B) PVAc macroCTA and PVAc-b-PVPv block copolymer prepared via microwave-assisted RAFT polymerization. Reproduced with permission from Ref. (55). Copyright 2011, Elsevier.

All three models were able to predict facets of the results observed in the experimental results. For instance, the model that relied on elevated reaction temperatures led to a large increase in initial radical concentrations, leading to accelerated reaction rates. However, after the initiator was completely consumed, the reaction slowed considerably as termination predominated. The model that accounted for microwave-specific initiation events again predicted the faster reaction rate due to higher radical concentrations. However, the molecular weight and molecular weight distributions deviated greatly from experimental values. The third mechanism most closely matched the experimental results. By enhancing the rates for propagation and addition to the CTA, the experimentally observed phenomenon of increased rate with retention of molecular weight control was reproduced. It was estimated that these conditions lead to a high degree of end group retention and "living" characteristics at high conversion.

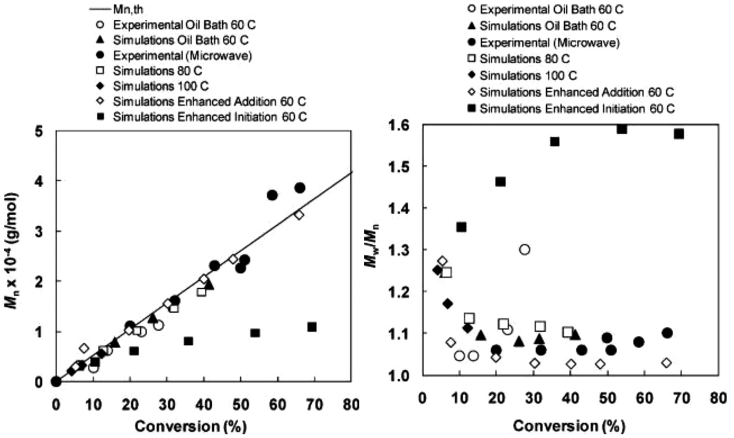

Figure 9. Number-average molecular weights (M_n) vs. conversion for RAFT polymerization of styrene using CPDB under microwave. ($[St]_o$ = 8.7 M (bulk), $[CPDB]_o = 1.74 \times 10^{-2}$ M, $[AIBN]_o = 4.35 \times 10^{-3}$ M), and theM_w/M_nvs. conversion for RAFT polymerization of styrene using CPDB under microwave. ($[St]_o$ = 8.7 M (bulk), $[CPDB]_o = 1.74 \times 10^{-2}$ M, $[AIBN]_o = 4.35 \times 10^{-3}$ M). Reproduced with permission from Ref. (65). Copyright 2011, American Chemical Society.

Outlook

Although the mechanism driving the accelerated reactions rates observed in many microwave-assisted RAFT polymerizations is still not entirely clear, the utility of the technique has been clearly demonstrated. It is likely rate acceleration is to the result of microwave-specific thermal effects that are difficult to reproduce by conventional heating. For the majority of microwave-assisted reactions reported in the literature, rates exhibited were up to an order of magnitude greater than reactions performed using conventional heating while often maintaining molecular weight and end group functionality control. Elucidating the driving force behind these enhanced reaction results will likely require a combination of computational studies and experimental observation. Although scale-up of microwave-assisted RAFT polymerizations may prove challenging, the technique may prove invaluable during rapid screening scenarios, where multiple homopolymers and copolymers can be prepared quickly and efficiently.

Acknowledgments

This material is based upon work supported by the National Science Foundation (CAREER DMR-0846792).

References

1. Boyer, C.; Stenzel, M. H.; Davis, T. P. *J. Polym. Sci., Part A: Polym. Chem.* **2010**, *49*, 551.
2. Georges, M. K.; Veregin, R. P. N.; Kazmaier, P. M.; Hamer, G. K. *Macromolecules* **1993**, *26*, 2987.
3. Odell, P. G.; Veregin, R. P. N.; Michalak, L. M.; Brousmiche, D.; Georges, M. K. *Macromolecules* **1995**, *28*, 8453.
4. Grubbs, R. B. *Polym. Rev.* **2011**, *51*, 104.
5. Kamigaito, M.; Ando, T.; Sawamoto, M. *Chem. Rev.* **2001**, *101*, 3689.
6. Kato, M.; Kamigaito, M.; Sawamoto, M.; Higashimura, T. *Macromolecules* **1995**, *28*, 1721.
7. Wang, J.-S.; Matyjaszewski, K. *J. Am. Chem. Soc.* **1995**, *117*, 5614.
8. Matyjaszewski, K.; Xia, J. *Chem. Rev.* **2001**, *101*, 2921.
9. Ouchi, M.; Terashima, T.; Sawamoto, M. *Chem. Rev.* **2009**, *109*, 4963.
10. Ayres, N. *Polym. Rev.* **2011**, *51*, 138.
11. Chiefari, J.; Chong, Y. K.; Ercole, F.; Krstina, J.; Jeffery, J.; Le, T. P. T.; Mayadunne, R. T. A.; Meijs, G. F.; Moad, C. L.; Moad, G.; Rizzardo, E.; Thang, S. H. *Macromolecules* **1998**, *31*, 5559.
12. Perrier, S.; Takolpuckdee, P. *J. Polym. Sci, Part A: Polym. Chem.* **2005**, *43*, 5347.
13. Destarac, M. *Polym. Rev.* **2011**, *51*, 163.
14. Stenzel, M. H. In *Handbook of RAFT Polymerization*; Wiley-VCH Verlag GmbH & Co. KGaA: Weinheim, Germany, 2008, p 315.
15. *Handbook of RAFT Polymerization*; Wiley-VCH Verlag GmbH & Co. KGaA: Darmstadt, Germany, 2008.
16. Ting, S. R. S.; Davis, T. P.; Zetterlund, P. B. *Macromolecules* **2011**, *44*, 4187.
17. McLeary, J. B.; Calitz, F. M.; McKenzie, J. M.; Tonge, M. P.; Sanderson, R. D.; Klumperman, B. *Macromolecules* **2004**, *37*, 2383.
18. McLeary, J. B.; McKenzie, J. M.; Tonge, M. P.; Sanderson, R. D.; Klumperman, B. *Chem. Comm.* **2004**, *17*, 1950.
19. Kappe, C. O.; Dullinger, D.; Murphree, S. S. *Practical Microwave Synthesis for Organic Chemists: Strategies, Instruments, and Protocols*; Wiley-VCH Verlag GmbH & Co. KGaA, Weinheim, Darmstadt, 2009.
20. Cohen-Arazi, N.; Hagag, I.; Kolitz, M.; Domb, A. J.; Katzhendler, J. *Adv. Sci. Technol.* **2010**, *76*, 30.
21. Hirao, K.; Masutani, K.; Ohara, H. *J. Chem. Eng. Jpn.* **2009**, *42*, 417.
22. Horie, M.; Luo, Y.; Morrison, J. J.; Majewski, L. A.; Song, A.; Saunders, B. R.; Turner, M. L. *J. Mater. Chem.* **2008**, *18*, 5230.
23. Kempe, K.; Becer, C. R.; Schubert, U. S. *Macromolecules* **2011**, *44*, 5825.
24. Kolitz, M.; Cohen-Arazi, N.; Hagag, I.; Katzhendler, J.; Domb, A. J. *Macromolecules* **2009**, *42*, 4520.
25. Saraf, R.; Lee, H. J.; Michielsen, S.; Owens, J.; Willis, C.; Stone, C.; Wilusz, E. *J. Mater. Sci.* **2011**, *46*, 5751.
26. Meuldijk, J.; van, d. K. B. H. P.; van, V. J. A. J. M.; Hulshof, L. A.; Duchateau, R.; Koning, C. E. *Macromol. Symp.* **2011**, *302*, 69.

27. Seo, R. S.; Vergani, C. E.; Giampaolo, E. T.; Pavarina, A. C.; Machado, A. L. *J. Appl. Oral Sci.* **2007**, *15*, 506.
28. Urban, V. M.; Machado, A. L.; Vergani, C. E.; Jorge, E. G.; Serejo, d. S. L. P.; Leite, E. R.; Canevarolo, S. V. *Mater. Res.* **2007**, *10*, 191.
29. Vergani, C. E.; Seo, R. S.; Pavarina, A. C.; dos, S. N. R. J. M. *J. Prosthet. Dent.* **2005**, *93*, 577.
30. Leenen, M.; Wiesbrock, F.; Hoogenboom, R.; Schubert, U. S. *e-Polymers* **2005**.
31. Li, J.; Zhu, X.; Zhu, J.; Cheng, Z. *Radiat. Phys. Chem.* **2006**, *75*, 253.
32. Li, J.; Zhu, X.; Zhu, J.; Cheng, Z. *Radiat. Phys. Chem.* **2006**, *76*, 23.
33. Rigolini, J.; Grassl, B.; Billon, L.; Reynaud, S.; Donard, O. F. X. *J. Polym. Sci., Part A: Polym. Chem.* **2009**, *47*, 6919.
34. Rigolini, J.; Grassl, B.; Reynaud, S.; Billon, L. *J. Polym. Sci., Part A: Polym. Chem.* **2010**, *48*, 5775.
35. Xu, W.; Zhu, X.; Cheng, Z.; Chen, G.; Lu, J. *Eur. Polym. J.* **2003**, *39*, 1349.
36. Li, N.; Lu, J.; Xu, Q.; Xia, X.; Wang, L. *Eur. Polym. J.* **2007**, *43*, 4486.
37. Delfosse, S.; Borguet, Y.; Delaude, L.; Demonceau, A. *Macromol. Rapid Commun.* **2007**, *28*, 492.
38. Hou, C.; Guo, Z.; Liu, J.; Ying, L.; Geng, D. *J. Appl. Polym. Sci.* **2007**, *104*, 1382.
39. Buruiana, E. C.; Murariu, M.; Buruiana, T. *J. Lumin.* **2010**, *130*, 1794.
40. Marcasuzaa, P.; Reynaud, S.; Grassl, B.; Preud'homme, H.; Desbrières, J.; Trchovà, M.; Donard, O. F. X. *Polymer* **2011**, *52*, 33.
41. Buruiana, E. C.; Jitaru, F.; Buruiana, T.; Olaru, N. *Des. Monomers Polym.* **2010**, *13*, 167.
42. Cheng, Z.; Zhu, X.; Chen, J.; Lu, J. *J. Macromol. Sci., Pure Appl. Chem.* **2003**, *A40*, 1157.
43. Hou, C.; Qu, R.; Ji, C.; Wang, C.; Sun, C. *J. Appl. Polym. Sci.* **2006**, *101*, 1598.
44. Li, X.; Zhu, X.; Cheng, Z.; Xu, W.; Chen, G. *J. Appl. Polym. Sci.* **2004**, *92*, 2189.
45. Zhu, X.; Zhou, N.; He, X.; Cheng, Z.; Lu, J. *J. Appl. Polym. Sci.* **2003**, *88*, 1787.
46. Zhang, H.; Schubert, U. S. *Macromol. Rapid Commun.* **2004**, *25*, 1225.
47. Zhu, J.; Zhu, X.; Zhang, Z.; Cheng, Z. *J. Polym. Sci, Part A: Polym. Chem.* **2006**, *44*, 6810.
48. Brown, S. L.; Rayner, C. M.; Perrier, S. *Macromol. Rapid Commun.* **2007**, *28*, 478.
49. Brown, S. L.; Rayner, C. M.; Graham, S.; Cooper, A.; Rannard, S.; Perrier, S. b. *Chem. Commun.* **2007**, 2145.
50. Assem, Y.; Greiner, A.; Agarwal, S. *Macromol. Rapid Commun.* **2007**, *28*, 1923.
51. Nguyen, C. T.; Nghiem, Q. D.; Kim, D.-P.; San Chang, J.; Hwang, Y. K. *Polymer* **2009**, *50*, 5037.
52. Paulus, R. M.; Becer, R.; Hoogenboom, R.; Schubert, U. S. *Aust. J. Chem.* **2009**, *62*, 254.
53. Roy, D.; Ullah, A.; Sumerlin, B. S. *Macromolecules* **2009**, *42*, 7701.

54. An, Z.; Shi, Q.; Tang, W.; Tsung, C.-K.; Hawker, C. J.; Stucky, G. D. *J. Am. Chem. Soc.* **2007**, *129*, 14493.
55. Roy, D.; Sumerlin, B. S. *Polymer* **2011**, *52*, 3038.
56. Fijten, M. W. M.; Meier, M. A. R.; Hoogenboom, R.; Schubert, U. S. *J. Polym. Sci, Part A: Polym. Chem.* **2004**, *42*, 5775.
57. Fijten, M. W. M.; Paulus, R. M.; Schubert, U. S. *J. Polym. Sci, Part A: Polym. Chem.* **2005**, *43*, 3831.
58. Herrero, M. A.; Kremsner, J. M.; Kappe, C. O. *J. Org. Chem.* **2007**, *73*, 36.
59. Favier, A.; Barner-Kowollik, C.; Davis, T. P.; Stenzel, M. H. *Macromol. Chem. Phys.* **2004**, *205*, 925.
60. Stenzel, M. H.; Cummins, L.; Roberts, G. E.; Davis, T. P.; Vana, P.; Barner-Kowollik, C. *Macromol. Chem. Phys.* **2003**, *204*, 1160.
61. Bunck, D. N.; Sorenson, G. P.; Mahanthappa, M. K. *J. Polym. Sci, Part A: Polym. Chem.* **2011**, *49*, 242.
62. Lipscomb, C. E.; Mahanthappa, M. K. *Macromolecules* **2009**, *42*, 4571.
63. Repollet-Pedrosa, M. H.; Weber, R. L.; Schmitt, A. L.; Mahanthappa, M. K. *Macromolecules* **2010**, *43*, 7900.
64. Hernández-Ortiz, J. C.; Jaramillo-Soto, G.; Palacios-Alquisira, J.; Vivaldo-Lima, E. *Macromol. React. Eng.* **2010**, *4*, 210.
65. Zetterlund, P. B.; Perrier, S. b. *Macromolecules* **2011**, 1340.

Chapter 19

Kinetic Simulations of RAFT-Mediated Microemulsion Polymerizations of Styrene

Zhongfan Jia and Michael J. Monteiro[*]

Australian Institute for Bioengineering and Nanotechnology,
The University of Queensland, Brisbane QLD 4972, Australia
[*]E-mail: m.monteiro@uq.edu.au

Downloaded by OHIO STATE UNIV LIBRARIES on June 1, 2012 | http://pubs.acs.org
Publication Date (Web): March 20, 2012 | doi: 10.1021/bk-2012-1100.ch019

Microemulsion polymerizations mediated by reversible addition-fragmentation chain transfer (RAFT) has the potential to produce small polymer particles with controlled molecular weight and molecular weight distributions. This work describes the kinetic simulations using the Smith-Ewart equations to examine the effect of RAFT agent concentration, number of initial droplets and partition coefficient on the rate of polymerization, rate of nucleation and average number of radicals per particle. The simulations showed that exit and reentry of the R radicals from the RAFT agent leaving group dominated the kinetics of microemulsions. The high rate of exit allowed all the droplets to be nucleated under 1% conversion for the high reactive RAFT agents. These simulations further suggest that true compartmentalization only starts upon consumption of the RAFT agent. Retardation and inhibition in the rate of polymerization can be explained through exit and reentry of the R radicals, and one does not require the additional mechanisms of either 'slow fragmentation' or 'intermediate radical termination' (IRT).

Introduction

Microemulsions of oil-in-water (o/w) form instantaneously when the surfactant (e.g. sodium dodecylsulfate) and a cosurfactant (e.g. 1-pentanol or 1-hexanol) are added to the mixture (*1*, *2*). These mixtures are thermodynamically stable, transparent and can remain unchanged for months (*3*), and consists of small

In Progress in Controlled Radical Polymerization: Mechanisms and Techniques; Matyjaszewski, K., et al.;
ACS Symposium Series; American Chemical Society: Washington, DC, 2012.

Downloaded by OHIO STATE UNIV LIBRARIES on June 1, 2012 | http://pubs.acs.org
Publication Date (Web): March 20, 2012 | doi: 10.1021/bk-2012-1100.ch019

spherical droplet size, usually from 5 to 40 nm. Microemulsion polymerization represent an interesting class of compartmentalized polymerizations, and allows small particles (10-50 nm) to be produced at very fast rates with very high molecular weights (in the millions). The term compartmentalization has been defined as the segregation of radicals in growing polymer particles, which through confinement cannot terminate with each other as found in a solution or bulk polymerization (*4*). In a microemulsion polymerization, the extremely high number of initial monomer-swollen micelles compared to that found in either ab initio, seeded or miniemulsions, results in the ultimate compartmentalized system. The probability of a radical entering a monomer-swollen micelle already containing a polymeric radical is extremely low, and thus, each entering radical will produce a new polymer particle (*5*). Nucleation of monomer-swollen micelles to form polymer particles, therefore, takes much longer than for ab initio or seeded emulsion polymerizations. The consequence of such a high monomer-swollen micelle and particle number is that radical termination within the particles is negligible, allowing the synthesis of very high molecular weight polymer with one or at most two polymer chains per particle. Should a radical enter a growing particle (i.e. one containing a polymeric radical), bimolecular radical termination should be instantaneous due to the very small particle size, adhering to the concept of zero-one kinetics (i.e. where only one or no radicals are allowed within the particle) (*4*, *6*).

The application of reversible addition-fragmentation chain transfer (RAFT) to heterogeneous systems is attractive from an industrial view point to make new and advance polymer products (*7–9*). The major advantage over other ‘living’ radical polymerization (LRP) techniques is that RAFT-based dispersion polymerizations can use existing industrial equipment and processes. The use of the low reactive RAFT agents (e.g. xanthates) have shown to be easily implemented into aqueous dispersions (*10–16*). However, the highly reactive RAFT agents in ab initio or seeded emulsion polymerizations has not been as easy as originally thought (*17*). The major problem encountered was particle instability, retardation and inhibition in rates of polymerization, and transportation of the RAFT agent to the growing particles, resulting in little or no control over the number-average molecular weight (M_n), the molecular weight polydispersity (PDI) and the particle size distribution. Miniemulsion polymerizations have shown success in controlling the molecular weight distribution (MWD) as the monomer, RAFT agent are co-located within the monomer droplet (*18–20*). The particle sizes are generally large with quite broad particle size distributions (PSDs). Microemulsion polymerization offers hope in this area, as the size and size distributions are small and much narrower.

Understanding the major kinetic events in a RAFT-mediated microemulsion polymerization will greatly aid in the control of both the molecular weight and particle size distributions (*21–23*). In a conventional microemulsion, only 1 in 20 monomer droplets are nucleated, suggesting that the RAFT agent (CTA) in the un-nucleated monomer-swollen micelles need to transport to the growing particles. Should transportation be slow as found in nearly all other aqueous dispersion polymerizations (*17*, *19*), control of both MWD and PSD will be difficult (if not impossible). To obtain excellent control of both the MWD and PSD, nucleation of the droplets must therefore be rapid to eliminate RAFT transportation dominating the kinetic process. In this work, we develop a kinetic model for the RAFT polymerization of styrene in a microemulsion. We aim to unravel the dominant kinetic process, and provide insight into why microemulsions and miniemulsions provide the best methodology to carry out RAFT polymerizations. These kinetic simulations can also provide some insight in the mechanisms found in other non-conventional dispersion polymerizations (including self-assembly (*24–30*) and nanoreactors (*31–33*)) that have been used to produce a living polymerization with excellent control over the MWD and PSD.

Downloaded by OHIO STATE UNIV LIBRARIES on June 1, 2012 | http://pubs.acs.org
Publication Date (Web): March 20, 2012 | doi: 10.1021/bk-2012-1100.ch019

Kinetic Model

The kinetic simulations solve the Smith-Ewart equations (*34*) for RAFT-mediated microemulsion polymerization of styrene. The kinetic model ignores the complexities found in microemulsion where monomer transports from the un-nucleated monomer-swollen micelles to the growing particles. As shown in the simulations, this assumption is valid for our polymerization systems. We will examine the effect of exit of the R-leaving group from the RAFT agent, initiator concentration (using a water soluble initiator), number of initial droplets and the reactivity of the RAFT agent (i.e. the chain transfer constant, $C_{tr,RAFT}$) on the rate of polymerization, average number of radicals per particle ($\overline{n}$) and the nucleation rate of initial monomer-swollen micelles ($N^{0}_{0,micelle}$). We assume the RAFT agents show little or no retardation in solution or bulk experiments with styrene (*35*), and therefore we can simplify the RAFT mechanism from including all the intermediate radicals to degenerative chain transfer (Scheme 1). This is an accurate method to simulate RAFT-mediated polymerizations providing that retardation in rate is not observed in solution or bulk (*7*, *36–38*). Our model assumes that the initial monomer-swollen micelle size is close to that of the final particle size. This assumption is valid after about 5 % conversion as the particle size remains relatively constant to full conversion as observed from our previous styrene emulsion experiments (*23*).

The main kinetic events for a RAFT-mediated microemulsion have been described elsewhere (*21–23*). First, a thermal initiator decomposes in the aqueous phase to form radicals, I•, that then adds to monomer. These radicals continue to add to monomer, and on their way to becoming surface active radicals survive termination events with all other radicals in the aqueous phase ($[T^{\bullet}]_{aq}$). At a critical chain length ('z-mer' consisting of z monomer units), these oligomers become surface active and can now enter a particle, assumed to be an irreversible process. This pseudo entry rate coefficient, $\rho_{initiator}$, for these z-mers is given by the following equation (*4*, *39*)

$$\rho_{initiator} = \frac{2k_d[I]N_A}{N_c} f_{efficiency} \tag{1}$$

Downloaded by OHIO STATE UNIV LIBRARIES on June 1, 2012 | http://pubs.acs.org
Publication Date (Web): March 20, 2012 | doi: 10.1021/bk-2012-1100.ch019

Where k_d is the rate coefficient for initiator decomposition, [I] is initiator concentration, N_A is Avogadro's number, N_c is the number of particles per liter, and $f_{efficiency}$ is the efficiency to form a z-mer radical from initiator derived radicals, $I^\bullet$.

In styrene emulsion polymerizations consisting of small particles sizes, the entry of z-mer into a growing particle already containing a radical results in instantaneous termination – denoted as 'zero-one' kinetics. This 'zero-one' condition permits zero or one radical to reside in a particle at any one time. More than one radical is not allowed. For the 'zero-one' condition to be met, the rate of propagation must be significantly lower to the rate of termination between two radicals. The 'zero-one' condition is satisfied when the rate coefficient for propagation, k_p, is low (e.g. for styrene) and the particle size small. For reactive monomers with a high k_p (e.g. butyl acrylate) there is a high probability that one or more radicals can coexist per particle even in very small particles (*40*). In microemulsions, 'zero-one' operates for most monomer systems due to (i) the small particle sizes and (ii) the probability of a second radical entering a growing particle is negligible.

There are numerous ways small radicals can form within a particle: through transfer to monomer, CTA or solvent. These small radicals have a high probability of exiting the micelles or particles that have a small size (*12*, *13*, *17*, *41*). The rate coefficient for exit is dependent on the diffusion coefficient (D_R) of the radical, its partition coefficient (q) between the oil and water phases and the radius of the swollen particle (r_s), and is given as follows (*42*):

$$k_{exit} = \frac{3D_R}{qr_s} \qquad (2)$$

These exited $R^\bullet$ radicals can either terminate in the aqueous phase or re-enter a micelle or particle with rate coefficient:

$$k_{re-entry} = 4\pi D_R N_A r_s \qquad (3)$$

and therefore,

$$\rho_{re-entry} = k_{re-entry}[R^\cdot]_{aq} \qquad (4)$$

The re-entry of $R^\bullet$ into a micelle occurs quite rapidly due to the great number of micelles but would also rapidly re-escape due to their very small size (*Limit 3* in emulsion polymerization (*4*)). This process will increase the probability of these R radicals being terminated in the aqueous phase. Exited radicals play an important role in emulsion systems for small particle sizes, and there is experimental evidence that they retard the rate of polymerization in seeded and ab initio emulsion polymerizations (*11*, *12*, *15*).

To simulate a RAFT-mediated microemulsion polymerization, we derived the Smith-Ewart equations in two dimensions, similar to the derivation by Butte et al (*43*) for NMP (*44*) and Luo et al. (*45*) for RAFT (but where *j* represents in their case the intermediate radical concentration). The equation used to describe the number fraction of particles N_i^j, in which there are *i* active polymeric radicals P• and *j* active R• radicals, is given as follows:

$$\begin{aligned}\frac{dN_i^j}{dt} &= \rho_{initiator}\left\{(1-\delta_i)N_{i-1}^j - N_i^j\right\} + k_{exit}\left\{(j+1)N_i^{j+1} - jN_i^j\right\} + k_{tr,RAFT}[CTA]\left\{(1-\delta_j)(i+1)N_{i+1}^{j-1} - iN_i^j\right\}\\ &+ \frac{k_t}{N_A v_p}\left\{(i+1)(i+2)N_{i+2}^j - i(i-1)N_i^j\right\} + \frac{k_{t1}}{N_A v_p}\left\{(i+1)(i+2)N_{i+1}^{j+1} - ijN_i^j\right\}\\ &+ \frac{k_{t1}}{N_A v_p}\left\{(j+1)(j+2)N_i^{j+2} - j(j-1)N_i^j\right\} + k_{p1}C_p\left\{(1-\delta_i)(j+1)N_{i-1}^{j+1} - jN_i^j\right\}\\ &+ \rho_{re-entry}\left\{(1-\delta_j)N_i^{j-1} - N_i^j\right\} + k_{tr,RAFT}[MacroCTA]\left\{(1-\delta_i)(j+1)N_{i-1}^{j+1} - jN_i^j\right\}\end{aligned} \qquad (5)$$

Where $k_{tr,RAFT}$ is the transfer rate coefficient to the RAFT agent (CTA), v_p is the volume of a swollen particle, C_p is the monomer concentration within the particles, k_t is the termination rate coefficient between two polymeric chains, k_{t1} is the termination rate coefficient dominated by short chains, and MacroCTA consisting of a polymer chain with a RAFT end-group. The Kronecker delta δ_i or δ_j in Eq 5 represents the condition if *i* or *j* equals 0 then the Kronecker delta value equals 1. We set that the initial particle number constant over the polymerization, but include in the model the number fraction of monomer-swollen micelles that are converted to particles by z-mers or exited R• radicals, N_0^0; those not yet stung or still existing as micelles, $N_{0\,micelles}^0$; and those micelles that have been entered by an R radical but do not yet contain any oligomeric or polymeric species, $N_{0micelles}^1$. This is an extension from our original equations given in reference (*23*), and provides a more accurate method of assessing nucleation. The initial conditions are $N_{0\,micelles}^0=1$, $N_{0micelles}^1=0$ and $N_0^0=0$, and therefore additional terms (Eq 6, 7 and 8) must be included in the full differential equation in Eq 5 for N_0^1.

$$\frac{dN_1^0}{dt} = \rho_{initiator}N_{0\,micelles}^0 \qquad (6)$$

$$\frac{dN_{0\,micelles}^0}{dt} = -\rho_{initiator}N_{0\,micelles}^0 - \rho_{reentry}N_{0\,micelles}^0 + k_{exit}N_{0micelles}^1 \qquad (7)$$

$$\frac{dN_{0,micelle}^1}{dt} = \rho_{re-entry}N_{0\,micelles}^0 - k_{exit}N_{0micelles}^1 - k_{p1}C_pN_{0micelles}^1 \qquad (8)$$

The average number of P• ($\overline{n}$) per particle is given by

$$\overline{n} = \sum_i\sum_j iN_i^j \qquad (9)$$

Downloaded by OHIO STATE UNIV LIBRARIES on June 1, 2012 | http://pubs.acs.org
Publication Date (Web): March 20, 2012 | doi: 10.1021/bk-2012-1100.ch019

Downloaded by OHIO STATE UNIV LIBRARIES on June 1, 2012 | http://pubs.acs.org
Publication Date (Web): March 20, 2012 | doi: 10.1021/bk-2012-1100.ch019

The differential equations for all other species are given as follows:

$$\frac{dC_p}{dt} = -k_{p1}C_p[R^{\cdot}] - k_pC_p[P^{\cdot}] \qquad (10)$$

$$\frac{d[I]}{dt} = -k_d[I] \qquad (11)$$

$$\frac{d[CTA]}{dt} = -k_{tr,RAFT}[CTA][P^{\cdot}] + k_{tr,RAFT}[MacroCTA][R^{\cdot}] \qquad (12)$$

$$\frac{d[R^{\cdot}]_{aq}}{dt} = k_{exit}[R^{\cdot}]N_c/N_A - k_{entry}[R^{\cdot}]_{aq}N_c/N_A - k_{t1}[R^{\cdot}]_{aq}[T^{\cdot}]_{aq} \qquad (13)$$

$$[T.]_{aq} = \left(\frac{k_d[I]}{k_{t1}}\right)^{0.5} \qquad (14)$$

The differential Equations 5 to 13 are solved iteratively using a high order Runge-Kutta method and using Matlab software to solve the stiffly coupled differential equations (*7*, *36*). Consistency checks are made to ensure that the total number of particles and micelles remained constant with time. We use eq. 14 to calculate $[T^{\bullet}]_{aq}$.

Results and Discussion

The first series of kinetic simulations of styrene were carried out using the parameters in Table 1 for RAFT agents with different $C_{tr,RAFT}$ chain transfer constants. Figure 1 shows the theoretical rate of loss of RAFT agent with conversion as a function of $C_{tr,RAFT}$ (*7*). At low $C_{tr,RAFT}$ value (i.e. 0.7 and 1) the RAFT agent is consumed nearly linearly with conversion. The rate of consumption of RAFT agent to a MacroCTA (or polymer with a RAFT end-group) becomes significantly faster as shown by increasing the $C_{tr,RAFT}$ to 5 and 100. The consumption of RAFT agent will influence the rate of polymerization in a microemulsion as the rate of exit of R radicals becomes dependent on $C_{tr,RAFT}$. The conversion vs time profiles for the different $C_{tr,RAFT}$ values at an initial monomer-swollen micelle size of 20 nm are given in Figure 2A. At low $C_{tr,RAFT}$ values of 0.7 and 1 (curves a and b, respectively), there is little or no inhibition period and a very small amount of retardation compared to the non-RAFT microemulsion polymerization (data not shown). Pepels et al. (*23*) provide detailed kinetic simulations at these low $C_{tr,RAFT}$ values. The increase of $C_{tr,RAFT}$ results in a faster rate of polymerization but with a short inhibition period, which became more pronounced at a higher $C_{tr,RAFT}$ value of 100. The average number of radicals per particle $\bar{n}$ also reflected this trend (Figure 2B). The simulations showed that at this RAFT agent concentration of 0.06 M and high

Downloaded by OHIO STATE UNIV LIBRARIES on June 1, 2012 | http://pubs.acs.org
Publication Date (Web): March 20, 2012 | doi: 10.1021/bk-2012-1100.ch019

monomer-swollen micelle number per unit volume ($N_c = 2.72 \times 10^{19}$), nucleation to form either oligomers or polymer chains in monomer-swollen micelles was complete in less than 8 % conversion even at the lowest $C_{tr,RAFT}$ value of 0.7. This result supports the assumption that we do not need to include monomer transportation from un-nucleated to nucleated particles in our model, and further suggests that microemulsions have a high probability of success to produce well-defined polymer chains. At the highest value of $C_{tr,RAFT}$ (i.e. 100) all the monomer-swollen micelles were nucleated within the first percent of conversion. In contrast, the simulation of a non-RAFT polymerization (data given in ref (*23*)) shows that only a few percent of monomer-swollen micelles were nucleated.

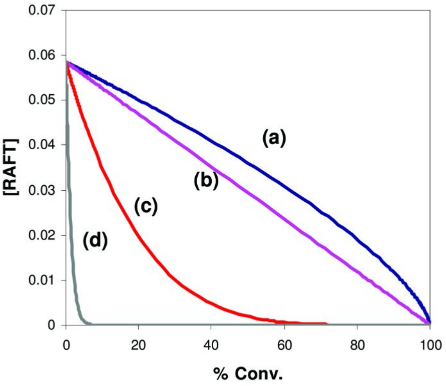

Figure 1. Loss of RAFT agent (CTA) with conversion in bulk or solution according to theory. Curves (a) to (d) represent $C_{tr,RAFT}$ values of 0.7, 1, 5 and 100, respectively.

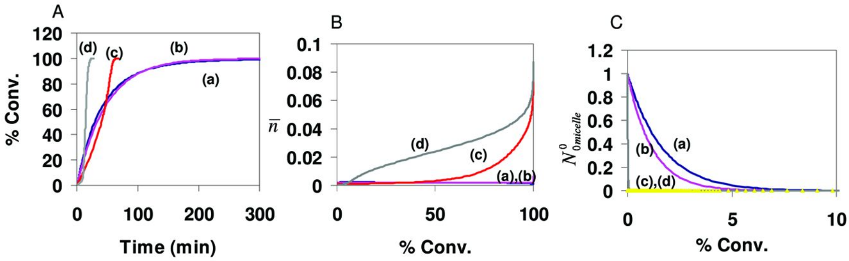

Figure 2. Kinetic simulations using parameters in Table 1 at a $[RAFT]_p = 0.06$ M (targeting $M_n = 15k$ at 100% conversion), $N_c = 2.72 \times 10^{19}$ particles L^{-1}, $[I] = 1 \times 10^{-3}$ mol L^{-1}, in which curves (a) to (d) represent $C_{tr,RAFT}$ values of 0.7, 1, 5 and 100, respectively. (A) conversion vs time; (B) number of radicals per particles ($\bar{n}$) vs conversion; (C) number fraction of initial droples converted to particles by z-mers or exited $R^{\bullet}$ radicals vs conversion.

Downloaded by OHIO STATE UNIV LIBRARIES on June 1, 2012 | http://pubs.acs.org
Publication Date (Web): March 20, 2012 | doi: 10.1021/bk-2012-1100.ch019

Since the simulations for the low reactive RAFT agents have already been described previously (*23*), we will examine the influence of the highly reactive RAFT agent ($C_{tr,RAFT}$ = 100) in microemulsion polymerizations. The simulations in Figure 3 show the effect of RAFT agent concentration (targeting M_n's of 5, 15 and 100 k) on the rate of polymerization and nucleation. When targeting 100 k (i.e. the lowest RAFT agent concentration), we found a short inhibition period of ~3 min and the time to reach 100% conversion was the shortest at approximately 15 min (curve a). Increasing the RAFT concentration (curve b and c) resulted in increasing inhibition periods, but the rate of polymerization after the inhibition period was similar for all RAFT concentrations. This was shown more clearly with the change in $\overline{n}$ with conversion (Figure 3B), in which $\overline{n}$ was the same after 40% conversion. These simulations suggest that once all the RAFT agent has been converted to MacroCTA, exit no longer occurred and thus inhibition or retardation was eliminated. For all the three RAFT agent concentrations, nucleation of all droplets was complete in less than 1% conversion (Figure 3C). These simulations further suggest that during the initial stages of polymerization, there is no true compartmentalization, but one cannot rule out some effects of segregation especially towards the end of the inhibition period. Once the RAFT agent has been consumed, exit will not occur from R radicals from the RAFT agent but through other transfer reactions.

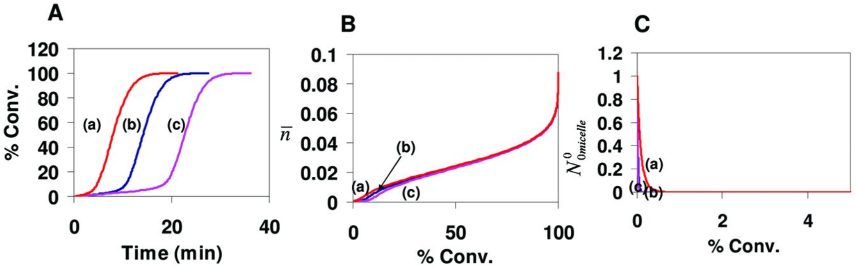

Figure 3. Kinetic simulations using parameters in Table 1 at a $C_{tr,RAFT}$ = 100, $N_c = 2.72 \times 10^{19}$ particles L^{-1}, [I] = 1×10^{-3} mol L^{-1}, in which curves (a) to (c) represent $[RAFT]_p$ of 0.009 M (targeting 100K), 0.06 M (targeting 15k) and 0.18 M (targeting 5k), respectively. (A) conversion vs time; (B) number of radicals per particles ($\overline{n}$) vs conversion; (C) number fraction of initial droples converted to particles by z-mers or exited $R^\bullet$ radicals vs conversion.

The effect of particle number (N_c) on the conversion vs time plots is given in Figure 4A. The change in N_c value from 2.72×10^{19} (curve a) to 1×10^{17} (curve c) showed that the time to reach 100% conversion became shorter. The inhibition period also decreased significantly. Lowering N_c also increased $\overline{n}$ from 0.02 at 50 % conversion (for $N_c = 2.72 \times 10^{19}$) to 0.3 at 50 % conversion (for $N_c = 1 \times 10^{17}$) as shown in Figure 4B. The reason for the faster rates of polymerization and lower inhibition time when using a lower N_c can be explained using Equation 1. The pseudo entry rate coefficient, $\rho_{initiator}$, is dependent on N_c; a lower N_c results in a higher $\rho_{initiator}$ that in turn will increase $\overline{n}$.

Downloaded by OHIO STATE UNIV LIBRARIES on June 1, 2012 | http://pubs.acs.org
Publication Date (Web): March 20, 2012 | doi: 10.1021/bk-2012-1100.ch019

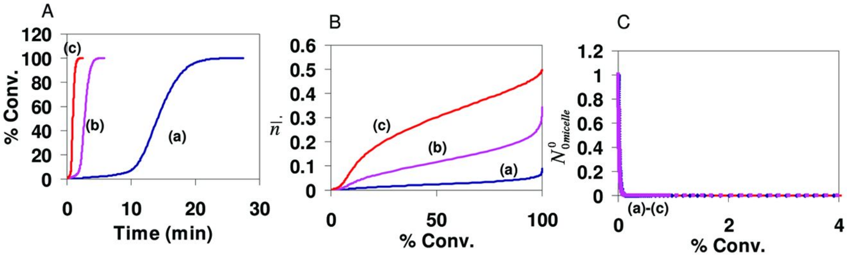

Figure 4. Kinetic simulations using parameters in Table 1 at a $C_{tr,RAFT}$ = 100, $[RAFT]_p$ of 0.06 M (targeting 15K), [I] = 1 x 10^{-3} mol L^{-1}, in which curves (a) to (c) represent N_c of 2.72 x10^{19}, 1 x10^{18}, and 1 x10^{17} particles L^{-1}, respectively. (A) conversion vs time; (B) number of radicals per particles ($\bar{n}$) vs conversion; (C) number fraction of initial droples converted to particles by z-mers or exited $R^{\bullet}$ radicals vs conversion.

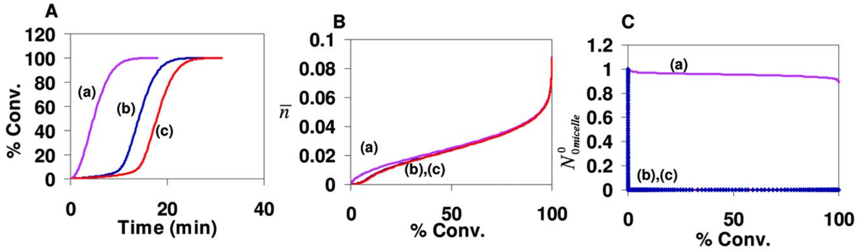

Figure 5. Kinetic simulations using parameters in Table 1 at a $C_{tr,RAFT}$ = 100, $[RAFT]_p$ of 0.06 M (targeting 15K), N_c of 2.72 x10^{19}, [I] = 1 x 10^{-3} mol L^{-1}, in which curves (a) to (c) represent partition coefficients of the R leaving group at 5.5 x 10^6, 1279 and 550, respectively. (A) conversion vs time; (B) number of radicals per particles ($\bar{n}$) vs conversion; (C) number fraction of initial droples converted to particles by z-mers or exited $R^{\bullet}$ radicals vs conversion.

The RAFT agents used in these simulations have an R-group that has a similar partition coefficient to the monomer styrene. This means that diffusion and adsorption into and out of the particles is the same as a monomer molecule, and thus we used a partition coefficient, q, equal to 1279. The next set of simulations examine the effect of the partition coefficient on the microemulsion kinetics. We do this because the range of R-groups on the RAFT agent are diverse. The partition coefficient is changed from 550 to 5.5 x 10^6 as shown in Figure 5. The lower the partition coefficient the more likely the R radical will exit. At the highest partition coefficient of 5.5 x 10^6, 100% conversion is reached in less than 10 min (Figure 5A, curve a). Decreasing q results in an increase in the inhibition period (curve b and c). Nucleation, as shown in Figure 5C, was very much dependent upon q. At the highest value of q (curve a in Figure 5C), nucleation resembled that of a non-RAFT microemulsion polymerization, in which only a small percentage (~12%) of droplets are nucleated. This would suggest that transportation of RAFT from the non-nucleated droplets would become a problem. It further suggests that all droplets will take a considerable time to nucleate, resulting in variable growth of particles and thus broader MWDs.

Table 1. Parameters used in the kinetic simulations for the RAFT-mediated microemulsion polymerization of styrene at 70 °C

Parameter	*Value*	*Description*	*Literature reference*
C_p	8.4 mol L^{-1}	Assuming bulk Monomer concentration within the particle	
D_p	20 nm	Diameter of the particle	
N_c	2.72 x 10^{19} particles L^{-1} (unless otherwise stated)	Number of particles per L (value calculated based on 100 g of styrene in 1 L water)	
k_p	477 L mol^{-1} s^{-1}	Propagation rate coefficient	(*46*)
k_{p1}	4770 L mol^{-1} s^{-1}	Propagation rate coefficient for $R^\bullet + M$	
k_t & k_{t1}	1.72 x 10^8 L mol^{-1} s^{-1}	Termination rate coefficient	(*47*)
k_d	2.2 x 10^{-6} s^{-1}	Initiator decomposition rate coefficient	(*48*)
D_R	1 x 10^{-7} dm^2 s^{-1}	Diffusion coefficient of $R^\bullet$	(*49*)
q	**1279 (unless otherwise stated)**	**Partition coefficient of $R^\bullet$**	(*12*)

Conclusion

In summary, we showed that in a RAFT-mediated microemulsion polymerization, compartmentalization no longer played a role due to the exit and reentry of R radicals from the leaving group on the RAFT agent. The simulations clearly show that $C_{tr,RAFT}$ has a marked effect on the rate of polymerization. The higher the $C_{tr,RAFT}$ value the faster the time to reach 100% conversion, but the inhibition time was found to increase with increasing $C_{tr,RAFT}$. At a $C_{tr,RAFT}$ of 100, the inhibition time increased with increasing RAFT concentration but the rate of polymerization after the inhibition period was similar. There was a significant effect of N_c on the rate of polymerization; the lower the N_c the faster the rate due to a greater $\rho_{initiator}$. The simulations also showed that the partition coefficient of the R radical influenced the rate of nucleation and the inhibition time. The simulations show that retardation in the rate of polymerization was due to exited radicals either terminating in the aqueous phase or through reentry. These simulations further suggest that there is no compartmentalization until the RAFT agent has been consumed. After this time, compartmentalization

Downloaded by OHIO STATE UNIV LIBRARIES on June 1, 2012 | http://pubs.acs.org
Publication Date (Web): March 20, 2012 | doi: 10.1021/bk-2012-1100.ch019

dominates the kinetics due to the absence of exit. As the model assumes a fast fragmentation rate constant for the RAFT process, the simulations show that one does not need to invoke either 'slow fragmentation' or 'intermediate radical termination' to explain retardation in heterogeneous emulsion polymerizations.

Acknowledgments

M.J.M acknowledges financial support from the ARC Discovery grant (DP0987315), Z.J acknowledges the UQ Postdoctoral Research Fellowship.

Downloaded by OHIO STATE UNIV LIBRARIES on June 1, 2012 | http://pubs.acs.org
Publication Date (Web): March 20, 2012 | doi: 10.1021/bk-2012-1100.ch019

References

1. Atik, S. S.; Thomas, J. K. *J. Am. Chem. Soc.* **1981**, *103*, 4279–4280.
2. Kuo, P. L.; Turro, N. J.; Tseng, C. M.; El-Aasser, M. S.; Vanderhoff, J. W. *Macromolecules* **1987**, *20*, 1216–1221.
3. Hoar, J. P.; Schulman, J. H. *Nature* **1943**, *152*, 102–103.
4. Gilbert, R. G. *Emulsion Polymerization: A Mechanistic Approach*; London: Academic Press, 1995.
5. Guo, J. S.; Sudol, E. D.; Vanderhoff, J. W.; El-Aasser, M. S. *J. Polym. Sci., Polym. Chem. Ed.* **1992**, *30*, 703–712.
6. Fitch, R. M. *Polymer Colloids*; Academic Press, 1997.
7. Monteiro, M. J. *J. Polym. Sci., Part A: Polym. Chem.* **2005**, *43*, 3189–3204.
8. Zetterlund, P. B.; Kagawa, Y.; Okubo, M. *Chem. Rev.* **2008**, *108*, 3747–3794.
9. Cunningham, M. F. *Prog. Polym. Sci.* **2008**, *33*, 365–398.
10. Charmot, D.; Corpart, P.; Adam, H.; Zard, S. Z.; Biadatti, T.; Bouhadir, G. *Macromol. Symp.* **2000**, *150*, 23–32.
11. Monteiro, M. J.; Adamy, M. M.; Leeuwen, B. J.; van Herk, A. M.; Destarac, M. *Macromolecules* **2005**, *38*, 1538–1541.
12. Smulders, W.; Gilbert, R. G.; Monteiro, M. J. *Macromolecules* **2003**, *36*, 4309–4318.
13. Smulders, W.; Monteiro, M. J. *Macromolecules* **2004**, *37*, 4474–4483.
14. Bell, C. A.; Smith, S. V.; Whittaker, M. R.; Whittaker, A. K.; Gahan, L. R.; Monteiro, M. J. *Adv. Mater.* **2006**, *18*, 582–586.
15. Monteiro, M. J.; de Barbeyrac, J. *Macromolecules* **2001**, *34*, 4416–4423.
16. Monteiro, M. J.; De Barbeyrac, J. *Macromol. Rapid Commun.* **2002**, *23*, 370–374.
17. Monteiro, M. J.; Hodgson, M.; De Brouwer, H. *J. Polym. Sci., Part A: Polym. Chem.* **2000**, *38*, 3864–3874.
18. de Brouwer, H.; Tsavalas, J. G.; Schork, F. J.; Monteiro, M. J. *Macromolecules* **2000**, *33*, 9239–9246.
19. Tsavalas, J. G.; Schork, F. J.; de Brouwer, H.; Monteiro, M. J. *Macromolecules* **2001**, *34*, 3938–3946.
20. Lansalot, M.; Davis, T. P.; Heuts, J. P. A. *Macromolecules* **2002**, *35*, 7582–7591.
21. Hermanson, K. D.; Liu, S.; Kaler, E. W. *J. Polym. Sci., Part A: Polym. Chem.* **2006**, *44*, 6055–6070.

22. Liu, S.; Hermanson, K. D.; Kaler, E. W. *Macromolecules* **2006**, *39*, 4345–4350.
23. Pepels, M. P. F.; Holdsworth, C. I.; Pascual, S.; Monteiro, M. J. *Macromolecules* **2010**, *43*, 7565–7576.
24. Ferguson, C. J.; Hughes, R. J.; Pham, B. T. T.; Hawkett, B. S.; Gilbert, R. G.; Serelis, A. K.; Such, C. H. *Macromolecules* **2002**, *35*, 9243–9245.
25. Burguiere, C.; Pascual, S.; Bui, C.; Varion, J.; Charleux, B.; Davis, K. A.; Matyjaszewski, K. *Macromolecules* **2001**, *34*, 4439–4451.
26. Stoffelbach, F.; Belardi, B.; Santos, J. M. R. C. A.; Tessier, L.; Matyjaszewski, K.; Charleux, B. *Macromolecules* **2007**, *40*, 8813–8816.
27. Stoffelbach, F.; Tibiletti, L.; Rieger, J.; Charleux, B. *Macromolecules* **2008**, *41*, 7850–7856.
28. Rieger, J.; Grazon, C.; Charleux, B.; Alaimo, D.; Jerome, C. *J. Polym. Sci., Part A: Polym. Chem.* **2009**, *47*, 2373–2390.
29. Rieger, J.; Stoffelbach, F.; Bui, C.; Alaimo, D.; Jerome, C.; Charleux, B. *Macromolecules* **2008**, *41*, 4065–4068.
30. Zhang, W.; D'Agosto, F.; Boyron, O.; Rieger, J.; Charleux, B. *Macomolecules* **2011**, *44*, 7584–7593.
31. Urbani, C. N.; Monteiro, M. J. *Macromolecules* **2009**, *42*, 3884–3886.
32. Monteiro, M. J. *Macromolecules* **2010**, *43*, 1159–1168.
33. Urbani, C. N.; Monteiro, M. J. *Aust. J. Chem.* **2009**, *62*, 1528–1532.
34. Smith, W. V.; Ewart, R. H. *J. Chem. Phys.* **1948**, *16*, 592–9.
35. Adamy, M.; van Herk, A. M.; Destarac, M.; Monteiro, M. J. *Macromolecules* **2003**, *36*, 2293–2301.
36. Monteiro, M. J. *J. Polym. Sci., Part A: Polym. Chem.* **2005**, *43*, 5643–5651.
37. Johnston-Hall, G.; Monteiro, M. J. *Macromolecules* **2007**, *40*, 7171–7179.
38. Johnston-Hall, G.; Monteiro, M. J. *Macromolecules* **2008**, *41*, 727–736.
39. Maxwell, I. A.; Morrison, B. R.; Napper, D. H.; Gilbert, R. G. *Macromolecules* **1991**, *24*, 1629–1640.
40. Maeder, S.; Gilbert, R. G. *Macomolecules* **1998**, *31*, 4410–4418.
41. Monteiro, M. J.; Charleux, B. In *Chemistry and Technology of Emulsion Polymerisation*; Herk, A. v., Ed.; Blackwell Publishing, Ltd.: Boston, 2005, pp 111−139.
42. Ugelstad, J.; Hanson, F. K. *Rubber Chem. Technol.* **1976**, *49*, 536–546.
43. Butte, A.; Storti, G.; Morbidelli, M. *DECHEMA Monogr.* **1998**, *134*, 497–507.
44. Zetterlund, P. B.; Okubo, M. *Macromolecules* **2006**, *39*, 8959–8967.
45. Luo, Y.; Wang, R.; Yang, L.; Yu, B.; Li, B.; Zhu, S. *Macromolecules* **2006**, *39*, 1328–1337.
46. Manders, B. G.; Chambard, G.; Kingma, W. J.; Klumperman, B.; German, A. L. *J. Polym. Sci., Part A: Poly. Chem.* **1996**, *34*, 2473–2479.
47. Johnston-Hall, G.; Monteiro, M. J. *J. Polym. Sci., Part A: Poly. Chem.* **2008**, *46*, 3155–3173.
48. Behrman, E. J.; Edwards, J. O. *Rev. Inorg. Chem.* **1980**, *2*, 179–182.
49. Griffiths, M. C.; Straunch, J.; Monteiro, M. J.; Gilbert, R. G. *Macromolecules* **1998**, *31*, 7835–7844.

Downloaded by OHIO STATE UNIV LIBRARIES on June 1, 2012 | http://pubs.acs.org
Publication Date (Web): March 20, 2012 | doi: 10.1021/bk-2012-1100.ch019

Chapter 20

Reversible Complexation Mediated Polymerization (RCMP) of Methyl Methacrylate

Atsushi Goto,* **Yoshinobu Tsujii, and Hironori Kaji**

Institute for Chemical Research, Kyoto University, Uji, Kyoto 611-0011, Japan
***E-mail: agoto@scl.kyoto-u.ac.jp**

Downloaded by CORNELL UNIV on May 31, 2012 | http://pubs.acs.org
Publication Date (Web): March 20, 2012 | doi: 10.1021/bk-2012-1100.ch020

A new family of living radical polymerization using amines as organic catalysts was introduced. It was based on a new reversible activation mechanism, *reversible complexation*. The polymer molecular weight (M_n being up to 30,000) and its distribution (M_w/M_n = 1.2–1.4) were well controlled in the polymerizations of methyl methacrylate. The catalysts included such common amines as triethylamine. Their low cost, good environmental safety, and ease of handling may be attractive for possible applications. The method using the alkyl iodide (low-mass dormant species) in situ generated in the polymerization was also successfully adopted to this polymerization.

Introduction

Living radical polymerization (LRP) has attracted growing interest as a powerful tool for synthesizing well-defined polymers (*1–4*). The basic concept of LRP is the reversible activation of the dormant species Polymer-X to the propagating radical Polymer$^\bullet$ (Scheme 1a). A sufficiently large number of activation-deactivation cycles are requisite for good control of chain length distribution (*5–7*).

Downloaded by CORNELL UNIV on May 31, 2012 | http://pubs.acs.org
Publication Date (Web): March 20, 2012 | doi: 10.1021/bk-2012-1100.ch020

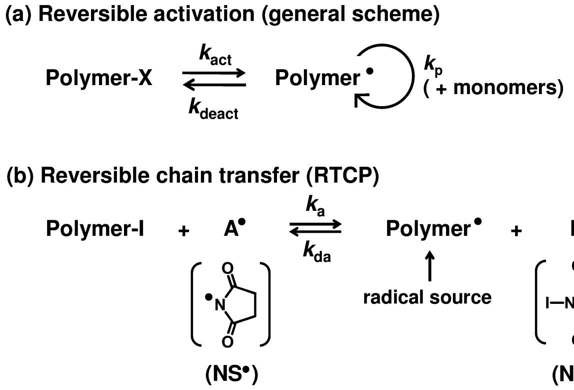

Scheme 1. Reversible Activation Processes. (a) General Scheme and (b) Reversible Chain Transfer.

We recently developed two new families of LRP, both of which use iodine as a capping agent (X) and an organic compound as a catalyst, but with different mechanisms. One (Scheme 1b) uses a reversible chain transfer agent such as *N*-iodosuccinimide (NIS) as a catalyst and is termed reversible chain transfer catalyzed polymerization (RTCP) (*8–16*). It consists of an alkyl iodide (Polymer-I) as a dormant species, a radical source (e.g., azo compound), and NIS as a catalyst. Polymer$^\bullet$, which is originally supplied from a radical source, reacts with NIS, in situ producing the *N*-centered radical (NS$^\bullet$). NS$^\bullet$ is an activator of Polymer-I to produce Polymer$^\bullet$ and NIS. This cycle is a *reversible chain transfer* to the catalyst, allowing a frequent activation of Polymer-I.

The other uses an amine as a catalyst (*17*). It was more recently developed and termed reversible complexation mediated polymerization (RCMP), which will be introduced in the present paper. The background of RCMP is atom transfer radical polymerization (ATRP) (Scheme 2a) that uses a halogen as an X and a transition metal compound ((*18–21*)) such as Cu(I)X (*18*, *19*) as an activator catalyst. Cu(I)X reversibly activates Polymer-X to generate Polymer$^\bullet$ and Cu(II)X$_2$. This is a redox reaction of copper. RCMP uses an amine as an activator catalyst (Scheme 2b) instead of Cu(I)X. The amine includes such simple amines as triethylamine (TEA), which has little or a much weaker redox ability. As a possible mechanism (Scheme 2b), the amine abstracts an iodine from Polymer-I to generate Polymer$^\bullet$ and a complex of the iodine radical and amine (I$^\bullet$/amine complex). Since the iodine radical is not a stable radical, it recombines with another iodine radical to form a complex of the iodine molecule and amine (I$_2$/amine complex) (*22–24*). Polymer$^\bullet$ reacts with these complexes (deactivators) to form Polymer-I and the amine. In this process, electron transfer from the amine to iodine would occur to a range of different degrees including full (redox), partial (coordination) and nearly no transfer, depending on the kind of amines. This process is *reversible complexation* of iodine and catalyst. Clearly, RCMP is mechanistically distinguished from both ATRP and RTCP.

Downloaded by CORNELL UNIV on May 31, 2012 | http://pubs.acs.org
Publication Date (Web): March 20, 2012 | doi: 10.1021/bk-2012-1100.ch020

Technically, RCMP is like ATRP in that they include only a dormant species and an activator catalyst. Unlike RTCP, it requires no conventional radical initiator, even though a conventional radical initiator would, as in other LRPs, work to decrease the concentration of deactivator and thus increase the polymerization rate R_p (*5–7*). A small amount of the deactivator $Cu(II)X_2$ is sometimes added in ATRP. In the same way, the deactivator I_2/amine complex is sometimes added in RCMP.

In the present paper, we briefly summarize the polymerization behaviors of RCMP. We show typical polymerization behaviors with some amine catalysts, as previously reported, but at slightly lower temperature than previously reported, and also show new results on higher molecular weights, another deactivator, and the use of an alkyl iodide (low-mass dormant species) in situ formed in the polymerization. We focus on methyl methacrylate (MMA) in the present paper.

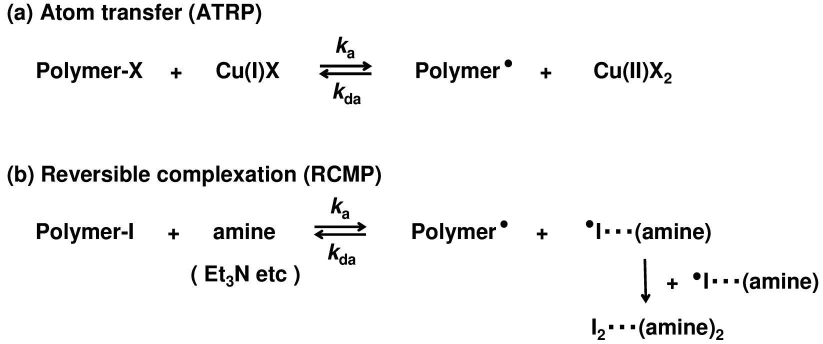

Scheme 2. Reversible Activation Processes. (a) Atom Transfer and (b) Reversible Complexation.

Experimental

Materials

MMA (99%, Nacalai Tesque, Japan) and azobis(isobutyronitrile) (AIBN) (99%, Nacalai) were purified by distillation and recrystallization, respectively. 2-Cyanopropyl iodide (CP-I) (99%, Tokyo Chemical Industry (TCI), Japan (contract service)), I_2 (99.8%, Wako Pure Chemical, Japan), TEA (99%, Wako), *N,N,N′,N′*-tetramethylethylenediamine (TMEDA) (98%, TCI), 1,4,8,11-tetramethyl-1,4,8,11-tetraazacyclotetradecane (TMTAC) (98%, Aldrich), NIS (98%, Wako) were used as received. The structures of CP-I and the amines are shown in Figure 1.

Gel Permeation Chromatography (GPC)

The GPC analysis was made on a Shodex GPC-101 liquid chromatograph (Tokyo, Japan) equipped with two Shodex KF-804L polystyrene mixed gel columns (300 × 8.0 mm; bead size = 7 μm; pore size = 20–200 Å). Tetrahydrofuran (THF) was used as eluent with a flow rate of 0.8 mL/min (40 °C). Sample

Downloaded by CORNELL UNIV on May 31, 2012 | http://pubs.acs.org
Publication Date (Web): March 20, 2012 | doi: 10.1021/bk-2012-1100.ch020

detection and quantification were made with a Shodex differential refractometer RI-101 calibrated with known concentrations of polymer in THF. The column system was calibrated with standard poly(methyl methacrylate)s.

Polymerization

In a typical run, a mixture of MMA (3 mL), CP-I, TEA, and I_2 in a Schlenk flask was heated at 80 °C under argon atmosphere. After a prescribed time *t*, an aliquot (0.1 mL) of the solution was taken out by a syringe, quenched to room temperature, diluted by THF to a known concentration, and analyzed by GPC. The conversion was determined from the GPC peak area.

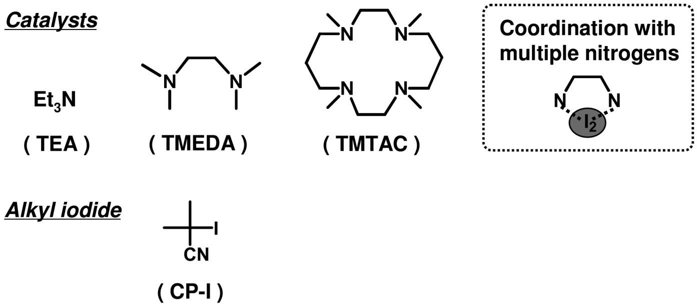

Figure 1. Structures of catalysts and alkyl iodides used in this work.

Results and Discussion

TEA as Catalyst

We studied the polymerizations of MMA with amine catalysts at 60-90 °C. The polydispersity control was essentially the same at these temperatures. We previously reported the results at 90 °C (*17*) and here present those at 80 and 60 °C as examples. Figures 2 (open circles) show the bulk polymerization of MMA (8 M) (100 eq) with CP-I (Figure 1) (80 mM) (1 eq) as a low-mass dormant species and TEA (40 mM) (0.5 eq) as an activator catalyst at 80 °C. The polymerization proceeded up to, e.g., 76% monomer conversion in 4 h (Figure 2a (open circle)), confirming the generation of the propagating radical from CP-I and TEA. The first order plot of the monomer concentration [M] was linear in the studied range of time *t*. However, M_n deviated from the theoretical value $M_{n,theo}$ and the polydispersity index (PDI) (M_w/M_n) was larger than 1.5 at an early stage of polymerization (Figure 2b (open circles)). This is because a sufficient amount of deactivator (I_2/amine complex) was not accumulated at an early stage of polymerization, at which many monomers added to Polymer•. Thus, we added a small amount of iodine molecule (I_2) as a stating compound, which will form the I_2/amine complex with TEA (Scheme 2b) (*25–27*). In fact (Figure 2 (filled circles)), with the addition of 2 mM of I_2 (as small as 1/20 equivalent to TEA), M_n agreed with $M_{n,theo}$ and PDI was about 1.3 from an early stage of polymerization.

Also importantly, PDI kept small (about 1.2) up to high conversions, e.g., 80% (Figure 2b (filled circles) and Table 1 (entry 1)), demonstrating the success of RCMP. The R_p with I_2 was slightly lower than that without it (Figure 2a), as expected from the equilibrium in Scheme 2b. The R_p at 80 °C was about 2/3 times lower than that at 90 °C, with other conditions being set the same.

Table 1. Bulk Polymerizations of MMA (8 M) with CP-I, amine, and I_2

entry	*Target DP*[a]	*amine*	*$[CP\text{-}I]_0/[amine]_0/[I_2]_0$ (mM)*[b]	*T (°C)*	*t (h)*	*c*[c] *(%)*	*M_n ($M_{n,theo}$)*[d]	*PDI*
1	100	TEA	80/40/2	80	5	80	8500 (8000)	1.25
2	100	TMEDA	80/40/2	80	6	68	7900 (6800)	1.32
3	100	TMTAC	80/40/2	80	2	80	9200 (8000)	1.39
4	100	TEA	80/80/20	60	24	81	10000 (8100)	1.26
5	200	TEA	40/80/20	60	24	67	17000 (14000)	1.29
6	400	TEA	20/80/20	60	24	62	30000 (25000)	1.42

[a] Target degree of polymerization at 100% monomer conversion = $[MMA]_0/[CP\text{-}I]_0$. [b] $[MMA]_0/[CP\text{-}I]_0/[amine]_0/[I_2]_0$ = 100/1/0.5/0.025 for entry 1, for example. [c] Monomer conversion. [d] Theoretical M_n calculated with $[MMA]_0$, $[CP\text{-}I]_0$, and conversion.

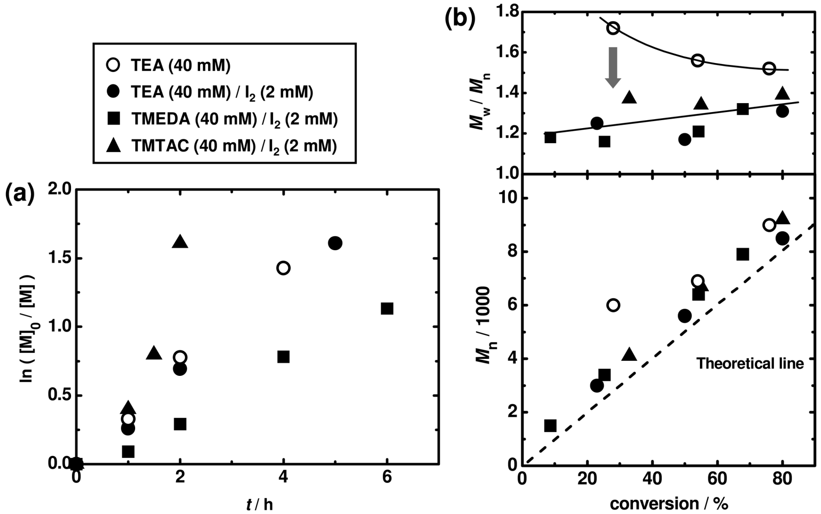

Figure 2. Plots of (a) $\ln([M]_0/[M])$ vs t and (b) M_n and M_w/M_n vs conversion for the MMA/CP-I/amine/I_2 systems at 80 °C: $[MMA]_0$ = 8 M, $[CP\text{-}I]_0$ = 80 mM, $[amine]_0$ = 40 mM, and $[I_2]_0$ = 0 (open circles) or 2 mM (filled symbols) for entries 1-3 in Table 1. The symbols are indicated in the figure. The solid lines in (b) are just guides for eyes.

Downloaded by CORNELL UNIV on May 31, 2012 | http://pubs.acs.org
Publication Date (Web): March 20, 2012 | doi: 10.1021/bk-2012-1100.ch020

Mechanistically, as an activation process, RCMP also includes degenerative chain transfer (DT) (activation of Polymer-I by Polymer•). However, the rate constant of DT is small (*17*), as the PDI in the pure DT system (iodide-mediated polymerization) (*28–31*) is generally relatively large (> 1.5) for MMA in bulk. Thus, the good polydispersity control observed in RCMP is mainly due to the work of the catalyst (reversible complexation (Scheme 2b)) with a small contribution of DT. The kinetic study previously reported (*17*) supported the existence of the reversible complexation process (Scheme 2b), while other catalytic mechanisms can also be involved.

Amines with Multiple Nitrogens as Catalysts

Iodine can be stabilized by using amines with multiple nitrogens (Figure 1), and such amines may work as good activators. The amines thus examined and their abbreviated names are shown in Figure 1. Compared with TEA with one nitrogen (Figure 2 (circles) and Table 1 (entry 1)), TMEDA with two nitrogens (Figure 2 (squares) and Table 1 (entry 2)) in fact afforded lower polydispersity at an early stage of polymerization, suggesting a larger activation rate constant for TMEDA. The smaller R_p for TMEDA (Figure 2a) also suggests an even larger deactivation rate constant for TMEDA than TEA, probably due to the small steric hindrance at the I_2 center for the I_2/TMEDA complex with the compactly bridged TMEDA. TMTAC with four nitrogens (Figure 2 (triangles) and Table 1 (entry 3)) led to the fastest polymerization. The PDI was relatively small (1.3-1.4) but somewhat larger than those with TEA and TMEDA.

The studied amines such as TEA and TMEDA are among the simplest and cheapest amines. The use of such common amines as catalysts may be attractive for possible applications. The small PDI achievable even at high conversions may also be an attractive feature.

Higher Molecular Weights

The polymer produced in RCMP contains iodine at the chain end. In the case of methacrylate polymers, upon heating, the decomposition (elimination of HI (Scheme 3)) occurs to produce a dead chain. A mild temperature like 60 °C can suppress this side reaction, and we may have relatively high molecular weight polymers. In fact (Table 1 (entries 4-6)), with TEA as a catalyst at 60 °C, when the target degree of polymerization at a full conversion was set to 100, 200, and 400, we obtained low polydispersity polymers up to high conversions (up to M_n = 30000 in the studied case), which was difficult at higher temperatures. With TEA, the polymerization was rather slow and took 24 h for high conversions (e.g., 60%) in the studied conditions. We are currently exploring more active catalysts which can lead to faster polymerization.

Downloaded by CORNELL UNIV on May 31, 2012 | http://pubs.acs.org
Publication Date (Web): March 20, 2012 | doi: 10.1021/bk-2012-1100.ch020

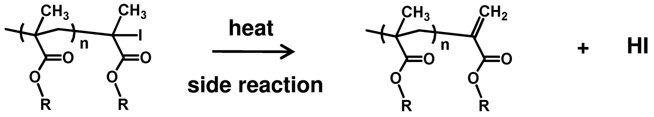

Scheme 3. Elimination of HI from Polymer-I for Methacrylates.

Downloaded by CORNELL UNIV on May 31, 2012 | http://pubs.acs.org
Publication Date (Web): March 20, 2012 | doi: 10.1021/bk-2012-1100.ch020

NIS as Deactivator

In the above-mentioned systems, we used I_2 as a starting compound. Here, instead of I_2, we used NIS as a starting deactivator compound. NIS reacts via the reversible chain transfer mechanism (Scheme 1b) (*10*). Thus, this system is a mixed system of RCMP and RTCP and includes two activators, amine and NS•, and two deactivators, I_2/amine complex (in situ accumulated) and NIS. This method would be useful for amines whose deactivation is slow and hence requiring a large amount of I_2 (sometimes a too large amount to dissolve).

To demonstrate this concept, we studied the polymerizations with CP-I, an amine, and NIS at 80 °C, using TEA, TMEDA, and TMTAC as amines. In all cases (Figure 3 and Table 2), with a small amount of NIS (5 mM (500ppm)), PDI was small (about 1.3) throughout the polymerization, demonstrating the effectiveness of this concept.

Table 2. Bulk Polymerizations of MMA (8 M) with CP-I, amine, and NIS

entry	*Target DP*[a]	*amine*	*[CP-I]$_0$/ [amine]$_0$ /[NIS]$_0$ (mM)*[b]	*T (°C)*	*t (h)*	*c*[c] *(%)*	*M_n ($M_{n,theo}$)*[d]	*PDI*
1	100	TEA	80/40/5	80	4	72	8300 (7200)	1.28
2	100	TMEDA	80/40/5	80	5	69	8300 (6900)	1.35
3	100	TMTAC	80/20/5	80	4	71	7800 (7100)	1.32

[a] Target degree of polymerization at 100% monomer conversion = $[MMA]_0/[CP\text{-}I]_0$. [b] $[MMA]_0/[CP\text{-}I]_0/[amine]_0/[NIS]_0$ = 100/1/0.5/0.0625 for entry 1, for example. [c] Monomer conversion. [d] Theoretical M_n calculated with $[MMA]_0$, $[CP\text{-}I]_0$, and conversion.

Downloaded by CORNELL UNIV on May 31, 2012 | http://pubs.acs.org
Publication Date (Web): March 20, 2012 | doi: 10.1021/bk-2012-1100.ch020

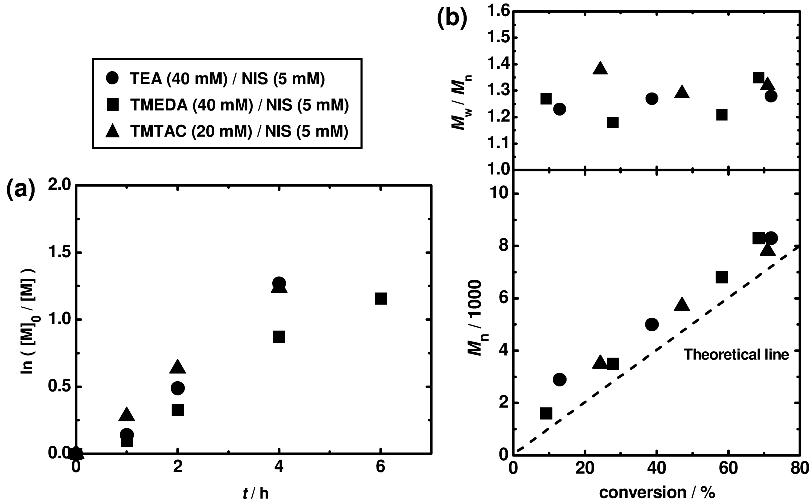

Figure 3. Plots of (a) ln([M]$_0$/[M]) vs t and (b) M_n and M_w/M_n vs conversion for the MMA/CP-I/amine/NIS systems at 80 °C for Table 2: [MMA]$_0$ = 8 M, [CPI]$_0$ = 80 mM, [amine]$_0$ as indicated in the figure, and [NIS]$_0$ = 5 mM. The symbols are indicated in the figure.

Use of in Situ Formed Alkyl Iodide

Instead of using a preformed alkyl iodide (R-I), we may add molecular iodine I_2 and an azo compound (R-N=N-R) to the system as starting compounds and use the alkyl iodide in situ formed in the polymerization. We previously demonstrated that this (I_2/azo) method is effective for RTCP (*10–12*). This method was originally invented by Lacroix-Desmazes et al. for the iodide-mediated LRP (*27*, *32*, *33*) and may be practically useful due to the general lack of the long-term stability of alkyl iodides upon storage. Here we adopted it to RCMP.

The polymerization of MMA was examined with I_2 (40 mM), AIBN (60 mM), and TEA (10 mM) at 80 °C (Figure 4 (filled circles) and Table 3 (entry 1)). AIBN gives 2-cyanopropyl radical CP$^\bullet$, and CP$^\bullet$ reacts with I_2 to form CP-I (*34*). Virtually no polymerization occurred for 3.5 h (Figure 4a), during which time CP$^\bullet$ predominantly reacted with I_2 (rather than monomer) and CP-I accumulated. Since the efficiency of AIBN to produce free CP$^\bullet$ is about 0.6, 60 mM of AIBN (used in this work) can give about 72 mM of free CP$^\bullet$ and hence about 72 mM (theoretical amount) of CP-I. After this period, the polymerization smoothly proceeded (Figure 4a). The M_n almost agreed with $M_{n,theo}$, and PDI was 1.2-1.4 from a low conversion to a high conversion (Figure 4b). Without TEA (catalyst) (Figure 4a (open circle)), no polymerization occurred. With a much larger amount (40 mM) of TEA (Figure 4 (triangles) and Table 3 (entry 2)), the polymerization began before all of AIBN was consumed to generate CP-I. The M_n was about 1.5 times larger than $M_{n,theo}$, while PDI was still relatively small (1.25-1.45). Thus, with the use of appropriate amounts of AIBN and TEA, this method was proved to be effective in RCMP.

Downloaded by CORNELL UNIV on May 31, 2012 | http://pubs.acs.org
Publication Date (Web): March 20, 2012 | doi: 10.1021/bk-2012-1100.ch020

Table 3. Bulk Polymerizations of MMA (8 M) with I_2, AIBN, and TEA

entry	*Target DP*[a]	*$[I_2]_0$/ $[AIBN]_0$ /$[TEA]_0$ (mM)*[b]	*T (°C)*	*t (h)*	*c*[c] *(%)*	*M_n ($M_{n,theo}$)*[d]	*PDI*
1	110	40/60/10	80	5.8	90	11000 (9900)	1.42
2	110	40/60/40	80	2.1	87	15000 (9600)	1.45

[a] Target degree of polymerization at 100% monomer conversion = $[MMA]_0/(2\times0.6\times[AIBN]_0)$. [b] $[MMA]_0/[I_2]_0/[AIBN]_0$ = 100/0.5/0.75/0.125 for entry 1, for example. [c] Monomer conversion. [d] Theoretical M_n calculated with $[MMA]_0$, $[I_2]_0$, and conversion, in which 72 mM of CP-I is assumed to be formed (as noted in the text).

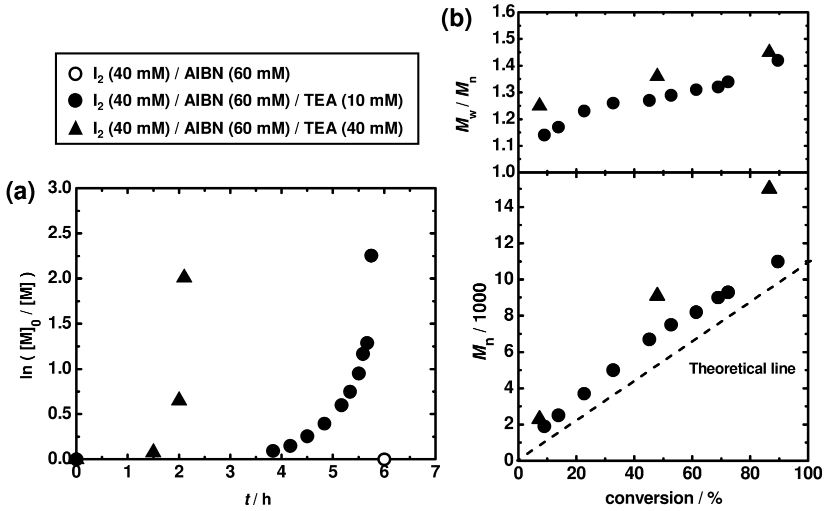

Figure 4. Plots of (a) ln($[M]_0$/[M]) vs t and (b) M_n and M_w/M_n vs conversion for the MMA/I_2/AIBN/amine systems at 80 °C for Table 3: $[MMA]_0$ = 8 M, $[I_2]_0$ = 40 mM, $[AIBN]_0$ = 60 mM, and $[TEA]_0$ = 0 (open circle), 10 mM (filled circles), and 40 mM (triangles).

Conclusions

The success of RCMP was demonstrated for MMA with three amines as catalysts. The PDI was small (1.2-1.4) up to high conversions and up to a few tens thousand molecular weights. Both I_2 and NIS were effective as deactivators. The CP-I in situ formed in the polymerization effectively worked as a low-mass dormant species. Attractive features of the amine catalysts include their low cost, low toxicity, and ease to handling (insensitivity to air).

Downloaded by CORNELL UNIV on May 31, 2012 | http://pubs.acs.org
Publication Date (Web): March 20, 2012 | doi: 10.1021/bk-2012-1100.ch020

Acknowledgments

This work was supported by Grants-in-Aid for Scientific Research, the Ministry of Education, Culture, Sports, Science and Technology, Japan, Industrial Technology Research Grant Program in 2007 from New Energy and Industrial Technology Development Organization (NEDO) of Japan, and Japan Science and Technology Agency (JST).

References

1. *Handbook of Radical Polymerization*; Matyjaszewski, K., Davis, T. P., Eds.; Wiley-Interscience: New York, 2002.
2. (a) *Controlled/Living Radical Polymerization: Progress in ATRP*; Matyjaszewski, K., Ed.; ACS Symposium Series 1023; American Chemical Society: Washington, DC, 2009. (b) *Controlled/Living Radical Polymerization: Progress in RAFT, DT, NMP & OMRP*; Matyjaszewski, K., Ed.; ACS Symposium Series 1024; American Chemical Society: Washington, DC, 2009.
3. *The Chemistry of Radical Polymerization*; Moad, G.; Solomon, D. H., Eds.; Elsevier, Amsterdam, 2006.
4. Braunecker, W. A.; Matyjaszewski, K. *Prog. Polym. Sci.* **2007**, *32*, 93–146.
5. For reviews on kinetics, see refs 5−7. Fukuda, T. *J. Polym. Sci., Part A: Polym. Chem.* **2004**, *42*, 4743−4755.
6. Fischer, H. *Chem. Rev.* **2001**, *101*, 3581–3618.
7. Goto, A.; Fukuda, T. *Prog. Polym. Sci.* **2004**, *29*, 329–385.
8. Goto, A.; Zushi, H.; Kwak, Y.; Fukuda, T. Germanium- and Tin-Catalyzed Living Radical Polymerizations of Styrene. In *Controlled/Living Radical Polymerization*; Matyjaszewski, K., Ed.; ACS Symposium Series 944; American Chemical Society: Washington, DC, 2006; pp 595−603.
9. Goto, A.; Zushi, H.; Hirai, N.; Wakada, T.; Tsujii, Y.; Fukuda, T. *J. Am. Chem. Soc.* **2007**, *129*, 13347–13354.
10. Goto, A.; Hirai, N.; Wakada, T.; Nagasawa, K.; Tsujii, Y.; Fukuda, T. *Macromolecules* **2008**, *41*, 6261–6264.
11. Goto, A.; Tsujii, Y.; Fukuda, T. *Polymer* **2008**, *49*, 5177–5185.
12. Goto, A.; Nagasawa, K.; Shinjo, A.; Tsujii, Y.; Fukuda, T. *Aust. J. Chem.* **2009**, *62*, 1492–1495.
13. Vana, P.; Goto, A. *Macromol. Theory Simul.* **2010**, *19*, 24–35.
14. Yorizane, M.; Nagasuga, T.; Kitayama, Y.; Tanaka, A.; Minami, H.; Goto, A.; Fukuda, T.; Okubo, M. *Macromolecules* **2010**, *43*, 8703–8705.
15. Goto, A.; Hirai, N.; Nagasawa, K.; Tsujii, Y.; Fukuda, T.; Kaji, H. *Macromolecules* **2010**, *43*, 7971–7978.
16. Wolpers, A.; Ackermann, L.; Vana, P. *Macromol. Chem. Phys.* **2011**, *212*, 259–265.
17. Goto, A.; Hirai, N.; Nagasawa, K.; Tsujii, Y.; Fukuda, T.; Kaji, H. *Macromolecules* **2011**, *44*, 8709–8715.
18. Wang, J. S.; Matyjaszewski, K. *J. Am. Chem. Soc.* **1995**, *117*, 5614–5615.
19. Lena, F.; Matyjaszewski, K. *Prog. Polym. Sci.* **2010**, *35*, 959–1021.

20. Kato, M.; Kamigaito, M.; Sawamoto, M.; Higashimura, T. *Macromolecules* **1995**, *28*, 1721–1723.
21. Ouchi, M.; Terashima, T.; Sawamoto, M. *Chem. Rev.* **2009**, *109*, 4963–5050.
22. For the combination of two free I•s (not I•/amine complexes) to generate an iodine molecule I_2, see refs 22−24. Rosman, H.; Noyes, R. M. *J. Am. Chem. Soc.* **1958**, *80*, 2410−2415.
23. LaVerne, J. A.; Wojnarovits, L. *J. Phys. Chem.* **1994**, *98*, 12635–12640.
24. Lacroix-Desmazes, P.; Tonnar, J.; Boutevin, B. *Macromol. Symp.* **2007**, *248*, 150–157.
25. Yada, H.; Tanaka, J.; Nagakura, S. *Bull. Chem. Soc. Jpn.* **1960**, *33*, 1660–1667.
26. Wan, J. K. S.; Jitts, J. N., Jr. *Tetrahedron Lett.* **1964**, *44*, 3245–3250.
27. Lacroix-Desmazes, P.; Severac, R.; Boutevin, B. *Macromolecules* **2005**, *38*, 6299–6309.
28. Yutani, T.; Tatemoto, M. European Patent Appl. 048937OA1, 1991.
29. Kato, M.; Kamigaito, M.; Sawamoto, M.; Higashimura, T. *Polym. Prepr., Jpn.* **1994**, *43*, 255.
30. Matyjaszewski, K.; Gaynor, S.; Wang, J. S. *Macromolecules* **1995**, *28*, 2093–2095.
31. David, G.; Boyer, C.; Tonnar, J.; Ameduri, B.; Lacroix-Desmazes, P.; Boutevin, B. *Chem. Rev.* **2006**, *106*, 3936–3962.
32. For other methods for in situ producing an alkyl iodide, see refs 32 and 33. J. Tonnar, P. Lacroix-Desmazes, *Angew. Chem., Int. Ed.* 2008, *47*, 1294-1297.
33. Tonnar, J.; Lacroix-Desmazes, P. *Soft Matter* **2008**, *4*, 1225–1260.
34. Balczewski, P.; Mikolajczyk, M. *New J. Chem.* **2001**, *25*, 659–663.

Downloaded by CORNELL UNIV on May 31, 2012 | http://pubs.acs.org
Publication Date (Web): March 20, 2012 | doi: 10.1021/bk-2012-1100.ch020

Downloaded by CORNELL UNIV on June 1, 2012 | http://pubs.acs.org
Publication Date (Web): March 20, 2012 | doi: 10.1021/bk-2012-1100.ch021

Chapter 21

Reverse Iodine Transfer Polymerization (RITP): From Kinetics and Mechanisms to Macromolecular Engineering

Patrick Lacroix-Desmazes,* Alejandro-Magno Villa-Hernandez, and David Rayeroux

**Institut Charles Gerhardt - UMR5253 CNRS/UM2/ENSCM/
UM1 - Ingénierie et Architectures Macromoléculaires,
Ecole Nationale Supérieure de Chimie de Montpellier,
8 rue de l'Ecole Normale, 34296 Montpellier Cedex 5, France
*E-mail: patrick.lacroix-desmazes@enscm.fr**

In recent studies, we focused on the kinetics and mechanisms of reverse iodine transfer polymerization (RITP) to control the iodine end-chain functionality of the polymer chains, allowing further macromolecular engineering. Indeed, we were able to synthesize ω-hydroxyl and ω-carboxyl poly(1,1,2,2-tetrahydroperfluorodecyl acrylate) chains, cationic poly(vinylbenzyl triethylammonium chloride)-*b*-polystyrene, ionogenic polystyrene-*b*-poly(acrylic acid) and non-ionic polystyrene-*b*-poly(2-methyl-2-oxazoline) diblock copolymers as well as triblock copolymers of butyl acrylate and styrene. Thus, RITP proves to be a promising tool for polymer chemists.

Introduction

Reverse iodine transfer polymerization (RITP) (Scheme 1) has emerged as an easy, efficient and robust method of controlled radical polymerization, applicable to a wide range of monomers and compatible with both homogeneous and heterogeneous processes, including the industrially relevant aqueous emulsion polymerization (*1–5*). RITP relies on the *in situ* formation of iodinated transfer agents starting from molecular iodine I_2 or its precursors (such as sodium iodide, NaI). In recent studies, we focused on the kinetics and mechanisms of RITP to control the iodine end-chain functionality of the polymer chains, which in turn has opened the door to macromolecular engineering thanks to the richness of the chemistry of iodo-compounds.

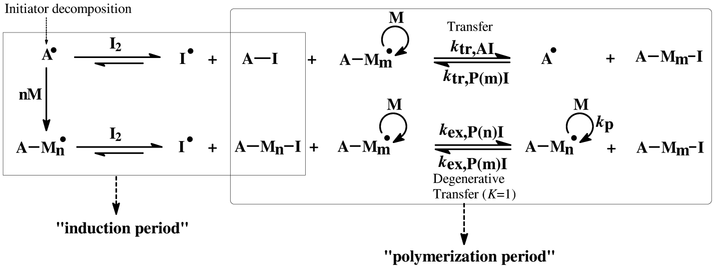

Scheme 1. Simplified mechanism of reverse iodine transfer polymerization in solution ($A^•$: radical from the initiator; I_2: molecular iodine; M: monomer unit; n: mean number degree of polymerization).

Experimental

Materials

All monomers were distilled prior to use. α,α′-Azobisisobutyronitrile (AIBN, Fluka, 98%) was purified by recrystallization in methanol. Dilaurylperoxide (LYP, Aldrich, 97%), bis(4-tert-butylcyclohexyl)peroxydicarbonate (P16S, Akzo Nobel, 95%), 2,5-bis(2-ethylhexanoylperoxy)-2,5-dimethylhexane (T141, Akzo Nobel, 90%), and iodine (I_2, Aldrich, 99.8%) were used as received.

Synthesis of Polymers by Reverse Iodine Transfer Polymerization (RITP)

Typically, iodine I_2, radical initiator, monomer and solvent (when applicable) were weighed in a round-bottom schlenk flask equipped with a magnetic stirrer. The schlenk flask was fitted with a septum and after three freeze-pump-thaw cycles, it was heated in an oil bath at the appropriate temperature for the radical initiator dissociation, in the absence of light and under argon atmosphere, for several hours. Conversion and molecular weight of crude and/or precipitated samples were obtained by ^1H NMR and SEC, respectively.

Synthesis of Block Copolymers by Iodine Transfer Polymerization (ITP)

Typically, radical initiator, the P-I polymer precursor prepared by RITP, monomer and solvent (when applicable) were weighed in a round-bottom schlenk flask fitted with a magnetic stirrer. The polymerization proceeded as mentioned above for RITP.

Downloaded by CORNELL UNIV on June 1, 2012 | http://pubs.acs.org
Publication Date (Web): March 20, 2012 | doi: 10.1021/bk-2012-1100.ch021

Synthesis of Block Copolymers by Cationic Ring-Opening Polymerization (CROP)

Typically, the P-I polymer precursor prepared by RITP, monomer (2-methyl-2-oxazoline, MOx) and solvent (when applicable) were weighed in a round-bottom schlenk flask fitted with a magnetic stirrer. The flask was then sealed with a septum and heated at the appropriate temperature (*e.g.* T=80°C) for several hours under argon atmosphere in the absence of light. The crude product was purified by a series of precipitation in selective solvents to get rid of any unreacted reactants and/or side products. ^{1}H NMR in $CDCl_3$ and SEC in DMF were performed on samples of the purified product.

Characterizations

^{1}H NMR (250 and 400 MHz) analyses were performed at room temperature on Bruker AC 250 and AC 400 spectrometers in deuterated chloroform $CDCl_3$ or DMSO-d^6 as solvent. Size exclusion chromatography (SEC) was used to determine molecular weights and molecular weight distributions of polymer samples. Size Exclusion Chromatography (SEC) with THF as eluent at a flow rate of 1.0 mL.min^{-1}, calibrated with polystyrene standards or poly(methyl methacrylate) from Polymer Laboratories, was done on a PL-GPC 50 plus equipped with a PL-AS RT autosampler from Polymer Laboratories. The SEC apparatus is fitted with two 300 mm long columns thermostated at 35°C (mixed-C PL-gel 5 µm columns from Polymer Laboratories: $2 \times 10^2 - 2 \times 10^6$ g.mol^{-1} molecular weight range) and comprises an integrated chromatography system: a micro-volume double piston pump, a deflection type refractometer detector and a variable wavelength UV detector (wavelength range: 190-740 nm). SEC with DMF as eluent, calibrated with poly(methyl methacrylate) standards from Polymer Laboratories, was run with a Varian Prostar (model 210) pump at a flow rate of 0.8 mL.min^{-1} using two 300 mm long, mixed-D PL-gel 5 µm columns (molecular weight range: $2 \times 10^2 - 4 \times 10^5$ g.mol^{-1} from Polymer Laboratories) thermostated at 70°C, connected to a Shodex (model RI-101) refractometer detector.

Results and Discussion

Kinetics and Mechanisms

RITP is a technique of controlled radical polymerization which relies on the use of molecular iodine as the control agent. Actually, the transfer agents are synthesized *in situ*. Schematically, the RITP process can be divided into two periods (Scheme 1). A first induction period during which the radicals produced by a radical initiator will react with iodine or propagate with very few monomer units before reacting with iodine. Then, when all the iodine has been consumed, the polymerization period starts. During this second period, the polymerization is governed by transfer to the A-I adduct and degenerative transfer to dormant chains. So, when using a symmetrical initiator (e.g. AIBN), one molecule of iodine is

Downloaded by CORNELL UNIV on June 1, 2012 | http://pubs.acs.org
Publication Date (Web): March 20, 2012 | doi: 10.1021/bk-2012-1100.ch021

able to control two polymer chains and the targeted molecular weight (excluding the contribution of the chain-ends) is given by Equation 1 (where $m_{monomer,0}$ is the initial mass of monomer and $n_{I2,0}$ the initial number of moles of iodine).

$$M_{n,targeted} = (m_{monomer,0}) / (2 \times n_{I2,0}) \qquad \text{(Eq. 1)}$$

We have tested this process with several classes of monomers and it happens that RITP is a very cheap and straightforward method to control the molecular weight and the structure of polymers such as styrenics, methacrylates, acrylates, and vinylidene halides.

One important feature of RITP is that it can also be conducted in emulsion starting with sodium iodide as control agent (*3*). Indeed, iodide ions are oxidized by persulfate to produce molecular iodine. Persulfate also produces some radicals which can propagate and the propagating radicals will be controlled by the molecular iodine produced *in situ*. In this system, we could obtain a living PBuA latex which could be chain extended with styrene to produce a block copolymer latex.

Regarding the kinetics of RITP, in theory, the induction period is the time needed to produce enough radicals to consume all the iodine. The theoretical duration of this induction period (during which the monomer conversion remains low provided that the targeted degree of polymerization is high enough) (*6*) is given by Equation 2 (where $[I_2]_0$ stands for the initial concentration of iodine, f is the initiator efficiency, $[\text{Initiator}]_0$ is the initial concentration of initiator and $k_{d,initiator}$ is the dissociation rate constant of the initiator) (*1*).

$$t_{induction\ period} = -\text{Ln}\ [1-([I_2]_0/(f\times[\text{Initiator}]_0))]/k_{d,initiator} \qquad \text{(Eq. 2)}$$

In the case of RITP of methyl acrylate, the induction period is very clear and its duration is in good agreement with the theoretical prediction given by Equation 2 (Figure 1). So, it confirms that the radicals favorably react with iodine. This is due to a nearly diffusion-controlled reaction of radicals with iodine (*2*). Importantly, for practical reasons, the induction period can be shortened. For instance, by increasing the temperature and thus the k_d of the initiator (*7*), the polymerization of butyl acrylate could be performed in 1h (at T=95°C) instead of 24 hours (at T=65°C), while still keeping a good control of the molecular weight (Table 1). Regarding the case of methyl methacrylate, we have found a very similar behavior during the induction period. Indeed, the duration of the induction period is well-predicted by the theoretical Equation 2.

In contrast, in the case of styrene, the experimental induction time $t_{ind,exp}$ was much shorter than the theoretical one $t_{ind,theo}$ predicted by Equation 2 (Figure 2). We have identified that the reversible formation of (1,2-diiodoethyl)benzene could be the reason for this shorter induction period (*8*). Indeed, the instantaneous concentration of free iodine is decreased because some iodine is temporarily transformed into (1,2-diiodoethyl)benzene. Actually, by using a numerical simulation (PREDICI software) and adapting the model previously elaborated for RITP of acrylates (*9*), we were promisingly able to match the experimental values by introducing this new reaction between styrene and iodine into the model (Figure 2, the simulation gives the dotted and solid lines; $t'_{ind,theo(PREDICI)} \cong t_{ind,exp}$).

Downloaded by CORNELL UNIV on June 1, 2012 | http://pubs.acs.org
Publication Date (Web): March 20, 2012 | doi: 10.1021/bk-2012-1100.ch021

Downloaded by CORNELL UNIV on June 1, 2012 | http://pubs.acs.org
Publication Date (Web): March 20, 2012 | doi: 10.1021/bk-2012-1100.ch021

Table 1. RITP of n-butyl acrylate (80% w/v versus butyl acetate) with $[AIBN]_0/[I_2]_0=1.9$

Run	*T (°C)*	$t_{loss\ of\ coloration}$	$t_{induction,theo}$[a]	t_{polym}	*Conv. (%)*[b]	$M_{n,theo}$ $(g.mol^{-1})$[c]	$M_{n,exp}$ $(g.mol^{-1})$[d]	M_w/M_n
1	65	>15h	20h 25min	24h	97	10 300	12 000	2.14
2	85	1h 40min	1h 34min	5h	95	9 500	9 700	1.83
3	95	30min	29min	1h	95	9 200	8 300	1.85

[a] Estimated by $t_{induction\ period}=-Ln[1-([I_2]_0/(f\times[AIBN]_0))]/k_{d,AIBN}$ (with f=0.7). [b] Determined by ^1H NMR. [c] Calculated by $M_{n,theo}$=(mass of monomer)× conversion/(2×(moles of I_2)) + M_{A-I} where $M_{A-I}=M_{chain-ends}=195$ g.mol^{-1}. [d] Determined by size exclusion chromatography with polystyrene calibration.

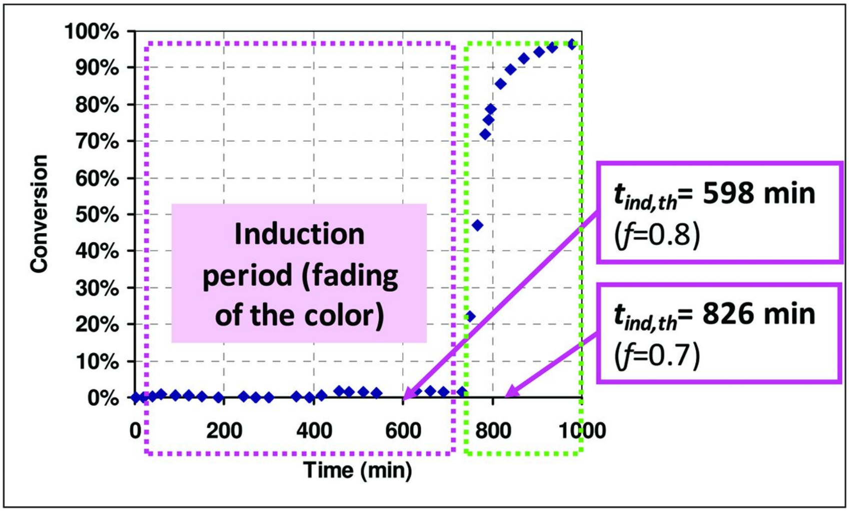

Figure 1. Evolution of monomer conversion versus time for the polymerization of methyl acrylate ($[methyl\ acrylate]_0=5.47M$, $[C_6D_6]_0=5.70\ M$) by reverse iodine transfer polymerization (RITP) initiated by 2,2'-azobis(isobutyronitrile) (AIBN) at T=70 °C ($k_{d,AIBN}=3.70\times10^{-5}\ s^{-1}$): $[AIBN]_0=3.78\times10^{-2}$ M and $[I_2]_0=2.22\times10^{-2}$ M. The duration of the induction period is estimated by $t_{induction\ period}=-Ln[1-([I_2]_0/(f\times[AIBN]_0))]/k_{d,AIBN}$.

Downloaded by CORNELL UNIV on June 1, 2012 | http://pubs.acs.org
Publication Date (Web): March 20, 2012 | doi: 10.1021/bk-2012-1100.ch021

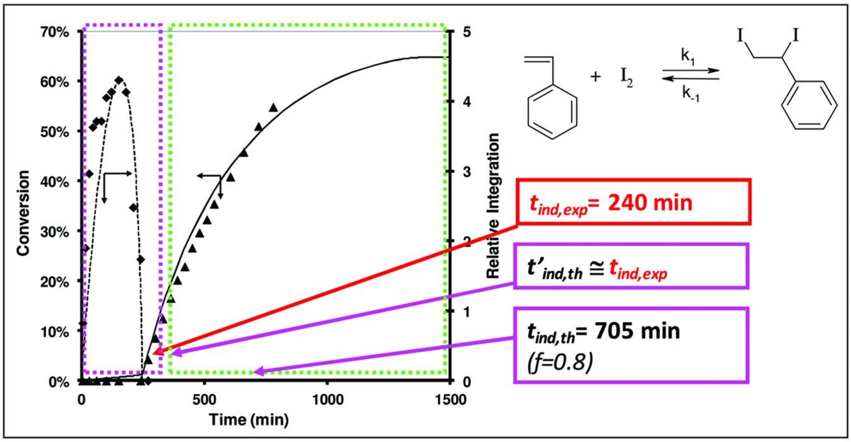

Figure 2. Evolution of monomer conversion (%) and the concentration of A-I adduct (i.e. $(CH_3)_2(CN)C$-I) (arbitrary unit) versus time in the polymerization of styrene by RITP at T=70°C ([Styrene] = 4.45M, $[C_6D_6]$ = 5.9M; $[I_2]$ = 2.2×10^{-2}M, [AIBN] = 3.49×10^{-2}M). Lines correspond to simulation with PREDICI software with $K_c = k_1/k_{-1} = 0.255$ L.mol^{-1}; $\alpha = 0.3$ (where α stands for the order of reaction relative to iodine) and $k_1 = 2.5\times10^{-6}$ L.mol^{-1}.s^{-1}.

Concerning the polymerization period, it is essentially governed by degenerative transfer to dormant chains P-I, for which typical evolution of M_n and PDI=M_w/M_n is given by Equation 3 and Equation 4, respectively (where ρ is the fractional conversion of monomer, $[M]_0$ is the initial concentration of monomer, $M_{monomer}$ is the molecular weight of the monomer, [P-I] is the concentration of the dormant chains and $C_{ex}=k_{ex}/k_p$ is the degenerative chain transfer constant) (*2*, *10*).

$$M_n=(\rho[M]_0M_{monomer})/([P\text{-}I](1-(1-\rho)^{Cex})) \qquad \text{(Eq. 3)}$$

$$PDI=(1+([M]_0/[P\text{-}I])(2+(2-\rho)(1-C_{ex})/C_{ex}))/(\rho[M]_0/([P\text{-}I](1-(1-\rho)^{Cex}))) \qquad \text{(Eq. 4)}$$

Note that Equation 3 and Equation 4 apply to RITP of methyl acrylate and methyl methacrylate but not to RITP of styrene. In the case of styrene, the additional reversible reaction between styrene and iodine to form (1,2-diiodoethyl)benzene makes the system more complex for analytical equations of M_n and PDI versus monomer conversion and it is beyond the scope of this article.

In addition to the control of the molecular weight, one important thing in controlled radical polymerization (or reversible-deactivation radical polymerization as recommended term by IUPAC) (*11*) is the proportion of living chains, i.e. the iodine functionality of the chains. Figure 3 shows a typical result for PMeA chains prepared by RITP. As in a previous publication (*1*), SEC values were obtained using the Mark-Houwink coefficients of polystyrene (K=11.4×10^{-5} dL.g^{-1}, alpha=0.716) and poly(methyl acrylate) (K=19.5×10^{-5} dL.g^{-1}, alpha=0.660). The structure of the polymer chains was confirmed by

MALDI-TOF MS analysis. The ^1H NMR spectrum shows a signal at 4.2 ppm attributed to the iodine functional chain-end. From these data and considering the value of $M_{n,SEC}$ as the reference, one can estimate that about 97% of the chains bear an iodine atom at the chain-end.

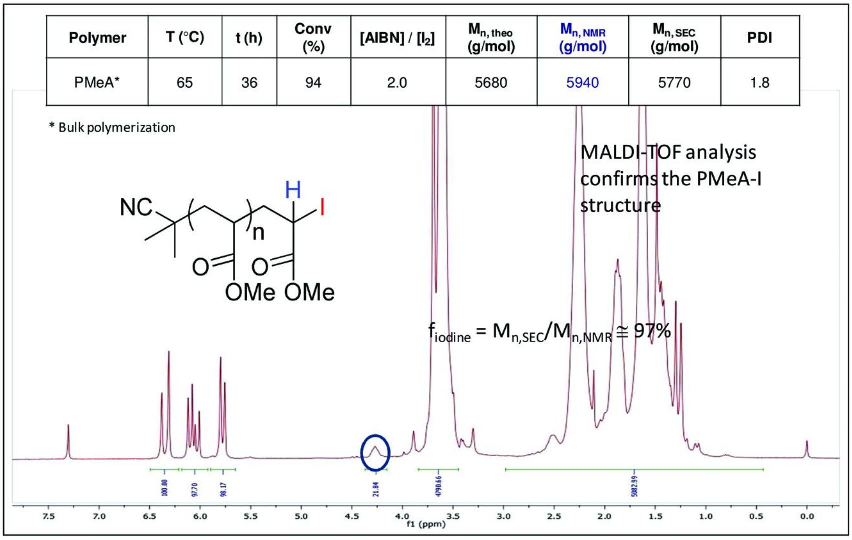

Polymer	T (°C)	t (h)	Conv (%)	[AIBN] / [I_2]	$M_{n, theo}$ (g/mol)	$M_{n, NMR}$ (g/mol)	$M_{n, SEC}$ (g/mol)	PDI
PMeA*	65	36	94	2.0	5680	5940	5770	1.8

* Bulk polymerization

MALDI-TOF analysis confirms the PMeA-I structure

$f_{iodine} = M_{n,SEC}/M_{n,NMR} \cong 97\%$

Figure 3. Characteristics of a poly(methyl acrylate) sample prepared by RITP of methyl acrylate in bulk at T=65°C.

In the case of styrene, the ESI-TOF MS analysis confirmed the presence of the iodinated polymer chains, but the chains undergo a major degradation during the analysis (*12*). Figure 4 shows an example of PS sample prepared by RITP. ^1H NMR spectrum shows a signal at 4.6 ppm attributed to the iodinated chain-end. Considering the experimental value of $M_{n,SEC}$ as the reference, a chain-end fidelity of 91% is obtained. During RITP of styrene, (1,2-diiodoethyl)benzene can act as a chain transfer agent leading to a dormant chain and a I-CH_2-CH(Ph)$^•$ radical. This radical however seems not prone to initiate the polymerization since we did not observe the corresponding I-M_n-I polymer structure by ESI-TOF MS analysis. Therefore, we assume that this radical is very unstable and decomposes instantaneously to styrene and iodine radical $I^•$.

In the case of poly(methyl methacrylate), as in the case of PS, the MALDI-TOF MS analysis also damages the polymer chains (*13*). On the ^1H NMR spectrum, the signal at 2.9 ppm is attributed to the two protons in beta position to the iodinated chain-end (Figure 5). From these results and considering the value of $M_{n,SEC}$ as the reference, a chain-end fidelity of about 86% is obtained. More importantly, in contrast to PMeA-I and PS-I, the stability of the PMMA-I chain-end seems to be a bigger issue. Actually, according to our latest results (*14*), the iodine functionality of PMMA chains decreased drastically when the monomer conversion increased (Figure 6). Some possible degradation reactions are elimination reaction or formation of lactone. A deeper investigation of the

Downloaded by CORNELL UNIV on June 1, 2012 | http://pubs.acs.org
Publication Date (Web): March 20, 2012 | doi: 10.1021/bk-2012-1100.ch021

degradation scheme would deserve attention. Anyway, for sure it is much easier to obtain a highly functional ω-iodo PBuA or PS than PMMA.

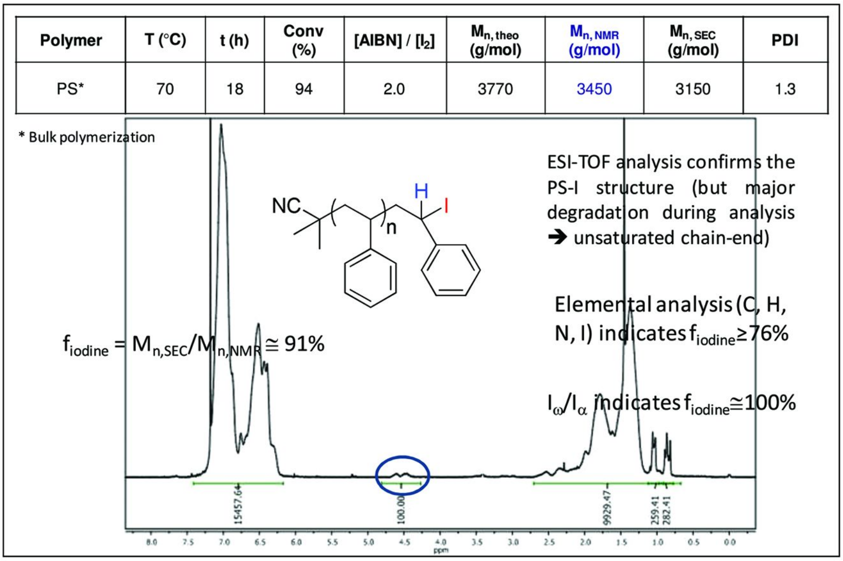

Polymer	T (°C)	t (h)	Conv (%)	[AIBN] / [I_2]	$M_{n,theo}$ (g/mol)	$M_{n,NMR}$ (g/mol)	$M_{n,SEC}$ (g/mol)	PDI
PS*	70	18	94	2.0	3770	3450	3150	1.3

* Bulk polymerization

$f_{iodine} = M_{n,SEC}/M_{n,NMR} \cong 91\%$

ESI-TOF analysis confirms the PS-I structure (but major degradation during analysis ➔ unsaturated chain-end)

Elemental analysis (C, H, N, I) indicates $f_{iodine} \geq 76\%$

I_ω/I_α indicates $f_{iodine} \cong 100\%$

Figure 4. Characteristics of a polystyrene sample prepared by RITP of styrene in bulk at T=70°C.

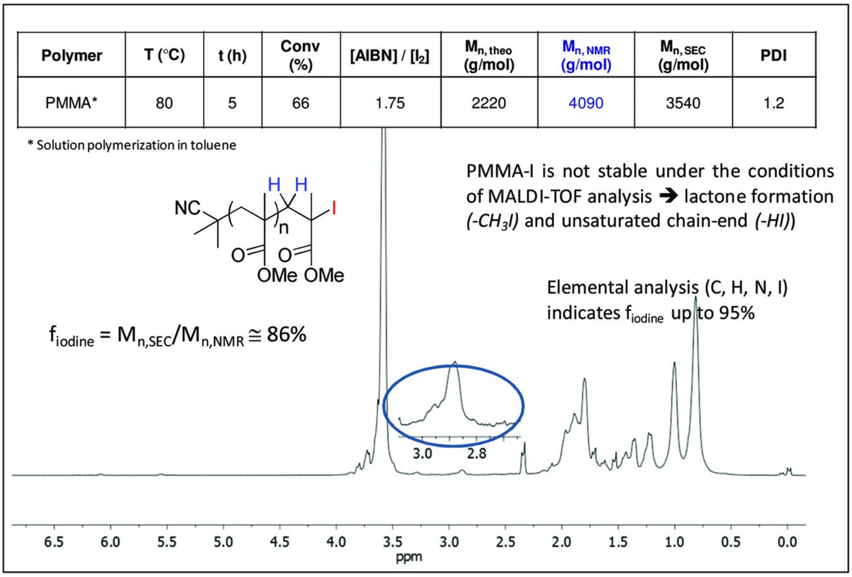

Polymer	T (°C)	t (h)	Conv (%)	[AIBN] / [I_2]	$M_{n,theo}$ (g/mol)	$M_{n,NMR}$ (g/mol)	$M_{n,SEC}$ (g/mol)	PDI
PMMA*	80	5	66	1.75	2220	4090	3540	1.2

* Solution polymerization in toluene

$f_{iodine} = M_{n,SEC}/M_{n,NMR} \cong 86\%$

PMMA-I is not stable under the conditions of MALDI-TOF analysis ➔ lactone formation *($-CH_3I$)* and unsaturated chain-end *($-HI$)*)

Elemental analysis (C, H, N, I) indicates f_{iodine} up to 95%

Figure 5. Characteristics of a poly(methyl methacrylate) sample prepared by RITP of methyl methacrylate in toluene at T=80°C.

Downloaded by CORNELL UNIV on June 1, 2012 | http://pubs.acs.org
Publication Date (Web): March 20, 2012 | doi: 10.1021/bk-2012-1100.ch021

Downloaded by CORNELL UNIV on June 1, 2012 | http://pubs.acs.org
Publication Date (Web): March 20, 2012 | doi: 10.1021/bk-2012-1100.ch021

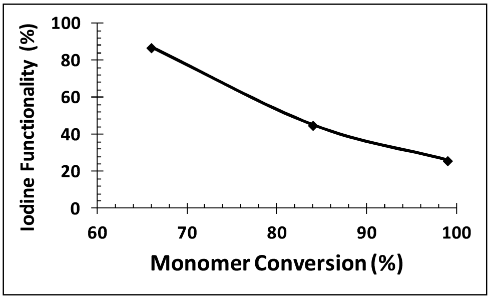

Figure 6. Evolution of the iodine functionality versus monomer conversion for poly(methyl methacrylate) prepared by RITP of methyl methacrylate in toluene at T=80°C ($M_{n,targeted}$≅3000 g/mole) (low PDI≤1.2 were obtained in all cases).

Since the RITP process requires a radical initiator, one can wonder whether a difunctional initiator can be used. To address this question, we have used a Trigonox difunctional initiator (T141) (Figure 7) (*15*). This initiator can dissociate into three fragments. In the RITP process, these fragments could lead to two monofunctional chains and one difunctional chain. By assigning the apparent coefficients of efficiency, α and β, to these fragments in the RITP process, the M_n can now be calculated by Equation 5.

$$M_{n,theoretical,\alpha,\beta}=(m_{monomer,0}\times\rho)/(((2\alpha+\beta)/2)\times n_{I_2,0}) \qquad \text{(Eq. 5)}$$

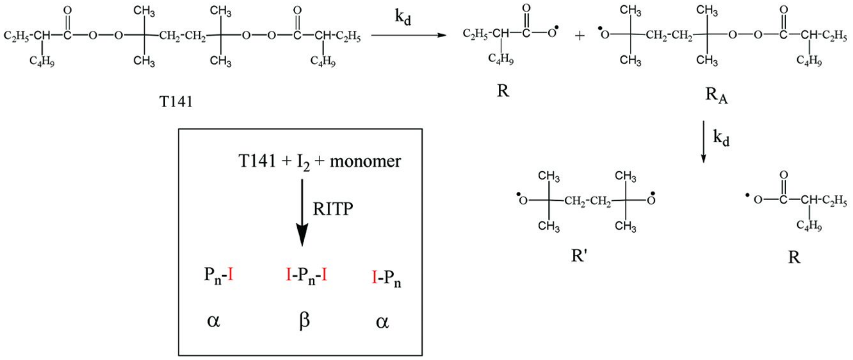

Figure 7. Structure and decomposition scheme of the difunctional initiator T141 used in RITP of styrene and methyl methacrylate.

Downloaded by CORNELL UNIV on June 1, 2012 | http://pubs.acs.org
Publication Date (Web): March 20, 2012 | doi: 10.1021/bk-2012-1100.ch021

To determine the coefficients α and β, two monofunctional initiators were used (lauroyl peroxide and Perkadox16S, respectively) leading to fragments with structural characteristics approaching those of the fragments from T141 decomposition. Bulk polymerizations were performed at 73°C and 59°C for LYP and P16S, respectively, and at a ratio [radical initiator]/[I_2] close to 1.8. The values were calculated by $\alpha = (m_{monomer,0} \times \rho)/(2 \times M_{n,SEC} \times n_{I_2,0})$ (with lauroyl peroxide) and $\beta = (m_{monomer,0} \times \rho)/(2 \times M_{n,SEC} \times n_{I_2,0})$ (with Perkadox 16S). Then, the so-obtained α and β values (α=0.41 and β=1 for styrene, α=0.14 and β=0.75 for methyl methacrylate) were successfully applied using Equation 5 to predict the molecular weights of PS and PMMA prepared by RITP initiated by the difunctional initiator T141 (Table 2). In both cases, a high conversion was reached and a good agreement was obtained between theoretical and experimental molecular weights. Interestingly, since some of the chains are difunctional, such polymers open the route to the synthesis of multiblock copolymers by either block copolymerization or coupling techniques. As α cannot be neglected, however, this means that a proportion of diblock copolymers would also be formed during the synthesis of a triblock copolymer in two steps. Similarly, a multiblock copolymer strategy would also be affected by these mono-iodinated polymer chains and this might have implications on the formation of the nanodomains involved in thermoplastic elastomer applications.

Table 2. RITP of styrene and methyl methacrylate in bulk with T141 as difunctional initiator at T=80°C ([T141]/[I_2]=1)

Run	*Monomer*	$M_{n,targ,\alpha,\beta}$ *(g. mol^{-1})*[a]	*Conv. (%)*[b]	$M_{n,theo,\alpha,\beta}$ *(g.mol^{-1})*[c]	$M_{n,exp}$ *(g.mol^{-1})*[d]	M_w/M_n
1	Styrene	20 530	98	20 120	20 600	1.5
2	MMA	34 850	93	32 150	28 870	1.7

[a] Calculated by $M_{n,targ,\alpha,\beta}$= (mass of monomer)/[((2α+β)/2) × (moles of I_2)]; [b] Determined by ^{1}H NMR; [c] Calculated by $M_{n,Theoretical,\alpha,\beta}$= (mass of monomer × ρ/[((2α+β)/2) × (moles of I_2)]; [d] Obtained by SEC analysis on the crude product.

Macromolecular Engineering

The interest in iodinated polymers prepared by RITP is that they can easily be used for macromolecular engineering. Indeed, thanks to the richness of the chemistry of iodinated compounds, they can undergo many reactions such as substitution reactions, further radical polymerization, or combination with other living polymerizations (Figure 8). Some of our studies focused on the preparation of polymeric surfactants and nanostructured polymers such as thermoplastic elastomers.

Downloaded by CORNELL UNIV on June 1, 2012 | http://pubs.acs.org
Publication Date (Web): March 20, 2012 | doi: 10.1021/bk-2012-1100.ch021

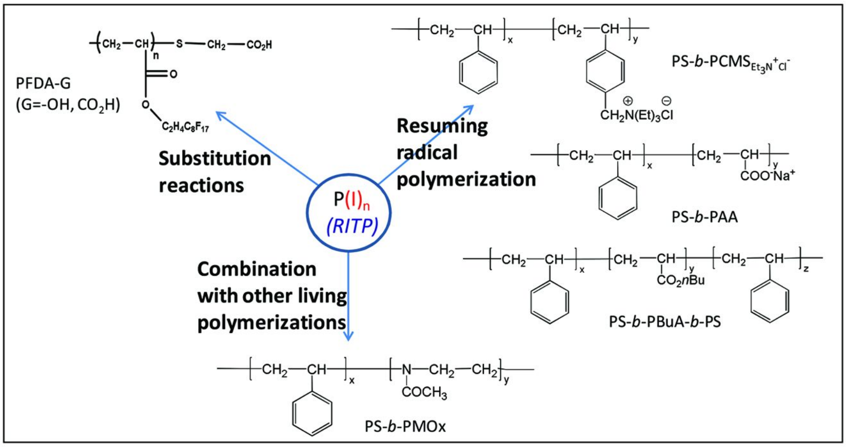

Figure 8. Macromolecular engineering from RITP-derived polymers.

Substitution Reaction

Fluoropolymers were synthesized by RITP of 1,1,2,2-tetrahydroperfluorodecyl acrylate (FDA) (*6*). The substitution reaction of the iodide chain-end with thiols was performed to prepare PFDA bearing a polar end-group. For instance, mercaptoacetic acid was used to afford a carboxylic acid $–CO_2H$ functionalized PFDA (Figure 9). The substitution reaction was executed at T=35°C in a trifluorotoluene/dimethylformamide mixture in the presence of K_2CO_3 to form the nucleophilic reactive thiolate. The structure of the resulting polymer was confirmed by MALDI-TOF MS analysis (M_n=7700 $g.mol^{-1}$, M_w/M_n=1.12). This leads a polymeric surfactant for applications in liquid or supercritical CO_2 (*16*) since the fluorinated tail is CO_2-philic while the polar head group is CO_2-phobic. Any other “iodo-click-chemistry” (i.e. click chemistry involving iodo-compounds represented here by the dormant chains $P(I)_n$) would also be applicable to build new architectures with potentially innovative properties.

Polymeric trithiocarbonates were also prepared from RITP-derived polymers. Thus, iodo-terminated polystyrene PS-I were reacted with Cs_2CO_3/CS_2 in acetonitile at T=40°C to afford PS-SC(S)S-PS polystyrene trithiocarbonates (*17*). However, the reaction yield decreased steadily with the molecular weight of the PS-I precursor, as usual in such coupling reactions between polymeric reactants.

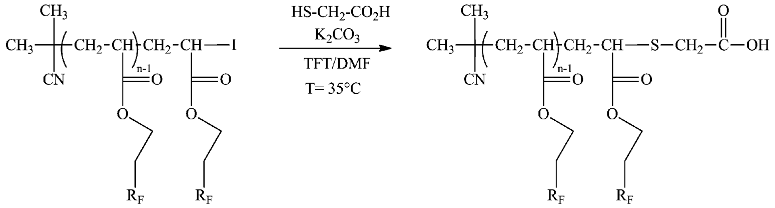

Figure 9. Chain-end substitution reaction on a poly(1,1,2,2-tetrahydroperfluorodecyl acrylate) sample prepared by reverse iodine transfer polymerization.

Downloaded by CORNELL UNIV on June 1, 2012 | http://pubs.acs.org
Publication Date (Web): March 20, 2012 | doi: 10.1021/bk-2012-1100.ch021

Block Radical Polymerization

Resuming radical polymerization from iodinated polymers prepared by RITP, $P(I)_n$, also affords the possibility of preparing block copolymers to serve in soft matter (e.g. macromolecular surfactants) or in nanostructured materials (e.g. thermoplastic elastomers).

Thus, cationic amphiphilic diblock copolymers PS-*b*-$PCMS_{Et3N+Cl-}$ (Figure 10) can be prepared by iodine transfer polymerization (ITP) of chloromethylstyrene (CMS) with AIBN radical initiator from a PS-I macromolecular transfer agent prepared by RITP, followed by quaternization with an amine (*18*).

Similarly, ionogenic (neutral/anionic) amphiphilic diblock copolymers PS-*b*-PAA can be easily prepared by iodine transfer polymerization (ITP) of tert-butyl acrylate with AIBN radical initiator from a PS-I macromolecular transfer agent prepared by RITP, followed by deprotection of the PtBuA block with trifluoroacetic acid (*19*).

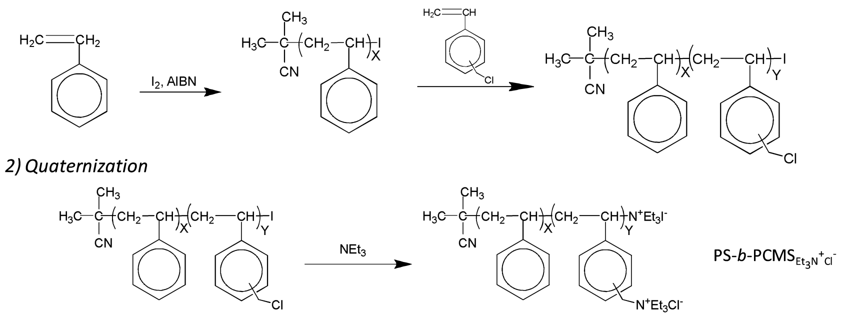

Figure 10. Synthesis of PS-I by RITP of styrene and PS-b-$PCMS_{Et3N+Cl-}$ by ITP of chloromethylstyrene and quaternization.

Some interesting preliminary results were also obtained from polymers prepared by RITP with the difunctional initiator T141. For instance, a hard-soft-hard triblock copolymer ($M_{n,SEC}$= 73 100 g.mol^{-1}, M_w/M_n=1.7) was synthesized by ITP of styrene starting from a poly(butylacrylate-*co*-styrene) precursor ($M_{n,SEC}$= 46 400 g.mol^{-1}, M_w/M_n=1.6) previously synthesized by RITP of butyl acrylate/styrene 95/5 w/w with T141 initiator (*20*). Thus, RITP with difunctional initiators opens the route to the design of copolymers which could serve as thermoplastic elastomers.

Combination with Other Living Polymerizations

The combination of RITP with other living radical polymerizations is also an attractive pathway. For instance, we were interested in the preparation of an amphiphilic non-ionic block copolymer of PS and PMOx, where PMOx can compete with the extensively studied poly(ethylene oxide) polymers. To this aim, we have investigated the polymerization of styrene by RITP followed by the cationic ring-opening polymerization (CROP) of 2-methyl 2-oxazoline (MOx) (Figure 11). The advantage of this strategy in comparison with other routes is that it is an all iodine route: it does not require the modification of the chain-end between the two stages of polymerization. Thus, RITP of styrene was performed in bulk at 70°C (styrene conversion = 95%, $M_{n,SEC}$=2 200 g.mol^{-1}, M_w/M_n=1.4) followed directly by CROP of MOx at 80°C in DMF (MOx conversion = 100%) (*21*). Regarding the mechanism of CROP, it is mainly reported as an ionic mechanism although a covalent mechanism is also possible. After a selective precipitation of the copolymer in diethyl ether and methanol, the size exclusion chromatogram confirmed the formation of the block copolymer ($M_{n,SEC}$=4 200 g.mol^{-1}, M_w/M_n=1.8) albeit a residual impurity was still present at lower molecular weight. This minor side-product was assigned to the formation of PMOx homopolymer, possibly due to transfer to monomer. So, RITP offers the feasibility of directly merging with CROP to synthesize amphiphilic copolymers.

Downloaded by CORNELL UNIV on June 1, 2012 | http://pubs.acs.org
Publication Date (Web): March 20, 2012 | doi: 10.1021/bk-2012-1100.ch021

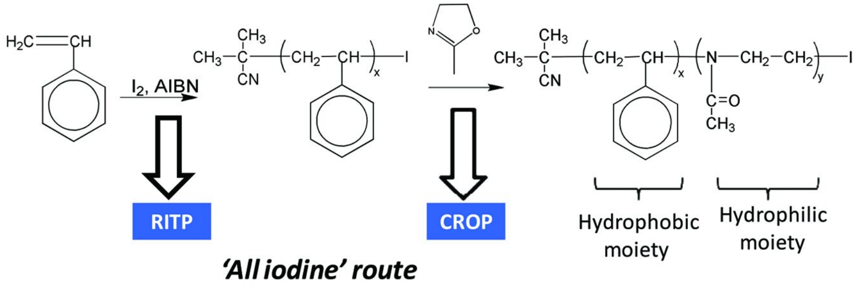

Figure 11. Synthesis of PS-b-PMOx by RITP of styrene and CROP of 2-methyl 2-oxazoline (the end-group in CROP can also be in the form of an oxazolinium species).

Conclusion

RITP is an easy-to-make and flexible method. It can be performed in bulk, solution and even emulsion polymerization. Styrenics have a peculiar behavior in RITP because the monomer interacts with iodine, leading to induction time shorter than expected. The stability of the iodo chain-end is very good for acrylates, good for styrenics, but might be an issue for methacrylates. Difunctional initiators can be used in RITP to prepare telechelic polymers. Finally, by playing with the very wide range of chemical reactions relevant to iodo-compounds, all these iodinated polymers easily prepared by RITP can be used to prepare useful architectures such as amphiphilic copolymers and thermoplastic elastomers. Thus, RITP proves to be a versatile and efficient method as a starting point for macromolecular engineering. It is undoubtedly a promising tool for polymer chemists both in academics and industry.

Acknowledgments

The authors of this paper thank the French Ministry of Research and the CONACYT (Consejo Nacional de Ciencia y Tecnologia, Mexico) for grants as well as CID and the Scientific Council of University Montpellier II (UM2) for their financial support of this research. The authors also thank the colleagues who took part in the studies on RITP (R. Severac, B. Boutevin, J. Tonnar, S. Clerc, C. Boyer, R. Guerrero-Santos, F.J. Enriquez-Medrano, B. Patra, C. Ladavière, F. Delolme) and CROP (V. Lapinte).

Downloaded by CORNELL UNIV on June 1, 2012 | http://pubs.acs.org
Publication Date (Web): March 20, 2012 | doi: 10.1021/bk-2012-1100.ch021

References

1. Lacroix-Desmazes, P.; Severac, R.; Boutevin, B. *Macromolecules* **2005**, *38*, 6299–6309.
2. Lacroix-Desmazes, P.; Tonnar, J.; Boutevin, B. *Macromol. Symp.* **2007**, *248*, 150–157.
3. Tonnar, J.; Lacroix-Desmazes, P. *Angew. Chem.* **2008**, *47*, 1294–1297.
4. Tonnar, J.; Lacroix-Desmazes, P. *Soft Matter* **2008**, *4*, 1255–1260.
5. Lacroix-Desmazes, P.; Tonnar, J. *Compr. Polym. Sci., 2nd Suppl.* **2012**, *3*, in press.
6. Clerc, S.; Tonnar, J.; Lacroix-Desmazes, P. *Polym. Prepr. (Am. Chem. Soc., Div. Polym. Chem.)* **2008**, *49*, 64–65.
7. Van Hook, J. P.; Tobolsky, A. V. *J. Am. Chem. Soc.* **1958**, *80*, 779–82.
8. Tonnar, J.; Severac, R.; Lacroix-Desmazes, P.; Boutevin, B. *Polym. Prepr. (Am. Chem. Soc., Div. Polym. Chem.)* **2008**, *49*, 68–69.
9. Tonnar, J.; Severac, R.; Lacroix-Desmazes, P.; Boutevin, B. *Polym. Prepr. (Am. Chem. Soc., Div. Polym. Chem.)* **2008**, *49*, 187–188.
10. David, G.; Boyer, C.; Tonnar, J.; Ameduri, B.; Lacroix-Desmazes, P.; Boutevin, B. *Chem. Rev.* **2006**, *106*, 3936–3962.
11. Jenkins, A. D.; Jones, R. G.; Moad, G. *Pure Appl. Chem.* **2010**, *82*, 483–491.
12. Ladaviere, C.; Lacroix-Desmazes, P.; Delolme, F. *Macromolecules* **2009**, *42*, 70–84.

13. Boyer, C.; Lacroix-Desmazes, P.; Robin, J.-J.; Boutevin, B. *Macromolecules* **2006**, *39*, 4044–4053.
14. Lacroix-Desmazes, P.; Rayeroux, D.; Villa-Hernandez, A. M. *Polym. Prepr. (Am. Chem. Soc., Div. Polym. Chem.)* **2011**, *52*, 582–583.
15. Villa-Hernandez, A. M.; Enrique-Medrano, F. J.; Guerrero-Santos, R.; Lacroix-Desmazes, P. *Polym. Prepr. (Am. Chem. Soc., Div. Polym. Chem.)* **2011**, *52*, 590–591.
16. Ma, Z.; Lacroix-Desmazes, P. *J. Polym. Sci., Part A: Polym. Chem.* **2004**, *42*, 2405–2415.
17. Enriquez-Medrano, F.; Garza-Ordaz, J. C.; Cabello-Romero, J.; Maldonado-Texle, H.; Hernandez-Valdez, M.; Lacroix-Desmazes, P.; Guerrero-Santos, R. *Polym. Prepr. (Am. Chem. Soc., Div. Polym. Chem.)* **2011**, *52*, 681–682.
18. Patra, B. N.; Rayeroux, D.; Lacroix-Desmazes, P. *React. Funct. Polym.* **2010**, *70*, 408–413.
19. Patra, B. N.; Lacroix-Desmazes, P. *Polym. Prepr. (Am. Chem. Soc., Div. Polym. Chem.)* **2008**, *49*, 345–346.
20. Enriquez-Medrano, F. J.; Guerrero-Santos, R.; Hernandez-Valdez, M.; Lacroix-Desmazes, P. *J. Appl. Polym. Sci.* **2011**, *119*, 2476–2484.
21. Rayeroux, D.; Lapinte, V.; Lacroix-Desmazes, P. *Polym. Prepr. (Am. Chem. Soc., Div. Polym. Chem.)* **2011**, *52*, 665–666.

Downloaded by CORNELL UNIV on June 1, 2012 | http://pubs.acs.org
Publication Date (Web): March 20, 2012 | doi: 10.1021/bk-2012-1100.ch021

Downloaded by 89.163.35.42 on May 30, 2012 | http://pubs.acs.org
Publication Date (Web): March 20, 2012 | doi: 10.1021/bk-2012-1100.ix002

Subject Index

A

Acrylate terminal chain ends fraction, 57*f*
Acrylates ATRP branching, 150*t*, 153*t*, 157*f*, 158*f*, 160*f*, 161*f*, 162*f*
Acrylates FRP branching, 152*t*, 153*t*, 156*f*
Activators regenerated by electron transfer (ARGET), 172
Active chain fraction, styrene terminal, 57*f*
Active species generation, 129*s*
AIBN concentration, *Ultimate ATRP*^{SM}, 207*f*
Alkyl iodide, 308*f*, 312
Aqueous RAFT/MADIX polymerization
  DADMAC, 272, 273*f*, 273*t*
  NVP, 267, 267*s*, 268*t*, 269*f*
  O-ethyl-S-(1-carboxy)methyl dithiocarbonate synthesis, 261
  overview, 259
  PVP, 271*f*, 272*t*
  VPA, 261, 262, 262*s*, 263*s*, 264*t*, 265*f*, 266*f*
Aqueous soluble switchable RAFT agent, 246*s*
ARGET. *See* activators regenerated by electron transfer (ARGET)
ARGET ATRP mechanism, 184*f*
Aryl trithiocarbonate RAFT agent, 248*s*
Atom transfer radical addition (ATRA), 44, 133, 134*s*
Atom transfer radical polymerization (ATRP)
  catalase, 177
  hemoglobin, 173
  hemoglobin-catalyzed polymerization, 174*f*
  horseradish peroxidase, 173, 177
  horseradish peroxidase-catalyzed polymerization, 174*f*, 176*f*, 177*f*
  laccase, 177
  overview, 171
  PEGA polymerizations, 178*f*
ATRA. *See* Atom transfer radical addition (ATRA)
ATRP. *See* Atom transfer radical polymerization (ATRP)

B

BA. *See* butyl acrylate (BA)
Benzene ring, 23*f*
Block copolymers, organic semiconductors, 250
BMA. *See* butyl methacrylate (BMA)
BMA vs. BA, 197
Bromopropionitrile (BPN), 177
Bulky methacrylates, free-radical polymerization
  benzene ring, 23*f*
  inherent tacticity, 19
    conformational analysis, 25
    π-stacking interactions, 27
    steric effects, 23
  isotactic poly(MMA), 27*f*
  isotactic trimeric poly(PhMA), 30*f*
  meso propagation, 18*s*, 20*f*, 21*t*, 24*f*, 25*f*
  monomers, 22*s*
  overview, 15
  PhMA, trimeric growing chains, 29*f*
  poly(FMA), 30*f*
  polymer tacticity nomenclature, 17*s*
  racemo propagation, 18*s*
  stereocontrol strategies, 16*s*
  syndiotactic poly(MMA), 26*f*
  trimeric poly(MMA) propagating radical, 19*f*
Butyl acrylate (BA)
  ARGET ATRP, 197*t*, 198*f*, 198*t*, 200*f*
    analytical methods, 187
    decreased catalyst effect, 189
    initiator loading, 187
    materials, 186
    overview, 183
    procedure, 186
    varying catalyst effect, 192
  MMD, 199*f*
Butyl methacrylate (BMA)
  ARGET ATRP, 188*f*, 188*t*, 190*f*, 190*t*, 192*t*, 193*f*, 194*f*, 195*f*, 197*t*, 198*f*
    analytical methods, 187
    decreased catalyst effect, 189
    initiator loading, 187
    materials, 186
    overview, 183
    procedure, 186
    varying catalyst effect, 192
  MMD, 189*f*, 195*f*

Downloaded by 89.163.35.42 on May 30, 2012 | http://pubs.acs.org
Publication Date (Web): March 20, 2012 | doi: 10.1021/bk-2012-1100.ix002

C

Carbon nanotubes, radical coupling, 219, 225, 227*f*
Catalase, 177
Catalytic activity (K_{ATRP}), 103
Cationic ring-opening polymerization (CROP), 319
Click chemistry classification, 74*f*
C/LRP. *See* controlled/living radical polymerization (C/LRP)
CMRP. *See* cobalt-mediated radical polymerization (CMRP)
Cobalt-mediated radical polymerization (CMRP)
  carbon nanotubes, radical coupling, 219, 225, 227*f*
  conjugated dienes, radical coupling, 218, 220
  CuAAC, 224*f*
  diblock graft copolymers, 226*f*
  fullerenes, radical coupling, 219
  nitrones, radical coupling, 219, 223
  overview, 217
  triblock copolymer, 221*f*
Conjugated dienes, radical coupling, 218, 220
Controlled radical polymerization (CRP)
  2011 state-of-the-art, 1
    new challenges, 8
    recent progress, 6
  aqueous media, 8
  commercialization, 9
  competing equilibria, 8
  energy and environment, 9
  monomer, polymerization time, 5*f*
  monomer conversion, 8
  orthogonal chemistry, functional groups, 9
  SciFinder search results, 3*f*
  smart-responsive systems, 9
  universal mediating agents, 9
Controlled/living radical polymerization (C/LRP), 60
Conventional radical copolymerization simulation, 52*t*
Copper-catalyzed azide-alkyne [3+2] cycloaddition (CuAAC)
  ATRA, 75, 87*s*, 88*t*, 89*t*, 90*t*, 91*f*, 92*t*
  ATRP, 78*f*, 84*s*, 85*s*
  click chemistry, 82*s*, 84*s*
  ^1H NMR, 93*f*
  HRMS, 93*f*
  macromolecular structures synthesis, 77
    ATRP, click chemistry, 79
    click chemistry, materials/polymer chemistry, 79
  mechanism, 75*s*
  overview, 73
  sequential ATRP, 80*s*, 82*s*
  small molecule synthesis, 86
    functionalized polytriazoles synthesis, 91
    triazolyl alkyl ester-Aryl compound synthesis, 86
  transition metal catalyzed ATRA, 76*s*
Copper-mediated atom transfer radical polymerization
  chain “killing” reactions, 102*f*
  chloridophilicity, 106*f*
  Et_2BrMM, 109*f*
  ethyl 2-bromoisobutyrate, 109*f*
  low catalyst concentration ATRP, 102
    catalytic activity (K_{ATRP}), 103
    catalytically-active complexes, 103
    initiator selection, 108
    polymerization control degree, 103
    reducing agent effect, 106
    solvent selection, 108
  mechanism, 100*f*
  overview, 203
  1-phenylethyl bromide, 108*f*
  poly(glycidyl methacrylate), 107*f*
  TsCl, 110*f*
CuAAC. *See* copper-catalyzed azide-alkyne [3+2] cycloaddition (CuAAC)
CuAAC, ATRA, 75
CuAAC, CMRP, 224*f*
Cu^I activator, 205*f*
Cyanoisopropyl dithiobenzoate, RAFT polymerization, 254*s*

D

DADMAC. *See* diallydimethylammonium chloride (DADMAC)
DEPN-based alkoxyamine, 54*f*
Diallydimethylammonium chloride (DADMAC), 272, 273*f*, 273*t*
Diblock graft copolymers, 226*f*
Diphenylphosphinoyl radical, activation energies, 42*t*
Diphenylphosphinoyl radical, Arrhenius plot, 41*f*
Dithiocarbamate, ATRP, 66*s*
Dithiocarbamate RAFT agents, 245*s*, 246*s*, 247*s*
Divinyl-dichloro compounds, 135, 135*s*

Downloaded by 89.163.35.42 on May 30, 2012 | http://pubs.acs.org
Publication Date (Web): March 20, 2012 | doi: 10.1021/bk-2012-1100.ix002

DMA polymerization, 283*t*, 284*f*
DMAm polymerizations, 246*f*

E

End-group transformation, RAFT polymerization, 253*s*
Ethyl 2-bromoisobutyrate, 109*f*
Ethylenolysis, 128*s*

F

Fullerenes, radical coupling, 219

G

Gel permeation chromatograms, RAFT polymerization, 247*f*

H

Hb. *See* hemoglobin (Hb)
Hemoglobin (Hb), 173
Hemoglobin-catalyzed polymerization, 174*f*
Homobimetallic ruthenium-ethylene complexes, ATRP, 116
  methyl methacrylate polymerisation, 117*t*, 119*f*, 120*t*
  NHC ligand, 117*s*
  styrene cross-metathesis, 118*s*, 118*t*
  tricyclohexylphosphine ligand, 116*s*
  triphenylphosphine ligand, 119*s*
Homobimetallic ruthenium-vinylidene complexes, ATRP, 121, 121*s*
  active species generation, 129*s*
  ethylenolysis, 128*s*
  methyl methacrylate polymerisation, 122*f*, 122*t*, 124*f*, 124*t*
  microwave-assisted syntheses, 128*s*
  ruthenium m-carbide complex, 127*s*
  ruthenium-carbenes, 126*s*
  unsaturated 16-electron ruthenium species, 126*s*
  vinylidene ligand, 121*s*, 123*s*
Homo-telechelic polymer synthesis, 139
Horseradish peroxidase (HRP), 173, 177
HRP. *See* horseradish peroxidase (HRP)
HRP-catalyzed polymerization, 174*f*, 176*f*, 177*f*

I

ICAR. *See* initiators for continuous activator regeneration (ICAR)
Initiators for continuous activator regeneration (ICAR), 172
Isotactic poly(MMA), 27*f*
Isotactic trimeric poly(PhMA), 30*f*

K

K_{ATRP}. *See* catalytic activity (K_{ATRP})
Kinetic model, polymer properties tuning
  acrylates CRP/FRP, 150
  acrylates CRP/FRP branching, 156
  ICAR ATRP, 154, 162

L

Laccase, 177
Low catalyst concentration ATRP, 102
  catalytic activity (K_{ATRP}), 103
  catalytically-active complexes, 103
  initiator selection, 108
  polymerization control degree, 103
  reducing agent effect, 106
  solvent selection, 108

M

MA. *See* methyl acrylate (MA)
Macromolecular structures synthesis, CuAAC, 77
  ATRP, click chemistry, 79
  click chemistry, materials/polymer chemistry, 77
Manganese decacarbonyl/alkyl iodide system, photoinduced controlled radical polymerizations, 70*s*
Meso propagation, bulky methacrylates, 18*s*, 20*f*, 21*t*, 24*f*, 25*f*
Metal-catalyzed step-growth radical polymerization
  ATRP, 134*s*
  divinyl-dichloro compounds, 135, 135*s*
  ^{1}H NMR spectra, 138*f*, 140*f*, 141*f*

  homo-telechelic polymer synthesis, 139
  overview, 133
  polyaddition, 134*s*, 137*t*
  sequence-regulated vinyl copolymers, 140
  toluene, 136*f*, 138*f*, 139*f*
Methyl acrylate (MA), 4
Methyl acrylate, FRcP, 51*s*
Methyl acrylate (MA) polymerization, minimal time, 5*t*
Methyl methacrylate (MMA), 4, 68*f*
  C/LRP, 61*s*
  polymerisation, 117*t*, 119*f*, 120*t*, 122*f*, 122*t*, 124*f*, 124*t*
  polymerization, minimal time, 5*t*
  RCMP, 305
  visible light-induced atom transfer radical polymerization, 69*t*
Microwave-irradiation, 278
MMA. *See* methyl methacrylate (MMA)
Monomers, bulky methacrylates, 22*s*
Monometallic ruthenium-p-cymene complexes, 116*s*

N

N-butyl acrylate, 55*f*
  ARGET ATRP, 214
  LRcP, 50*s*
  RITP, 321*t*
N-butyl acrylate polymerization, *Ultimate ATRP^{SM}*, 210, 211*f*, 212*f*, 214
Newman projections, radical polymerizations, 36*f*
NHC ligand, 117*s*
N-iodosuccinimide (NIS), 306, 311
NIPAM homopolymerization, 283*t*
NIS. *See* *N*-iodosuccinimide (NIS)
Nitrones, radical coupling, 219, 223
Nitroxide mediated copolymerization simulation, 52*t*
Nitroxide-mediated radical polymerization (NMRP), 60
  photoinduced, 61
Nitroxide-terminated chains, 55*f*
NMRP. *See* nitroxide-mediated radical polymerization (NMRP)
N-vinylpyrrolidone (NVP), 267, 267*s*, 268*t*, 269*f*
NVP. *See* N-vinylpyrrolidone (NVP)

O

O-ethyl-S-(1-carboxy)methyl dithiocarbonate synthesis, 261
Organotellurium-mediated, photoinduced controlled radical polymerizations, 70*s*

P

PEGA. *See* poly(ethylene glycol) methyl ether acrylate (PEGA)
PEGA polymerizations, 178*f*
Perylene diimide macro-RAFT agents, 252*s*
PhMA, trimeric growing chains, 29*f*
Photochemical generation, ATRP, 67*s*
Photoinduced ATRP, 65
Photoinduced controlled radical polymerizations
  dithiocarbamate, ATRP, 66*s*
  manganese decacarbonyl/alkyl iodide system, 70*s*
  methyl methacrylate, 68*f*
    visible light-induced atom transfer radical polymerization, 69*t*
  methyl methacrylate, C/LRP, 61*s*
  organotellurium-mediated, 70*s*
  overview, 59
  photochemical generation, ATRP, 67*s*
  photoinduced ATRP, 65
  photoinduced degenerative-transfer polymerization, 69
  photoinduced NMRP, 61
  photoinduced RAFT polymerization, 64
  photoiniferters, 60, 60*c*
  photoinitiated RAFT polymerization, 65*s*
  photoinitiated reverse ATRP process, 66*s*
  photosensitive alkoxyamines, 63*c*
  photosensitive RAFT agents, 64*c*
  photosensitive TEMPO-based alkoxyamines, 62*c*
  PMMA, 69*f*
  vinyl monomers, 63*s*
Photoinduced degenerative-transfer polymerization, 69
Photoinduced NMRP, 61
Photoinduced RAFT polymerization, 64
Photoiniferters, 60, 60*c*
Photoinitiated RAFT polymerization, 65*s*
Photoinitiated reverse ATRP process, 66*s*
Photosensitive alkoxyamines, 63*c*
Photosensitive RAFT agents, 64*c*

Downloaded by 89.163.35.42 on May 30, 2012 | http://pubs.acs.org
Publication Date (Web): March 20, 2012 | doi: 10.1021/bk-2012-1100.ix002

Downloaded by 89.163.35.42 on May 30, 2012 | http://pubs.acs.org
Publication Date (Web): March 20, 2012 | doi: 10.1021/bk-2012-1100.ix002

- Photosensitive TEMPO-based alkoxyamines, 62*c*
- PMMA, photoinduced controlled radical polymerizations, 69*f*
- Poly(ethylene glycol) methyl ether acrylate (PEGA), 177
- Poly(FMA), bulky methacrylates, 30*f*
- Poly(glycidyl methacrylate), 107*f*
- Poly(3-hexylthiophene) macro-RAFT agents, 251*s*
- Poly(3-hexylthiophene)-block-polystyrene, 251*s*
- Polymer properties tuning
  - acrylates ATRP branching, 150*t*, 153*t*, 157*f*, 158*f*, 160*f*, 161*f*, 162*f*
  - acrylates FRP branching, 152*t*, 153*t*, 156*f*
  - ATRP, 146*s*, 149*s*, 159*f*
  - CRP model, 147*s*
  - FRP, 159*f*
  - ICAR ATRP, 149*s*
  - kinetic model
    - acrylates CRP/FRP, 150
    - acrylates CRP/FRP branching, 156
    - ICAR ATRP, 154, 162
  - MMA ICAR ATRP, 154*t*, 156*t*, 163*f*, 164*f*, 165*f*, 166*f*, 167*f*
  - NMP, 146*s*
  - overview, 145
  - RAFT polymerization, 146*s*
- Polymer tacticity nomenclature, 17*s*
- Poly(methyl methacrylate), RAFT polymerization, 255*f*
- Poly(N-vinylpyrrolidone) (PVP), 271*f*, 272*t*
- Poly(triarylamine) block copolymer, 252*s*
- PSt macroinitiators, *Ultimate ATRP*^{SM}, 209, 210*f*, 214
- PVP. *See* poly(N-vinylpyrrolidone) (PVP)

R

- Racemo propagation, bulky methacrylates, 18*s*
- Radical polymerizations, electron spin resonance
  - diphenylphosphinoyl radical, activation energies, 42*t*
  - diphenylphosphinoyl radical, Arrhenius plot, 41*f*
  - newman projections, averaged structures, 36*f*
  - overview, 33
  - SS ESR spectra, 36*f*, 37*f*
  - SS ESR/ATRP combination method, 35, 44
  - TMDPO, TR ESR spectrum, 38*f*, 43*f*
  - TR ESR measurements, 37, 44
  - TR ESR spectra, 39*f*, 40*f*, 41*f*
- RAFT polymerization
  - aqueous soluble switchable RAFT agent, 246*s*
  - aryl trithiocarbonate RAFT agent, 248*s*
  - block copolymers, 285*f*, 287*f*
  - block copolymers, organic semiconductors, 250
  - chain transfer agents, 280*f*
  - cyanoisopropyl dithiobenzoate, 254*s*
  - dithiocarbamate RAFT agents, 245*s*, 246*s*, 247*s*
  - DMA polymerization, 283*t*, 284*f*
  - DMAm polymerizations, 246*f*
  - end-group transformation, 253*s*
  - gel permeation chromatograms, 247*f*
  - microwave oven, 279*f*
  - microwave-irradiation, 278
  - MMA polymerization, 282*f*
  - monomers, 280*f*
  - NIPAM homopolymerization, 283*t*
  - overview, 243, 277
  - perylene diimide macro-RAFT agents, 252*s*
  - poly(3-hexylthiophene) macro-RAFT agents, 251*s*
  - poly(3-hexylthiophene)-block-polystyrene, 251*s*
  - poly(methyl methacrylate), 255*f*
  - poly(triarylamine) block copolymer, 252*s*
  - RAFT-click reaction, 253, 255*s*
  - S-benzyl trithiocarbonate, 248*s*
  - single unit monomer insertion, 248, 249*s*
  - styrene, 288*f*
  - styrene macro-RAFT agent, 250*f*
  - switchable raft agents, 244
  - thiocarbonylthio end group removal, 251*s*
  - thiocarbonylthio RAFT agents, 244*s*
  - vinyl acetate, 286*f*
  - ‘Z’ group agents, 245*f*
- RAFT-click reaction, 253, 255*s*
- RAFT-mediated microemulsion polymerization
  - kinetic model, 295
  - kinetic simulations, 299*f*, 300*f*, 301*f*, 302*t*
  - overview, 293
  - *See also* RAFT polymerization
- RCMP. *See* reversible complexation mediated polymerization (RCMP)

Downloaded by 89.163.35.42 on May 30, 2012 | http://pubs.acs.org
Publication Date (Web): March 20, 2012 | doi: 10.1021/bk-2012-1100.ix002

- Reverse iodine transfer polymerization (RITP)
  - block copolymer synthesis, 318, 319
  - chloromethylstyrene, 328*f*
  - CROP, 319
  - derived polymers, 327*f*
  - kinetics, 319
  - macromolecular engineering, 326
    - block radical polymerization, 328
    - living polymerization combination, 329
    - substitution reaction, 327
  - mechanisms, 318*s*, 319
  - methyl acrylate, 323*f*
  - MMA, 321*f*, 324*f*, 325*f*, 326*t*
  - n-butyl acrylate, 321*t*
  - overview, 317
  - polymer synthesis, 318
  - poly(1,1,2,2-tetrahydroperfluorodecyl acrylate), 328*f*
  - styrene, 322*f*, 324*f*, 325*f*, 326*t*
- Reversible complexation mediated polymerization (RCMP)
  - alkyl iodide, 308*f*, 312
  - amines, 310
  - GPC, 307
  - HI elimination, 311*s*
  - higher molecular weights, 310
  - MMA, 309*f*, 309*t*, 311*t*, 312*f*, 313*f*, 313*t*
  - NIS, 311
  - overview, 305
  - reversible activation processes, 306*s*, 307*s*
  - TEA, 308
- Ruthenium μ-carbide complex, 127*s*

S

- S-benzyl trithiocarbonate, 248*s*
- Sequence-regulated vinyl copolymers, 140
- Single unit monomer insertion, 248, 249*s*
- Small molecule synthesis, CuAAC, 86
  - functionalized polytriazoles synthesis, 91
  - triazolyl alkyl ester-Aryl compound synthesis, 86
- SS ESR spectra, radical polymerizations, 36*f*, 37*f*
- SS ESR/ATRP combination method, radical polymerizations, 35, 44
- St. *See* styrene (St)
- Stereocontrol strategies, bulky methacrylates, 16*s*
- Styrene (St), 4
  - cross-metathesis, 118*s*, 118*t*
  - FRcP, 51*s*
  - LRcP, 50*s*
  - macro-RAFT agent, 250*f*
  - polymerization, minimal time, 5*t*
  - polymerization, *Ultimate ATRP*^{SM}, 208, 208*f*, 209*f*, 214
  - RAFT-mediated microemulsion polymerizations, 293
- Switchable RAFT agents, 244
- Syndiotactic poly(MMA), 26*f*
- Syndiotactic poly(MMA), bulky methacrylates, 26*f*

T

- Tacticity, bulky methacrylates, 19
  - conformational analysis, 25
  - π-stacking interactions, 27
  - steric effects, 23
- TEA. *See* triethylamine (TEA)
- Terminal monomer units
  - acrylate terminal chain ends fraction, 57*f*
  - active chain fraction, styrene terminal, 57*f*
  - conventional radical copolymerization simulation, 53*t*
  - DEPN-based alkoxyamine, 54*f*
  - methyl acrylate, FRcP, 51*s*
  - n-butyl acrylate, 55*f*
  - n-butyl acrylate, LRcP, 50*s*
  - nitroxide mediated copolymerization simulation, 52*t*
  - nitroxide-terminated chains, 55*f*
  - overview, 47
  - simulations, 49
  - styrene, FRcP, 51*s*
  - styrene, LRcP, 50*s*
- Thiocarbonylthio end group removal, RAFT polymerization, 251*s*
- Thiocarbonylthio RAFT agents, 244*s*
- TMDPO, TR ESR spectrum, 38*f*, 43*f*
- TR ESR measurements, radical polymerizations, 37, 44
- TR ESR spectra, radical polymerizations, 39*f*, 40*f*, 41*f*
- Triblock copolymer, 221*f*
- Tricyclohexylphosphine, 116*s*
- Tricyclohexylphosphine ligand, 116*s*
- Triethylamine (TEA), 306, 308
- Trimeric poly(MMA) propagating radical, 19*f*
- Triphenylphosphine ligand, 119*s*

U

Ultimate ATRP^{SM}
  AIBN concentration, 207*f*
  Cu^{I} activator, 205*f*
  features, 206
  mechanism, 206*f*
  n-butyl acrylate, ARGET ATRP, 214
  n-butyl acrylate polymerization, 210, 211*f*, 212*f*, 214
  new technology, 205
  overview, 203
  PSt macroinitiators, 209, 210*f*, 214
  styrene polymerization, 208, 208*f*, 209*f*, 214
Unsaturated 16-electron ruthenium species, 126*s*

V

Vinyl monomers, 63*s*
Vinylidene ligand, 121*s*, 123*s*
Vinylphosphonic acid (VPA), 261, 262, 262*s*, 263*s*, 264*t*, 265*f*, 266*f*
VPA. *See* vinylphosphonic acid (VPA)

Z

'Z' group agents, RAFT polymerization, 245*f*

Downloaded by 89.163.35.42 on May 30, 2012 | http://pubs.acs.org
Publication Date (Web): March 20, 2012 | doi: 10.1021/bk-2012-1100.ix002